

SHORT PAPERS IN—

- Analytical methods
- Economic geology
- Engineering geology
- Geochemistry
- Geomorphology
- Glaciology
- Ground water
- Hydrologic instrumentation
- Limnology
- Marine geology
- Mineralogy
- Paleontology
- Petrology
- Photogeology
- Pleistocene geology
- Quality of water
- Stratigraphy
- Structural geology
- Surface water
- Volcanology

GEOLOGICAL SURVEY RESEARCH 1967

Chapter C



PROPERTY OF:
U. S. BUREAU OF MINES

AREA VI MINERAL RESOURCE OFFICE

GEOLOGICAL SURVEY RESEARCH 1967

Chapter C

GEOLOGICAL SURVEY PROFESSIONAL PAPER 575-C

Scientific notes and summaries of investigations in geology, hydrology, and related fields



UNITED STATES GOVERNMENT PRINTING OFFICE, WASHINGTON: 1967

UNITED STATES DEPARTMENT OF THE INTERIOR

STEWART L. UDALL, Secretary

GEOLOGICAL SURVEY

William T. Pecora, Director

CONTENTS

GEOLOGIC STUDIES

Mineralogy and petrology

	Page
Upside-down metamorphic zonation, blueschist facies, along a regional thrust in California and Oregon, by M. C. Blake, Jr., W. P. Irwin, and R. G. Coleman.....	C1
The occurrence of green iron-rich muscovite and oxidation during regional metamorphism in the Grandfather Mountain window, northwestern North Carolina, by Bruce Bryant.....	10
Tetrasilicic dioctahedral micas—celadonite from near Reno, Nev., by M. D. Foster.....	17
A computer-based procedure for deriving mineral formulas from mineral analyses, by E. D. Jackson, R. E. Stevens, and R. W. Bowen.....	23
Spheroidal weathering of thermally metamorphosed limestone and dolomite, White Mountains, Calif., by V. C. LaMarche, Jr.....	32
Rare-earth mineral occurrence in marine evaporites, Paradox basin, Utah, by O. B. Raup, A. J. Gude 3d, and H. L. Groves, Jr.....	38
Volcanism and tectonism as reflected by the distribution of nonopaque heavy minerals in some Tertiary rocks of Wyoming and adjacent States, by Yoshiaki Sato and N. M. Denson.....	42
Petrology of a late Quaternary potassium-rich andesite flow from Mount Adams, Washington, by R. A. Sheppard.....	55

Structural geology

Precambrian wrench fault in central Arizona, by C. A. Anderson.....	60
Breccia pipes in the West Tintic and Sheeprock Mountains, Utah, by H. T. Morris and R. W. Kopf.....	66

Marine geology

Description and use of an underwater television system on the Atlantic Continental Shelf, by J. E. Eddy, V. J. Henry, John Hoyt, and Edward Bradley.....	72
Heavy-mineral assemblages in the nearshore surface sediments of the Gulf of Maine, by D. A. Ross.....	77
High-efficiency subbottom profiling, by G. A. Rusnak.....	81
Subsurface morphology of Long Island Sound, Block Island Sound, Rhode Island Sound, and Buzzards Bay, by A. R. Tagg, and Elazar Uchupi.....	92
Origin of Redondo submarine canyon, southern California, by R. F. Yerkes, D. S. Gorsline, and G. A. Rusnak.....	97

Geochemistry

Activity coefficients from emf measurements, by C. L. Christ and P. B. Hostetler.....	106
Possible role of sulfur-oxidizing bacteria in surficial acid alteration near hot springs, by G. G. Ehrlich and Robert Schoen... ..	110
Spectrographic data on the composition of basaltic rocks, by T. G. Lovering, M. S. Niles, and M. L. Graves.....	113
Calculation of ion activity products for a brine from the Bonneville Salt Flats, Utah, by W. L. Polzer and C. E. Roberson... ..	116

Paleontology and stratigraphy

Lower Permian plants from the Arroyo Formation in Baylor County, north-central Texas, by S. H. Mamay.....	120
Age and regional significance of basal part of Milligen Formation, Lost River Range, Idaho, by C. A. Sandberg, W. J. Mapel, and J. W. Huddle.....	127

Analytical techniques and instrumentation

Spectrographic determination of volatile elements in silicates and carbonates of geologic interest, using an argon d-c arc, by Charles Annell.....	132
Determination of phosphorus in silicate rocks by neutron activation, by L. P. Greenland.....	137
Determination of palladium in the parts-per-billion range in rocks, by F. S. Grimaldi and M. M. Schnepfe.....	141

Glacial geology and glaciology

Glaciation at Wallowa Lake, Oreg., by D. R. Crandell.....	145
Observations on the Teton Glacier, Grand Teton National Park, Wyoming, 1965 and 1966, by J. C. Reed, Jr.....	154

Economic geology

Revised correlation of the No. 4 (Dawson Springs No. 6) coal bed, Western Kentucky coal field, by T. M. Kehn, J. E. Palmer, and G. J. Franklin.....	160
---	-----

	Page
Engineering geology	
Kaolinization of bedrock of the Boston, Mass., area, by C. A. Kaye.....	C165
Volcanology	
May 1963 earthquakes and deformation in the Koae fault zone, Kilauea Volcano, Hawaii, by W. T. Kinoshita.....	173
Geomorphology	
The great sand dunes of southern Colorado, by R. B. Johnson.....	177
Photointerpretation	
Measurement of the abundance of fracture traces on aerial photographs, by F. W. Trainer.....	184
HYDROLOGIC STUDIES	
Ground water	
Use of an infiltration gallery to obtain fresh water at Ocean Cape, Alaska, by A. J. Feulner, H. H. Heyward, and C. G. Angelo.....	189
Immobility of connate water in permeable sandstone, by G. E. Manger and W. T. Wertman.....	192
Surface water	
The underside of river ice, St. Croix River, Wis., by K. L. Carey.....	195
Analytical approaches to computation of discharge of an ice-covered stream, by K. L. Carey.....	200
Two methods of estimating base flow at ungaged stream sites in Kansas and adjacent States, by L. W. Furness and M. W. Busby.....	208
Characteristics of summer base flow of the Potomac River, by R. L. Hanson.....	212
The construction and use of flow-volume curves, by E. G. Miller.....	216
Bed-material movement, Middle Fork Eel River, Calif., by J. R. Ritter.....	219
Quality of water	
Chemical characteristics of bulk precipitation in the Mojave Desert region, California, by J. H. Feth.....	222
Winter loss and spring recovery of dissolved solids in two prairie-pothole ponds in North Dakota, by J. H. Ficken.....	228
Hydrogeologic significance of calcium-magnesium ratios in ground water from carbonate rocks in the Lancaster quadrangle, southeastern Pennsylvania, by Harold Meisler and A. E. Becher.....	232
Limnology	
Shoreline features as indicators of high lake levels, by D. D. Knochenmus.....	236
Hydrologic instrumentation	
Magnetic tape recording of geophysical logs, by W. S. Keys.....	242
INDEXES	
Subject	247
Author	251

GEOLOGICAL SURVEY RESEARCH 1967

This collection of 44 short papers is the second published chapter of "Geological Survey Research 1967." The papers report on scientific and economic results of current work by members of the Geologic and Water Resources Divisions of the U.S. Geological Survey.

Chapter A, to be published later in the year, will present a summary of significant results of work done during fiscal year 1967, together with lists of investigations in progress, reports published, cooperating agencies, and Geological Survey offices.

"Geological Survey Research 1967" is the eighth volume of the annual series Geological Survey Research. The seven volumes already published are listed below, with their series designations.

Geological Survey Research 1960—Prof. Paper 400
Geological Survey Research 1961—Prof. Paper 424
Geological Survey Research 1962—Prof. Paper 450
Geological Survey Research 1963—Prof. Paper 475
Geological Survey Research 1964—Prof. Paper 501
Geological Survey Research 1965—Prof. Paper 525
Geological Survey Research 1966—Prof. Paper 550

UPSIDE-DOWN METAMORPHIC ZONATION, BLUESCHIST FACIES, ALONG A REGIONAL THRUST IN CALIFORNIA AND OREGON

By M. C. BLAKE, Jr., W. P. IRWIN, and R. G. COLEMAN,
Menlo Park, Calif.

*Work done in cooperation with the
California Division of Mines and Geology*

Abstract.—Low-grade metamorphic rocks of the blueschist facies grade upward to the sole of a great thrust fault along the eastern margin of the Coast Ranges in northern California and southwestern Oregon. The gradation is defined by three textural zones of increasing reconstitution in metagraywacke, and by two metamorphic mineral zones, lawsonite and pumpellyite. The metagraywacke of textural zones 1 and 2 is clearly Franciscan Formation on the basis of lithology and age, and grades into thoroughly reconstituted rocks of textural zone 3 that herein are named the South Fork Mountain Schist. The blueschist probably formed in a zone of cataclasis and anomalously high water pressures under the thrust fault, rather than in the generally postulated zone of extreme depth of burial. Water in excess of that required to form pumpellyite and lawsonite was available for serpentinization of ultramafic rocks emplaced in the thrust fault.

Depth of burial is commonly thought to be the primary factor in the development of regionally metamorphosed rocks. Under this concept the metamorphic grade should increase downward in response to the normal gradients of pressure and temperature. This view of regional metamorphism, however, does not seem to apply to a belt of blueschist several hundred miles long in northwestern California and southwestern Oregon, where rather than increasing downward, the metamorphism increases upward to the sole of a low-angle thrust fault along the eastern side of the belt. The upward increase in metamorphism is both textural and mineralogic, and thus the thrusting is thought to have been more important with regard to metamorphism than was depth of burial. The term

“blueschist” as used herein refers to rocks of the blueschist metamorphic facies of Bailey and others (1964).

Three widely spaced parts of the blueschist belt (the Yolla Bolly area and the Pickett Peak quadrangle in California and the Agness area in Oregon) have been studied in detail by one or more of the authors, and most of the remaining parts of the belt have been sampled in reconnaissance. The authors have benefited by discussions and field trips with B. L. Wood of the New Zealand Geological Survey, and E. D. Ghent of Victoria University, New Zealand. We are indebted to E. H. Bailey, J. O. Berkland, H. R. Blank, Jr., Preston E. Hotz, and Salem Rice for the generous loan of specimens.

GEOLOGIC SETTING

The thrust fault along the eastern side of the blueschist belt generally forms the boundary between the Coast Range province on the west, and the Klamath Mountains and the Great Valley provinces on the east (fig. 1). The Klamath Mountains are a structurally complex terrane of Paleozoic and earlier-than-latest Mesozoic (pre-Tithonian) strata that are widely intruded by granitic, mafic, and ultramafic rocks. The Mesozoic rocks of the Great Valley are a thick sequence of clastic sedimentary strata, ranging from latest Jurassic (Tithonian) to Late Cretaceous in age, whose upturned edge crops out in a broad band adjacent to the Coast Ranges along the west side of the valley. These strata, called the Great Valley sequence, were deposited on the continental shelf and slope, on base-

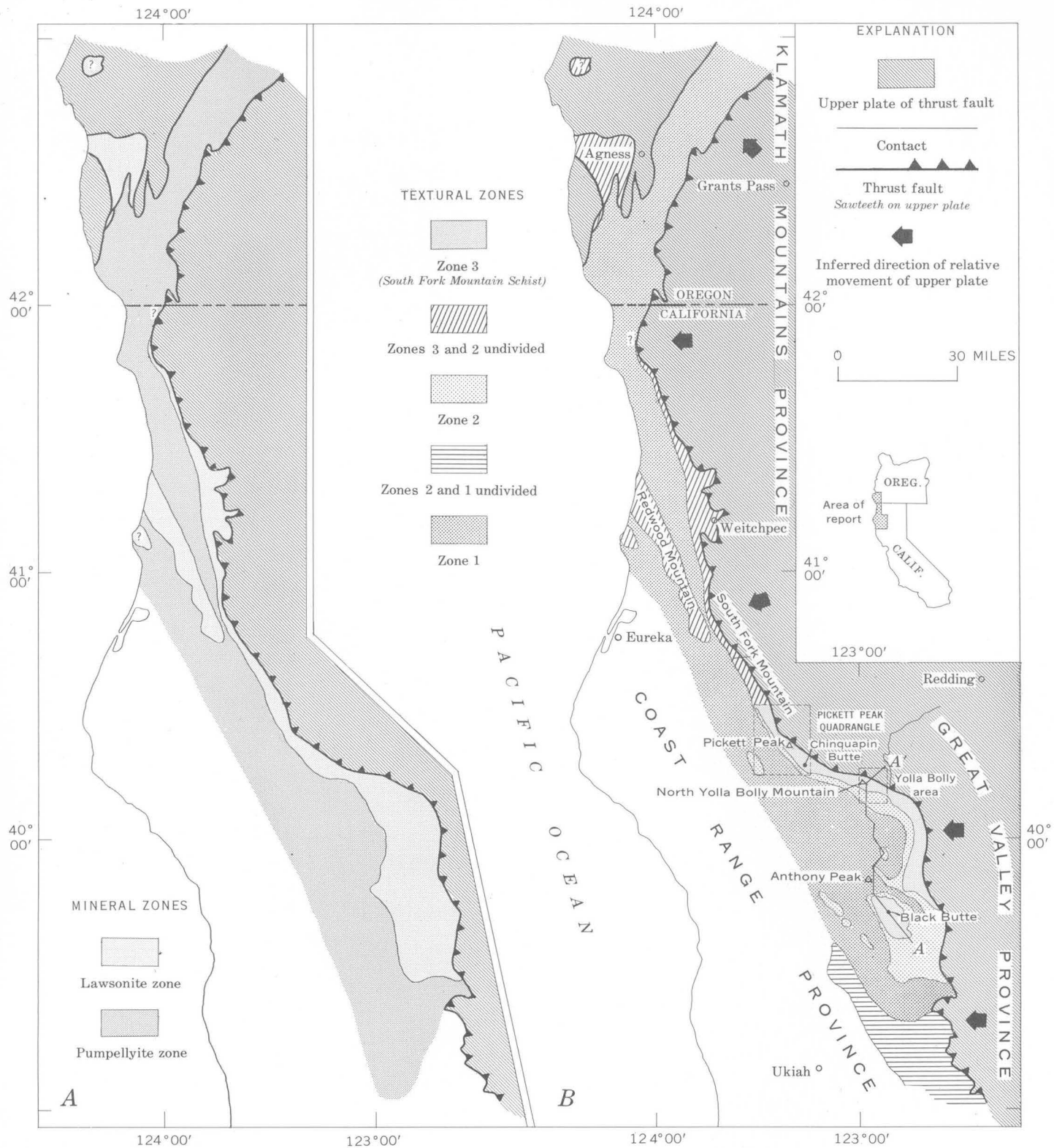


FIGURE 1.—Maps of part of California and Oregon, showing mineralogic (A) and textural (B) zones in metamorphic rocks of the blueschist facies.

ment rocks comparable to the Klamath Mountains terrane. The Coast Ranges, lying west of the boundary thrust fault, consist chiefly of the Franciscan Formation, a highly deformed eugeosynclinal equivalent of the Great Valley sequence. The Franciscan consists predominantly of a thick prism of graywacke and shale, with locally abundant volcanic rocks and radiolarian chert. Along the boundary fault the rocks of the Klamath Mountains and Great Valley provinces are thrust westward, virtually as a single plate, over the Franciscan of the Coast Ranges. The trace of the thrust is marked along much of its length by linear masses of ultramafic rocks. The thrusting is thought to have occurred during the Late Cretaceous. These relations were described more fully elsewhere (Irwin, 1964; Bailey and others, 1964).

METAMORPHIC ZONATION

The Franciscan Formation has been metamorphosed to the blueschist facies (Bailey and others, 1964) in a belt along the west side of the trace of the thrust fault, the metamorphism increasing progressively toward the fault. The progressive metamorphism includes both increasing reconstitution (cataclasis and recrystallization) and increasing metamorphic grade. The reconstitution is zoned in the field chiefly on the basis of megascopic textures of the graywacke. The metamorphic grade is zoned in the laboratory on the presence of the metamorphic minerals pumpellyite and lawsonite in metagraywacke. Coincident with increasing metamorphism, the Franciscan becomes more folded until near the thrust fault the folds are tightly isoclinal with axial planes that dip toward the trace of the fault.

Three textural zones of progressive metamorphism have been mapped (fig. 1). The rocks of these zones correspond texturally to the chlorite subzones 1, 2, and 3 in metagraywacke of the greenschist facies of the Otago area of New Zealand (Turner, 1938). However, they differ mineralogically from those of the Otago area, and thus we will refer informally to the textural zonation in California and Oregon as textural zones 1, 2, and 3. In essence, the metagraywacke typical of textural zone 1 appears unmetamorphosed, and shows no evidence of cataclasis, either in outcrop or under the hand lens. That typical of textural zone 2 shows well-developed platy cleavage in outcrop, and is clearly cataclastic under the hand lens. Metagraywacke of textural zone 3 is completely recrystallized to quartz-mica schist. Transitional types exist between textural zones 1 and 2, and between textural zones 2 and 3, although parts of the complete transition locally are absent owing to postmetamorphic faulting.

Although the metagraywacke typical of textural zone 1 appears unmetamorphosed in outcrop, and texturally unmodified in thin section (fig. 2A), microscopic and X-ray diffraction studies show that it is truly metagraywacke consisting for the most part of the mineral assemblage quartz-albite-muscovite-chlorite-pumpellyite. The pumpellyite occurs as minute felted aggregates in the matrix and as a replacement of relict plagioclase grains. Prehnite has not been recognized, but lawsonite, together with pumpellyite, is found in some metagraywacke transitional into textural zone 2. Calcite is the common carbonate mineral, but at a few places metamorphic aragonite has been found in rocks containing pumpellyite but no lawsonite. The belt of pumpellyite-bearing metagraywacke is known to be many miles wide, but the western limit is not clearly known.

The metagraywacke transitional into textural zone 2 develops a subtle platy cleavage that can be distinguished in outcrop and that is generally parallel to bedding. The lower boundary of textural zone 2 is placed where a mild platy cleavage is seen both in outcrop and under the hand lens. In thin section (fig. 2B), the platy cleavage is seen to be caused by incipient cataclasis. In metagraywacke typical of textural zone 2, cataclastic texture is clearly seen (fig. 2C). Lawsonite is the only common calcium-aluminum silicate, and aragonite is the stable carbonate.

In the upper part of textural zone 2, the original sedimentary texture of the graywacke is almost completely destroyed, and recrystallization and incipient segregation into quartzofeldspathic and mafic micaeous layers that average about 0.2 millimeter in thickness are seen (fig. 2D). The boundary between textural zones 2 and 3 is at the point where recrystallization becomes complete and segregation banding well developed. In textural zone 3 the degree of metamorphic segregation is even greater, and the typical rock is an intensely crumpled, fine-grained quartz-albite-muscovite-chlorite schist. The schist commonly encloses abundant segregation quartz lenses. In thin section, much of the schist shows extreme internal deformation marked by small-scale isoclinal folding of the mafic layers (fig. 2E). Lawsonite occurs in much of the schist, and is coarse grained relative to that of textural zone 2. Some is seen to be oriented parallel to the axial planes of the isoclinal folds. Carbonate is very scarce in the schists of textural zone 3. Primary aragonite, mantled by later calcite, has been recognized in a number of thin sections, but at least one small lens of calcite marble has been found in the North Yolla Bolly area. It may be that calcite was the stable carbonate in part of the area under consideration. Garnet, epi-

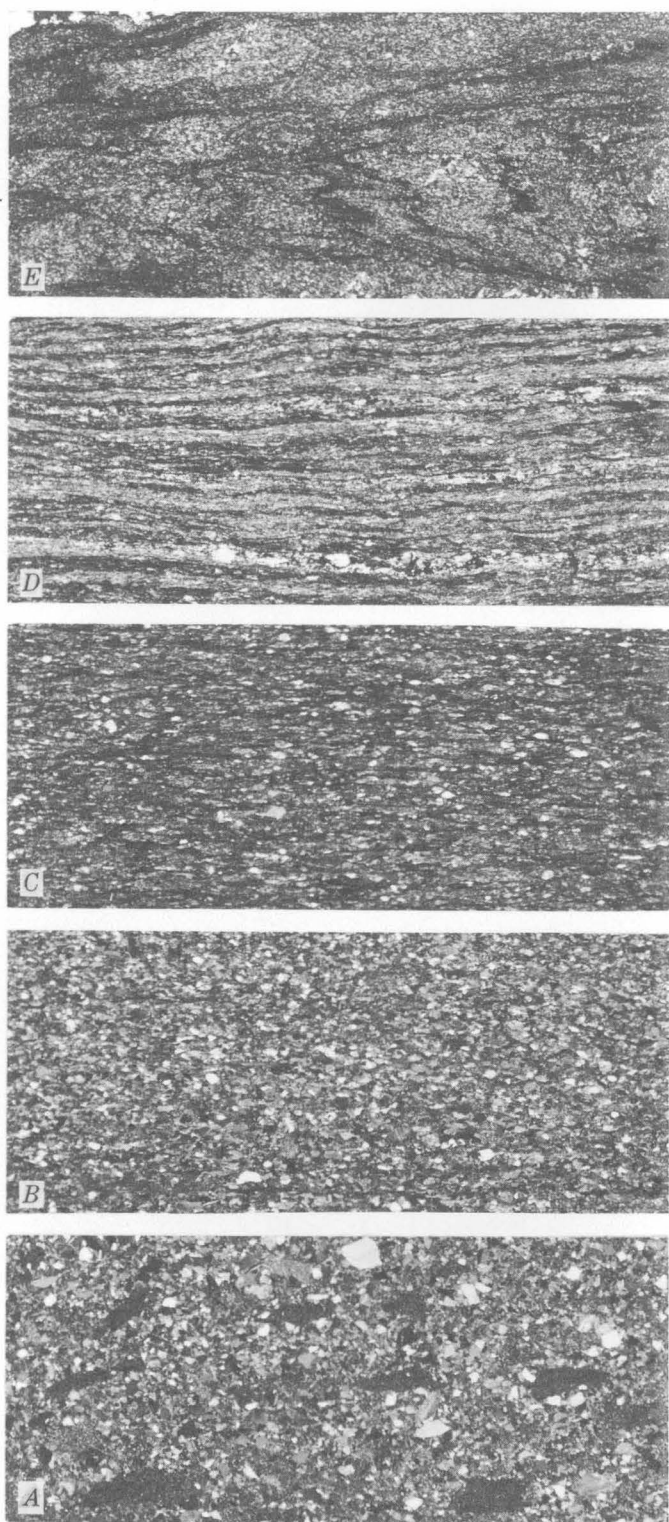


FIGURE 2.—Photomicrographs showing progressive development of metamorphic fabric from textural zones 1 to 3: (A) typical textural zone 1; (B) lower part of textural zone 2; (C) typical textural zone 2; (D) lower part of textural zone 3; (E) typical textural zone 3.

dote, sphene, and hematite have been recognized in some mafic varieties of the mica schist.

Although the textural zones are defined by the degree of cataclasis and recrystallization in graywacke, differences in the enclosed volcanic rocks and chert are also recognized. The volcanic rock and chert of textural zone 1 are megascopically similar to the same rock types elsewhere in the Franciscan. Pillow structure is seen in some outcrops, but many of the volcanic rocks are quartz keratophyre that consists largely of felted laths of cloudy twinned albite (0.1 to 0.25 mm in length) with subordinate fine-grained interstitial material recrystallized to quartz, chlorite, pumpellyite, and dusty sphene. Whole-rock X-ray diffraction patterns of the chert indicate minor albite, muscovite, and chlorite, in addition to quartz. In textural zone 2 the igneous texture of the volcanic rocks is clearly recognized only in thin section. Unlike the metagraywacke, the volcanic rocks are not visibly schistose in outcrop. However, in thin section, the volcanic rocks are seen to be broken by closely spaced fine-grained shear zones made up of clear albite, pumpellyite, chlorite, and quartz which have disrupted and rotated the relict plagioclase laths. The chert is noticeably sheared and locally contains spots of recrystallized quartz.

The metavolcanic rocks associated with the schist of textural zone 3 are basaltic in composition, and their metamorphic character is obvious both in outcrop and in thin section. The metabasalt is commonly a well-banded, light-green to greenish-brown, fine-grained gneiss that consists chiefly of albite, chlorite, actinolite, and epidote, with subordinate stilpnomelane, pumpellyite, muscovite, sphene, and quartz. Locally within the gneiss are bluish layers or segregations that consist largely of crossite, epidote, chlorite, and stilpnomelane, with subordinate quartz, albite, muscovite, and sphene. Metachert locally is found with the metabasalt, usually along contacts with mica schist. The most common variety of metachert is light blue and consists of quartz, riebeckite, hematite, and magnetite. Aegerine, garnet, barite, and stilpnomelane are common accessories.

The combined thickness of textural zones 2 and 3, measured nearly normal to the surface of the thrust fault, ranges from $1\frac{1}{2}$ to 3 miles, as shown in the geologic section through the North Yolla Bolly Mountain-Black Butte area (fig. 3). The outcrop width of textural zones 2 and 3 is much greater in this area than it is along the west face of South Fork Mountain (fig. 1B). A similar relation is seen in the mineral zonation (fig. 1A). The outcrop width of these zones,

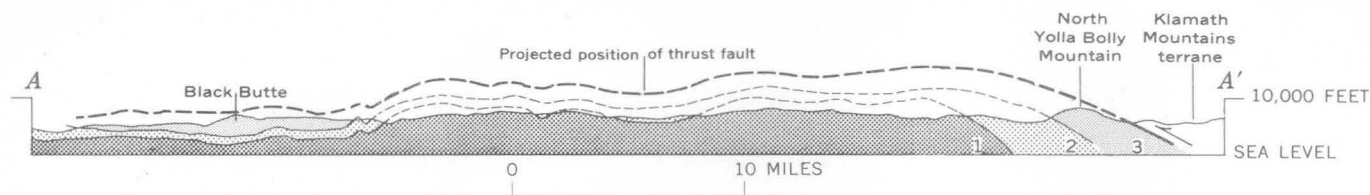


FIGURE 3.—Section through North Yolla Bolly Mountain and Black Butte, showing textural zones 1, 2, and 3.

however, is a circumstance of the intersection of structure and topography, and the actual difference in thickness of the transition zone is not as great as the disparity in outcrop width might suggest.

The mineral zonation shown on figure 1 is based on the presence of pumpellyite and lawsonite in the metagraywacke. The transition from pumpellyite- to lawsonite-bearing metagraywacke is toward the thrust fault, thus indicating an increase in metamorphic grade in that direction. The mineral zones also generally follow the trace of the thrust fault, but their boundaries do not coincide exactly with those of the textural zones. An increase in metamorphic grade toward the fault also is indicated by the transition from calcite, the predominant carbonate in textural zone 1, to aragonite in textural zones 2 and 3. A summary of mineral parageneses in relation to textural zonation is given in figure 4.

Buchias of latest Jurassic and Early Cretaceous age occur in rocks of both textural zones 1 and 2, and several are in rocks that contain lawsonite and aragonite (Irwin, 1960; Ghent, 1963; Blake, 1965). The fossil shells are now aragonite, whereas the shells of identical fossils in the unmetamorphosed Franciscan Formation and the Great Valley sequence are calcite. Fossils have not been found in rocks of textural zone 3; their preservation in these rocks would seem unlikely owing to the extreme cataclasis and recrystallization.

	TEXTURAL ZONES		
	1	2	3
Quartz			
Albite			
Chlorite			
White mica			
Pumpellyite		---	
Lawsonite		----	
Calcite	---		?
Aragonite		-----	
Texture	Nonschistose	Semischistose, nonsegregated	Schistose, segregated
Average grain size of lawsonite	0.01-0.02mm	0.02-0.03mm	0.05-0.08mm

FIGURE 4.—Summary of mineral parageneses of metagraywacke of textural zones 1, 2, and 3.

SOUTH FORK MOUNTAIN SCHIST

To formalize the original usage, rocks referred to as the schist of South Fork Mountain by Diller (1903a) are here named the South Fork Mountain Schist. This name is restricted to the rocks of textural zone 3. The type locality is Pickett Peak (sec. 26, T. 29 N., R. 7 E.) on South Fork Mountain in Pickett Peak quadrangle, California (fig. 1). The distribution of the South Fork Mountain Schist is shown as textural zone 3 (fig. 1) where the blueschist belt has been mapped in sufficient detail to differentiate textural zones 2 and 3. North of Pickett Peak quadrangle, rocks of textural zones 2 and 3 have not been divided, and have been called the Weitchpec Schist for exposures near Weitchpec (Hershey, 1904, 1906), Kerr Ranch Schist for exposures on Redwood Mountain (Manning and Ogle, 1950), and Colebrooke Schist in southwestern Oregon (Diller, 1903b).

Metabasaltic rocks in the South Fork Mountain Schist are here named the Chinquapin Metabasalt Member after its type locality, Chinquapin Butte (sec. 21, T. 28 N., R. 8 E., and sec. 18, T. 28 N., R. 12 W.), in the southeast corner of the Pickett Peak quadrangle. The Chinquapin Metabasalt Member occurs as mappable, discontinuous lenses throughout the South Fork Mountain Schist.

The South Fork Mountain Schist was long thought to be older rock of the complexly deformed Klamath terrane (Diller, 1903a; Hershey, 1906; Irwin, 1960; and others). Early workers thought that the schist was affiliated with rocks of the Klamath terrane because (1) pebbles of suspected Colebrooke Schist were thought to occur in nearby unmetamorphosed conglomerate of Early Cretaceous age along the coast of southern Oregon (Diller, 1903b), and (2) there was a supposed gradation between the schist and the Galice Formation of Late Jurassic age along the Trinity River near Weitchpec (Hershey, 1906). We have reexamined both localities. Although the conglomerate described by Diller contains pebbles of fine-grained quartz-sericite schist, none typical of the South Fork Mountain Schist was seen, nor did thin sections of the matrix of the conglomerate reveal blue amphibole or lawsonite. The supposed gradation between the schist

and Galice Formation could be neither readily confirmed nor disproved along the Trinity River south of Weitchpec, but exposures in new roadcuts along the Klamath River to the east of Weitchpec, where such a gradation also had been reported (Irwin, 1960), show that the transition from schist to the Galice Formation is abrupt and that the two formations are separated by sheared ultramafic rock. At all places where we have seen the relation between the schist and the Galice Formation clearly exposed, the two formations are separated by either ultramafic rock or a fault. Furthermore, it is perhaps of equal significance that nowhere is the South Fork Mountain Schist intruded by granitic dikes and plutons, although such intrusive rocks are widespread in the Galice and other pre-Nevadan formations of the Klamath terrane.

Locally, however, some metagraywacke of the Galice Formation might easily be mistaken for Franciscan metagraywacke high in textural zone 2 that is transitional into the South Fork Mountain Schist. Along much of the contact we have examined between the Galice and the schist, reconstitution equivalent to textural zone 2 is well developed in metagraywacke of the Galice. But at some places, such as in central Pickett Peak quadrangle, recrystallization and crude micaceous foliation approaching that of textural zone 3 develop within a few hundred feet of the fault contact. Here the Galice is intruded by felsic dikes, but nowhere have these dikes been seen to intrude the South Fork Mountain Schist. Secondary kink folds are a common feature of the more highly metamorphosed graywacke of the Galice. None of the Galice metagraywacke we have examined contains pumpellyite or lawsonite. Whole-rock X-ray patterns show it to consist almost entirely of quartz, albite, and well-crystallized muscovite and chlorite. Although this article emphasizes an upward increase in metamorphism of Franciscan rocks in the lower plate of the thrust fault, some evidence also suggests a downward increase in metamorphism (reconstitution) of the Galice Formation in the upper plate adjacent to the fault. This relation has been obscured by postmetamorphism faulting along much of the boundary between the Galice Formation and the South Fork Mountain Schist, and in some places the faults even have cut out the serpentine.

Strong doubt as to the affiliation of the South Fork Mountain Schist with pre-Nevadan rocks of the Klamath terrane was first raised during studies of the blueschist along the west side of the Great Valley (Blake and Ghent, 1964; also see Ghent, 1965, and Blake, 1965) that earlier had been mapped as metamorphosed Franciscan (Irwin, 1960). Here some of the more highly

metamorphosed rocks were found to be texturally and mineralogically similar to the mica schist and metabasalt typically exposed along South Fork Mountain, and were found to grade into the Franciscan Formation to the west. Ghent's work in the Anthony Peak-Black Butte area substantiated earlier work by Voloshin and Kilmer¹, who reported that the more highly metamorphosed rocks commonly are topographically higher than the less metamorphosed. Once the metamorphic gradation between the Franciscan and its higher metamorphic facies—the South Fork Mountain Schist—had been established, it became evident that the boundary between the Klamath terrane and Franciscan rocks is on the east side of the belt of the South Fork Mountain Schist rather than on the west.

Rubidium-strontium analyses of metagraywacke of both textural zones 1 and 2 in the Yolla Bolly area give an isochron age of 105 ± 16 million years (Z. E. Peterman and others, unpub. data), and this age conforms with the regional geologic relations. This metagraywacke contains *Buchia* of Early Cretaceous age, and grades into rocks of textural zone 3. Thus the metamorphic age of the South Fork Mountain Schist is later-than-earliest Cretaceous, and as the metamorphism is related to the Coast Range orogeny (Irwin, 1964), the schist is believed to have formed during the Late(?) Cretaceous. However, conflicting evidence of the age of metamorphism has been obtained in southwestern Oregon, where two whole-rock K/Ar ages on the Colebrooke Schist give 125 ± 6 m.y. and 138 ± 10 m.y. (Dott, 1965; Koch, 1966). Isotopic ages of coexisting white mica and glaucophane of 133 ± 15 m.y. have been obtained from schist in the Cazadero area, south of the area on figure 1 (Lee and others, 1964). The schist in the Cazadero area lies within the Franciscan Formation more than 50 miles southwest of the belt of South Fork Mountain Schist. It differs mineralogically and structurally from the South Fork Mountain Schist and cannot now be related. Even though the radiometric data are preliminary and need further verification, the geochronologic isotope evidence suggests two periods of blueschist-facies metamorphism in California and Oregon.

STRUCTURAL INTERPRETATION

The concept of inverted metamorphic zonation along a low-angle thrust fault, rather than a normal increase in metamorphism with increasing depth of burial, is based on several factors. Metamorphism of the Franciscan Formation clearly increases toward a fault

¹ Vadim Voloshin and Frank Kilmer, 1960, Engineering geology of the Eel-Glenn Tunnel: California Dept. Water Resources unpub. prelm. rept., 27 p.

boundary with Klamath terrane and Great Valley sequence, and the boundary generally is marked by serpentine. Axial planes of folds in the metamorphosed rock generally dip gently to moderately toward the boundary fault, and the sense of drag (or vergence) of the folds suggests westward translation of the Klamath terrane and Great Valley sequence over the Franciscan. West of the main belt of South Fork Mountain Schist, and generally occupying topographic highs, are isolated patches of rocks of textural zones 2 and 3. The isolated patches of rocks of textural zone 3 (South Fork Mountain Schist) were earlier (Irwin, 1964) thought to be klippen of Klamath terrane. But, as the South Fork Mountain Schist along the main belt is now considered to be a metamorphic facies of the Franciscan, the isolated patches of schist are also now considered metamorphosed Franciscan, and are thought to indicate the proximity of the Franciscan Formation to a regionally overlying plate of Klamath terrane that has been removed by erosion. Here the order of magnitude of westward transport of the upper plate may be comparable to that farther south in the Coast Ranges, where klippen of Great Valley sequence are found as much as 50 miles west of the trace of the thrust fault along the west side of the Great Valley.

BLUESCHIST-FACIES METAMORPHISM

The rocks of all three textural zones are tentatively assigned to the blueschist facies. Our inclusion of all these rocks in the blueschist facies is debatable, but the mineral assemblages in all three zones indicate recrystallization under high pressures and low temperatures. Within the metagraywacke of textural zone 1, pumpellyite and aragonite associated with quartz, albite, and chlorite cannot be placed in the prehnite-pumpellyite facies because of the absence of prehnite. The metagraywacke of textural zones 2 and 3 contains lawsonite and aragonite in equilibrium with quartz, albite, and chlorite, and thus belongs to the blueschist facies (Bailey and others, 1964). Seki (1965) has noted the lack of prehnite in blueschist metamorphic belts, and has suggested that higher pressures exclude prehnite. Transitions between blueschist and greenschist or prehnite-pumpellyite facies are to be expected. However, the mineral assemblages in rocks of textural zone 3 indicate pressure-temperature conditions more representative of blueschist. It is now well established that blueschist terranes form elongate belts that are developed as a result of high pressures and low temperatures in active tectonic zones, whereas the greenschist facies is developed at lower pressure-to-temperature ratios (Ernst, 1963; Coleman and Lee, 1962, 1963; Miyashiro, 1961). The blueschist facies is estimated to have

formed at temperatures beginning at 200°C and extending to perhaps 350° or 400°C. on the basis of O^{18}/O^{16} fractionation temperature curves as applied to equilibrium assemblages (H. P. Taylor, written commun., 1966).

Experimental studies of the aragonite-calcite transition indicate that at temperatures of 200° to 300°C, the pressure necessary for the formation of aragonite is on the order of 6,000 to 9,000 bars (Jamieson, 1953; Clark, 1957). Similar studies made on the stability of lawsonite (Crawford and Fyfe, 1965; Newton and Kennedy, 1963) and jadeite (Birch and LeComte, 1960) have shown that these minerals, common to the blueschist facies, are favored by high pressures.

Rocks of the blueschist facies are restricted to continental margins and island arcs, but their local tectonic environment and mode of formation are controversial. Most recent workers (Bailey and others, 1964; Ernst, 1965; Essene and others, 1965) have concluded that this metagraywacke was formed during extreme downwarping of a geosynclinal prism. If one assumes temperatures of formation were 200° to 300°C and lithostatic pressure was equal to total pressure, the experimental data on metamorphic aragonite indicate that these rocks must have been buried to depths of 20 to 30 kilometers.

If blueschist is formed by simple depth-of-burial (load) metamorphism, one would expect to find areas in the world where this is substantiated by field evidence. However, where the structural relations are described in the geologic literature, the anomalous situation of more completely metamorphosed schist structurally overlying less metamorphosed rocks is the rule rather than the exception. In the central Coast Ranges, south of the area on figure 1, blueschist has a great extent in the Diablo Range where glaucophane-bearing phyllonite appears to be related to the Tesla-Ortogonalita fault (Briggs, 1953), and in the Pacheco Pass area where jadeitized metagraywacke overlies unmetamorphosed graywacke (McKee, 1958). Similar structural relations have been described from blueschist areas in Europe (Egeler, 1956), Venezuela (Seiders, 1962), and Japan (Iwasaki, 1963; Seki, 1961).

A tectonic origin for the blueschist rocks is strongly suggested by their geographic distribution, outcrop pattern, and lithic associations. On a worldwide basis, the blueschist rocks generally crop out in long narrow belts associated with linear masses of ultramafic rocks. In addition to blueschist rocks in California, examples are seen in the Sanbagawa belt of Japan (Miyashiro, 1966), the marginal synclinal belt of New Zealand (Coombs and Landis, 1966), the blueschist ultramafic

belt of northern New Caledonia (Coleman, 1966), and the Kamchatka and Ural belts of the USSR (Dobretsov and others, 1966). The common association of blueschist and ultramafic rocks has led many geologists to suggest a genetic relation. It is our belief that on a regional scale the ultramafic rocks mark the sites of major low-angle thrusts into which they have been emplaced, and that blueschist is developed along the sole of the thrusts. However, the exact process by which pressure-temperature conditions of the blueschist field are restricted to a narrow zone is obscure.

Proposed conditions for development of rocks of the blueschist facies in northern California and southwestern Oregon are shown in figure 5. This model requires that the high-pressure-low-temperature conditions necessary for the development of the blueschist minerals must have been met in the zone immediately below the fault. In order to create such conditions, some means of developing tectonic overpressures must be called upon, for great depth of burial alone will not satisfy the geometry of the model. Overpressures in excess of twice the lithostatic pressures are theoretically possible (Coleman and Lee, 1962), assuming that the rocks have sufficient strength. A related factor may be the development of anomalously high water pressures in the rocks below the thrust fault. During thrusting the reorganization of the sedimentary fabric due to cataclasis would result in a considerable reduction of pore space in the rocks of the lower plate. If the interstitial water was detained by an impermeable boundary, such as ultramafic rock in the fault zone, fluid pressure might exceed the lithostatic pressure long enough to allow crystallization of the dense hydrous mineral lawsonite. The importance of the thrusting to the development of the pumpellyite-bearing metagraywacke of textural zone 1 is not entirely clear. The pumpellyite may develop as a result of tectonic thicken-

ing caused by thrusting, the rocks below the zones of pronounced reconstitution being buried to appropriate depths for the crystallization of pumpellyite.

In a recent paper (Heard and Rubey, 1966), it has been suggested that thrust faults may arise through dehydration reactions such as gypsum→anhydrite and serpentine→peridotite. They have demonstrated that during such a reaction, there occurs a marked decrease in the strength of the rocks, together with a corresponding increase in pore pressure. In our example, however, we are dealing with a hydration reaction such as anorthite + 2H₂O→lawsonite. In this situation, much of the interstitial water is presumably incorporated into the silicate structure (lawsonite, 11.3 percent H₂O; pumpellyite, 7.3 percent H₂O). An interesting corollary is that under this concept the remainder of the interstitial water not used for such reactions would also be available for the serpentinization of the peridotite in the fault zone.

REFERENCES

- Bailey, E. H., Irwin, W. P., and Jones, D. L., 1964, Franciscan and related rocks and their significance in the geology of western California: California Div. Mines and Geology Bull. 183, 177 p.
- Birch, A. F., and LeComte, Paul, 1960, Temperature-pressure plane for albite composition: Am. Jour. Sci., v. 258, p. 209-217.
- Blake, M. C., Jr., 1965, Structure and petrology of low-grade metamorphic rocks, blueschist facies, Yolla Bolly area, northern California: Stanford Univ. unpub. Ph.D. thesis, 91 p.
- Blake, M. C., Jr., and Ghent, E. D., 1965, Regional glaucophane schist facies metamorphism in the northern Coast Ranges of California [abs.]: Geol. Soc. America Spec. Paper 82, p. 241.
- Briggs, L. I., Jr., 1953, Geology of the Ortigalita Peak quadrangle: California Dept. Nat. Resources, Div. Mines Bull. 167, 61 p.
- Clark, S. P., Jr., 1957, A note on the calcite-aragonite equilibrium: Am. Mineralogist, v. 42, p. 564-566.
- Coleman, R. G., 1966, Glaucophane schists from California and New Caledonia [abs.]: Pacific Sci. Cong., 11th, Tokyo 1966, Proc. 4, p. 11.
- Coleman, R. G. and Lee, D. E., 1962, Metamorphic aragonite in the glaucophane schists of Cazadero, California: Am. Jour. Sci., v. 260, p. 577-595.
- 1963, Glaucophane-bearing metamorphic rock types of the Cazadero area, California: Jour. Petrology, v. 4, no. 2, p. 260-301.
- Coombs, D. S., and Landis, C. A., 1966, Metamorphic belts and orogenesis in New Zealand [abs.]: Pacific Sci. Cong., 11th Tokyo 1966, Proc. 4, p. 13.
- Crawford, W. A., and Fyfe, W. S., 1965, Lawsonite equilibria: Am. Jour. Sci., v. 263, p. 262-270.
- Diller, J. S., 1903a, Klamath Mountain section: Am. Jour. Sci., ser. 4, v. 15, p. 342-362.
- 1903b, Description of the Port Orford quadrangle: U.S. Geol. Survey Geol. Atlas, Folio 89, 6 p.

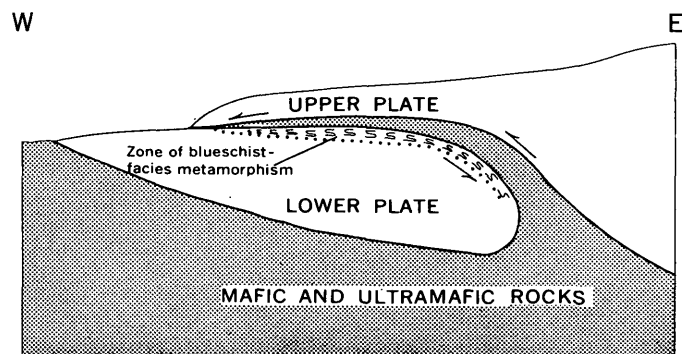


FIGURE 5.—Schematic diagram showing development of metamorphic rocks of the blueschist facies. Arrows indicate relative movement.

- Dobretsov, N. L., and others, 1966, Karta metamorficheskikh fatzi SSSR [Metamorphic facies map of the USSR]: Izdatel'stvo Nauka, Siberskoe Otdel, Novosibirsk, scale 1: 7,500,000.
- Dott, R. H., Jr., 1965, Mesozoic-Cenozoic tectonic history of the southwestern Oregon coast in relation to Cordilleran orogenesis: *Jour. Geophys. Research*, v. 70, no. 18, p. 4687-4707.
- Egeler, C. G., 1956, The alpine metamorphism in Corsica: *Geol. Mijnb.* v. 18, no. 4, p. 115-117.
- Ernst, W. G., 1963, Petrogenesis of glaucophane schists: *Jour. Petrology*, v. 4, p. 1-30.
- 1965, Mineral paragenesis in Franciscan metamorphic rocks, Panoche Pass, California: *Geol. Soc. American Bull.*, v. 76, no. 8, p. 879-914.
- Essene, E. J., Fyfe, W. E., and Turner, F. J., 1965, Petrogenesis of Franciscan glaucophane schists and associated metamorphic rocks, California: *Beitr. Zur. Mineralogie und Petrographie*, v. 11, p. 695-704.
- Ghent, E. D., 1963, Fossil evidence for maximum age of metamorphism in part of the Franciscan Formation, northern Coast Ranges, California: *California Div. Mines and Geology Spec. Rept.* 82, p. 41.
- 1965, Glaucophane-schist facies metamorphism in the Black Butte area, northern Coast Ranges, California: *Am. Jour. Sci.*, v. 263, p. 385-400.
- Heard, H. C., and Rubey, W. W., 1966, Tectonic implications of gypsum dehydration: *Geol. Soc. America Bull.*, v. 77, p. 741-760.
- Hershey, O. H., 1904, The Bragdon formation in northwestern California: *Am. Geologist*, v. 33, p. 248-256, 347-360.
- 1906, Some western Klamath stratigraphy: *Am. Jour. Sci.*, ser. 4, v. 21, p. 58-66.
- Irwin, W. P., 1960, Geologic reconnaissance of the northern Coast Ranges and Klamath Mountains, California, with a summary of the mineral resources: *California Div. Mines Bull.* 179, 80 p.
- 1964, Late Mesozoic orogenesis in the ultramafic belts of northwestern California and southwestern Oregon, in *Geological Survey Research 1964: U.S. Geol. Survey Prof. Paper 501-C*, p. C1-C9.
- Iwasaki, Masao, 1963, Metamorphic rocks of the Kotu-Bizan area, eastern Shikoku, Japan: *Tokyo Univ. Fac. Sci. Jour.*, Sec. 2, v. 15, part 1, 90 p.
- Jamieson, J. C., 1953, Phase equilibrium in the system calcite-aragonite: *Jour. Chem. Physics*, v. 21, p. 1385-1390.
- Koch, J. G., 1966, Late Mesozoic stratigraphy and tectonic history, Port Orford-Gold Beach area, southwestern Oregon Coast: *Am. Assoc. Petroleum Geologists Bull.*, v. 50, no. 1, p. 25-71.
- Lee, D. E., Thomas, H. H., Marvin, R. F., and Coleman, R. G., 1964, Isotopic ages of glaucophane schists from the area of Cazadero, California: *Art. 142 in U.S. Geol. Survey Prof. Paper 475-D*, p. D105-D107.
- McKee, E. B., Jr., 1958, The geology of the Pacheco Pass area, California: *Stanford Univ. Ph.D. thesis*, 88 p.
- Manning, G. A., and Ogle, B. A., 1950, Geology of the Blue Lake quadrangle, California: *California Dept. Nat. Resources, Div. Mines Bull.* 148, 36 p.
- Miyashiro, Akiho, 1961, Evolution of metamorphic belts: *Jour. Petrology*, v. 2, p. 277-311.
- 1966, Some aspects of peridotite and serpentinite in orogenic belts: *Japanese Jour. Geology and Geography*, v. 37, no. 1, p. 45-61.
- Newton, R. C., and Kennedy, G. C., 1963, Some equilibrium reactions in the join $\text{CaAl}_2\text{Si}_2\text{O}_8\text{-H}_2\text{O}$: *Jour. Geophys. Research*, v. 68, p. 2967-2983.
- Seiders, V. M., 1962, Geology of the central Miranda, Venezuela: *Princeton Univ., Ph.D. thesis*, 255 p.
- Seki, Yotaro, 1961, Geology and metamorphism of Sanbagawa crystalline schists in the Tenryu district, central Japan: *Saitama Univ., Urwa, Japan, Sci. Rept.*, ser. B, v. 4, no. 1, p. 75-92.
- 1965, Prehnite in low-grade metamorphism: *Saitama Univ., Urwa, Japan, Sci. Rept.*, v. 5, no. 1, p. 29-43.
- Turner, F. J., 1948, Mineralogical and structural evolution of the metamorphic rocks: *Geol. Soc. America Mem.* 30, 342 p.



THE OCCURRENCE OF GREEN IRON-RICH MUSCOVITE AND OXIDATION DURING REGIONAL METAMORPHISM IN THE GRANDFATHER MOUNTAIN WINDOW, NORTHWESTERN NORTH CAROLINA

By BRUCE BRYANT, Denver, Colo.

Abstract.—Assemblages containing (1) magnetite, magnetite and hematite, or hematite, (2) variable and generally high Fe_2O_3/FeO ratios, and (3) green muscovite rich in ferric iron in various rock types in progressively and retrogressively metamorphosed rocks suggest that the rocks in the Grandfather Mountain window were open to oxygen during metamorphism. Metamorphism apparently took place under conditions of high shearing stress, low temperature, and high P_{H_2O} .

Metamorphosed plutonic, sedimentary, and volcanic rocks beneath the Blue Ridge thrust sheet are exposed in the Grandfather Mountain window in northwestern North Carolina (fig. 1). In the window, Precambrian plutonic rocks that were formed 1,000–1,100 million years ago are unconformably overlain by a thick sequence of interbedded arkose, siltstone, shale, conglomerate, graywacke, and felsic and mafic volcanic rocks, all of late Precambrian age. In the southern part of the window, the autochthonous Precambrian rocks are separated from the tectonically overlying Blue Ridge thrust sheet by a thin intermediate thrust sheet composed of quartzite and shale of the Chilhowee Group of Cambrian and Cambrian(?) age and the Shady Dolomite of Cambrian age. During the Paleozoic, the Cambrian and upper Precambrian sedimentary and volcanic rocks were progressively metamorphosed to low grades; at the same time, the underlying plutonic rocks were retrogressively metamorphosed to the same grade. All the rocks are strongly cleaved and display a strong northwest-trending mineral lineation that marks the direction of the tectonic transport (Bryant, 1962, 1963; Bryant and Reed, 1962; Reed, 1964a, 1964b).

Sedimentary, volcanic, and plutonic textures are partly preserved in many of the rocks. The plutonic rocks have especially varied textures ranging from gneissic granitic rock to blastomylonite and phyllonite.

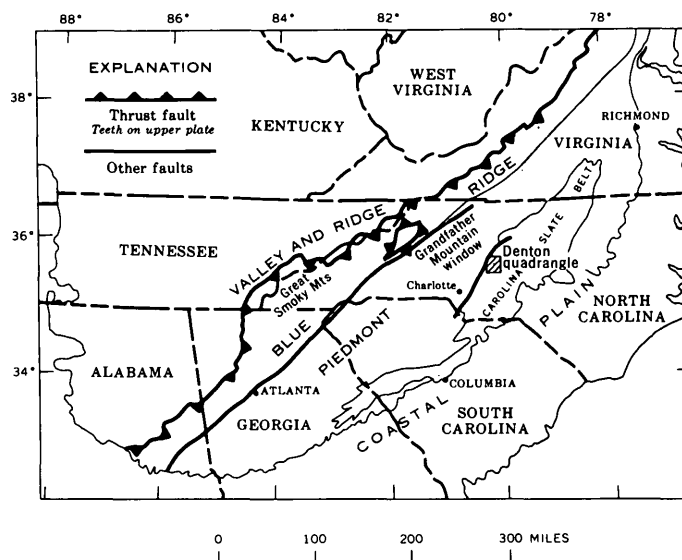


FIGURE 1.—Map showing location of the Grandfather Mountain window, the Great Smoky Mountains, and the Denton, N.C., quadrangle. Generalized from the tectonic map of the United States (Cohee and others, 1962).

The principal metamorphic minerals are epidote, albite, chlorite, and actinolite in mafic rocks; quartz, albite, microcline, biotite, and sericite in sandstones and felsic volcanic and plutonic rocks; and quartz, albite, sericite, biotite, and chlorite in predominantly argillaceous sedimentary rocks.

Green muscovite rich in ferric iron (Foster and others, 1960) is a common rock-forming mineral in many of the intensely sheared rocks of low metamorphic grade. A thorough study of the chemical variations of the mica in the different rock types was impracticable because of the difficulty in separating the mica, but chemical analyses of the rocks containing the green mica suggest the relations discussed below.

Mineral assemblages and approximate modes of some representative rocks are given in table 1. The pyrox-

TABLE 1.—Modal analyses and iron oxide ratios of metamorphic rocks in the Grandfather Mountain window, North Carolina, and beta index of contained muscovite

Sample	Field No.	Rock type	Modal analyses (volume percent)															FeO/FeO (weight percent)	β index (± 0.002), muscovite	Textural notes		
			Quartz	Potassic feldspar	Plagioclase	Quartz sericite and opaque groundmass	Muscovite	Epidote	Chlorite	Biotite	Actinolite	Pyroxene	Sphene and leucoxene	Ilmenite	Magnetite	Hematite	Calcite				Pyrite	Other
1	Q-11-1	Phyllite	18				31					36								100	1.597	Ilmenite in aggregates. Ilmenite rimmed by sphene. Some ilmenite rimmed by sphene.
2	GML-3	Metadiabase			14		8	23	23		1		20						1	100	1.603	
3	GML-1	Greenstone			4			25	8				54	1						100	.23	
4	6-960	Gray phyllite: Chilhowee Group					79													100		1.596
5	20-1959-C	Phyllonite	14	6			30					4								100		1.601
6	24-34	Felsic metavolcanic rock	54				6							2						100	1.1	1.609
7	M-52-3	Meta-arkose	29	36	17		1					5								100		1.594
8	GMB-6	Greenstone	42	2	16		19					1			11					100	.82	1.596
9	U-67-2a	Phyllite					36													100		1.600
10	GMB-5	Felsic metavolcanic rock	6				26					60								100		1.600
11	12-0-19-B	Green phyllite: Chilhowee Group	16	8	1	73	1												Tr.	100	1.6	1.609
12	R-63-4-B	Felsic metavolcanic rock	30				66												2	100		1.618
13	GML-2	Greenstone	16	26	21		25	1	Tr.	Tr.	Tr.									100	6.4	1.608
14	T-31-1	Phyllite			14		1	30	17				26							100	1.9	
15	Z-15-1-B	Phyllonite	18				70													100		1.604
16	GMB-2	Phyllite	35				57													100		1.609
17	ZA-8-1-b	Quartzitic gneiss	11		8		75													100	3.1	1.613
18	ZD-4-4	Phyllonite	69	6			22													100		1.618
19	W-32-2	Phyllite	24				41	2	10											100		1.593
20	J-20-1	do	7		13		28		25											100		1.605
21	H-49-2-b	Sandy phyllite	5				82													100	11.5	1.614
22	RE-03-1	Meta-arkose																		100		1.614
23	GML-8	do	36	10	2		50													100		1.614
24	GML-7	do	54	14	6		22													100		1.617
25	J-8-4-a	do	42	8	13		35													100	14.3	1.618
			51	16	7		25													100	3.4	1.619
			25	16	16		41													100	3.9	1.614
																				100		1.614

¹ Rutile included.² Analyzed mica, table 2.

ene in sample 3 is relict from the original volcanic rock and is out of equilibrium with the metamorphic mineral assemblage. Other relict minerals, such as detrital grains or phenocrysts of quartz, or possibly of potassic feldspar, are in equilibrium with the metamorphic conditions. Plagioclase and amphibole have been altered to albite or actinolite, respectively. Most of the rocks in table 1 were selected for polished-section study because they have an abundance of opaque minerals. Except for the high opaque-mineral content and lack of less metamorphosed basement rock, these rocks are representative of the range of lithic types and mineral suites found in the Grandfather Mountain window.

The iron and titanium oxide minerals were identified in polished sections. A hand magnet was run over a powdered sample of the rock to confirm the presence and to approximate the proportion of magnetite. Magnetite and hematite were not likely to be confused with magnetite in polished section because of its anisotropic character.

Magnetite forms equidimensional subhedral to euhedral grains. Hematite occurs as smaller platy crystals, anhedral grains, or aggregates of grains. Where hematite and magnetite occur together, the hematite is on the margins of and along fractures in magnetite and appears to be younger than the magnetite. In a few of the volcanic rocks larger grains of magnetite or ilmenite are probably premetamorphic, because their grain size contrasts with that of the metamorphic minerals. Some of the larger magnetite grains are partly replaced by hematite, and compose part of a matrix of minerals recrystallized during metamorphism. In most of the rocks of table 1, the oxides apparently have crystallized during metamorphism.

OCCURRENCE OF IRON-RICH MUSCOVITE

Fine-grained green iron-rich muscovitic mica (Foster and others, 1960) is widespread in the rocks of the Grandfather Mountain window and in the plutonic rocks and intercalated slices of rocks of the Chilhowee Group in the Blue Ridge thrust sheet, north and west of the window. Minerals and textures produced by the latest metamorphism in rocks outside the window are similar to those in the window. The green mica is widespread in metamorphosed sandstones and interbedded shales, felsic volcanic rocks, and plutonic rocks, and gives many of these rocks a markedly green color.

The analysis and optical properties of green muscovite from the Grandfather Mountain area are given in table 2. Although the muscovitic micas with high indices of refraction generally have a high ferric and total-iron content, the relations between these param-

eters are not close enough to allow composition to be precisely determined from optical data (Foster and others, 1960). Beta refractive indices and pleochroism of many of the green micas in rocks of the Grandfather Mountain window are similar to those of the mica in table 2, but a wide range in β index of other samples of green to colorless muscovitic mica (table 1) indicates that some of them have different iron contents. It is likely that all the green muscovites contain more ferric than ferrous iron (Foster and others, 1960, p. 850).

In a review of phengitic micas in low-grade schists, Ernst (1963) points out that such micas are common in glaucophane schists and that a few have been reported in greenschists. The analyzed mica from the Grandfather Mountain window is more ferruginous than any in Ernst's compilation. Kanehira and Banno (1960), however, report a mica from a glaucophane schist facies terrane with a higher β index of refraction (1.624), and that it contains 9.10 percent Fe_2O_3 , 1.96 percent FeO, and 2.87 percent MgO.

TABLE 2.—Analysis, in weight percentage adjusted for impurities, and optical properties of green muscovite

[From Foster and others, 1960, table 2 and p. 841]

Analysis	Optical properties ¹
SiO ₂ 47.62	α 1.580 ± 0.001, colorless.
Al ₂ O ₃ 24.74	
Fe ₂ O ₃ 8.11	β 1.6195 ± 0.0005, light green.
FeO..... 2.55	γ 1.6230 ± 0.0005, light green.
MgO..... 1.88	$\gamma - \alpha$ 0.043 ± 0.01.
Na ₂ O..... .11	Optic sign... Negative.
K ₂ O..... 10.72	2V..... 35° ± 3°.
H ₂ O..... 4.05	
F..... .14	
Total..... 100.00	

¹ Indices determined in Na light at 25°C.

The relation between the occurrence of iron-rich muscovite and the ratio $\text{K}_2\text{O}/\text{Fe}_2\text{O}_3/\text{FeO} + \text{MgO}$ in sedimentary and volcanic rocks in the Grandfather Mountain window is shown in figure 2. The formation of iron-rich muscovite is favored by the presence of microcline and a $\text{Fe}_2\text{O}_3/\text{FeO} + \text{MgO}$ ratio of 1 or more. In mafic rocks the ferric iron is taken up in larger amounts of epidote, magnetite, and hematite (table 1).

The β index of the muscovite shows a very general increase with increase in oxidation of the rocks as shown by the Fe-Ti oxide minerals (fig. 3) and increase in $\text{Fe}_2\text{O}_3/\text{FeO}$ ratios (table 1). However, the range of the index of the mica associated with each oxide assemblage indicates that other compositional parameters in the rock, such as K_2O , Al_2O_3 , or MgO contents, may

also control the iron content of the muscovite. The Fe_2O_3/FeO ratios are related to the quantity as well as the nature of the iron-bearing minerals in the rock.

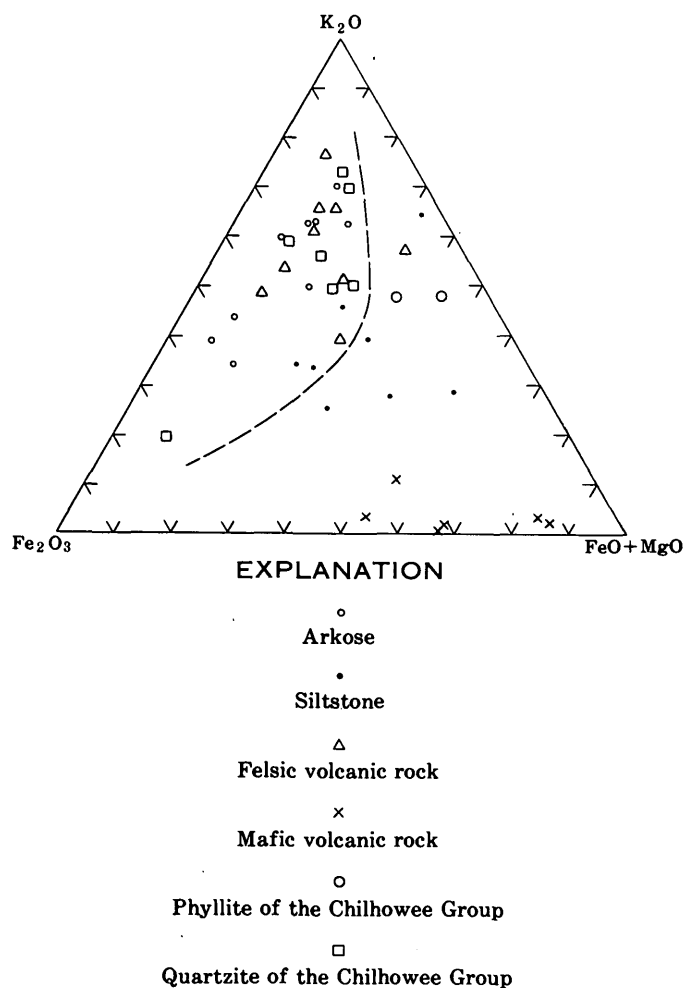


FIGURE 2.—Ratios of K_2O , Fe_2O_3 , and $FeO+MgO$ in metamorphosed sedimentary and felsic volcanic rocks in the Grandfather Mountain window. Samples to the left of the dashed line contain green muscovite rich in ferric iron. Rocks to the right of the line contain biotite, colorless sericite, and chlorite. Some rocks immediately to the left of the line contain iron-rich muscovite and biotite and (or) chlorite. Rocks near the $Fe_2O_3-FeO+MgO$ side contain epidote, actinolite, and chlorite.

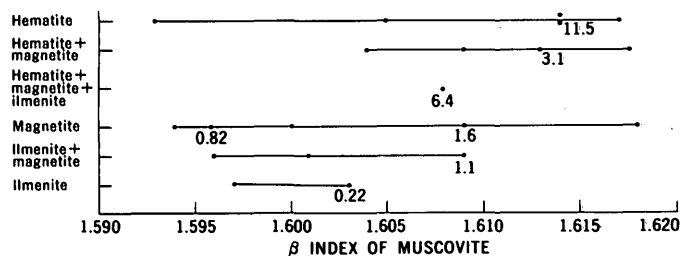


FIGURE 3.—Relation between β index of muscovite and Fe-Ti oxide minerals of rock. Numbers beneath points are Fe_2O_3/FeO ratios for rocks where analysis is available.

Fe_2O_3/FeO RATIOS IN ROCKS OF THE GRANDFATHER MOUNTAIN WINDOW—AN OXIDIZED TERRANE?

Chemical analyses of the sedimentary and volcanic rocks in the Grandfather Mountain window show that the rocks have varied but generally high Fe_2O_3/FeO ratios (fig. 4A). The variation is independent of the total-iron content. This variation is especially well shown by the mafic volcanic rocks, which have about 13

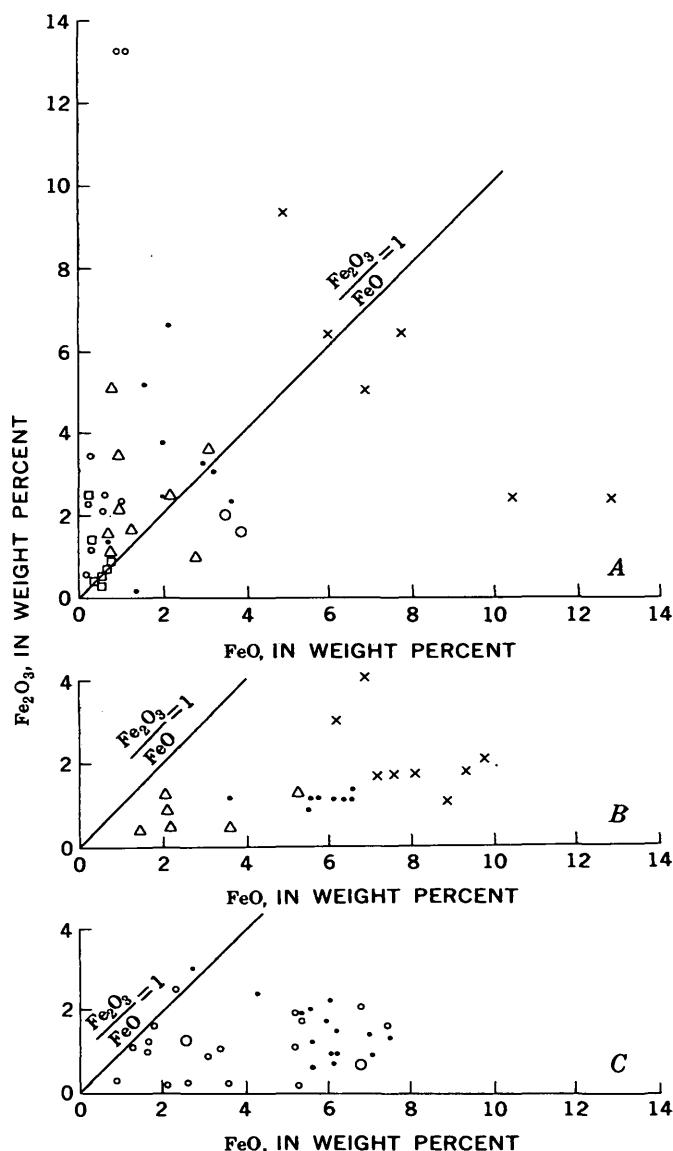


FIGURE 4.—Oxidation state of iron in some suites of rocks of low metamorphic grade. A. Grandfather Mountain window: small circle, arkose; dot, siltstone; triangle, felsic volcanic rock; X, mafic volcanic rock; large circle, phyllite of the Chilhowee Group; square, quartzite of the Chilhowee Group. B. Slate belt in the Denton quadrangle, North Carolina (Arvid Stromquist, written commun., 1962): X, mafic volcanic rock; triangle, felsic volcanic rock; dot, argillite. C. Great Smokey Mountains, Tenn.-N.C. (Hamilton, 1961; Hadley and Goldsmith, 1963; King, 1964): small circle, sandstone; dot, siltstone; large circle, shale.

percent total $\text{FeO} + \text{Fe}_2\text{O}_3$ content but various $\text{Fe}_2\text{O}_3/\text{FeO}$ ratios. The oxidation state of the iron in the rocks before metamorphism is not known, and the $\text{Fe}_2\text{O}_3/\text{FeO}$ ratios in the premetamorphic sedimentary and volcanic rocks certainly were not the same. Some idea as to the general values of the ratios may be drawn by analogy with ratios from unmetamorphosed rock of the same type (table 3).

TABLE 3.— $\text{Fe}_2\text{O}_3/\text{FeO}$ ratios of typical unmetamorphosed rocks and of various metamorphic rocks in the Grandfather Mountain window

Rock type	Typical ratio in unmetamorphosed rock		Ratio in rocks of the Grandfather Mountain window	
	Range	Average	Range	Average
Arkose.....	¹ 0.45-6.7	2.1	2-14.....	7.6
Graywacke and siltstone.....	¹ 0.1-1.3	.45	0.2-3.2.....	1.7
Basalt flows.....	² 1; often 0.5	.5	0.2-1.9 (includes one intrusive rock).	0.9
Felsic volcanic rocks.....	Variable; may be very high for subaerially deposited tuffs. ⁴		³ 0.2-6.4.....	2.3
Orthoquartzite....	¹ 0.20-4.5	2.0	1.1-9.3.....	3.3

¹ Pettijohn (1963); data on siltstone lacking.

² Of 333 rocks identified as basalt in the field and recently analyzed in the laboratories of the U.S. Geological Survey, 80 percent have ratios of Fe_2O_3 to FeO less than 1, and 52 percent have ratios of less than 0.5. These include altered and vesicular basalts, which commonly have higher ratios than massive basalts. Basalts extruded subaerially show similar relations (see recent analyses of Columbia River basalts in Waters, 1961; Hamilton, 1963a).

³ Includes flows and tuffs, but whether deposited subaerially or subaqueously is not certain.

⁴ For examples of subaerial flows and tuffs see Hamilton (1963b) and Lipman (1965).

If, in the Grandfather Mountain window, the original volcanic rocks were deposited subaerially and the original arkoses were red beds, the $\text{Fe}_2\text{O}_3/\text{FeO}$ ratios of many of the rocks may reflect the premetamorphic oxidation state of the iron in those rocks. However, the ratios in the basalt flows, graywackes and siltstones, and, perhaps, the quartzites are higher than might be expected for such rocks.

In irregularly distributed areas and local zones in the Grandfather Mountain window, blastomylonite and phyllonite derived from basement rock have high contents of green iron-rich muscovite. Chemical analyses of these metamorphosed basement rocks are not available, but it is reasonable to assume that rocks rich in green muscovite have $\text{Fe}_2\text{O}_3/\text{FeO}$ ratios greater than 1. Blastomylonitic and recrystallized mortar gneiss containing biotite generally have $\text{Fe}_2\text{O}_3/\text{FeO}$ ratios of less than 0.5 (Bryant, 1966, table 1). Comparison of chemical analyses of phyllonite and metamorphosed basement rock lacking green mica shows that the iron in

the phyllonite is more oxidized than in the less altered granitic gneiss (Bryant, 1966, table 1). Some phyllonite zones in the basement rocks are locally rich in hematite (table 1, samples 15 and 18). Thus, during the retrogressive metamorphism of the basement rocks and the progressive metamorphism in the overlying sedimentary and volcanic rocks, the terrane was apparently open to oxygen.

Compared with the metamorphosed rocks of similar grade of nearby terranes, the rocks of the Grandfather Mountain window are highly oxidized. Regionally metamorphosed argillite and felsic and mafic volcanic rock of low metamorphic grade in the Carolina slate belt of central North Carolina (in the Denton quadrangle), and the sandstone, siltstone, and shale in the western margin of the Blue Ridge thrust sheet in the Great Smoky Mountains have markedly lower $\text{Fe}_2\text{O}_3/\text{FeO}$ ratios (figs. 4B and 4C) than rocks in the Grandfather Mountain window (fig. 4A).

ORIGIN OF IRON-RICH MUSCOVITE

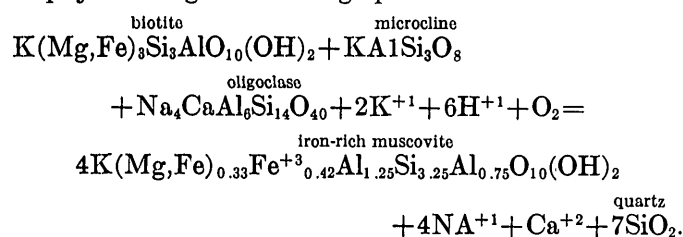
Several studies have related the formation of iron-rich muscovite to metamorphism under oxidizing conditions. Chinner (1960) found that in pelitic gneisses of sillimanite grade in the Glen Clova area, Scotland, the more oxidized the rocks, the higher the indices of refraction and ferric iron contents in the muscovite. Lambert (1959) in Scotland and Miyashiro (1958) in Japan found that muscovites were richer in Fe_2O_3 in rocks of low metamorphic grade than in those of higher grade. Lambert (1959, p. 561, 583) attributed the ferric iron content of the muscovite to metamorphism at low temperature accompanied by strongly oxidizing conditions and high chemical activity of hydroxyl ion. McNamara (1965, p. 361-362) found, statistically, that white micas from the rocks of the upper greenschist facies (biotite zone; corresponding to the metamorphic grade of the rocks in the Grandfather Mountain window) had larger ratios of Fe^{+3} to Fe^{+2} than micas from lower greenschist facies (chlorite zone) rocks. He attributed the difference in this ratio between micas of the two zones to higher total pressure of oxygen (P_{O_2}), from greater thermal dissociation of water in the higher grade or upper greenschist facies zone.

Ernst (1963) concludes that high fluid pressure and low temperature encourage solid solution between muscovite and celadonite, resulting in phengitic mica, such as the green iron-rich muscovite from the Grandfather Mountain area. On the basis of experimental work and a review of the occurrence of phengites, Velde (1965, p. 910-911) concludes that high pressure ($\approx P_{\text{H}_2\text{O}}$) is responsible in most cases for the formation of phen-

gitic micas. The experimental work of Velde agrees with Lambert's observation that at high metamorphic grade conditions the phengitic micas converge toward compositions close to those of muscovite.

Plas (1959, p. 538) gives a possible reaction for the formation of phengite from biotite, muscovite, microcline, and quartz in metamorphosed granitic rocks. The resulting phengite gneisses have $\text{Fe}_2\text{O}_3/\text{FeO}$ ratios of 0.8 to 3.5, and most of the ratios are greater than 2. Although the phengite in those gneisses has an infinite ratio of Fe_2O_3 to FeO , due to lack of FeO its Fe_2O_3 to $\text{FeO} + \text{MgO}$ ratio is only 1.2 compared to 1.8 for the iron-rich muscovite from the Grandfather Mountain area. Plas concludes that the iron in the biotite is completely converted to ferric iron by oxygen derived from water available during metamorphism.

Petrographic study of least metamorphosed basement rocks in the Grandfather Mountain area indicates that muscovite was not widespread before metamorphism. Apparently iron-rich muscovite in the metamorphosed basement rocks formed by destruction of biotite and various amounts of feldspar. A possible reaction leading to formation of iron-rich muscovite in a phyllonite or phyllonitic gneiss lacking epidote or albite is



Part of the iron is oxidized by oxygen from water available during metamorphism, and feldspars are converted to mica by H^{+1} and K^{+1} ions from the water. The H^{+1} and O_2 necessary for the reaction must be available by the dissociation of water (Eugster, 1959, p. 407). The conversion of granitic rock to phyllonite requires that potassic feldspar be sericitized, which results in the liberation of K^{+1} (Bryant, 1966). During sericitization more H^{+1} ions are consumed than O atoms, leaving a net surplus of O in unreacted water. This could furnish a source and mechanism for relatively high P_{O_2} during the metamorphism of the overlying sedimentary and volcanic rocks and in parts of the phyllonite zones.

Reactions involved in the formation of iron-rich muscovite in overlying sedimentary and volcanic rocks can only be surmised because of lack of knowledge of original mineralogy. The reactions could be much simpler than the reaction shown here and involve merely clay minerals and iron oxide minerals or biotite without affecting feldspar.

SUMMARY

Rocks in the Grandfather Mountain window have various $\text{Fe}_2\text{O}_3/\text{FeO}$ ratios, at least some of which are probably substantially greater than those in the original premetamorphic rocks. The rocks in the terrane, as a whole, have higher $\text{Fe}_2\text{O}_3/\text{FeO}$ ratios than rocks in nearby terranes of similar metamorphic grade, thus suggesting that the rocks in the Grandfather Mountain window behaved as a system locally open to oxygen.

Structural evidence suggests that deformation and metamorphism in the Grandfather Mountain window could have taken place over a considerable length of time, and it may have been associated with earlier phases of thrusting. In contrast, rocks of the Carolina slate belt and those of the Great Smoky Mountain area (fig. 3) are products of regional metamorphism not directly associated with thrusting. Intense α lineations and well-developed foliation in rocks of diverse types in the Grandfather Mountain window show that shear stress was relatively high. The uniform occurrence of mineral assemblages of the greenschist facies throughout the Grandfather Mountain window suggests that temperature was relatively low and no marked temperature gradients existed between different parts of the area. The mineral assemblages containing such hydrous minerals as mica, chlorite, actinolite, and epidote indicate that the $P_{\text{H}_2\text{O}}/P_{\text{rock}}$ ratio was high. The range in iron oxide minerals from ilmenite to hematite in the rocks indicates that P_{O_2} was variable but locally high in many rock types in various localities throughout the Grandfather Mountain window.

REFERENCES

- Bryant, Bruce, 1962, Geology of the Linville quadrangle, North Carolina-Tennessee (preliminary report): U.S. Geol. Survey Bull. 1121-D, 30 p.
- 1963, Geology of the Blowing Rock quadrangle, North Carolina: U.S. Geol. Survey Geol. Quad. Map GQ-243.
- 1966, Formation of phyllonites in the Grandfather Mountain area, northwestern North Carolina, in Geological Survey Research, 1966: U.S. Geol. Survey Prof. Paper 550-D, p. D144-D150.
- Bryant, Bruce, and Reed, J. C., Jr., 1962, Structural and metamorphic history of the Grandfather Mountain area, North Carolina—A preliminary report: Am. Jour. Sci., v. 260, p. 161-180.
- Chinner, G. A., 1960, Pelitic gneisses with varying ferrous/ferric ratios from Glen Clova, Angus, Scotland: Jour. Petrology, v. 1, no. 2, p. 178-217.
- Cohee, G. V., and others, 1962, Tectonic map of the United States, exclusive of Alaska and Hawaii: U.S. Geol. Survey and Am. Assoc. Petroleum Geologists.
- Ernst, W. G., 1963, Significance of phengitic micas from low-grade schists: Am. Mineralogist., v. 48, p. 1357-1373.

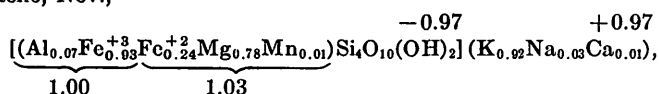
- Eugster, H. P., 1959, Reduction and oxidation during metamorphism, in Abelson, P. H., ed., *Researches in geochemistry*: New York, John Wiley and Sons, p. 397-426.
- Foster, M. D., Bryant, Bruce, and Hathaway, John, 1960, Iron-rich muscovitic mica from the Grandfather Mountain area, North Carolina: *Am. Mineralogist.*, v. 45, p. 839-851.
- Hadley, J. B., and Goldsmith, Richard, 1963, Geology of eastern Great Smoky Mountains, North Carolina and Tennessee: U.S. Geol. Survey Prof. Paper 349-B, 118 p.
- Hamilton, Warren, 1961, Geology of the Richardson Cove and Jones Cove quadrangles, Tennessee: U.S. Geol. Survey Prof. Paper 349-A, 55 p.
- 1963a, Columbia River basalt in the Riggins quadrangle, western Idaho: U.S. Geol. Survey Bull. 1141-L, 37 p.
- 1963b, Petrology of rhyolite and basalt, northwestern Yellowstone Plateau: Art. 80 in U.S. Geol. Survey Prof. Paper 475-C, p. C78-C81.
- Kanehira, K., and Banno, S., 1960, Ferriphengite and aegerin-jadeite in a crystalline schist of the Iimori district, Kii peninsula: *Geol. Soc. Japan Jour.*, v. 66, p. 654-659.
- King, P. B., 1964, Geology of the central Great Smoky Mountains, Tennessee: U.S. Geol. Survey Prof. Paper 349-C, 148 p.
- Lambert, R. St. J., 1959, The mineralogy and metamorphism of the Moine schists of the Morar and Knoyclart districts of Inverness-Shire: *Royal Soc. Edinburgh Trans.*, v. 63, p. 553-588.
- Lipman, P. W., 1965, Chemical comparison of glassy and crystalline volcanic rocks: U.S. Geol. Survey Bull. 1201-D, 24 p.
- McNamara, Malcolm, 1965, The lower greenschist facies in the Scottish Highlands: *Geol. Fören. Stockholm Förh.*, v. 87, p. 347-389.
- Miyashiro, Akiho, 1958, Regional metamorphism of the Gotsaisyo-Takanuki district in the Central Abukuma Plateau: *Tokyo Univ. Fac. Sci. Jour.*, sec. 2, v. 11, p. 219-272.
- Pettijohn, F. J., 1963, Chemical composition of sandstones—excluding carbonate and volcanic sands; in Fleischer, Michael, ed., *Data of geochemistry*, 6th ed: U.S. Geol. Survey Prof. Paper 440-S, p. S1-S21.
- Plas, L. van der, 1959, Petrology of the northern Adula region, Switzerland (with particular reference to the glaucophane-bearing rocks): *Leidse Geol. Mededeel.*, v. 24, p. 418-598.
- Reed, J. C., Jr., 1964a, Geology of the Lenoir quadrangle, North Carolina: U.S. Geol. Survey Geol. Quad. Map GQ-242.
- 1964b, Geology of the Linville Falls quadrangle, North Carolina: U.S. Geol. Survey Bull. 1161-B, 53 p.
- Velde, B., 1965, Phengitic micas—synthesis, stability, and natural occurrence: *Am. Jour. Sci.*, v. 263, p. 886-913.
- Waters, A. C., 1961, Stratigraphic and lithologic variations in the Columbia River basalt: *Am. Jour. Sci.*, v. 259, p. 583-611.



TETRASILICIC DIOCTAHEDRAL MICAS—CELADONITE FROM NEAR RENO, NEVADA

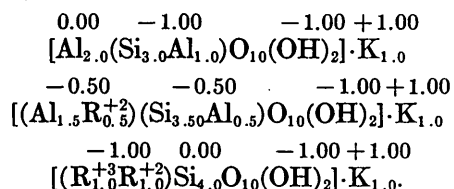
By MARGARET D. FOSTER, Washington, D.C.

Abstract.—The end result of replacement of 2 R⁺³ by R⁺² Si in muscovite is tetrasilicic mica in which half the octahedral cations are trivalent and half are bivalent, as for example in Al_{1.0}Mg_{1.0}, Al_{1.0}Fe_{1.0}⁺², Fe_{1.0}⁺³Mg_{1.0}, or Fe_{1.0}⁺³Fe_{1.0}⁺². A comparative study of the formulas calculated from seven published analyses of tetrasilicic or near-tetrasilicic dioctahedral micas shows that the formula calculated from the analysis of celadonite from near Reno, Nev.,



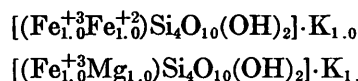
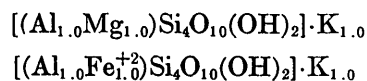
is closer to that of the theoretical (Fe⁺³Mg) tetrasilicic end member than are the formulas calculated from any other analyses. This celadonite gives a well-resolved X-ray diffraction pattern and consists of a single phase.

Foster (1956) has shown that progressive replacement of the trivalent octahedral cations by bivalent cations is accompanied by a simultaneous increase in Si, decrease in tetrahedral Al, and a gradual shift in the seat of the charge from the tetrahedral layers to the octahedral layer. The end result of this replacement is a tetrasilicic dioctahedral mica in which half the octahedral cations are trivalent and half are bivalent as shown by:



The fact that half the octahedral cations are bivalent in the tetrasilicic Si₄ end member in no way relates these Si₄ micas to biotites. Replacement in the octahedral layer is ion for ion, and the Si₄ micas are dioctahedral, just as muscovite is, and not trioctahedral, as are the biotites.

Possible tetrasilicic end members containing the cations most commonly found in natural micas are:



Analyses of natural dioctahedral potassium micas indicate that the dominant trivalent octahedral cation is Al⁺³ at the muscovite or trisilicic end, and is usually Fe⁺³ at the celadonite or tetrasilicic end; neither Al⁺³ nor Fe⁺³ seem to extend from one end of the range to the other as the dominant trivalent octahedral cation. Thus the trisilicic-tetrasilicic dioctahedral micas apparently do not represent a single series, but rather two series—one starts with muscovite and is characterized by replacement of 2 Al by MgSi, and the other starts with celadonite and is characterized by replacement of R⁺²Si by 2 Al, but neither extends much beyond the middle of the range.

The aluminum trisilicic end member, muscovite, Al₂(Si₃Al)O₁₀(OH)₂·K, is the most common of the micas, and numerous published analyses yield formulas in which the number of tetrahedral positions occupied by Si is between 3.00 and 3.10. The number of published analyses of micas in which Si occupies more than 3.10 tetrahedral positions decreases sharply with increase in Si content, and very few analyses have been published of dioctahedral micas in which Si occupies more than 3.80 (out of 4.00) positions in a half-cell formula.

NATURAL TETRASILICIC MICAS

A search of the literature revealed only seven analyses that yield formulas in which Si occupies more than 3.80 tetrahedral positions, and in which the interlayer charge is 0.85 or more. These analyses are given in table 1. The atomic ratios calculated from these analyses are given in table 2, and the compositions indicated by the atomic ratios are represented graphically in figure 1.

Analyses 1 through 5 (tables 1 and 2) yield atomic ratios that indicate tetrasilicic micas of the (Fe⁺³Mg), or celadonite type. In the formulas for analyses 1 and

TABLE 1.—Analyses of tetrasilicic dioctahedral micas with high K₂O content

Constituent	1	2	3	3a ¹	3b ¹	4	5	6	7
SiO ₂ -----	55.61	56.20	56.41	54.50	52.57	54.38	52.26	55.30	56.02
Al ₂ O ₃ -----	.79	2.05	2.14	2.23	2.32	5.41	1.62	10.90	17.82
TiO ₂ -----		.10				.14	(²)		.43
Fe ₂ O ₃ -----	17.19	19.18	14.07	14.63	15.28	14.22	21.84	6.95	1.14
FeO-----	4.02	3.19	5.10	5.30	5.54	3.56	4.45	3.54	2.79
MgO-----	7.26	5.42	5.91	6.15	6.42	6.40	5.25	6.56	5.21
MnO-----	.09	Tr.	.23	.24	.25	.25	(²)		.03
CaO-----	.21	.27	.60	.62	.65	.42	Tr.	.47	.68
Na ₂ O-----	.19	.64				.05	(²)	.00	Tr.
K ₂ O-----	10.03	8.26	8.83	9.18	9.59	9.23	10.04	9.38	9.17
H ₂ O-----	.48	4.86	6.80	7.07	7.38	1.16	10.10	6.51	1.51
H ₂ O ⁺ -----	4.40	.25				4.80			3.4.15
Total-----	100.27	100.42	100.09	99.92	100.00	⁴ 100.17	99.71	99.61	⁵ 99.96

1. Reno, Nev.; 23 miles east of Reno, Nev. (Wells, 1937, p. 102). In vesicular basalt. Collected by W. F. Foshag. Analyst: Roger C. Wells.
 2. Krivoi Rog, USSR (Serduchenko, 1965, p. 566). Replacing aegerine and riebeckite along fractures in iron-bearing quartzite. Analyst: M. M. Stukalova.
 3, 3a, and 3b. Giant's Causeway, Northern Ireland (Heddlé, 1880, p. 102). Filling druses and coating chalcedony associated with chlorophaeite in basalt. Analyst not given.

¹ Adjusted analyses, assuming the presence of 4 percent (3a), and 8 percent (3b) excess SiO₂, respectively, in original analysis.
² Not found.

4. Wind River quadrangle, sec. 3, T. 3 N., R. 73 W., Washington (Wise and Eugster, 1964, p. 1034, no. 15). Amygdulite filling in basalt. Analyst: O. von Knorring.
 5. Kursk Mountain, USSR; 80 km northwest of Kursk Mountain (Sudovikova, 1956, p. 544). Seams in iron-bearing quartzite of the Kursk magnetic anomaly. Analyst: B. S. Kopelevich.
 6. Vesuvius, Italy (Maegdefrau and Hoffman, 1937, p. 41). Analyst: not given.
 7. Barcza, Poland (Kardymowicz, 1960, p. 610). Chief component of tuffite in sandstone. Analyst: I. Sznajder.

³ Loss on ignition.

⁴ Includes 0.15 percent Li₂O, (=0.04 octahedral sites).

⁵ Includes 0.12 percent P₂O₅.

TABLE 2.—Atomic ratios for tetrasilicic dioctahedral micas with high K₂O content

Analysis	Octahedral cations					Tetrahedral cations			Negative layer charge	Interlayer cations			Positive interlayer charge
	Al	Fe ³⁺	Fe ²⁺	Mg	Mn	Si	Al	Fe ³⁺		K	Na	Ca	
1-----	0.07	0.93	0.24	0.78	0.01	4.00	---	---	0.94	0.92	0.03	0.01	0.97
	1.00		1.03										
2-----	.16	1.03	.19	.57	---	4.00	---	---	.91	.75	.09	.02	.88
	1.19		.76										
3-----	.18	.77	.31	.64	.01	4.08	---	---	.91	.81	---	.04	.89
	.95		.96										
3a-----	.19	.81	.33	.67	.02	4.00	---	---	.96	.86	---	.05	.96
	1.00		1.02										
3b-----	.12	.86	.34	.71	.02	3.91	0.09	---	1.01	.91	---	.05	1.01
	.98		1.07										
4-----	.34	.76	.21	.68	.01	3.88	.12	---	.98	.84	.01	.03	.91
	1.10		¹ .94										
5-----	---	1.18	.27	.57	---	3.83	.14	0.03	.95	.94	---	---	.94
	1.18		.84										
6-----	.78	.37	.21	.68	---	3.88	.12	---	.89	.84	---	.04	.92
	1.15		.89										
7-----	1.25	.06	.16	.53	---	3.82	.18	---	.87	.80	---	.04	.88
	1.31		.69										

¹ Includes 0.04 Li.

2, Si exactly and completely occupies all four tetrahedral sites, but the atomic ratio for Si calculated from analysis 3, an old analysis dating from 1880, is 4.08, suggesting the presence of SiO₂ extraneous to the mica structure. Adjusted values, based on an assumed extraneous SiO₂ of 4 percent and 8 percent, yield atomic ratios for Si of 4.00 and 3.91, and octahedral occupancies of 2.02 and 2.05, respectively, compared to an octahedral occupancy of only 1.91 yielded by the origi-

nal analysis. Formulas for analyses 4 through 7 contain a little tetrahedral Al, amounting to 0.12 to 0.18 sites, and the formula for analysis 5 also contains a little tetrahedral Fe³⁺ (0.03). Thus in all these analyses, Si occupies 95 percent or more of the tetrahedral sites.

In the celadonite from near Reno, Nev., 49 percent of the octahedral sites are occupied by trivalent cations and 51 percent by bivalent cations. The 1.00 trivalent octahedral cation is made up of 0.93 Fe³⁺ and 0.07

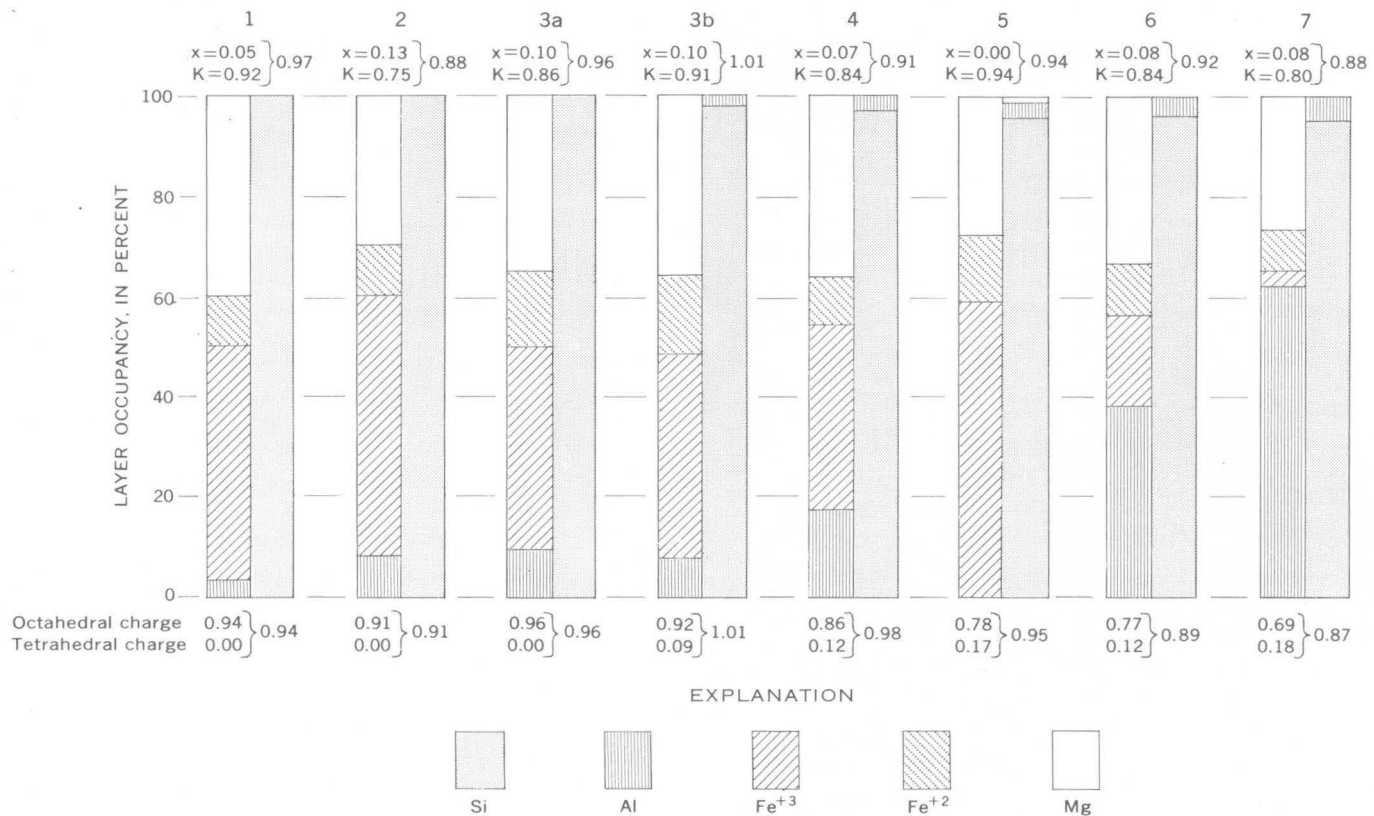


FIGURE 1.—Composition of natural tetrasilicic dioctahedral micas with high K_2O content. The left-hand column of the diagrams represents the percentage occupancy of the octahedral layer by Al^{+3} , Fe^{+3} , Fe^{+2} , and Mg^{+2} ; the right-hand column represents the percentage occupancy of the tetrahedral layers by Si^{+4} and Al^{+3} . Analyses sources are given in explanation to table 1. Exchange cations, x.

Al^{+3} , and Mg^{+2} makes up more than three-fourths of the 1.03 bivalent cations. In none of the other formulas is the ratio of trivalent to bivalent octahedral cations so close to 1:1, except in formulas for 3a and 3b. In the other formulas, the respective percentages of trivalent and bivalent cations in the octahedral layer are: 54 and 46 percent in the formula for analysis 4; 56.5 and 43.5 percent in formula 6; 58 and 42 percent in formula 5; 60 and 40 percent in formula 2; and 62 and 38 percent in formula 7.

The celadonite from near Reno, Nev., also has the highest interlayer charge, 0.97, and the number of interlayer sites occupied by K, 0.92, is exceeded only by the interlayer sites occupied by K in the formula for analysis 5, 0.94.

Of the other (Fe^{+3}, Mg) tetrasilicic micas, the formula for analysis 3 is almost as close to the (Fe^{+3}, Mg) end member as the celadonite from Reno, but in formula 3 the calculated tetrahedral occupancy by Si is 4.08, slightly in excess of the 4.00 sites available. The ratio between trivalent and bivalent octahedral cations is very close to 1:1, but the interlayer charge is only 0.89 and K is only 0.81. The formula for analysis 4 is also close to the (Fe^{+3}, Mg) end member, with only 0.12

tetrahedral sites occupied by Al, with a trivalent-bivalent octahedral cation ratio very close to 1:1 and with an interlayer charge of 0.91. Potassium, however, occupies only 0.84 interlayer sites. The "green mica" from the Kursk magnetic anomaly (analysis 5, table 2) is the most ferruginous of these micas, with Fe^{+3} and Fe^{+2} occupying more than 70 percent of the octahedral sites. In it Si occupies 3.83; Al, 0.14; and Fe^{+3} , 0.03 tetrahedral sites. Octahedral trivalent ions in the Kursk mica are somewhat in excess of bivalent ions, but less so than in the Krivoi Rog mica (analysis 2, table 2). The Kursk mica also has a higher interlayer charge (0.94) than mica 2 (0.88), and a higher K content, 0.94, as compared with 0.75 for mica 2.

Five celadonites (analyses 1–5, table 1) are all high in iron, especially trivalent iron, and thus are more comparable to the (Fe^{+3}, Mg) end member than to the other tetrasilicic end members. On the other hand, in the formulas for analyses 6 and 7, Al^{+3} is the dominant trivalent octahedral cation. In formula 6, Al^{+3} occupies 0.78 octahedral sites. The dominant bivalent cation, Mg^{+2} , occupies 0.68 sites, leaving only 0.58 sites occupied by trivalent and bivalent Fe. Thus, this mica is closer to the (Al, Mg) end member than are the pre-

ceding celadonites. It stands in about the same relation to the (Al,Mg) end member as mica 4 stands to the (Fe³⁺,Mg) end member. Analysis 7 is even higher in octahedral Al than analysis 6, and very low in iron; Al³⁺ makes up more than 60 percent of the octahedral cations, and Fe³⁺ only 3 percent.

In micas 1 and 3, the octahedral cations are equally divided between trivalent and bivalent (table 2), but in micas 2, 4, 5, and 6, the number of trivalent octahedral cations is somewhat greater than the number of bivalent cations. In these 4 micas it is possible that there has been some oxidation, that the Fe²⁺ content may at one time have been higher, and that the number of trivalent and bivalent octahedral cations may have been more evenly balanced. It is possible also, that the FeO value reported may be somewhat low. The correct determination of FeO requires a very precise analytical technique, which, if not observed, results in low values for FeO, with proportionately higher values for Fe₂O₃. Thus, in micas 1 through 5 (table 2), the octahedral cations are, or may once have been, equally divided between trivalent and bivalent.

On the other hand, the high content of octahedral Al in the formula for analysis 7 rules out the possibility of former equality between trivalent and bivalent cations. The composition of this mica could also be interpreted as the result of a slight interlayering of the (Al,Mg) tetrasilicic end member with montmorillonite. A comparison of the first, second, and third diagrams in figure 2 shows that a slight interlayering of the (Al,Mg) tetrasilicic end member with montmorillonite would increase octahedral Al, decrease Mg, and introduce tetrahedral Al to produce a composition similar to that shown by the formula calculated from analysis 7.

CELADONITE FROM NEAR RENO, NEV.

The specimen from near Reno was collected by W. F. Foshag in 1935, 23 miles east of Reno, Nev., where it occurs in vesicles in basalt. It was analyzed by R. C. Wells. Foster (1956) has shown that it represents the tetrasilicic end of the natural dioctahedral micas. The present comparative study of analyses of celadonites with high K₂O content shows that it is closer, compositionally, to the hypothetical (Fe³⁺,Mg) end member than any other (Fe³⁺,Mg) tetrasilicic or near-tetrasilicic mica for which an analysis has been published. It is the only one that combines Si_{4.00} tetrahedral layers and a 1:1 ratio between trivalent and bivalent octahedral cations, and has an interlayer charge close to 1.00 and interlayer K close to 1.00.

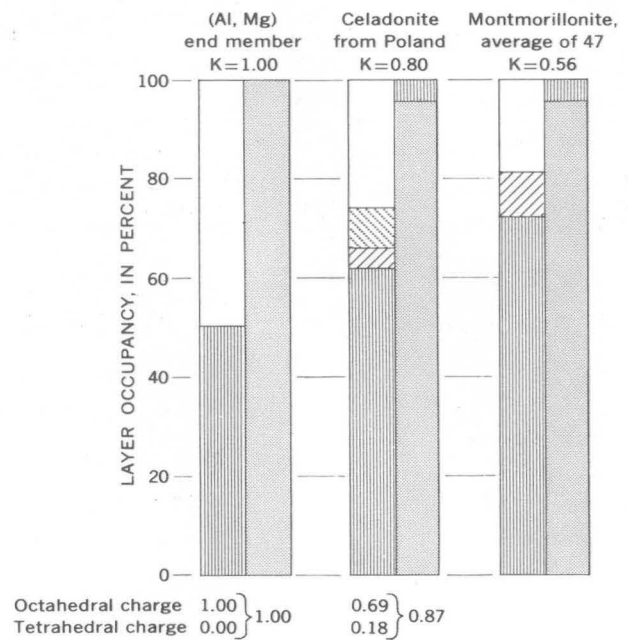


FIGURE 2.—Compositional relation between the celadonite from Poland (analysis 7), the (Al,Mg) tetrasilicic end member, and the average of 47 montmorillonite analyses (from Ross and Hendricks, 1945, p. 34).

A semiquantitative spectrographic analysis (table 3) shows that the trace elements in this mica amount to only 0.077 percent; this includes 0.015 percent Ti and 0.03 percent Zn. None of the other elements that were looked for were found in amounts greater than 0.007 percent (Ni and V).

TABLE 3.—Semiquantitative spectrographic trace-element analysis of celadonite from near Reno, Nev.

[Analyst: Helen Worthing]

Element	Percent	Element	Percent	Element	Percent
Ag	0.00005	Hf	0	Sa	.0003
As	0	Hg	0	Sr	.001
Au	0	In	0	Ta	0
B	.003	La	0	Te	0
Ba	.002	Mo	.0007	Ti	.015
Be	.00007	Nb	0	Th	0
Bi	0	Ni	.007	Tl	0
Cd	0	P	0	U	0
Ce	0	Pb	0.001	V	.007
Co	.003	Pd	0	W	0
Cr	.0003	Pt	0	Y	0
Cu	.001	Re	0	Yb	0
Ga	.0007	Sb	0	Zn	.03
Ge	0	Sc	0	Zr	.005

David R. Wones, U.S. Geological Survey (oral commun., 1966), makes the following statement with respect to the unit-cell dimensions of the Reno, Nev., celadonite:

"This material gives a well-resolved X-ray diffraction pattern [fig. 3 and table 4]. Its fine grain size allows a smear mount to be made with a minimum of preferred orientation. However, the peaks are broader than the typical muscovite pattern, although much better resolved than the typical biotite pattern. The standard error of observation after least-squares refinement of 19 reflections is $0.03^\circ 2\theta$. The pattern was measured using NaF and CaF_2 as internal standards. The results are as follows (in angstrom units):

a	b	c	β	Internal standard
5.237 ± 0.007	0.052 ± 0.003	10.143 ± 0.004	$100^\circ 34' \pm 4'$	NaF
5.233 ± 0.003	9.051 ± 0.003	10.141 ± 0.004	$100^\circ 38' \pm 3'$	CaF_2

The above standard errors measure the internal consistency of the data. The average values for the unit cell are (in Å):

a	b	c	β
5.235 ± 0.01	9.052 ± 0.005	10.142 ± 0.005	$100^\circ 36' \pm 5'$

A noteworthy feature of the pattern is that the reflections $00l$, $l=2n$, are quite weak, as opposed to ferriannite $\text{KFe}_3^{+2}\text{Fe}^{+3}\text{Si}_3\text{O}_{10}(\text{OH})_2$ where they are quite strong."

The unit-cell dimension for the celadonite from Reno compare very well with those given by Wise and Eugster (1964) for the material from Wind River quad-

range, Washington, which are:

a	b	c	β
5.23 ± 0.02	9.02 ± 0.01	10.13 ± 0.02	$100^\circ 55' \pm 0.10'$

but differ somewhat from those given by Serdyuchenko (1965):

a	b	c sin β	β
5.22	9.11	9.96	-----

The X-ray diffraction patterns indicate that both the Reno material and the Washington material of Wise and Eugster (1964) are single-phase material; no other crystalline phase was detected in either pattern.

CONCLUSION

The celadonite from near Reno, Nev. was shown by Foster (1956) to be the (Fe^{+3}Mg) tetrasilic end member of trisilicic-tetrasilic dioctahedral micas of which muscovite is the trisilicic end member. The present comparative study shows that it is more the (Fe^{+3}Mg) tetrasilic end member than any other high-silica mica for which an analysis has been published. The tetrahedral layers are completely occupied by Si, the octahedral cations are evenly divided between trivalent and bivalent, and the interlayer charge and the K are both close to 1.00. It is much closer to the (Fe^{+3}Mg) tetrasilic end member than "Svitalskite" named by Nikol'skii (Nikol'skii and Efimov, 1960), and called by Serdyuchenko (1965) the (Fe^{+3}Mg) tetrasilic end member of the trisilicic dioctahedral micas. "Svital-

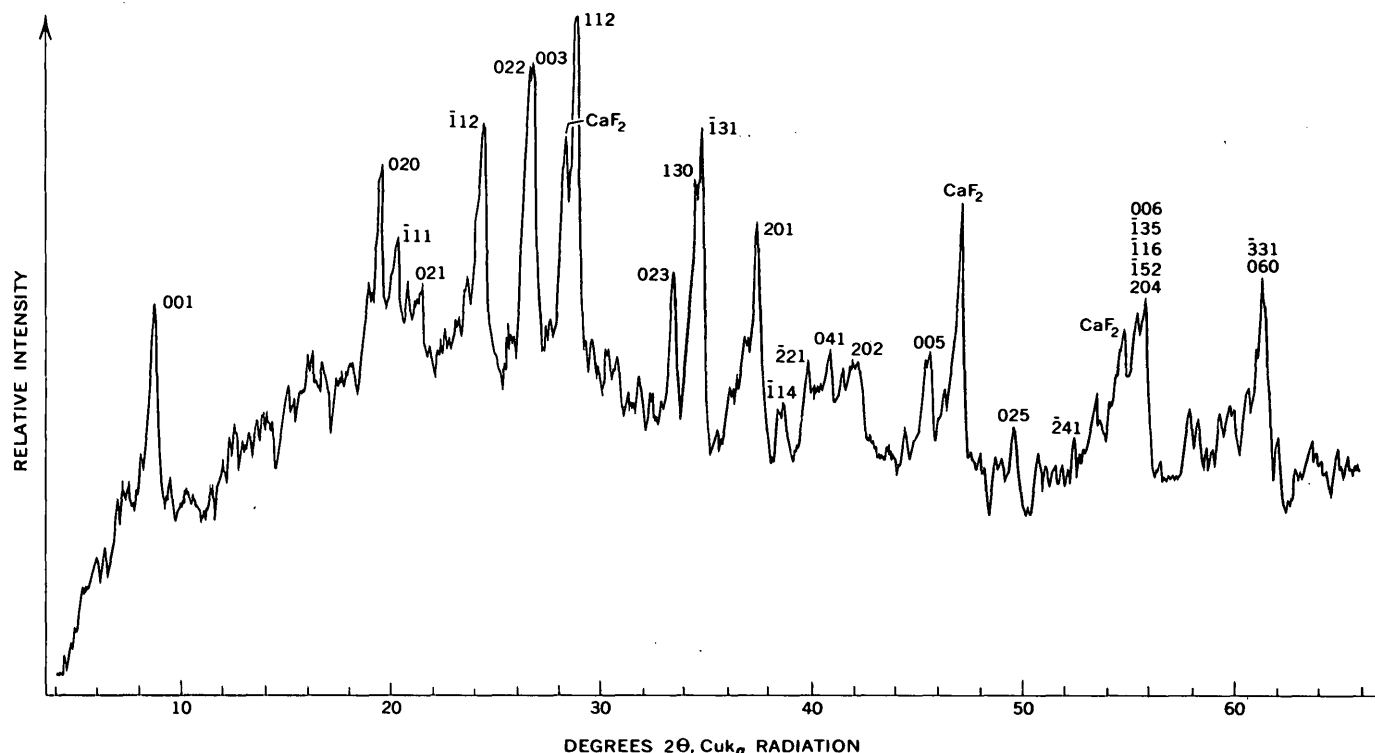


FIGURE 3.—X-ray diffractometer pattern for celadonite from Reno, Nev., by D. R. Wones. For d -spacings of this pattern see table 4.

TABLE 4.—X-ray powder pattern of celadonite from Reno, Nev., in angstrom units

[Prepared by David R. Wones]

hkl	d ¹ (calculated)	d ² (observed)	I/I ₀ ²	d ³ (observed)	I/I ₀ ³
001	9.969	10.033	50	9.979	55
002	4.984	—	—	—	—
020	4.526	4.536	45	4.534	40
110	4.473	—	—	—	—
111	4.349	4.355	15	4.353	30
021	4.121	4.127	10	4.126	25
111	3.857	—	—	—	—
112	3.630	3.635	60	3.637	65
022	3.351	3.352	25	3.355	20
003	3.323	3.327	80	3.328	90
112	3.092	3.093	80	3.093	100
113	2.899	2.902	10	—	—
023	2.679	2.679	25	2.678	55
201	2.610	—	—	—	—
130	2.603	2.602	20	2.602	40
131	2.578	2.576	100	2.577	100
200	2.573	—	—	—	—
004	2.492	—	—	—	—
113	2.484	—	—	—	—
202	2.480	—	—	—	—
131	2.463	—	—	—	—
132	2.401	2.399	80	2.398	65
201	2.387	2.383	25	—	—
114	2.342	—	—	—	—
040	2.263	—	—	—	—
221	2.261	2.260	5	—	—
203	2.244	—	—	—	—
220	2.237	—	—	—	—
132	2.224	—	—	—	—
041	2.207	2.205	5	2.206	5
024	2.183	—	—	—	—
222	2.175	—	—	—	—
133	2.148	—	—	2.149	5
202	2.132	2.132	5	—	—
221	2.112	—	—	—	—
042	2.061	—	—	—	—
114	2.043	—	—	—	—
223	2.010	—	—	—	—
005	1.994	1.992	15	1.994	15
204	1.981	—	—	—	—
(4)	—	—	—	—	—
006	1.661	—	—	—	—
135	1.659	1.658	10	1.658	10
(5)	—	—	—	—	—
331	1.510	—	—	—	—
060	1.509	1.509	50	1.509	40

¹ a=5.235, b=9.052, c=10.142, and β=100°36'.² CaF₂ (a₀=5.4620 Å) internal standard.³ NaF (a₀=4.6327 Å) internal standard.⁴ No reflections observed—22 lines.⁵ No reflections observed—17 lines.

skite" is also tetrasilicic, but the octahedral cations are not evenly divided between trivalent and bivalent, and the interlayer charge and K are both low, 0.88 and 0.75 respectively. The fact that the genesis of "svitalskite" is different from that of the celadonite from Reno does not justify a different species name. They are sufficiently similar in composition that both can be classified as celadonites.

The celadonite from Reno represents the mica form of celadonite. Ordinary celadonites, having lower SiO₂ and K₂O contents, are normally interlayered minerals—the mica interlayered with montmorillonite.

REFERENCES

- Foster, M. D., 1956, Correlation of dioctahedral potassium micas on the basis of their charge relations: U.S. Geol. Survey Bull. 1036-D, p. 57-67.
- Hedde, M. F., 1880, The mineralogy of Scotland, chap. 6, "Chloritic" minerals: Royal Soc. Edinburgh Trans. v. 29, p. 102.
- Kardymowicz, Irena, 1960, Celadonite from Barcza in the Swietokrzysz Mountains: Poland Geol. Inst. Quart. v. 4, p. 610.
- Maegdefrau, Edmund, and Hofmann, Ulrich, 1939, Glimmerartige Mineralien als Tonsubstanzen: Zeitschr. f. Kristallographie, Band 98, p. 41.
- Nikol'skii, A. P., and Efimov, A. I., 1960, Geological metallogenic features of the eastern part of the Ukrainian Shield: Vses. Nauchno-Issled. Geol. Inst. Trudy, v. 37., 163 p. [In Russian]
- Ross, C. S., and Hendricks, S. B., 1945, Minerals of the montmorillonite group, their origin and relation to soils and clays: U.S. Geol. Survey Prof. Paper 205-B, p. 23-79.
- Serdyuchenko, D. P., 1965, Svitalskite and its position in the series of tetrasilicic micas: Vses. Mineralog. Obsch. Zapiski, v. 94, p. 566-570. [In Russian]
- Sudovikova, E. N., 1956, A green mica of the iron ore series of the Kursk magnetic anomaly: Vses. Mineralog. Obsch. Zapiski, v. 85, p. 544 [In Russian]
- Wells, R. C., 1937, Analyses of rocks and minerals from the laboratory of the United States Geological Survey, 1914-36: U.S. Geol. Survey Bull. 878, 134 p.
- Wise, W. S., and Eugster, H. P., 1964, Celadonite—synthesis, thermal stability, and occurrence: Am. Mineralogist, v. 49, p. 1031-1083.



A COMPUTER-BASED PROCEDURE FOR DERIVING MINERAL FORMULAS FROM MINERAL ANALYSES

By EVERETT D. JACKSON, ROLLIN E. STEVENS,
and ROGER W. BOWEN, Menlo Park, Calif.

Abstract.—The anion-based, hydrogen-equivalent method for deriving formulas from chemical analyses of minerals has been programmed in Extended Algol for the Burroughs B5500 computer. Input data consist of the weight percentage of oxides or halogens and, if desired, the density and cell volume of the mineral. From these data the computer calculates the number of ions per formula, ratios of ions, normalized values of ions, gram-formula weight, calculated density, and (or) calculated cell volume. The program is designed to provide a maximum flexibility of output with a minimum of input data. It eliminates tedious hand calculations, reduces the chances for error, provides a standardized basis of comparison of mineral norms, and permits systematic searches for integral numbers of anions per formula or of formulas per unit cell, if these parameters are unknown.

CALCULATION OF IONS PER FORMULA

Our method for deriving the number of ions per mineral formula consists of calculating the ratios of hydrogen equivalents of the analyzed constituents and normalizing these values to twice the sum of the anions per unit formula. The basic assumptions are that anion vacancies do not occur in minerals and that the total ionic valency charges in minerals are balanced. A method based on these assumptions is, for most minerals, in better accord with current concepts of crystal structure than methods based on the assumption that the sum of the cations per formula (Hurlbut, 1959) is fixed, and the calculations in this method are simpler and more straightforward than calculations in methods based on molecular proportions (Groves, 1951).

The anion-based, hydrogen-equivalent method was used by Miser and Stevens (1938) in formulating the composition of taeniolite and later applied to other micas by Stevens (1938, 1945). We have generalized the method for application to all minerals whose con-

stituents are reported principally as oxides and have found it advantageous for five reasons:

1. The weight percentages of oxides in the chemical analyses are immediately converted to units having equal combining power (hydrogen equivalents) irrespective of the valence of the constituents.
2. The method is straightforward; adjusted equivalents directly give the charge carried by each cation and anion in the formula; and division of the adjusted equivalents by the valences of the respective cations gives the number of ions of each element per unit formula.
3. The formula-calculation problem posed by monovalent anions such as fluorine, is simplified.
4. The number of vacant cation positions in minerals that have defect structures is a direct product of the calculation.
5. Only two numerical arrays, the atomic weights and valences of the constituents, are required to calculate the number of ions per formula and the gram-formula weight.

A chemical analysis of a calcic labradorite recently published by Stewart and others (1966) was selected to illustrate the hydrogen-equivalent method of calculation. The analysis, in weight percent oxides, is given in table 1, column 1. Column 2 lists the weight of one equivalent¹ of each constituent reported. Column 3 gives the ions and the number of equivalents per

¹The weight of one equivalent of an element or compound, in any weight unit, is equal in combining capacity to 7.9997 units of oxygen measured in the same weight unit. The equivalent weight of an element is calculated by dividing its atomic weight by its valence; the equivalent weight of a compound is calculated by dividing the molecular weight of the compound by the positive valences expressed in the formula. A list of equivalent weights was compiled by Stevens and others (1960), but the values in column 2 of table 1 have been calculated from the 1961 revised atomic weights of the Commission on Atomic Weights of the International Union of Pure and Applied Chemistry (Cameron and Wichers, 1962).

TABLE 1.—*Example of the anion-based hydrogen-equivalent method of calculating ions per formula*[Calcic labradorite, Lake County, Oreg. (Stewart, and others, 1966): type formula $W_4Z_{16}O_{32}$]

Oxide	1	2	3		4	5
	Weight percentage	Weight of one equivalent	Ion	Equivalents per hundredweight	Equivalents per formula (=charge)	Ions per formula
SiO ₂	51.42	15.021	Si ⁴⁺	3.4232	37.459	9.365
Al ₂ O ₃	30.76	16.9935	Al ³⁺	1.8101	19.808	6.603
Fe ₂ O ₃24	26.615	Fe ³⁺	.0090	.099	.033
TiO ₂04	19.97	Ti ⁴⁺	.0020	.022	.006
MgO.....	.05	20.156	Mg ²⁺	.0025	.027	.014
FeO.....	.17	35.923	Fe ²⁺	.0047	.051	.026
CaO.....	13.42	28.04	Ca ²⁺	.4786	5.237	2.619
Na ₂ O.....	3.52	30.9895	Na ⁺	.1136	1.243	1.243
K ₂ O.....	.23	47.102	K ⁺	.0049	.054	.054
¹ H ₂ O.....	.04					
Total.....	99.89			5.8486	64.000	19.963
Anions.....			O ⁻²	-5.8486	-64.000	-32.000

Normalizing factor = 10.9428

Weight percentage of oxygen = 46.79

Extended formula = $(K_{0.05} Na_{1.24} Ca_{2.62} Mg_{0.01} Fe_{0.03}^{+2} Fe_{0.03}^{+3} Ti_{0.01})(Al_{4.60}^{IV} Si_{9.37}) O_{32}$
3.99 15.97¹ Rejected from the calculations.

hundredweight (in any weight unit) obtained by dividing the weight percentages of the constituents by their respective equivalent weights. The numbers of equivalents per hundredweight are next multiplied by the normalizing factor to give numbers of equivalents per formula weight, whose total balances the anion equivalents in the type formula. In the example (table 1), the type formula is taken as $W_4Z_{16}O_{32}$, and therefore the numbers of equivalents per formula weight are normalized to total 64.000 (table 1, column 4). It is apparent that the number of equivalents per formula for each ion is equal to the positive or negative charge contributed by that ion, if it is assumed that the total charge of the mineral is balanced. Finally, the number of equivalents of each ion per formula is divided by the valence of that ion to obtain the ions per formula of the mineral (table 1, column 5). The sum of the cations obtained in column 5 is slightly less than the expected total of 20 given by the type formula. Under the assumptions that the type formula is correctly chosen, that the anion positions in the mineral structure are completely filled, and that the charges of the mineral do balance, observed cation deficiencies may be due (1) to vacant cation positions in the mineral structure, or (2) to analytical error. (Under the same assumptions, any calculated excess of cations may only be due to analytical error.) The weight percentage of oxygen shown in table 1 is obtained by multiplying the sum of the number of equivalents per hundredweight by the equivalent weight of oxygen (7.9997).

The hydrogen-equivalent method of calculation also readily simplifies the problem posed by minerals that

have multiple anion groups. For example, we may consider a system in which the anions in the formula vary between $O_{10}(OH)_2$ and O_{12} , both having 12 oxygens but having 22 and 24 anion equivalents respectively, OH being counted as an anion. Obviously, calculation of atomic ratios for a mineral having these two anion groups in solid solution cannot be correctly made on either the basis of 22 or 24 anion equivalents, OH being counted as one of the anions. However, both formulas contain 12 oxygens, and if we calculate to balance the 12 oxygens (24 equivalents), in effect counting the H of OH as a cation, solid solutions having the two anion groups can be properly formulated. Similarly, formulas of minerals containing fluorine and other monovalent anions can be derived simply by calculating the oxygen before calculating the formula. Let us consider the anion group $O_{10}(OH)_2$ and the corresponding fluorine group $O_{10}F_2$. The first group has 24 equivalents of oxygen; the second, $O_{10}F_2$, has 22 anion equivalents. However, if fluorine is arbitrarily included in the cation equivalents and the analysis is calculated as if 24 anion equivalents (O_{12}) were actually present, the proper formula can be obtained. To evaluate multiple anion groups, therefore, one simply normalizes the number of equivalents per formula to twice the total number of anions.

In the computer program for the anion-based, hydrogen-equivalent method, a great deal of flexibility was desired to accommodate the extreme ranges of structure and chemical composition among natural minerals. (Our program seems to offer more flexibility than one recently reported by Howarth, 1966, which

TABLE 2.—Chemical constituents that can be used in the computer program and their coordination categories

Constituent	Ion	Constituent	Ion
III- and IV-coordinated cations			
N ₂ O ₅ -----	N ⁺⁵	SO ₃ -----	S ⁺⁶
N ₂ O ₃ -----	N ⁺³	BeO-----	Be ⁺²
CO ₂ -----	C ⁺⁴	P ₂ O ₅ -----	P ⁺⁵
B ₂ O ₃ -----	B ⁺³	SiO ₂ -----	Si ⁺⁴
N ₂ O-----	N ⁺¹	Al ₂ O ₃ (if as- signed).	Al ⁺³
VI-coordinated trivalent cations			
Al ₂ O ₃ -----	Al ⁺³	Ho ₂ O ₃ -----	Ho ⁺³
Gd ₂ O ₃ -----	Gd ⁺³	Dy ₂ O ₃ -----	Dy ⁺³
Ga ₂ O ₃ -----	Ga ⁺³	Y ₂ O ₃ -----	Y ⁺³
Cr ₂ O ₃ -----	Cr ⁺³	Tb ₂ O ₃ -----	Tb ⁺³
Fe ₂ O ₃ -----	Fe ⁺³	Tl ₂ O ₃ -----	Tl ⁺³
Mn ₂ O ₃ -----	Mn ⁺³	Bi ₂ O ₃ -----	Bi ⁺³
V ₂ O ₃ -----	V ⁺³	Eu ₂ O ₃ -----	Eu ⁺³
Sc ₂ O ₃ -----	Sc ⁺³	Nd ₂ O ₃ -----	Nd ⁺³
In ₂ O ₃ -----	In ⁺³	Pr ₂ O ₃ -----	Pr ⁺³
Lu ₂ O ₃ -----	Lu ⁺³	Sm ₂ O ₃ -----	Sm ⁺³
Yb ₂ O ₃ -----	Yb ⁺³	Ce ₂ O ₃ -----	Ce ⁺³
Tm ₂ O ₃ -----	Tm ⁺³	La ₂ O ₃ -----	La ⁺³
Er ₂ O ₃ -----	Er ⁺³		
VI-coordinated 4-, 5-, and 6-valent cations			
SeO ₂ -----	Se ⁺⁴	As ₂ O ₅ -----	As ⁺⁵
GeO ₂ -----	Ge ⁺⁴	V ₂ O ₅ -----	V ⁺⁵
MnO ₂ -----	Mn ⁺⁴	Sb ₂ O ₅ -----	Sb ⁺⁵
VO ₂ -----	V ⁺⁴	Nb ₂ O ₅ -----	Nb ⁺⁵
TiO ₂ -----	Ti ⁺⁴	Ta ₂ O ₅ -----	Ta ⁺⁵
TeO ₂ -----	Te ⁺⁴	CrO ₃ -----	Cr ⁺⁶
SnO ₂ -----	Sn ⁺⁴	TeO ₃ -----	Te ⁺⁶
HfO ₂ -----	Hf ⁺⁴	WO ₃ -----	W ⁺⁶
ZrO ₂ -----	Zr ⁺⁴	MoO ₃ -----	Mo ⁺⁶
ThO ₂ -----	Th ⁺⁴	UO ₃ -----	U ⁺⁶
VI-coordinated monovalent and bivalent cations			
MgO-----	Mg ⁺²	RhO-----	Rh ⁺²
NiO-----	Ni ⁺²	PdO-----	Pd ⁺²
CoO-----	Co ⁺²	PtO-----	Pt ⁺²
CuO-----	Cu ⁺²	IrO-----	Ir ⁺²
FeO-----	Fe ⁺²	ReO-----	Re ⁺²
ZnO-----	Zn ⁺²	OsO-----	Os ⁺²
MnO-----	Mn ⁺²	Li ₂ O-----	Li ⁺¹
Large cations			
Cu ₂ O-----	Cu ⁺¹	Ag ₂ O-----	Ag ⁺¹
CdO-----	Cd ⁺²	Hg ₂ O-----	Hg ⁺¹
CaO-----	Ca ⁺²	K ₂ O-----	K ⁺¹
HgO-----	Hg ⁺²	Au ₂ O-----	Au ⁺¹
SrO-----	Sr ⁺²	(NH ₄) ₂ O-----	(NH) ⁺¹
PbO-----	Pb ⁺²	Rb ₂ O-----	Rb ⁺¹
BaO-----	Ba ⁺²	Cs ₂ O-----	Cs ⁺¹
Na ₂ O-----	Na ⁺¹		
Anions			
H ₂ O+-----	OH ⁻¹	Cl-----	Cl ⁻¹
H ₂ O-----	OH ⁻¹	Br-----	Br ⁻¹
F-----	F ⁻¹	I-----	I ⁻¹

where G is the gram-formula weight in grams, m is the number of constituents, n_i is the number of ions per formula for ion i , and a_i is the atomic weight of ion i . If the density of an analyzed mineral has been determined and the cell volume is desired, one enters the numbers of formulas per unit cell and the measured density (see fig. 1, option 1), and the volume is calculated by the relation

$$V_c = \frac{GN}{10^{-24}A\rho_o},$$

where V_c is the calculated cell volume in cubic angstroms, G is the gram-formula weight in grams, N is the number of formulas per unit cell, A is Avogadro's number, and ρ_o is the observed density in grams per cubic centimeter. If the cell volume has been measured, however, the density can be calculated from the relation

$$\rho_c = \frac{GN}{10^{-24}AV_o},$$

where ρ_c is the calculated density in grams per cubic centimeter, V_o is the observed cell volume in cubic angstroms, and the other symbols are the same as above. Finally, if both the density and cell volume have been measured, both these parameters can be calculated by the computer as a check on the internal consistency of all the chemical and physical data (Hey, 1939).

CALCULATION OF ION RATIOS AND NORMALIZED IONIC VALUES

Provision has been made in the computer program for the calculation of as many as eight ionic ratios, such as $Mg^{+2}/(Mg^{+2}+Fe^{+2})$ or $Fe^{+3}/(Fe^{+2}+Fe^{+3})$ (see fig. 1, option 2). Any such ratios may be requested, including those involving the ionic oxygen remainder and those involving IV- and VI-coordinated Al⁺³, if this ion has been partitioned during the calculation of ions per formula. Similarly, as many as 12 normative notations, such as Ca⁺²Mg⁺²Fe⁺² in pyroxene or K⁺¹Na⁺¹Ca⁺² in feldspar may be routinely requested (see fig. 1, option 3).

THE COMPUTER PROGRAM

The program has been written in Extended Algol for the Burroughs B5500 computer. Because of the inherent simplicity of the anion-based, hydrogen-equivalent method, only two numerical arrays are required: (1) the atomic weights of the elements (the 1961 revised atomic weights of the Commission on Atomic Weights of the International Union of Pure and Applied Chemistry have been used; see Cameron and Wichers, 1962) and (2) the valence assigned to each constituent. In addition, two name (alpha) arrays are

required: (1) the symbols of the reported constituents and (2) the ionic forms of these constituents. Additional constituents other than those listed in table 2 may be added with very little reprogramming, and a large number of parameters for one variable of a data set may be run without resubmitting the whole set. For simplicity, mnemonic names are used throughout for program variables.

The output speed of the Burroughs lineprinter is 800 lines per minute. At this rate, data for about 20 minerals can be processed per minute.

Data forms and program documentation may be obtained from R. W. Bowen or any representative of the U.S. Geological Survey Computer Branch.

EXAMPLES OF CALCULATIONS

The versatility, as well as the limitations, of the anion-based, hydrogen-equivalent method and of the computer program can best be shown by specific examples.

Figure 2 is a copy of the computer printout of the reduction of the calcic labradorite used as the example in table 1. (Figure 1 is the input-data and instruction form for this sample). The given data are printed at

the top and at the upper left of figure 2, the calculated data to the right of the given data and at the bottom. In this example, the number of ions of Al³⁺ was insufficient to make up the total of 16 cations in the IV-coordination requested on the input-data form (fig. 1). The program is so designed that if this occurs, the available Si⁴⁺ and Al³⁺ are simply summed. The practice of successively assigning ions of Fe⁺³, Ti⁴⁺, or other ions to IV-coordination until all such positions total the desired value is not followed because of the lack of evidence that ions having radii larger than Al³⁺ consistently do enter IV-coordinated structural positions. The extended formula is derived simply by inspection of the ions of the figure. Our results for the ions per formula, K⁺¹ Na⁺¹ Ca⁺² values, and calculated density are virtually identical with the published values (Stewart and others, 1966). The extreme closeness of the values in the extended formula to the theoretical values and the good agreement between the measured and the calculated densities and cell volumes indicate that the chemical and physical data for this mineral were of very high quality.

As another example of the method and the program, a formula was derived for a mineral containing

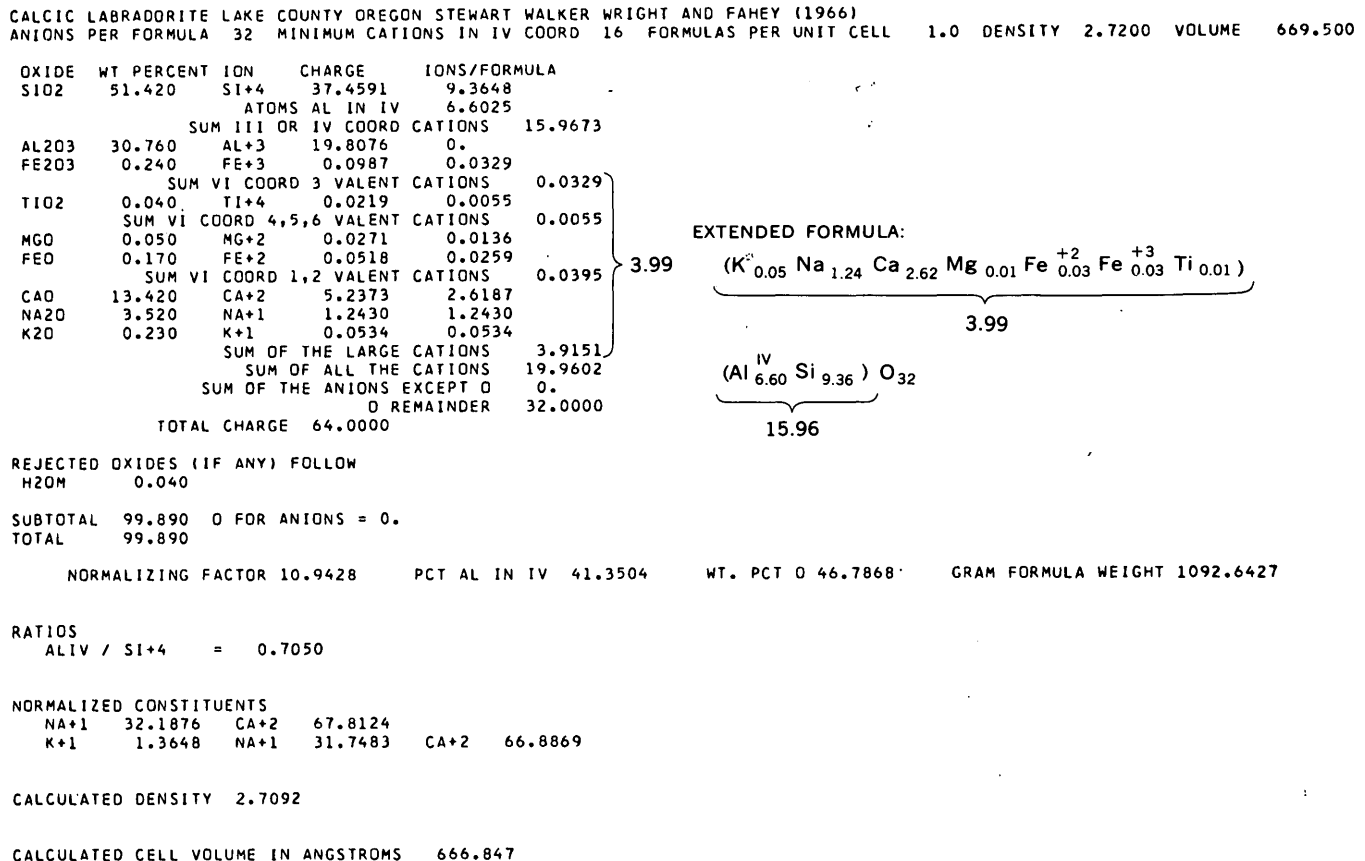


FIGURE 2.—Computer printout of calculations for a calcic labradorite. The derived extended formula is on the right.

monovalent anions. The chemical and physical data for an alkali amphibole were supplied by R. G. Coleman, U.S. Geological Survey (written commun., July 1966); chemical analysis by Leonice Beatty; unit-cell data by J. J. Papike; and density by D. E. Lee. The chemical analysis (fig. 3) was normalized to twice the number of anions per formula, and the monovalent anions were calculated in the same way as the cations. Ions of OH^{-1} and F^{-1} are then summed and subtracted from total anions per formula to obtain the oxygen remainder. The weight percentage of oxygen is obtained by adding the ions of OH^{-1} and O remainder and by reversing the calculation procedure, as previously described. Again, the closeness of the computer results to the theoretical values confirms the accuracy of the chemical and physical measurements.

The program was also used to calculate data and derive a formula for a mineral whose number of unit cells per formula is uncertain. The density and chemical analysis of an antigorite, from Mikonui, New Zea-

land, were published by Aruja (1945) and Zussman (1954), respectively. We calculated the cell volume from cell parameters of the same material published by Kunze (1956). The ions per formula (fig. 4) are almost identical with those calculated for this same mineral analysis by Deer and others (1962) but differ significantly (when adjusted to the same formula) from those of Faust and Fahey (1962), which were calculated on the basis of a fixed cation charge. The calculated cell volume and calculated density are both considerably larger than the measured values when determined on the basis of 17 formulas per unit cell, the number proposed by Zussman (1954) and Kunze (1956). It is unlikely that the observed density and cell volume are in error in the same direction and to the same degree. Thus, either the chemical analysis is in error so as to yield an erroneously large gram-formula weight, or there are less than 17 formulas per unit cell as measured. Deer and others (1962) suggested that the a parameter of serpentines may be spaced at even multiples of $5.3/2$ A. If this is correct,

38CZ 59 ALKALI AMPHIBOLE CAZADERO CALIF UNPUBLISHED DATA R G COLEMAN
ANIONS PER FORMULA 24 MINIMUM CATIONS IN IV COORD 8 FORMULAS PER UNIT CELL 2.0 DENSITY 3.2700 VOLUME 895.000

OXIDE	WT PERCENT	ION	CHARGE	IONS/FORMULA
SiO ₂	54.200	Si ⁺⁴	31.7887	7.9472
		ATOMS AL IN IV		0.0528
		SUM III OR IV COORD CATIONS		8.0000
Al ₂ O ₃	4.500	Al ⁺³	2.3330	0.7248
Fe ₂ O ₃	12.100	Fe ⁺³	4.0053	1.3351
		SUM VI COORD 3 VALENT CATIONS		2.0599
TiO ₂	0.030	Ti ⁺⁴	0.0132	0.0033
		SUM VI COORD 4,5,6 VALENT CATIONS		0.0033
MgO	5.000	Mg ⁺²	2.1855	1.0927
FeO	14.000	Fe ⁺²	3.4335	1.7167
MnO	0.760	Mn ⁺²	0.1888	0.0944
		SUM VI COORD 1,2 VALENT CATIONS		2.9039
CaO	0.600	Ca ⁺²	0.1885	0.0943
Na ₂ O	6.600	Na ⁺¹	1.8763	1.8763
		SUM OF THE LARGE CATIONS		1.9706
		SUM OF ALL THE CATIONS		14.9377
H ₂ OP	1.700	OH ⁻¹	1.6627	1.6627
F	0.700	F ⁻¹	0.3246	0.3246
		SUM OF THE ANIONS EXCEPT O		1.9873
		O REMAINDER		22.0127
		TOTAL CHARGE	48.0000	

REJECTED OXIDES (IF ANY) FOLLOW
H₂OM 0.190

SUBTOTAL 100.380 O FOR ANIONS = 0.295
TOTAL 100.085

NORMALIZING FACTOR 8.8100 PCT AL IN IV 0.6604 WT. PCT O 42.9955 GRAM FORMULA WEIGHT 880.0943

RATIOS
 FE+2 / FE+2 + MG+2 + MN+2 = 0.5912
 MG+2 / MG+2 + FE+2 + FE+3 + MN+2 = 0.2578
 FE+3 / FE+3 + FE+2 = 0.4375
 FE+3 / FE+3 + ALVI + TI+4 = 0.6471

NORMALIZED CONSTITUENTS
 FE+2 40.4989 MG+2 25.7788 FE+3 31.4957 MN+2 2.2267
 FE+3 64.7090 ALVI 35.1307 TI+4 0.1603

CALCULATED DENSITY 3.2648

CALCULATED CELL VOLUME IN ANGSTROMS 893.570

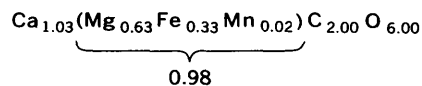
EXTENDED FORMULA:
 (Na_{1.88} Ca_{0.09}) (Mg_{1.09} Fe_{1.72}⁺² Mn_{0.09} Fe_{1.34}⁺³ Al_{0.72}^{VI})
 1.97 4.96
 (Al_{0.05}^{IV} Si_{7.95}) O_{22.01} (OH_{1.66} F_{0.32})
 8.00 1.98

FIGURE 3.—Computer printout of calculations for an alkali amphibole. The derived extended formula is on the right.

ANKERITE OLDHAM LANCASHIRE HOWIE AND BROADHURST (1958)
 ANIONS PER FORMULA 6 MINIMUM CATIONS IN IV COORD -0 FORMULAS PER UNIT CELL 1.0 DENSITY 2.9700 VOLUME 108.000

OXIDE	WT PERCENT	ION	CHARGE	IONS/FORMULA
CO2	44.700	C+4	7.9921	1.9980
		ATOMS AL IN IV		0.
		SUM III OR IV COORD CATIONS		1.9980
		SUM VI COORD 3 VALENT CATIONS		0.
		SUM VI COORD 4,5,6 VALENT CATIONS		0.
MGO	12.850	MG+2	1.2541	0.6271
FEO	12.060	FE+2	0.6604	0.3302
MNO	0.770	MN+2	0.0427	0.0214
		SUM VI COORD 1,2 VALENT CATIONS		0.9786
CAO	29.230	CA+2	2.0507	1.0253
		SUM OF THE LARGE CATIONS		1.0253
		SUM OF ALL THE CATIONS		4.0020
		SUM OF THE ANIONS EXCEPT O		0.
		O REMAINDER		6.0000
		TOTAL CHARGE		12.0000

EXTENDED FORMULA:



REJECTED OXIDES (IF ANY) FOLLOW

SiO2	0.150
Al2O3	0.280
Fe2O3	0.100
Na2O	0.060
K2O	0.010
H2O	0.020

SUBTOTAL 100.230 O FOR ANIONS = 0.
 TOTAL 100.230

NORMALIZING FACTOR 1.9672 PCT AL IN IV 0.

WT. PCT O 48.7992 GRAM FORMULA WEIGHT 195.9499

RATIOS

$$\frac{\text{C}+4}{\text{Mg}+2 + \text{Fe}+2 + \text{Mn}+2 + \text{Ca}+2} = 0.9970$$

$$\frac{\text{Mg}+2}{\text{Fe}+2} = 1.8990$$

NORMALIZED CONSTITUENTS

MG+2	31.2915	FE+2	16.4776	MN+2	1.0655	CA+2	51.1654
MG+2	65.5058	FE+2	34.4942				
MG+2	37.9489	CA+2	62.0511				

CALCULATED DENSITY 3.0119

CALCULATED CELL VOLUME IN ANGSTROMS 109.523

FIGURE 5.—Computer printout of calculations for an analyzed ankerite. The derived extended formula is on the right.

tematic errors in the chemical analysis that result in too large a gram-formula weight.

CONCLUSION

The anion-based, hydrogen-equivalent method for deriving formulas from chemical analyses of minerals provides a standard basis of comparison for mineral norms. The basic assumptions of the method are simple and in accord with current concepts of crystal structure. The computer program based on this method eliminates tedious hand calculations and reduces the chances for error. The speed and flexibility of the program (1) permit recalculation of large numbers of previously published analyses, (2) allow systematic searches for integral numbers of anions that produce rational numbers of cations per formula or searches for numbers of formulas per unit cell that cause agreement between measured and calculated cell volumes and densities, and (3) permit trial-and-error rejection of constituents suspected of being impurities.

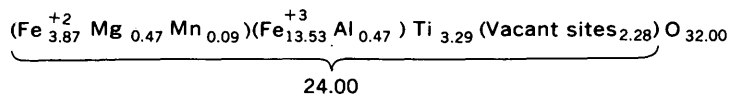
REFERENCES

- Aruja, Endel, 1945, An X-ray study of the crystal-structure of antigorite: *Mineralog. Mag.*, v. 27, p. 65-74.
- Barrett, C. S., 1952, *Structure of metals*, 2d ed.: New York, McGraw-Hill Book Co., Inc., 661 p.
- Basta, E. Z., 1959, Some mineralogical relationships in the system $\text{Fe}_2\text{O}_3\text{-Fe}_3\text{O}_4$ and the composition of titanomaghemite: *Econ. Geology*, v. 54, p. 698-719.
- Cameron, A. E., and Wichers, Edward, 1962, Report of the International Commission on Atomic Weights (1961): *Am. Chem. Soc. Jour.*, v. 84, p. 4175-4197.
- Deer, W. A., Howie, R. A., and Zussman, Jack, 1962, *Rock-forming minerals*, v. 3, Sheet silicates: New York, John Wiley and Sons, Inc., 270 p.
- Faust, G. T., and Fahey, J. J., 1962, The serpentine group minerals: U.S. Geol. Survey Prof. Paper 384-A, 92 p.
- Groves, A. W., 1951, *Silicate analysis*: London, Allen and Unwin, Ltd., 336 p.
- Hey, M. H., 1939, On the presentation of chemical analysis of minerals: *Mineralog. Mag.*, v. 25, p. 402-412.
- Howarth, R. J., 1966, Calculation of mineral unit cell contents: *Mineralog. Mag.*, v. 35, p. 787.
- Howie, R. A., and Broadhurst, F. M., 1958, X-ray data for dolomite and ankerite: *Am. Mineralogist*, v. 43, p. 1210-1214.

TITANOMAGHEMITE BON ACCORD SOUTH AFRICA WALKER (1930) BASTA (1959)
 ANIONS PER FORMULA 32 MINIMUM CATIONS IN IV COORD -0 FORMULAS PER UNIT CELL 1.0 DENSITY 4.7000 VOLUME 580.510

OXIDE	WT PERCENT	ION	CHARGE	IONS/FORMULA
			ATOMS AL IN IV	0.
			SUM III OR IV COORD CATIONS	0.
AL2O3	1.420	AL+3	1.4153	0.4718
FE2O3	63.760	FE+3	40.5765	13.5255
			SUM VI COORD 3 VALENT CATIONS	13.9973
TiO2	15.500	Ti+4	13.1435	3.2859
			SUM VI COORD 4,5,6 VALENT CATIONS	3.2859
MGO	1.120	Mg+2	0.9412	0.4706
FEO	16.430	FE+2	7.7468	3.8734
MNO	0.370	MN+2	0.1767	0.0883
			SUM VI COORD 1,2 VALENT CATIONS	4.4323
			SUM OF THE LARGE CATIONS	0.
			SUM OF ALL THE CATIONS	21.7155
			SUM OF THE ANIONS EXCEPT O	0.
			O REMAINDER	32.0000
			TOTAL CHARGE	64.0000

EXTENDED FORMULA:



REJECTED OXIDES (IF ANY) FOLLOW

SiO2	0.500
H2O	1.340

SUBTOTAL 100.440 O FOR ANIONS = C.
 TOTAL 100.440

NORMALIZING FACTOR 16.9379 PCT AL IN. IV 0. WT. PCT O 30.2270 GRAM FORMULA WEIGHT 1670.0740

RATIOS

FE+3 / FE+2 + FE+3	=	0.7774
Mg+2 + Mn+2 + FE+2 / FE+3 + AL+3	=	0.3167
FE+2 + FE+3 / Ti+4	=	5.2951
FE+2 + FE+3 + Ti+4 / OREM	=	0.6464

NORMALIZED CONSTITUENTS

AL+3	3.3705	FE+3	96.6295
Mg+2	10.6174	FE+2	87.3894
		MN+2	1.9932

CALCULATED DENSITY 4.7758

CALCULATED CELL VOLUME IN ANGSTROMS 589.868

FIGURE 6.—Computer printout of calculations for an analyzed titanomaghemite. The derived extended formula is on the right.

Hurlburt, C. S., Jr., 1959, Dana's manual of mineralogy, 17th ed.: New York, John Wiley and Sons, Inc., 609 p.
 Kunze, Gunther, 1956, Die gewellte Struktur des Antigorits, I: Zeitschr. Kristallographie, v. 108, p. 82-107.
 Miser, H. D., and Stevens, R. E., 1938, Taeniolite from Magnet Cove, Arkansas: Am. Mineralogist, v. 23, p. 104-110.
 Stevens, R. E., 1938, New analyses of lepidolites and their interpretation: Am. Mineralogist, v. 23, p. 607-628.
 ——— 1945, A system for calculating analyses of micas and related minerals to end members, in Wells, R. C., and others, Contributions to geochemistry, 1942-45: U.S. Geol. Survey Bull. 950, p. 101-119.

Stevens, R. E., Neil, S. T., and Roberson, C. F., 1960, Gravitric conversion factors and other data used in interpreting analyses of rocks, minerals, and waters: Geotimes, v. 4, no. 7, p. 41-43; no. 8, p. 23.
 Stewart, D. B., Walker, G. W., Wright, T. L., and Fahey, J. J., 1966, Physical properties of calcic labradorite from Lake County, Oregon: Am. Mineralogist, v. 51, p. 177-197.
 Walker, T. L., 1930, Lodestone from Bon Accord, Transvaal: Toronto Univ. Studies, Geol. Ser., no. 29, p. 17-19.
 Zussman, Jack, 1954, Investigation of the crystal structure of antigorite: Mineralog. Mag., v. 30, p. 498-512.



SPHEROIDAL WEATHERING OF THERMALLY METAMORPHOSED LIMESTONE AND DOLOMITE, WHITE MOUNTAINS, CALIFORNIA

By VALMORE C. LoMARCHE, JR., Menlo Park, Calif.

Abstract.—Silicate-free carbonate rocks in the White Mountains, Calif., weather spheroidally only in contact aureoles near intrusive bodies. Comparison of the textures of the bedrock and soil indicates that the spheroidal weathering is the result of granular disintegration of joint blocks. Selective grain-boundary corrosion during weathering probably causes this disintegration and is thought to be the result of intergranular stresses that developed on cooling, following high-temperature recrystallization. Exfoliation is regarded as an indirect consequence of increased porosity near the margins of a weathering block.

Massive silicate rocks commonly weather by small-scale exfoliation and granular disintegration to yield rounded outcrops and residual spheroidal boulders. A mechanism involving the hydration and alteration of primary silicate minerals postulated by Blackwelder (1925), and investigated by Chapman and Greenfield (1949), has been widely accepted as the explanation for this weathering phenomenon (Reiche, 1950, p. 10). However, the spheroidal weathering of silicate-free dolomite and limestone beds in the White Mountains, Calif., requires a different explanation.

The White Mountains are located in the arid rain shadow east of the Sierra Nevada, in southeastern California (fig. 1, index map). The southern part of the range is composed mainly of folded Precambrian and Lower Cambrian sedimentary rocks and by granitic rocks of probable Jurassic age (Emerson, 1966, p. 134). Tertiary (Dalrymple, 1963, p. 387) basalt flows and underlying tuff and gravel are locally preserved as a resistant capping on buttes and ridge-crests. Although the sedimentary strata have apparently been subjected to low-grade regional metamorphism (Emerson, 1966, p. 129), pronounced textural and mineralogical effects of metamorphism are restricted to the

contact aureoles around the igneous intrusions. This report discusses spheroidal weathering, near the intrusions, of the Reed Dolomite of Precambrian age and of a limestone bed in the underlying Wyman Formation, also of Precambrian age (Stewart, 1965).

EFFECTS OF METAMORPHISM AND NATURE OF THE WEATHERING

The Reed Dolomite is exposed over a large area in the southern White Mountains (fig. 1). The formation is about 2,000 feet thick (Nelson, 1963) and ranges from dark-gray medium-grained dolomite near the base to light-gray fine-grained dolomite at the top. Bedding is indistinct, and exposures in areas distant from intrusive contacts break down along closely spaced joints and irregular fractures (fig. 2), yielding large, angular fragments. Near the northern and southern edges of the Sage Hen Flat pluton (fig. 1), an adamellite (quartz monzonite) stock (Emerson, 1966, p. 145), the Reed Dolomite has been recrystallized to form a spheroidally weathered medium- to coarse-grained dolomite marble. The formation has undergone similar thermal metamorphism near the western border of the Cottonwood quartz monzonite pluton (Emerson, 1966, p. 134) despite the presence of a narrow band of the Deep Springs and Campito Formations lying between the pluton and the dolomite. A calcite marble bed in the Wyman Formation also weathers spheroidally in at least one locality (fig. 1, rock sample 14). Although the outcrop is about 1,500 feet east of the Sage Hen Flat pluton, the limestone here has been intruded by sills and dikes of a fine-grained mafic rock. To the south, the marble grades into a grossularite-rich skarn, apparently the product of reaction with the intrusive silicate rock.

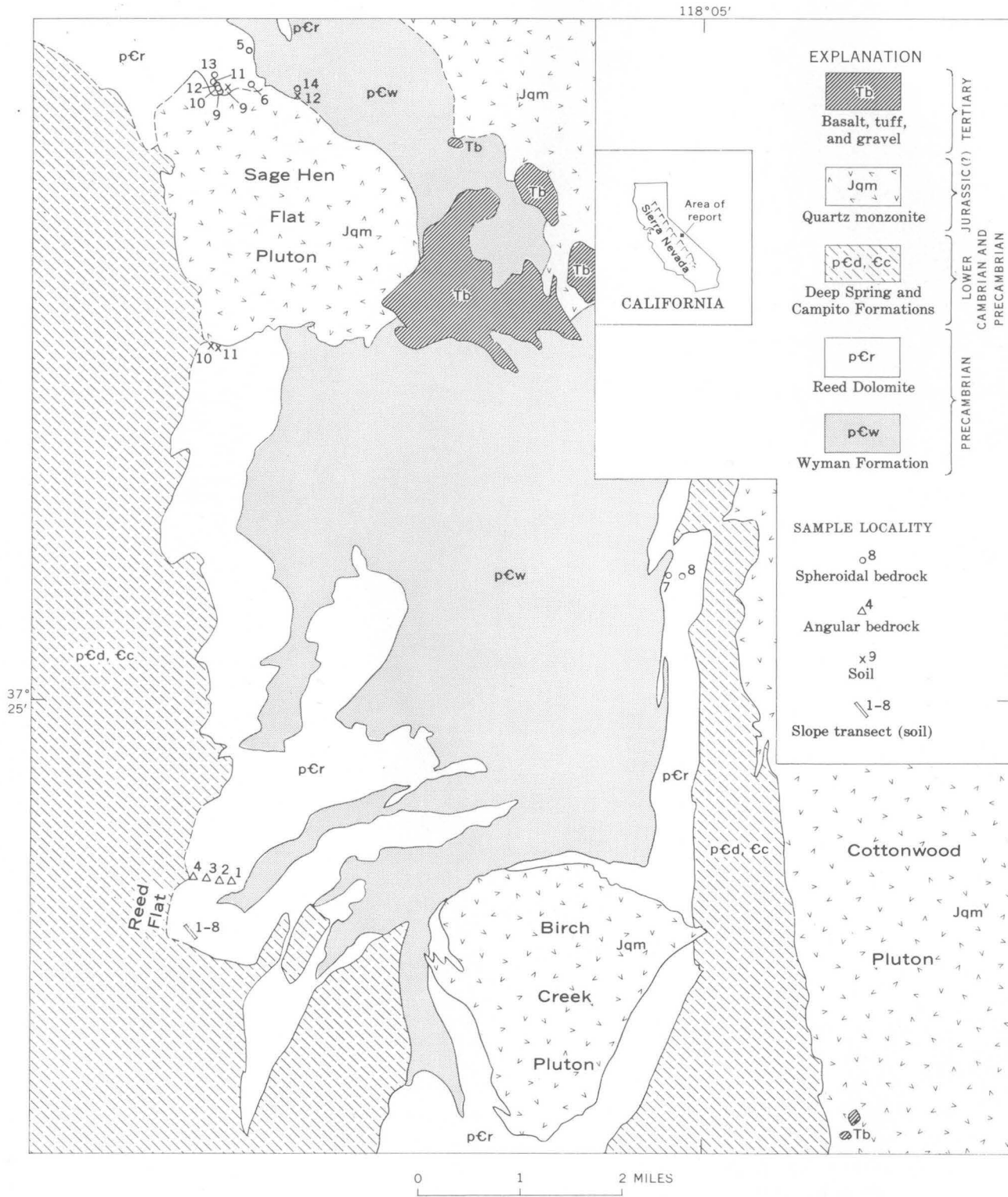


FIGURE 1.—Generalized geologic map of part of the southern White Mountains, Calif., showing rock and soil sample localities. Soil samples 1 through 8 are from angularly weathered rocks and 9 through 12 are from spheroidally weathered rocks. Geology modified after Nelson (1963) and Hall (1964).



FIGURE 2.—Angular weathering of unmetamorphosed dolomite.

Near intrusive contacts, spheroidally weathered dolomite is well exposed along the crests of ridges and it also crops out sporadically as cliffs and irregular rocky spurs on canyon slopes. Steeply sloping outcrops are composed mainly of joint-bounded hemispheroidal blocks ranging from several inches to a few feet in size (fig. 3). Crevices and depressions between the larger blocks contain subangular to rounded rock fragments in a loose matrix of coarse soil. On ridge crests and gentle slopes, the soil that mantles the bedrock (closely resembling the grüß of many granitic terranes) is thicker and more extensive than the soil on steeply sloping outcrops and it contains few large fragments.

The spheroidally weathered Reed Dolomite is creamy white in marked contrast to the gray or buff surface

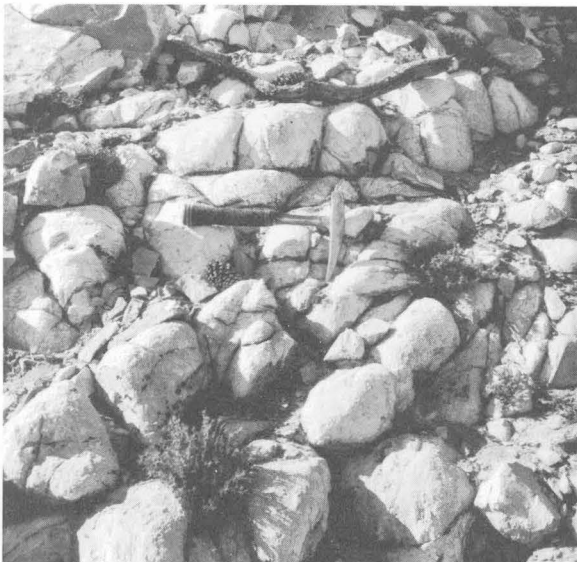


FIGURE 3.—Spheroidal weathering of joint blocks of thermally metamorphosed dolomite.

of angularly weathered rock. The surface of a spheroidal joint block is rough and friable, and grains are easily detached by rubbing, whereas the exposed surface of an angularly weathered outcrop is comparatively smooth and hard.

Although granular disintegration seems to characterize the spheroidal weathering process in the White Mountains, another mechanism also contributes to the development of rounded outcrop forms. In part, the rounded surfaces result from spalling along closely spaced concentric fractures that have developed near the surface in some joint blocks and residual boulders of both the calcite and dolomite marble (fig. 4). This concentric fracturing closely resembles the small-scale "chemical" exfoliation of many spheroidally weathered silicate rocks (Blackwelder, 1925).



FIGURE 4.—Dolomitic "boulder of weathering" showing exfoliation.

TEXTURAL COMPARISON OF BEDROCK AND SOILS

Possible causes of the contrasting modes of weathering of the sedimentary and metamorphic carbonate rocks were investigated. To study the textural changes that may have accompanied metamorphic recrystallization, crude comparative measurements were made of grain sizes in samples from spheroidally weathered and angularly weathered Reed Dolomite. Thin sections were made from four rock specimens representing a broad stratigraphic range in the formation in an area of "normal," angular weathering (fig. 1). The apparent diameters of 20 randomly selected dolomite crystals in each thin section were measured by an eyepiece micrometer; the results are given in table 1. The same procedure was followed with nine specimens of

spheroidally weathered Reed Dolomite from contact aureoles and one of spheroidally weathered calcite marble (fig. 1, table 1). The results of grain-size measurements show that the dolomite marbles are generally coarser and more nearly uniform in grain size than the unmetamorphosed rocks. However, one specimen (B-29) of angularly weathered sedimentary dolomite is coarser grained than most of the spheroidally weathering marbles, and two (SD-4, SD-8) of the dolomite marbles are about as fine grained as the average unmetamorphosed dolomite.

TABLE 1.—Summary of measurements of apparent grain size of carbonate rocks in the White Mountains, Calif.

Rock sample (fig. 1)	Field designation	Apparent grain size (millimeters)	
		Mean	Mean deviation (percent)
Angularly weathered dolomite (unmetamorphosed)			
1-----	B-29	0.7	51
2-----	B-24	.1	55
3-----	B-19	.07	58
4-----	B-12	.04	81
Spheroidally weathered dolomite (metamorphosed)			
5-----	SD-10	1.8	37
6-----	SD-11	.8	27
7-----	SD-1	.7	38
8-----	SD-2	.7	36
9-----	SD-3	.6	29
10-----	SD-5	.4	35
11-----	SD-7	.3	29
12-----	SD-4	.2	55
13-----	SD-8	.2	54
Spheroidally weathered limestone (metamorphosed)			
14-----	SL-1	1.3	36

The textures of weathering products are related to weathering processes as well as to the original textural and mineralogical features of the parent rock. Therefore, soil samples from areas of both angularly and spheroidally weathered dolomite were used to study mechanisms of weathering. Samples of the upper 6 inches of soil were collected at intervals of about 200 feet along a transect from the base to the crest of a north-facing Reed Dolomite slope in an area of angular weathering (fig. 1). The air-dried samples were passed through a series of graded sieves without preliminary treatment. The results (table 2) show that pebble-sized and larger particles constitute nearly half the weight of each sample. Most of the remainder consists of very fine sand. Furthermore, microscopic examination of each individual weight fraction shows that the intermediate size classes consist primarily of

calcite-cemented aggregates of smaller dolomite grains. Thus, the initial products of the breakdown of the sedimentary dolomite have an even more pronounced bimodal grain-size distribution than is indicated by these figures.

TABLE 2.—Grain-size distribution of samples of surface soil from the White Mountains, Calif.

Soil sample (fig. 1)	Field designation	Distribution of size fractions (weight percent)					
		Silt and clay (<0.062 mm)	Sand			Granules (2.0-4.76 mm)	Pebbles and cobbles (>4.76 mm)
			Fine to very fine (0.062-0.25 mm)	Medium to coarse (0.25-1.0 mm)	Very coarse (1.0-2.0 mm)		
Angularly weathered Reed Dolomite transect							
1-----	DS-14	10	28	5	2	5	50
2-----	DS-15	6	20	3	1	6	64
3-----	DS-16	6	20	6	2	6	60
4-----	DS-17	10	23	8	2	6	51
5-----	DS-18	9	26	9	6	13	37
6-----	DS-19	9	33	6	5	10	37
7-----	DS-20	5	25	6	5	12	47
8-----	DS-21	5	29	8	6	15	39
Spheroidally weathered dolomite marble							
9-----	SDS-1	7	12	52	6	4	19
10-----	SDS-2A	4	31	55	1	1	8
11-----	SDS-2B	7	32	50	1	1	9
Spheroidally weathered calcite marble							
12-----	SLS-1	8	14	38	20	6	14

Comparison of the particle-size distribution in the soil samples with the average grain sizes in samples of angularly weathered parent rock (fig. 5) clearly shows that the abundant (averaging 45 percent of total sample weight) coarse soil particles must represent polycrystalline fragments. These are apparently dislodged along joints and irregular intersecting fractures. Much less abundant (averaging 26 percent of total sample weight), but making up a secondary mode, are fine to very fine sand-sized grains that probably correspond to cleavage fragments and individual crystals.

A similar comparison can also be made for soils derived from spheroidally weathered dolomite marble (fig. 5). In contrast to soils derived from angularly weathered rock, these samples show a consistently unimodal particle-size distribution. More than 50 percent by weight of each of the dolomitic soils consists of unaggregated particles of medium- to coarse-sand size. The mean grain sizes in 6 of the 9 measured specimens of spheroidal dolomite also fall in this size range

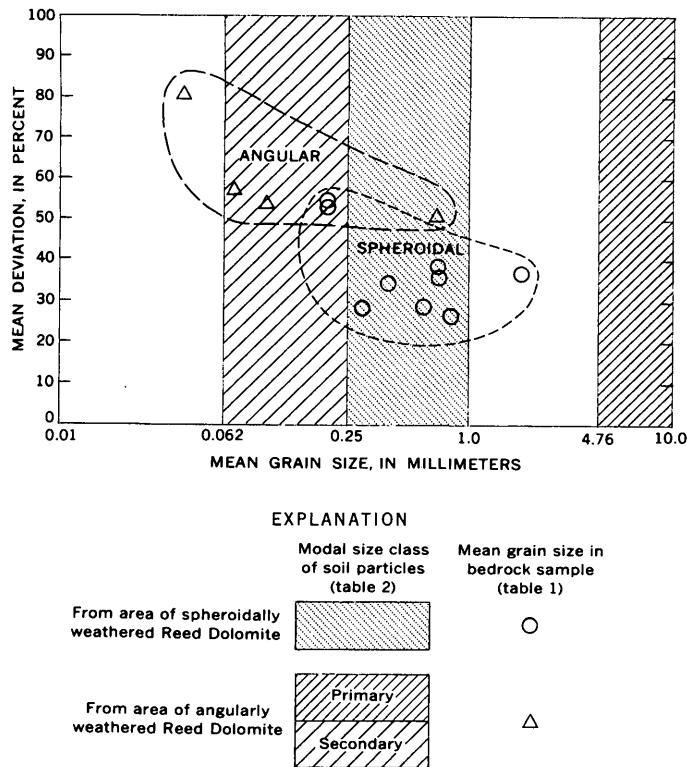


FIGURE 5.—Textural comparison of soils and parent rock.

(fig. 5), implying that spheroidal weathering produces a soil containing a large proportion of individual dolomite crystals from the parent rock. Dislodgment of discrete component grains along grain boundaries thus seems to be the dominant mode of breakdown of the larger joint blocks in areas of spheroidal weathering in the White Mountains. Spalls detached from the local exfoliating blocks are friable and apparently do not persist, but are rapidly reduced by granular disintegration.

DISCUSSION

The properties of outcrop surfaces and the textures of locally derived soils show that thermally metamorphosed carbonate rocks in the White Mountains react to weathering agencies in a manner different from that of their unmetamorphosed counterparts. Both rock types are obscurely bedded but strongly jointed, and break down initially along intersecting planar fractures into irregular blocks that remain in place. In the unmetamorphosed rock, these joint blocks are further reduced by minute fracturing and produce angular polycrystalline fragments and subsidiary amounts of much finer debris. Because the fracturing tends to parallel certain joint directions, and because the fragments are comparatively large, the outcrops are dominated by planar facets and sharp edges. In

contrast, individual joint blocks of dolomite marble or calcite marble outcrops are decomposed into their constituent mineral grains. Because the individual particles are small, and because they are preferentially removed at the edges and corners of a block, the resulting residual rock masses are rounded.

The difference in weathering mechanisms of these carbonate rocks is clearly related to their different metamorphic histories. However, as shown by textural evidence, the general increase in grain size that accompanied thermal metamorphism does not explain the granular disintegration of the dolomite marble. The marble must have undergone a large drop in temperature—from the temperature of recrystallization near the intrusive contact to that prevailing at the earth's surface. This possibly explains the ease of detachment of individual weathered grains from the surface of the marble, because, as has been pointed out (Leopold and others, 1964, p. 99), intergranular stresses can be expected to develop on cooling in rocks that have crystallized at high temperatures.

The rates of thermal contraction are different in different directions in adjacent randomly oriented anisotropic crystals. The rhombohedral carbonate minerals, including calcite and dolomite, are strongly anisotropic. Calcite, for example, shrinks about 1.8 percent in the direction perpendicular to the *c* crystallographic axis on cooling from 600°C to 20°C, while expanding about 0.2 percent parallel to the *c* axis (Skinner, 1966, p. 82). Thus two adjacent calcite grains, crystallographically perpendicular and of the same size, in a contact marble could differ as much as 2 percent in length along their mutual boundary after cooling to earth surface temperatures. Because stress increases the solubility of minerals (Turner and Verhoogen, 1960, p. 476), rapid solution might occur along such misfit grain boundaries during weathering. Stress relief by fracturing along the boundaries would further decrease intergrain cohesion and promote grain-boundary corrosion by permitting the penetration of water. The phenomenon may be similar to the intergranular corrosion that takes place in metals that have been rapidly cooled from high temperatures (Copson, 1963, p. 18). A similar explanation may be indicated for other metamorphic or igneous rocks that weather spheroidally in circumstances that inhibit or preclude clay-mineral development.

The predominance of granular disintegration in the spheroidal weathering of contact-metamorphosed marbles can be plausibly explained on the basis of their distinctive thermal history. However, it is more difficult to explain the local occurrence of typical "chemical" exfoliation in these rocks. Blackwelder (1925,

p. 803) did not observe chemical exfoliation in "quartzites, limestones, or other rocks of simple and unfavorable mineral composition." In silicate rocks, he attributed exfoliation to the expansion of the outer part of a weathering block, due to hydration and clayey alteration of primary silicates. Obviously, however, an exfoliation mechanism based on alteration of silicate minerals cannot be effective in the sedimentary and metamorphic facies of the Reed Dolomite and the calcite marble bed in the Wyman Formation, which contain only sporadic trace amounts of detrital quartz and feldspar. Furthermore, there are no weathering products of calcite or dolomite which might be analogous to the clay minerals formed during weathering of silicates to provide a mechanism of expansion.

The exfoliation in blocks of spheroidally weathered marble may be an indirect consequence of intergranular corrosion. The increased porosity near the margins of such blocks can be observed on the surfaces of transverse cuts. An expansion mechanism related to the difference in porosity between the outside and inside of the rock would explain the development of concentric fractures. On the other hand, penetration by plant roots and swelling of interstitial colloids (Blackwelder, 1925, p. 795) are probably not effective because vegetation is generally sparse in the White Mountains, and it is virtually absent from spheroidally weathered outcrops. Although casehardening of the outer surface is associated with exfoliation in these rocks, interstitial secondary precipitates in the porous outer shells, which might cause a net volume increase, have not been observed. Weather data from a station in the study area¹ show that air temperatures drop from above the freezing point to 32°F or less, on an average of

219 days per year. The repeated freezing of pore water with consequent volume increase, is therefore probably effective in expanding the outer surface of the marble.

REFERENCES

- Blackwelder, Eliot, 1925, Exfoliation as a phase in rock weathering: *Jour. Geology*, v. 33, p. 793-806.
- Chapman, R. W., and Greenfield, M. A., 1949, Spheroidal weathering of igneous rocks: *Am. Jour. Sci.*, v. 247, p. 407-429.
- Copson, H. R., 1963, Forms of corrosion, in La Que, F. C., and Copson, H. R., eds., *Corrosion resistance of metals and alloys*: *Am. Chem. Soc. Mon.* 158, 2d ed., p. 7-44.
- Dalrymple, G. B., 1963, Potassium-argon dates of some Cenozoic volcanic rocks of the Sierra Nevada, California: *Geol. Soc. America Bull.*, v. 74, p. 379-390.
- Emerson, D. O., 1966, Granitic rocks of the Mt. Barcroft quadrangle, Inyo Batholith, California-Nevada: *Geol. Soc. America Bull.*, v. 77, p. 127-152.
- Hall, M. L., 1964, Intrusive truncation of the Precambrian-Cambrian succession in the White Mountains, California: *California Univ., Berkeley, M. A. thesis.*
- Leopold, L. B., Wolman, M. G., and Miller, J. P., 1964, *Fluvial processes in geomorphology*: San Francisco, Freeman, 522 p.
- Nelson, C. A., 1963, Preliminary geologic map of the Blanco Mountain quadrangle, Inyo and Mono Counties, California: *U.S. Geol. Survey Mineral Inv. Field Studies Map MF-256.*
- Reiche, Parry, 1950, A survey of weathering processes and products: Albuquerque, N. Mex., Univ. New Mexico Press, *Geology Pub.* 3, 95 p.
- Skinner, B. J., 1966, Thermal expansion, in Clark, S. P., ed., *Handbook of physical constants*: *Geol. Soc. America Mem.* 97, p. 75-96.
- Stewart, J. H., 1965, Precambrian and Lower Cambrian formations in the Last Chance Range area, Inyo County, California, in Cohee, G. V., and West, W. S., *Changes in stratigraphic nomenclature by the U.S. Geological Survey 1964*: *U.S. Geol. Survey Bull.* 1224-A, p. A60-A70.
- Turner, F. J., and Verhoogen, John, 1960, *Igneous and metamorphic petrology*, 2d ed.: New York, McGraw-Hill, 694 p.

¹ Nello Pace, 1963, Climatological data summary for the decade 1 January, 1953 through 31 December, 1962 from the Crooked Creek Laboratory and the Barcroft Laboratory: *California Univ. White Mtn. Research Sta., Berkeley, Calif.* (duplicated rept., 52 p.).



RARE-EARTH MINERAL OCCURRENCE IN MARINE EVAPORITES, PARADOX BASIN, UTAH

By OMER B. RAUP, ARTHUR J. GUDE 3d,
and H. LEON GROVES, Jr., Denver, Colo.

Abstract.—A new calcium rare-earth borate mineral has been found in the marine evaporites in the Paradox Member of the Hermosa Formation of Pennsylvanian age in southeastern Utah. This is the first known occurrence of any rare-earth mineral from marine evaporites. The mineral occurs in nodules in a 6-inch zone in anhydrite which immediately overlies the potash deposit in the Cane Creek mine of the Texas Gulf Sulphur Co. near Moab, Utah. The occurrence of this mineral and its relation to the host rock indicates that it is a diagenetic mineral, most likely formed through incorporation of rare-earth elements concentrated in the evaporites and derived from sea water.

A rare-earth mineral has been found in marine evaporites in the Paradox Member of the Hermosa Formation of Pennsylvanian age in southeastern Utah. This preliminary report describes only the geologic setting of this mineral. The mineral was first recognized by the senior author during mineralogical studies of the potash deposit in the Cane Creek mine of the Texas Gulf Sulphur Co. near Moab, Utah. A review of the literature on marine evaporites, particularly Lotze (1957), Braitsch (1962), Stewart (1963), Borchert and Muir (1964), as well as discussions with Michael Fleischer, of the U.S. Geological Survey (oral commun., 1966), indicate this is a new mineral and is the first known occurrence of a rare-earth mineral in marine evaporites. Preliminary X-ray and spectrographic chemical data support the determination of a unique mineral species. A paper describing the physical and chemical characteristics of this mineral and proposing a name is in preparation.

The writers wish to acknowledge the assistance and cooperation of H. V. W. Donohoo, Kurt O. Linn, and George R. Grandbouche, of the Texas Gulf Sulphur Co. who made the mine workings available for sample collecting, made core material available, and granted permission to publish the data. Arthur L. Sutton, of

the U.S. Geological Survey, made the preliminary spectrographic determinations.

GEOLOGIC SETTING

A rare-earth mineral occurs in rocks that are part of a thick sequence of marine evaporites in the Paradox basin. The basin covers an area of 11,000 square miles in southeastern Utah and southwestern Colorado. The boundaries of the basin are defined by the limit of the salt deposits in the Paradox Member of the Hermosa Formation of Pennsylvanian area (fig. 1).

The original thickness of the Paradox Member ranged from 0 at the basin margins to about 7,000 feet in the deepest part of the basin. The salt has been locally thickened to as much as 14,000 feet in diapiric anticlines (Hite, 1961, p. D135).

The saline rocks of the Paradox Member consist of 29 known evaporite cycles. The rock types in these cycles include limestone, dolomite, anhydrite, black shale, and halite with or without potash salts (Hite, 1961, p. D135). Hite (1960) has numbered the salt beds of the saline section from 1 through 29 from top to bottom.

The rare-earth mineral was found in rocks closely associated with the potash deposit in salt bed 5 in the Cane Creek mine of the Texas Gulf Sulphur Co. This mine is on the northeast flank of the Cane Creek anticline, one of the northwest-trending structures in the basin, and is about 8 miles southwest of Moab, Utah. The potash is being mined at depths of 3,000 to 3,500 feet. Salt beds 2 through 5 are exposed in the workings of the mine (fig. 2).

OCCURRENCE OF RARE-EARTH MINERAL

The rare-earth mineral was found at the base of the penesaline and clastic unit overlying salt bed 5. The mineral occurs in reddish-pink nodules distributed

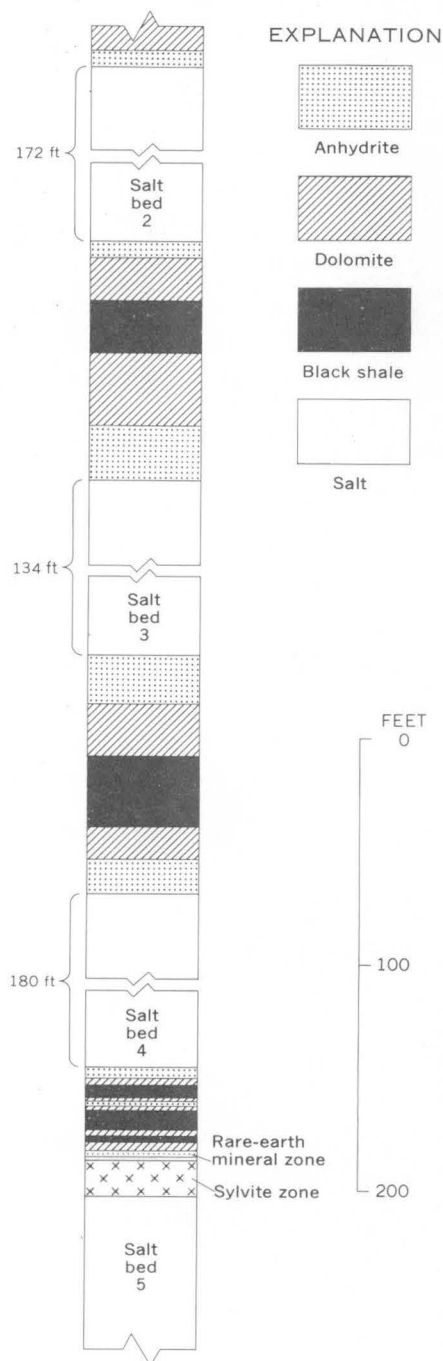


FIGURE 2.—Stratigraphic column of rocks exposed in the Texas Gulf Sulphur Co. potash mine.

through a 6-inch layer in anhydrite that immediately overlies the salt (fig. 3). The nodules are in this stratigraphic position throughout the mine workings, as well as in the same zone in drill core from a hole approximately 1 mile south of the mine shaft. Although the nodules are confined to the 6-inch bed described above (fig. 3), the individual nodules cut



FIGURE 3.—Contact of salt bed 5 with overlying anhydrite. Pocketknife is standing on contact. Arrows indicate thickness of rare-earth-mineral zone in anhydrite.

across thin varve-like primary layering of the enclosing rock (fig. 4).

The nodules occur in rock that is predominantly anhydrite containing varied amounts of dolomite, halite, small amounts of pyrite, and detrital quartz and mica. The nodules are roughly spherical, range in size from about 0.05 to 8 millimeters (fig. 4), and are composed of a finely crystalline aggregate of the rare-earth mineral, anhydrite, halite, and a small amount of finely disseminated hematite. The nodules are composed of about 65 percent rare-earth mineral. The hematite gives the nodules a color ranging from pink to red. Very small nodules appear to contain little or no hematite, and are white. Many of the larger nodules contain small sulfide crystals which have been identified as chalcopyrite (E. J. Dwornik, oral commun., 1966).

The chemical composition of the rare-earth mineral has not yet been fully determined, but preliminary data from qualitative chemical analyses and a semiquantitative spectrophotographic analysis indicate that the mineral is a calcium rare-earth borate.

ORIGIN

The origin of this rare-earth-bearing mineral in these marine evaporite rocks is difficult to explain. The mineral is restricted to a thin stratigraphic zone, yet has a fairly wide areal extent. The thick sequence of bedded salt below this mineral-bearing zone makes it unlikely that ascending hydrothermal solutions were the source of rare-earth elements. The nodules crosscut primary layering and indicate a younger age than the enclosing rock, thus eliminating a detrital origin. Therefore, the nodules probably formed as

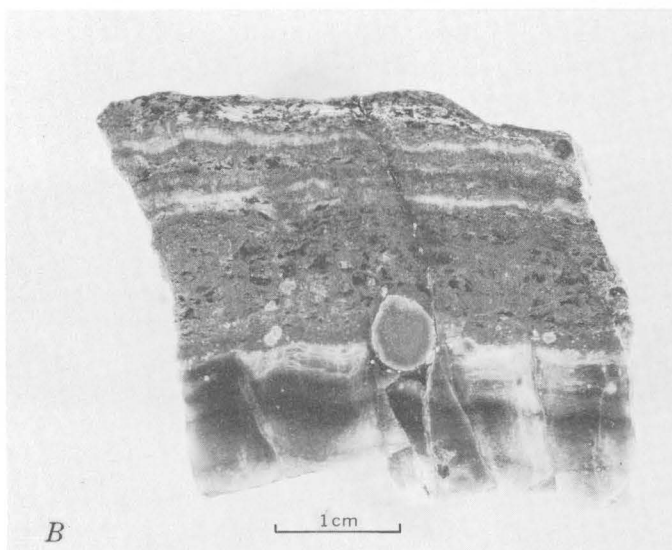
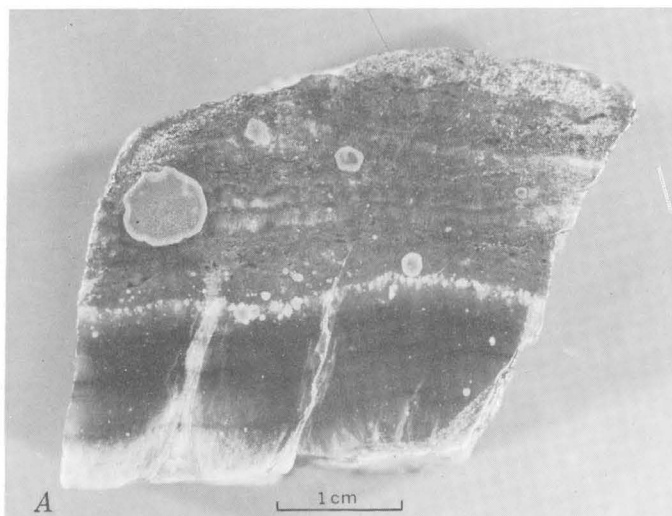


FIGURE 4.—Polished specimens of anhydrite rock with nodules containing rare-earth mineral. A. Large nodules and concentration of small nodules along bedding plane. B. Large nodule cutting across bedding plane.

the result of a diagenetic process, and the elements involved were derived from sea water.

The data are insufficient at present to determine the origin of the rare-earth mineral. However, the rare-earth elements may have been concentrated in at least two ways: (1) Continued concentration of bittern brine through several evaporite cycles could have caused an abnormally high concentration of rare-earth elements. This brine could have occupied the interstitial space in the crystal "mush" of sylvite and halite at the top of salt bed 5, and during lithification the brine might have been expelled against the overlying anhydrite to react with it and form nodules (K. O. Linn, oral commun., 1966). (2) The rare-earth elements could have been concentrated by organic agents such as macro-organisms washed into the basin, or floating micro-organisms (Milton and others, 1965, p. 611; Rankama and Sahama, 1950, p. 531).

REFERENCES

- Borchert, Hermann and Muir, R. O., 1964, Salt deposits: London, D. Van Nostrand Company, Ltd., 338 p.
- Braitsch, Otto, 1962, Entstehung und Stoffbestand der Salzlagerstätten: Berlin-Gottinger-Heidelberg, Springer Verlag., 232 p.
- Hite, R. J., 1960, Stratigraphy of the saline facies of the Paradox member of the Hermosa formation of southeastern Utah and southwestern Colorado, in *Geology of the Paradox basin fold and fault belt: Four Corners Geol. Soc. 3d Field Conf. 1960, Guidebook*, p. 86-89.
- 1961, Potash-bearing evaporite cycles in the salt anticlines of the Paradox basin, Colorado and Utah: *Art 337 in U.S. Geol. Survey Prof. Paper 424-D*, p. D135-D138.
- Lotze, Franz, 1957, *Steinalz und Kalisalze*: Berlin-Nikolassee, Gebrüder Borntraeger, 465 p.
- Milton, Charles, Ingram, Blanche, Clarke, J. R., and Dwornik, E. J., 1965, Mckelveyite, a new hydrous sodium barium rare-earth uranium carbonate mineral from the Green River Formation, Wyoming: *Am. Mineralogist*, v. 50, p. 593-612.
- Rankama, Kalervo and Sahama, Th. G., 1950, *Geochemistry*: Chicago, Univ. Chicago Press, 912 p.
- Stewart, F. H., 1963, Marine evaporites, in *Fleischer, Michael, ed., Data of geochemistry*, 6th ed.: U.S. Geol. Survey Prof. Paper 440-Y, 52 p.



VOLCANISM AND TECTONISM AS REFLECTED BY THE DISTRIBUTION OF NONOPAQUE HEAVY MINERALS IN SOME TERTIARY ROCKS OF WYOMING AND ADJACENT STATES

By YOSHIAKI SATO¹ and N. M. DENSON, Tokyo, Japan, Denver, Colo.

Abstract.—Tertiary rocks in the middle Rocky Mountains and northern High Plains contain two distinct assemblages of nonopaque heavy minerals. A volcanic assemblage is characterized by oxy- and green-brown hornblende, augite, hypersthene, and red-brown biotite, and generally constitutes 60–70 percent of the nonopaque heavy minerals in lower Miocene rocks (Arikaree Formation). A plutonic assemblage is characterized by blue-green hornblende, garnet, epidote, sillimanite, sphene, tourmaline, zircon, and gray-green biotite and generally constitutes more than 55 percent of the nonopaque heavy minerals in middle Tertiary, Oligocene (White River Formation), and upper Miocene and Pliocene rocks (Ogallala Formation). These heavy-mineral assemblages substantiate postulated regional Tertiary geologic history and aid in correlating units throughout the northern High Plains.

Continental rocks of Oligocene, Miocene, and Pliocene age unconformably overlie the truncated edges of older rocks in parts of the middle Rocky Mountains and Great Plains areas. These rocks range in thickness from about 600 to 1,900 feet in southeastern Wyoming and adjacent parts of western Nebraska and northeastern Colorado (Denson and Bergendahl, 1961), and from about 1,500 to 2,800 feet in the intermontane basins of central Wyoming and northwestern Colorado (Love, 1960). In the southwestern part of the Williston basin of eastern Montana and adjacent parts of North and South Dakota, they have an average thickness of about 800 feet (Denson and Gill, 1965).

In general, the older rocks in this sequence (Oligocene) are finer grained, more uniformly sized, and have a higher carbonate content than the younger rocks. Oligocene rocks (White River Formation) are chiefly siltstone; lower Miocene rocks (Arikaree Formation) are chiefly very fine grained tuffaceous sand-

stone; and upper Miocene and Pliocene rocks (Ogallala, Browns Park, and Flaxville Formations) are chiefly medium- to coarse-grained sandstone and conglomerate. Lenticular beds of volcanic ash, bentonite, and limestone occur locally in all these formations. Conglomerate and coarse-grained sandstone occur as channel-fill and fanlike deposits throughout the sequence but are most common in the upper Miocene and Pliocene rocks.

A twofold stratigraphic division of the Miocene is used in this report. On the northern High Plains, sediments deposited in late Tertiary time are included in either the Arikaree (lower Miocene) or the Ogallala (upper Miocene and Pliocene). The writers believe that, at or near the type locality of the "middle Miocene" of Wood and others (1941) near Hemingford, Nebr., the rocks are divisible into a lower unit, the Marsland of Lugn (1939), which is lithologically allied to the rocks assigned to the Arikaree, and an upper unit, the Sheep Creek, which is lithologically allied to the rocks assigned to the Ogallala. (See Matthew, 1924, p. 61; and Matthew and Cook, 1909, p. 363, lines 8 and 9.) Because the Marsland and Sheep Creek of Lugn (1939) cannot be differentiated on lithologic criteria from the rocks assigned to the underlying and overlying formations, the term "middle Miocene" seemingly has only a faunal connotation and is not used in this report.

Heavy minerals are present in various proportions in all the middle and upper Tertiary rocks but are most abundant in the Arikaree Formation. In the Arikaree, about 75 percent of the total nonopaque heavy minerals were derived from volcanic source areas, whereas the heavy minerals in the lower Tertiary rocks came largely from metamorphic and plutonic rocks.

¹ Geological Survey of Japan.

Minerals derived largely from the weathering of Precambrian metamorphic and plutonic rocks and their sedimentary cover are referred to in this report as plutonic minerals. The term, as used here, includes minerals of both plutonic and metamorphic origin. Minerals that are largely the products of explosive volcanic eruptions are referred to here as volcanic minerals. Some grains of both types probably have undergone more than one cycle of deposition. Because most of the volcanic minerals may have been distributed largely through the atmosphere to their present locations, they generally are angular to subangular in shape, whereas the plutonic minerals were transported mostly by water and are generally rounded to subrounded.

Acknowledgments.—The writers are indebted to D. M. Sheridan, G. M. Richmond, W. A. Chisholm, and H. J. Hyden for the loan of their samples collected from terrace deposits along present-day streams draining Precambrian metamorphic and igneous terrane in Colorado, Wyoming, and South Dakota. Laura W. McGrew supplied information on the Wheatland area, Wyoming, and loaned rock samples from several wells. J. R. Donnell and M. J. Bergin collected surface samples and supplied well data on the Browns Park Formation in the Maybell-Lay-Burro Mountain area of northwestern Colorado, and Wallace R. Hansen loaned samples of vitric tuff from the Browns Park Formation in the Flaming Gorge area of northeastern Utah. James R. Gill collected many samples from the uranium-bearing lignite areas in the Williston basin, North and South Dakota. Seven-hundred-fifty size analyses, prepared slides, and thin sections of the Tertiary rocks were made by Robert F. Gantnier, James A. Thomas, Phillip G. Hanna, and Thomas D. Hessin. Mineral counts for all samples reported from the Williston basin, from the Oregon Buttes area in central Wyoming, and from the Maybell-Lay area in northwestern Colorado were made by W. A. Chisholm. Sato did most of the petrographic work, whereas the organization and interpretation of the field and laboratory data were the responsibility of Denson.

PURPOSE, SCOPE, AND SAMPLE PREPARATION

Approximately 700 samples of Tertiary rocks were collected from measured stratigraphic sections in the Williston basin of North and South Dakota, the High Plains of eastern Wyoming and western Nebraska, and the intermontane basins of central Wyoming and northeastern Colorado (fig. 1). A microscopic study of the variety and characteristics of the nonopaque heavy-mineral grains of the samples was undertaken for three purposes:

1. Determine whether differences in the heavy-mineral assemblage of successive formations were great enough to be used as a criterion for correlating a formation in one area with a formation in another.
2. Establish, insofar as possible, the relative proportion of volcanic minerals to plutonic minerals in any particular suite of samples.
3. Determine whether the nonopaque heavy minerals in the Tertiary rocks reflect specific periods of volcanism and tectonism in the middle Rocky Mountains, as Stow (1938) described in the Bighorn Basin of northwestern Wyoming and southwestern Montana.

Heavy-mineral suites from terrace deposits along streams draining Precambrian igneous and metamorphic rocks in the Front Range of Colorado, the Black Hills of South Dakota, and the Wind River Mountains of Wyoming were studied and compared with the heavy-mineral suites from the Tertiary rocks in order to establish which assemblages in the Tertiary rocks were derived from the Precambrian. Many samples were also analyzed for grain size and carbonate content, and thin sections of selected samples were examined to aid in interpreting the heavy-mineral data.

Most of the samples collected were selected at arbitrary stratigraphic intervals of about 15–25 feet in measured sections. Lenses or thin beds of texturally different material within thick, otherwise homogeneous beds were not sampled. Lenticular, channel-like sandstone and conglomerate, common throughout the Tertiary, were also excluded in the sampling.

The locations of the stratigraphic sections and localities at which rocks were collected for heavy-mineral analyses are given on figure 1 and table 1.

The samples were disaggregated in dilute hydrochloric acid, and the heavy minerals were concentrated in bromoform. Only heavy minerals in the very fine sand-size fraction (0.062–0.125 mm) of most of the samples were studied. A few samples, however, yielded too few grains of this size for adequate evaluation, so grains in the coarse silt-size fraction (0.031–0.062 mm) were also studied. Comparisons made between different groups of samples are, therefore, for heavy minerals from about the same size range. Quantitative determinations were made from approximately equal amounts of samples, and mineral ratios were determined on a percentage basis by counts of 100 or more grains per sample mounted in Arochlor ($N=1.66$). Very few of the samples had minerals coated with iron oxide or clay; they were warmed in dilute hydrochloric or nitric acid and agitated in an ultrasonic vibrator to clean them and facilitate identification.

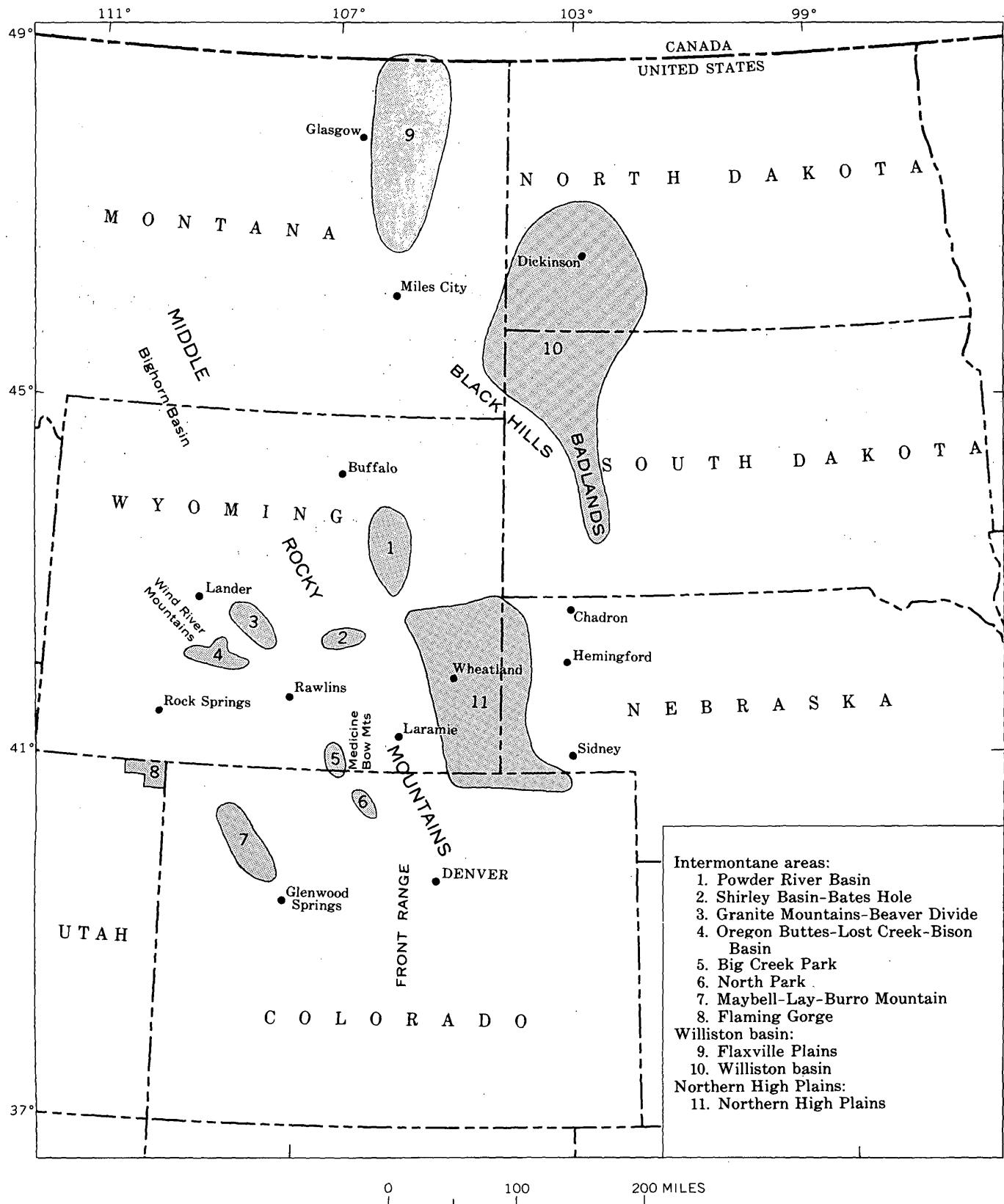


FIGURE 1.—Index map showing general areas where samples of Tertiary rocks were collected for heavy-mineral analysis.

The magnetic opaque minerals, as much as 50 percent of the concentrate in some samples, were removed with an electromagnet before the nonopaque minerals were studied. These magnetic minerals, which include magnetite, ilmenite, ferruginous and clay aggregates, leucoxene, and pyrite, were not studied in detail.

MIDDLE AND UPPER TERTIARY ROCKS

Physical characteristics

As shown on figure 2, the Oligocene, Miocene, and Pliocene rocks in the intermontane basins and High Plains of Wyoming, Colorado, and Nebraska, differ markedly in average grain-size distribution, carbonate content, the percentage of total heavy minerals. The Oligocene rocks, for example, are mostly siltstones of which 20-25 percent is carbonate. The very fine grained sand fraction of these rocks also has the smallest percentage of heavy minerals among any of the Tertiary rocks studied. The lower Miocene rocks are mostly well-sorted moderately calcareous sandstone and contain the largest percentage of very fine grained heavy minerals. The upper Miocene and Pliocene are mostly poorly sorted, moderately calcareous sandstone having relatively small content of very fine grained heavy minerals.

Heavy minerals

Heavy minerals from the middle and upper Tertiary rocks of the middle Rocky Mountains and High Plains regions are mixtures of two mineral suites of widely different origins: (1) minerals derived largely from Precambrian cores of the mountain ranges and their sedimentary cover, and (2) minerals largely of volcanic origin. Minerals of the first suite commonly include blue-green hornblende, garnet, epidote, sillimanite, sphene, tourmaline, zircon, and gray-green biotite (fig. 3A). Minerals in the second suite commonly include green-brown and red-brown hornblende, augite, hypersthene, and red-brown biotite (fig. 3B).

As shown graphically on figure 3A, very fine grained heavy minerals of the first suite are characteristic of terrace deposits along present-day streams draining only Precambrian igneous and metamorphic terranes in the Front Range of Colorado, Medicine Bow and Wind River Mountains in Wyoming, and the Black Hills of South Dakota. Blue-green hornblende and garnet or epidote predominate in this suite. Mineral suites in Tertiary sedimentary rocks contain a similar assemblage and probably had the same sources; they are described here as plutonic suites. Minerals of the second suite are common in some of the Tertiary rocks but are absent or sparse in terrace deposits derived

from metamorphic and igneous terranes. This suite includes hypersthene, augite, and red-brown (basaltic) hornblende and green-brown hornblende. In this report, these minerals are considered to be volcanically derived.

The sparsity of green-brown hornblende in the Precambrian igneous rocks was questioned by colleagues who contended that in thin sections, the green-brown variety was present in much greater quantities than we reported in our grain counts of samples from the Precambrian. The apparent cause of the discrepancy was revealed when a fine-grained sand fraction of the rock from which the thin sections were made was crushed and separated. As seen in thin sections, much of the hornblende in the Precambrian rocks transmits a green-brown color. In mounts of separated grains, however, it is clearly blue green. Because the percentages of minerals as used in this report were uniformly determined from grain mounts, any discrepancy that might occur from use of thin sections was eliminated.

Shown graphically on figure 3B are the varieties of very fine grained nonopaque heavy minerals in samples of vitric tuff and volcanic ash from middle and upper Tertiary rocks in the Uinta Mountains and the High Plains. High percentages of pyroxene and green-brown amphibole characterize these mineral concentrates, which are beyond doubt largely of volcanic origin. A striking similarity is found between the relative proportions of the various species of nonopaque heavy minerals in tuff from the Uinta Mountains (fig. 3B) and in the Arikaree Formation of the intermontane basins (fig. 4), and between the relative proportion of heavy-mineral species in beds of volcanic ash from the Northern Plains and in those from the Arikaree Formation in the same region.

Figure 4 shows graphically the predominance of volcanic minerals in the siltstone and very fine grained sandstone which make up the bulk of the Oligocene and lower Miocene rocks. The abundance of green-brown hornblende and pyroxene (augite and hypersthene) is in marked contrast to the paucity of these minerals in samples of plutonic origin. A small proportion of some minerals such as sphene, zircon, and allanite, which are interpreted on figure 4 as plutonic, may be of volcanic origin. Conversely, a small proportion of the green-brown hornblende, interpreted on figure 4 as volcanic, may be plutonic. In either case, however, the percentages are too small to affect significantly the interpretation placed upon the ratio of volcanic minerals to plutonic minerals in any particular sample group. Apatite, which occurs in small quantities in both the volcanic and detrital assemblages,

TABLE 1.—Locations of stratigraphic sections and localities at which samples from Tertiary formations were collected for heavy-mineral analyses

System or series	Intermontane basins	Williston basin	Northern High Plains																																																																																																						
Upper Tertiary	<p>Browns Park¹</p> <ol style="list-style-type: none"> Burro Mountain, Rio Blanco County, Colo., Tps. 1 and 2 S., R. 91 W. Maybell-Lay area, Moffat County, Colo., secs. 5 and 31, Tps. 6 and 7 N., R. 95 W. (two test holes). 	<p>Flaxville</p> <ol style="list-style-type: none"> Big Sheep Mountain, Prairie County, Mont., sec. 24, T. 15 N., R. 47 E. Flaxville Plains, Daniels County, Mont., sec. 14, T. 37 N., R. 49 E. Flaxville Plains, Valley County, Mont., sec. 24, T. 35 N., R. 42 E. 	<p>Ogallala</p> <p>Pine Ridge, Goshen County, Wyo., sec. 2, T. 26 N., R. 63 W.</p> <p>Wheatland Flats, Platte County, Wyo., sec. 33, T. 24 N., R. 68 W. (core hole).</p> <p>Simpson Creek, Weld County, Colo., sec. 22, T. 12 N., R. 65 W.</p> <p>Kennesaw Point, Logan County, Colo., sec. 27, T. 12 N., R. 55 W.</p> <p>Flattop Butte, Platte County, Wyo., sec. 1, T. 30 N., R. 66 W.</p>																																																																																																						
Lower Miocene	<p>Arikaree</p> <ol style="list-style-type: none"> Twin Buttes, Natrona County, Wyo., sec. 7, T. 29 N., R. 79 W. Stratton, Natrona County, Wyo., sec. 27, T. 29 N., R. 82 W. Oregon Buttes, Fremont County, Wyo., sec. 24, T. 27 N., R. 100 W. Beaver Divide, Fremont County, Wyo., sec. 26, T. 32 N., R. 95 W. Granite Mountains, Fremont County, Wyo., sec. 35, T. 29 N., R. 90 W. Lost Creek, Sweetwater County, Wyo., sec. 13, T. 95 W., R. 26 N. Big Creek Park, Carbon County, Wyo., sec. 10, T. 12 N., R. 82 W. 	<p>Arikaree</p> <ol style="list-style-type: none"> Long Pine Hills, Carter County, Mont., secs. 16 and 17, T. 3 S., R. 62 E. Chalky Buttes, Slope County, N. Dak., sec. 25, T. 134 N., R. 101 W. Killdeer Mountains, Dunn County, N. Dak., secs. 27 and 28, T. 146 N., R. 96 W. West Rainy Butte, Slope County, N. Dak., sec. 20, T. 135 N., R. 98 W. Coffin Butte, Grant County, N. Dak., sec. 2, T. 131 N., R. 90 W. Slim Buttes, Harding County, S. Dak., sec. 17, T. 18 N., R. 8 E. Short Pine Hills, Harding County, S. Dak., sec. 26, T. 17 N., R. 1 E. 	<p>Arikaree</p> <table border="1"> <thead> <tr> <th>Sec.</th> <th>T.(N.)</th> <th>R.(W.)</th> <th>Sec.</th> <th>T.(N.)</th> <th>R.(W.)</th> </tr> </thead> <tbody> <tr> <td>Converse County, Wyo.</td> <td></td> <td></td> <td>Platte County, Wyo.</td> <td></td> <td></td> </tr> <tr> <td>23</td> <td>31</td> <td>69</td> <td>24</td> <td>20</td> <td>68</td> </tr> <tr> <td>26</td> <td>32</td> <td>69</td> <td>33</td> <td>24</td> <td>68</td> </tr> <tr> <td>18</td> <td>32</td> <td>71</td> <td>1</td> <td>25</td> <td>69</td> </tr> <tr> <td>Goshen County, Wyo.</td> <td></td> <td></td> <td>5</td> <td>27</td> <td>68</td> </tr> <tr> <td>5</td> <td>20</td> <td>63</td> <td>6</td> <td>29</td> <td>66</td> </tr> <tr> <td>15</td> <td>26</td> <td>63</td> <td>Banner County, Nebr.</td> <td></td> <td></td> </tr> <tr> <td>Laramie County, Wyo.</td> <td></td> <td></td> <td>10</td> <td>18</td> <td>58</td> </tr> <tr> <td>35</td> <td>15</td> <td>62</td> <td>Scotts Bluff County,</td> <td></td> <td></td> </tr> <tr> <td>3</td> <td>16</td> <td>65</td> <td>Nebr.</td> <td></td> <td></td> </tr> <tr> <td>Niobrara County, Wyo.</td> <td></td> <td></td> <td>6</td> <td>20</td> <td>55</td> </tr> <tr> <td>7</td> <td>33</td> <td>64</td> <td>Sioux County, Nebr.</td> <td></td> <td></td> </tr> <tr> <td>36</td> <td>34</td> <td>61</td> <td>17</td> <td>32</td> <td>55</td> </tr> <tr> <td>Weld County, Colo.</td> <td></td> <td></td> <td>Logan County, Colo.</td> <td></td> <td></td> </tr> <tr> <td>2</td> <td>11</td> <td>66</td> <td>15</td> <td>11</td> <td>52</td> </tr> </tbody> </table>	Sec.	T.(N.)	R.(W.)	Sec.	T.(N.)	R.(W.)	Converse County, Wyo.			Platte County, Wyo.			23	31	69	24	20	68	26	32	69	33	24	68	18	32	71	1	25	69	Goshen County, Wyo.			5	27	68	5	20	63	6	29	66	15	26	63	Banner County, Nebr.			Laramie County, Wyo.			10	18	58	35	15	62	Scotts Bluff County,			3	16	65	Nebr.			Niobrara County, Wyo.			6	20	55	7	33	64	Sioux County, Nebr.			36	34	61	17	32	55	Weld County, Colo.			Logan County, Colo.			2	11	66	15	11	52						
Sec.	T.(N.)	R.(W.)	Sec.	T.(N.)	R.(W.)																																																																																																				
Converse County, Wyo.			Platte County, Wyo.																																																																																																						
23	31	69	24	20	68																																																																																																				
26	32	69	33	24	68																																																																																																				
18	32	71	1	25	69																																																																																																				
Goshen County, Wyo.			5	27	68																																																																																																				
5	20	63	6	29	66																																																																																																				
15	26	63	Banner County, Nebr.																																																																																																						
Laramie County, Wyo.			10	18	58																																																																																																				
35	15	62	Scotts Bluff County,																																																																																																						
3	16	65	Nebr.																																																																																																						
Niobrara County, Wyo.			6	20	55																																																																																																				
7	33	64	Sioux County, Nebr.																																																																																																						
36	34	61	17	32	55																																																																																																				
Weld County, Colo.			Logan County, Colo.																																																																																																						
2	11	66	15	11	52																																																																																																				
Oligocene	<p>White River</p> <ol style="list-style-type: none"> Dishpan Butte, Fremont County, Wyo., sec. 29, T. 31 N., R. 95 W. Bates Hole, Carbon County, Wyo., sec. 6, T. 27 N., R. 80 W. Red Canyon, Fremont County, Wyo., sec. 3, T. 30 N., R. 96 W. Owl Ridge, Jackson County, Colo., sec. 28, T. 7 N., R. 78 W. 	<p>White River</p> <ol style="list-style-type: none"> Short Pine Hills, Harding County, S. Dak., sec. 26, T. 17 N., R. 1 E. Slim Buttes, Harding County, S. Dak., sec. 17, T. 18 N., R. 8 E. Chalky Buttes, Slope County, N. Dak., sec. 15, T. 134 N., R. 101 W. Little Badlands, Stark County, N. Dak., sec. 7, T. 137 N., R. 97 W. Big Bedlands, Pennington County, S. Dak., sec. 5, T. 4 S., R. 13 E. 	<p>White River</p> <table border="1"> <thead> <tr> <th>Sec.</th> <th>T.(N.)</th> <th>R.(W.)</th> <th>Sec.</th> <th>T.(N.)</th> <th>R.(W.)</th> </tr> </thead> <tbody> <tr> <td>Albany County, Wyo.</td> <td></td> <td></td> <td>Larimer County, Colo.</td> <td></td> <td></td> </tr> <tr> <td>17</td> <td>24</td> <td>73</td> <td>27</td> <td>12</td> <td>69</td> </tr> <tr> <td>Converse County, Wyo.</td> <td></td> <td></td> <td>Logan County, Colo.</td> <td></td> <td></td> </tr> <tr> <td>33</td> <td>31</td> <td>70</td> <td>2</td> <td>11</td> <td>54</td> </tr> <tr> <td>10</td> <td>32</td> <td>68</td> <td>Weld County, Colo.</td> <td></td> <td></td> </tr> <tr> <td>12</td> <td>32</td> <td>73</td> <td>17</td> <td>11</td> <td>65</td> </tr> <tr> <td>Goshen County, Wyo.</td> <td></td> <td></td> <td>Scotts Bluff County,</td> <td></td> <td></td> </tr> <tr> <td>17</td> <td>20</td> <td>62</td> <td>Nebr.</td> <td></td> <td></td> </tr> <tr> <td>Laramie County, Wyo.</td> <td></td> <td></td> <td>12</td> <td>21</td> <td>56</td> </tr> <tr> <td>32</td> <td>17</td> <td>69</td> <td>22</td> <td>21</td> <td>58</td> </tr> <tr> <td>Niobrara County, Wyo.</td> <td></td> <td></td> <td>Sioux County, Nebr.</td> <td></td> <td></td> </tr> <tr> <td>35</td> <td>35</td> <td>64</td> <td>17</td> <td>33</td> <td>56</td> </tr> <tr> <td>Platte County, Wyo.</td> <td></td> <td></td> <td></td> <td></td> <td></td> </tr> <tr> <td>19</td> <td>22</td> <td>66</td> <td></td> <td></td> <td></td> </tr> <tr> <td>13</td> <td>27</td> <td>70</td> <td></td> <td></td> <td></td> </tr> <tr> <td>30</td> <td>29</td> <td>69</td> <td></td> <td></td> <td></td> </tr> </tbody> </table>	Sec.	T.(N.)	R.(W.)	Sec.	T.(N.)	R.(W.)	Albany County, Wyo.			Larimer County, Colo.			17	24	73	27	12	69	Converse County, Wyo.			Logan County, Colo.			33	31	70	2	11	54	10	32	68	Weld County, Colo.			12	32	73	17	11	65	Goshen County, Wyo.			Scotts Bluff County,			17	20	62	Nebr.			Laramie County, Wyo.			12	21	56	32	17	69	22	21	58	Niobrara County, Wyo.			Sioux County, Nebr.			35	35	64	17	33	56	Platte County, Wyo.						19	22	66				13	27	70				30	29	69			
Sec.	T.(N.)	R.(W.)	Sec.	T.(N.)	R.(W.)																																																																																																				
Albany County, Wyo.			Larimer County, Colo.																																																																																																						
17	24	73	27	12	69																																																																																																				
Converse County, Wyo.			Logan County, Colo.																																																																																																						
33	31	70	2	11	54																																																																																																				
10	32	68	Weld County, Colo.																																																																																																						
12	32	73	17	11	65																																																																																																				
Goshen County, Wyo.			Scotts Bluff County,																																																																																																						
17	20	62	Nebr.																																																																																																						
Laramie County, Wyo.			12	21	56																																																																																																				
32	17	69	22	21	58																																																																																																				
Niobrara County, Wyo.			Sioux County, Nebr.																																																																																																						
35	35	64	17	33	56																																																																																																				
Platte County, Wyo.																																																																																																									
19	22	66																																																																																																							
13	27	70																																																																																																							
30	29	69																																																																																																							

TABLE 1.—Locations of stratigraphic sections and localities at which samples from Tertiary formations were collected for heavy-mineral analyses—Continued

System or series	Intermontane basins	Williston basin	Northern High Plains																																																																													
Eocene	<p>Wind River²</p> <p>1. Red Canyon, Fremont County, Wyo., sec. 2, T. 30 N., R. 96 W. 2. Dry Creek, Carbon County, Wyo., sec. 33, T. 28 N., R. 81 W. 3. Shirley Basin, Carbon County, Wyo., sec. 9, T. 27 N., R. 78 W. 4. Soap Holes, Fremont County, Wyo., secs. 3 and 14, T. 28 N., R. 94 W.</p>	<p>Golden Valley</p> <p>1. Killdeer Mountains, Dunn County, N. Dak., sec. 28 T. 146 N., R. 96 W. 2. Antelope Butte, Stark County, N. Dak., sec. 14, T. 139 N., R. 91 W. 3. Little Badlands, Stark County, N. Dak., sec. 31, T. 139 N., R. 97 W.</p>	<p>Wasatch³</p> <table border="1"> <thead> <tr> <th>Sec.</th> <th>T.(N.)</th> <th>R.(W.)</th> <th>Sec.</th> <th>T.(N.)</th> <th>R.(W.)</th> </tr> </thead> <tbody> <tr> <td colspan="3">Converse County, Wyo.</td> <td colspan="3">Campbell County, Wyo.</td> </tr> <tr> <td>20</td> <td>34</td> <td>73</td> <td>10</td> <td>41</td> <td>74</td> </tr> <tr> <td>3</td> <td>37</td> <td>73</td> <td colspan="3">Johnson County, Wyo.</td> </tr> <tr> <td>13</td> <td>37</td> <td>74</td> <td>8</td> <td>45</td> <td>76</td> </tr> <tr> <td>36</td> <td>37</td> <td>74</td> <td></td> <td></td> <td></td> </tr> <tr> <td>8</td> <td>37</td> <td>75</td> <td></td> <td></td> <td></td> </tr> <tr> <td>27</td> <td>38</td> <td>73</td> <td></td> <td></td> <td></td> </tr> <tr> <td>34</td> <td>38</td> <td>73</td> <td></td> <td></td> <td></td> </tr> <tr> <td>36</td> <td>38</td> <td>74</td> <td></td> <td></td> <td></td> </tr> <tr> <td>2</td> <td>38</td> <td>75</td> <td></td> <td></td> <td></td> </tr> <tr> <td>6</td> <td>40</td> <td>75</td> <td></td> <td></td> <td></td> </tr> </tbody> </table>						Sec.	T.(N.)	R.(W.)	Sec.	T.(N.)	R.(W.)	Converse County, Wyo.			Campbell County, Wyo.			20	34	73	10	41	74	3	37	73	Johnson County, Wyo.			13	37	74	8	45	76	36	37	74				8	37	75				27	38	73				34	38	73				36	38	74				2	38	75				6	40	75			
	Sec.	T.(N.)	R.(W.)	Sec.	T.(N.)	R.(W.)																																																																										
Converse County, Wyo.			Campbell County, Wyo.																																																																													
20	34	73	10	41	74																																																																											
3	37	73	Johnson County, Wyo.																																																																													
13	37	74	8	45	76																																																																											
36	37	74																																																																														
8	37	75																																																																														
27	38	73																																																																														
34	38	73																																																																														
36	38	74																																																																														
2	38	75																																																																														
6	40	75																																																																														
Paleocene	<p>Fort Union</p> <p>1. Bison Basin, Fremont County, Wyo., secs. 27 and 28, T. 27 N., R. 95 W.</p>	<p>Fort Union</p> <p>1. Sentinel Butte, Golden Valley County, N. Dak., sec. 8, T. 139 N., R. 104 W. 2. Chalky Buttes, Slope County, N. Dak., sec. 31, T. 134 N., R. 100 W. 3. Rocky Ridge, Billings County, N. Dak., sec. 34, T. 137 N., R. 100 W. 4. North Cave Hills, Harding County, S. Dak., sec. 26, T. 22 N., R. 5 E. 5. South Cave Hills, Harding County, S. Dak., sec. 28, T. 20 N., R. 4 E.</p>	<p>Fort Union³</p> <table border="1"> <thead> <tr> <th>Sec.</th> <th>T.(N.)</th> <th>R.(W.)</th> </tr> </thead> <tbody> <tr> <td colspan="3">Converse County, Wyo.</td> </tr> <tr> <td>15</td> <td>36</td> <td>75</td> </tr> <tr> <td>9</td> <td>37</td> <td>74</td> </tr> <tr> <td>12</td> <td>38</td> <td>77</td> </tr> <tr> <td>10</td> <td>39</td> <td>71</td> </tr> <tr> <td>5</td> <td>40</td> <td>70</td> </tr> </tbody> </table>						Sec.	T.(N.)	R.(W.)	Converse County, Wyo.			15	36	75	9	37	74	12	38	77	10	39	71	5	40	70																																																			
Sec.	T.(N.)	R.(W.)																																																																														
Converse County, Wyo.																																																																																
15	36	75																																																																														
9	37	74																																																																														
12	38	77																																																																														
10	39	71																																																																														
5	40	70																																																																														

¹ In some areas the Browns Park is composed of a lower tuffaceous part and an upper predominantly detrital part (Hanson, 1965, p. 128). Only sample from the upper part of the Browns Park are included in this report.

² Includes samples from the Eocene Battle Spring and Wagon Bed Formations.
³ Samples from Powder River Basin; data from Sharp and Gibbons (1964).

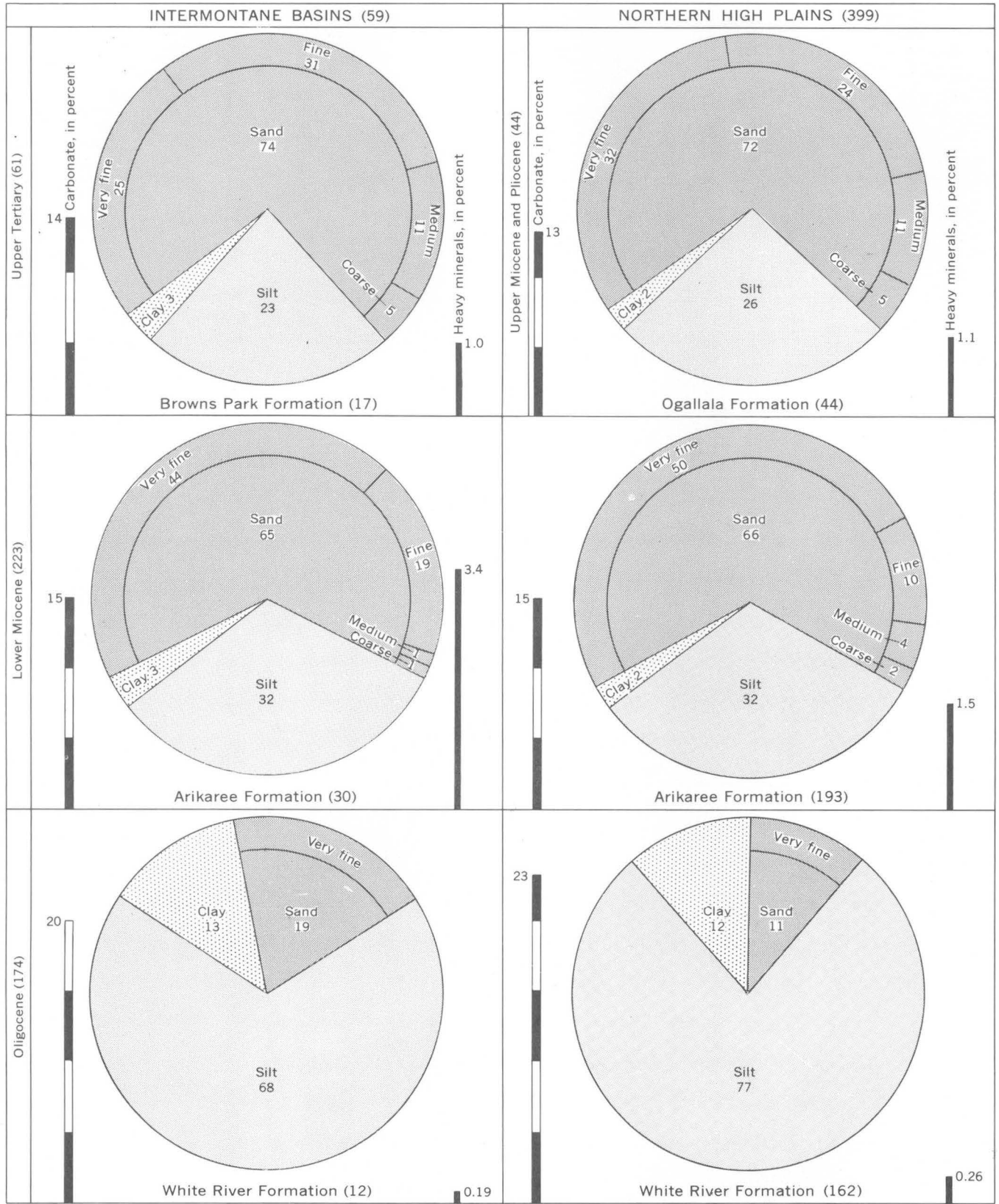
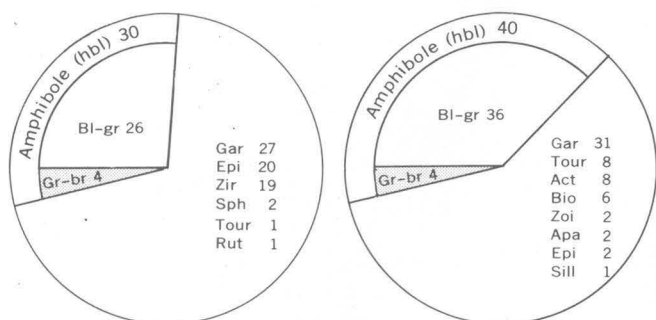
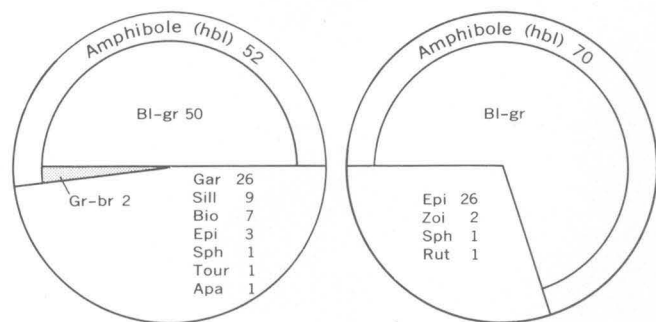


FIGURE 2.—Average grain-size distribution, carbonate content, and very fine grained heavy-mineral content for grab samples of Oligocene, Miocene, and Pliocene rocks from parts of the middle Rocky Mountains and northern High Plains. Numbers within circles and at top of bar scales are percentages. Numbers in parentheses represent number of samples studied.



Wind River Mountains, Wyo. (6)

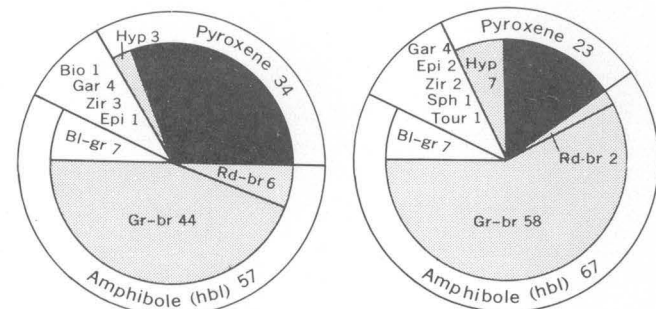
Black Hills, S. Dak. (10)
(After W. J. Mapel and others, 1964, p. C34)



Front Range, Colo. (7)

Medicine Bow Mountains, Wyo. (1)

A



Uinta Mountains (3)

Northern High Plains (7)

B

MINERALS

Actinolite—Act	Hornblende—Hbl	Sphene—Sph
Apatite—Apa	Hypersthene—Hyp	Tourmaline—Tour
Biotite—Bio	Pyroxene—Px	Zircon—Zir
Epidote—Epi	Rutile—Rut	Zoisite—Zoi
Garnet—Gar	Sillimanite—Sill	

COLORS

Blue—Bl	Brown—Br	Green—Gr	Red—Rd
---------	----------	----------	--------

FIGURE 3.—Average percentages of nonopaque heavy minerals in the very fine sand fraction of samples (A) from deposits of streams draining Precambrian igneous and metamorphic rocks in selected areas in Colorado, Wyoming, and South Dakota, and (B) of vitric tuff and volcanic ash from middle and upper Tertiary rocks in the Uinta Mountains and the northern High Plains. Black pattern is augite. Numbers in parentheses represent number of samples studied.

may have been partly destroyed in disaggregation of the samples with hydrochloric acid and is not reported.

Figure 5 shows graphically the average abundance and stratigraphic distribution of varieties of heavy minerals which are considered diagnostic and important in determining specific periods of volcanism and tectonism in the middle Rocky Mountains during Tertiary time. These data are summarized and discussed at the end of this report.

Boundary correlations of fossils and heavy-mineral assemblages

The faunal and floral succession from the Tertiary rocks in the areas of this report is, in general, well established, and although paleontologists disagree on the application and use of some time, rock, and faunal terms they are in general agreement on the major tripartite subdivision of the middle and upper Tertiary rocks of the areas described in this report. The boundaries of these subdivisions are marked by lithologic and mineralogic changes that can be observed and mapped in the field. In order to compare the validity and regularity of the boundaries determined from the assemblages of heavy minerals with boundaries based on paleontologic criteria, samples for petrographic study were collected from vertebrate quarries as well as from the matrices of fossils in museum collections. These samples were studied along with samples collected at or near the type locality of each of the named stratigraphic units. The results of heavy-mineral analyses of the samples show that the heavy-mineral and paleontologic data are compatible and supplement one another to a degree remarkable in nonmarine rocks. The faunas establish the age of the rocks from which samples were collected and are supported by the potassium-argon-age determinations of the associated volcanic tuffs reported by Evernden and others (1964). Samples collected at fossil localities or at nearby places contain suites of heavy minerals that are distinctive of the major subdivisions.

The diagnostic faunas that establish the stratigraphic paleontology of the middle and upper Tertiary rock units from which most of the samples were collected are described and discussed extensively by Black (1961), Collier and Thom (1918), Cook and Cook (1933), Denson and Gill (1965), Elias (1942), Galbreath (1953), L. W. McGrew (1963), P. O. McGrew (1951), Moore (1959), Rachou (1951), Rich (1962), Schultz and Falkenbach (1949), Schultz and Stout (1955), Stecher and others (1962), Van Houten (1964), Voorhees (1965), and Wilson (1960).

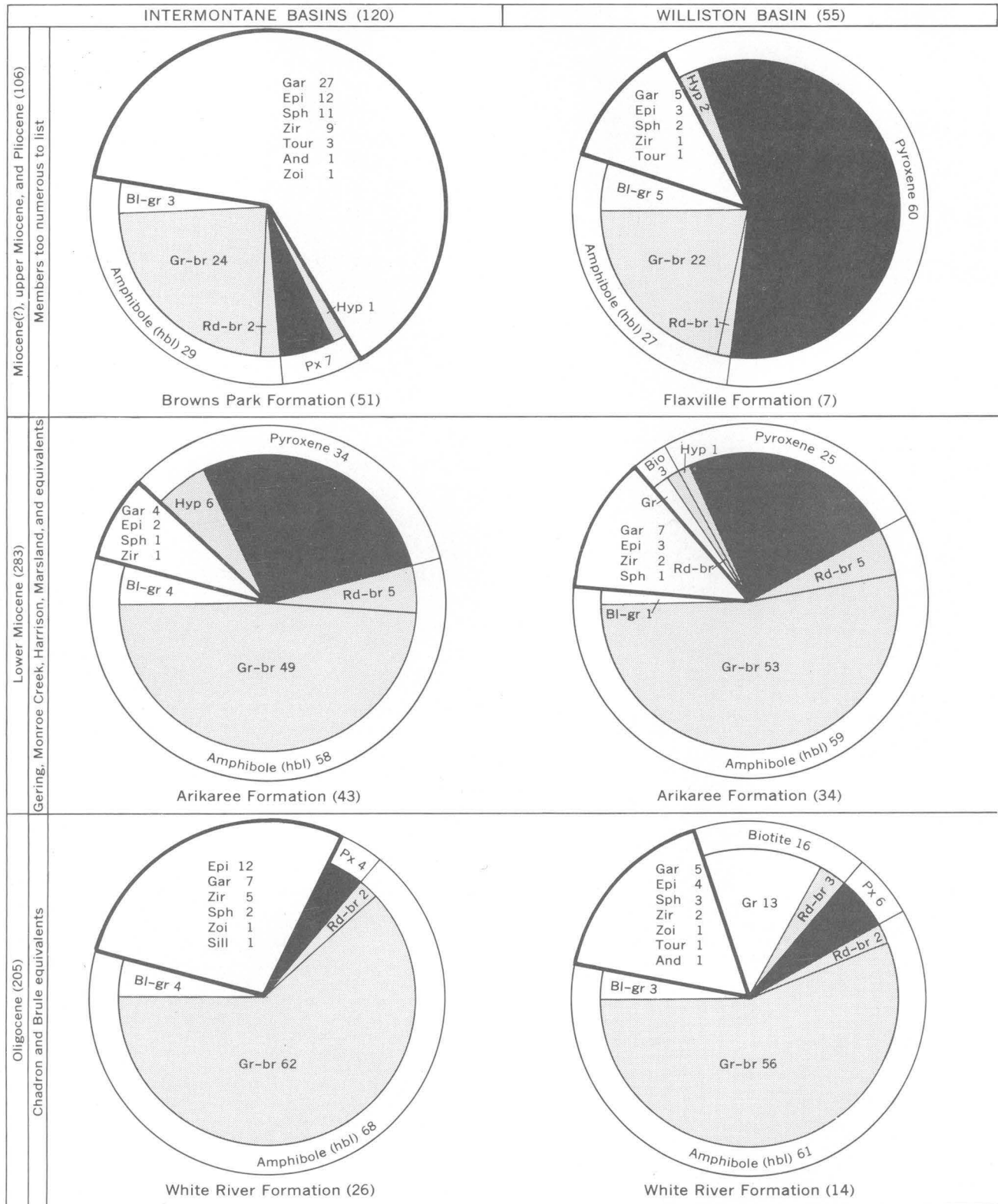
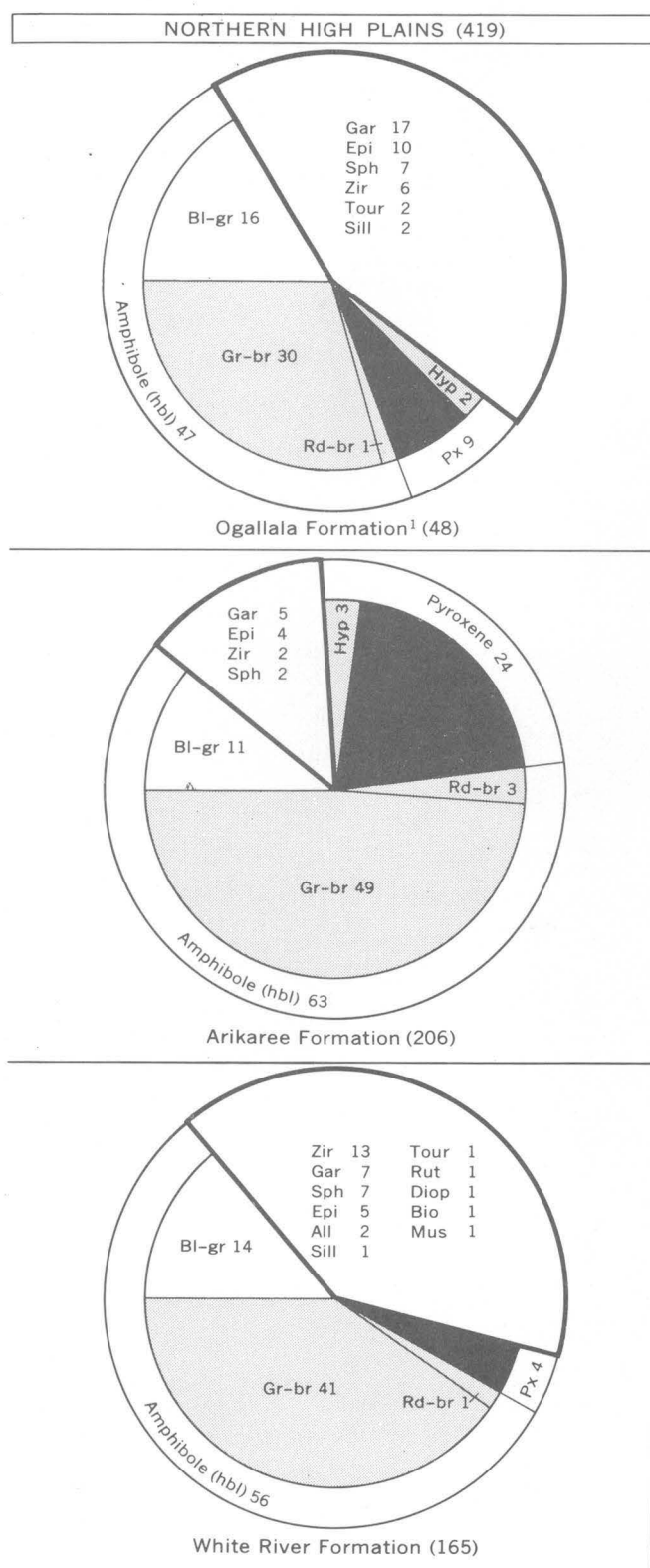


FIGURE 4.—Average percentages of very fine grained nonopaque heavy minerals in middle and upper Tertiary rocks from parts of the middle Rocky Mountains and northern High Plains. White, mostly plutonic and metamorphic minerals; stippled, mostly volcanic minerals; black, augite. (Total very fine grained nonopaque minerals=100 percent.) Numbers within circles are percentages. Numbers in parentheses represent number of samples studied.



¹ Of Mathew and Cook (1909) and Mathew (1924).

FIGURE 4

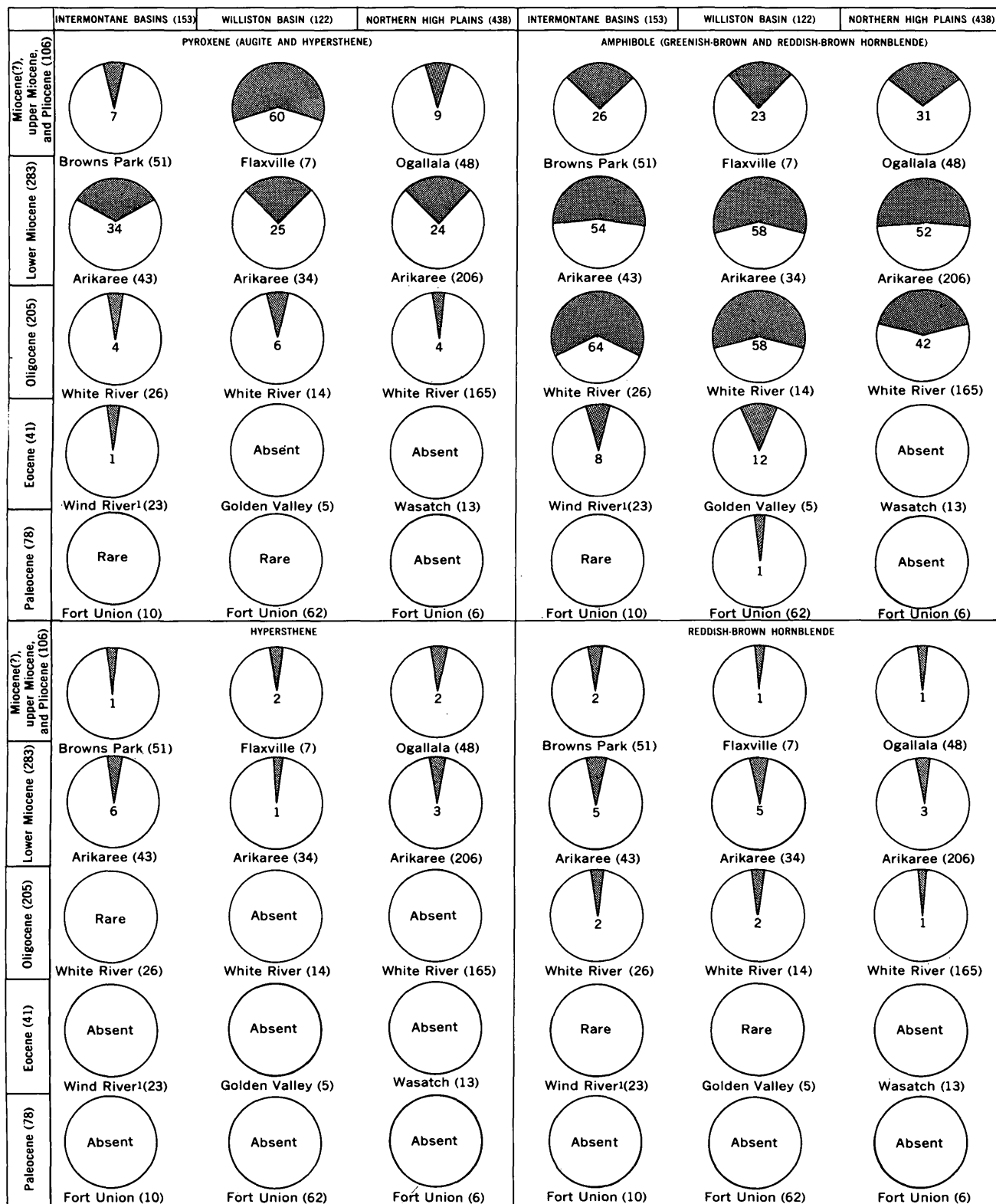
SUMMARY AND CONCLUSIONS

From the summary of heavy-mineral data shown on figure 5, several conclusions can be made.

A roughly simultaneous uncovering of Precambrian rocks in widely separated mountain uplifts in Eocene time is shown clearly by the abrupt appearance of blue-green hornblende, a ubiquitous constituent in Precambrian cores of the mountains (fig. 3A). The sudden appearance of this mineral reflects uplift and exposure of Precambrian cores during the Laramide orogeny. In most areas, such as Bison Basin of central Wyoming, the Powder River Basin of eastern Wyoming, or the Williston basin in western North and South Dakota, fossiliferous rocks assigned to the Fort Union Formation (Paleocene) were derived largely from the weathering of preexisting sediments. Although locally, as at Whiskey Gap, north of Rawlins, in central Wyoming (M. W. Reynolds, oral commun., 1966), some constituents of the Paleocene rocks may have been derived from Precambrian rocks, the amount contributed by crystalline sources in most of the areas sampled was extremely small compared to that from sedimentary rocks. This conclusion agrees with that of Stow who worked in the Bighorn Basin of northwest Wyoming and southwest Montana; Stow (1938, p. 157) stated

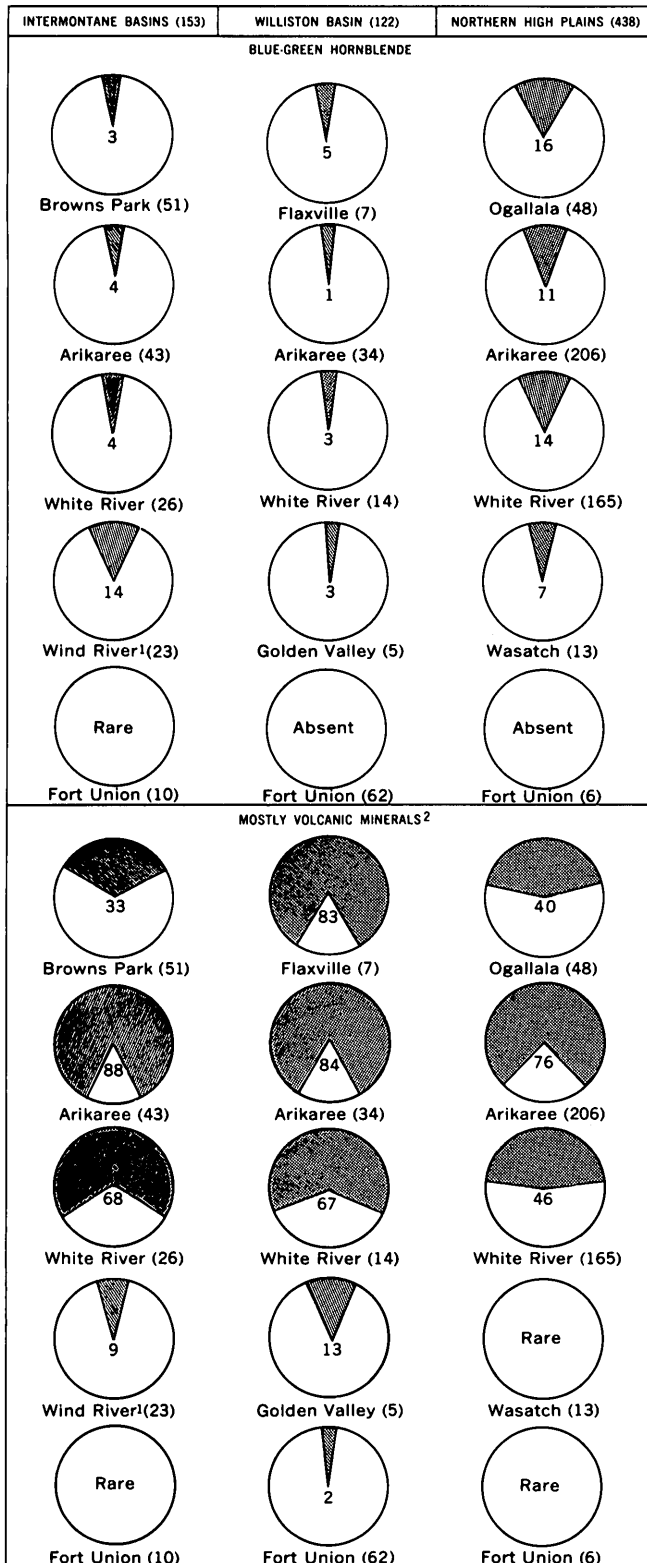
In the Wasatch (lower Eocene) extreme persistence and abundance of minerals derived from a crystalline rock and the scarcity of those derived from a sedimentary rock establishes an area predominantly of crystalline rocks as the source of the sediments composing this formation. The sudden appearance and high persistence of hornblende (blue-green and yellow-green) in the Wasatch denotes a new source of sediment, rather suddenly made available.

Widespread volcanic activity in and adjacent to the middle Rocky Mountains that began with Oligocene time is clearly reflected by a regional influx of heavy minerals of volcanic origin in about the same proportion over thousands of square miles. As shown



¹ Includes samples from the Eocene Battle Spring and Wagon Bed Formations.

FIGURE 5.—Average abundance of diagnostic very fine grained nonopaque heavy minerals from Tertiary rocks in Wyoming and adjacent areas. (Total very fine grained nonopaque heavy minerals=100 percent.) Numbers within circles are percentages. Numbers in parentheses represent number of samples studied. Names under circles are formations sampled.



² Includes red-brown biotite, hypersthene, augite, and red-brown and green-brown hornblende.

FIGURE 5

on figure 5, the important changes in heavy minerals during White River time were the abrupt increase in amount of green-brown hornblende and the appearance of augite.

Volcanism, as indicated on figure 5, reached its peak in early Miocene time and resulted in a heavy concentration of pyroxene, making up 25-35 percent of the total very fine grained nonopaque heavy-mineral suite, in the Arikaree Formation. This concentration is fairly constant throughout the formation in a stratigraphic interval locally as thick as 1,000 feet. Inasmuch as pyroxene occurs in appreciably lesser amounts in the underlying White River Formation, its sudden abundance in the Arikaree denotes some change in the volcanic source at the beginning of Miocene time.

The small percentage of minerals of plutonic and metamorphic derivation in the heavy-mineral suites from the Arikaree Formation suggests that the rocks containing the suites were not derived to any large extent from the Precambrian cores of the mountains as has been postulated by some geologists. Precambrian rocks had been, in fact, so extensively buried by lower and middle Tertiary sediments in early Miocene time that they could not have contributed significantly to the volume of Miocene sediments deposited across the sites of present-day mountain ranges.

Tectonism and uplift of regional significance during late Miocene or early Pliocene are suggested by differences in the percentage of plutonic and metamorphic minerals. The Ogallala and Browns Park Formations contain 60-70 percent minerals of plutonic and metamorphic derivation, whereas the underlying Arikaree Formation contains only 25 percent or less. Some of the volcanic material in the Ogallala and Browns Park Formations was probably derived from the reworking of the White River and Arikaree Formations. Uplift in late Miocene or early Pliocene in local areas may have been accompanied by extensive volcanism. Evidence for this is the relatively high proportions of volcanic minerals in the few samples reported from the Flaxville, as well as the local occurrence of many volcanic ash beds in some upper Miocene and lower Pliocene rocks.

A westerly source for the sediments comprising the White River and Arikaree Formations is suggested by noticeably higher percentages of volcanic minerals in heavy-mineral concentrates from samples from the western part of the region as compared with percentages of volcanic minerals in concentrates from samples from the eastern part. This conclusion is also corroborated, as shown on figure 2, by a corresponding, but very slight, increase in the average size of the mineral

grains in the samples collected in the west as compared with those collected in the east.

The events that led to the distribution of heavy minerals in the Tertiary have long been known in general outline from more direct evidence than that provided by the average proportions of heavy minerals shown on figure 5. Uplift and tectonism during late Miocene and Pliocene time, for example, are corroborated by a significant increase in grain size, as shown on figure 2, accompanied by a noticeably less uniform distribution of the sand-size fractions. The greater frequency of conglomerate and coarse-grained sandstone throughout the upper Miocene and Pliocene rocks also confirms this interpretation. The results of this study show that the distribution of heavy minerals substantiates these well-known regional events and that the assemblages are distinct enough to help correlate units in one area with units in another.

REFERENCES

- Black, C. C., 1961, New rodents from the early Miocene deposits of Sixty-Six Mountain, Wyoming: *Breviora*, Harvard Coll. Mus. Comp. Zoology, no. 147, p. 1-7.
- Collier, A. J., and Thom, W. T., Jr., 1918, The Flaxville gravel and its relation to other terrace gravels of the Northern Great Plains: U.S. Geol. Survey Prof. Paper 108-J, p. 179-184.
- Cook, H. J., and Cook, M. C., 1933, Faunal lists of the Tertiary vertebrata of Nebraska and adjacent areas: *Nebraska Geol. Survey Paper* 5, 58 p.
- Denson, N. M., and Bergendahl, M. H., 1961, Middle and upper Tertiary rocks of southeastern Wyoming and adjoining areas: Art. 209 in U.S. Geol. Survey Prof. Paper 424-C, p. C168-C172.
- Denson, N. M., and Gill, J. R., 1965, Uranium-bearing lignite and carbonaceous shale in the southwestern part of the Williston basin—a regional study, *with a section on heavy minerals* by W. A. Chisholm: U.S. Geol. Survey Prof. Paper 463, 75 p.
- Elias, M. K., 1942, Tertiary prairie grasses and other herbs from the high plains: *Geol. Soc. America Spec. Paper* 41, 176 p., pls. 1-17.
- Evernden, J. F., Savage, D. E., Curtis, G. H., and James, G. T., 1964, Potassium-argon dates and the Cenozoic mammalian chronology of North America: *Am. Jour. Sci.*, v. 262, p. 145-198.
- Galbreath, E. C., 1953, A contribution to the Tertiary geology and paleontology of northeastern Colorado: *Kansas Univ. Paleont. Contr.* [13], *Vertebrata*, art. 4, 120 p., 2 pls., 26 figs.
- Hansen, W. R., 1965, Geology of the Flaming Gorge area, Utah-Colorado-Wyoming: U.S. Geol. Survey Prof. Paper 490, 196 p.
- Love, J. D., 1960, Cenozoic sedimentation and crustal movement in Wyoming: *Am. Jour. Sci.*, v. 258-A, p. 204-214.
- Lugn, A. L., 1939, Classification of the Tertiary System in Nebraska: *Geol. Soc. America Bull.*, v. 50, p. 1245-1276, 1 pl.
- McGrew, L. W., 1963, Geology of the Fort Laramie area, Platte and Goshen Counties, Wyoming: U.S. Geol. Survey Bull. 1141-F, p. F1-F39.
- McGrew, P. O., 1951, Tertiary stratigraphy and paleontology of south-central Wyoming, in *Wyoming Geol. Assoc. Guidebook*, 6th Ann. Field Conf., South-central Wyoming: p. 54-57.
- Mapel, W. J., Chisholm, W. A., and Bergenback, R. E., 1964, Nonopaque heavy minerals in sandstone of Jurassic and Cretaceous age in the Black Hills, Wyoming and South Dakota: U.S. Geol. Survey Bull. 1161-C, p. C1-C59.
- Matthew, W. D., 1924, Third contribution to Snake Creek fauna: *Am. Mus. Nat. History Bull.*, v. 50, p. 59-425.
- Matthew, W. D., and Cook, H. J., 1909, A Pliocene fauna from western Nebraska: *Am. Mus. Nat. History Bull.*, v. 26, p. 361-414.
- Moore, F. E., 1959, The geomorphic evolution of the east flank of the Laramie Range, Colorado and Wyoming: *Wyoming Univ. unpub. Ph. D. thesis*, 123 p.
- Rachou, J. F., 1951, Tertiary stratigraphy of the Rattlesnake Hills, central Wyoming: *Wyoming Univ. unpub. M.A. thesis* 70 p.
- Rich, E. I., 1962, Reconnaissance geology of Hiland-Clarkson Hill area, Natrona County, Wyoming: U.S. Geol. Survey Bull. 1107-G, p. 447-540.
- Schultz, C. B., and Falkenbach, C. H., 1949, *Promerycochoerinae*, a new subfamily of oreodonts: *Am. Mus. Nat. History Bull.*, v. 93, art. 3, p. 69-198, figs. 1-26, 8 tables, 6 charts.
- Schultz, C. B., and Stout, T. M., 1955, Classification of Oligocene sediments in Nebraska, a guide for the stratigraphic collecting of fossil mammals: *Nebraska Univ. Mus. Bull.*, v. 4, no. 2, p. 17-52, figs. 1-12.
- Sharp, N. S., and Gibbons, A. B., 1964, Geology and uranium deposits of the southern part of the Powder River Basin, Wyoming: U.S. Geol. Survey Bull. 1147-D, p. D1-D60.
- Stecher, R. M., Schultz, C. B., and Tanner, L. G., 1962, A Middle Miocene rhinoceros quarry in Morrill County, Nebraska (with notes on hip disease in *Diceratherium*): *Nebraska Univ. Mus. Bull.*, v. 4, no. 7, p. 101-111, figs. 1-6.
- Stow, M. H., 1938, Dating Cretaceous-Eocene tectonic movements in Big Horn Basin by heavy minerals: *Geol. Soc. America Bull.*, v. 49, p. 731-762.
- Van Houten, F. B., 1964, Tertiary geology of the Beaver Rim area, Fremont and Natrona Counties, Wyoming: U.S. Geol. Survey Bull. 1164, 99 p.
- Voorhies, M. R., 1965, The carnivora of the Trail Creek fauna: *Wyoming Univ. Contr. Geology*, v. 4, no. 1, p. 21-25.
- Wilson, R. W., 1960, Early Miocene rodents and insectivores from northeastern Colorado: *Kansas Univ. Paleont. Contr.* [24], *Vertebrata*, art. 7, 92 p., 131 figs.
- Wood, H. E., 2d, Chaney, R. W., Clark, John, Colbert, E. H., Jepsen, G. L., Reeside, J. B., and Stock, Chester, 1941, Nomenclature and correlation of the North American continental Tertiary: *Geol. Soc. America Bull.*, v. 52, p. 1-48.

PETROLOGY OF A LATE QUATERNARY POTASSIUM-RICH ANDESITE FLOW FROM MOUNT ADAMS, WASHINGTON

By RICHARD A. SHEPPARD, Denver, Colo.

Abstract.—A single thick flow of augite-hypersthene andesite crops out in the Klickitat River canyon. The flow is characterized by an upper dark-gray vesicular zone that is succeeded downward by a light-gray platy and massive zone, and then a columnar zone. Chemical analyses indicate that the andesite contains more K_2O and TiO_2 and less MgO than most andesites of similar SiO_2 content from other volcanoes of the High Cascade Range.

Mount Adams in south-central Washington (figs. 1 and 2) is one of the conspicuous Quaternary volcanoes of the High Cascade Range. Unlike adjacent volcanoes, Mount Adams has received only cursory geological study—partly because of its poor accessibility and partly because of the lack of adequate topographic maps. The volcanic rocks south and east of Mount Adams were examined by Sheppard (1964), and the southeast flank of Mount Adams was also reconnoitered.

A single flow of andesite crops out in the Klickitat River canyon southeast of Mount Adams (fig. 2), and reconnaissance indicates that it was extruded from the southeast flank of Mount Adams. Prior to this most recent filling of the Klickitat River canyon by the andesite flow, flows of olivine basalt from King Mountain, south of Mount Adams, filled the canyon and were subsequently partly dissected. About 350 feet of the andesite flow is exposed, but the Klickitat River has not yet eroded through the base of the flow. The upper 30 feet of the andesite is highly vesicular and dark gray because of abundant glass in the groundmass. This vesicular zone grades downward into a light-gray platy and massive zone that in turn is succeeded downward by well-developed columnar joints. The columns are about 2 feet in diameter and generally vertical; however, nearly horizontal columns are locally perpendicular to the old canyon walls.

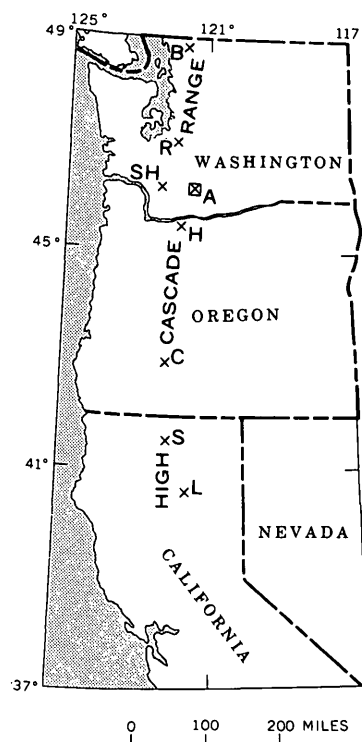


FIGURE 1.—Index map showing location of area of figure 2 (A) and places mentioned in this report: A, Mount Adams, Wash.; B, Mount Baker, Wash.; C, Crater Lake, Oreg.; H, Mount Hood, Oreg.; L, Lassen Peak region, California; R, Mount Rainier, Wash.; S, Mount Shasta, Calif.; SH, Mount St. Helens, Wash.

PETROGRAPHY

The andesite is porphyritic with phenocrysts of plagioclase, hypersthene, augite, and rarely olivine that are set in a groundmass of plagioclase laths, pigeonite, magnetite, tridymite, and glass. The pink to pale-brown glass ($n = 1.51-1.52$) appears fresh and accounts for 20-40 percent of the rock. Phenocrysts make up 20-30 percent of the rock and occur in de-

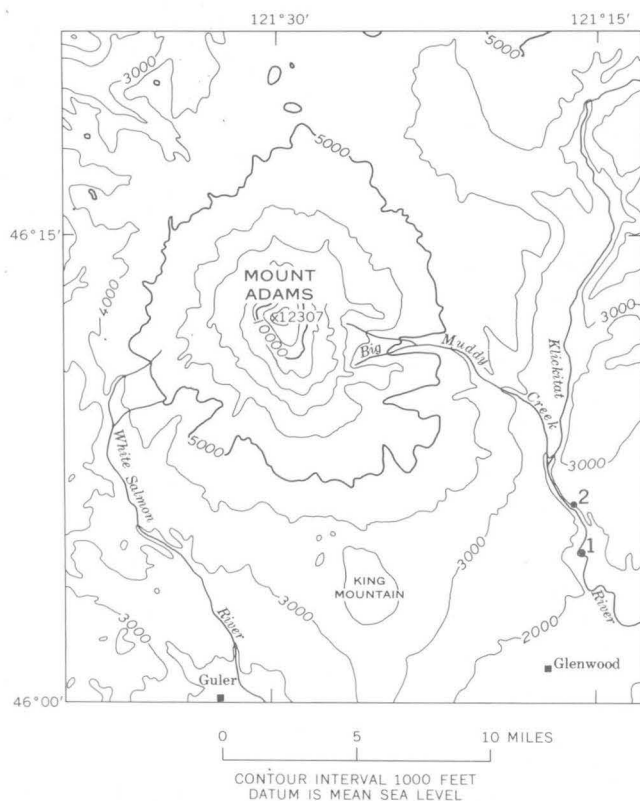


FIGURE 2.—Index map of Mount Adams, showing location (numbered dots) of specimens analyzed.

creasing abundance in the order listed above. Glomeroporphyritic clusters are rare and generally consist of mafic phenocrysts. A flow alinement of groundmass plagioclase laths is parallel with that of the phenocrysts but is less well developed than that of the phenocrysts. This suggests that most of the flow movement had ceased, perhaps by the time the laths crystallized.

Plagioclase was determined with the universal stage by first measuring the maximum extinction angle in the zone perpendicular to (010) and then utilizing the "high temperature" curve of van der Kaaden (1951, p. 51).

Plagioclase phenocrysts are subhedral, 2–3 millimeters long, and generally have normal oscillatory zoning. The cores (An_{50-34}) are sharply bounded from the normal zoned rims (An_{32-28}). Plagioclase in the groundmass seldom exceeds 0.2 mm in length and shows the same compositional range as the rims of the phenocrysts, indicating that crystallization of rims continued briefly after extrusion. The plagioclase phenocrysts, including their rims, and the laths, did not stain by sodium cobaltinitrite solution treatment, suggesting that the plagioclase is not potassium rich.

All measurements of optic angles of pyroxenes were

made with the universal stage. Hypersthene phenocrysts are resorbed, unzoned (uniform $2V$ from center to rim), and commonly smaller than the associated plagioclase phenocrysts. Their optic angle is negative and ranges from 60° to 64° . An average n_γ of 1.704 corresponds to a composition of En_{67} (Kuno, 1954, p. 40). Pleochroism is distinct: X = pale rose, Y = brownish pink, Z = pale green. Hypersthene is surrounded by a reaction rim of randomly oriented granular pigeonite, except for that included within plagioclase phenocrysts or in glomeroporphyritic clusters (fig. 3). Magnetite commonly accompanies pigeonite in the reaction rim.

Augite is pale green, resorbed, unzoned (uniform $2V$ from center to rim), and generally smaller than the associated plagioclase phenocrysts. Twinning is common with (100) as the twin plane. The optic angle is positive and ranges from 49° to 51° . Optically continuous pigeonite surrounds augite as a reaction rim and has the same crystallographic orientation as the augite even though it is sharply bounded from the phenocryst and appears granular (fig. 3). Twinning is continuous across augite phenocrysts and through their pigeonite rim. The pigeonite rim is absent from augite enclosed by plagioclase and that portion of augite phenocrysts in contact with other phenocrysts within a glomeroporphyritic cluster (fig. 3).

The groundmass proxene is pigeonite (positive optic angle 4° – 13°) that occurs as minute pale-green granules in andesite with a low glass content. Pigeonite having the same $2V$ range rims both hypersthene and augite phenocrysts. If the groundmass pigeonite crys-

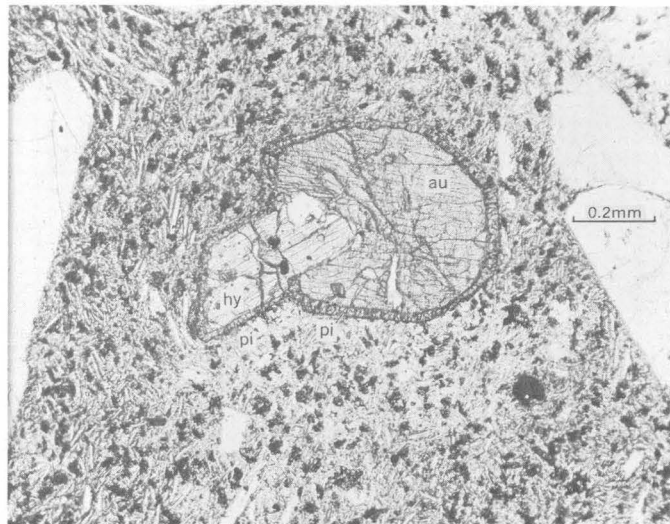


FIGURE 3.—Photomicrograph of glomeroporphyritic cluster of augite (au) and hypersthene (hy) in andesite from the platy zone of the flow. Reaction rim of pigeonite (pi) surrounds the cluster but is absent at the contact of the phenocrysts. Ordinary light.

tallized during the effusive stage, the rimming pigeonite probably also crystallized contemporaneously because (1) the $2V$ of the groundmass pigeonite and the rimming pigeonite is similar, (2) augite and hypersthene that are enclosed by plagioclase lack a pigeonite rim, (3) pigeonite surrounds only those parts of augite and hypersthene phenocrysts that project outward from a glomeroporphyritic cluster—those portions of the phenocrysts that were in contact with the liquid, and (4) augite and hypersthene phenocrysts in the upper, quickly chilled portion of the flow lack reaction rims or have very narrow ones. Groundmass pigeonite is also absent in this chilled phase.

From these features, it is apparent that plagioclase, augite, and hypersthene crystallized simultaneously during the intratelluric stage. After extrusion the crystallization was relatively rapid and pigeonite precipitated from the liquid as groundmass crystals and as overgrowths. Augite and hypersthene were unstable during the groundmass crystallization and were resorbed, accompanied by precipitation of pigeonite. Study by Kuno (1950, p. 974) of pyroxenes in lavas of Hakone indicated that augite phenocrysts were surrounded by pigeonite only in those rocks whose groundmass pyroxene was greatly enriched in iron.

The rare occurrences of deeply embayed olivine phenocrysts suggests that they may have been the earliest mafic minerals to crystallize. Only two such phenocrysts were observed, and neither had an orientation that would permit the determination of $2V$ and, consequently, their composition. Olivine is surrounded by randomly oriented coarse hypersthene. The part of the hypersthene in contact with the groundmass has reaction rims of granular randomly oriented pigeonite (fig. 4). Because the $2V$ of hypersthene surrounding olivine is somewhat larger than that of isolated hypersthene phenocrysts, magnesium enrichment is indicated. Kuno (1936, p. 137) has suggested that such enrichment is due to the slowness with which the magnesium ions of the resorbed olivines diffused into the surrounding liquid, allowing hypersthene to then crystallize from this magnesium-enriched liquid layer adjacent to the olivine. Hypersthene rims around olivine apparently formed prior to eruption because the individual hypersthene crystals of the rims are the same size as isolated phenocrysts and hypersthene is absent in the groundmass. After eruption, hypersthene was unstable and reacted with the liquid to produce a second reaction rim of pigeonite (fig. 4).

Magnetite and apatite occur as microphenocrysts in the andesite. The apatite is slightly pleochroic and contains abundant rods of an unidentified brown mineral aligned parallel to the c axis. Similar apatite has

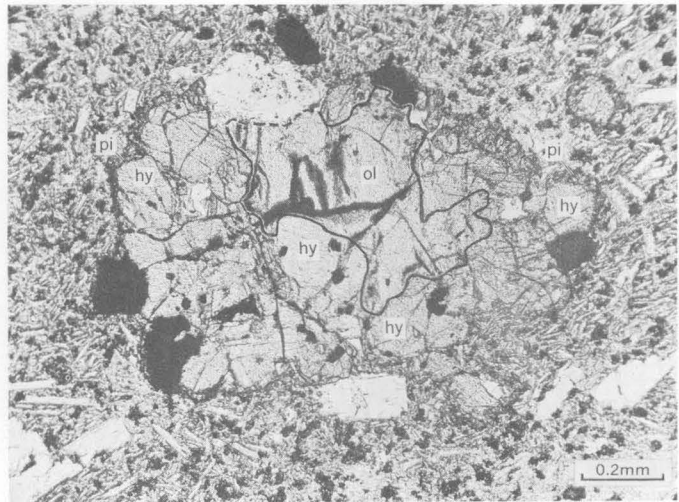


FIGURE 4.—Photomicrograph of resorbed phenocryst of olivine (ol) surrounded by randomly oriented coarse hypersthene (hy). A narrow reaction rim of randomly oriented pigeonite (pi) surrounds those portions of the hypersthene that are in contact with the groundmass. Ordinary light.

been described from andesites of other areas by Coats (1952, p. 492) and Kuno (1950, p. 983).

CHEMISTRY

Chemical analyses and corresponding molecular norms for two specimens of andesite from the Klickitat River are given in table 1. Specimens 1 and 2 are from 50 feet and 10 feet, respectively, below the top of the flow. The lower and columnar part of the flow was not sampled. Semiquantitative spectrographic analyses of the same specimens are given in table 2.

DISCUSSION

Inasmuch as the chemical analyses were prepared by the same analyst at the same time, differences in the alkali content, though relatively small, can be discussed with some confidence. Recent work by Lipman (1965) and Noble (1967) indicates that sodium is lost and potassium is gained in secondarily hydrated, silicic, natural glasses. The relatively high H_2O+ content of specimen 2 from the glassy vesicular zone indicates that the glass is hydrated. The Na_2O and K_2O contents of specimen 1 probably are closer to the original values of the lava, and the slightly higher K_2O content and lower Na_2O content of specimen 2 probably is due to secondary hydration by ground water accompanied by ion exchange. Thus, the data suggest that even very young rocks of intermediate composition that have glassy groundmasses undergo some secondary changes in alkali content.

A comparison of the two analyses of this study with analyses of andesites from other volcanoes of the High

TABLE 1.—Chemical analyses and molecular norms of augite-hypersthene andesite from the Klickitat River at Mount Adams, Wash.

[Analyst: Christel L. Parker. Quantities in percent]

	1	2
Standard rock analyses		
SiO ₂	59.67	59.11
Al ₂ O ₃	18.01	17.80
Fe ₂ O ₃	2.61	1.56
FeO.....	3.28	4.25
MgO.....	1.95	2.03
CaO.....	5.57	5.63
Na ₂ O.....	4.47	4.22
K ₂ O.....	2.41	2.54
H ₂ O+.....	.22	.91
H ₂ O-.....	.22	.12
TiO ₂	1.11	1.14
P ₂ O ₅32	.33
MnO.....	.10	.10
CO ₂01	.01
Cl.....	.01	.06
F.....	.06	.06
Subtotal.....	100.02	99.87
Less O.....	.04	.04
Total.....	99.98	99.83
Norms		
Q.....	9.69	8.84
Or.....	14.30	15.20
Ab.....	40.30	38.35
An.....	22.05	22.40
Wo.....	1.46	1.50
En.....	5.44	5.72
Fs.....	1.72	3.96
Mt.....	2.73	1.65
Il.....	1.56	1.60
Ap.....	0.67	0.69
Total.....	99.92	99.91

1. Lab. No. D101152, field No. RS-325B; platy zone, about 50 feet below top of flow. Locality: east canyon wall of Klickitat River, NE $\frac{1}{4}$ SE $\frac{1}{4}$ sec. 23, T. 7 N., R. 12 E., Yakima County, Wash.
2. Lab. No. D101153, field No. RS-328; vesicular zone, about 10 feet below top of flow. Locality: east canyon wall of Klickitat River, SW $\frac{1}{4}$ SE $\frac{1}{4}$ sec. 11, T. 7 N., R. 12 E., Yakima County, Wash.

Cascade Range indicates some differences. The andesite from the Klickitat River contains more K₂O and TiO₂ but less MgO than most andesites of similar SiO₂ content. The TiO₂ content of andesite from the High Cascades ranges from 0.17 to 0.95 percent and averages 0.60 percent; the MgO content ranges from 1.64 to 4.46 percent and averages 3.06 percent. Figure 5 is a plot of weight percentage K₂O against weight percentage SiO₂ for the two analyses of andesite from the Klickitat River and other analyses of andesite from the volcanoes of the High Cascade Range, north and south of Mount Adams. The analysis of specimen 2 is plotted even though the K₂O content may have increased slightly after solidification of the flow.

TABLE 2.—Semiquantitative spectrographic analyses of augite-hypersthene andesite from the Klickitat River at Mount Adams, Wash.

[Analyst: Harriet Neiman. Field and lab. Nos. given in table 1]

	1	2
Ba.....	0.05	0.05
Co.....	.0015	.002
Cr.....	.002	.003
Cu.....	.005	.002
Ga.....	.002	.003
La.....	.003	.003
Mo.....	0	.0005
Nb.....	.0015	.002
Ni.....	.002	.002
Se.....	.0015	.0015
Sr.....	.07	.07
V.....	.015	.02
Y.....	.003	.003
Yb.....	.0003	.0003
Zr.....	.03	.03

Results are reported in percent to the nearest number in the series 1, 0.7, 0.5, 0.3, 0.2, 0.15, and 0.1, and so forth; which represent approximate midpoints of group data on a geometric scale. The assigned group for semiquantitative results will include the quantitative value about 30 percent of the time.

The following elements were looked for but not found: Ag, As, Au, B, Be, Bi, Cd, Ce, Eu, Ge, Hf, Hg, In, Li, Pb, Pd, Pt, Re, Sb, Sn, Ta, Te, Th, Tl, U, W, and Zn.

The andesite from the Klickitat River has a higher K₂O content than any other andesite of comparable SiO₂ content from the High Cascade Range. The K₂O content of the High Cascade andesites is between 1 and 2 percent, except in 2 analyses from the Lassen Peak region, California, and 1 from Mount Baker, Wash. Niggli's *k* value (the molecular ratio, K₂O/K₂O + Na₂O) has been used by Moore (1962) to show a general increase in potassium relative to sodium from west to east for the Cenozoic igneous rock of the West-

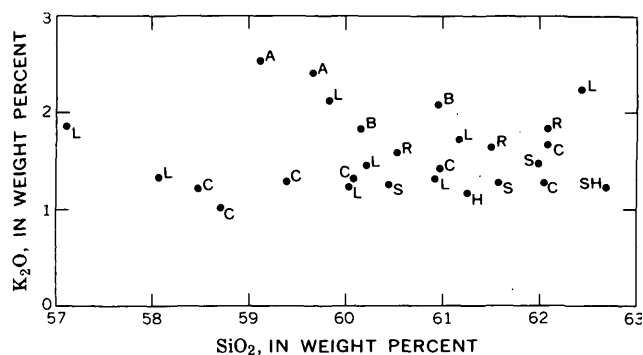


FIGURE 5.—Plot, in weight percentages of K₂O against SiO₂ for andesite of High Cascade Range. Source of data as follows: A, Klickitat River at Mount Adams, Wash. (this report); B, Mount Baker, Wash. (Coombs, 1939, p. 1506); C, Crater Lake, Oreg. (Williams, 1942, p. 149-150); H, Mount Hood, Oreg. (A. C. Waters, 1966, written commun.); L, Lassen Peak region, California (Clarke, 1904, p. 213-216); R, Mount Rainier, Wash. (Coombs, 1939, p. 1506); S, Mount Shasta, Calif. (Williams, 1934, p. 250); SH, Mount St. Helens, Wash. (Verhoogen, 1937, p. 293).

ern United States. The k values for those volcanoes adjacent to Mount Adams are given by Moore (1962, p. 106 and 108) as follows: Mount Rainier, 0.19; Mount St. Helens, 0.14; and Mount Hood, 0.17. The average k value for this andesite from the Klickitat River at Mount Adams is 0.27—significantly higher than that for the adjacent volcanoes.

REFERENCES

- Clarke, F. W., 1904, Analyses of rocks from the laboratory of the United States Geological Survey 1880 to 1903: U.S. Geol. Survey Bull. 228, 375 p.
- Coats, R. R., 1952, Magmatic differentiation in Tertiary and Quaternary volcanic rocks from Adak and Kanaga Islands, Aleutian Islands, Alaska: Geol. Soc. America Bull., v. 63, p. 485-514.
- Coombs, H. A., 1939, Mt. Baker, a Cascade volcano: Geol. Soc. America Bull., v. 50, p. 1493-1510.
- Kaaden, Gerrit van der, 1951, Optical studies on natural plagioclase feldspars with high- and low-temperature optics: Univ. Utrecht., Dissert, 105 p.
- Kuno, Hisashi, 1936, Petrological notes on some pyroxene andesites from Hakone volcano, with special reference to some types with pigeonite phenocrysts: Japanese Jour. Geology and Geography, v. 13, p. 107-140.
- 1950, Petrology of Hakone volcano and the adjacent areas, Japan: Geol. Soc. America Bull., v. 61, p. 957-1020.
- 1954, Study of orthopyroxenes from volcanic rocks: Am. Mineralogist, v. 39, p. 30-46.
- Lipman, P. W., 1965, Chemical comparison of glassy and crystalline volcanic rocks: U.S. Geol. Survey Bull. 1201-D, p. D1-D24.
- Moore, J. G., 1962, K/Na ratio of Cenozoic igneous rocks of the western United States: Geochim. et Cosmochim. Acta, v. 26, p. 101-130.
- Noble, D. C., 1967, Sodium, potassium, and ferrous iron contents of some secondarily hydrated natural silicic glasses: Am. Mineralogist, v. 52, p. 280-286.
- Sheppard, R. A., 1964, Geologic map of the Husum quadrangle, Washington: U.S. Geol. Survey Mineral Inv. Field Studies Map MF-280.
- Verhoogen, Jean, 1937, Mount St. Helens—A Recent Cascade volcano: California Univ. Pub. Geol. Sci., v. 24, p. 263-302.
- Williams, Howel, 1934, Mount Shasta, California: Zeitschr. Vulkanologie, v. 15, 225-253.
- 1942, The geology of Crater Lake National Park, Oregon, with a reconnaissance of the Cascade Range southward to Mount Shasta: Carnegie Inst. Washington Pub. 540, 157 p.



PRECAMBRIAN WRENCH FAULT IN CENTRAL ARIZONA

By C. A. ANDERSON, Menlo Park, Calif.

Abstract.—The major north-trending high-angle Shylock fault zone, 17 miles east of Prescott, Ariz., displaces Precambrian rocks. It is interpreted as a wrench fault with a minimum right-lateral slip of 5 miles. A piercement structure in the fault zone is implied by a fault slice of tightly folded and highly deformed incompetent rhyolitic tuff and slate that is in contact with younger andesitic breccia and tuff. The fault zone is covered by unbroken Cambrian Tapeats Sandstone at its north end.

The Shylock fault in the Mingus Mountain quadrangle in central Arizona is a straight high-angle fault separating diverse rocks of Precambrian age (Anderson and Creasey, 1958, p. 77). New data added by geologic mapping to the south in the Mayer quadrangle indicate that the Shylock fault is a major wrench fault, following E. M. Anderson's terminology (1951, p. 15). Evidence in the Mingus Mountain quadrangle indicates a right-lateral slip.

Acknowledgments.—Much of the detailed mapping of the Shylock fault zone in the Mingus Mountain quadrangle was done by my associate S. C. Creasey, and I am indebted to him for many helpful suggestions in the structural interpretation of this Precambrian terrane. I am most appreciative of the encouragement and helpful comments of Mason L. Hill in the preparation of the manuscript; I should state, however, that he does not agree with all of my terminology.

GENERAL GEOLOGY OF THE AREA

The geologic setting is shown in figure 1. Originally the Shylock fault was limited to the sharp break along the eastern margin of a complex faulted zone (Anderson and Creasey, 1958, p. 77). Following Noble's distinction (1926, p. 416-17) between "fault" and "fault zone," "Shylock fault zone" is used for the belt of branching, interlacing, and roughly parallel faults to the west of the Shylock fault. The Shylock fault zone is approximately 1 mile wide at the exposed north end and somewhat wider at the south margin of figure 1.

Where the fault zone contains rocks of diverse lithology and age, its branching and interlacing pattern is apparent on geologic maps (figs. 2, 3, 4). This pattern is obscure in the area (central part, fig. 1) where only the Spud Mountain Volcanics are exposed along and within the fault zone.

The Yavapai Series (fig. 1) consists largely of volcanic rocks that are metamorphosed to the greenschist facies. Relict textures and structures permit the identification of the original character of the volcanic rocks ranging from basalt to rhyolite, and the distinction between flows and pyroclastics. The Yavapai Series is divided into the Alder and Ash Creek Groups. The Alder Group is exposed on both sides of the Shylock fault, and in the southern half of the area (fig. 1) and east of the fault, the Spud Mountain Volcanics of this group are intruded by a quartz diorite pluton. The Ash Creek Group is exposed only east of the Shylock fault and north of the quartz diorite pluton which cuts southeasterly plunging folds developed in the Ash Creek (fig. 1). The Ash Creek Group is typically non-foliated, whereas the Alder Group is isoclinally folded and is foliated parallel to the overturned folds.

The oldest formation in the Alder Group, the Texas Gulch Formation, is unconformable above the Brady Butte Granodiorite (Blacet, 1966). Elsewhere various types of plutonic rocks intrude the Alder Group (fig. 1). At present, no evidence is available to determine the age relationships of the Alder and Ash Creek Groups because they are separated either by the Shylock fault or by the quartz diorite which intrudes both groups.

SHYLOCK FAULT ZONE

Because of its width of approximately 1 mile, its known length of more than 30 miles, and its separation in part of dissimilar rocks, the Shylock fault zone is a major structural feature of the region. The Cambrian Tapeats Sandstone and Devonian Martin Formation were deposited on a widespread surface of low

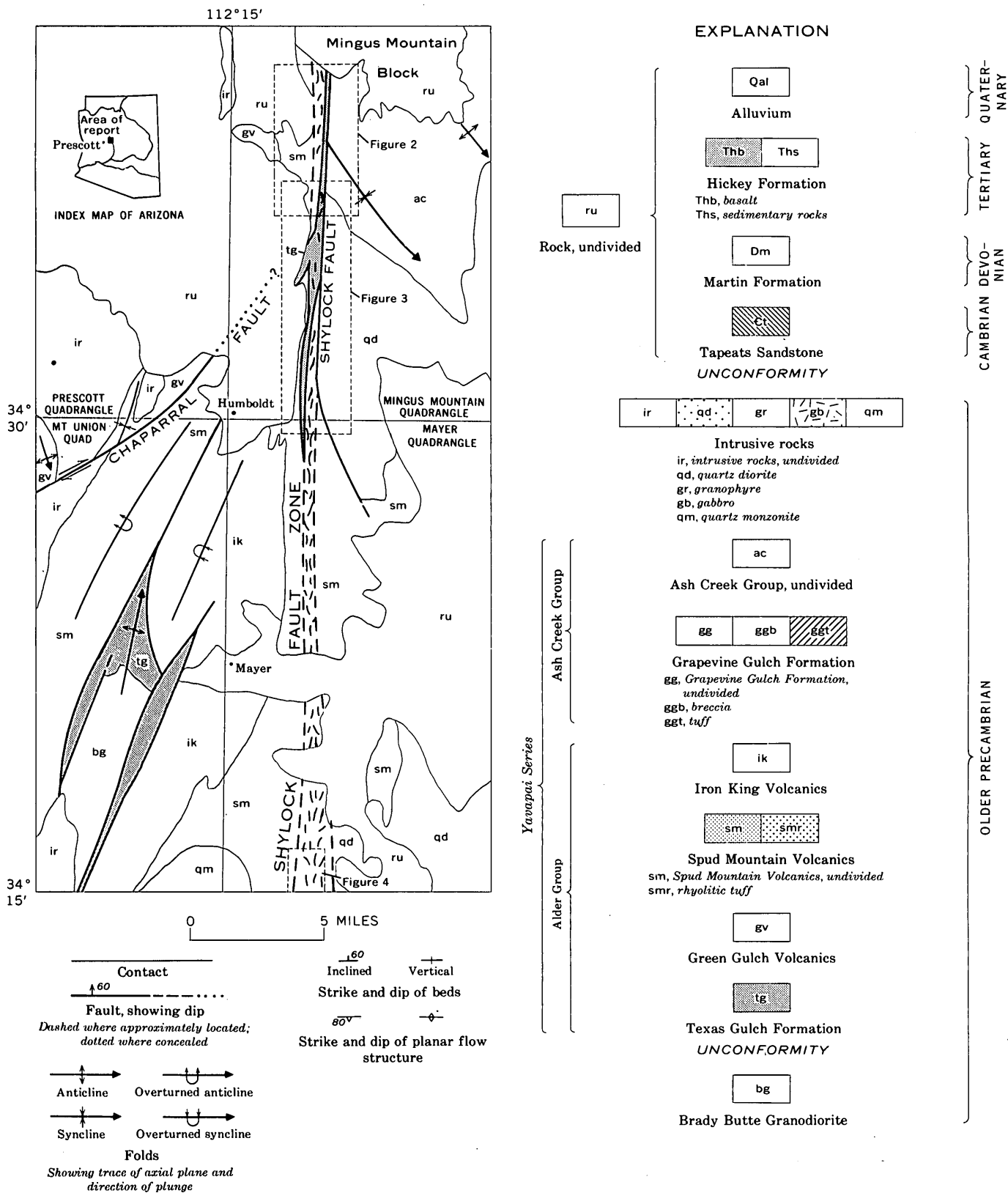


FIGURE 1.—Generalized geologic map of parts of the Mingus Mountain, Prescott, Mount Union, and Mayer quadrangles, Yavapai County, central Arizona, showing the geologic setting of the Shylock fault zone and Chaparral fault. Explanation applies to figures 1, 2, and 3. Only the pattern for the Texas Gulch Formation is shown on figure 1.

relief. The northern end of the exposed Shylock fault zone is covered by the Tapeats Sandstone, and therefore the faulting is of Precambrian age (fig. 2). Three narrow slices of quartz diorite and one of the Spud Mountain Volcanics illustrate the exotic character of some of the fault slices within the fault zone (fig. 2). These fault slices have schistose margins, and only in their exposed cores are relict minerals and textures preserved.

The best key to the displacement along the Shylock fault is provided by the quartz diorite fault slices within the fault zone north of the crudely planar,

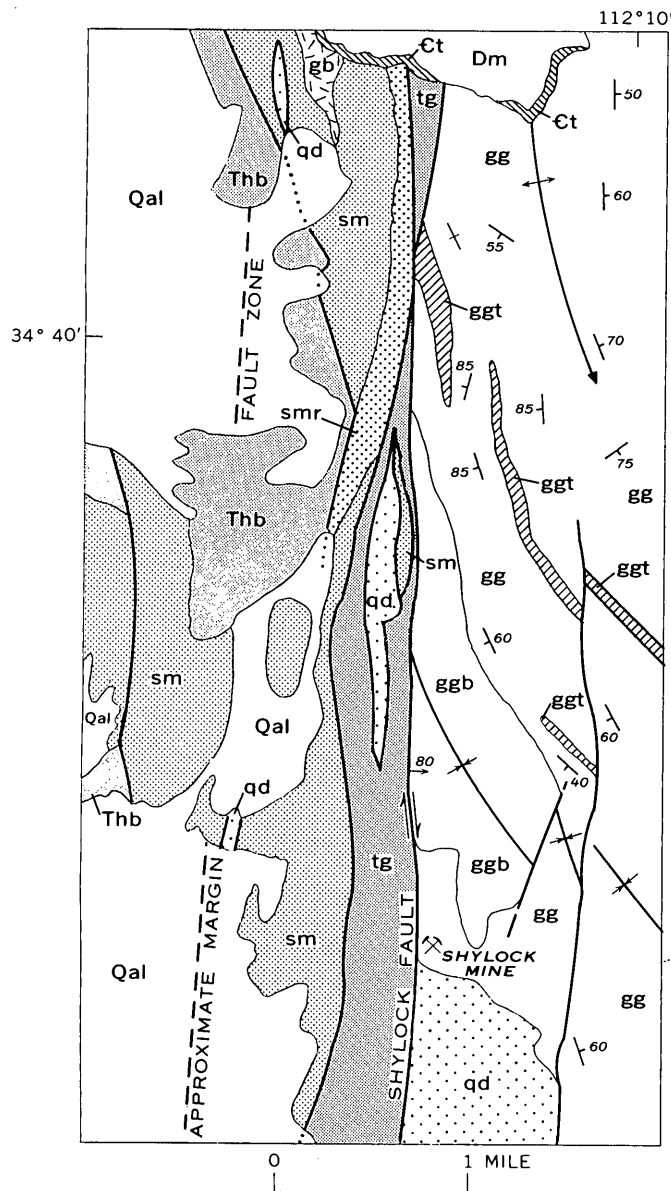


FIGURE 2.—Geologic map of the northern part of the Shylock fault zone. Patterns and map units are explained in figure 1.

steeply dipping contact of the quartz diorite pluton that extends southeastward from the Shylock fault for a distance of 7 miles (figs. 1, 2). A minimum of 5 miles of right-lateral slip is indicated, measured in the fault zone from the steeply dipping planar quartz diorite contact southeast of the Shylock fault to the most northerly quartz diorite fault slice (fig. 2). The total displacement is not known because no faulted segment of the pluton has been found west of the fault zone; it may be buried by Phanerozoic rocks to the north. The quartz diorite pluton east of the Shylock fault clearly is truncated by the fault, as shown by the sharp discordance between the fault and the planar flow structures within the quartz diorite (fig. 3). The bending northward of the synclinal axial trace, (outlined by the tuff beds in the Grapevine Gulch Formation) next to the Shylock fault also is consistent with right-lateral slip.

The Texas Gulch Formation is the dominant unit in the northern part of the Shylock fault zone (figs. 2, 3). This formation consists of intertonguing rhyolitic tuff and slate, and within the fault zone these two lithologic units are, in general, separated by faults. The formation is tightly folded and shows reversals of plunge (fig. 3). In places, slaty cleavage (S2) is folded and cut by a younger cleavage (S3) that has axial-plane symmetry with the folded slate. Fault slices of the Spud Mountain Volcanics appear within the larger fault slice of the Texas Gulch Formation (fig. 3); those on the west are largely andesitic tuff and those on the east are andesitic breccia. The most southerly exposures of the Texas Gulch Formation in the Shylock fault zone end abruptly about a mile south of the area shown in figure 3 (fig. 1).

Faults of north and northwest trends displace basalts of the Tertiary Hickey Formation (fig. 2), and northward they bound the Mingus Mountain block (fig. 1). In the area shown in figure 2, these young faults converge with the Shylock fault zone, and some late movement may have occurred along the westerly faults in the Shylock fault zone. Several miles south of the Shylock mine (fig. 3), the Hickey Formation covers the entire Shylock fault zone, but farther south this formation is in fault contact with the Spud Mountain Volcanics. Presumably the fault contact represents small activation along an older fault.

A splay fault off the Shylock fault dies out southeastward in the Spud Mountain Volcanics (fig. 1), diverging from the main fault by an acute angle, typical of splay faults associated with wrench faults (Anderson, 1951, p. 167).

In the Mayer quadrangle (fig. 1), much of the Shylock fault zone is in the Spud Mountain Volcanics;

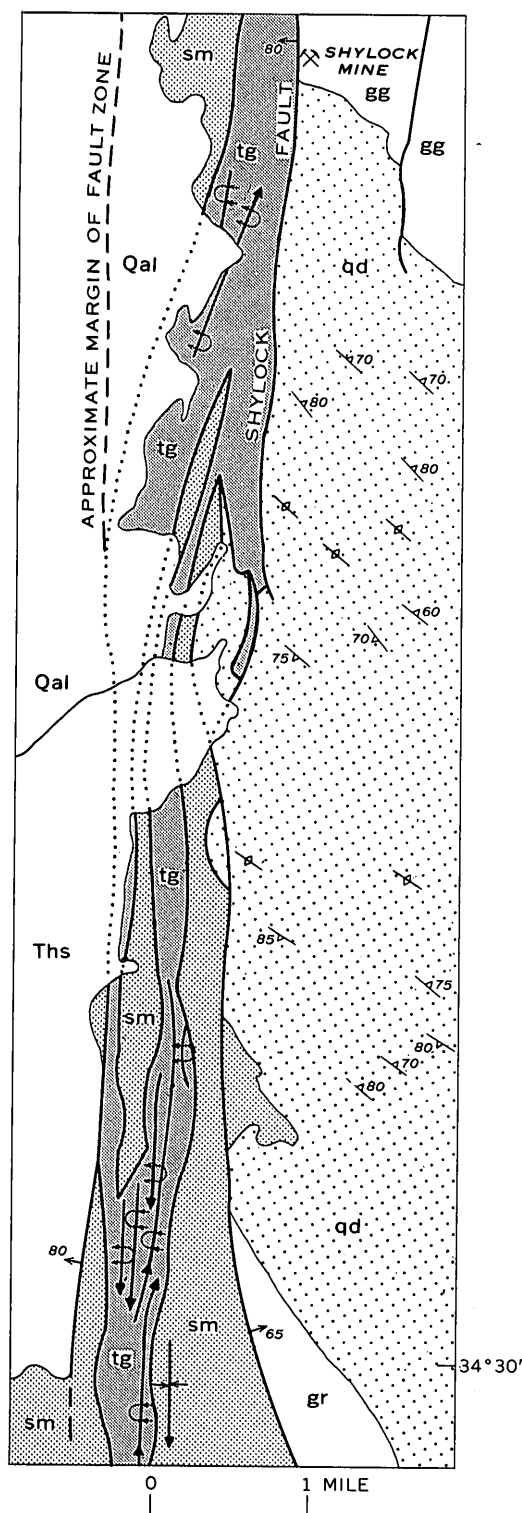


FIGURE 3.—Geologic map of elongate area along the Shylock fault zone, south of area shown in figure 2. Patterns and map units are explained in figure 1.

the bedded units of this formation are almost parallel to the fault zone, as revealed by the north-trending contact between the Spud Mountain Volcanics and Iron King Volcanics north of Mayer and west of the fault zone (fig. 1). In this segment of the fault zone, some minor folds have been mapped, and one north-trending fault can be traced for $2\frac{1}{2}$ miles.

At the southern margin of the Mayer quadrangle (fig. 4), the Spud Mountain Volcanics are in fault contact with a pluton of coarse-grained quartz diorite. Near the fault, this quartz diorite is appreciably granulated and cut by subparallel veinlets of sericite and chlorite, whereas at the fault, the rock is highly foliated. West of the Shylock fault (fig. 4), the Spud Mountain rocks are largely mixed andesitic and rhyolitic tuff, recrystallized to well-foliated chlorite schist, quartz-sericite schist, and quartz-chlorite-sericite schist. Amygdaloidal basalt in part crops out in very irregular outlines that contrast with the regular and continuous pattern of intertonguing flows exposed elsewhere distant from the Shylock fault zone. Alteration and foliation mask the amygdaloids in the margins of the basalt. Small fault slices of the coarse-grained quartz diorite and gabbro also appear in the foliated andesitic-rhyolitic tuff.

Masses of quartz porphyry crop out in the Shylock fault zone south of the area shown in figure 3 (fig. 1). Three elongate masses mapped northeast of Mayer (Anderson, 1959) have their long dimensions almost north. The margins of these masses are highly foliated quartz-sericite schist, but relict textures are present throughout most of the masses. The general concordance of these quartz porphyry masses with the bedded tuffs and breccias of the Spud Mountain Volcanics and their strongly foliated margins suggest that they are fault slices, particularly because elsewhere in the Yavapai Series, other quartz porphyry masses are largely discordant with their host rocks and presumably had an intrusive origin.

As shown in the western part of figure 4, at the southern margin of the Mayer quadrangle (fig. 1) rhyolitic flows and breccias are associated with quartz porphyry and other amygdaloidal basalt. Whether or not these quartz porphyry and basalt masses are fault slices is debatable, particularly because the pattern of the quartz porphyry outcrops in part can be interpreted as normal intrusive relations (fig. 4). However, all these rocks are foliated and contain zones of chlorite schist and quartz-sericite schist. It may be

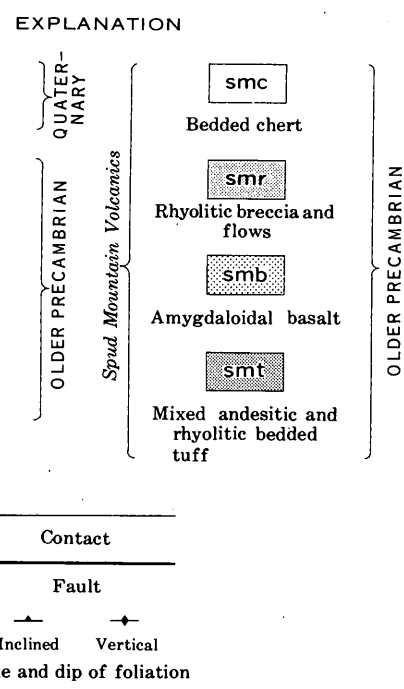
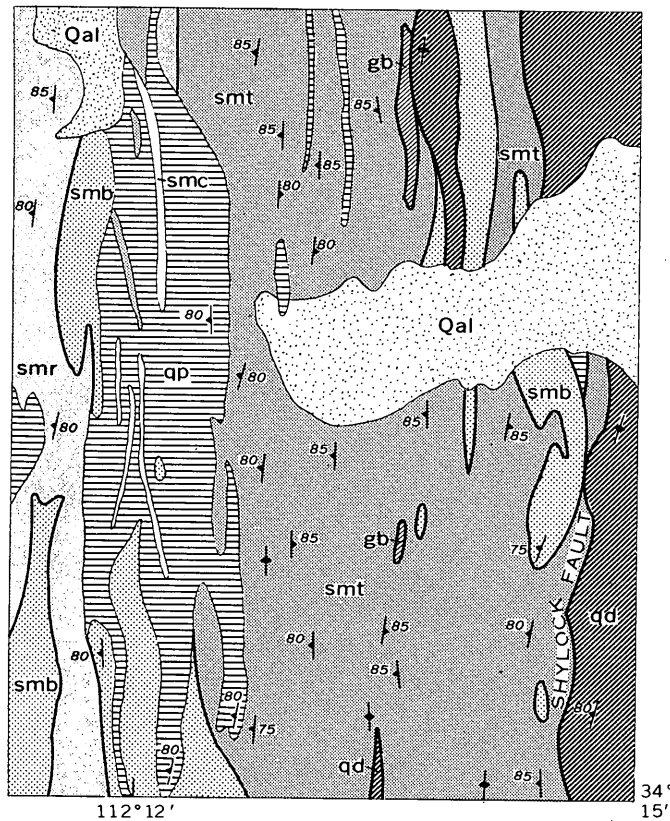


FIGURE 4.—Geologic map of the Shylock fault zone at the southern margin of the Mayer quadrangle.

that all the contacts shown in figure 4, except those of the alluvium, are faults.

PIERCEMENT STRUCTURE

The Texas Gulch Formation in the Shylock fault zone forms a long narrow fault slice in contact with the younger Spud Mountain Volcanics. To the west, where the regional stratigraphic relations can be established, the Green Gulch Volcanics, about 6,000 feet thick, separate the older Texas Gulch Formation from the younger Spud Mountain Volcanics. Therefore, formation of the fault slice of Texas Gulch Formation required an appreciable component of upward displacement. The large displacement justifies the interpretation that the fault slice is a piercement structure in the Shylock fault zone.

Upward squeezing of rocks appears to be a common feature in wrench faults. Kingma (1959, p. 15) reported such small-scale piercement structures in wrench faults in New Zealand. Crowell (1962, p. 48) noted that in the San Andreas fault zone the shape and orientation of phacoids and rare minor structural features suggest upward squeezing. Wallace (1949, p. 796, 805) related ridges of sedimentary rocks in the San Andreas fault zone to upward squeezing of plastic fault gouge and breccia; this squeezing raised the covering sedimentary rocks above the rift zone.

Because of the incompetent character of the Texas Gulch Formation, it is not surprising to find the elongated fault slice in the Shylock fault zone. To the west (fig. 1) the Texas Gulch Formation is in a north-plunging anticline where it rests on the Brady Butte Granodiorite. The margins of this fold are in fault contact with the Spud Mountain Volcanics to the west and with the Iron King Volcanics to the east. The single fault line shown extending northward toward Humboldt from the outcrop area of the Texas Gulch Formation on figure 1 represents a narrow fault slice of Texas Gulch Formation, another piercement structure but one related to the underlying anticline.

CHAPARRAL FAULT

The Chaparral fault (fig. 1) is another wrench fault with right-lateral slip, as shown by the pattern of deformation in the Green Gulch Volcanics along the fault. Vertical separation is indicated by the older Green Gulch Volcanics in fault relationship with the younger Spud Mountain Volcanics, but vertical slip cannot be proven. The terrane north of the Chaparral fault includes a large volume of rock intrusive into the Alder Group, implying an appreciable right-lateral separation as these rocks are common to the southwest on the south side of the Chaparral fault. The fault

itself does not have any of the spectacular fault slices typical of the Shylock fault zone, and much of the fault is a narrow mylonite zone in which cataclasis is dominant. The relation of the Chaparral fault to the Shylock fault is unknown because of the cover of Phanerozoic rocks in the critical area.

AGE OF THE SHYLOCK FAULT

The evidence is clear that the Shylock fault is older than the Cambrian Tapeats Sandstone and is therefore Precambrian. The faulting is later than the intrusion of the two quartz diorite plutons, and the northerly pluton was clearly intruded after the folding of the Ash Creek Group. West of the Shylock fault zone at the south end of the area (fig. 1), the northern end of a quartz monzonite pluton is exposed. This pluton has many associated pegmatite dikes, and the grade of metamorphism is high around the nose of the pluton in Spud Mountain Volcanics west of the Shylock fault zone. Coarse muscovite-biotite schist, locally containing abundant garnet and staurolite, indicates the high rank. In the Shylock fault zone to the east, chlorite, albite, and sericite are common metamorphic minerals and imply either retrograde metamorphism at the time of faulting or the southward displacement of green-schist facies in juxtaposition with high-rank

metamorphic Spud Mountain Volcanics. Thus the wrench fault is younger than the quartz monzonite pluton. No evidence is available to establish the time interval between the folding of the Yavapai Series and intrusion of the plutons and the later deformation creating the Shylock wrench fault.

REFERENCES

- Anderson, C. A., 1959, Preliminary geologic map of the NW $\frac{1}{4}$ Mayer quadrangle, Yavapai County, Arizona: U.S. Geol. Survey Map MF-228, scale 1:24,000.
- Anderson, C. A., and Creasey, S. C., 1958, Geology and ore deposits of the Jerome area, Yavapai County, Arizona: U.S. Geol. Survey Prof. Paper 308, 184 p.
- Anderson, E. M., 1951, The dynamics of faulting: 2d ed. Edinburgh, Oliver and Boyd, 206 p.
- Blacet, P. M., 1966, Unconformity between gneissic granodiorite and overlying Yavapai Series (older Precambrian), central Arizona, *in* Geological Survey Research, 1966: U.S. Geol. Survey Prof. Paper 550-B, p. B1-B5.
- Crowell, J. C., 1962, Displacement along the San Andreas fault, California: Geol. Soc. America Spec. Paper 71, 61 p.
- Kingma, J. T., 1959, The tectonic history of New Zealand: New Zealand Jour. Geology and Geophysics, v. 2, p. 1-55.
- Noble, L. F., 1926, The San Andreas rift and some other active faults in the desert region of southeastern California: Carnegie Inst. Washington Year Book 25, p. 415-428.
- Wallace, R. E., 1949, Structure of a portion of the San Andreas rift in southern California: Geol. Soc. America Bull., v. 60, p. 781-806.



BRECCIA PIPES IN THE WEST TINTIC AND SHEEPROCK MOUNTAINS, UTAH

By HAL T. MORRIS and RUDOLPH W. KOPF, Menlo Park, Calif.

Abstract.—Three large breccia pipes of volcanic origin cut folded and faulted sedimentary rocks of Precambrian and Paleozoic age and volcanic rocks of Tertiary age in the Cherry Creek area, Juab County, Utah. Their most characteristic feature is the presence of giant inclusions of quartzite, argillite, boulder phyllite, shale, and limestone that have been transported upward from strata that are several thousand feet below the surface. The inclusions range in size from microscopic dust to a block that is 1,200 feet long and 500 feet wide; they constitute about one-third of the material filling the pipes. The matrix in which the larger inclusions are embedded resembles arkosic tuff, consisting of shattered fragments of quartz, potassium feldspar, plagioclase, sparse biotite, and pumiceous shards in addition to the particles of exotic rocks. Locally this matrix has been chloritized, pyritized, and silicified, but no ore deposits are known to be associated with the pipes.

Breccia pipes characterized by giant blocks of Precambrian and Paleozoic sedimentary rocks embedded in a matrix of quartz-rich tuffaceous material and rock fragments have recently been recognized in the Cherry Creek area of west-central Utah (fig. 1). These intrusive masses are noteworthy because of their large size, and because of the great distances, as much as several thousand feet or more, that even the largest of the exotic inclusions have been transported upward from depth.

Cherry Creek is a short perennial stream about 15 miles west-southwest of Eureka, Utah, that separates the central and southern parts of the West Tintic Mountains from the southern tip of the en echelon Sheeprock Mountains. Three breccia pipes have been recognized to date in the area; the Hassel pipe is near the southeastern edge of the Sheeprock Mountains, the Cherry Creek pipe extends southeastward across the ridge dividing Cherry and West Cherry Creeks, and the Maple Peak pipe, largest of the three, underlies the greater part of the high, backbone ridge of the

southern West Tintic Mountains including Maple Peak (fig. 2).

Acknowledgments.—The observations and interpretations presented in this report are largely in variance with earlier conclusions about the geology of the West Tintic and Sheeprock Mountains; however, we have made frequent use of the reports of Butler and others (1920), Stringham (1942), Cohenour (1959), and, particularly, Groff (1959).

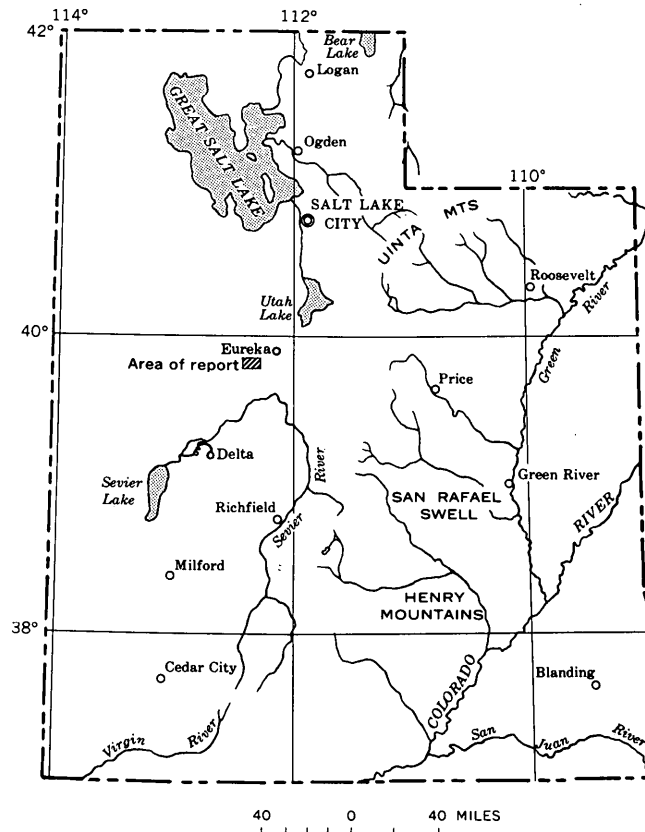


FIGURE 1.—Index map of Utah, showing location of Cherry Creek area (diagonal pattern).

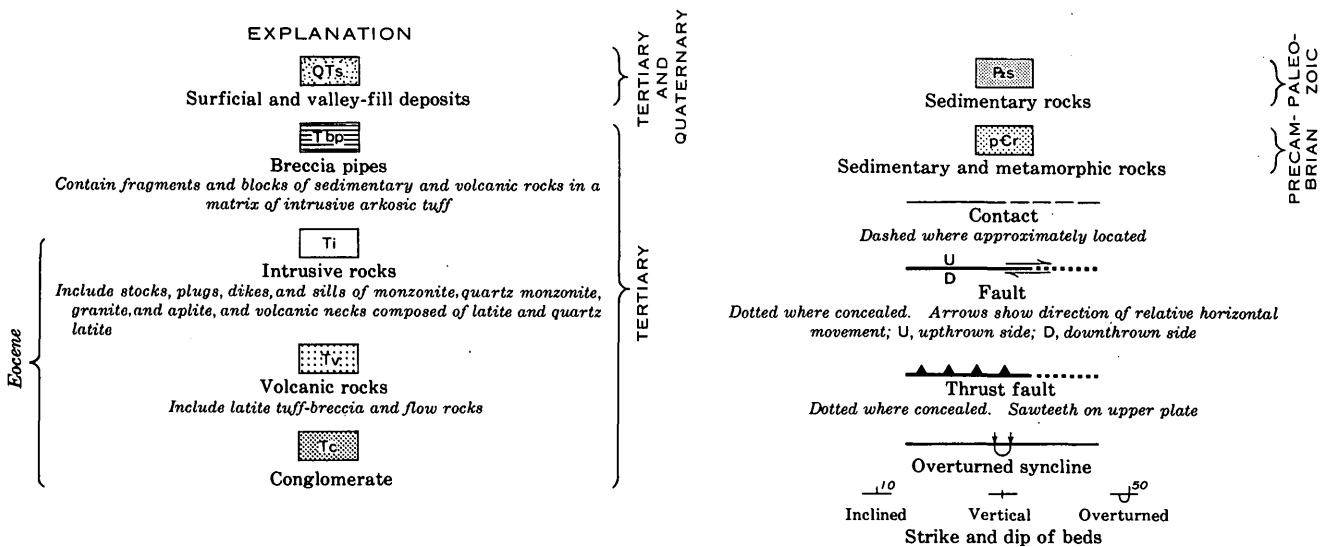
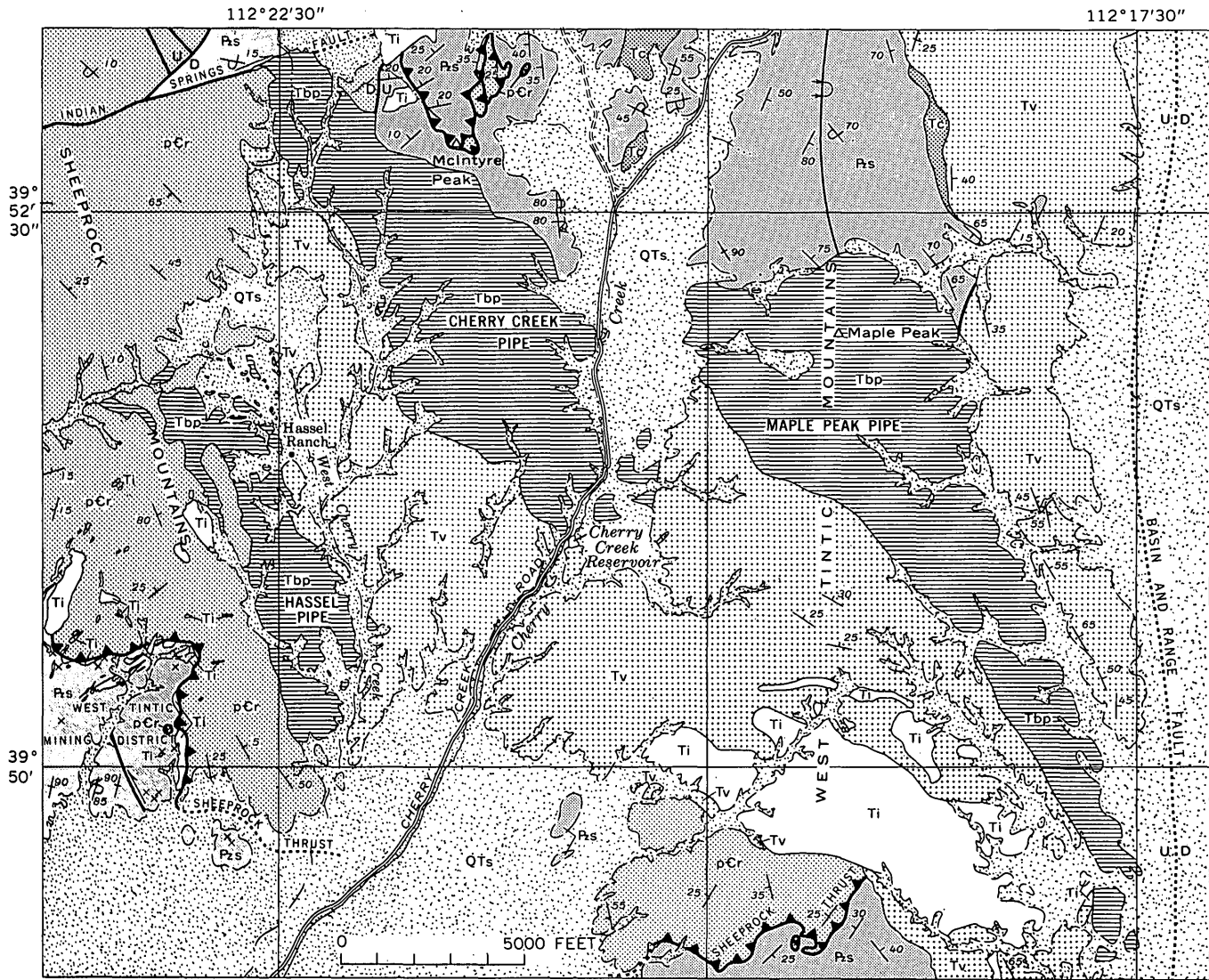


FIGURE 2.—Generalized geologic map of the Cherry Creek area, West Tintic and Sheeprock Mountains, Utah.

Capable assistance during the field investigations leading to the present report was furnished by J. T. Abbott, L. T. Benton, Rodney Wilson, T. T. Sumida, and Rubem Cibré.

GEOLOGIC SETTING

The West Tintic and Sheeprock Mountains are parts of a complex, fault-broken horst located in the east-central part of the Great Basin. The rocks exposed in the area range in age from late Precambrian to Recent. The Precambrian rocks consist of argillites, boulder phyllites of glacial origin, quartzites, and quartzite conglomerates with an aggregate thickness of more than 13,500 feet; they have been assigned to the Sheeprock, Dutch Peak, and Mutual Formations by Cohenour (1959, p. 17-28) and Groff (1959, p. 12-28). The Paleozoic rocks include strata of each geologic period from the Cambrian to the Mississippian and have an aggregate thickness of approximately 20,000 feet. Except for about 3,500 feet of quartzite and shale in the lower part of the Cambrian section and about 1,400 feet of carbonaceous shale and quartzite in the upper part of the Mississippian section, the Paleozoic rocks are chiefly limestones and dolomites.

Unconformably overlying the Precambrian and Paleozoic rocks, and an intervening discontinuous unit of Tertiary conglomerate, is a sequence of latitic and quartz latitic volcanic rocks comparable in composition and stratigraphic and structural relationships with the middle Eocene volcanic rocks of the East Tintic Mountains (Morris and Lovering, 1961, p. 124-126). The lowest volcanic units in both areas consist of pyroclastic deposits that fill eastward- and south-eastward-draining valleys, some of which were hundreds of feet deep prior to the volcanic eruptions (Morris and Anderson, 1962, p. C1-C4).

Cutting the volcanic and older rocks are many igneous intrusive bodies ranging in composition from latite and monzonite to granite, and in size from narrow dikes to plugs and stocks. These intrusive bodies form part of an eastward-trending zone of intrusions that extends from the Deep Creek Range to the Wasatch Mountains (Mabey and others, 1964; and Hilpert and Roberts, 1964, p. 30). Many of the latite intrusions in the Cherry Creek area were obviously the source vents for the petrographically similar volcanic rocks, but most of the other intrusives apparently crystallized at depth during the waning stages of volcanic activity. Some of these rocks and all the older volcanic and sedimentary rocks are cut by the breccia pipes and locally are overlain by valley-fill and upland alluvial deposits of Pliocene to Recent age.

The general geologic structure of the Cherry Creek area consists of imbricate plates of thrust-faulted and folded Precambrian and Paleozoic strata that are cut by tear faults and broken and delimited by normal faults of the Basin and Range fault system. The Precambrian and lower Paleozoic rocks of the area form the upper plate of the Sheeprock thrust fault that originally extended across folded and faulted strata of Ordovician to Mississippian age that are believed to be in the upper plate of the concealed Tintic Valley thrust (Roberts and others, 1965, p. 1946-1948, 1952-1953).

The Basin and Range fault bordering the West Tintic Mountains (fig. 2) is inferred from geophysical data presented by Mabey and Morris (1967) and is probably similar to concealed faults near the southwestern border of the Sheeprock Mountains.

BRECCIA PIPES

Form and character

The breccia pipes in the Cherry Creek area are elongate in plan, the long axes striking about N. 30° W. The smallest breccia pipe, here termed the Hassel pipe from the nearby Hassel Ranch, is 11,000 feet long and 2,500 feet wide at its widest outcrop; the Cherry Creek pipe is about 16,000 feet long and 5,500 feet wide in the central part; the Maple Peak pipe, which is tadpole shaped in general outline, is more than 22,000 feet long and 6,800 feet wide near Maple Peak. Most of the contacts of the breccia pipes with their wallrocks are moderately well defined and readily followed except where they are concealed beneath surficial deposits. However, in areas underlain by volcanic rocks that superficially resemble the tuffaceous matrix of the breccia pipes, the contact may be recognized by close-spaced fractures in the wall rocks, zones of weak alteration parallel to the edge of the breccia pipe, and locally by small globs and stringers of remelted country rock.

The material filling the breccia pipes is characteristically a massive chaotic breccia of highly variable grain size and composition. Locally a steep planar structure that developed in response to lamellar flow in the fluidized breccia filling is strongly developed parallel to the walls of the pipes. In some parts of the Hassel and Cherry Creek breccia pipes, this planar structure was intricately folded during the last stages of injection of the breccia.

Composition

The most distinctive and impressive feature of the breccia pipes of the Cherry Creek area is the presence of giant inclusions of exotic rocks, some of which

have been displaced several thousand feet upward from underlying strata. These inclusions locally constitute virtually all the material filling the pipes, but more commonly they are embedded in a matrix of light-gray to buff tuffaceous breccia and rock fragments. Overall, the exotic inclusions probably constitute approximately 35 percent of the bulk composition of the breccia pipes, although locally a superficial examination would suggest a higher proportion. Not all the inclusions are large, however, and some parts of the pipes contain such an abundance of small angular rock fragments that they resemble concrete.

The exotic inclusions range in size from irregular-shaped blocks and slabs more than 1,000 feet long to particles that are barely discernible with a hand lens. One of the largest masses noted is an unbroken slab of limestone exposed near the western base of Maple Peak that is at least 1,200 feet long and 500 feet wide. Irregular-shaped blocks and slabs 50 feet or more in length are common, although they are less abundant than rounded, boulder-shaped masses 2–20 feet in diameter (fig. 3).

The inclusions were obviously derived from all the older rocks recognized in the West Tintic and Sheep-rock Mountains. These rocks include quartzite, phyllite, argillite, and conglomerate of Precambrian age; quartzite, limestone, shale, and chert of Paleozoic age; and latite, quartz latite, monzonite, quartz monzonite, and aplitic granite of Tertiary age. Massive siliceous rocks, such as quartzite and chert, appear to have resisted crushing and abrasion; commonly the

inclusions composed of these rocks are well rounded and have smooth surfaces that are polished and striated. Some of the smaller masses of phyllite and limestone are also rounded but generally are not polished because of their softness and susceptibility to solution and reaction.

No sorting of the inclusions is discernible except for a slightly greater abundance of fragments near the edge of the breccia pipes that were obviously derived from the nearby wallrocks. The larger inclusions are more resistant to erosion than the tuffaceous and fragmental matrix and locally cap hills and ridges. A particularly large cluster of giant quartzite fragments underlies Maple Peak and has led to the erroneous impression that these rocks are a klippen of the Sheep-rock thrust fault.

Under the microscope the fine-grained matrix of the breccia pipes is seen to consist of unsorted angular and broken crystals of quartz, orthoclase, andesine, biotite, and fragments of rock, all embedded in a rock powder that locally is silicified, calcitized, and chloritized. A few of the igneous minerals preserve entire crystal outlines, but most of them have been fractured into sharp-edged particles ranging in size from 0.5 mm to the finest dust. The largest and least broken of the igneous minerals are the quartz grains, which constitute as much as 25 percent of selected samples of the tuff. Apparently many of the quartz grains were rounded by resorption prior to eruption and may have resisted crushing and breaking as much as by their sphericity as by their hardness.

Zonation

A rude compositional zonation is recognized particularly across the Maple Peak breccia pipe. The central area of this pipe is dominantly composed of tuffaceous material and rare boulder-sized clasts of sedimentary rocks. Peripheral to this core is an irregular zone containing abundant exotic inclusions of Precambrian and Paleozoic rocks, including the largest blocks of these rocks. Outward from this zone these inclusions progressively diminish in number and become subordinate to less rounded blocks and fragments of the wallrocks, which locally become so numerous that they make the selection of the contact between the breccia pipe and the country rocks somewhat arbitrary. A similar zonal arrangement of a tuffaceous core, an intermediate zone of exotic inclusions, and a border zone of brecciated contact rocks is also primitively developed in the Cherry Creek and Hassel breccia pipes.

The central zone of the breccia pipes closely resembles ashfall arkosic tuffs and commonly has been mistaken for a pyroclastic deposit. It is less resistant

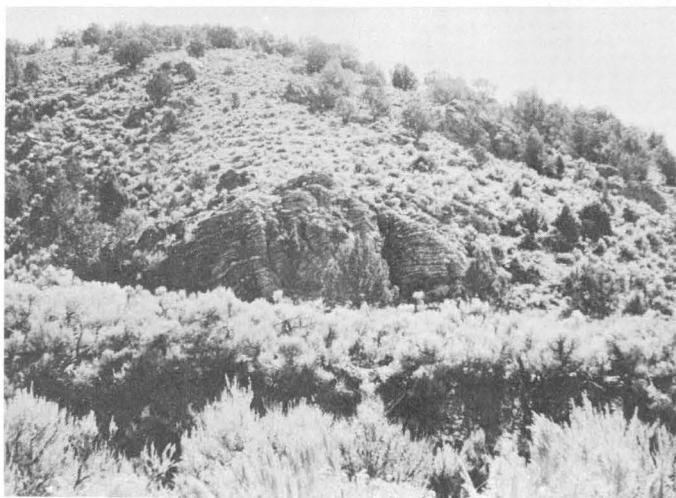


FIGURE 3.—Outcrop of the Cherry Creek breccia pipe near the Cherry Creek Reservoir. The exposed part of the large banded inclusion, which is limestone of Mississippian age, is 15 feet high and 35 feet wide. The other partly exhumed inclusions consist of Cambrian quartzite and Cambrian to Mississippian limestone in a matrix of tuffaceous breccia and rock fragments. Cherry Creek has been entrenched into flood plain in foreground.

than the adjacent zone of abundant inclusions and locally is cut by canyons and gulches. The intermediate zone of inclusion-rich breccia typically weathers in relief and is characterized by a chaotic assemblage of exotic blocks of all sizes and composition. In this zone, blocks of fossiliferous Mississippian limestone may lie adjacent to Precambrian boulder phyllites, or any other rock that may be hundreds or even thousands of feet higher or lower in the stratigraphic column, and indicate a thorough mixing or churning of the breccias. Toward the edge of the pipe, the zone of inclusions gradually merges with the narrow border zone that consists chiefly of brecciated wall rocks. In areas where the pipes cut volcanic rocks that superficially resemble the tuffaceous and fragmental matrix of the pipes, the contact is commonly placed at the limit of rotated blocks and the few scattered exotic inclusions.

ORIGIN

The thorough brecciation of the matrix and inclusions of the breccia pipes of the Cherry Creek area, as well as the chaotic nature of the pipes, their shattered wallrocks, abundance of rounded inclusions, and association with rhyolitic or quartz latitic igneous material, all suggest an explosive emplacement. Such an emplacement is also supported by the occurrence of arkosic ashfall and welded tuffs in the Cherry Creek area (Groff, 1959, p. 118) that were apparently derived from material erupted through these vents. It is conceivable that the breccia pipes were formed when a partly crystallized, gas-rich magma reached fissures that extended to the surface. The initial phase was probably the development of the vents in the manner originally proposed by Daubreé (1891), who postulated that diatreme channelways were drilled by escaping gas and steam and the vents were produced by volcanic explosions. After the channelways had been developed to the surface, the magma probably continued to evolve gas, which became charged with crystal fragments, pieces of country rock, and pumiceous shards. During this and succeeding phases, surficial eruptions deposited welded and ashfall tuffs, and the channelways doubtlessly were enlarged through abrasion by the churning mass of debris.

The inclusions of sedimentary rocks probably were derived from giant slabs that had been stoped-out at depth by the invading magma; however, some slabs and blocks may have originated through rock bursts that doubtless took place when the velocity of the gas and debris column increased sufficiently to create a sharp drop in pressure across the walls of the pipe. Heat derived from the rising gasses and through fric-

tion of the churning mass of debris pyrometasomatically case-hardened the surface of some boulders and locally remelted the volcanic wallrocks and formed irregular patches and stringers of partly fused tuff.

Unlike the down-dropped inclusions in the diatremes of the Navajo and Hopi Indian Reservations (Shoemaker, 1956, p. 182), which resulted from repeated eruption and collapse of the diatremes, the inclusions of sedimentary rocks in the breccia pipes of the Cherry Creek area are all from underlying rock units. This fact is confirmed by the sparseness of inclusions composed of volcanic rocks, which overlay the sedimentary rocks at the time of the eruptions. The occurrence of slabs of readily identified Precambrian quartzite, boulder phyllite, argillite, and conglomerate adjacent to the Mississippian strata forming the northern and northeastern wallrocks of the Cherry Creek and Maple Peak pipes indicate an upward dislocation of many thousand feet. The absence of fragments derived from older Precambrian crystalline rocks may probably be explained by the great thickness of the late Precambrian and younger sedimentary rocks, which have been repeated by thrust faulting in the Cherry Creek area, and by the possibly high level that was reached by the parent magma prior to the formation of the breccia pipe.

The upper parts of the Cherry Creek breccia pipes have long since been removed by erosion, but it may be conjectured that craters were formed at the original surface, first by explosion, and possibly later by subsidence. Any crater deposits that may have been laid down during this interval, such as stratified tuffs, siltstones, or marly limestones, have been eroded.

ECONOMIC ASPECTS

The breccia pipes in the Cherry Creek area are similar in many respects to mineralized breccia pipes in other areas, particularly the Braden pipe in Chile, which is the localizing feature of one of the largest copper ore deposits in South America, if not the world (Lindgren and Bastian, 1922; Howell and Molloy, 1960). However, no evidence of ore deposits closely associated with the pipes, or of fragments of older ore bodies, was recognized in the Cherry Creek area. The weak hydrothermal alteration of the tuffaceous matrix and of some of the wallrocks adjacent to the pipes is suggestive, however, of some hydrothermal activity. The most obvious alteration is a bleaching of the mafic minerals and groundmass of both the volcanic rocks and the matrix material, apparently resulting principally from the weathering of introduced pyrite and the action of weak primary argillizing solutions. Incipient patches of hydrothermal chlorite minerals and

some secondary calcite, which probably originated from the limestone inclusions and rock flour, were also observed in thin sections of the tuffaceous and fragmental matrix. The abundance of unaltered limestone fragments in the pipes indicates the relative weakness and general paucity of hydrothermal solutions associated with the pipes of the Cherry Creek area, as well as the absence of ore bodies at depth in the subsurface limestones that were incorporated into the breccia pipes.

REFERENCES

- Butler, B. S., Loughlin, G. F., Heikes, V. C., and others, 1920, The ore deposits of Utah: U.S. Geol. Survey Prof. Paper 111, 672 p.
- Cohenour, R. E., 1959, Sheeprock Mountains, Tooele and Juab Counties: Utah Geol., Mineralog. Survey Bull. 63, 201 p.
- Daubré, Auguste, 1891, Recherches Expérimentales sur le Rôle des Gaz à Hautes Températures, doués de très fortes pressions et animés d'un mouvement forte rapide dans divers phénomènes géologiques: Soc. géol. France Bull., 3d ser., v. 19, p. 313-354.
- Groff, S. L., 1959, Geology of the West Tintic Range and vicinity, Tooele and Juab Counties, Utah: Utah Univ. unpub. Ph. D. thesis, 183 p.
- Hilpert, L. S., and Roberts, R. J., 1964, Economic geology, in Mineral and water resources of Utah, Report to the Committee on Interior and Insular Affairs, United States Senate: Washington, U.S. Govt. Printing Office, 275 p.
- Howell, F. H., and Molloy, J. S., 1960, Geology of the Braden ore body, Chile, South America: Econ. Geology, v. 55, no. 5, p. 863-905.
- Lindgren, Waldemar, and Bastian, E. S., 1922, Geology of the Braden mine, Rancagna, Chile: Econ. Geology, v. 17, p. 75-79.
- Mabey, D. R., Crittenden, M. D., Jr., Morris, H. T., Roberts, R. J., and Tooker, E. W., 1964, Aeromagnetic and generalized geologic map of part of north-central Utah: U.S. Geol. Survey Geophys. Inv. Map GP-422.
- Mabey, D. R., and Morris, H. T., 1967, Aeromagnetic and gravity maps of Tintic Valley and adjacent areas, Tooele and Juab Counties, Utah: U.S. Geol. Prof. Paper 516-D.
- Morris, H. T., and Anderson, J. A., 1962, Eocene topography of the central East Tintic Mountains, Utah: Art. 60 in U.S. Geol. Survey Prof. Paper 450-C, p. C1-C4.
- Morris, H. T., and Lovering, T. S., 1961, Stratigraphy of the East Tintic Mountains, Utah: U.S. Geol. Survey Prof. Paper 361, 145 p.
- Roberts, R. J., Crittenden, M. D., Jr., Tooker, E. W., Morris, H. T., Hose, R. K., and Cheney, T. M., 1965, Pennsylvanian and Permian basins in northwestern Utah, northeastern Nevada, and south-central Idaho: Am. Assoc. Petroleum Geologists Bull., v. 49, no. 11, p. 1926-1956.
- Shoemaker, E. M., 1956, Occurrence of uranium in diatremes on the Navajo and Hopi Reservations, Arizona, New Mexico and Utah in Page, L. R., Stocking, H. E., and Smith, H. B., compilers, Contributions to the geology of uranium and thorium by the United States Geological Survey and Atomic Energy Commission for the United Nations International Conference on peaceful uses of atomic energy, Geneva, Switzerland, 1955: U.S. Geol. Survey Prof. Paper 300, p. 179-185.
- Stringham, B. F., 1942, Mineralization in the West Tintic mining district, Utah: Econ. Geology, v. 53, p. 267-290.



DESCRIPTION AND USE OF AN UNDERWATER TELEVISION SYSTEM ON THE ATLANTIC CONTINENTAL SHELF¹

By J. E. EDDY,¹ V. J. HENRY,² JOHN HOYT,²
and EDWARD BRADLEY¹

¹Washington, D.C., ²Sapelo Island, Ga.

*Work done in collaboration with the
University of Georgia Marine Institute, Sapelo Island, Ga.*

Abstract.—Relatively inexpensive underwater closed-circuit television cameras and a monitor, which were adapted first for use in boreholes, were used to obtain a 500-line-resolution picture of the Continental Shelf off the Georgia coast. Illumination for viewing the bottom at night or on deep parts of the shelf was provided by 1,000-watt quartz lights mounted with the television camera on a steel-framed sled. The sled rested on the sea floor or was towed slowly behind a ship. Physical characteristics of the bottom as well as considerable biological activity were recorded by photographing the television monitor using both 35-mm still pictures and 16-mm motion pictures.

Probably the most widespread uses of underwater television in the oceans are in salvage work—particularly on sunken ships or aircraft—and in underwater engineering construction work. Some reports of such work can be found in recent issues of various industrial journals. Stamp (1953) discussed underwater television operations in the identification and salvage work of H.M. Submarine *Affray* in the North Sea; he also pointed out that underwater television may be used for scientific studies of the bottom and for reading underwater instruments. Use of underwater television in a stationary instrument system for measuring sea-floor boundary conditions was discussed by Sternberg and Creager (1965).

A series of closed-circuit television observations of the sea floor off the Georgia coast were made to determine the efficiency of such equipment in marine geologic and biologic studies. Observations were made in water from about 18 to 90 meters (60 to 300 feet)

deep with the television camera mounted on a specially designed sled. Successful observations were made with the sled stationary and also under tow. During a preliminary cruise, several stations were occupied on the shallow shelf seaward of Sapelo Island, Ga.; a second cruise was made to examine the sea floor near the edge of the Continental Shelf and at intermediate points on the shelf. This report primarily describes the equipment and the results of the second cruise.

All observations were made from the Research Vessel *Kit Jones* under command of Capt. B. J. Rouse, whose assistance is gratefully acknowledged. The television equipment used was modified for underwater use by the senior author. This study was made possible through research-vessel support provided by National Science Foundation Grant GP-4599.

DESCRIPTION OF EQUIPMENT

Television camera and housing

The underwater television apparatus was designed to be simple and to operate at a maximum hydrostatic pressure of 305 m (1,000 ft) of water. The system uses high-resolution cameras and a monitor manufactured by the Kin Tel Division of Cohu Electronics, Inc., modified for use in boreholes (Eddy, 1964). The monitor and cameras furnish a full 500-line resolution, which is about twice that of home television receivers. A 14-inch aluminized picture tube, mounted with a Polaroid filter in front of it, provides bright, clear pictures.

The control unit is designed to provide a high degree of flexibility for both cameras and the monitor. The

¹Contribution No. 126 of the University of Georgia Marine Institute, Sapelo Island, Ga.

unit employs a video amplifier of 8-megacycle bandwidth to furnish the 500-line resolution and has a number of remote camera controls, including horizontal and vertical centering controls, that can be used to shift the field of vision electronically. Full automatic electronic target control provides self-adjustment of the image intensity over a range of 4,000 to 1. Service and operation of the unit have been simplified by placing all the adjustment controls on the front panel and by building the chassis so that it can be removed readily from the front of the mount.

Two cameras were used in the development of the system. The first was a Kin Tel model 1990 enclosed in a metal tube, 45 centimeters ($17\frac{3}{4}$ -inches) long by 15 cm (6 in.) in diameter. This camera was fitted with a lens that has motor-driven focus and iris adjustments. The second was built from a Kin Tel model 1986-C studio camera modified to fit into a 11.4-cm ($4\frac{1}{2}$ -in.) diameter aluminum tube. The tube is 91 cm (36 in.) long and has an 11.4-cm ($4\frac{1}{2}$ -in.) outside diameter and an 8.9-cm ($3\frac{1}{2}$ -in.) inside diameter. The lower end is fitted with a quartz-glass plate 8.3 millimeters ($\frac{1}{4}$ -in.) thick, specially cut from high-strength glass (reported tensile strength of 2,000 pounds per square inch). Both the viewing end and the upper end of the camera case are fitted with O-rings which are sealed with silastic rubber. A high-pressure coupling with neoprene sleeves joins the camera case to a 24-conductor 1.9-cm ($\frac{3}{4}$ -in.) cable that is connected to the monitor. The camera-case assembly has been tested successfully to simulated water depths of 290 m (950 ft) in a high-pressure chamber.

The second camera has a French-made Kinoptik "fish-eye" lens with a focal length of 5.7 mm, a wide viewing field of 117° , and an overall diameter of 8.9 cm ($3\frac{1}{2}$ -in.). The fixed focus, from 10 cm (4 in.) to infinity, of this lens keeps most of the lighted area several feet in front of the camera in focus.

Towing sled

The television cameras and light were placed on a steel-framed sled (fig. 1) about 1.8 m long, about 91 cm in both width and height, and weighing about 182 kilograms (400 pounds). The runners of the sled were 10 cm (4 in.) wide and were turned up about 30 cm (12 in.) in the front. This shape of runner is satisfactory for smooth sandy bottoms found over most of the Continental Shelf. However, for rocky areas, provision should be made to prevent the runners from snagging.

When the sled was towed, a chain bridle was attached to the forward end. The bridle is shifted to the top of

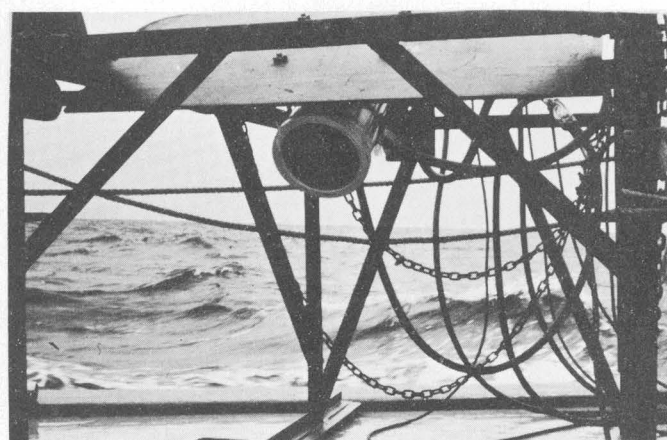
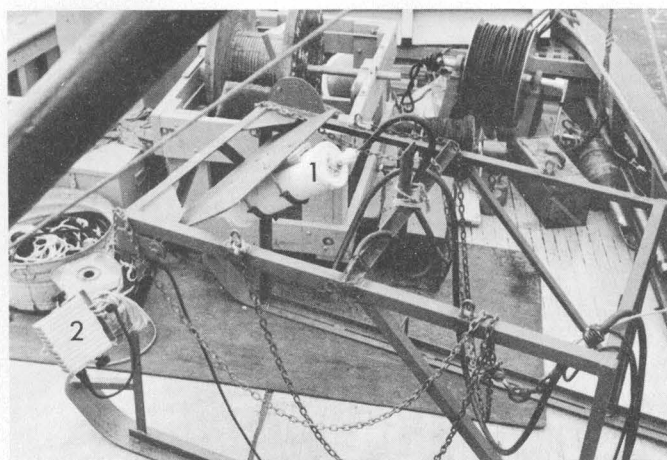


FIGURE 1.—Towing sled and television camera. *Top*, Sled with television camera (1) mounted at an angle of about 45° for towing and with 1,000-watt quartz light (2) attached to the front of the sled. *Bottom*, Front view of television camera mounted on the sled in towing position.

the sled when the sled remains stationary. A float attached to the top of the bridle keeps some tension on the chains and prevents them from falling into the sled when the cable is slack.

Underwater lighting

One of the factors responsible for reduced visibility in sea water is the absorption of light by water, which reduces the intensity of light with increasing distance. Another factor that is particularly difficult to overcome can be called foreground back-scatter. Back-scatter results from light scattering by small marine organisms and silt and clay particles which cause a reduction in contrast. Thus a source of illumination for viewing the bottom should be relatively close to the object or objects to be observed and also the direction of maximum illumination should be at an angle that minimizes light scattering. Ideally, to avoid foreground back-

scatter as much as possible, the source should be well to one side and pointed down at about an angle of 45° .

In the present study, a 1,000-watt quartz light was used at each of the stations. Many of the observations were made at night, but at the deeper stations artificial light was used in the daytime as well. Good results were obtained with the light pointing at about a 45° angle from the bottom and somewhat to the side of the center of the image being viewed.

Photography of television image

The television image was photographed with a conventional 35-mm single-lens reflex camera and with 16-mm movie equipment. Proper exposure was obtained by increasing the exposure by approximately $\frac{1}{2}$ f stop from the indicated light-meter reading. Because of the rapid scan rate, fast shutter speeds should not be used. One-thirtieth of a second was found to give satisfactory results without noticeable variations in light intensity.

OPERATION OF THE SYSTEM

At station 2 (fig. 2) where the water depth was about 60 m (195 ft), the observations were made at night and the camera was mounted vertically for viewing with the sled in a stationary position. As the ship swung at anchor, however, the sled and camera were moved so that a rather sizable area was covered during approximately 2 hours of viewing, even though the width of the area seen on the television screen at a given instant was only about 40 cm (16 in.). The current was from the south and moved over the bottom at approximately half a knot. Current velocities were observed using a Savonius-type rotor current meter attached to the sled at anchor stations. The meter had read-out and recorder capabilities for both speed and direction.

The sea floor at station 2 is covered with coarse sand that is rippled in asymmetrical forms oriented normal to the current flow and has wavelengths of 15–20 cm (6–8 in.). Ripple crests (fig. 3A) are generally sinu-

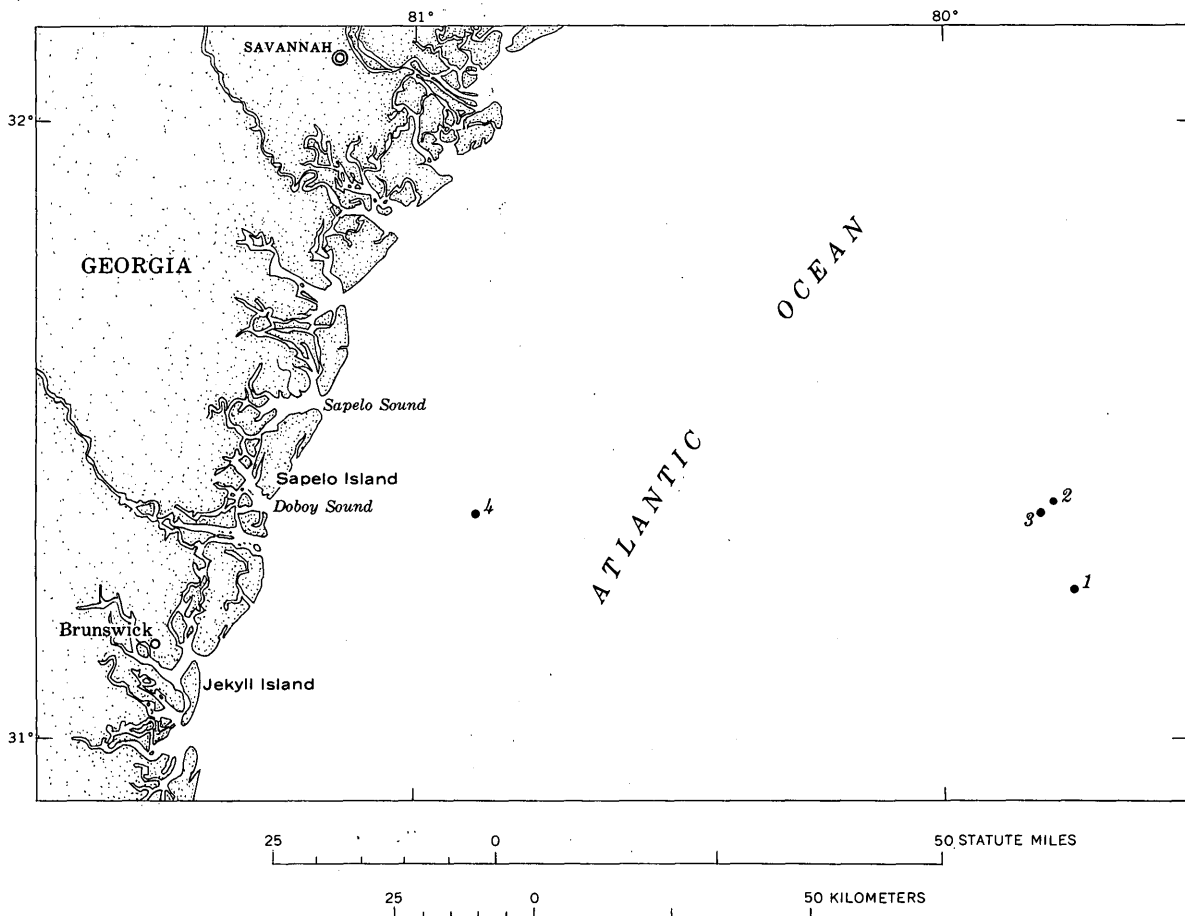


FIGURE 2.—Map of the southern part of the Atlantic Continental Shelf, showing stations (numbered) where underwater television observations were made.

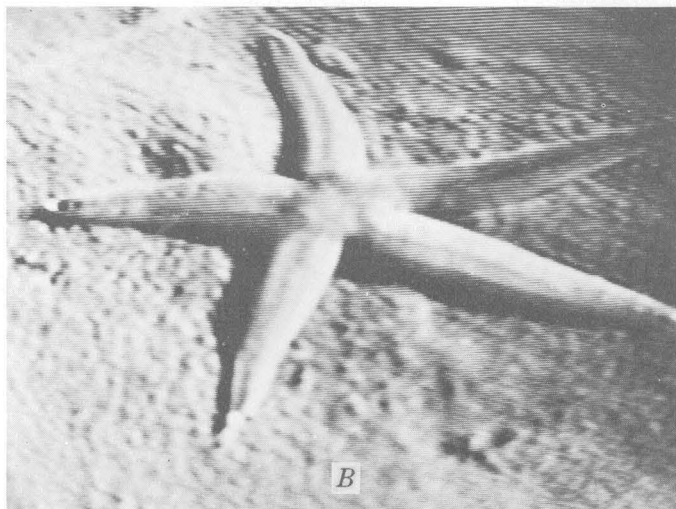
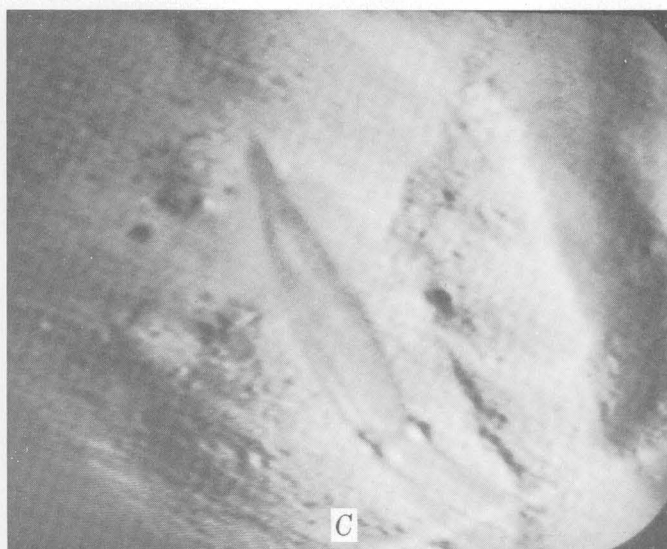
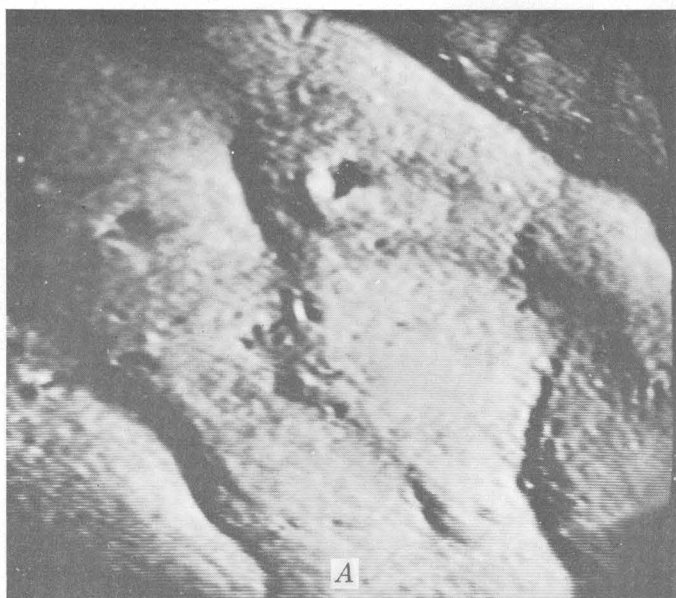


FIGURE 3.—Views of the flow on the Continental Shelf at station 2. *A*, Sinuous ripple marks in bottom sediment consisting largely of coarse sand; note burrow openings on sides of ripples. *B*, Starfish about 37 cm (15 in.) in diameter. *C*, Squid about 30 cm (1 ft) long searching for food on or in the bottom sediment.

ous. Sediment and organic debris could be seen flowing over the ripple crests and accumulating in the troughs, but the period of observation at any one spot was not long enough to detect ripple movement.

A large variety of benthic and nektonic organisms was present at station 2. Most abundant were small 8.3- to 38-mm ($\frac{1}{4}$ - to $1\frac{1}{2}$ -in.) arthropods and fish that darted about just above the bottom. During one period of observation, a small animal swam rapidly into view and quickly burrowed into the sand. It was followed immediately by a large squid (fig. 3*C*), which vigorously pursued it into the sand and apparently captured the animal. Several crabs 1-3 in. in size were seen, and a hermit crab, occupying a whelk shell about 6 in. long, came into view. Many starfish were observed (fig. 3*B*), and burrow openings 8.3-16.6 mm ($\frac{1}{4}$ - $\frac{1}{2}$

in.) (fig. 3*A*) in diameter and averaging about two per square foot were abundant.

Station 3 (fig. 2) is at the edge of the shelf where there is a pronounced change in slope and where the water depth is from about 45 to 50 m (150 to 170 ft). Although the observations were made during the day, it was necessary to use artificial lighting. The sled and television camera were towed slowly with the camera tilted at about a 45° angle to observe the nature of the bottom in selected areas.

The sled was towed at about 2 knots up the slope. Large blocks of rock several feet thick and encrusted with calcareous growth were observed. The blocks, partly covered by sand through which they projected about 30-90 cm (1-3 ft), had no consistent orientation and probably have slid or tumbled to their present positions from elsewhere. The sand between the blocks contained many asymmetrical ripples 15-20 cm (6-8 in.) in wavelength. Although current velocity was not measured, a substantial drift of the sand stirred up by the sled runners suggested a northeast flow. Sea fan, sea whip, corals, and sponges were attached to the blocks. Small fish and many arthropods also darted about among the blocks. One relatively large fish—perhaps about 75 cm long—passed the camera rapidly. As the sled and camera moved up the slope, the blocks became more numerous and when the sled runners caught on the larger blocks, the sled overturned.

At station 1 (fig. 2) the ship was anchored in 150 m (485 ft) of water. The Gulf Stream current was

slightly greater than 3 knots at the surface and was about 1 knot at the bottom. Considerably more than 160 m (about 500 ft) of cable was let out with the fixed-focus television camera in a vertical viewing position. The pull of the current on the equipment was so strong that the sled did not reach bottom. No pictures were taken but during both descent and ascent an abundance of plankton was seen drifting rapidly past the television camera.

No pictures were obtained at station 4 (fig. 2) where the water is about 20 m (65 ft) deep because strong winds and moderately heavy seas caused the vessel to jerk the cable suddenly and the sled was overturned just after it reached the bottom.

CONCLUSIONS

Observation of the sea floor by closed-circuit television is a practical and useful method of obtaining biologic and geologic information over large areas of the Continental Shelf and slope. Compared to that in SCUBA diving, human risk is minimal, and diving skills and conditioning are not necessary. Viewing can continue for extended periods at one location, and sizable areas can be observed by towing the equipment. Under certain circumstances, geological conditions such as sediment transport, ripple marks, particle shapes and size, and similar bottom characteristics can be observed directly. Benthic and nektonic biota and their behavior can be studied and photographed rela-

tively simply. Perhaps one of the best uses for underwater television is for viewing conditions on the bottom and thus being able to better plan and direct investigative techniques.

Several improvements in the technique of station tending and in the design of the equipment—particularly in the sled to hold the camera and lights—were found to be desirable during these operations. Briefly they are (1) stabilization of the position of the vessel by both bow and stern anchors to prevent swinging while making stationary observations; (2) improvement of the design of the sled runners to prevent snagging during towing; (3) use of a buoy or a spring-controlled sleeve for the television and light cables above the sled to avoid entanglement and jerking; (4) provision for fastening the lights inside and near the back of the sled frame, both for better lighting and to avoid damage to them if the sled overturns; and (5) use of video tape to record all observations for later study.

REFERENCES

- Eddy, J. E., 1964, Television apparatus for borehole exploration: Art. 172 in U.S. Geol. Survey Prof. Paper 475-D, p. D219-D220.
- Stamp, W. R., 1953, Underwater television. *Scientific American*, v. 188, no. 6, p. 32-37.
- Sternberg, R. W., and Creager, J. S., 1965, An instrument system to measure boundary layer conditions at the sea floor: *Marine Geology*, v. 3, no. 6, p. 475-482.



HEAVY-MINERAL ASSEMBLAGES IN THE NEARSHORE SURFACE SEDIMENTS OF THE GULF OF MAINE¹

By DAVID A. ROSS, Woods Hole, Mass.

Abstract.—Nearshore sediments adjacent to the mouths of three rivers entering the Gulf of Maine have heavy-mineral suites similar to those in the rivers. The heavy-mineral assemblages found both in the rivers and in the adjacent nearshore areas correspond with those expected from the rocks exposed in the drainage areas of the rivers. The distribution of the light-mineral components, although not diagnostic in differentiating between source areas, is helpful in understanding environments of deposition. These sediments are interpreted as Recent in origin, whereas the sediments farther offshore are presumably Pleistocene or glacial in origin.

The Gulf of Maine (fig. 1), situated off the northeast coast of the United States, is an irregular depression containing numerous shallow basins and banks which are mainly of glacial origin. As part of the United States Geological Survey–Woods Hole Oceanographic Institution's joint study of the continental margin off the east coast of the United States (Emery and Schlee, 1963), the general mineral composition, texture, and other characteristics of about 800 bottom-sediment samples from the Gulf of Maine area have been determined. This paper discusses the results of detailed mineral analyses made on the sand-sized fraction (2 to 0.062 mm) of 57 of these samples.

The writer is grateful to J. C. Hathaway, K. O. Emery, and J. V. A. Trumbull for critical reading of the manuscript. Grain-size determinations were made by John Schlee.

MINERALOGY

Heavy minerals

The sand-size material in the surface samples from the Gulf of Maine was divided into heavy and light fractions, using standard heavy-mineral separation techniques. Heavy minerals (density greater than 2.89 grams per cubic centimeter) were identified using a

¹ Contribution No. 1897 of the Woods Hole Oceanographic Institution.

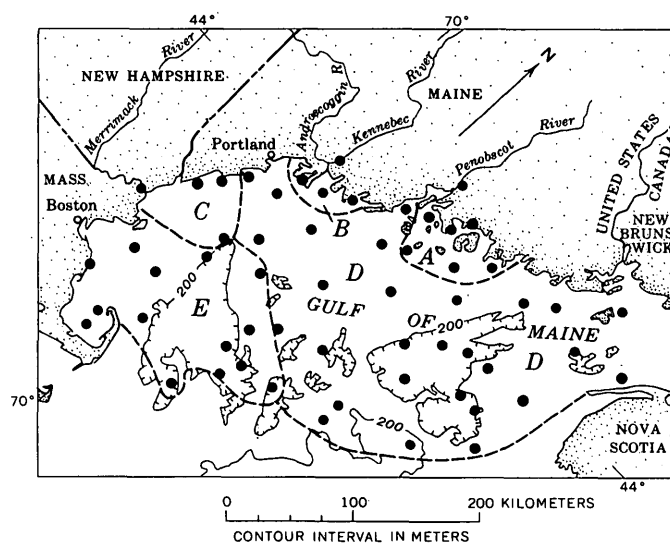


FIGURE 1.—Location map of samples (dots) from the Gulf of Maine. The letters refer to mineral associations discussed by name in the text: A, Penobscot amphibole, B, Kennebec amphibole, C, Merrimack garnet, D, Gulf of Maine, augite, and E, Gulf of Maine amphibole.

petrographic microscope. Garnet, amphiboles (mainly green hornblende), augite, hypersthene, and staurolite were the most common heavy minerals.

The heavy minerals were separated into several typical associations. Preliminary associations were based on the dominant mineral or minerals and the areal position of the samples. Means and standard deviations of percentages of individual minerals in all samples from each association were calculated. When individual samples had statistics considerably different from those of their original association, new categories or associations were established. This technique has resulted in five associations (table 1).

Three associations consist of a river sample and adjacent nearshore samples. These associations (the Penobscot amphibole, Kennebec amphibole, and Merri-

TABLE 1.—Average composition of heavy-mineral associations from the Gulf of Maine and from three rivers flowing into the Gulf
 [\bar{x} , mean; σ , standard deviation]

Mineral association or sample type (fig. 1)	Heavy Minerals (percent)									Number of samples	
	Epidote ¹	Amphibole	Augite	Hypersthene	Garnet	Staurolite	Andalusite	Sillimanite	Others		
Gulf of Maine											
A. Penobscot amphibole.	\bar{x}	5.6	39.0	13.4	20.0	6.4	2.7	6.4	1.3	5.2	7
	σ	2.2	6.1	4.9	7.8	4.1	5.2	2.6	1.4	5.4	4
B. Kennebec amphibole.	\bar{x}	3.5	55.0	9.5	7.2	11.0	4.2	1.2	3.0	9.0	4
	σ	1.9	13.7	2.9	5.1	3.2	3.0	1.5	2.8	8.1	4
C. Merrimack garnet.	\bar{x}	3.7	20.2	16.5	1.5	36.2	8.2	2.2	2.5	11.0	28
	σ	2.1	4.5	9.5	1.0	9.7	5.2	1.7	2.9	11.0	14
D. Gulf of Maine augite.	\bar{x}	6.5	28.5	29.2	4.9	15.7	3.2	2.1	1.3	11.0	28
	σ	3.2	11.0	10.4	4.3	9.7	2.7	2.2	1.8	11.0	14
E. Gulf of Maine amphibole.	\bar{x}	9.6	36.9	9.1	3.6	17.1	5.4	3.9	3.4	11.0	14
	σ	5.1	10.4	4.6	2.2	8.7	3.2	3.1	1.8	11.0	14
Rivers											
Penobscot		3	43	10	28	2	0	8	4	2	1
Kennebec		6	40	6	14	15	7	3	1	8	1
Merrimack		5	20	5	2	50	6	3	5	4	1

¹A line-counting technique was used to obtain mineral frequency. This is an approximation to area or volume percentage.

mack garnet) are interpreted as representing recent material carried by these rivers.

The Penobscot, Kennebec (with the Androscoggin), and Merrimack Rivers drain large areas of Paleozoic and older sedimentary and metamorphic rocks as well as smaller areas of Paleozoic and older intrusive rocks. The mineral composition of sediments from these rivers generally reflects the composition of their respective drainage areas as is seen by comparing the nearshore and river samples in figure 2.

The drainage area of the Penobscot includes volcanic rocks in the upper parts of the river and andalusite hornfels in the lower part; relatively large quantities of volcanic minerals, such as hypersthene and augite, and the metamorphic mineral andalusite occur in the Penobscot River sample. Areas drained by the Kennebec and Androscoggin Rivers have higher quantities of intrusive rocks than do the other rivers; the heavy minerals in the Kennebec sample are a mixed assemblage containing high percentages of intrusive minerals. The Merrimack River drains some garnet metamorphic zones in the coastal regions of its drainage basin, and metamorphic minerals are common in the sample from the Merrimack River. The samples from the Merrimack and Penobscot Rivers are so near the river mouth that tidal mixing of material is possible, but the one from the Kennebec River is upstream from the area of tidal mixing.

Two exceptions to the general similarity of mineral

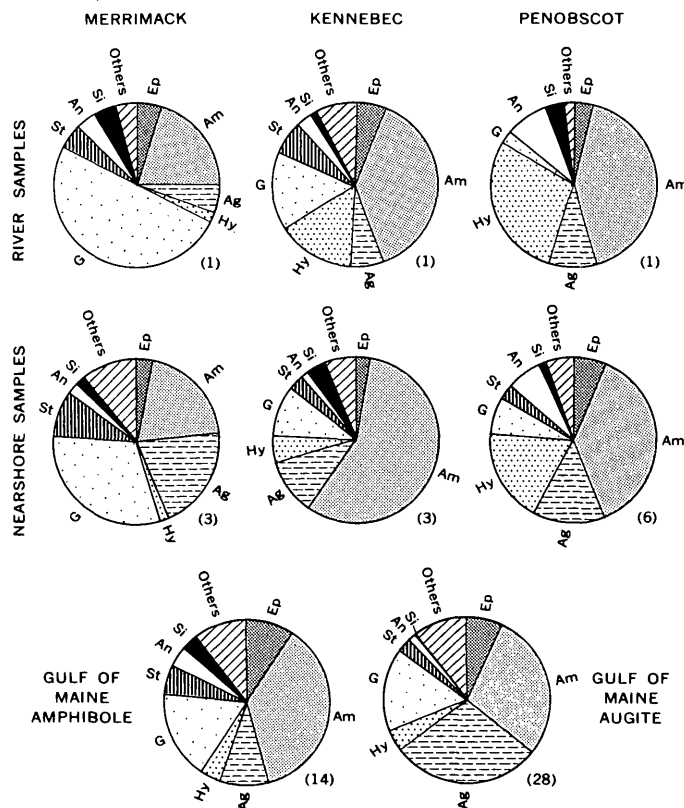


FIGURE 2.—Heavy-mineral composition of samples collected from the Gulf of Maine and rivers flowing into the gulf. Ep, epidote; Am, amphiboles; Ag, augite; Hy, hypersthene; G, garnet; St, staurolite; An, andalusite; Si, sillimanite; others include zircon, tourmaline, and sphene. The numbers in parentheses refer to the number of samples.

compositions in the river and nearshore samples are significant. One occurs off the Kennebec River, where the nearshore sediments contain somewhat more amphibole than the river sediments, and the other occurs in the Merrimack River, where garnet is more abundant than in the nearshore sediments.

Augite and amphibole assemblages, which cover the central parts of the Gulf of Maine, are mixtures of volcanic, igneous, and metamorphic minerals, and in this respect are similar to the nearshore heavy-mineral assemblages. The Gulf of Maine amphibole assemblage is similar to that of the Kennebec River sample, but its geographic position, in the southwest part of the gulf far from the Kennebec River, suggests no genetic relationship between the two areas.

Light minerals

Light minerals (density less than 2.89 g per cm³) compose the bulk of the sand fraction; however, they generally consist of only a few mineral species and therefore have limited application in determination of source areas. The light material is mainly quartz and feldspar (undifferentiated) with minor amounts of rock fragments, mica, and biogeneous material (table 2). Samples from the Penobscot and Kennebec Rivers have large quantities of wood fibers and black rock fragments, possibly coal. Some coallike material is also found in the sample from the Merrimack River. Commercial activity could contribute coal to these rivers.

Except in the Merrimack, the light-mineral assemblages in the river sediments are different from both the nearshore sediments and the Gulf of Maine assemblages (table 2). The Merrimack River sediment is

similar to the more seaward sediments. Stained quartz and feldspar are more common in the Gulf of Maine assemblages than in the nearshore samples; otherwise the samples are rather similar. Mica is common in the samples off the Kennebec River but is lacking in the river sample.

The grain size of sediments, which has been determined by settling-tube and pipet techniques, is shown in table 2. The grain size of the samples taken from the rivers is generally coarser than that of other sediment samples. The difference in grain size may explain some of the differences in light-mineral content. The nearshore sediments and the Gulf of Maine material have similar grain size. However, the large standard deviations of the median grain size indicate considerable spread in the grain sizes (table 2). Sorting is generally poor in all sediments except in the coarse sand from the Merrimacks and Kennebec Rivers.

DISCUSSION

Heavy-mineral data suggest different sources for some nearshore sediments of the Gulf of Maine. Sediments in three nearshore regions off rivers have heavy-mineral compositions similar to those found in samples obtained from the rivers and the heavy-mineral assemblages are representative of the rivers' present drainage areas. The presence in the river samples of wood fibers and possibly coal suggests that the river material is of Recent origin. Thus the nearshore sediment may also be Recent. If it were glacial in origin, a heavy-mineral assemblage more typical of the entire hinterland rather than that of a local river would be expected.

Other hypotheses can be proposed for the similarity in heavy minerals of the nearshore and river sediments

TABLE 2.—Light-mineral composition and grain size of samples collected from the Gulf of Maine

[\bar{x} , mean; σ , standard deviation]

Sample type or mineral association (fig. 1)	Quartz and feldspar (percent)	Stained quartz and feldspar (percent of total quartz and feldspar)	Rock fragments (percent)	Biogeneous material (percent)	Mica (percent)	Median grain size (phi)	Sorting ¹ (phi)	Number of samples
Penobscot River.....	46.0	8.0	² 32.0	0.0	5.0	3.2	3.3	1
Nearshore samples..... \bar{x}	81.2	21.8	7.4	7.2	2.0	5.7	3.5	5
..... σ	13.1	13.2	5.6	8.4	1.9	3.1	0.2	
Kennebec River.....	47.0	53.0	² 53.0	0.0	0.0	1.0	0.6	1
Nearshore samples..... \bar{x}	67.3	11.7	5.0	6.0	21.7	6.9	3.4	3
..... σ	7.6	10.9	3.6	1.0	4.2	2.0	0.6	
Merrimack River.....	90.0	41.0	³ 10.0	0.0	0.0	0.4	0.8	1
Nearshore samples..... \bar{x}	87.0	15.0	4.0	4.7	4.3	4.3	2.8	3
..... σ	4.6	5.6	2.6	3.1	4.0	1.4	0.5	
D. Gulf of Maine augite..... \bar{x}	84.7	44.1	10.8	3.5	0.8	5.1	3.3	28
..... σ	10.4	15.1	6.5	9.6	2.3	2.3	1.2	
E. Gulf of Maine amphibole..... \bar{x}	83.3	24.7	6.9	1.1	1.4	4.8	2.2	14
..... σ	24.7	10.0	6.6	1.9	2.5	2.4	1.1	

¹ Standard deviation.

² Many wood fibers and black rock fragments.

³ Some black rock fragments.

and the difference between the nearshore and Gulf of Maine sediments. The influence of grain size on mineral composition, generally thought to be minor (van Andel, 1959), can be locally important. The differences and similarities in grain size and mineral composition in the study area are relatively complex; they cannot be explained fully by either the similarity of mineral composition and difference in grain size between nearshore and river samples or by the similarity in grain size between the nearshore and the more offshore Gulf of Maine samples.

Removal of unstable minerals by weathering can modify mineral assemblages. This process may be important in the outer parts of the Gulf of Maine, near Georges Bank, but closer to shore within the main area of study, little evidence of removal of unstable or moderately stable minerals is observed. The heavy minerals are those generally considered as fairly stable.

Errors introduced by visual grouping of samples and by sampling and laboratory techniques may account for some of the sample variability. These undoubtedly affect the variability within the associations. Mixing between assemblages certainly also must occur. Probably, however, the main cause of differences in heavy-mineral content between associations is due to differences in source area.

The small number of samples does not allow ade-

quate definition of dispersal patterns. The surface currents in the nearshore regions are generally from east to west and of low velocity (usually less than 5 miles/day or about 10 cm/sec). Distribution of heavy minerals in the nearshore samples off the Penobscot River, however, suggests dispersion from west to east. Possibly here local sources of sediment such as cliff erosion or more local glacial effects may be important.

The distribution of the light-mineral components, aside from the wood fibers and coal-like material in the river sediments, does not aid in differentiating between source areas but can help in understanding environments of deposition. An example is the sample from the Kennebec River with median grain size of 1.0 phi (0.5 mm), indicating a high-energy environment. Mica, usually an indication of a low-energy environment, is not present in the river sample, but it is very common in the nearshore sediments where finer grain sizes and presumably lower energy environments prevail.

REFERENCES

- Emery, K. O., and Schlee, J. S., 1963, The Atlantic Continental Shelf and Slope, a program for study: U.S. Geological Survey Circ. 481, 11 p.
- van Andel, T. H., 1959, Reflections on the interpretation of heavy mineral analyses: *Jour. Sed. Petrology*, v. 29, p. 153-163.



HIGH-EFFICIENCY SUBBOTTOM PROFILING

By GENE A. RUSNAK, Menlo Park, Calif.

Abstract.—Difficulty because of side echoes and their multiple reflections when making seismic subbottom profiles in narrow fiords (width-to-depth ratio of 4/1 or less) can be overcome by beamforming, or focusing, with suitable source and receiver geometry. A multiple-electrode sparker system increases sound-source propagation area and improves signal directivity. Signal directivity is achieved by the additive nature of reflected signals whose travel time is equidistant from the source. A four-unit sparker system in a square planar format, with discharge units spaced at half a wave length from each other and a quarter of a wave length from the water surface, improves the signal and directivity and increases resolution. Freefield measurement with a calibrated hydrophone is planned for experiments to provide a quantitative evaluation of the apparent gains so far observed qualitatively.

The extensive highly localized wave damage which accompanied the Alaska earthquake of March 27, 1964, in numerous fiords of Prince William Sound and adjacent areas suggested that local slumping of submerged land must have occurred (Grantz and others, 1964). Plans were immediately formulated for extensive and detailed submarine sampling and profiling studies intended to lead to a better understanding of some of the marine geological processes generated by the earthquake. During the summer field season of 1964 and 1965, these studies were made from the U.S. Geological Survey R/V *Don J. Miller*, a 105-foot-long power barge.

Sea-floor sampling and bottom profiling were carried out in Orca Inlet, Port Valdez, Passage Canal, Blackstone Bay, Kings Bay, Nellie Juan, and Ice Bay off Chenega in Prince William Sound, as well as in Resurrection Bay near Seward. Standard coring and grab-sampling equipment, plus recording fathometers and a sonoprobe were used in 1964. The original subbottom profiling done with the sonoprobe was accomplished through the kindness of Dr. George G. Shor of the Scripps Institution of Oceanography, who loaned this subbottom profiling gear to the Geological Survey. Although much data were collected in profiling to

suggest mechanisms and resulting behavior of the fiord sea floor during the earthquake, few of the subbottom records were of a quality acceptable for definitive analysis. The common working depths found in the fiords, at approximately 200–400 meters, were beyond the design capability of the sonoprobe (McClure and others, 1958). Most of the outgoing sonic energy was attenuated by the water column; only feeble returns were gotten from beneath the water-sediment interface. In addition, the self-generated noise of the receiving element coupled with the noise generated by the vessel degraded the signal-to-noise ratio beyond the limits of usefulness. The experience from this work demonstrated the need for equipment of greater energy output to obtain records of higher quality. Subsequently, tests with electrical discharge sources provided records of outstanding clarity from these same fiords, as well as from the very narrow confines of the Redondo submarine canyon of southern California (Yerkes and others, 1967) (p. C97–C105, this chapter).

Acknowledgments.—The author wishes to thank Capt. Robert Stacey of the U.S. Geological Survey Research Vessel *Don J. Miller* and Capt. Fred Ziessenhenie of the University of Southern California R/V *Velevo IV* for their help and sincere interest in the collection of data for this experiment. Dr. Donn Gorsline of the University of Southern California provided various facilities with which this work could be accomplished. Charles I. Wingard contributed willingly of his time and energies during the many hours of preparation and data gathering. On various occasions in the fieldwork involved, the author had the helpful assistance of John Muttart, Roland von Heune, and many of the members in the ships' crews. Particular thanks are extended to Hartley Hoskins for kindly providing the author with a copy of his notes compiling his personal studies with those of the Woods Hole Oceanographic Institution's Geophysics Department as of the spring of 1965. The helpful review of

this manuscript by S. T. Knott, is gratefully acknowledged. The author accepts sole responsibility for any errors or omissions.

EQUIPMENT REQUIREMENTS

Analysis of the records in the light of other experience, fiord geometry, and available commercial apparatus for seismic profiling, indicated that high-voltage electrical-discharge devices such as the Arcer system (manufactured by the Rayflex Corp.), the GEP (Geological Echo Profiler of Alpine Geophysical Corp.), or the sparker and boomer (manufactured by Edgerton, Germeshausen and Grier Corp.; see Hoskins and Knott, 1961; Van Reenan, 1964) could provide a most convenient profiling unit. For various expedient and design reasons, the sparker and boomer combination was selected for use during the 1965 field season. The narrow confines imposed by the geometry of the fiords predicated the need for a system with some directional control of the outgoing signal if side echoes were to be reduced. The boomer provided such directionality, but the multiple-source techniques of explosive seismology (Dobrin, 1960) could provide sparker directionality with higher and more efficient energy coupling (S. T. Knott, personal commun.; Caulfield, 1962; Caulfield and others, 1964). A consideration of continuous-wave theory applied to phase enhancement characteristics of sound demonstrates that a given frequency (and its harmonics) can be made directional through use of multiple synchronous-discharge sources operating at sound-source separation distances of even half wave lengths $\frac{(n\lambda)}{2}$. Although continuous-wave theory does not apply directly to short-pulse acoustical sources, considerable gains in directivity are possible (Dobrin, 1960). Similar separation of receiving elements could improve the signal-to-noise ratio of the desirable frequency return signal.

In view of the theoretical gains to be made in the reduction of side echoes and the improvement of signal-to-noise ratios through the use of multiple output and receiving elements, a second sparker array transducer and a multiple-element (individually selectable) hydrophone array was included for experimentation. The complete system thus assembled was composed of a boomer transducer, two sparker arrays for beam-forming by $\frac{(n\lambda)}{2}$ spacing, a Rayflex amplifier system utilizing mixed outputs from two Geospace 111 seismic amplifiers, and a Rayflex-designed neutrally buoyant hydrophone array consisting of four individually selectable, preamplified piezoelectric receiving elements.

Received data are recorded graphically and mag-

netically as a continuous subbottom profile and as a permanent file copy. The graphic recording is made with an Alden Precision Graphic Recorder (PGR), (Knott and Witzell, 1960) or a T. H. Giffit Graphic Depth Recorder Transceiver (GDRT) on a 19-inch wet paper. The incoming alternating-current voltages are recorded direct or are rectified to print out only the positive or negative component of the received signal. Half-wave rectification has the advantage of being more easily read and providing an easy distinction between multiples because these undergo a phase reversal with each reflection (Officer, 1958).

Magnetic tape recording is made of all received data for later additional signal processing and for the permanent files. For this purpose, an Ampex SP-300 tape recorder capable of recording seven channels of information on $\frac{1}{4}$ -inch tape is used. Only three channels are used at one time. One channel is used at $1\frac{7}{8}$ inches per second for low-frequency FM recording (DC-312 Hertz, or cycles per second), the second channel is used for high-frequency AM recording (50-3500 Hz), and the third channel records both the 60-Hz reference signal for synchronization and the voice identification of fixes on the record. With the magnetic tape recorder operating at $1\frac{7}{8}$ ips, full fidelity is obtained for the desired frequencies. Thus, a total recording time of 12 hours is obtained on 3,600 feet of tape by recording three channels per side. Slow recording speeds reduce the amount of tape that has to be stored for reference and thus eliminates the need for large magnetically protective storage cabinets.

The complete electronic package of power source, receivers, recorders, and shortwave radio receivers for National Bureau of Standards WWV time checks was housed in a portable deck-mounted laboratory (fig. 1). This self-contained instrument pod could be mounted aboard any ship of opportunity having a free deck area of 8×12 feet. Permanent installation of a similar assembly was made within a compact cabinet arrangement aboard the U.S. Geological Survey R/V *Polaris* (fig. 2).

The towed hydrophone-receiver elements can be used individually or interconnected to provide optimum signal-to-noise reception. Spacing between the individual piezoelectric elements, however, was fixed at equal 1.5-m intervals so that the multiple hydrophones could be made most highly directional only for selective frequencies of 2000, 1000, and 500 Hz that correspond to half wave lengths of 1.5, 3.0, and 4.5 m ($\lambda/2 = 1.5$ m) and higher harmonics; that is, any combination of two receivers when $\lambda = 2(1.5)$ m or $\lambda = 3(1.5)$ m.

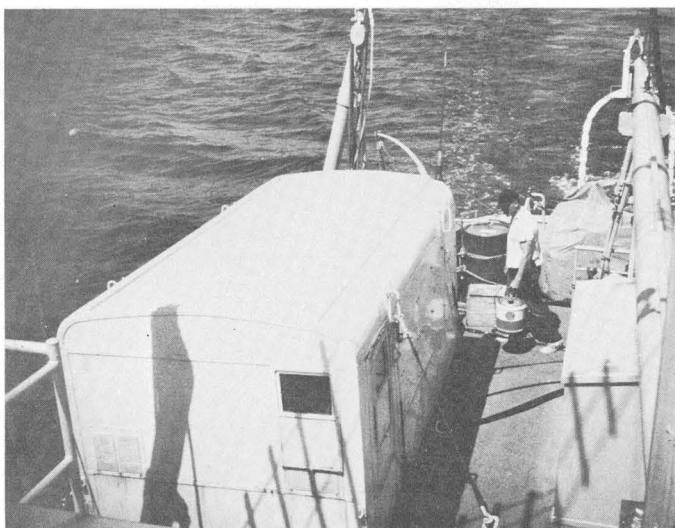


FIGURE 1.—Portable self-contained geophysical laboratory used aboard the *Don J. Miller* is shown here aboard the University of Southern California R/V *Veleo IV*. All instrumentation—such as power supplies, trigger bank, capacitor banks, graphic and magnetic recorders, and communications equipment—is contained within this laboratory. Ship's power and auxiliary generators are used for electrical power.



FIGURE 2.—Geophysical instrumentation installed in the laboratory of the U.S. Geological Survey R/V *Polaris*. From left to right are the radio-communications receivers for time fixes, an Ampex SP-300 magnetic tape recorder, a Rayflex seismic amplifier system, and the T. H. Giff GDRT graphic recorder. The energy storage units for the electrical-discharge sparker source are enclosed in cabinets adjacent to the console shown.

The sparker units in the system consist of three small-diameter rubber-insulated anodes whose tips are separated from each other, within the large ground-return cage, by a distance of 50 centimeters (fig. 3). A single unit thus produces an almost cylindrical wave front perpendicular to the axis of that array for low frequencies. A pair of individual units could be physi-

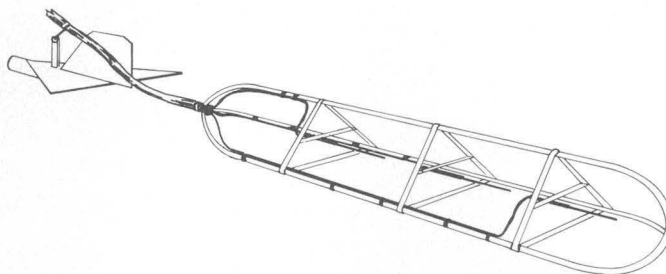


FIGURE 3.—Diagrammatic sketch of the sparker array. It can be used singly or in any combination of multiple units desired. Spacing between center electrode tips is fixed at 50 cm. The distance between the center electrodes to the grounding triangular frame remains constant and for the electrical potential used, 3,750 volts direct current, the unit will function in water with a salinity of less than 2.0 percent. The Kolstrand Supply Co. depressor at the front allows the flight depth to be varied as is desired. Not drawn to scale.

cally spaced at any given $\lambda/2$ distance desired within the optimum range of sound frequencies provided by the energy source. For the specific experiment here, the spacing of approximately 9 m (30 feet) was chosen because it falls near ($\lambda/2$ in fig. 4) the lowest principal frequency in use within the broad spectrum of sound generated by electrical-discharge devices of the sparker type (Hersey, 1963). The estimated efficiency of conversion of electrical energy to acoustical energy is 10 percent for a single electrode discharge when careful attention is given to electrode polarity, low inductance cables, and other electrical parameters (Caulfield and others, 1964). Multiple-electrode efficiency apparently is greater. Power output from our combination of power supplies, storage capacitors, and trigger bank could be varied from 500 to 5,000 watt-second. Thus, the discharge energy could be varied between about 130 w-sec to 1,300 w-sec per electrode for a single (3-electrode) unit to a minimum of about 33 w-sec and a maximum of 330 w-sec for a four-unit (12-electrode) sparker array. Besides increasing the sound energy linearly, the multiple-electrode, multiple-array system has a lower erosion rate for the electrode tips. The hydrophone elements could not be adjusted for the desired frequency and therefore were used as omnidirectional receivers.

DISCUSSION OF METHOD

The technique of beam-forming with multiple arrays of sound sources is analogous to wave-front diffraction phenomena as described by Huygen's principle in the treatment of light interference. Here, however, it applies to constructive interference of sound energy through use of multiple sound-source transmission and an analogous highly directional group of detectors (multiple hydrophones). The mathematical proofs

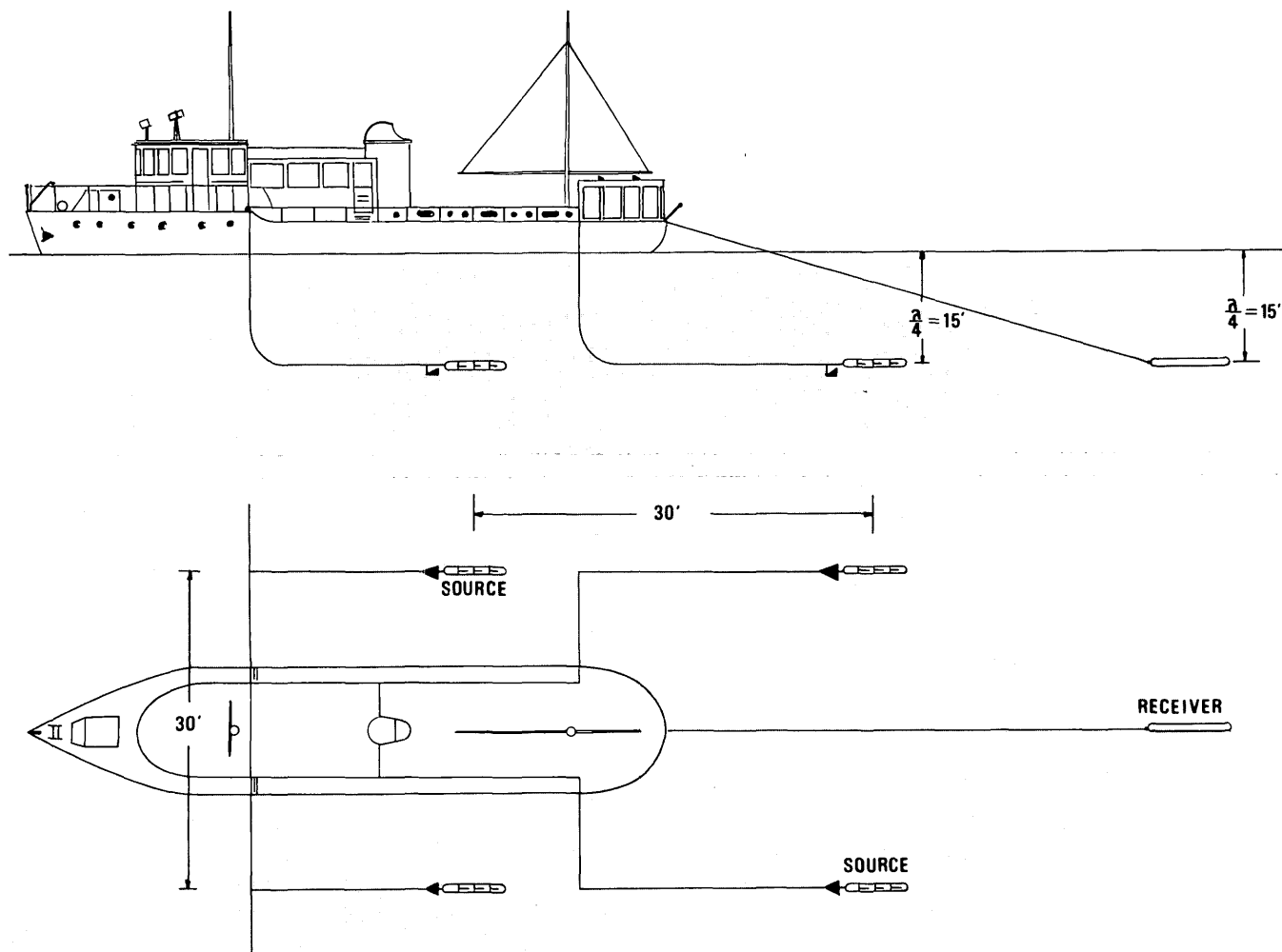


FIGURE 4.—Diagrammatic sketch of source and receiver geometry used for optimum transmission and reception of acoustical energy centered on a frequency of approximately 85 Hz (cycles per second). Use of two sources provides a cylindrical array, whereas, use of four sources provides a planar array that is more directional.

for composite signal enhancement are treated according to Fresnel in standard texts dealing with diffraction theory (see, for example, Lamb, 1945) and apply equally well, within prescribed boundary conditions, to continuous-wave sound propagation and reception (see, for example, Officer, 1958). For short-pulse sound sources, constructive interference applies only to the finite length of the signal, thus, geometrically representing a larger area pulsed wave front.

It can be readily demonstrated that for a given wave length (λ) a line array of multiple sources or receivers is most highly directionally perpendicular around such a line when the spacing (d) of the elements in the array is equal to half a wave length ($d = \lambda/2$). A single lobe around the linear array is thus generated perpendicular to the line so that the greatest transmission or reception of sound energy occurs only from within this lobe. Caulfield and others (1964) demon-

strated that substantial gains can be derived at the source of a single-electrode discharge system by varying the electrical parameters and the towing configuration. The acoustical-pulse shape can be modified from a short-pulse train rich in higher frequencies to a long-pulse train having most of its energy at frequencies near 100 Hz. In addition, adjustment of the towing depth of the source and receiver beneath the water surface to one-quarter the nominal wave length ($\lambda/4$) introduces four-fold reflective enhancement of in-phase energy and minimizes destructive reflecting signals that are out of phase (Caulfield, and others, 1964). A planar array is more highly directive than a linear array and, in its simplest form, would consist of three sources or receivers spaced at distances of half a wave length from each other (that is, an equilateral triangle). Multiple sources have also the benefit of being additive in power (Dobrin, 1960; Knott and Witzell,

1966). The towing depth for such a planar array again should be approximately a quarter of the lowest wave length of principal interest ($\lambda/4$).

For fixed frequency sources, the multiple-unit directional array is designed to be responsive to its tuned fundamental frequency, but for broad-band frequency sources producing a wide spectrum of sound energy (such as the sparker or a similar device) the directional array is also responsive to all the harmonics of the tuned frequency (that is, $d=N\frac{\lambda}{2}$, where N is a whole integer). The contribution of harmonics has the disadvantage of creating side lobes, but these lobes can be eliminated by selective band-pass filtering.

Depressors¹ such as those shown in figure 3 can be used to maintain towed sources and receivers at a fixed depth at high speeds (about 10 knots), although the cable weight alone is sufficient to depress streamers at slow speeds (4 knots). Earlier experiments (1965 Alaskan fiord runs) were conducted with spark arrays fastened near the bow of the vessel at a fixed depth of approximately 2.5 m (that is, $\lambda/4=2.5$ m for a frequency of 150 Hz). Standard model Scripps Institute of Oceanography (SIO) type bronze depressors were experimented with but were found unnecessary for the configuration adopted above.

EXAMPLES OF SEISMIC PROFILES

The reproduced profile in figure 5 is an east-southeast cross section from the east side of Resurrection Bay to the southern margin of Lowell Creek delta just south of Seward, Alaska. The clarity of this record and absence of side echoes from the fiord walls demonstrate the benefits of using a two-sparker array separated by 9 m in beam-forming geometry. The particularly broad signal signature of the combined direct arrival and water-surface-reflected arrival is due to the separation of the direct arrival and its surface multiple caused by deep towing (approximately 60 feet, or 18 m) of the hydrophone array. The water-surface-reflected bottom return is clearly identified as a phase-inverted "multiple" underlying the direct bottom return. Careful attention to hydrophone towing depth eliminates the doublet and increases the resolving power of the system.

Figure 6 is a reproduction of an east-west seismic reflection profile from the east side of Resurrection Bay to the northern margin of Lowell Point just south of Seward, Alaska. This profile shows also the "mul-

multiple" effect. The deep towing of the hydrophone array separates the direct arrival from the surface reflected arrival by approximately 25 milliseconds. This record is of particular interest because it demonstrates distorted sediment drapery over a bedrock salient as well as in the grabenlike trough.

An example of the resolution and penetration which is possible with the multiple-array sparker system can be seen better in a north-south seismic-reflection profile taken across Redondo submarine canyon, west of Redondo Beach, Calif. (fig. 7). The sediments just north of Redondo canyon are considerably more transparent acoustically than those south of the Redondo canyon fault boundary (Yerkes and others, 1967) (p. C97-C105, this chapter). Signal multiples of the outgoing pulse are eliminated and the record is here clearer because hydrophone depth-of-flight was better adjusted to approximately 4.5 m (15 feet). The depth adjustment also enhances the received signal. It might be added here that the surface-reflected multiple at the receiver can be eliminated also by towing the hydrophone at the surface (for velocity sensors) or very near the water surface (for pressure sensors). Surface streaming, however, has the disadvantage of being very noisy, reducing the constructive interference of the reflected signal and thus degrading the signal-to-noise ratio. For comparison, a more nearly east-west profile of Redondo canyon, shown in figure 8, was taken under conditions similar to those of the profile shown in figure 7. A relatively clean record was obtained from this apparently very narrow slot.

The relative efficiency of using beam-forming geometry in sparker profiling can perhaps best be seen by a direct comparison between two different acoustical profiling systems. It has been the author's observation, as well as that of others who have participated in such experiments, that a pneumatic source such as the Bolt Associates air gun equals or betters the acoustical penetration of a single-electrode electrical-discharge source when the discharge is driven by a 20,000-w-sec source and the air gun is operated at 1,700-1,800 pounds per square inch with a 10-cubic-inch pressure chamber. Not only was the acoustical penetration better, but the resolution was considerably improved because apparently the air gun did not exhibit a strong disturbing bubble pulse. The experience of using beam-forming geometry has demonstrated that the 5,000-w-sec sparker system with a 4-unit (12-electrode) array provides subbottom profiles equal to or better than a single air gun, both in depth penetration and in resolution. Thus, the 5,000-w-sec sparker system used by the Geological Survey can be considered more efficient than single-electrode electrical-discharge systems

¹ The depressor illustrated in figure 3 is a relatively inexpensive galvanized steel unit manufactured by the Kolstrand Supply Co., Seattle, Wash. These are comparable to the 15-pound bronze SIO depressors distributed by Kahl Scientific, El Cajon, Calif. The Kolstrand depressors are made to be used for mechanical stabilizers on outriggers of small vessels.

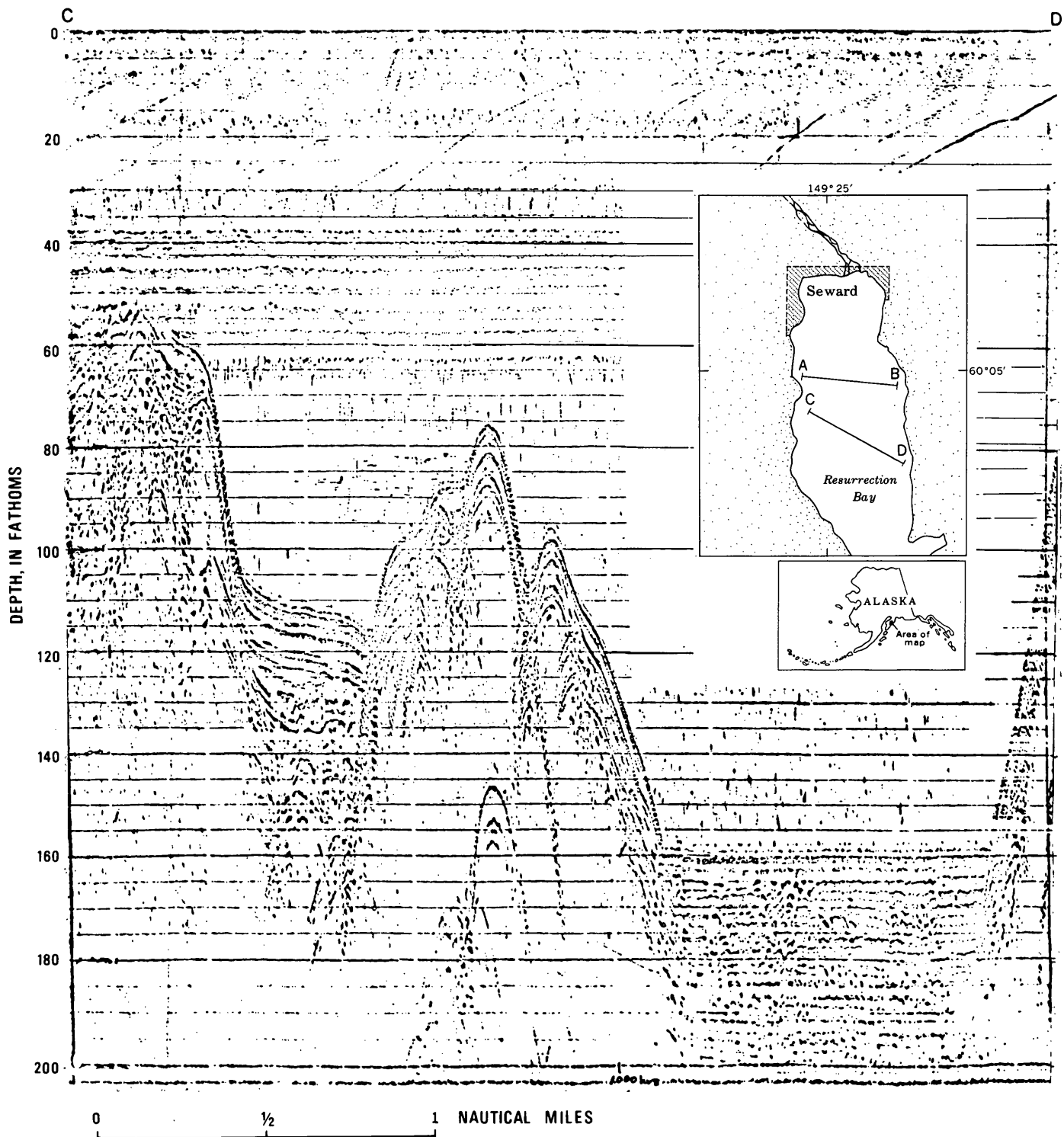


FIGURE 5.—An east-southeast cross section from the east side of Resurrection Bay to the southern margin of Lowell Point just south of Seward, Alaska. Two-sparker array of 5,000 w-sec firing at a 4-sec interval. Recording frequency band-pass is 80–125 Hz through a Rayflex amplifier system from a Rayflex miniature hydrophone to an Alden Precision Graphic Recorder. Half-wave rectification here allows only the negative half of the received signal to be recorded.

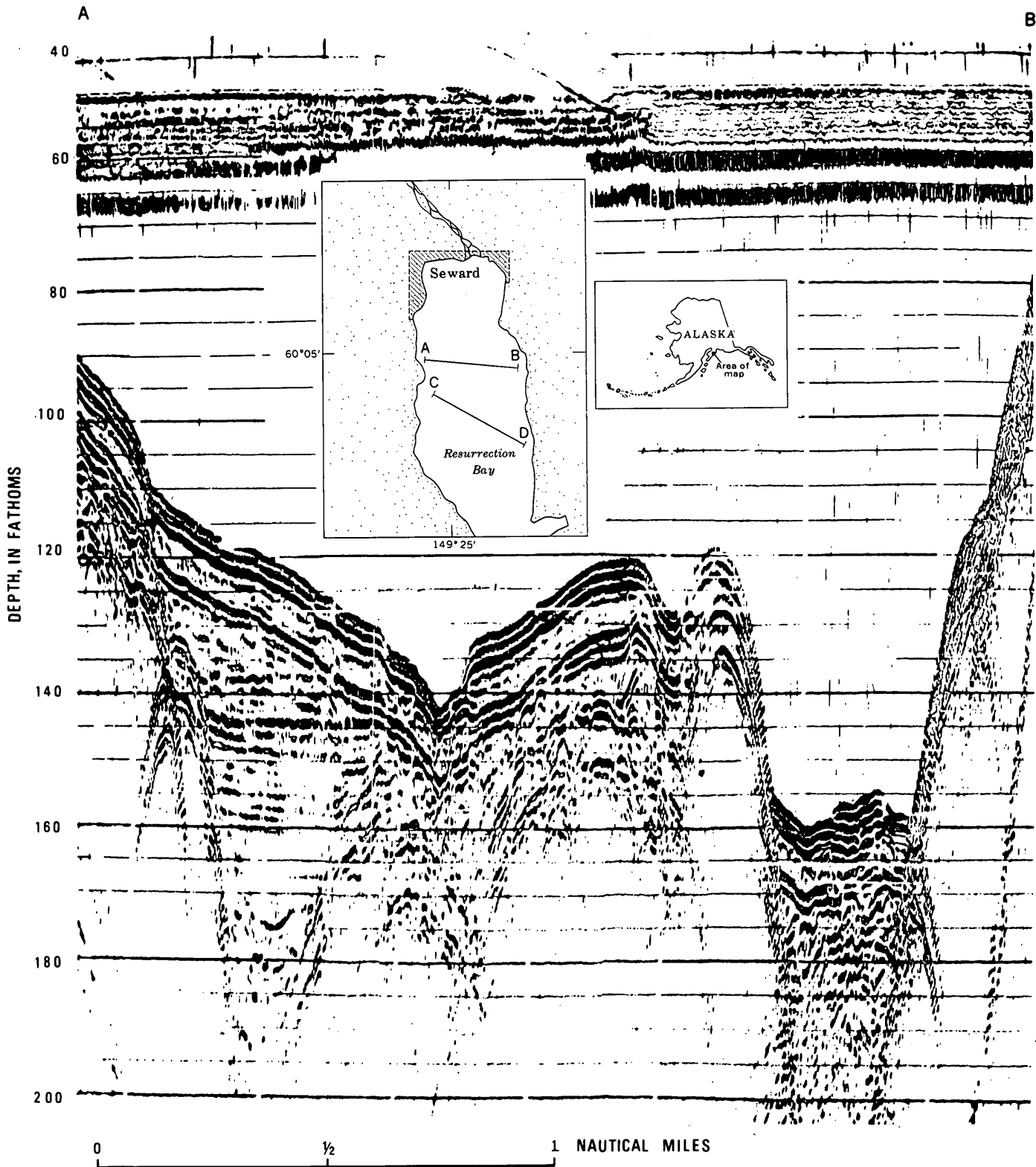


FIGURE 6.—An east-west cross section from the east side of Resurrection Bay to the northern margin of Lowell Point just south of Seward, Alaska. Two-sparker array with 5,000 w-sec operating at a 4-sec repetition rate. Recording frequency band-pass is 80-125 Hz through a Rayflex amplifier from a Rayflex miniature hydrophone to an Alden Precision Graphic Recorder. Half-wave rectification here allows only the negative half of the received signal to be recorded.

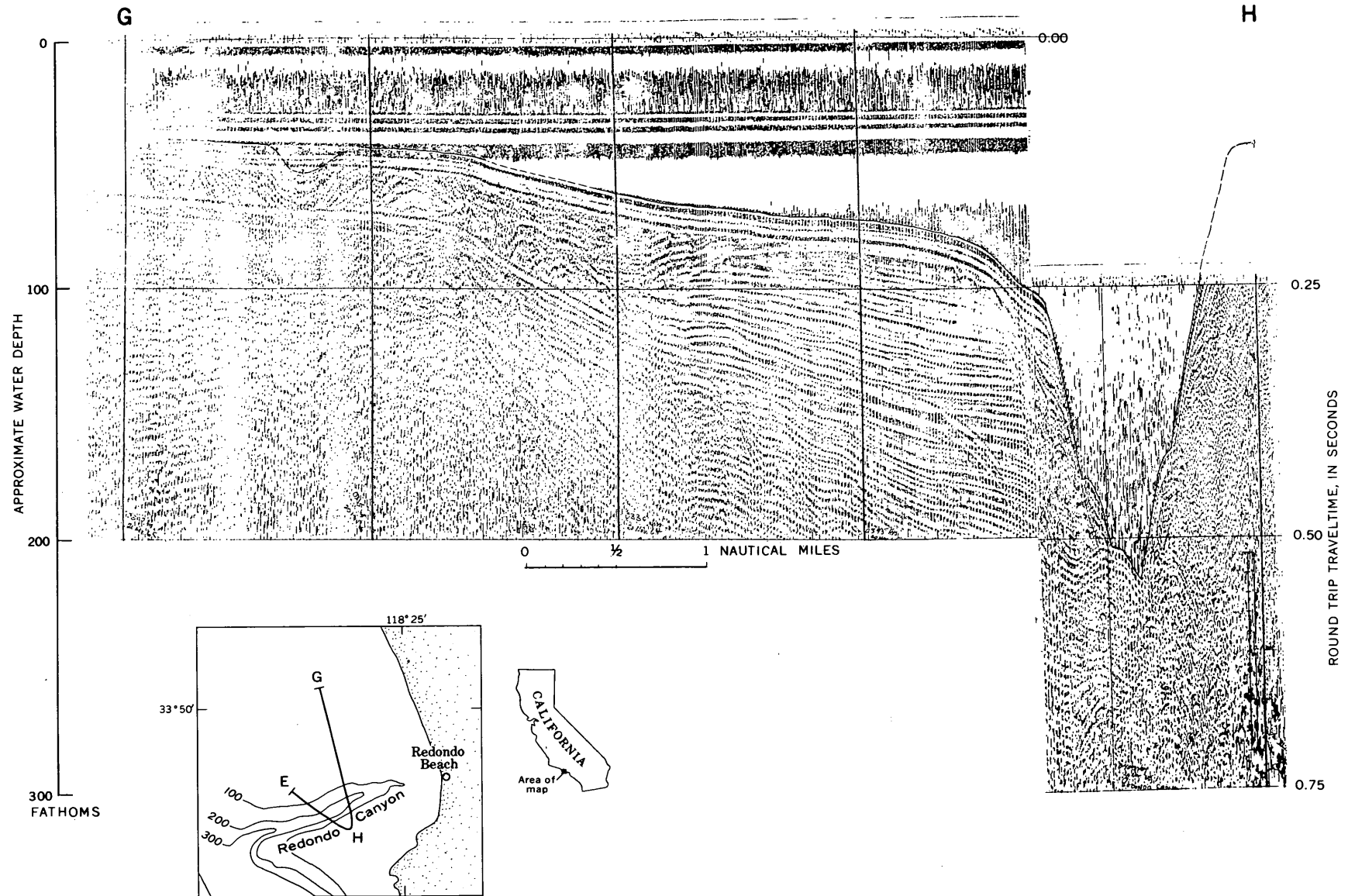


FIGURE 7.—Seismic profiles from north to south across Redondo submarine canyon, west of Redondo Beach, Calif. Vertical scale is two-way traveltime. Horizontal scale is indicated beneath the profile. The ship's speed was 6.5 knots. Two-sparker array separated by a distance of approximately 9 m (30 feet). The length of the sparker signature or outgoing pulse, is 24 msec. The Bolt Associates 10-element hydrophone array is towed 150 feet behind the source. Recording frequency is set at a band-pass of 80–125 Hz with half-wave rectification on a T. H. Giff GDRT recorder.

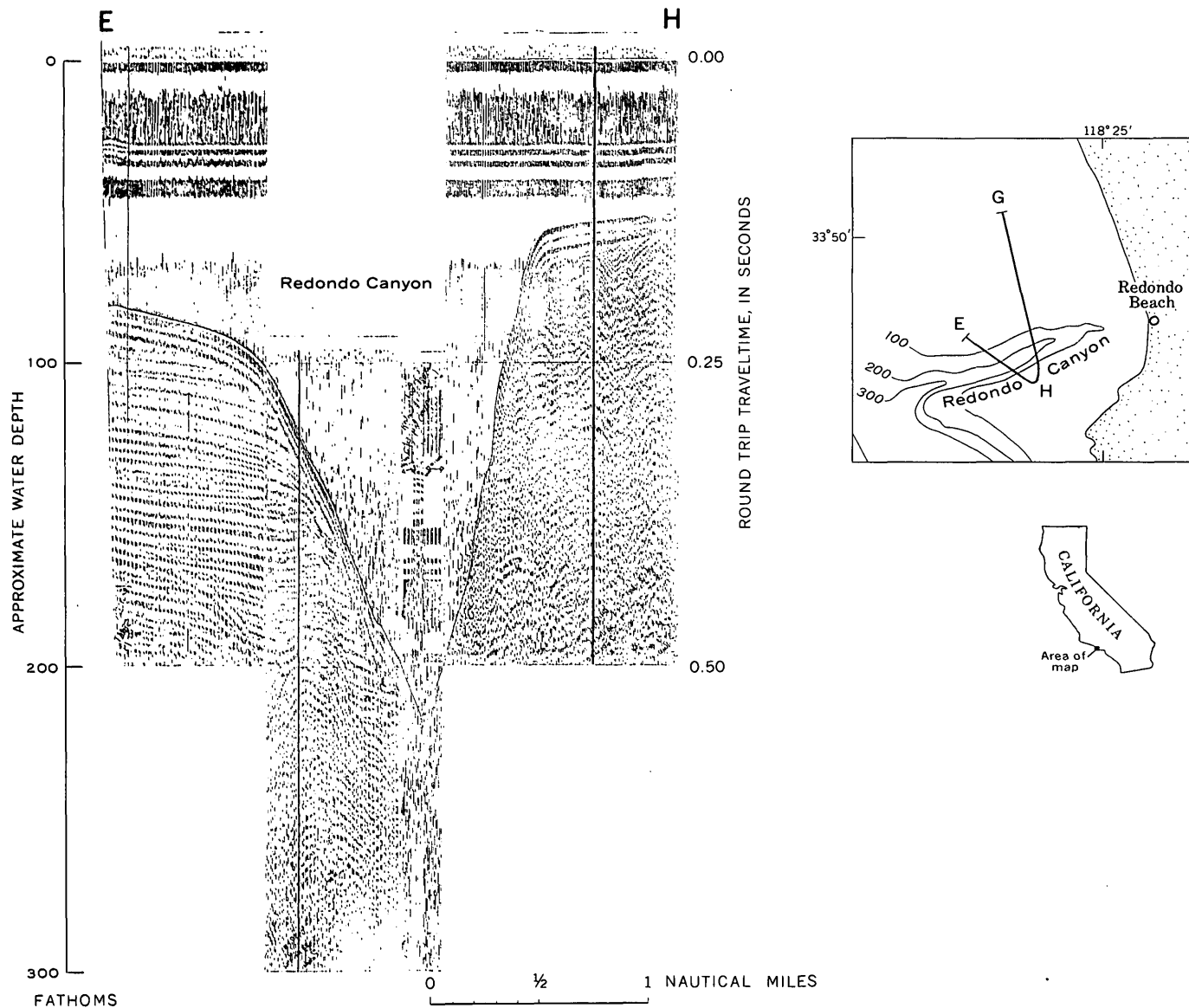


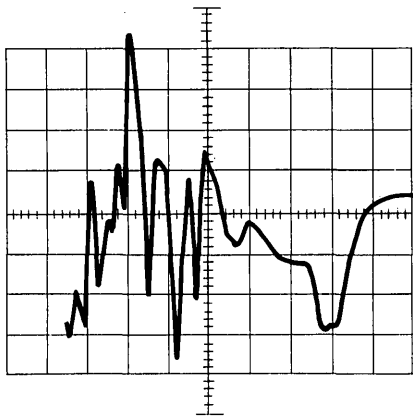
FIGURE 8.—Seismic profile northwest to southeast across Redondo submarine canyon west of Redondo Beach, Calif., from along line *E-H* on the inset diagram. As in figure 7, vertical scale is about 14 times horizontal scale. Two-sparker array separated by a distance of approximately 9 m (30 feet). The signal is received on a Bolt Associates 10-element hydrophone and recorded with half-wave rectification on a T. H. Giff GDRT recorder at a band-pass of 80–125 Hz.

which use four times more electrical energy. Quantitative comparisons are required to support what here can be specified only qualitatively at present.

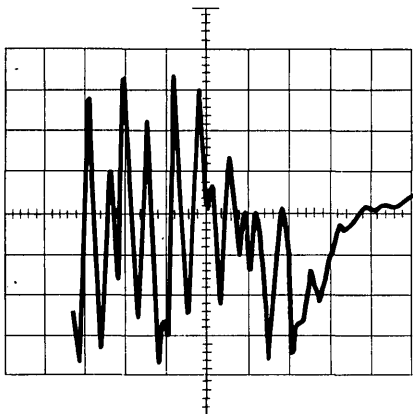
Because graphic recordings can sometimes be deceiving to the eye and therefore be subjectively interpreted, oscilloscope photographic records are used to show qualitatively the relative signal strength and the signal character depicted in figure 9. In each of the photographic records shown, the received signal is reproduced from one magnetic tape record. The recorded signals are band passed at 85–125 Hz with no changes in the recording except the manner of producing the acoustic signal; that is, all electrical controls were kept

constant and only the source was changed. The receiver was a Bolt Associates 10-element hydrophone towed at a depth of approximately 12 m, with a source-to-receiver separation of 50 m. The hydrophone towing depth was greater than optimum because depth control was dependent entirely upon lead-in cable weight to depress the hydrophone. Cable lengths which were short enough to give the optimum towing depth at the towing speed used caused insufficient source-to-receiver separation and created amplifier saturation. It was necessary, therefore, to forgo optimum tow depth in favor of better separation.

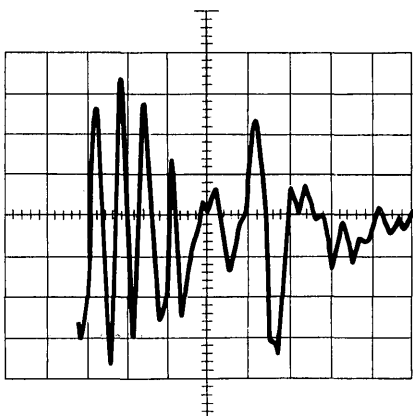
The profiling was done in the open water of Santa



Four-sparker array
at 5,000 watt-sec



Two-sparker array
at 5,000 watt-sec



Air gun discharging 1,750 psi
from a 10-cubic-inch chamber

FIGURE 9.—Oscilloscope traces recording the output from various acoustical sources. The ordinate represents 0.1 volt per division, and the abscissa represents 10 msec per division in each trace. Note especially the higher peak pressure and the greater peak width of the four-unit sparker array.

Monica Basin where water depths exceed 600 m. These recorded traces are not free-field measurements, however, because the signal observed represents both the direct arrival and its water-surface reflection as detected at the streaming hydrophone. The relative strength of the different acoustic sources is none the less clear. The marked peakedness (although the main pulse is broader) of the four-unit sparker array and the absence of a degrading bubble pulse is an advantage not shared by other methods of single-source high-energy acoustic sources.

CONCLUSIONS

Beam-forming techniques using multiple sources and receivers, according to the principles of continuous-wave propagation theory, can be applied with advantage to broad-band short-pulse signal propagation in electrical-discharge seismic profiling at sea.

A multiple-electrode sparker system consisting of two discharge units, spaced half a nominal wave length from each other, increases sound-source propagation area and improves signal directivity. Signal directivity is achieved by the additive nature of reflected signals whose travel time is equidistant from the source. When the two sources are parallel to the water surface and spaced a quarter wave length beneath the surface, the outgoing pulse is enhanced also by the water-surface reflected wave. The best signal-to-noise ratio is then achieved by reflections from points directly beneath the source. A four-unit sparker system set up in a square planar format, with discharge units spaced at half a wave length from each other and a quarter wave length from the water surface, improves both signal and directivity and increases resolution.

The precise quantitative improvement observed requires additional study, but experiments indicate that a two-unit array discharging 5,000 w-sec of electrical energy is equal in peak pressure output to a pneumatic acoustic source discharging compressed air at 1,750 psi from a 10-cubic-inch chamber. A four-unit array discharging 5,000 w-sec of electrical energy produces higher acoustic peak pressures than the pneumatic source. These results may be compared to higher energy single-electrode discharge sources operating at energies of 20,000 w-sec. Seismic profiles obtained by single-electrode 20,000-w-sec sources have been equaled with a pneumatic source operating at 2,000 psi from a 10-cubic-inch chamber over the geology. Therefore, the apparent increase in acoustic peak pressure implies an increased efficiency of energy transfer with multiple arrays.

The increase in peak pressures is probably due to the additive quality of multiple electrodes and also to the increased area of the acoustic source provided by the wide spacing of the discharge units. The character of the signal received at the hydrophone (from the direct arrival and its surface reflection) suggests that the multiple-electrode four-unit array emits a broad-band group of acoustic signals at each discharge point which are integrated with mutual interference into a broader but higher peaked pressure-pulse wave front than the two-unit array. Free-field measurements with a calibrated hydrophone are planned for experiments to provide a quantitative evaluation of the apparent gains so far observed qualitatively. The apparent principal peak width is approximately 6–10 msec wide and exhibits a very subdued bubble pulse.

REFERENCES

- Caulfield, D. D., 1962, Predicting sonic pulse shapes of underwater spark discharges: *Deep-Sea Research*, v. 9, p. 339–348.
- Caulfield, D. D., Hoskins, Hartley, and Nowak, R. T., 1964, Improvements in the continuous seismic profiler: *Geophysics*, v. 30, p. 133–138.
- Dobrin, Milton, 1960, *Geophysical prospecting*: 2d ed., New York, McGraw-Hill Book Co., Inc., 446 p.
- Grantz, Arthur, Plafker, George, and Kachadoorian, Reuben, 1964, Alaska's Good Friday earthquake, March 27, 1964, a preliminary geologic evaluation: U.S. Geol. Survey Circ. 491, 35 p.
- Hersey, J. B., 1963, Continuous reflection profiling chap. 4 of Hill, M. N., ed., *The Sea*: New York, John Wiley and Sons, p. 47–72.
- Hoskins, Hartley, and Knott, S. T., 1961, Geophysical investigation of Cape Cod Bay, Massachusetts, using the continuous seismic profiler: *Jour. Geology*, v. 69, p. 330–340.
- Knott, S. T., and Witzell, W. E., 1960, Instruction manual for precision graphic recorder (PGR): Woods Hole Oceanog. Inst. Ref. 60–38, 125 p.
- 1966, Multiple electrode spark source: U.S. Patent 3,245,032 [granted by the U.S. Patent Office, Apr. 5, 1966, on application filed May 19, 1961, Ser. 111,372, making 9 claims].
- Lamb, Horace, 1945, *Hydrodynamics*: 6th ed., New York, Dover Publications, 1945, 748 p.
- McClure, C. D., Nelson, H. F., and Huckaby, W. B., 1958, Marine sonoprobe, new tool for geologic mapping: *Am. Assoc. Petroleum Geologists Bull.*, v. 42, p. 701–716.
- Officer, C. B., 1958, Introduction to the theory of sound transmission with application to the ocean: New York, McGraw-Hill Book Co., Inc., 284 p.
- Van Reenan, E. D., 1964, Subsurface exploration by sonar seismic systems: *Am. Soc. Testing Materials Spec. Tech. Pub.* 351, p. 1–14.
- Yerkes, R. F., Gorsline, D. S., and Rusnak, G. A., 1967, Origin of Redondo submarine canyon, southern California, in *Geological Survey Research, 1967*: U.S. Geol. Survey Prof. Paper 575-C, p. C97–C105.



SUBSURFACE MORPHOLOGY OF LONG ISLAND SOUND, BLOCK ISLAND SOUND, RHODE ISLAND SOUND, AND BUZZARDS BAY¹

By A. RICHARD TAGG and ELAZAR UCHUPI, Woods Hole, Mass.

Abstract.—Continuous seismic profiles from Long Island Sound, Block Island Sound, Rhode Island Sound, and Buzzards Bay show a widespread reflector ranging in depth from 16 to 200 m below sea level or 0 to 160 m beneath the bottom. This reflector delineates the top of the pre-Cretaceous rocks. Relief of the reflector appears to be due mainly to fluvial erosion modified by glacial erosion.

Long Island Sound and Long Island and the other sounds and islands to the east have been interpreted in the past as lowlands and cuestas carved subaerially out of the shelf strata and later modified by glacial erosion and deposition. Dana (1890) suggested that the "Sound River" that carved the trough occupied by Long Island Sound flowed eastward and reached the sea by way of Mattituck, N.Y., and Great Peconic Bay. Evidence cited by Dana for the existence of such a river was the narrow depressions along the axis of Long Island Sound. Fuller (1914, p. 58) also believed that the "Sound River" flowed to the east, but he stated that the river reached the sea between Fishers Island and Greenport, N.Y. He also stated that the depressions believed by Dana to mark the valley of the former "Sound River" were much younger and were formed, at the earliest, during the last glacial advance. The trough carved by the "Sound River" supposedly was eroded during late Tertiary or early Pleistocene time. In 1906 Veatch (p. 31, pl. VI) suggested that the "Sound River" flowed west rather than east and reached the sea across western Long Island. Well data from this area (Suter and others, 1949, p. 38; Swarzenski, 1963, pls. 2, 3), however, show no evidence of a continuous channel in this section of Long Island. Channels cut into the Cretaceous rocks extend only about 20 kilometers south and have been cut by streams that drained northward into the sound.

¹ Contribution No. 1860 of the Woods Hole Oceanographic Institution.

These early speculations as to the origin of Long Island Sound and the other sounds were based on the surface and subsurface morphology of the islands and the bathymetry of the sounds. At that time no data were available from the subsurface of the sounds. Within the last two decades, geophysical methods have yielded information on the sub-surface morphology of these areas. A seismic refraction survey of Long Island Sound by Oliver and Drake (1951) showed that the pre-Cretaceous rocks were 50–260 meters below sea level. Relief of at least 60 m was found on the pre-Cretaceous rocks. Above the Paleozoic rocks, Oliver and Drake (1951) found a single seismic horizon that designated as "unconsolidated sediments." These sediments are probably Pleistocene in age, suggesting that the Cretaceous deposits of Long Island may not extend into Long Island Sound, at least not as far as the seismic lines of study. Using seismic reflection techniques, Smith (1963) and Drake and Smith (1964) showed that the surface of the pre-Cretaceous rocks is irregular and characterized by flat-bottomed, north-south-trending troughs that Smith (1963) believed were formed by glacial erosion. They also reported evidence of a valley of an eastward-flowing stream having a thalweg 122 m below sea level. J. B. Hersey, A. H. Nalwalk, and D. R. Fink (written commun., 1961) in a survey of Narragansett Bay with a continuous seismic profiler found several valleys on the pre-Cretaceous rocks more than 100 m below sea level.

SEISMIC-PROFILE STUDY

The present paper describes some seismic-profiling results obtained in Long Island Sound, the other sounds to the east, and Buzzards Bay, and supplements data already published about this region. About 450 km of continuous seismic profiles were made in Long

Island Sound, Block Island Sound, Rhode Island Sound, and Buzzards Bay with a 3,000-joule (watt-seconds) sparker in November 1965. The speed of the ship was about 9 km per hour. The sparker was programmed to discharge every 3 seconds; thus a sound pulse was produced every 6 m along the ship's track. Bottom and subbottom reflections were received by a five-element hydrophone array towed behind the ship. The returning signals were amplified and simultaneously recorded unfiltered on magnetic tape for later playback and filtered at frequencies of 75–150 cycles per second for visual recording. Profiles shown on figure 1 are interpretations of records obtained during this survey.

RESULTS AND CONCLUSIONS

All the profiles (fig. 1, p. C94–C95) show a strong reflecting horizon 16–200 m below sea level, or 0–160 m below the bottom. A chart (fig. 2B) showing the depth to this reflector was constructed by assuming velocities of 1,500 m per second in water and 1,800 m per second in the sediments above the reflector. Outcrops along the mainland shore and compressive velocities of sediment from Long Island Sound (Oliver and Drake, 1951) indicate that this strong reflector marks the top of the pre-Cretaceous rocks. The signals reflected from layers above the reflector were weak and discontinuous. The low seismic velocities reported by Oliver and Drake (1951) suggest that these sediments are unconsolidated. None of the seismic recordings show any evidence of pre-Pleistocene deposits.

Except for some deep channels southeast of Narragansett Bay, the pre-Cretaceous rocks in Block Island Sound, Rhode Island Sound, and in Buzzard Bay have little relief. The channels along profile 165 (fig. 1) may be seaward extensions of channels described by J. B. Hersey, A. H. Nalwalk, and D. R. Fink (written commun., 1961) at the entrance of Narragansett Bay. The pre-Cretaceous rocks display their greatest relief near Stratford Shoal. Here the rocks are deeply cut by flat-bottomed, broad, U-shaped troughs whose axes are more than 200 m below sea level, or about 160 m below the bottom of Long Island Sound. The U-shaped troughs are separated by narrow ridges that have side slopes of about 7–10°. Stratford Shoal, which has a minimum depth of 3 m, lies at the crest of one of these ridges. Smith (1963) reported that these depressions have closures and do not extend under Long Island. The U-shaped cross section and lack of seaward gradient suggest that these depressions were probably formed by glacial erosion,

along preglacial fluvial valleys. Because of a lack of seismic lines near the north shore of Long Island, it is impossible to determine whether these valleys extend under the island. The drainage indicated by these valleys may be pre-Cretaceous in age, or may be part of the drainage system that formed Long Island Sound in post-Cretaceous time, or a combination of both. The marked relief shown on the seismic profiles of the pre-Cretaceous rocks in this section of Long Island Sound contrasts with the low relief from well data of the same rocks in the subsurface in Long Island (fig. 2B, p. C96). This contrast may be partly due to the greater amount and continuous nature of the information now available from the sound, whereas the configuration of the surface of the pre-Cretaceous rocks under Long Island is based on a few scattered wells.

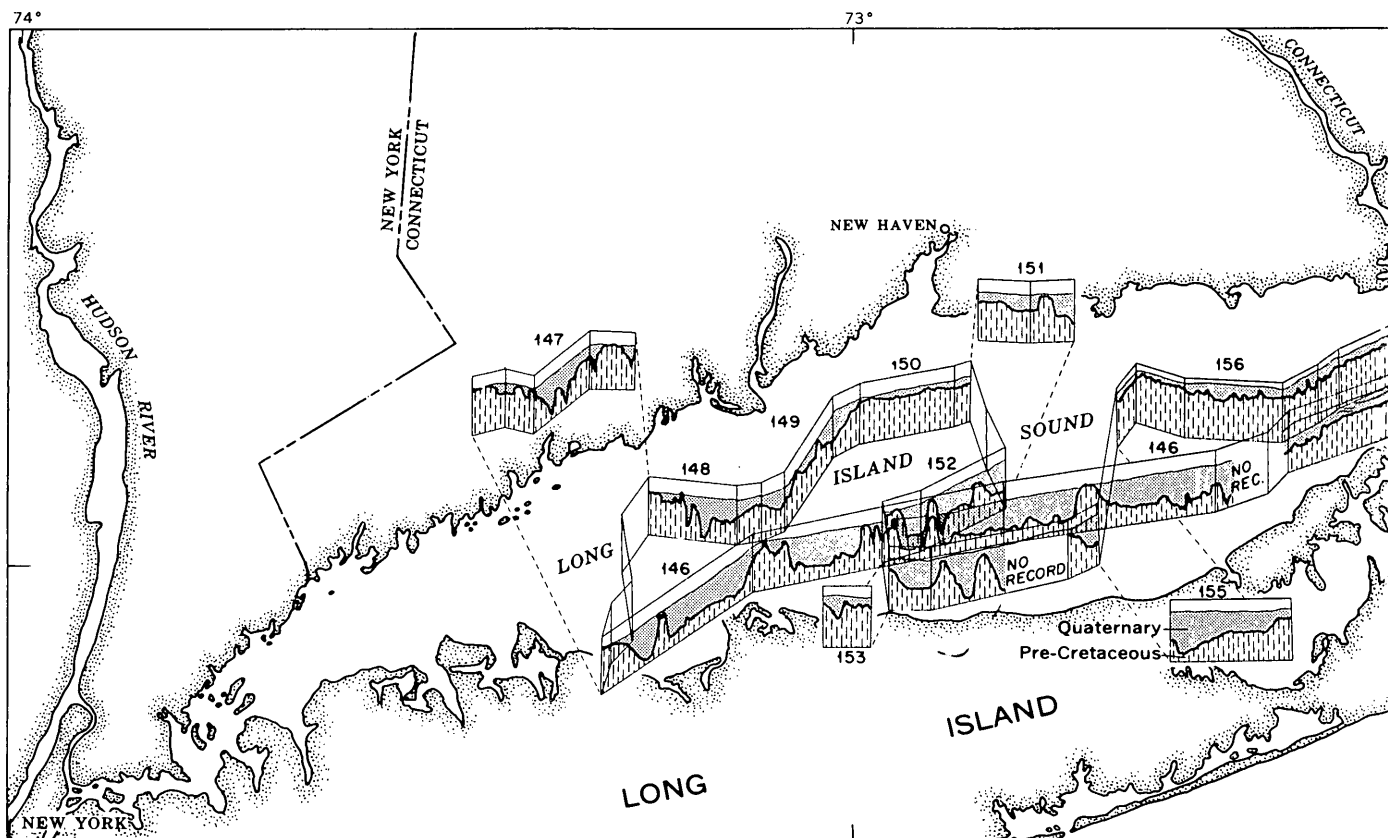
The depressions west of Stratford Shoal are in that area where Sanders (1960) and Zurflueh (1962) suggested that Triassic sediments may be present. The presence of relatively soft sedimentary rocks rather than crystalline or metamorphic rocks might account for the rather extensive erosion west of Stratford Shoal in contrast to the low relief displayed by the same reflector east of the shoal. However, none of the profiles near Stratford Shoal indicates bedded sediments below the widespread reflector, in contrast to profiles in the Acadian Triassic Basin in the Bay of Fundy where well-developed reflectors were found (Tagg and Uchupi, 1966).

The drainage system suggested by Dana (1890), Fuller (1914), and Veatch (1906) is not discernible on the pre-Cretaceous surface in the profiles taken during the present survey, possibly because the profiles are too far apart, because Pleistocene glacial erosion has obscured the earlier fluvial topography, or because the Valley occurs above the pre-Cretaceous surface. The present results differ from those of Drake and Smith (1964) who stated that they found evidence of a valley having a thalweg 122 m below sea level.

The present topography of the sounds is believed to be due to fluvial erosion that formed a lowland (sounds) and cuesta (islands) out of the shelf sediments. Later the fluvial topography was modified by glacial erosion and deposition. Glacial erosion deepened the lowlands to some degree and built up the cuesta by deposition of sediments removed from the sounds.

REFERENCES

- Dana, J. D., 1890, Long Island Sound in the Quaternary, with observations on the submarine Hudson River Channel: *Am. Jour. Sci.*, 3d ser., v. 4, p. 425–437.



- Drake, C. L., and Smith, M. C., 1964, Subbottom study of Long Island Sound [abs]: Geol. Soc. America Ann. Mtg., 77th, Miami, 1964, Program, p. 49-50.
- Fuller, M. L., 1914, The geology of Long Island, New York: U.S. Geol. Survey Prof. Paper 82, 231 p.
- Oldale, R. N., and Tuttle, C. R., 1964, Seismic investigations on Cape Cod, Massachusetts: Art. 145 in U.S. Geol. Survey Prof. Paper 475-D, p. D118-D122.
- Oliver, J. E., and Drake, C. L., 1951, Geophysical investigations in the emerged and submerged Atlantic Coastal Plain, pt. VI, The Long Island Sound area: Geol. Soc. America Bull., v. 62, p. 1287-1296.
- Sanders, J. E., 1960, Structural history of Triassic rocks of the Connecticut Valley and its regional implications: New York Acad. Sci. Trans., v. 23, p. 119-132.
- Smith, M. C., 1963, The Long Island Sound sub-bottom topography in the area between 73°00' W. and 73°30' W.: Columbia Univ. Fac. Pure Sci. unpub. M.S. thesis, 25 p.
- Suter, Russell, Laguna, Wallace de, and Perlmutter, N. M., 1949, Mapping of geologic formations and aquifers of Long Island, New York: New York Dept. Conserv. Water Power and Control Comm. Bull. GW-18, 212 p.
- Swarzenski, W. V., 1963, Hydrogeology of northwestern Nassau and northeastern Queens Counties, Long Island, New York: U.S. Geol. Survey Water-Supply Paper 1657, 90 p. [1964].
- Tagg, A. R., and Uchupi, Elazar, 1966, Distribution and geologic structure of Triassic rocks in the Bay of Fundy and the northeastern part of the Gulf of Maine, in Geological Survey Research, 1966: U.S. Geol. Survey Prof. Paper 550-B, p. B95-B98.
- Veatch, A. C., 1906, Outlines of the geology of Long Island, in Veatch, A. C., Slichter, C. S., Bowman, Isaiah, Crosby, W. O., and Horton, R. E., Underground resources of Long Island: U.S. Geol. Survey Prof. Paper 44, 394 p., Chap. I, p. 15-52.
- Zurflueh, E. G., 1962, A magnetic map of Long Island Sound and the southward continuation of geologic units in Connecticut [abs.]: Am. Geophys. Union Trans., v. 43, p. 435.

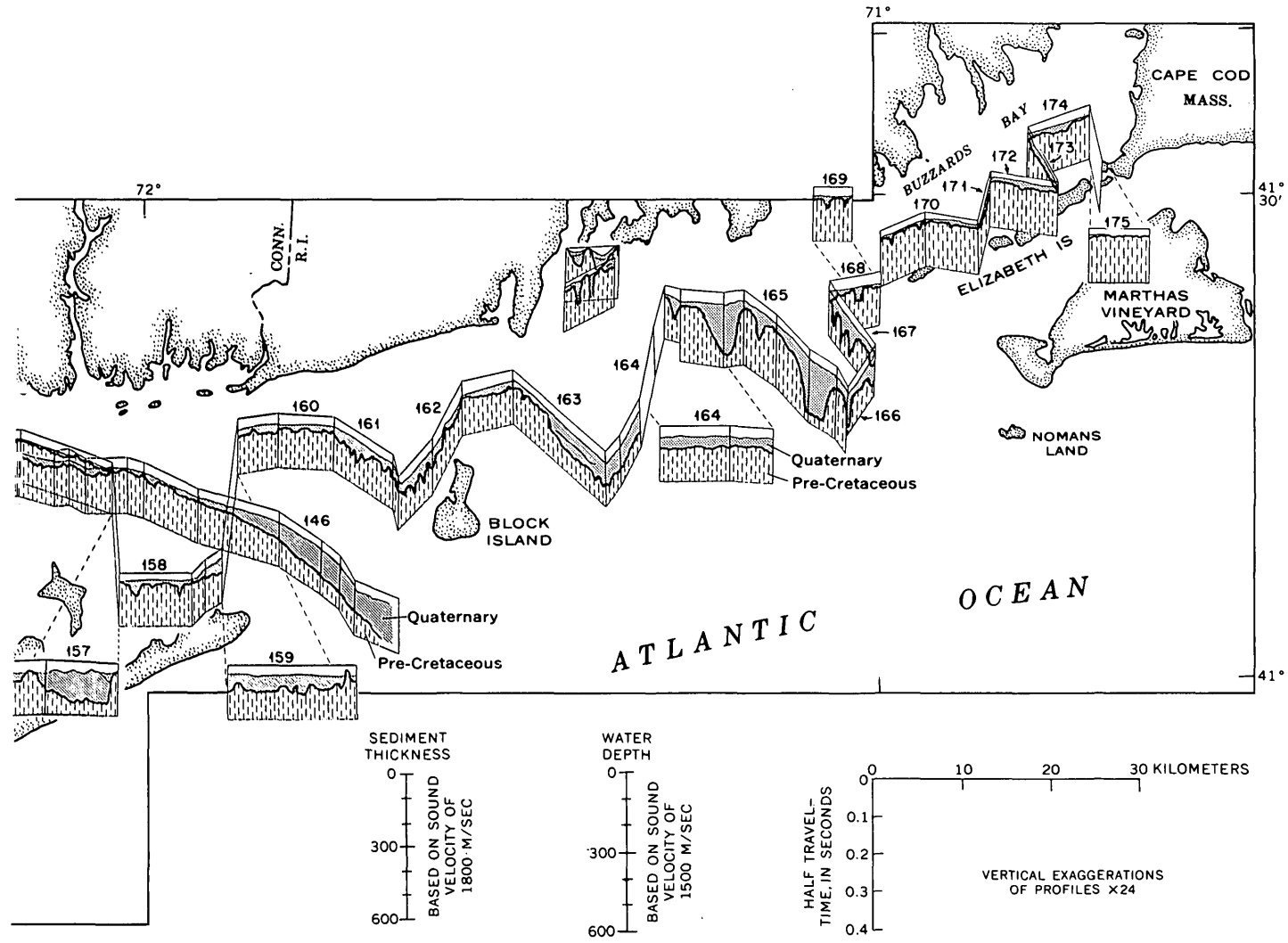


FIGURE 1.—Seismic profiles showing configuration of the most widespread reflector in Long Island Sound, Block Island Sound, Rhode Island Sound, and Buzzards Bay. This reflector delineates the surface of the pre-Cretaceous rocks. See figure 2A for geographic names. Profiles at the entrance of Narragansett Bay from J. B. Hersey, A. H. Nalwalk, and D. R. Fink (written commun., 1961).

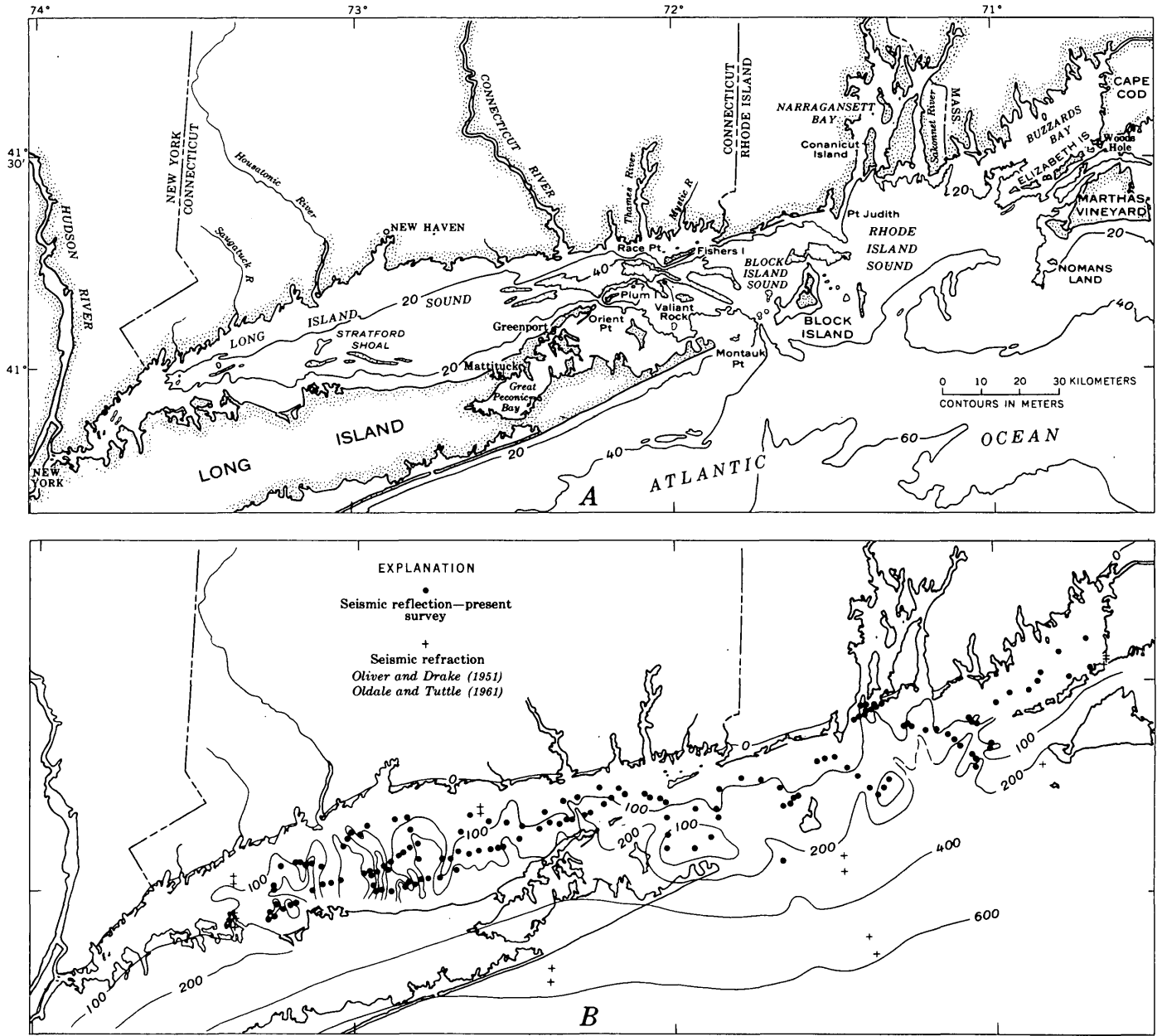


FIGURE 2.—A, Bathymetry of Long Island Sound, Block Island Sound, Rhode Island Sound, and Buzzards Bay. B, Depth of pre-Cretaceous rocks, in meters below sea level. Data for Long Island are from Suter and others (1949).



ORIGIN OF REDONDO SUBMARINE CANYON, SOUTHERN CALIFORNIA

By R. F. YERKES, D. S. GORSLINE,¹ and G. A. RUSNAK,
Menlo Park, Calif., Los Angeles, Calif., Menlo Park, Calif.

Abstract.—Redondo submarine canyon trends west-southwest for about 15 km from its head near the shoreline at Redondo Beach, 4 km north of the Palos Verdes Hills and about 45 km southwest of Los Angeles, Calif. The canyon is unusually straight and has a V-shaped cross section. Continuous reflection profiles show that the canyon formed along a structural trough that was created chiefly by faulting in middle Pleistocene time during relative uplift of the Palos Verdes Hills structural block south of the canyon. Subaerial erosion of the canyon head early in the late Pleistocene time is suggested by the presence, directly inland from the canyon head, of a buried westward-sloping channel. Down-canyon movement of longshore-drifted sediment has modified the canyon head, maintained the canyon below the level of low sea stands, contributed sediment to the extensive submarine fan at the canyon mouth, and eroded or maintained the leveed channels that incise the length of the fan.

Redondo submarine canyon (fig. 1) heads in water about 15 meters deep, about 300 m from the shoreline, and about 4 kilometers north of the Palos Verdes Hills on the southern California coast (about 45 km southwest of Los Angeles). The canyon has no present continuation on land (see cross section, fig. 1). It extends seaward (S. 70° W.) for about 15 km to the head of an extensive submarine fan at a depth of about 580 m; the fan slopes from the canyon mouth about 15 km southeastward to merge with the almost flat floor of the closed San Pedro basin at a depth of about 825 m (Emery, 1960, p. 48). The canyon is as much as 1.6 km wide, and its south wall is steeper, straighter, and higher than the north wall (figs. 2-6). Relief across the canyon at its deepest part is about 395 m. The longitudinal gradient decreases with increasing water depth from a maximum of about 15 percent at its head to less than 2 percent at its mouth, an average of about 3.6 percent.

At least three longitudinal leveed channels or valleys, only one of which is presently continuous, incise

the submarine fan. Emery (1960, p. 47) estimated the volume of the fan to be about 20×10^9 cubic yards (15.3×10^9 cubic meters) or 1.8 times the volume of the canyon. The area of the fan above the 403-fathom (740-m) contour (the depth of the large San Pedro basin to the south) is about 130 square kilometers. Three continuous reflection profiles made during this investigation show that the fan is at least 360 m thick; these dimensions yield a volume of about 47×10^9 cu m, or about 5.5 times that of the canyon. Comprehensive descriptions of the physiography of the canyon, its relation to the adjacent sea floor, its submarine fan, and the general character of the sediments and water have been given by Emery (1960) and Emery and Hulsemann (1963).

Submarine canyons are common features of continental margins. Although most are short and steep and head far from shore, a few head at or within the shoreline; some are as long as 240 km and as deep as 1,520 m below adjacent slopes. Although most major rivers have large submarine canyons associated with their mouths, the Continental Shelf off California and Baja California is characterized by relatively small submarine canyons that are not necessarily associated with rivers. Several of these canyons are being actively downcut along their axes (Dill, 1964), a process that appears to be related to coastal longshore drift. Redondo is typical of these latter canyons in that it is not associated with a modern stream valley, but lies at the downdrift (south) end of a coastal sediment cell (Crowell, 1952). Like most of the small, active California canyons studied by divers and by means of detailed echo sounding, Redondo has a steep, deep, cirquelike head. However, Redondo differs from other California canyons in that it has a relatively straight channel and no important tributaries, features that suggest structural control.

Three current hypotheses on the origin of submarine canyons are: (1) subaerial erosion followed by dia-

¹ Department of Geology, University of Southern California.

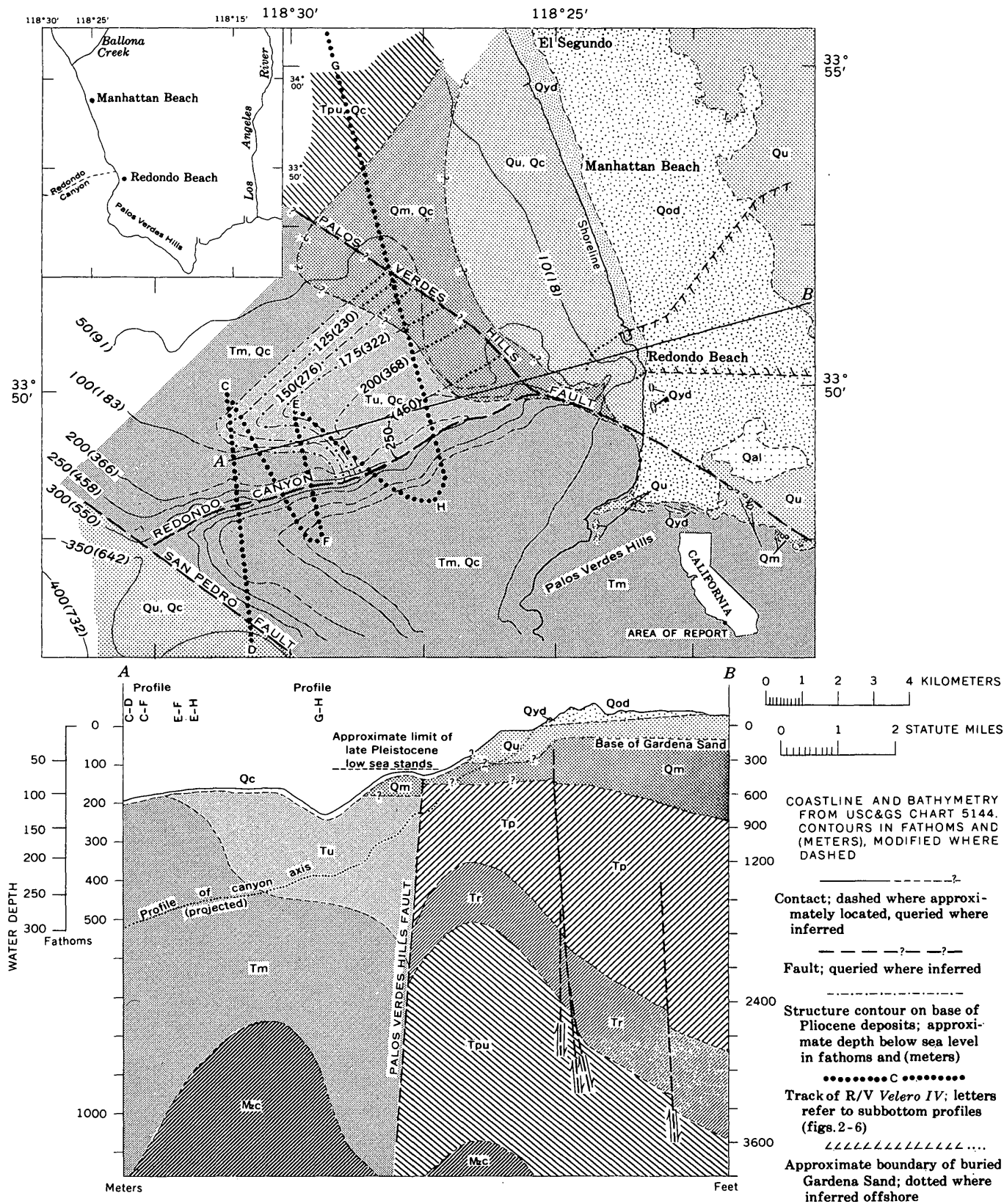
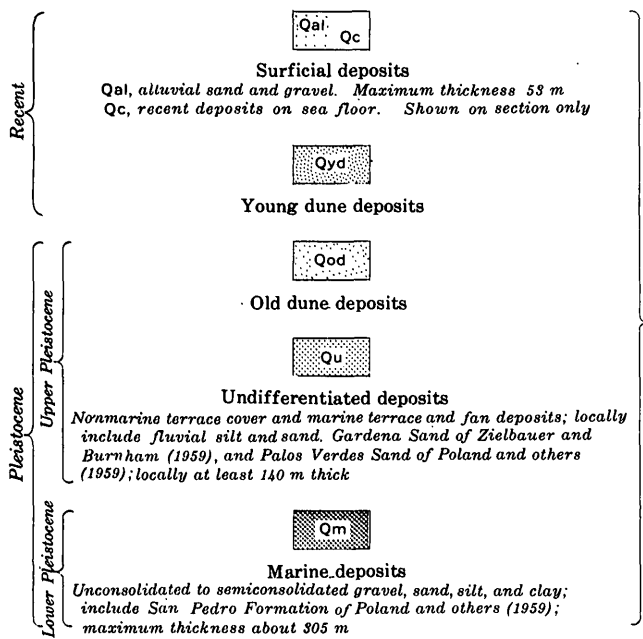


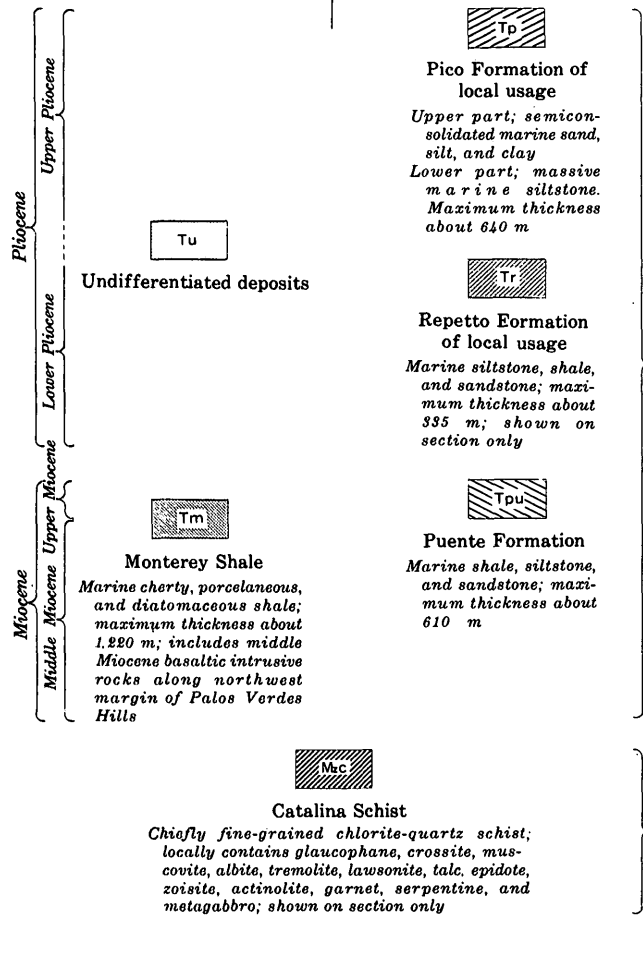
FIGURE 1.—Geologic map of Redondo submarine canyon area, California, showing November 1965 track of RV *Velero IV*, and geologic section along line A-B. Vertical scale is about $\times 11$ horizontal.

EXPLANATION



QUATERNARY

SOUTH WEST OF PALOS VERDES HILLS FAULT | NORTHEAST OF PALOS VERDES HILLS FAULT



TERTIARY

MESOZOIC OR OLDER

strophic or eustatic drowning and maintenance by submarine processes, (2) erosion entirely by submarine processes, or (3) structural control combined with some erosive process (Emery, 1960). No single hypothesis satisfactorily explains all canyons, or even all parts of some individual canyons. The upper parts (submerged less than 120 m) of many canyons were probably cut by subaerial erosion during glacially lowered sea levels (Emery, 1960, p. 50), but their heads must since have been modified by submarine processes to account for their very steep gradients, their cirque-like shape, and the evidence of active erosion.

This report presents evidence of structural control of Redondo canyon and subaerial erosion of the canyon head early in late Pleistocene time by a stream whose channel is now backfilled and buried. The report is based on a geologic map and section of the Redondo canyon area (fig. 1), the offshore parts of which are in turn based on continuous reflection sub-bottom (sparker) profiles (figs. 2-6).

METHODS AND SOURCES

The continuous reflection profiles were made by G. A. Rusnak, assisted by C. I. Winegard and R. F. Yerkes, of the U.S. Geological Survey, in November 1965 and June 1966 from the University of Southern California Research Vessel *Velero IV*, through the courtesy of D. S. Gorsline. The basic principles and techniques of continuous reflection profiling have been reviewed by Moore (1966, app.); equipment design and techniques used in this survey are described in a report by Rusnak (1967) (p. C81-C91, this chapter).

The geologic map and section (fig. 1) were prepared by Yerkes and were based on reflection profiles for the offshore areas and on the following sources for the onshore areas: California Department of Water Resources (1961), Crowder (1956), Poland and others (1959), Woodring and others (1946), Yerkes and others (1965), Zielbauer and Burnham (1959), and unpublished data from exploratory drill holes.

The velocity of the compressional sonic wave in water is close to 1,500 meters per second, but it varies with temperature, pressure at depth, and salinity. In sediment or sedimentary rock it varies with porosity and modulus of elasticity (degree of saturation and lithification) and ranges between about 1,460 and 4,000 m per sec (Hamilton, 1959; Shumway, 1960). Because specific values for velocity of sonic waves in the profiled media are not available, the vertical scales of the profiles represent only the uncorrected conven-

tional velocity of sound in sea water or the most porous and saturated unconsolidated sediment (about 1,500 m per sec), and therefore represent minima for the sediment-rock columns profiled. The actual thickness of the sediment-rock columns may be nearly three times as great as that of a water column of the same apparent length because of variation in velocity of the compressional sonic wave; for this reason the true dip of the faults illustrated cannot be determined.

The limit of resolution of the profiling method used is approximately 10 m at the assumed velocity of 1,500 m per sec, as determined by the nominal frequency of the seismic receivers; the frequency was limited by band-pass filtering to 80–125 cycles per second. Although higher frequencies would have provided greater theoretical resolution, they were rejected in favor of the longer, less rapidly attenuated, and therefore more deeply penetrating wavelengths.

The accuracy of location of the ship's track is dependent on the resolution of the ship's 16-inch radar—about ± 5 percent of the distance between the ship and identifiable geographic landmarks; all parts of the track are considered to be accurately located to about 0.5 km. The bathymetry of the base map (fig. 1), based on U.S. Coast and Geodetic Survey Chart 5144, was monitored by the ship's precision depth recorder and modified (indicated by dashed contours) where disparities were greater than permitted by the uncertainty of location.

INTERPRETATION OF PROFILES

Several types of lithology and the contacts between them are delineated by their distinctive acoustical signatures on the profiles. The Monterey Shale is characterized by relatively closely spaced, sharply defined sonic reflectors that are folded in a similar manner. The configuration of the upper surface of the Monterey conforms to the shape of the folds.

Profile *C-D* (fig. 2) crosses the Palos Verdes Hills anticline, which is underlain by the Monterey Shale, as are the adjacent Palos Verdes Hills. The Monterey there consists of laminated to thin-bedded silty, cherty, and phosphatic shale, diatomite, diatomaceous shale, and massive mudstone of middle and late Miocene age (Woodring and others, 1946).

In contrast to the Monterey, adjoining units are relatively unfolded, and the sonic reflectors within them are more widely spaced and persistent and give the appearance of thick-bedded strata (see Pliocene undifferentiated deposits on profile *G-H*, fig. 6). The undifferentiated Pliocene deposits are probably equivalent in large part to the upper Pliocene Pico Forma-

tion of local usage which, in the adjacent Redondo Beach-Torrance oil field, consists chiefly of siltstone and claystone with streaks of interbedded sandstone (Crowder, 1956).

A previously unreported wedge of undifferentiated Pliocene deposits, unconformably overlying the Monterey Shale, is well delineated north of Redondo canyon (fig. 1). This unit was deposited in an east-plunging structural depression in the Monterey Shale (see profile *C-F*, fig. 3). The inferred geologic history of the area indicates that the Monterey was folded in early Pliocene time (Yerkes and others, 1965, p. 18). In contrast, because the undifferentiated Pliocene deposits are virtually unfolded, little later folding has occurred in this area.

A unit of lower Pleistocene marine deposits (fig. 1) is distinguished on the profiles (fig. 6) by its clearly unconformable relation to the undifferentiated Pliocene deposits. The onshore equivalent of these marine deposits consists chiefly of unconsolidated silt, sand, and gravel (Poland and others, 1959).

The material of the Redondo fan at the base of the San Pedro escarpment (undifferentiated Pleistocene deposits and recent sea-floor deposits shown in the southwest corner of fig. 1 and right-hand, or south, end of fig. 2) is acoustically similar to the undifferentiated Pliocene deposits. However, estimates of the amount of sediment delivered to the canyon and ultimately available for deposit on the fan¹ and the inferred rate of sedimentation in the fan area (greater than 0.4 m per thousand years; Emery and Bray, 1962, fig. 10) suggest that at least the upper 140 m of the fan accumulated in the last 350,000 years and is therefore late Pleistocene to Recent in age. The more gently sloping parts of the sea floor in the area are mantled by a thin layer (10–20 m thick) of unconsolidated recent deposits that transgress all geologic contacts (see, for example, fig. 2). Moore (1960, p. 1126) indicated that such a layer on the slope south of the Palos Verdes Hills is about 12 m thick.

The profiles also reveal a fault that trends S. 70° W. along the axis of Redondo canyon (figs. 3–6); it extends from the Palos Verdes Hills fault on the east to the San Pedro fault on the west. The Redondo canyon fault dips northward and exhibits a minimum vertical separation of about 395 m (fig. 6). The fault cuts the undifferentiated Pliocene deposits (fig. 6) but does

¹ About 110,000 cu m per year of sediment may be delivered to the upper part of the canyon by longshore drifting. Johnson (1956, fig. 6) measured 124,000 cu m per year at El Segundo, 10 km north of the canyon head, and only 23,000 cu m per year at Redondo Beach, directly inland from the canyon head.

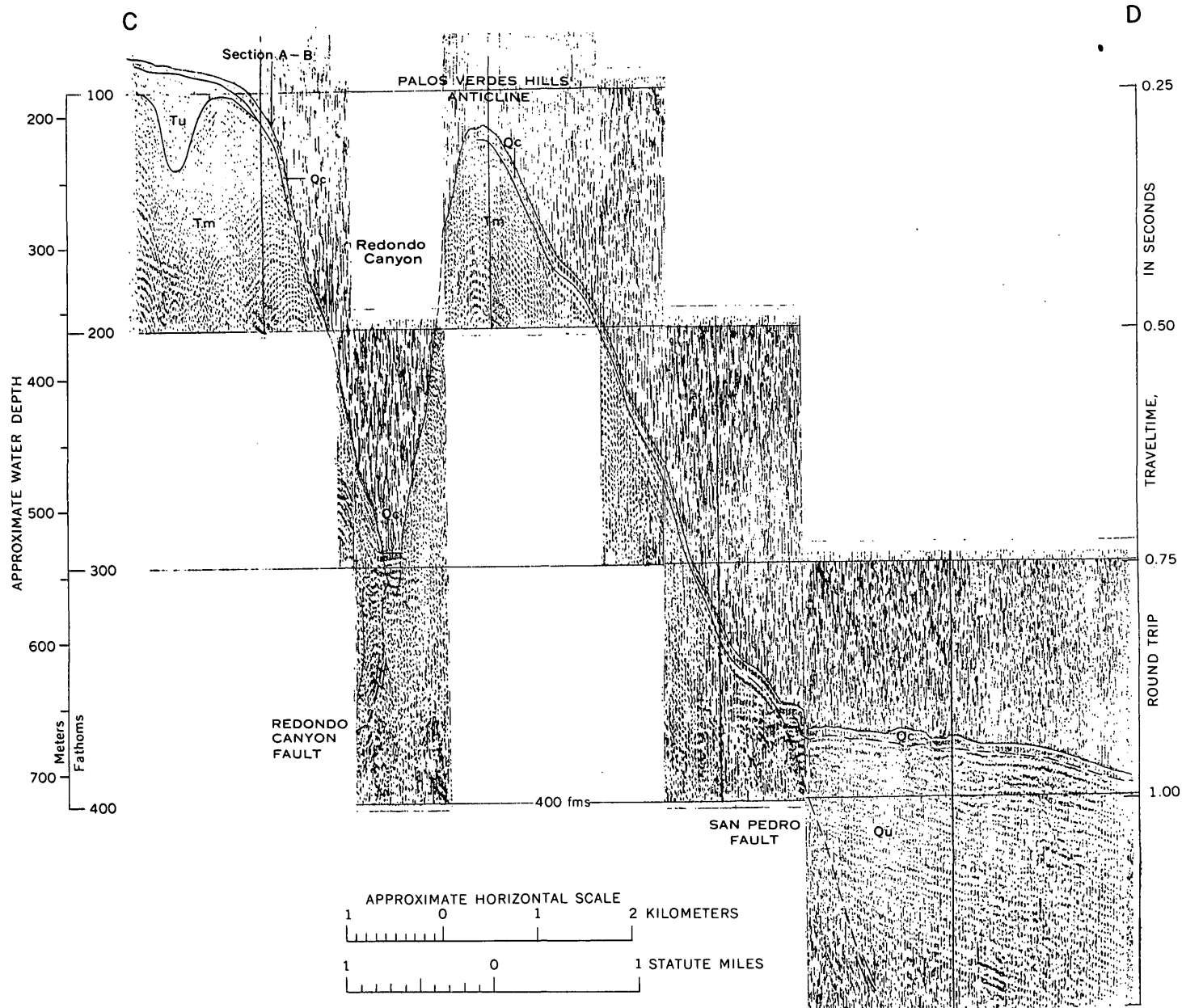


FIGURE 2.—Continuous reflection profile along line C-D. Vertical scale approximately $\times 14$ horizontal. Tm, Monterey Shale; Tu, undifferentiated Pliocene deposits; Qu, undifferentiated upper Pleistocene deposits; Qc, recent deposits on sea floor. See figure 1 for description of units and location of line C-D.

not appear to disrupt the recent deposits (fig.2). The fault forms the northwest boundary of the Palos Verdes Hills structural block which, on the basis of elevated marine terraces that flank the hills, has been uplifted about 395 m relative to present sea level since mid-Pleistocene time.

A unit of lower Pleistocene marine deposits is unconformable on both the undifferentiated Pliocene deposits and the Monterey Shale (middle or late Miocene) on either side of the inferred trace of the Palos Verdes Hills fault (fig. 6).

INFERRED GEOLOGIC HISTORY AND ORIGIN OF THE CANYON

The pre-Pleistocene geologic history of the Palos Verdes Hills area has been reviewed by Yerkes and others (1965, p. 18), who noted that activity along the Palos Verdes Hills fault in the area dates from at least early Pliocene time. This activity is indicated by a hiatus in the lower Pliocene section and unconformities in the upper Pliocene near the fault; the area north of the fault received as much as 610 m of upper Pliocene marine sediment, and areas both north

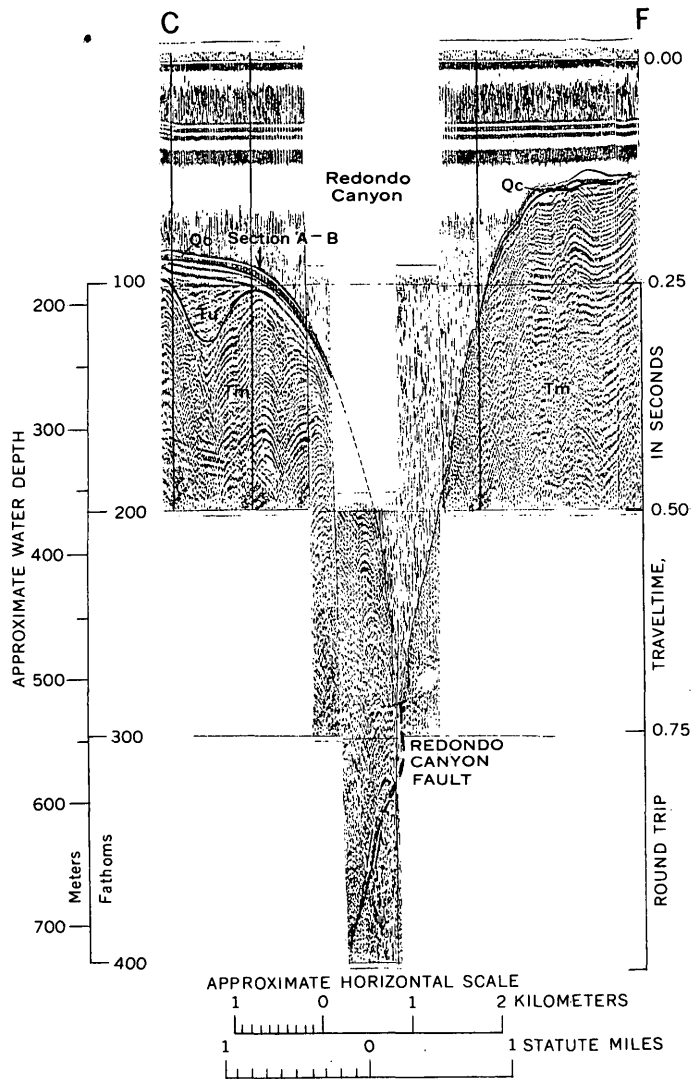


FIGURE 3.—Continuous reflection profile along line C-F. Tm, Monterey Shale; Tu, undifferentiated Pliocene deposits; Qc, recent deposits on sea floor. See figure 1 for description of units and location of line C-F.

and south of the fault received as much as 315 m of lower Pleistocene shallow-water clastic marine sediment.

In middle Pleistocene time, the time of the "Pasadenan orogeny," renewed uplift of the Palos Verdes Hills anticline occurred by downfolding of the flanks and subsidence of marginal areas. The folded upper Pliocene and lower Pleistocene strata ruptured along the Palos Verdes Hills, Redondo canyon, and the San Pedro faults as the hills were uplifted. Thirteen recognized marine terraces were cut around the periphery of the island formed by the hills during stillstands that interrupted the relative uplift. The highest and oldest of the platform is now at an altitude of about 395 m; the lowest and youngest is at an altitude of

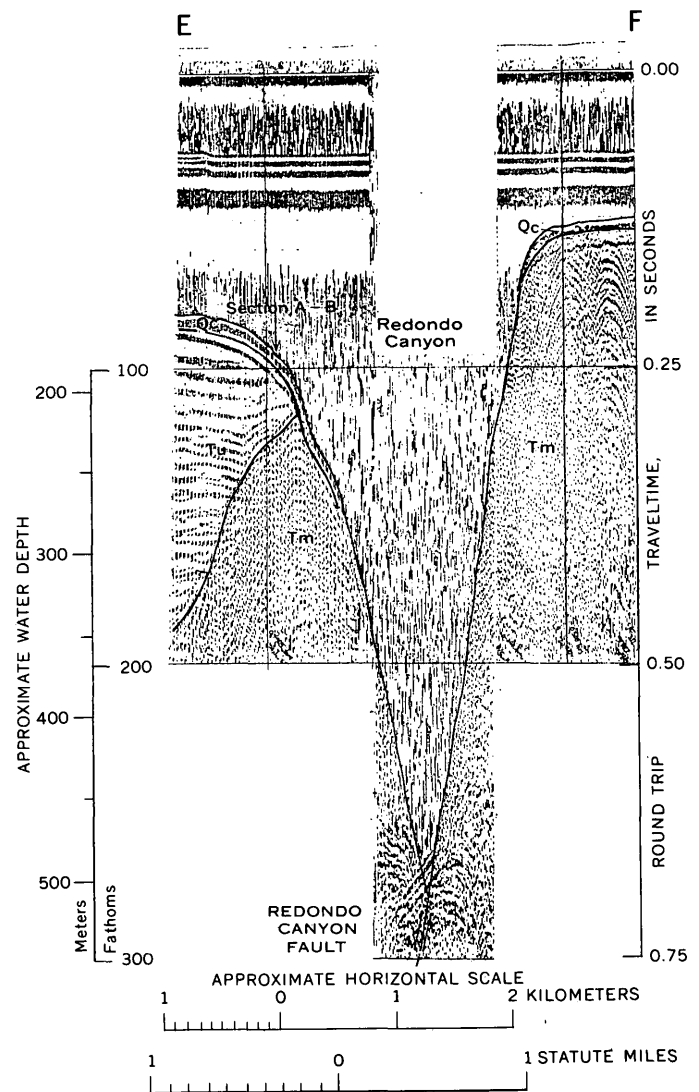


FIGURE 4.—Continuous reflection profile along line E-F. Tm, Monterey Shale; Tu, undifferentiated Pliocene deposits; Qc, recent deposits on sea floor. See figure 1 for description of units and location of line E-F.

about 40 m, and marine deposits on it (Palos Verdes Sand, mapped as part of the lower Pleistocene marine deposits) are about $91,000 \pm 15,000$ years old as determined by uranium-series disequilibrium dating of shell material (open-system model of J. N. Rosholt; reported by Yerkes and Wentworth, 1965, p. C-1, as 110,000 years and since revised to 91,000).

Although the head of Redondo canyon lies in an area where no land river debouches, Zielbauer and Burnham (1959) recognized and mapped a buried deposit of fluvial alluvium, their Gardena Sand (fig. 1) directly opposite the head of the canyon, as a result of a detailed drilling program. The Gardena Sand occupies a channellike depression about 1.5 km wide at the shoreline; the base of the sand slopes west-

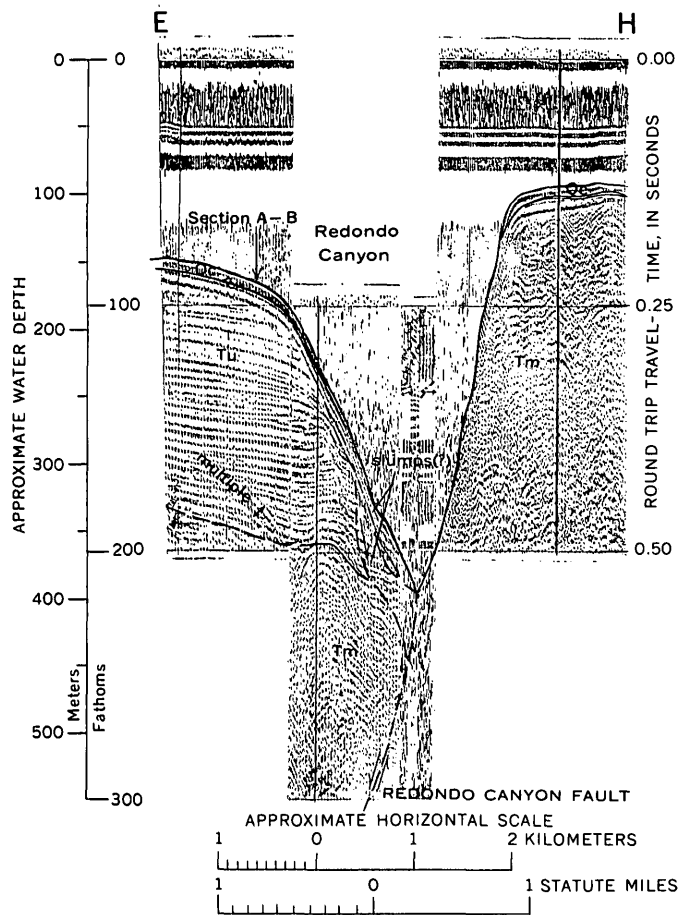


FIGURE 5.—Continuous reflection profile along line *E-H*. *T_m*, Monterey Shale; *T_u*, undifferentiated Pliocene deposits; *Q_c*, recent deposits on sea floor. See figure 1 for description of units and location of line *E-H*.

ward from an altitude of about 37 m below present sea level 1.6 km east of the shoreline to about 73 m below present sea level at the shoreline (fig. 1, cross section). The position, orientation, and altitude of the channel occupied by the Gardena indicate that it was formed by a stream that drained into the area now occupied by the head of Redondo canyon.

Crowell (1952, p. 66-67), on the evidence then available, suggested that (1) no river flowed to the upper part of the canyon during the time of its erosion and (2) the canyon heads at an altitude above the base of nearby alluvium-filled channels of Ballona Creek and Los Angeles River (fig. 1) that were cut into Pleistocene deposits during a Wisconsin(?) low sea stand. The canyon head was therefore inferred to postdate the Wisconsin(?) low sea stand. However, the Gardena channel was cut into deposits older than the Palos Verdes Sand and the channel fill was locally buried by deposits equivalent to the Palos Verdes,

whereas the Ballona and Los Angeles River channels were cut into deposits equivalent to the Palos Verdes. The Gardena channel was evidently formed by a river that was subsequently diverted to these or other channels (Calif. Dept. Water Resources, 1961, p. 39-40). The Gardena Sand was deposited by backfilling of the channel after the diversion early in late Pleistocene time, and then locally buried by later Pleistocene marine deposits in part equivalent to the radiometrically dated Palos Verdes Sand.

This sequence requires at least two low stands of the sea, one before and one after deposition of the Palos Verdes Sand (approximately 91,000 years Before Present). The inferred sequence is supported by reconstructions of late Quaternary sea-level fluctuations, which indicate minus (relative to present) sea stands at about 20,000, 55,000, and 120,000 years B.P. (Curry, 1965; Fairbridge, 1961, fig. 10).

If this reconstruction is valid, the canyon area has passed through at least three low sea stands, the earliest of which predated Palos Verdes Sand time and postdated most of the middle and late Pleistocene uplift of the Palos Verdes Hills along the Redondo canyon fault. During the earlier low stand, the upper parts of the canyon trend received their general form through subaerial erosion by the "Gardena" river along a preexisting structural trough that was created chiefly by the mid-Pleistocene faulting.

The Redondo canyon area possesses the three conditions considered by Crowell (1952) to be prerequisites for the formation of canyons by submarine erosion: (1) a source of sediment that reaches the upper parts of the canyon by longshore processes; (2) a steep near-shore submarine slope; and (3) a reduction in longshore current capacity, caused here by the headland of the Palos Verdes Hills block immediately south of the canyon.

As a result of an important regional investigation of the submarine basins off southern California, Moore (1966) concluded that turbidity currents have been the dominant process over the last million years; that relatively dense, high-velocity turbidity currents form in submarine canyons that head in zones of longshore sand transport; and that such currents can abrade rock-walled canyons and incise submarine fans (Moore, 1966, p. 96, 101).

Shepard and Dill (1966, p. 332-335) presented evidence that those canyons so situated that they intercept longshore-drifted sediment are eroded by sediment movement such as slow creep, sloughing as on the slip face of dunes, or occasional wholesale slides of sand masses; such movement is inferred to be cap-

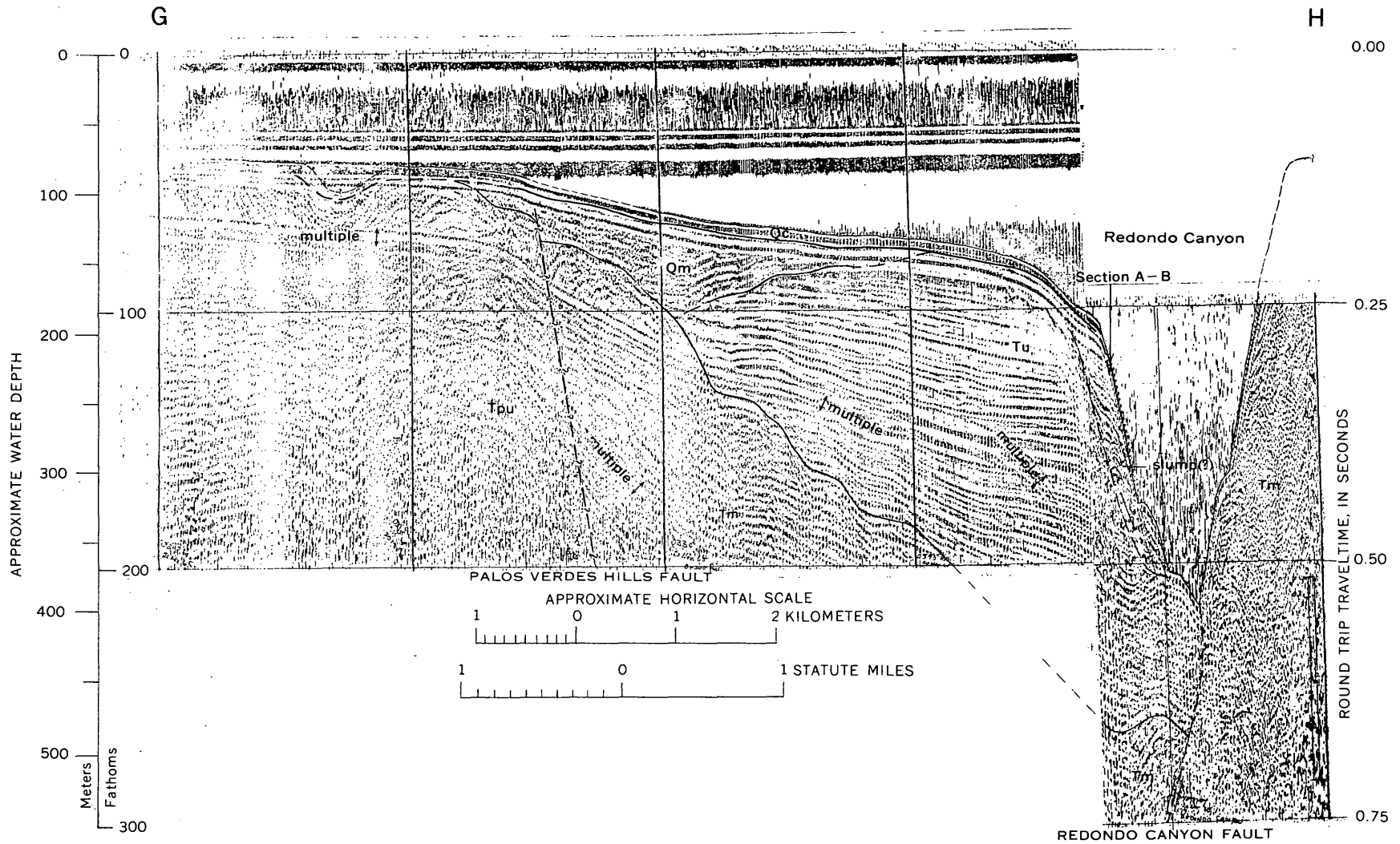


FIGURE 6.—Continuous reflection profile along line G-H. Tpu, Puente Formation; Tm, Monterey Shale; Tu, undifferentiated Pliocene deposits; Qm, Lower Pleistocene marine deposits; Qc, recent deposits on sea floor. See figure 1 for description of units and location of line G-H.

able of cutting back the canyon head and producing its cirquelike shape.

In Scripps submarine canyon near San Diego, small chutes have been cut into the cirquelike head; Dill (1964) noted that these chutes are migrating in an updrift direction, a process attributed to movement of longshore-drifted sand. And at Scripps, submarine erosion of Eocene sedimentary rocks has produced a canyon having vertical or overhanging walls for virtually its entire length of 2 km (Shepard, 1965, p. 304). Such erosional processes should be exceedingly effective in the less resistant material that underlies much of the Redondo Canyon area, and continuation of such erosion, if the sea level remains stabilized, should cause updrift (northward) migration of the canyon head. Such a migration of the head may have already begun, as suggested by the slight northward hook of the axis of the canyon head (fig. 1).

REFERENCES

- California Department of Water Resources, 1961, Ground water geology, in *Planned utilization of the ground water basins in the coastal plain of Los Angeles County*: California Dept. Water Resources Bull. 104, app. A, 191 p.
- Crowder, R. E., 1956, Torrance oil field: *California Oil Fields*, v. 42, no. 2, p. 5-8.
- Crowell, J. C., 1952, Submarine canyons bordering central and southern California: *Jour. Geology*, v. 60, no. 1, p. 58-83.
- Curray, J. R., 1965, Late Quaternary history, continental shelves of the United States, in Wright, H. E., Jr., and Frey, D. G., eds., *The Quaternary of the United States*, a review volume for the VII Congress of the International Association for Quaternary Research: Princeton Univ. Press, p. 723-735.
- Dill, R. F., 1964, Contemporary submarine erosion in Scripps submarine canyon [abs.]: *Dissert. Abs.*, v. 26, no. 8, p. 4569.
- Emery, K. O., 1960, The sea off southern California, a modern habitat of petroleum: New York, John Wiley and Sons, Inc., 366 p.
- Emery, K. O., and Bray, E. E., 1962, Radiocarbon dating of California basin sediments: *Am. Assoc. Petroleum Geologists Bull.*, v. 46, p. 1839-1856.
- Emery, K. O., and Hulsemann, Jobst, 1963, Topography, water, and sediments, pt. 1 of *Submarine Canyons of southern California*: Allan Hancock Foundation Sci. Research, Allan Hancock Pacific Exped., v. 27, pt. 1, p. 1-80.
- Fairbridge, R. W., 1961, Eustatic changes in sea level, in Ahrens, L. H., and others, eds., *Physics and chemistry of the earth*, v. 4: New York, Pergamon Press, p. 99-185.
- Hamilton, E. L., 1959, Thickness and consolidation of deep-sea sediments: *Geol. Soc. America Bull.*, v. 70, no. 11, p. 1399-1424.
- Johnson, J. W., 1956, Dynamics of nearshore sediment movement: *Am. Assoc. Petroleum Geologists Bull.*, v. 40, no. 9, p. 2211-2232.
- Moore, D. G., 1960, Acoustic-reflection studies of the continental shelf and slope off southern California: *Geol. Soc. America Bull.*, v. 71, no. 8, p. 1121-1136.
- 1966, Structure, litho-orogenic units and postorogenic basin fill by reflection profiling—California continental borderland: San Diego, Calif., U.S. Navy Electronics Lab., [Netherlands, Groningen, Univ., unpub. Ph. D. thesis] 151 p.
- Poland, J. F., Garrett, A. A., and Sinnott, A., 1959, Geology, hydrology, and chemical character of ground waters in the Torrance-Santa Monica area, California: U.S. Geol. Survey Water-Supply Paper 1461, 425 p.
- Rusnak, G. A., 1967, Geological survey high efficiency sub-bottom profiling, in *Geological Survey Research 1967*: U.S. Geol. Survey Prof. Paper 575-C, p. C81-C91.
- Shepard, F. P., 1965, Submarine canyons explored by Cousteau's diving saucer, in Whittard, W. F., and Bradshaw, R., eds., *Submarine geology and geophysics*, Proceedings of the Seventeenth Symposium of the Colston Research Society, University of Bristol, Apr. 5-9, 1965: London, Butterworth's, p. 303-309.
- Shepard, F. P., and Dill, R. F., 1966, Submarine canyons and other sea valleys: Chicago, Ill., Rand McNally and Co., 381 p.
- Shumway, George, 1960, Sound speed and absorption studies of marine sediments by a resonance method, pt. 1: *Geophysics*, v. 25, no. 2, p. 451-467.
- U.S. Coast and Geodetic Survey, 1964, Santa Monica Bay: U.S. Coast and Geodetic Survey Chart 5144, 9th ed., revised Sept. 28, 1964, scale 1:40,000.
- Woodring, W. P., Bramlette, M. N., and Kew, W. S. W., 1946, Geology and paleontology of the Palos Verdes Hills, California: U.S. Geol. Survey Prof. Paper 207, 145 p.
- Yerkes, R. F., and Wentworth, C. M., 1965, Structure, Quaternary history, and general geology of the Corral Canyon area, Los Angeles County, California: U.S. Geol. Survey open-file report 864, 228 p.
- Yerkes, R. F., McCulloh, T. H., Schoellhamer, J. F., and Vedder, J. G., 1965, Geology of the Los Angeles basin, California—an introduction: U.S. Geol. Survey Prof. Paper 420-A, 57 p.
- Zielbauer, E. J., and Burnham, W. L., 1959, West coast barrier basin project geologic investigation—Manhattan Beach to Palos Verdes Hills [California]: Los Angeles County Flood Control Dist. unnumbered rept., 22 p., 19 pls.



ACTIVITY COEFFICIENTS FROM EMF MEASUREMENTS

By C. L. CHRIST and PAUL B. HOSTETLER, Menlo Park, Calif.

Abstract.—Mean activity coefficients, γ_{\pm} , are readily determinable from measurements of potential on emf cells employing cation-sensitive electrodes, and having no liquid junction. Accurate results are obtained only when successive measurements are made on solutions having relatively small incremental differences in concentration. Recognition of this fact leads to a new graphical method for treating the experimental data, which is superior, both in principle and in practice, to previous methods.

Knowledge of the values of activity coefficients of electrolytes in aqueous solution is of fundamental importance in the study of geochemical equilibria (Hem, 1961; Garrels and Christ, 1965). The values for a large number of electrolytes at 25°C are given in the literature (see, for example, Parsons, 1959; Robinson and Stokes, 1959); however, for many electrolytes the data are both incomplete and of indifferent quality. In addition, for problems of practical geochemical importance, one needs to know the values of the activity coefficients over as wide a range of temperature as possible, as well as the values for mixed electrolyte solutions. Thus, any convenient and rapid method of determining these quantities is of considerable value.

The recent development of cation-specific membrane electrodes makes possible just such a convenient and rapid method. For example, Eisenman (1966) has determined the mean activity coefficients of sodium chloride, $\gamma_{\pm\text{NaCl}}$, in aqueous solution at 0°, 25°, and 50°C, and over a molality range of 0.13 to 6.14, using a Na^{+1} -sensitive glass electrode paired with an Ag-AgCl electrode. Hostetler and others (1967) used a K^{+1} -sensitive glass electrode paired with an Ag-AgCl electrode to determine aqueous $\gamma_{\pm\text{KCl}}$ over temperature and molality ranges of 10° to 50°C and 0.01 to 1.0 molal.

During the course of this latter investigation a new graphical method was developed for obtaining the values of γ_{\pm} from the measurements of the electromotive force of the cell employed. It is the primary purpose of the present paper to describe this graphical procedure.

BACKGROUND AND THEORETICAL BASIS

Eisenman (1966) has reviewed, in comprehensive fashion, both the electrochemical theory and practical applications of cation-sensitive electrodes; a discussion of glass electrodes sensitive to Ca^{+2} and other divalent cations was given by Truesdell and Christ (1967). Recently, nonglass membrane electrodes have been developed commercially by Corning Glass Works, Corning, N. Y., and Orion Research, Inc., Cambridge, Mass. Generally speaking, electrodes sensitive to H^{+1} , Li^{+1} , Na^{+1} , K^{+1} , Rb^{+1} , Cs^{+1} , NH_4^{+1} , Ag^{+1} , Tl^{+1} , Mg^{+2} , Ca^{+2} , Sr^{+2} , and Ba^{+2} are available.

To determine the mean activity coefficient, $\gamma_{\pm\text{CA}}$, of an electrolyte, CA, a C^{+z} -sensitive membrane electrode is paired with an electrode reversible to the anion, A^{-z} , to form an emf cell, known here as cell 1 and written as

C^{+z} -sensitive electrode, $\text{CA}(m)$, C^{-z} -sensitive electrode, where $\text{CA}(m)$ denotes the electrolyte in solution at molal concentration m . For example, cell 2, the cell used for determining $\gamma_{\pm\text{KCl}}$, was (Hostetler and others, 1967)

K^{+1} -sensitive electrode, $\text{KCl}(m)$, Ag-AgCl electrode.

It is an important feature that cells of this kind are without liquid junction.

Similarly, electrolytes of type formula MX , M_2Y , NX_2 , or NY , can be investigated with presently available electrodes; here M and N are monovalent and divalent cations, and X and Y are monovalent and divalent anions respectively. Thus, the cation-sensitive electrodes listed in the foregoing can be combined with various anion-sensitive electrodes, including the Ag-Ag halide electrodes and various electrodes reversible to sulfate ions, and possibly others (Ives and Janz, 1961), to determine the activity coefficients of a variety of electrolytes in either monoelectrolyte or polyelectrolyte solutions.

The potential, E , developed by cell 1 is given by the equation:

$$E = E' + S(T) \log(\gamma m), \quad (1)$$

where $(\gamma m) = (\gamma_{\pm} m_{\pm})_{CA}$, and $S(T) = 2(2.303RT)/nF$. R is the gas constant, n is the charge on the cation C (equal to that of the anion A), T is the absolute temperature, F is the Faraday, and m is the molality of the CA solution. Equations for the potentials developed in cells containing unsymmetrical electrolytes (M_2Y or NX_2), and for polyelectrolyte solutions, are similar in form to equation 1, and can be derived readily by analogy to the equations given in Harned and Owen (1958) for cells using the hydrogen electrode.

In the following, we consider the example of the determination of $\gamma_{\pm KCl}$ using cell 2. For this cell, $n=1$ and, therefore, $S(T) = 2(2.303RT)/F$.

GRAPHICAL PROCEDURE

The customary procedure for using equation 1 is to compare the potential, E_s , of a standard solution of molality, m_s , and of known γ_s , with the potential, E_x , of a solution of molality, m_x , to determine γ_x , in this way eliminating E' . Equation 1 then yields the equation

$$\frac{E_x - E_s}{S(T)} - \log \frac{m_x}{m_s} + \log \gamma_s = \log \gamma_x. \quad (2)$$

This method, which is analogous to that employed in pH determinations, was used by Eisenman (1966) in his determination of $\gamma_{\pm NaCl}$. It is seen from equation 2, that some one single value of the activity coefficient, γ_s , for a solution of molality, m_s , must be assumed in order to solve the equation for the γ_x . Eisenman (1966) used, for example, the value $\gamma_s = 0.657$ for 1.00*m* NaCl at 25°C.

In the derivation of equation 2 from equation 1, it is necessary to assume that E' is a constant. However, the value of E' does not remain constant over the long periods of time and over the wide range of solution concentrations found in experimental practice. E' can be treated accurately as a constant only when successive measurements of potential are made on solutions of relatively small incremental differences in concentration. Recognition of this fact leads to the new treatment which follows.

As previously stated by Hostetler and others (1967), for successive measurements of potentials E_{n-1} and E_n , of solutions of concentrations m_{n-1} and m_n , equation 1 on elimination of E' leads to

$$\frac{E_n - E_{n-1}}{S(T)} - \log \frac{m_n}{m_{n-1}} = \log \gamma_n - \log \gamma_{n-1} \quad (3)$$

or,

$$(\Delta \log \gamma)_{n,n-1} = \frac{\Delta E_{n,n-1}}{S(T)} - (\Delta \log m)_{n,n-1}. \quad (4)$$

From the experimental values of $\Delta E_{n,n-1}$ and $(\Delta \log m)_{n,n-1}$ (for a given temperature), the values of $(\Delta \log \gamma)_{n,n-1}$ are calculated using equation 4. The values of $-(\Delta \log \gamma / \Delta m)_{n,n-1}$ are then plotted as chords of length, $\Delta \log m_{n,n-1}$, against $\log m$, as shown in figure 1. The resulting plot is differentiated graphically using the "chord-equal area" method (Klotz, 1964; Running, 1927) to yield the continuous curve, $-(d \log \gamma) / dm$ versus $\log m$. This differentiation is carried out by drawing a smooth curve through the chords in such a way that the sum, (ΣA_u) , of all the areas of the upper triangles, such as U, is equal to the sum, (ΣA_l) , of all the areas of the lower triangles such as L. The mathematical justification for this method is given in Running (1927).

In actual practice, as a guide to drawing the final experimental curve of $-(d \log \gamma) / dm$ versus $\log m$, a preliminary curve based upon Debye-Hückel theory is drawn. The two area sums, ΣA_u and ΣA_l , are then determined; the difference between these two sums is noted, and the experimental curve then adjusted by trial and error until this difference is minimized.

The preliminary-guide curve was calculated from the Debye-Hückel expression (for KCl, a symmetrical monovalent electrolyte):

$$-\frac{d \log \gamma}{dm} = \frac{A}{2m^{1/2}(1 + aBm^{1/2})^2} = S_{D-H}, \quad (5)$$

corresponding to the integral expression (Garrels and Christ, 1965)

$$-\log \gamma = \frac{Am^{1/2}}{1 + aBm^{1/2}}. \quad (6)$$

Values of A and B, on a molal basis, were obtained from the Robinson and Stokes (1959, p. 468) values, which are on a molar basis, by multiplying these latter values by d_w^2 , where d_w is the density of water. The value, $a = 4.0$ angstroms (Hornibrook and others, 1942), was used. This leads to $\gamma_{25^\circ C}(0.01 \text{ m KCl}) = 0.901$, identical with the "best" experimental value (Lewis and Randall, revised ed., 1961, p. 643).

Adjusting the curve, $-(d \log \gamma) / dm = S_{D-H}$ versus $\log m$, to minimize the difference $|\Sigma A_u - \Sigma A_l|$ is not difficult in practice. Advantage is taken of the fact that the Debye-Hückel expression, equation 5, will be obeyed to a high degree of accuracy in dilute solution. In drawing the curve in figure 1, we used the Debye-Hückel value calculated at 0.01 *m*; for KCl, at $m = 0.01$ and at 25°C, $S_{D-H} = 1.988$. Because the Debye-Hückel

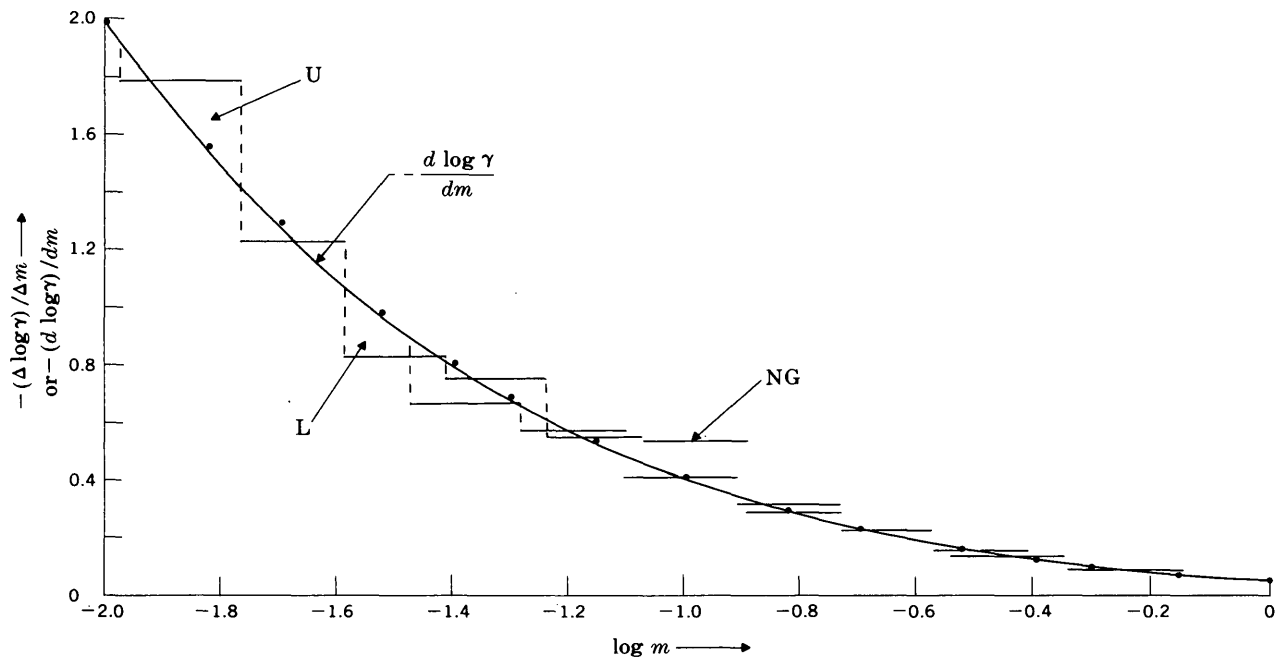


FIGURE 1.—Plots of $-(\Delta \log \gamma)/\Delta m$ or $-(d \log \gamma)/dm$ versus $\log m$ for KCl at 25°C. The horizontal bars denote the experimental results, $-(\Delta \log \gamma)/\Delta m$, plotted as lengths, $\Delta \log m$; the continuous curve is $-(d \log \gamma)/dm$ versus $\log m$. The vertical dotted lines, together with the horizontal bars, form a series of upper triangles such as U, and a series of lower triangles such as L. The curve is drawn so that $\Sigma(\text{areas of upper triangles}) = \Sigma(\text{areas of lower triangles})$; not all of the triangles are indicated. The dots represent the Debye-Hückel values calculated from equation 5. A preliminary-guide curve was drawn through these points to aid in drawing the final experimental curve; for clarity this guide curve is not shown. The experiment represented by the bar labeled NG is clearly inconsistent with the other results and is discarded. Data are from Hostetler and others (1967).

equation will be at least approximately obeyed in solutions slightly more concentrated than 0.01 m , the shape of the experimental curve in this concentration range is relatively fixed. At the other end of the concentration scale, as $\log m$ approaches zero (fig. 1), the slope of the curve also approaches zero. Thus, the shape of the curve is fairly well constrained at the lower and higher concentration ends, and any significant adjustment must be made in the intermediate concentration region. For the curve of figure 1, it was found that on the second adjustment from the Debye-Hückel curve the total area of the upper triangles differed from the total area of the lower triangles by 3 percent, and that no significant change could be made in the curve to lower this difference further.

To derive the values of $\log \gamma$ (and subsequently the values of γ), from the curve of figure 1, the curve is integrated graphically (by measuring the area under the curve over an appropriately small interval, $d \log \gamma$). In order to carry out this procedure, the value of $\log \gamma$ at some single value of $\log m$ must be assigned as a constant of integration. Again, advantage is taken of the validity of Debye-Hückel theory for dilute solutions, and the value of $-\log \gamma$ at 0.01 m KCl is calculated from equation 6, and used. For 0.01 m KCl at 25°C, calculated $-\log \gamma = 0.0455$.

The same graphical procedure illustrated in figure 1 for KCl at 25°C, was used in determining $\gamma_{\pm \text{KCl}}$ at 10°, 18°, 38°, and 50°C, by Hostetler and others (1967) and, as noted by them, excellent results were obtained. For the values obtained and a comparison of these values with previously determined values, as reported in the literature, reference may be made to these authors.

SUMMARY AND CONCLUSIONS

In the determination of activity coefficients from measurements of potentials of emf cells, it must be recognized that accurate results are obtained only when successive measurements are made on solutions having small incremental changes in concentration. This conclusion is given quantitative expression in equations 3 and 4. The problem then becomes one of how best to treat the quantities, $(\Delta \log \gamma)_{n,n-1}$ of equation 4 to extract accurate values of γ . The graphical method outlined herein, which is of general application, was most successful in yielding accurate values of $\gamma_{\pm \text{KCl}}$ (Hostetler and others, 1967).

The graphical method has several apparent desirable features. Each value of $-(\Delta \log \gamma)/\Delta m$, plotted as a bar in figure 1, contributes to the overall curve, $-(d \log \gamma)/$

dm versus $\log m$. Errors in the measurements, $\Delta E_{n,n-1}$, and hence in $(\Delta \log \gamma)_{n,n-1}$, do not accumulate. Any obviously poor experimental result, such as that indicated by NG in figure 1, is apparent at sight, and can be disregarded. The actual plotting of the curve, and its integration, presents no difficulties.

REFERENCES

- Eisenman, George, 1966, The electrochemistry of cation-sensitive glass electrodes, in Reilley, C. A., ed., *Advances in analytical chemistry and instrumentation*: New York, Interscience, v. 4, p. 213-369.
- Garrels, R. M., and Christ, C. L., 1965, *Solutions, minerals, and equilibria*: New York, Harper and Row, 450 p.
- Harned, H. S., and Owen, B. B., 1958, *The physical chemistry of electrolytic solutions*: New York, Reinhold Pub. Corp., 803 p.
- Hem, J. D., 1961, Calculation and use of ion activity: U.S. Geol. Survey Water-Supply Paper 1535-C, 17 p.
- Hornibrook, W. J., Janz, G. J., and Gordon, A. R., 1942, *The thermodynamics of aqueous solutions of potassium chloride at temperatures from 15 to 45° from E.M.F. measurements on cells with transference*: Am. Chem. Soc. Jour., v. 64, p. 513-516.
- Hostetler, P. B., Truesdell, A. H., and Christ, C. L., 1967, Activity coefficients of aqueous KCl measured with a potassium-sensitive glass electrode: *Science*, v. 155, p. 1537-1539.
- Ives, D. J. G., and Janz, G. J., 1961, *Reference electrodes*: New York, Academic Press, 651 p.
- Klotz, I. M., 1964, *Chemical thermodynamics*: New York, W. A. Benjamin, Inc., 468 p.
- Lewis, G. N., and Randall, Merle, 1961, *Thermodynamics*, revised by K. S. Pitzer and L. Brewer: New York, McGraw-Hill Book Co., 723 p.
- Parsons, Roger, 1959, *Handbook of electrochemical constants*: London, Butterworths Sci. Pubs., 113 p.
- Robinson, R. A., and Stokes, R. H., 1959, *Electrolyte solutions*: New York, Academic Press, 559 p.
- Running, T. R., 1927, *Graphical mathematics*: New York, John Wiley and Sons, Inc., p. 65-66.
- Truesdell, A. H., and Christ, C. L., 1967, Glass electrodes for calcium and other divalent cations, in Eisenman, George, ed., *Glass electrodes for hydrogen ion and other cations*: New York, Marcel Dekker, chap. 11, p. 293-321.



POSSIBLE ROLE OF SULFUR-OXIDIZING BACTERIA IN SURFICIAL ACID ALTERATION NEAR HOT SPRINGS

By GARRY G. EHRLICH and ROBERT SCHOEN, Menlo Park, Calif.

Abstract.—Explanations of sulfuric acid production near hot springs on the basis of purely inorganic mechanisms have not been convincing because of slow reaction rates. Presence of sulfuric acid producing bacteria in the soil of Steamboat Springs, Nev., was confirmed by comparing cultures inoculated with natural soil samples containing bacteria to cultures inoculated with sterilized soil. Involvement of these bacteria in surficial acid alteration is suggested.

Surficial alteration due to acid is a conspicuous aspect of the ground around many areas of hot-spring activity. It is manifested as stark white bleaching of otherwise dark rocks and is caused by the solubilizing action of dilute H_2SO_4 on the rocks. Schoen and White (1965) have described the process in detail. In general, all the primary minerals in the rock (except quartz) are destroyed and replaced by opal, kaolinite, and sometimes alunite. Few rocks are so refractory as to be immune to this sulfuric acid leaching. The assumed processes by which this acid is produced usually involve the near-surface oxidation of H_2S rising from the water table (Allen and Day, 1935; Sigvaldason and White, 1962; Steiner and Rafter, 1966). The H_2SO_4 thus formed near the surface combines with water from precipitation or condensing steam and then percolates back down to the water table, reacting with minerals on its way.

The exact chemical mechanism for the oxidation of H_2S to H_2SO_4 under these conditions is obscure. Allen and Day (1935) suggested either direct atmospheric oxidation of H_2S or oxidation through the agency of bacteria. Of these two possibilities, they favored atmospheric oxidation and cited experimental evidence reported by Dumas in 1846 and Maly in 1880 to show the plausibility of this mechanism. More detailed work (Sidgwick, 1950, p. 880) indicated, however, that H_2S is rapidly oxidized to elemental sulfur, but elemental sulfur is extremely resistant to further oxidation. For example, powdered sulfur remains un-

changed after years of exposure to the atmosphere under normal ambient conditions. Sulfur ignites in air at $260^\circ C$ and forms SO_2 , but such high temperatures are not found near the surface in hot springs areas. SO_2 reacts slowly with oxygen to form SO_3 , the anhydride of H_2SO_4 . The rate of oxidation of SO_2 is accelerated by high temperatures and noble-metal catalysts such as are used in the commercial production of H_2SO_4 . The authors are unaware of any critical studies on the catalytic properties of natural minerals in the oxidation of H_2S to H_2SO_4 .

Certain bacteria also accelerate the oxidation of various forms of sulfur, including H_2S to H_2SO_4 (Thieman, 1963, p. 714-717). These remarkable microorganisms are able to produce large quantities of H_2SO_4 at ordinary ambient temperatures and can exist under very acidic conditions (pH of 1-3). Some of the acidophilic sulfur-oxidizing bacteria are: *Thiobacillus thiooxidans* (Waksman and Joffe, 1922), *T. ferrooxidans* (Colmer and others, 1950), *Ferrobacillus ferrooxidans* (Silverman and Lundgren, 1959), and *F. sulfuroxidans* (Kinsel, 1960).

The questionable adequacy of the theory of atmospheric oxidation of H_2S in the absence of exotic catalysts led us to investigate the possibilities of biological involvement in the surficial acid alteration at Steamboat Springs, Nev.

Steamboat Springs is near the California border about 10 miles south of Reno, Nev. Hot springs, steam vents, and altered rock cover an area of approximately 4 square miles. Pre-Tertiary granodiorite and metasediments were intermittently buried by Tertiary and Quaternary volcanic rocks and alluvium and were dissected as well (White and others, 1964). The high heat flow at Steamboat Springs keeps much of the ground surface from freezing during the winter; some areas have a relatively constant soil temperature as high as $90^\circ C$ at a given point. Few living things can

exist in the inhospitable environment of warm, acid soil; stunted yellow pine is the most notable (Billings, 1950).

METHODS OF STUDY AND RESULTS

During a preliminary survey of the area, soil temperature was measured by burying the bulb of a maximum-reading thermometer just beneath the surface and soil pH was measured in slurries of approximately equal volumes of soil and distilled water. A Beckman Model-N portable pH meter equipped with glass and calomel electrodes was used.

Samples of soil (disintegrated siliceous sinter) for laboratory studies were collected at a point 3 feet away from a steaming fissure. The soil temperature at the collection point was 36°C and the pH was 2.20. The soil temperature adjacent to the fissure was 62°C and the pH was 3.40.

To demonstrate that microbiota living in the soil, rather than the soil itself, produce the acid, small samples of soil were inoculated into a culture medium that was designed to enhance selectively the growth of sulfur-oxidizing bacteria.

Two-day-old samples were inoculated into 100 milliliters of Medium C (Kaplan, 1956), which has the composition NH_4Cl , 0.2 gram; KH_2PO_4 , 3.0 g; $\text{MgCl}_2 \cdot 6\text{H}_2\text{O}$, 0.1 g; powdered sulfur, 10 g; and distilled water, 1,000 ml. Medium C is colorless and has a faint white turbidity and a layer of sulfur floating on the surface. The pH of several different batches of Medium C ranged from 4.37 to 4.59. The medium was not sterilized prior to inoculation. Cultures were incubated at room temperature for 21 days without shaking. After incubation, the contents of the flasks were filtered through Whatman-42 filter paper, and the filtrate was forced through Millipore HA membrane filters (mean pore size 0.45 micron) under nitrogen pressure. Sulfate content in the filtrate was determined as BaSO_4 by the method of Kolthoff and Sandell (1952). The results for two different levels of inoculation and a control are given below:

Amount of inoculum (grams)	Initial pH	Final pH	SO_4^{2-} found (grams)
0.1-----	4.59	1.43	0.240
1.0-----	4.59	1.39	.253
Control-----	4.59	4.38	.017

In subsequent more detailed studies, it was found that soils bearing sulfur-oxidizing organisms can be sterilized by autoclaving at 121°C for 15 minutes. No sulfur oxidation was noted when the sterilized soil was inoculated into an appropriate medium, whereas un-

sterilized specimens of the same soil showed very active sulfur oxidation.

In another experiment, 5 ml of a soil-sample culture (pH of 2.55) was transferred to 100 ml of fresh culture medium. Care was exercised to avoid transferring solids from the bottom of the flask. The pH of the fresh culture medium decreased from 4.37 to 3.80 after the addition of the old culture; after incubation at room temperature for 4 days the pH had decreased to 1.90. Later work showed that the capacity for sulfur oxidation is retained through repeated serial transfers and, furthermore, the rate of acid production accelerates from transfer to transfer.

Microscopic inspection of hanging-type drop slides prepared from young cultures disclosed the presence of many motile small rods (approximately 0.5 μ in diameter by 1–2 μ long) in the medium. The organisms appeared to be colorless and devoid of chlorophyll or carotenoids characteristic of algae and higher plants. They persisted through several serial transfers, but no attempt was made to correlate acid production with the number of organisms present.

DISCUSSION OF RESULTS

For the following reasons the results are interpreted to mean that sulfur-oxidizing bacteria were present in the Steamboat Springs soil:

1. Studies showed that addition of soil to an appropriate culture medium led to more rapid acid production than that noted in either an uninoculated control culture medium or a culture medium inoculated with sterilized soil. The increase in sulfate concentration was coincident with a decrease of pH. Old acid-producing medium had the ability to initiate acid production in fresh culture medium in the absence of soil through several serial transfers.
2. Microscopic examination disclosed motile organisms of a size characteristic of the class Schizomycetes (bacteria). The organisms appeared to lack the pigments characteristic of algae and higher plants. Both morphological evidence and the lack of organically combined carbon in the original culture medium would appear to unequivocally rule out participation by members of the animal kingdom in the observed sulfur-oxidation process.

One important point to be noted is that the strongly acid soil is probably inimical to the survival of most other species of bacteria. This is most important because under normal soil conditions sulfate-reducing organisms, such as plants and other bacteria, coexist with sulfur-oxidizing bacteria and lead to the natural sulfur cycle (Frobisher, 1963, p. 511–515). Several

important questions remain unanswered. The absence of other bacteria, particularly sulfate reducers, was not shown; the bacterial count of the soil was not determined; and finally, the source of phosphate which is important for sustaining the growth of sulfur-oxidizing bacteria (Vishniac and Santer, 1957) remains obscure. Work is currently in progress to provide answers for some of these questions.

Although it has been postulated that H_2S escaping from the water table is the precursor of the H_2SO_4 involved in surficial acid alteration and our evidence is based on the ability of the microorganisms to oxidize elemental sulfur, this does not constitute a serious discrepancy in our arguments, because direct atmospheric oxidation of H_2S to sulfur would probably be sufficient to supply an adequate energy source for the bacteria even if they were unable to utilize H_2S directly.

The quantitative importance of sulfur-oxidizing bacteria in surficial acid alteration remains an open question. At Steamboat Springs, for example, it appears that almost ideal conditions for such bacteria exist: warm, relatively constant soil temperatures throughout the year and points of optimum temperature at several places in the area near the springs; and continuous supply of H_2S , CO_2 and NH_3 from the underlying thermal water. Consequently, bacteria are likely to be major producers of acid. In other areas where similar conditions prevail, bacteria may also be important acid producers. Attempts to explain sulfuric acid production in hot-springs areas should include the possibilities of biogenic acid production.

REFERENCES

- Allen, E. T., and Day, A. L., 1935, Hot springs of the Yellowstone National Park: Carnegie Inst. Washington Pub. 466, 525 p.
- Billings, W. D., 1950, Vegetation and plant growth as affected by chemically altered rocks in the western Great Basin: Ecology, v. 31, p. 62-74.
- Colmer, A. R., Temple, K. L., and Hinkle, M. E., 1950, An iron-oxidizing bacterium from the acid drainage of some bituminous coal mines: Jour. Bacteriology, v. 59, p. 317-328.
- Frobisher, Martin, 1963, Fundamentals of microbiology: Philadelphia, W. B. Saunders Co., 610 p.
- Kaplan, I. R., 1956, Evidence of microbiological activity in some of the geothermal regions of New Zealand: New Zealand Jour. Sci. and Technology, v. 37, p. 639-662.
- Kinsel, N. A., 1960, New sulfur oxidizing iron bacterium—*Ferrobacillus sulfooxidans* sp. N.: Jour. Bacteriology, v. 80, p. 628-632.
- Kolthoff, I. M., and Sandell, E. B., 1952, Textbook of quantitative inorganic analysis: New York, Macmillan Co., 759 p.
- Schoen, Robert, and White, D. E., 1965, Hydrothermal alteration in GS-3 and GS-4 drill holes, main terrace, Steamboat Springs, Nevada: Econ. Geology, v. 60, p. 1411-1421.
- Sidgwick, N. V., 1950, The chemical elements and their compounds: London, Oxford Univ. Press, 1703 p.
- Sigvaldason, G. E., and White, D. E., 1962, Hydrothermal alteration in drill holes GS-5 and GS-7, Steamboat Springs, Nevada: Art. 153 in U.S. Geol. Survey Prof. Paper 450-D, p. D113-D117.
- Silverman, M. P., and Lundgren, D. G., 1959, Studies on the chemolithotrophic iron bacterium *Ferrobacillus ferrooxidans*, I. An improved medium and a harvesting procedure for securing high cell yields: Jour. Bacteriology, v. 77, p. 642-647.
- Steiner, A., and Rafter, T. A., 1966, Sulfur isotopes in pyrite, pyrrolite, alunite and anhydrite from steam wells in the Taupo volcanic zone, New Zealand: Econ. Geology, v. 61, p. 1115-1129.
- Thimann, K. V., 1963, The life of bacteria: New York, Macmillan Co., 909 p.
- Vishniac, Wolf, and Santer, Marvin, 1957, The *Thiobacilli*: Bacteriological Rev., v. 21, p. 195-213.
- Waksman, S. A., and Joffe, J. S., 1922, Microorganisms concerned in the oxidation of sulfur in the soil, II. *Theobacillus thiooxidans*, a new sulfur oxidizing organism isolated from the soil: Jour. Bacteriology, v. 7, p. 239-256.
- White, D. E., Thompson, G. A., and Sandberg, C. H., 1964, Rocks, structure, and geologic history of Steamboat Springs thermal area, Washoe County, Nevada: U.S. Geol. Survey Prof. Paper 458-B, 63 p., map.



SPECTROGRAPHIC DATA ON THE COMPOSITION OF BASALTIC ROCKS

By T. G. LOVERING, M. S. NILES, and M. L. GRAVES, Denver, Colo.

Abstract.—Grouped spectrographic analyses of 408 samples of basaltic rocks, from 16 States and 6 foreign countries, provide data on 34 elements. These data are summarized to furnish geologists with a background for comparison of spectrographic analyses on basalt.

Analytical data derived from grouped (6-step) spectrographic analyses of 408 samples of basaltic rocks, analyzed by the U.S. Geological Survey between 1961 and 1966, are summarized in this paper to provide geologists with a yardstick for comparison of spectrographic data for basalt. This summary does not provide an adequate basis for a petrochemical investigation of the composition of basalt, nor is it intended to do so. These samples were collected from 16 States and 6 foreign countries. They range in age from Precambrian to Recent, although most of them are Tertiary or younger.

The distribution of these samples by State or country of origin and by geologic age is shown in table 1. Localities are listed in order of decreasing abundance of samples; geologic ages are listed chronologically. Although a third of the samples analyzed come from

Hawaii, the remaining two-thirds represent widely scattered localities, and the distributions for the various elements should give an indication of typical concentrations of these elements in basaltic rocks.

Data obtained by 6-step semiquantitative spectrographic analysis are reported in weight percent to the nearest number in the series: 1, 0.7, 0.5, 0.3, 0.2, 0.15, 0.1, and so on; these represent approximate midpoints of group data on a geometric scale. The assigned group includes the quantitative value about 30 percent of the time.

No analyses were made for certain elements in some samples, so the total number of samples analyzed differs from element to element. Elements present as major constituents are reported only as greater than 10 percent. The lower limit of analytical determinations for the minor elements differs with the element. Table 2 summarizes data on the concentrations of 34 elements reported on grouped spectrographic analysis of basaltic rock samples in the order of their apparent abundance. Table 3 lists 27 elements that were looked for but not found in any of these samples, in alphabetical order of their chemical symbols.

The analytical data summarized in tables 2 and 3 represent samples of rock that were called basalt, on the basis of their appearance and field relations, by the submitters. Because there is some inconsistency in the usage of "basalt" as a field rock name, we use the term "basaltic rocks" for these samples. The maximum values reported for the concentrations of the various elements may not be representative of typical basalt for the same reason and also because some of the analyzed samples may have been partly altered. The truncated distributions given by the interdecile range should, however, provide a valid estimate of the normal variations in the commonly detected elements in basalt as reported in grouped spectrographic analysis. The median concentrations should also provide good typical values for most of

TABLE 1.—Distribution of basaltic rock samples by locality and by age

<u>Locality</u>	<u>No. of samples</u>	<u>Locality</u>	<u>No. of samples</u>
Hawaii.....	136	Puerto Rico.....	1
Oregon.....	48	Greenland.....	1
Antarctica.....	37		
Washington.....	35	<u>Geologic age</u>	<u>No. of samples</u>
Idaho.....	29	Recent.....	111
Arizona.....	22	Pleistocene.....	33
Virginia.....	19	Quaternary and	
Nevada.....	18	Tertiary.....	25
Alaska.....	16	Pliocene.....	13
Colorado.....	15	Miocene.....	16
California.....	7	Oligocene.....	16
New Mexico.....	6	Eocene.....	69
Utah.....	5	Tertiary undi-	
British Columbia..	3	vided.....	75
New Zealand.....	3	Cretaceous.....	7
Texas.....	2	Triassic.....	3
Costa Rica.....	2	Paleozoic.....	5
Georgia.....	1	Precambrian.....	15
Montana.....	1	Unknown.....	20
North Carolina....	1		

TABLE 2.—Distribution of elements in basaltic rock samples by grouped spectrographic analysis

[Concentrations in percent]

Elements	No. of analyses	Amount detected		Interdecile range of concentration values ¹		Modes ²	Median	Abundance ³	Proportion of samples below indicated limit of detection (percent)
		Maximum	Minimum	Upper	Lower				
Major elements (median concentration >0.1 percent)									
Si	177	>10.	>10.	-----	>10.	>10.	>10.	23.	0
Al	177	>10.	5.	>10.	7.	>10. (7)	>10.	7.8	0
Fe	187	>10.	2.	>10.	5.	>10. (7)	10.	8.65	0
Ca	181	>10.	.7	>10.	3.	>7.	7.	7.6	0
Mg	181	>10.	.3	>10.	2.	(>10.) 5	5.	4.6	0
Na	174	5.	.15	3.	1.	1.5	1.5	1.8	0
K	125	5.	.5	2.	1.	1.	1.5	.83	0
Ti	187	5.	.2	1.5	.5	1.5 (0.7)	1.	1.38	0
Mn	187	.2	.02	.15	.05	.15	.15	.15	0
Commonly detected minor elements (median concentration <0.1 percent)									
Sr	399	0.07	0.0005	0.07	0.001	0.07 (0.001)	0.03	0.0465	0
Ba	407	.7	.002	.1	.01	.015 (0.1)(0.03)	.03	.033	0
V	408	.1	<.0015	.05	.015	.02	.03	.025	2½ = <0.0015
Cr	408	.15	<.0001	.07	.001	.05 (0.001)	.03	.017	1¾ = <0.0001
Zr	399	.15	<.0015	.03	.007	.01	.015	.014	¼ = <0.0015
Ni	408	.15	<.0003	.03	.0003	.02 (<0.0003)	.015	.013	11 = <0.0003
Cu	408	.15	.00015	.02	.003	.015 (0.003)	.01	.0087	0
Co	408	.015	<.0005	.007	.002	.005	.005	.0048	2½ = <0.0005
Sc	391	.007	<.0003	.005	.002	.003	.003	.003	1¾ = <0.0003
Y	406	.015	<.001	.005	.002	.003	.003	.0021	1¾ = <0.001
Ga	399	.03	.00015	.003	.0015	.002	.002	.0017	0
Nb	404	.03	<.0003	.005	<.0003	<.0003 (0.001)	.001	.0019	31¼ = <0.0003
Yb	281	.0007	<.0001	.0005	.0001	.0003	.0003	.00021	4¼ = <0.0001
Less commonly detected minor elements (median below limit of detection)									
Zn	408	0.03	-----	<0.03	-----	-----	-----	0.01	99¾ = <0.03
Ce	394	.07	-----	.03	-----	-----	-----	.0048	78½ = <0.005
Nd	171	.03	-----	.02	-----	-----	-----	.002	58½ = <0.005
La	407	.05	-----	.01	-----	-----	-----	.0015	66½ = <0.002
Pb	408	.1	-----	.0015	-----	-----	-----	.0006	75 = <0.0002
B	399	.07	-----	<.001	-----	-----	-----	.0005	94 = <0.001
Mo	408	.03	-----	.0007	-----	-----	-----	.00015	69 = <0.00015
Sn	408	.005	-----	<.0005	-----	-----	-----	.00015	97½ = <0.0005
Be	408	.0015	-----	.0002	-----	-----	-----	.0001	67 = <0.0001
W	408	.007	-----	<.007	-----	-----	-----	.00007	99½ = <0.007
Sb	408	.02	-----	<.01	-----	-----	-----	.00002	99¾ = <0.01
Ag	407	.0015	-----	<.00005	-----	-----	-----	.00001	95¾ = <0.00005

¹ Excludes the highest 10 percent and the lowest 10 percent of the values.² Secondary modes in parentheses.³ Abundance from Turekian and Wedepohl (1961, table 2) converted to percent.

TABLE 3.—*Elements not detected*

Element	No. of analyses	Limit of detection (percent)	Abundance ¹
As.....	408	0.1	0.0002
Au.....	407	.002	.0000004
Bi.....	408	.001	.0000007
Cd.....	408	.005	.00002
Dy.....	60	.005	.0004
Er.....	60	.005	.0002
Eu.....	269	.05	.00008
Gd.....	60	.005	.0005
Ge.....	399	.001	.0001
Hf.....	398	.01	.0002
Hg.....	407	1.0	.000009
Ho.....	60	.01	.0001
In.....	399	.001	.00002
Li.....	407	.02	.0017
Lu.....	60	.01	.00006
Pd.....	407	.0003	.00002
Pr.....	157	.05	.0005
Pt.....	407	.003	-----
Re.....	398	.005	-----
Sm.....	163	.01	.0005
Ta.....	407	.02	.0001
Tb.....	60	.1	.00008
Te.....	398	.1	-----
Th.....	397	.02	.0004
Tl.....	407	.01	.00002
Tm.....	60	.01	.00002
U.....	398	.05	.0001

¹ Abundance from Turekian and Wedepohl (1961, table 2) converted to percent.

the elements, especially those in which they correspond to the major mode. Many of the major and commonly detected elements exhibit irregular distributions, as indicated by the existence of secondary modes. Strontium shows the most abnormal distribution, having two strong modes at 0.07 percent and 0.001 percent and a deep intermodal trough at 0.005 percent.

Data compiled by Turekian and Wedepohl (1961, p. 175, 176, 186) on the abundance of elements in basaltic rocks, have been converted to percent and rounded to facilitate comparison with the median spectrographic values in table 2 and to indicate how far below the limit of detection the not-detected elements listed in table 3 probably are. The abundance figures given by Turekian and Wedepohl are derived from published quantitative analyses of basalt, dolerite, and gabbro (Turekian and Wedepohl, 1961, p. 175, 176), and hence are not strictly comparable with our data. They do, however, provide a rough standard for comparison.

REFERENCE

Turekian, K. K., and Wedepohl, Hans, 1961, Distribution of the elements in some major units of the earth's crust: Geol. Soc. America Bull., v. 72, p. 175-192.



CALCULATION OF ION ACTIVITY PRODUCTS FOR A BRINE FROM THE BONNEVILLE SALT FLATS, UTAH

By W. L. POLZER and C. E. ROBERSON, Menlo Park, Calif.

Abstract.—Ion activity products for the dissolution of gypsum, halite, mirabilite, and some carbonate minerals were calculated for a Bonneville Salt Flats brine with an ionic strength of 6.3. Environmental conditions of the brine at the time of sampling and of analysis indicated near equilibrium with respect to most of these minerals; the agreement between the ion activity products and equilibrium constants was good. These results indicate that calculation of activity coefficients and ionic complex concentrations can be made with a reasonable degree of accuracy for waters of high ionic strength.

The solubility of salts varies greatly with a variation of the dissolved-solids content of waters. In brines and in waters from which evaporites are formed, the solubility of salts may be greatly enhanced or reduced owing to a high dissolved-solids content. The precipitation of soluble salts depends primarily on the ionic strength of the water and the nature of solute complexes, as well as the concentration of solutes. Therefore, an ion activity product (IAP) is more useful in the prediction of soluble-salt precipitation than a solubility product based on an apparent concentration alone. The determination of IAP's, however, is difficult for waters of high dissolved-solids content because of the formation of complex ions and because of the difficulty in the determination of activity coefficients of individual species. Ionic activities can be measured by means of electrodes, but the determination of single ion activities depends on the assumed constancy of the liquid-junction potential between the unknown and the calibrating standard, usually a chloride solution of low ionic strength for which the activity coefficients can be accurately calculated. If there is a large difference in ionic strength between the unknown and the standard, the liquid-junction potential is probably not con-

stant, and the measured activity could be grossly in error.

Despite the difficulties encountered in such complex systems (brines), an attempt has been made to calculate the IAP's for the solubility of gypsum, halite, mirabilite, and some carbonate minerals in a concentrated brine. The sample brine was from the Bonneville Salt Flats approximately 20 miles east of Wendover, Utah. The sample was filtered through a Whatman No. 42 filter paper into a gallon glass bottle at the time of collection. It was then taken to the laboratory for chemical analysis, the results of which are shown in table 1. Before the analysis was made, however, a white precipitate, which proved from X-ray diffraction analysis to be gypsum ($\text{CaSO}_4 \cdot 2\text{H}_2\text{O}$), had formed at the bottom of the sample bottle. This suggests that at the time of chemical determinations the brine was near equilibrium with respect to gypsum and

TABLE 1.—Analysis of brine from the Bonneville Salt Flats, east of Wendover, Utah

Constituent	Concentration (ppm)	Total molality ($\times 10^3$)
Silica (SiO_2)	10	0.23
Calcium (Ca)	1,130	38.34
Magnesium (Mg)	1,430	80.07
Strontium (Sr)	57	.88
Sodium (Na)	96,800	5,729.00
Potassium (K)	2,660	92.56
Lithium (Li)	41	8.08
Bicarbonate (HCO_3)	42	.94
Sulfate (SO_4)	3,680	52.10
Chloride (Cl)	159,000	6,095.06
Dissolved Solids (calc.)	265,000	-----

pH at 25°C..... 7.1
 Density at 20°C..... g/ml. 1.203
 Temperature at collection..... °C. 12

that the calculated IAP should therefore be equal to the equilibrium constant.

GYPSUM

For the purpose of comparison, the dissolution of gypsum can be written as follows:



At equilibrium, the IAP is equal to the equilibrium constant (K_{eq})

$$\text{IAP}_{\text{eq}} = K_{\text{eq}} = a_{\text{Ca}^{+2}} a_{\text{SO}_4^{-2}} a_{\text{H}_2\text{O}}^2 \quad (2)$$

where the symbols $a_{\text{Ca}^{+2}}$, $a_{\text{SO}_4^{-2}}$, and $a_{\text{H}_2\text{O}}$ represent the activities of respective species. The activities also may be written in terms of molalities and activity coefficients so that

$$K_{\text{eq}} = m_{\text{Ca}^{+2}} \gamma_{\text{Ca}^{+2}} m_{\text{SO}_4^{-2}} \gamma_{\text{SO}_4^{-2}} m_{\text{H}_2\text{O}}^2 \gamma_{\text{H}_2\text{O}}^2 \quad (3)$$

where $m_{\text{Ca}^{+2}}$, $m_{\text{SO}_4^{-2}}$, and $m_{\text{H}_2\text{O}}$ are the molalities of the respective species and $\gamma_{\text{Ca}^{+2}}$, $\gamma_{\text{SO}_4^{-2}}$, and $\gamma_{\text{H}_2\text{O}}$ represent the activity coefficients of the same species.

In waters of high ionic strength, the amounts of the aqueous species of equation (1) can be greatly influenced by other ionic species in the solution because of formations of complexes. Therefore, not only is an estimate of the activity coefficient necessary, but also an estimate of the molality of the individual ions in equation (1) is needed. Most of the activity coefficients of the individual ions were estimated from the mean activity coefficients (γ_{\pm}) of the related salts (Garrels and Christ, 1965). Table 2 gives the mean activity coefficients of the salts used in calculating the activity coefficient of individual ion species and the references from which the data were obtained. Table 3 lists the individual ion activity coefficients used

TABLE 2.—Mean activity coefficients (γ_{\pm}) for pure solutions of various salts at ionic strengths (μ) 2.13 and 6.3

Salt	γ_{\pm} for $\mu=2.13$	γ_{\pm} for $\mu=6.3$	Reference
NaCl	0.67	1.0	Harned and Owen (1958, p. 735); Lanier (1965, p. 3995).
KCl	.575		Harned and Owen (1958, p. 731).
CaCl ₂	.47	.82	Harned and Owen (1958, p. 735).
MgCl ₂		1.12	Do.
CaSO ₄	.10	.16	Templeton (1960, p. 516).
MgSO ₄		.043	Do.

in this study and also the method for estimating these values.

In order to obtain an estimate of $\gamma_{\pm\text{KCl}}$ at $\mu=6.3$ molal (a hypothetical solution for KCl) we measured $\gamma_{\text{K}^{+1}}$ in 6.3-molal solutions of KI and assumed that $\gamma_{\text{Cl}^{-1}} = \gamma_{\text{K}^{+1}}$ at this ionic strength. Complexing of K^{+1} in the KI solution was assumed to be negligible (Bjerrum and others, 1958). As mentioned earlier, measured activities may be grossly in error for large differences in ionic strength between the unknown and the standards. We measured the emf of a series of KI solutions using a K^{+1} -sensitive glass electrode. For the more dilute of the series, where activity coefficients could be calculated, one can plot emf against log activity of K^{+1} . The resulting straight line was then extrapolated to an activity corresponding to the measured emf of 6.3-molal KI. Then $a_{\text{K}^{+1}}/m_{\text{K}^{+1}} = \gamma_{\text{K}^{+1}}$.

The activity coefficients of MgSO_4^0 and CaSO_4^0 (uncharged ion pairs) were assumed to be the same as that for H_2CO_3 . This value is in turn an extrapolation from data by Harned and Davis (1943). The activity coefficients of the KSO_4^{-1} and NaSO_4^{-1} complexes were assumed to be the same as that of the Cl^{-1} ion. An assumption that these activity coefficients are the same as that of HCO_3^{-1} , because of the similar size of these ions, would have been more logical. However, the HCO_3^{-1} data are only available to 2.5-molal ionic strength (Walker and others, 1927). At this ionic strength, the activity coefficient appears to have reached a minimum (0.62) and should therefore be larger at 6.3-molal ionic strength. A value of 0.8 appears to be a fair approximation of the activity coefficients of the KSO_4^{-1} and NaSO_4^{-1} complexes.

TABLE 3.—Individual ion and ion-pair activity coefficients (γ) estimated for solutions of ionic strengths (μ) 2.13 and 6.3 at 25° C

Species	γ for $\mu=2.13$	γ for $\mu=6.3$	Method of calculation
K^{+1}		0.8	K^{+1} sensitive electrode, this study.
Na^{+1}	0.61	1.3	$\gamma_{\text{Na}^{+1}} = \gamma_{\pm\text{NaCl}}^2 / \gamma_{\text{Cl}^{-1}}$
Ca^{+2}	.31	.9	$\gamma_{\text{Ca}^{+2}} = \gamma_{\pm\text{CaCl}_2}^3 / \gamma_{\text{Cl}^{-1}}^2$
Mg^{+2}		2.2	$\gamma_{\text{Mg}^{+2}} = \gamma_{\pm\text{MgCl}_2}^3 / \gamma_{\text{Cl}^{-1}}^2$
SO_4^{-2}	.03	.03	$\gamma_{\text{SO}_4^{-2}} = \gamma_{\pm\text{CaSO}_4}^2 / \gamma_{\text{Ca}^{+2}}$
Cl^{-1}		.8	Assumed equal to $\gamma_{\text{K}^{+1}}$
KSO_4^{-1}		.8	Assumed equal to $\gamma_{\text{Cl}^{-1}}$
NaSO_4^{-1}		.8	Do.
HCO_3^{-1}		.8	Do.
$\text{Ca}(\text{HCO}_3)^{+1}$.8	Do.
$\text{Mg}(\text{HCO}_3)^{+1}$.8	Do.
NaHCO_3^0		3.0	Assumed equal to $\gamma_{\pm\text{H}_2\text{CO}_3}$
CaSO_4^0		3.0	Do.
MgSO_4^0		3.0	Do.

In the determination of the molality of various species of solutions of high ionic strength, consideration has to be given to complexes. Of the two anions of any significance, SO_4^{-2} and Cl^{-1} , the latter is assumed to be uncomplexed. This appears to be a safe assumption because workers have reported no evidence of complexes or only weak complexes of Cl^{-1} with the major ions (Na^{+1} , Ca^{+2} , K^{+1} , and Mg^{+2}) found in the Bonneville Salt Flats brine (Bjerrum and others, 1958). Sulfate does complex with some cations, however, and formation constants are reported for the ion pairs: NaSO_4^{-1} , KSO_4^{-1} , CaSO_4^0 , and MgSO_4^0 . No values were found for such species as $\text{Na}(\text{SO}_4)_2^{-3}$ and $\text{K}(\text{SO}_4)_2^{-3}$. Dissociation reactions with their equilibrium constants (Garrels and Thompson, 1962) for the ion pairs mentioned are:

Reaction	$-\log K_{eq}$	
$\text{KSO}_4^{-1} = \text{K}^{+1} + \text{SO}_4^{-2}$ -----	0.96	(4)
$\text{NaSO}_4^{-1} = \text{Na}^{+1} + \text{SO}_4^{-2}$ -----	.72	(5)
$\text{CaSO}_4^0 = \text{Ca}^{+2} + \text{SO}_4^{-2}$ -----	2.37	(6)
$\text{MgSO}_4^0 = \text{Mg}^{+2} + \text{SO}_4^{-2}$ -----	2.36	(7)

The 4 above reactions yield 4 equations with 9 unknowns. The additional equations can be obtained from the stoichiometric relations among the ions and their complexes. Methods for making such calculations are illustrated by Garrels and Thompson (1962).

An IAP for the dissolution of gypsum can be calculated by substituting numerical values into equation (3). The uncomplexed SO_4^{-2} was calculated as 0.017 molal and uncomplexed Ca^{+2} as 0.037. The activity of water was estimated as 0.75 from the data for the $\text{NaCl-H}_2\text{O}$ system listed by Robinson and Stokes (1959).

The effect of the complexed species may contribute significantly to the evaluation of the ionic strength of the brine. In such cases, the activity coefficients and molalities of the individual species have to be re-evaluated until a good approximation of the ionic strength is obtained. The SO_4^{-2} complexes of the predominantly NaCl brine only change the calculated ionic strength from 6.3 to 6.2. Therefore, these complexes do not change the ionic strength significantly.

An IAP of 0.9×10^{-5} was obtained for the dissolution of gypsum in the brine from Bonneville Salt Flats. The

equilibrium constant is 2.4×10^{-5} (table 4). This difference is probably due to the uncertainties in the data used for calculating the IAP. The difference, however, is not considered excessive in view of the large correction for activity. The apparent solubility product ($K'_{sp} = m_{\text{Ca total}} m_{\text{SO}_4 \text{ total}}$) is 2×10^{-3} and differs from the equilibrium constant by a factor of nearly 100.

HALITE

At the time of sampling, the brine was in contact with halite (NaCl). The IAP should, therefore, approximate the equilibrium constant for the dissolution of halite where

$$\text{IAP}_{eq} = K_{eq} = m_{\text{Na}^{+1}} m_{\text{Cl}^{-1}} \gamma_{\text{Na}^{+1}} \gamma_{\text{Cl}^{-1}}. \quad (8)$$

The amount of NaSO_4^{-1} was calculated to be only 0.03 molal; therefore, $m_{\text{Na}^{+1}}$ (uncomplexed) is approximately equal to $m_{\text{Na total}}$. The Cl^{-1} ion was assumed to be uncomplexed, therefore $m_{\text{Cl}^{-1}} = m_{\text{Cl total}}$. Substituting numerical values into equation (8) results in an IAP of 36.2. This value is very close to the equilibrium constant of 37.9 obtained from standard free energy of formation data for the dissolution of halite (table 4). The effect of a difference of 13°C in temperature between that at which the brine was sampled and standard conditions is less than 1 percent.

MIRABILITE

On the basis of its association with halite in the Bonneville Salt Flats, mirabilite ($\text{Na}_2\text{SO}_4 \cdot 10\text{H}_2\text{O}$) also should be in near equilibrium with the brine. The IAP for the dissolution of mirabilite at 12°C was calculated as 0.002, where

$$\text{IAP} = m_{\text{Na}^{+1}}^2 m_{\text{SO}_4^{-2}} \gamma_{\text{Na}^{+1}}^2 \gamma_{\text{SO}_4^{-2}} a_{\text{H}_2\text{O}}^{10}. \quad (9)$$

From solubility data (Hodgman, 1955) at 12°C , an equilibrium constant can be calculated for the dissolution of mirabilite on which equation (9) is based. It is necessary to obtain values of $\gamma_{\text{Na}^{+1}}$ and $\gamma_{\text{SO}_4^{-2}}$ for the solution containing 101.0 grams mirabilite (as Na_2SO_4)

TABLE 4.—Equilibrium constants for minerals with water

Mineral	Reactions	K_{eq}	General sources for calculation of K_{eq}
Gypsum-----	$\text{CaSO}_4 \cdot 2\text{H}_2\text{O}_{(s)} = \text{Ca}_{(aq)}^{+2} + \text{SO}_4^{-2}_{(aq)} + 2\text{H}_2\text{O}_{(l)}$	2.4×10^{-5}	Latimer (1952).
Halite-----	$\text{NaCl}_{(s)} = \text{Na}_{(aq)}^{+1} + \text{Cl}_{(aq)}^{-1}$	37.9	Do.
Mirabilite-----	$\text{Na}_2\text{SO}_4 \cdot 10\text{H}_2\text{O}_{(s)} = 2\text{Na}_{(aq)}^{+1} + \text{SO}_4^{-2}_{(aq)} + 10\text{H}_2\text{O}_{(l)}$	7.8×10^{-2}	Rossini and others (1952).
Calcite-----	$\text{CaCO}_3_{(s)} + \text{H}_{(aq)}^{+1} = \text{Ca}_{(aq)}^{+2} + \text{HCO}_3^{-1}_{(aq)}$	97	Garrels and Christ (1965).
Dolomite-----	$\text{Ca, Mg}(\text{CO}_3)_2_{(s)} + 2\text{H}_{(aq)}^{+1} = \text{Ca}_{(aq)}^{+2} + \text{Mg}_{(aq)}^{+2} + 2\text{HCO}_3^{-1}_{(aq)}$	7.59×10^3	Hostetler (1964).
Magnesite-----	$\text{MgCO}_3_{(s)} + \text{H}_{(aq)}^{+1} = \text{Mg}_{(aq)}^{+2} + \text{HCO}_3^{-1}_{(aq)}$	2.63×10^2	Do.
Hydromagnesite-----	$\text{Mg}_4(\text{CO}_3)_3(\text{OH})_2 \cdot 3\text{H}_2\text{O}_{(s)} = 4\text{Mg}_{(aq)}^{+2} + 50\text{H}_{(aq)}^{-1} + 3\text{HCO}_3^{-1}_{(aq)}$	1.32×10^{-47}	Do.

per 1,000 grams H_2O (solubility of mirabilite). To do this one must estimate the ionic strength of the solution. The ionic strength, in turn, is affected significantly by the $NaSO_4^{-1}$ complex. The molalities of Na^{+1} and $NaSO_4^{-1}$ and SO_4^{-2} can be calculated on the assumption that the ionic strength is independent of the complex. Activity coefficients are taken from data obtained from the references listed in table 2. Another ionic strength can then be determined on the basis of the calculated molalities including $m_{NaSO_4^{-1}}$. A series of successive approximations of such calculations results in almost constant values for the molalities, activity coefficients, and ionic strength which represent the true values of the solution.

The activity of water for a $Na_2SO_4-H_2O$ system was assumed to be about the same as for a $CaCl_2-H_2O$ system. The activity used (0.86) was taken from Robinson and Stokes (1959). All values for the activity of water were based on data obtained at $25^\circ C$. Since the activity of water appears in the equilibrium constant and IAP for mirabilite to the 10th power, a 1.3-percent difference in a_{H_2O} gives a 15-percent difference in the equilibrium constant (or IAP). Substitution of the appropriate values into equation (9) results in an equilibrium constant of 0.01.

At $12^\circ C$ the calculated IAP of the brine (0.002) was found to be lower than the calculated equilibrium constant (0.01). This difference suggests that the brine may be slightly undersaturated with respect to mirabilite if the accuracy in calculating activity coefficients and molalities was reasonable.

As a test for the validity of activity coefficients and the calculated concentrations of free Na^+ , SO_4^{-4} , and of $NaSO_4^{-1}$, the equilibrium constants at $25^\circ C$ were calculated from other data. An equilibrium constant calculated from solubility data at $25^\circ C$ (Hodgmen, 1955) was 0.13 ($\mu=4.5$) and the constant from standard free energy data (table 4) was 0.08. This agreement suggests that the calculated activity coefficients and molalities are reasonable and that the brine is slightly undersaturated with respect to mirabilite.

CARBONATE MINERALS

IAP's were calculated for some calcium- and magnesium-bearing carbonate minerals. The results are as follows where the IAP refers to the same reactions shown in table 4:

Mineral	IAP
Calcite.....	62
Dolomite.....	2.3×10^4
Magnesite.....	3.0×10^2
Hydromagnesite.....	7.1×10^{-50}

Comparison of these values with the equilibrium constants (table 4) suggests that at $25^\circ C$ the brine is near saturation with respect to calcite, magnesite, and dolomite. Equilibrium with carbonate minerals would be expected on the basis of the common association of traces of these minerals with evaporites.

This admittedly nonrigorous treatment of a very complex system does suggest that, for waters of high ionic strength, reasonably good estimates of activity coefficients and ionic complex concentrations can be made. From a practical point of view, these estimates can be used to determine the degree of saturation of soluble salts in water of high ionic strength.

REFERENCES

- Bjerrum, Jannik, Schwarzenbach, Gerold, and Sillén, L. G., 1958, Stability constants of metal-ion complexes, pt. 2, Inorganic ligands: London, Chem. Soc. Spec. Pub. 7, 131 p.
- Garrels, R. M., and Christ, C. L., 1965, Solutions, minerals, and equilibria: New York, Harper & Row, 450 p.
- Garrels, R. M., and Thompson, M. E., 1962, A chemical model for sea water at $25^\circ C$ and one atmosphere total pressure: Am. Jour. Sci., v. 260, p. 57-66.
- Harned, H. S., and Davis, Raymond, 1943, The ionization constant of carbonic acid in water and the solubility of carbon dioxide in water and aqueous salt solutions from 0° to $50^\circ C$: Am. Chem. Soc. Jour., v. 65, no. 10, p. 2030-2037.
- Harned, H. S., and Owen, B. B., 1958, The physical chemistry of electrolytic solutions: New York, Reinhold Pub. Corp., 803 p.
- Hodgman, C. D., ed., 1955-56, Handbook of chemistry and physics: 37th ed., Cleveland, Ohio, Chemical Rubber Pub. Co., 3156 p.
- Hostetler, P. B., 1964, The degree of saturation of magnesium and calcium carbonate minerals in natural waters: Internat. Assoc. of Sci. Hydrology Pub. 64, p. 34-49.
- Lanier, R. D., 1965, Activity coefficients of sodium chloride in aqueous three-component solutions by cation-sensitive glass electrodes: Jour. Phys. Chemistry, v. 69, p. 3992-3998.
- Latimer, W. M., 1952, Oxidation potentials: Englewood Cliffs, N.J., Prentice-Hall, Inc., 392 p.
- Robinson, R. A., and Stokes, R. H., 1959, Electrolyte solutions: London, Butterworths Pub. Ltd., 559 p.
- Rossini, F. D., Wagman, D. D., Evans, W. H., Levine, Samuel, and Jaffe, Irving, 1952, Selected values of chemical thermodynamic properties: Natl. Bur. Standards Circ. 500, 1268 p.
- Templeton, C. C., 1960, Solubility of barium sulfate in sodium chloride solutions from $25^\circ C$ to $95^\circ C$: Jour. Chem. Eng. Data, v. 5, no. 21, p. 514-516.
- Walker, A. C., Bray, V. B., and Johnston, John, 1927, Equilibrium in solutions of alkali carbonates: Am. Chem. Soc. Jour., v. 49, p. 1235-1256.



LOWER PERMIAN PLANTS FROM THE ARROYO FORMATION IN BAYLOR COUNTY, NORTH-CENTRAL TEXAS

By SERGIUS H. MAMAY, Washington, D.C.

Abstract.—The first fossil plants to be found in the Arroyo Formation of the Clear Fork Group (Leonard Series, Lower Permian) are described. The plants were found in a small shale deposit near Lake Kemp in Baylor County, Tex. The assemblage is limited and poorly preserved, but nonetheless it contains two taxonomic novelties: *Brachyphyllum* (?) *densum*, n. sp. and *Wattia texana*, n. gen. and sp. *Brachyphyllum* (?) is obviously coniferous, but *Wattia* is problematical, both morphologically and taxonomically. The flora is mixed, with indications of affinities with the Permian floras of Europe, Cathaysia, and Angaraland. The relatively high proportion of new taxa in this small collection suggests that the Arroyo Formation may ultimately produce a diversified flora of much morphologic and phytogeographic interest.

Prior to 1963 Permian plant megafossils had been obtained from several rock units in Baylor County and adjacent parts of north-central Texas. Fossiliferous units included (in ascending order) the Moran and Admiral Formations (Wolfcamp), the Belle Plains and Clyde Formations and the Lueders Limestone (all of Leonard? age), and the Vale Formation of the Clear Fork Group (Leonard). The youngest Permian plants were found in the upper part of the Vale Formation in Knox County, but none had been known from the subjacent Arroyo Formation. However, A. D. Watt, of the U.S. Geological Survey, and I discovered a shale deposit in 1963 in Baylor County that contained the first flora known from the Arroyo Formation. This small assemblage is not exceptionally well preserved but nonetheless contains distinctive forms and constitutes a potentially important link in the succession of Paleozoic floras of this continent.

SOURCE OF MATERIAL

The collecting site (USGS paleobotany loc. 10055) is approximately 1 mile northwest of the mouth of Big Moonshine Creek where it becomes an arm of the south side of Lake Kemp in Baylor County (see fig.

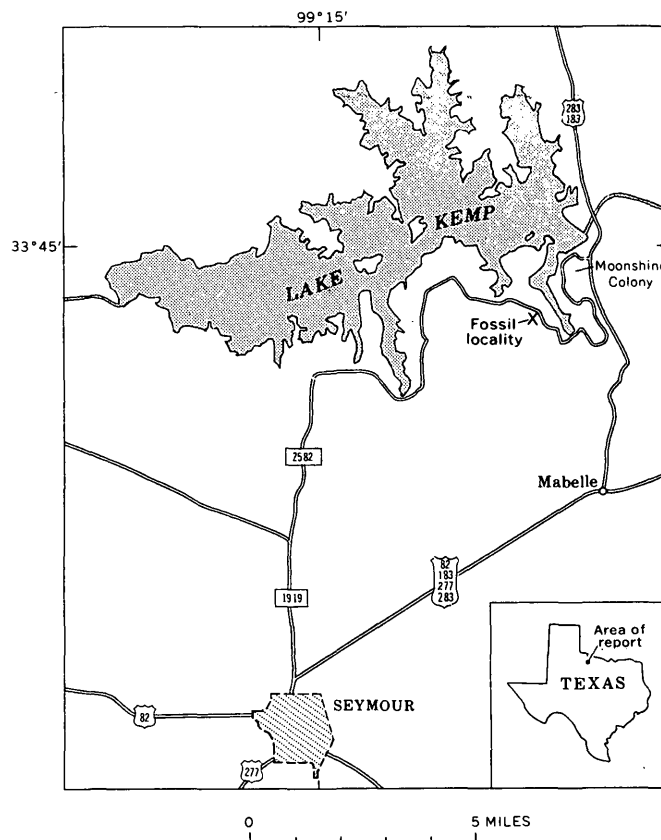


FIGURE 1.—Index map of part of Baylor County, Tex., showing fossil plant locality.

1). The fossiliferous outcrop was exposed in a low bank 15 feet west of a road that parallels the arm and is about 1/4 mile west of it. The locality is reached by entering the toll gate at Moonshine Colony, 5.6 miles north of Mabelle, on U.S. Highway 183-283, and upon passing the gate, following the main road and the first fork to the south for a total distance of 5.2 miles from the gate to the fossil plant locality. The locality is on the property of the W. T. Waggoner

Estate. Thanks are extended to Mr. John Biggs, Trustee, for permission to collect on the Waggoner properties.

For a 50-yard distance along the roadbank in this area there are several thin exposures of bluish-gray and tan clayey shales, 6 to 15 inches thick and as much as 10 feet wide. With the exception of one deposit, however, these exposures were barren of fossils.

The plants were found in moderate abundance as coalified compressions in a small lens of dark, bluish-gray shale, which is badly weathered and friable making removal of fossils difficult. The lens was virtually destroyed by our collecting efforts; originally it did not exceed 1 foot in thickness or 5 feet laterally. It was partly capped by a 2- to 6-inch layer of poorly indurated light-tan siltstone that contains abundant unidentifiable, coalified plant material intermixed with many small bits of bone and teeth. The latter were identified as paleoniscoid fish remains (D. H. Dunkle, oral commun., 1966). The only other animal remains associated with the plants are disarticulated estherid valves; these are fairly common in the plant-bearing shale.

Extensive rock exposures are rare in this area, and a detailed geologic map of Baylor County is not available. However, there seems to be no doubt that the plant deposit is within the Arroyo Formation. The collecting site is stratigraphically above the Lake Kemp limestone, the uppermost member of the Lueders Formation (usages of Garrett and others, 1930), and thus is an undetermined distance above the bottom of the superjacent Arroyo Formation. This is in agreement with Romer (1958; map facing p. 178).

COMPOSITION AND DESCRIPTION OF THE FLORA

Eight entities are recognizable in the Arroyo flora. Four of these are definitely gymnospermous, 1 is probably a gymnosperm, and 3 are in uncertain systematic position. Ferns, lycopods, and sphenopsids are absent, a fact that may indicate derivation of this assemblage from an upland environment, if the ecological interpretations of Cridland and Morris (1963) are applicable here.

The gymnospermous elements include the cordaitan structure known as *Artisia*, one *Samaropsis* seed, several specimens of *Walchia*, and abundant coniferous remains provisionally assigned to *Brachyphyllum* (fig. 2). Numerous detached scalelike organs, possibly of coniferous origin, are also present.

The genus *Taeniopteris* is represented by a few small but recognizable fragments. Other plant fossils of uncertain relationships include one small fragment of a *Gigantopteris* frond and a large number of pecu-

liar foliar appendages that evidently represent a new form and are designated here as the new genus *Wattia*.

Plants of known position

The following are plants of known position of the Arroyo flora:

Cordaitales

Genus *Artisia* Sternberg

Artisia sp.

Figure 2a

The name *Artisia* is applied to internal pith casts of cordaitan stems. Since cordaitan piths are characterized by closely spaced parenchymatous septae, the fossilized pith casts are easily recognized by their numerous transverse striations. This feature is clearly shown by the one specimen present in the Arroyo collection, illustrated in figure 2a.

Several species of *Artisia* have been described, but they are distinguished on the basis of very minor differences. Because of this, and the presence on hand of only one specimen, no specific determination is attempted.

Figured specimen.—USNM 42621a.

Genus *Samaropsis* Goeppert

Samaropsis sp.

Figure 2g

One small winged seed is present in the collection; because of the breadth of its winged margin and its bifid apex, the specimen is referred to *Samaropsis*. The specimen is 11 millimeters long, 9 mm wide, and broadest at its base. The central nucellar region is 3.5 mm wide, 5.5 mm long, and similarly broadest at the base. The broadest part of the winged margin is 4.0 mm wide, and the apex appears to be deeply notched.

Samaropsis and *Cordaicarpus* are similar seed types, but are usually separated on the basis of relative width of the marginal wing, that of *Samaropsis* being the wider. There is considerable morphological variation in this seed complex, so that a specific determination is not offered here on the basis of the one available specimen.

Seeds of the *Samaropsis* type have been found among the pteridosperms, cordaitaleans, and conifers. However, Florin (1950) has demonstrated that, where known, cordaitan female reproductive organs usually bear seeds of the *Samaropsis* type, and accordingly the Arroyo specimen is assigned to the Cordaitales.

Figured specimen.—USNM 42627.

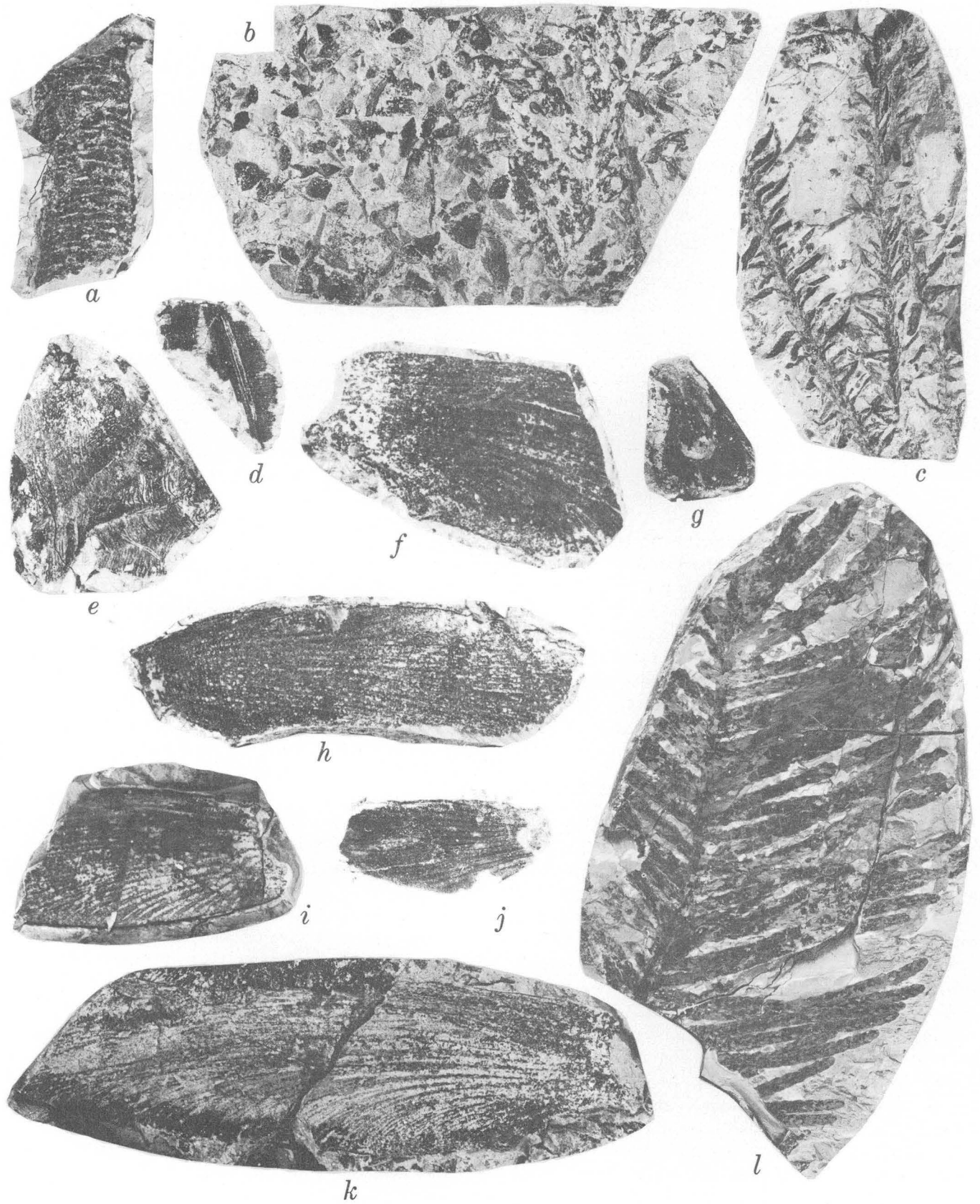


FIGURE 2.

Coniferales

Genus *Walchia* Sternberg*Walchia Schlotheimii* Brongniart

(See Florin, 1939, p. 205–210, pls. 128–132)

Figure 2o

Eight specimens of *Walchia* are present in the collection, all easily recognizable by the characteristic appearance and arrangement of the ultimate leafy shoots. The largest specimen consists of a group of 12 ultimate branchlets, reaching 9 centimeters in length, and arranged parallel to each other in a manner that suggests original pinnate attachment to a common penultimate shoot. Another specimen consists of a group of 10 ultimate branchlets, 4 of which are organically attached to a penultimate shoot; the latter is 8 mm to 10 mm wide. The branchlets are closely spaced, at intervals of 1.0 cm to 1.5 cm. The ultimate branchlets are fairly stout, reaching widths of 3.0 mm to 3.5 mm at their points of attachment to the penultimate branch.

As shown in figure 2c, the leaves are arranged in a dense spiral, reaching lengths of 8.0 mm to 10.0 mm and widths of 1.0 mm to 1.5 mm. Most leaves depart decurrently at a broad angle to the stem, assume angles of 60° to 80° and then bend upwards rather abruptly near their sharp tips.

Florin (1939, p. 206) pointed out that there always is a certain size variability among walchian species. Consequently it is sometimes difficult to identify species in this complex. However, judging from the dimensions and spatial relationships of the leaves and branches of the material from the Arroyo, the material compares closely with *Walchia Schlotheimii*, and in particular with the specimens figured by Florin (1939, plate 131) from the Autunian of France.

Figured specimen.—USNM 42623.

Genus *Brachyphyllum* Brongniart*Brachyphyllum(?) densum*, n. sp.

Figure 2l

Specific diagnosis.—Coniferous branch systems with densely arranged distichous ultimate branchlets. Penultimate axes as much as 7.0 mm broad, with sparse needlelike leaves as much as to 8.0 mm long closely appressed to the axis. Ultimate branchlets, 6.0 mm to 8.0 mm long and 2.0 mm to 3.0 mm broad, densely inserted on penultimate branches with scarcely any intervening space; branchlets straight or only slightly curved, of rigid appearance, parallel to each other, inserted at ascending angles ranging from 30° to 80°. Branchlets densely clothed with small, closely imbricated, spirally arranged, and tightly appressed scalelike leaves; leaves 2.0 mm to 2.2 mm long and 1.0 mm to 1.2 mm wide, broadest at the bases, with sharp acuminate tips.

Reproductive parts unknown.

Holotype.—USNM 42632.

Remarks.—This plant apparently was a dominant element in the Arroyo flora and is represented in the collection by about 50 specimens of penultimate branches, each with several to many attached branchlets. The small scalelike leaves, their densely imbricate distribution and tight appression to the ultimate branchlets distinguish this plant from the walchian conifers with their more laxly arranged, long and slender needlelike leaves.

Brachyphyllum is a poorly understood taxon with wide geographic and stratigraphic distribution. It is mostly characteristic of Mesozoic rocks, with few records of occurrence in the Paleozoic. One thus might question the propriety of referring this material to *Brachyphyllum*. However, despite the age of the Ar-

FIGURE 2.—Fossils of Lower Permian plants from the Arroyo Formation in Baylor County, north-central Texas.

- a. *Artisia* sp., fragment of pith cast showing discoid structure resulting from transverse septae in pith. USNM 42621, natural size.
- b. Slab of matrix covered with numerous detached (?) coniferous scales (cf. *Lepeophyllum* sp.); at right is a fragmentary shoot system of *Brachyphyllum(?) densum*. USNM 42622, × 2.
- c. Slab with two leafy ultimate shoots of *Walchia Schlotheimii* Brongniart. USNM 42623, natural size.
- d. Small fragment of leaf of *Taeniopteris* sp. USNM 42624, × 2.
- e. Small fragment of leaf of *Gigantopteris* n. sp. B. USNM 42625, × 2.
- f. Basal part of appendage of *Wattia texana*, showing concavely crescentic outline of basal end and asymmetrical venation. Paratype, USNM 42626, × 2.
- g. *Samaropsis* sp., showing broad wing and bifid apex. USNM 42627, × 2.
- h. Nearly complete appendage of *Wattia texana*, showing slightly falcate shape and asymmetrical venation. Paratype, USNM 42628, × 2.
- i. Basal fragment of appendage of *Wattia texana*, showing concavely crescentic base, asymmetrical venation, and forking of veins near lower edge of specimen. Paratype, USNM 42629, × 2.
- j. Small incomplete fragment of appendage of *Wattia texana*. Paratype, USNM 42630, × 2.
- k. Large nearly complete appendage of *Wattia texana*, showing concavely crescentic base, gradationally asymmetrical and forking venation, and slightly falcate shape. Holotype, USNM 42631, × 2.
- l. Specimen of *Brachyphyllum(?) densum*, showing a penultimate axis bearing numerous distichous, slender, closely set, and rigid ultimate axes clothed with abundant, closely appressed and scalelike leaves. Holotype, USNM 42632, natural size.

rojo material, it seems to fit reasonably well into the broad concept of this artificial generic designation which is applied to sterile coniferous branches with distichous arrangement of the ultimate branchlets and small, densely imbricate scalelike leaves.

Whether or not the provisional generic assignment made here is correct, the species is distinct from any Paleozoic plants known to me from North America. White (1929) described two species of *Brachyphyllum* (*B. arizonicum* and *B. tenue*) from the Permian Hermit Shale of the Grand Canyon, and, though the preservation of those species is very poor, they are easily distinguished from the Arroyo plants on the basis of branching habit, leaf size, and leaf attitude. A closer comparison of *B. (?) densum* might be drawn with the species *B. confusum*, from the Jurassic of Portugal (Saporta, 1894, pl. 21, fig. 8), on the basis of comparable densities of branchlet distribution. However, the branchlets of Saporta's material are somewhat thicker than those of *B. (?) densum* and the leaves appear to be sufficiently broader, relative to length, to warrant a specific distinction.

Plants of uncertain position

The following are plants of uncertain position of the Arroyo flora:

Detached gymnospermous(?) leaves

Figure 2b

Several slabs in the collection are covered by numerous detached foliar appendages whose size and shape suggest coniferous origin. They vary in shape from lanceolate to deltoid, and some attain lengths of nearly 5 mm and widths of 3 mm. Because many are considerably larger than the scales of *Brachyphyllum (?) densum* it is assumed that another plant, of unknown identity, is represented by these detached appendages. Some specimens show evidence of fine closely set parallel venation; in this aspect, in addition to their shape, they seem to resemble small specimens of the supposedly cordaitan species *Lepeophyllum trigonum* described by Neuberg (1965) from the Upper Permian of the Pechora Basin, USSR.

Figured specimen.—USNM 42622.

Genus *Gigantopteris* Schenk

Gigantopteris n. sp. B

Figure 2e

This important Permian genus is represented in the collection by one small distorted frond fragment consisting only of secondary and tertiary veins. The tertiary veins are mostly unforked and show no anasto-

moses. On the basis of the simplicity of venation it seems appropriate to discount an alliance of this specimen with *G. americana* White and ascribe it to *G.* n. sp. B, an as yet undescribed but distinctive member of the gigantopterids (figured by Read and Mamay, 1964, pl. 19, fig. 2). Its occurrence in the Arroyo assemblage is not surprising, because this occurrence is intermediate between the known limits of the stratigraphic range of this species.

On the basis of association with seeds of the *Cardiocarpon* type, White (1912) regarded *Gigantopteris* as a pteridosperm; other authors consider it to be a fern. Because no concrete evidence of the fruiting habit of this genus has yet been produced, a supergeneric assignment is not made here.

Figured specimen.—USNM 42625.

Genus *Taeniopteris* Brongniart

Taeniopteris sp.

Figure 2d

The form genus *Taeniopteris* is represented in the collection by several small fragments, none of which is sufficiently complete for specific identification. The genus is easily recognized, however, by its broad midrib and closely spaced lateral veins that depart at wide angles.

Taeniopteris is common in Upper Pennsylvanian and Lower Permian floras in the United States, but only in one instance has the natural affinity of American material been established. Cridland and Morris (1960) found seeds attached to specimens of *T. coriacea* Goeppert, from the Upper Pennsylvanian of Kansas, and established the new pteridospermous genus *Spermopteris*. Although the Arroyo material is likely pteridospermous, its assignment to that group would only be speculative.

Figured specimen.—USNM 42624.

Genus *Wattia*, n. gen.

Type species: *Wattia texana*, n. sp.

Figure 2f, h-k.

The available material of *Wattia* offers no clear basis for differentiation of more than one species; consequently a combined diagnosis is given. Because the orientation of attachment of appendages to the parent axis is yet unknown, the use of the terms "upper" and "lower" in reference to margins and veins must be regarded as arbitrary.

Combined diagnosis.—Long, narrow, asymmetrical foliar appendages of unknown morphologic rank or affinity, with unequally arching, simple or forking veins, and concavely crescentic basal abscission out-

lines. Appendages up to 10 cm in length and 2.5 cm. in width, linear-ovate to linear-obovate, slightly falcate and tapering gently toward apices. Margins entire, the lower usually showing more curvature than the upper; apices bluntly rounded.

Midrib absent; several stout veins entering bases of appendages, some simple, but most dichotomizing one to several times. Upper veins gently arched, in general conformity with upper margin of appendage, terminating at margin near apex of appendage; lower veins more abruptly arched downward, more often forked than upper veins, terminating at margin near base of appendage; intermediate veins following courses gradational between extremes.

Holotype.—USNM 42631.

Paratypes.—USNM 42626, 42628, 42629, 42630.

Remarks.—About 40 specimens of *Wattia* were found, and, though none is complete and the mode of their attachment to an axis is not known, the asymmetry of these appendages is sufficiently distinctive to warrant their recognition as a new genus. The asymmetrical gradational curvature of the veins and their bifurcations are shown in figure 2, *i* and *k*; the concavely crescentic basal ends are shown in figure 2, *f*, *i*, and *k*. Although these features render identification of *Wattia* relatively simple, they are of little assistance in morphologic or systematic interpretations of the genus. The question of whether the appendages rank morphologically as true leaves or as detached pinnae of a compound frond cannot be determined until more complete material is available. The clear-cut and concavely crescentic basal outline suggests a clasping habit and seasonal abscission, which in turn may indicate that the appendages are true leaves. On the other hand, the asymmetrical form and venation suggest that the appendages are detached pinnae of a compound frond.

Whatever the morphological nature of *Wattia* may prove to be, its systematic affiliation will be difficult to establish. Should it prove to be a simple leaf, the long narrow form and broad clasping base might suggest cordaitan affinity except for the asymmetrical features that are not known among the cordaites. Alternatively, if *Wattia* is a pinnate frond, its possible systematic affiliation should probably include the ferns, pteridosperms, cycadophytes, and noeggerathialeans. The last possibility is currently favored because of the asymmetrical pinnae in the genus *Noeggerathia* and the known existence of the noeggerathialean fructification *Discinities* in the somewhat older Permian Belle Plains Formation of Baylor County (Mamay, 1954). Actual identity of *Wattia* with *Noeggerathia* is not considered here, however, because the pinnae of

Noeggerathia have, for the most part, strongly toothed margins (see Hirmer, 1940, p. 19), whereas those of *Wattia* are entire.

With one exception, a search of the literature for forms that compare favorably with *Wattia* was unsuccessful. Radchenko and Shvedov (1940, pl. 6, fig. 3) illustrated a single specimen from the Lower Permian of the Tunguska basin, USSR, which, except for a slight difference in size, bears a remarkable likeness to the Arroyo specimen illustrated here in figure 2*h*. They identified their specimen as *Cardioneura magna* Zalesky, but I believe this to be a misidentification because the specimen fails to show the neuropteroid or cardiopteroid venation and outline included in Zalesky's diagnosis and figures of the genus (1934, p. 1105, figs. 4-6) or of the species *C. magna* (Zalesky, 1937, p. 131). In general shape, proportions, and asymmetrical venation, the Tunguska specimen is very similar to *Wattia*, and a close relationship probably exists between the two. Were it not for the obscurity of the base of the Tunguska specimen as shown in the Radchenko and Shvedov photograph, there would be ample justification for transferring the specimen to the genus *Wattia*.

Wattia is named after my assistant, A. D. Watt, U.S. Geological Survey.

DISCUSSION

Despite its limited taxonomic composition and poor preservation, the Arroyo assemblage is significant from several standpoints. Phytogeographically it tends to strengthen the original viewpoint of White (1912) regarding a relationship between the Permian floras of Asia and North America. The presence of *Gigantopteris* in the Arroyo flora is an important point of comparison with the flora of eastern Asia. Other elements in the Arroyo flora (*Wattia* and the *Lepeophyllum*-like structure) suggest links between the American assemblages and those of Siberia. The evidence of cordaites and walchians in the Arroyo flora not only establishes affinities with the floras of Europe, but also constitutes the youngest known occurrence of the North American cordaites. In North America they are abundant in the Pennsylvanian but rare in the Permian, whereas abundant Permian occurrences are known in eastern Asia and Siberia. Also notable is the presence in this flora of abundant *Brachyphyllum*(?); this Permian occurrence seems discordant with the majority of occurrences of conifers of that type and lends a Mesozoic aspect to the Arroyo flora.

The discovery of two taxonomic novelties in as limited an assemblage as that discussed here suggests the presence elsewhere in the Arroyo Formation of a

diversified flora with other new elements and emphasizes the importance of continued searches of the rocks of the Arroyo and adjacent formations. It also suggests that the Permian of the United States, as compared with the Pennsylvanian, was a period of rapid plant evolution and complex-facies relationships. Genera as distinctive as *Gigantopteris*, *Wattia*, and *Tingia* (see Darrah, 1938) seem to have evolved suddenly from unknown progenitors, persisted for relatively short segments of geologic time, and disappeared leaving no obvious lineages of succession. Although biologically perplexing, this circumstance promises eventually to make possible a relatively refined system of biostratigraphic correlations wherever plant-bearing Permian rocks are exposed in the United States. The known stratigraphic succession and geographic distribution of Permian floras in the United States were recently summarized (Read and Mamay, 1964), and three Permian floral zones (Zones 13-15) were recognized. The Arroyo flora clearly falls within the uppermost of these, and may provide a basis for subdivision of Zone 15.

REFERENCES

- Cridland, A. D., and Morris, J. E., 1960, *Spermopteris*, a new genus of pteridosperms from the Upper Pennsylvanian Series of Kansas: *Am. Jour. Botany*, v. 47, no. 10, p. 855-859, 15 figs.
- 1963, *Taeniopteris*, *Walchia* and *Dichophyllum* in the Pennsylvanian System of Kansas: *Univ. Kansas Sci. Bull.*, v. 44, no. 4, p. 71-85, 2 figs.
- Darrah, W. C., 1938, The occurrence of the genus *Tingia* in Texas: *Botanical Mus. Leaflets*, Harvard Univ., v. 5, no. 10, p. 173-188, 2 pls.
- Florin, Rudolf, 1939, Die Koniferen des Oberkarbons und des Unteren Perms, no. 4: *Palaeontographica*, v. 85, sec. B, p. 41-53, 175-241, pls. 111-150. Stuttgart.
- 1950, On female reproductive organs in the Cordaitinae: *Acta Horti Bergiana*, v. 15, no. 6, p. 111-134, pls. 1-6. Uppsala.
- Garrett, M. M., Lloyd, A. M., and Laskey, G. E., 1930, Map of Baylor County (revised 1937): Texas Bur. Econ. Geology.
- Hirmer, Max, 1940, Die Karbon-Flora des Saargebietes, sec. 3. Filicales und Verwandte. Noeggerathiineae (mit Beitrag von P. Guthörl): *Palaeontographica*, supp., v. 9, no. 1, p. 3-60, pls. 1-13, 12 text figs.
- Mamay, S. H., 1954, A Permian *Discinites* cone: *Washington Acad. Sci. Jour.*, v. 44, no. 1, p. 7-11, 5 figs.
- Neuburg, M. F., 1965, Permian flora of Pechora Basin, pt. 3: *Acad. Sci. USSR, Geol. Inst. Trans.*, v. 116, p. 5-144, pls. 1-48. [In Russian]
- Radchenko, G. P., and Shvedov, N. A., 1940, Upper Paleozoic flora of the coalbearing deposits of the western part of the lower Tunguska Basin: *Arctic Inst. of the Chief Adm. of the Northern Sea Route Trans.*, v. 157, p. 5-140, pls. 1-23. [In Russian]
- Read, C. B., and Mamay, S. H., 1964, Upper Paleozoic floral zones and floral provinces of the United States: *U.S. Geol. Survey Prof. Paper* 454-K, p. K1-K35, pls. 1-19 (with a glossary of stratigraphic terms by Grace C. Kerohar).
- Romer, A. S., 1958, The Texas Permian redbeds and their vertebrate fauna, chap. 9 of Westoll, T. S., ed., *Studies on fossil vertebrates*: *Univ. Lond., Athlone Press*, p. 157-179.
- Saporta, Gaston, 1894, *Flore fossile du Portugal*: Lisbon, Roy. Acad. Sci. Press, p. 1-288, pls. 1-39.
- White, David, 1912, The characters of the fossil plant *Gigantopteris* Schenk and its occurrence in North America: *U.S. Natl. Mus. Proc.*, v. 41, p. 493-516, pls. 43-49.
- 1929, *Flora of the Hermit Shale, Grand Canyon, Arizona*: *Carnegie Inst. of Washington*, pub. 405, p. 3-221, pls. A-D, 1-51.
- Zalessky, M. D., 1934, Sur quelques végétaux fossiles nouveaux du terrain houiller du Donetz: *Bull. de l'Acad. des Sciences de l'URSS; Classe des Sciences Math. et Nat., ser. 7, no. 7*, p. 1105-1117, 12 figs.
- 1937, Contribution à la flore Permienne du Bassin de Kousnetz: *Moscow Univ. Problems of Paleontology, Lab. of Paleontology Pub.* v. 2-3, p. 125-142, 25 figs.



AGE AND REGIONAL SIGNIFICANCE OF BASAL PART OF MILLIGEN FORMATION, LOST RIVER RANGE, IDAHO

By CHARLES A. SANDBERG, WILLIAM J. MAPEL, and JOHN W. HUDDLE,
Denver, Colo.; Washington, D.C.

Abstract.—A conodont fauna assigned to the Lower *Siphonodella crenulata* Zone (lower *cuIIa*), which is indicative of an Early Mississippian (Kinderhook) age, was found 13 feet above the base of the Milligen Formation near Mackay, Idaho. The conodonts are the first pre-Permian conodonts reported from Idaho and the first diagnostic fossils recovered from the Milligen. The fauna is identical with that in the basal part of the Lodgepole Limestone near Logan, in southwestern Montana. The occurrence of this fauna so far west of Logan and so near the Idaho batholith proves that the Milligen is no older than Mississippian in most of east-central Idaho.

The basal 26 feet of the Milligen Formation of Mississippian age and the upper 700 feet of Upper Devonian rocks are well exposed near the mouth of the canyon of Lower Cedar Creek on the west side of the Lost River Range, 4 miles northeast of Mackay, Idaho (fig. 1). An interbed of crinoidal limestone, 13–14 feet above the base of the Milligen at this locality, contains a large, well-preserved conodont fauna that represents the Lower *Siphonodella crenulata* Zone (lower *cuIIa*). The locality from which the conodonts were collected is at an altitude of 7,920 feet in the NE $\frac{1}{4}$ SW $\frac{1}{4}$ sec. 2 (unsurveyed), T. 7 N., R. 24 E., Custer County, in the Mackay 15-minute quadrangle. A detailed section was measured there by Sandberg and Mapel in July 1966. This section is summarized below.

<i>Unit</i>	<i>Thickness (feet)</i>
Mississippian:	
Milligen Formation (part).....	26+
Unconformity.	
Devonian:	
Trident Member of Three Forks Formation.....	267
Conformable contact.	
Birdbear Member of Jefferson Formation.....	313
Gradational contact.	
Lower member of Jefferson Formation (part).....	113
Bedding plane fault.	

A bold cliff formed by the Birdbear Member of the Jefferson Formation is plainly visible from Mackay, and the conodont locality lies a few hundred feet higher on the hillside (fig. 2). The measured section is approached by passenger car on a dirt road that extends northeast from Mackay, turns southeast around the town dump, and then heads due north across an alluvial fan to the mouth of the canyon of Lower Cedar Creek. From there the conodont locality is reached after a moderate climb.

LOWER CEDAR CREEK CONODONT LOCALITY

At Lower Cedar Creek the basal 10 feet of the Milligen Formation consists of grayish-black nonfossiliferous and noncalcareous argillite interlaminated with medium-dark-gray siltstone. These lithologies characterize most of the formation elsewhere in the Lost River Range. The next higher 16 feet is mostly dark-gray and dark-yellowish-orange limonitic calcareous siltstone and subordinate sandstone that weather light brown to dark yellowish orange and contain broken phosphatic plates, about $\frac{1}{8}$ -inch thick, and megascopically visible conodonts. Interbedded with the calcareous siltstone are at least three beds, 6–12 inches thick, of medium-dark-gray to dark-gray crinoidal bioclastic limestone that is very finely crystalline, finely to medium fossil-fragmental, silty, and carbonaceous. Besides abundant crinoid columnals, the limestone contains scattered ostracodes and small silicified horn corals and brachiopods. The limestone is lithologically similar to the crinoidal limestone in the basal part of the Lodgepole Limestone in western Montana and extreme western Wyoming. The megafauna resembles that reported from a basal unit of the Lodgepole by Sando and Dutro (1960).

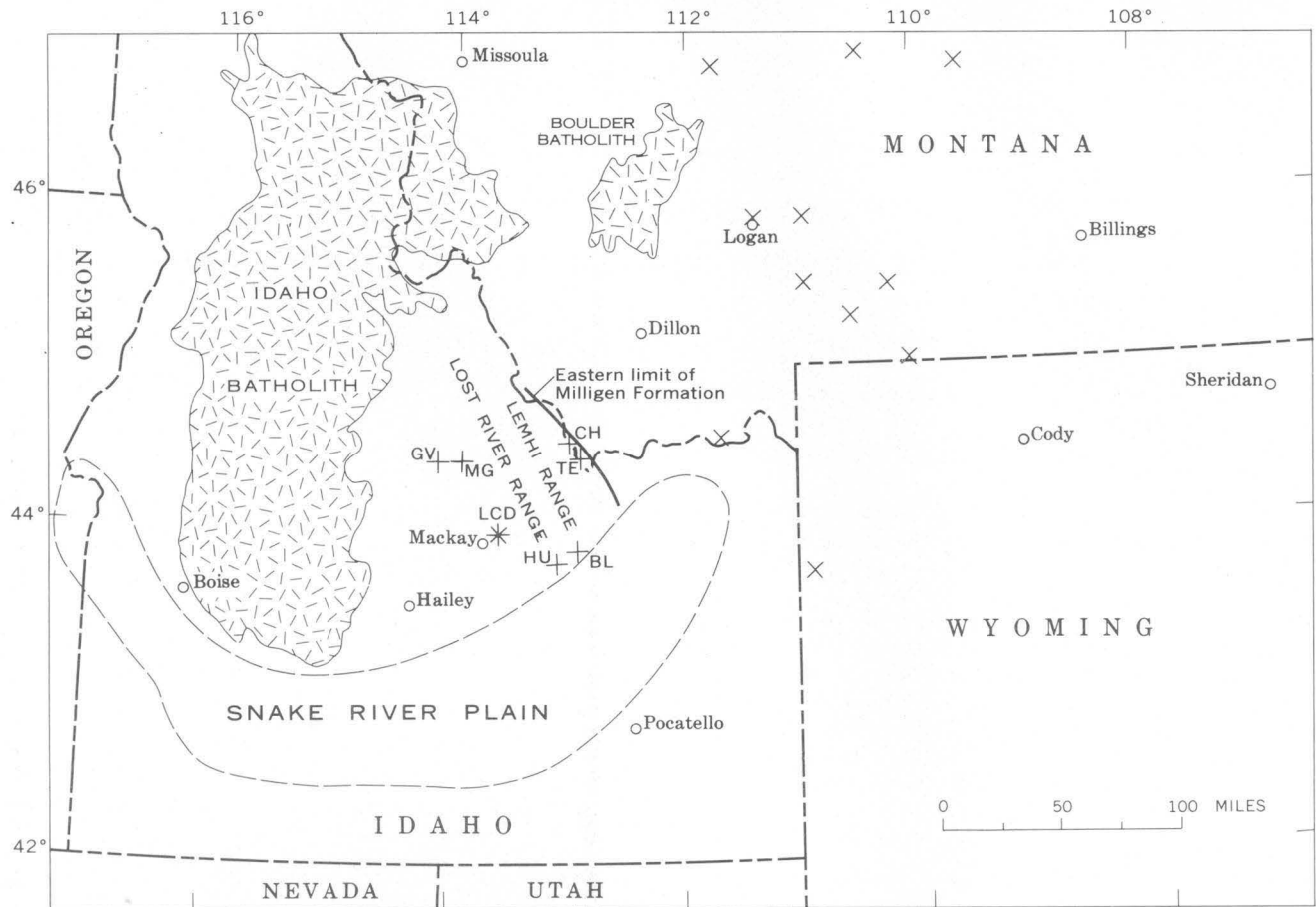


FIGURE 1.—Index map of parts of Idaho and adjacent States, showing Lower Cedar Creek conodont locality (LCD) and eastern limit of Milligen Formation. ×, location of basal Lodgepole Limestone sections that contain conodont faunas assigned to the Lower *Siphonodella crenulata* Zone. + location of Milligen Formation sections: GV, Grandview Canyon; MG, McGowan Creek; HU, Hurst Canyon; BL, Black Canyon; CH, Chamberlain Creek; and TE, Tendoy Creek.

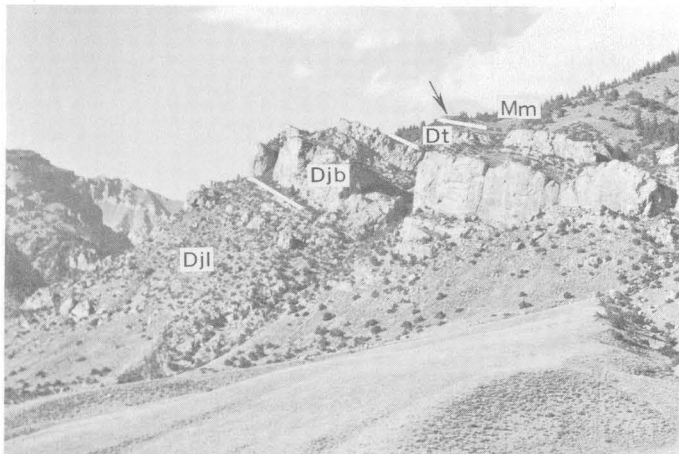


FIGURE 2.—Devonian and Mississippian rocks at south side of Lower Cedar Creek on west side of Lost River Range, 4 miles northeast of Mackay, Idaho. Conodont locality, indicated by arrow near base of Milligen Formation (Mm), is 1,100 feet above dirt road that ends at mouth of canyon to left of photograph. Milligen Formation unconformably overlies slope-forming Trident Member of Three Forks Formation (Dt), which conformably overlies Jefferson Formation. Bold cliff is formed by Birdbear Member (Djb) and underlying ledges by lower member (Djl) of Jefferson Formation.

Conodonts are present throughout the sequence from 10 to 26 feet above the base of the Milligen Formation, but the least silty and most carbonaceous limestone interbed, which is represented by sample LCD-16 from 13 to 14 feet above the base of the Milligen, yielded a large and well-preserved fauna. Several thousand conodonts were recovered by Sandberg from 3 kilograms of this sample. Although this large fauna has not yet been entirely sorted and prepared, representative specimens were examined and determined by Sandberg and Huddle.

The conodont fauna consists predominantly of Mississippian siphonodellids, pseudopolygnathids, and polygnathids, and subordinately of reworked Devonian palmatolepids, polylophodontids, and *nodocostata*-group polygnathids. The indigenous fauna is characterized by abundant *Siphonodella crenulata* (Cooper) together with *Pseudopolygnathus marginata* (Branson and Mehl) and abundant *P. triangula triangula* Voges. This association is diagnostic of the Lower *Siphonodella crenulata* Zone in Wyoming and Montana, accord-

ing to current work by C. A. Sandberg and Gilbert Klapper. This zone is indicative of an Early Mississippian (Kinderhook) age, equivalent to a part of the *Pericyclus*-Stufe (lower *cuIIa*) of Europe.

The conodont determinations confirm earlier conclusions, based solely on stratigraphic relations, that the Milligen includes no rocks as old as Devonian in the northern part of the Lost River Range and in some other parts of east-central Idaho (Ross, 1947, p. 1113; 1961, p. 217; 1962a, p. 781-782; Sloss and Moritz, 1951, p. 2161; Mapel and others, 1965).

REGIONAL SIGNIFICANCE

Lost River and Lemhi Ranges

The stratigraphy of the Milligen Formation and adjacent rocks in the Lost River and Lemhi Ranges has been described in some detail by Ross (1934, 1947, and 1961) and Shannon (1961). Outcrops of the Milligen and underlying rocks in both ranges were examined by Sandberg and Mapel in mapping or reconnaissance.

Grayish-black argillite and siltstone that form the bulk of the Milligen Formation constitute an eastward-thinning wedge in the Lost River and Lemhi Ranges. These rocks are 3,200 feet thick at McGowan Creek on the west side of the Lost River Range (Mapel and others, 1965) and probably are as thick or thicker several miles farther west near Grandview Canyon (fig. 1). The Milligen thins abruptly to only a little more than 500 feet near Lower Cedar Creek. Along the east side of the Lost River Range, northeast of Lower Cedar Creek, the grayish-black argillite in the Milligen thins southward from 460 to 340 feet. Farther south, at Hurst Canyon (fig. 1), the Milligen is estimated to be only about 200 feet thick. The Milligen generally is considerably thinner in the Lemhi Range than in the Lost River Range, but few reliable measurements have been made in the Lemhi Range because of poor exposures and faults (Ross, 1961, p. 217). At Black Canyon, near the south end of the Lemhi Range (fig. 1), the thickness of grayish-black argillite probably is 200 feet or less, as estimated by the writers.

At Lower Cedar Creek, throughout the Lost River and Lemhi Ranges, and at Grandview Canyon, the Milligen Formation overlies fossiliferous limestone at the top of the Three Forks Formation. The Three Forks is represented in these areas only by its Trident Member of Late Devonian age. This identification is based on the lithologic, faunal, and sequential similarity of the strata to the type Trident (Sandberg, 1965) at Logan, Mont. (fig. 1). The overlying Devonian and Mississippian Sappington Member and underlying Devonian Logan Gulch Member of the Three Forks

that are present at Logan and as far west as Dillon, Mont. (fig. 1), apparently were not deposited in Idaho. In southwestern Montana, the Trident contains a conodont fauna that was assigned to the *Scaphignathus velifera* Zone (to III-IV) by Klapper (1966). This zone is separated from the Lower *Siphonodella crenulata* Zone, which there occurs at or near the base of the Lodgepole Limestone, by four conodont zones—two Devonian and two Mississippian, as recognized by C. A. Sandberg and Gilbert Klapper.

The stratigraphic and faunal evidence indicates that in east-central Idaho the contact between the Milligen and Three Forks Formations is an unconformity that represents a latest Devonian to earliest Mississippian hiatus. Consequently, the Milligen is not partly Devonian anywhere in Idaho east of the Lost River Range.

Hailey area

The correlation of the type Milligen near Hailey, Idaho (fig. 1), with rocks mapped as Milligen in the Lost River Range and areas to the east is based on similar stratigraphic position and general lithologic similarity (Ross, 1934, p. 967). The exact stratigraphic relations are obscured by thrust faulting, possibly of considerable horizontal displacement (Roberts and Thomasson, 1964), and by a fairly extensive cover of Tertiary rocks. The base of the Milligen near Hailey apparently is not exposed. Its lower part was dated tentatively as Devonian (?) because of a handful of badly broken and rolled fossils, which were questionably regarded as Jefferson, from a single locality (Umpleby and others, 1930, p. 28). Ross (1934, p. 972; 1962b, p. 384) later discounted the value of these fossils for dating the Milligen; he suggested that the probability of any part of the formation being as old as Devonian was so slight as to be disregarded (Ross, 1962b, p. 384). The writers agree with Ross' later opinion. The widespread occurrence and nearly uniform thickness of the Trident Member of the Three Forks Formation between the Milligen and Jefferson Formations as far west as Grandview Canyon indicate a strong possibility of the same stratigraphic relations at Hailey, 55 miles nearly due south.

Beaverhead Mountains

The Beaverhead Mountains, which are not named on figure 1, have a northwest trend along the Idaho-Montana line (fig. 1).

Scholten and others (1955), Scholten (1957), Ross (1962a, p. 781-782), and Ramspott (1962) have discussed the geology of parts of the Beaverhead Mountains and the distribution of Mississippian rocks. Sandberg and Mapel, in 1966, examined basal Missis-

Mississippian and older rocks in this area to determine the stratigraphic relations.

The eastern limit of the miogeosynclinal Milligen Formation is partly depositional and partly structural; it approximately follows the irregular trace of a major low-angle thrust or gravity fault system. On the east side of the Beaverhead Mountains, only scattered outliers of the Milligen have been found (Scholten and others, 1955). There the Mississippian is represented largely by the cratonic Madison Group, which comprises the thin-bedded Lodgepole Limestone below and the massive Mission Canyon Limestone above. On the west side of the range, the Milligen locally is highly deformed and is found largely in fault slices (Sloss and Moritz, 1951, p. 2161).

The original depositional thickness of the allochthonous Milligen in the Beaverhead Mountains probably was on the order of 100 feet. At a section near Tendo Creek (fig. 1) in the NE $\frac{1}{4}$ NE $\frac{1}{4}$ NE $\frac{1}{4}$ sec. 21, T. 16 S., R. 11 W., Beaverhead County, Mont., at least 100 feet of gently-dipping Milligen Formation caps a high divide and rests with apparent fault contact on Ordovician Kinnikinic Quartzite.

The exact relation between the miogeosynclinal Milligen Formation and the cratonic Lodgepole Limestone is plainly evident on the west side of the Beaverhead Mountains in a series of outcrops along the crest of a ridge south of Chamberlain Creek (fig. 1) in the E $\frac{1}{2}$ sec. 31 (unsurveyed), T. 14 N., R. 29 E., Lemhi County, Idaho. There, a 50-foot-thick fault breccia, comprising mostly large angular blocks of the Jefferson Formation, Fish Haven Dolomite (Ordovician), Kinnikinic Quartzite, and Precambrian rocks, which are intermingled near the top of the breccia with small fragments of Lodgepole Limestone and Milligen Formation, is overlain by a gently dipping unfaulted sequence of Mississippian rocks. The lower part of this sequence consists of grayish-black argillite of the Milligen which grades and intertongues upward through a transitional zone containing beds of pinkish-gray siltstone and yellowish-gray and medium-gray argillaceous limestone to characteristically medium-dark-gray thin-bedded crinoidal Lodgepole Limestone. This gradational and intertonguing relation between the Milligen below and the Lodgepole above explains the presence of beds of Lodgepole-like bioclastic limestone, such as those that yielded conodonts at Lower Cedar Creek, farther west in the thick wedge of the Milligen Formation.

Southwestern Montana and western Wyoming

The Lodgepole Limestone is recognized as the lower formation of the Madison Group in southwestern Mon-

tana and extreme western Wyoming. The lower part of the Lodgepole Limestone comprises a persistent bed, 2–10 feet thick, of bioclastic limestone and a local underlying basal bed, 0.1–4 feet thick, of black carbonaceous shale. The bioclastic limestone is medium gray to medium dark gray, microcrystalline to cryptocrystalline, and glauconitic. It contains abundant medium to coarse fragments of fossils—largely crinoids. Farther east the dark shale thickens and the bioclastic limestone becomes lighter in color, less glauconitic and crinoidal, and more dolomitic.

The crinoidal bioclastic limestone at or near the base of the Lodgepole Limestone contains conodont faunas assigned to the Lower *Siphonodella crenulata* Zone at nearly 20 measured sections in southwestern and central Montana and western Wyoming (Sandberg, 1963; Klapper, 1966). In these areas, the basal shale contains the same faunas except at one section where the bottom 4 inches of the shale contains a fauna that probably represents the top of the underlying Early Mississippian upper *cu*I zone. Some of the more widely spaced sections that contain the Lower *S. crenulata* Zone are shown on figure 1; they include the type section of the Madison Group at Logan, Mont. The Lower *S. crenulata* Zone also is present in the basal part of the Lodgepole Limestone at its type locality, which lies about 100 miles northeast of the northeasternmost section shown on figure 1.

The distribution of sections in which the lower part of the Lodgepole Limestone contains the Lower *S. crenulata* Zone establishes an Early Mississippian (Kinderhook) age for basal Mississippian rocks in an area of Montana and Wyoming extending more than 300 miles from north to south and more than 150 miles from east to west. The presence of the Lower *S. crenulata* Zone in the Milligen Formation at Lower Cedar Creek extends this large area in which basal Mississippian rocks are confined largely to a single conodont zone for 165 miles southwest of Logan, Mont., and to within 50 miles of the Idaho batholith (fig. 1).

CONCLUSIONS

1. The base of the Milligen Formation and the base of the Lodgepole Limestone are virtually synchronous.
2. The age of the Milligen Formation in the Beaverhead Mountains and Lemhi and Lost River Ranges is exclusively Early Mississippian.
3. The age of the basal part of the Milligen Formation in the narrow area between the Lost River Range

and the east side of the Idaho batholith is not known but is considered to be Mississippian.

REFERENCES

- Klapper, Gilbert, 1966, Upper Devonian and Lower Mississippian conodont zones in Montana, Wyoming, and South Dakota: *Kansas Univ. Paleont. Contr.*, Paper 3, 43 p., 6 pl.
- Mapel, W. J., Read, W. H., and Smith, R. K., 1965, Geologic map and sections of the Doublespring quadrangle, Custer and Lemhi Counties, Idaho: U.S. Geol. Survey Geol. Quad. Map GQ-464.
- Ramsrott, L. D., 1962, Geology of the Eighteen Mile Peak area and petrology of the Beaverhead pluton, Idaho-Montana: Pennsylvania State Univ., unpub. Ph.D. thesis, 237 p.
- Roberts, R. J., and Thomasson, M. R., 1964, Comparison of late Paleozoic depositional history of northern Nevada and central Idaho: Art. 122 in U.S. Geol. Survey Prof. Paper 475-D, p. D1-D6.
- Ross, C. P., 1934, Correlation and interpretation of Paleozoic stratigraphy in south-central Idaho: *Geol. Soc. America Bull.*, v. 45, no. 5, p. 937-1000.
- 1947, Geology of the Borah Peak quadrangle, Idaho: *Geol. Soc. America Bull.*, v. 58, no. 12, p. 1085-1160.
- 1961, Geology of the southern part of the Lemhi Range, Idaho: U.S. Geol. Survey Bull. 1081-F, p. 189-260.
- 1962a, Paleozoic seas of central Idaho: *Geol. Soc. America Bull.*, v. 73, no. 6, p. 769-794.
- 1962b, Upper Paleozoic rocks in central Idaho, in *Geological notes*: *Am. Assoc. Petroleum Geologists Bull.*, v. 46, no. 3, p. 384-387.
- Sandberg, C. A., 1963, Dark shale unit of Devonian and Mississippian age in northern Wyoming and southern Montana: Art. 64 in U.S. Geol. Survey Prof. Paper 475-C, p. C17-C20.
- 1965, Nomenclature and correlation of lithologic subdivisions of the Jefferson and Three Forks Formations of southern Montana and northern Wyoming: U.S. Geol. Survey Bull. 1194-N, p. N1-N18.
- Sando, W. J., and Dutro, J. T., Jr., 1960, Stratigraphy and coral zonation of the Madison Group and Brazer Dolomite in northeastern Utah, western Wyoming, and southwestern Montana, in *Overthrust belt of southwestern Wyoming and adjacent areas*: Wyoming Geol. Assoc. Guidebook 15th Ann. Field Conf., 1960, p. 117-126.
- Scholten, Robert, 1957, Paleozoic evolution of the geosynclinal margin north of the Snake River Plain, Idaho-Montana: *Geol. Soc. America Bull.*, v. 68, no. 2, p. 151-170.
- Scholten, Robert, Keenmon, K. A., and Kupsch, W. O., 1955, Geology of the Lima region, southwestern Montana and adjacent Idaho: *Geol. Soc. America Bull.*, v. 66, no. 4, p. 345-404.
- Shannon, J. P., 1961, Upper Paleozoic stratigraphy of east-central Idaho: *Geol. Soc. America Bull.*, v. 72, no. 12, p. 1829-1836.
- Sloss, L. L., and Moritz, C. A., 1951, Paleozoic stratigraphy of southwestern Montana: *Am. Assoc. Petroleum Geologists Bull.*, v. 35, no. 10, p. 2145-2169.
- Umpleby, J. B., Westgate, L. G., and Ross, C. P., 1930, Geology and ore deposits of the Wood River region, Idaho: U.S. Geol. Survey Bull. 814, 250 p.



SPECTROGRAPHIC DETERMINATION OF VOLATILE ELEMENTS IN SILICATES AND CARBONATES OF GEOLOGIC INTEREST, USING AN ARGON D-C ARC

By CHARLES ANNELL, Washington, D.C.

Abstract.—A quantitative spectrographic method using a d-c arc in an argon atmosphere to determine trace amounts of Ag, Au, Bi, Cd, Ge, In, Pb, Sb, Tl and Zn in geologic samples is described. A 20-mg sample is mixed with 30 mg of anhydrous Na₂CO₃ and 5 mg of powdered graphite. The mixture subjected to a 25 amp d-c arc in an ambient argon atmosphere generally gives lower detection limits than those obtained with normal air arcings. Detection limits, in parts per million, are: Ag, 0.20; Au, 0.25; Cd, 8; Sb, 100; Zn, 4, and the remaining elements, 1.

Volatile elements such as Ag, Pb, and Zn can provide clues to the thermal history of materials of astrogeologic interest such as tektites, impactites, and meteorites. The term "volatile elements" is used here in a relative sense only for spectrochemical purposes. These elements have been found to volatilize earlier in the arcing period than the bulk of elements normally determined in silicate rocks. The quantitative spectrographic method used for silicates in the U.S. Geological Survey has a detection limit of 300 parts per million of Zn, which is far above the 1- to 20-ppm Zn content reported for 42 tektites from various strewn-fields (Schnetzler and Pinson, 1963).

A special procedure for the quantitative spectrographic analyses of geological samples is described which provides lower detection limits than normally obtained with the general method used (Bastron and others, 1960) for determining Ag, Au, Bi, Cd, Ge, In, Pb, Tl, and Zn. The detection limit for Sb is not improved by the method described here. Application to limestones and dolomites has also been found successful, provided standards having a similar carbonate matrix are used for comparison.

The effect of inert atmospheres, especially that of argon, on the line intensities of volatile elements has been reported by Vallee and others (1950) and Vallee and Baker (1956). Although their interest was cen-

tered upon the ash of human and animal organs, the principles involved in their method were found to be applicable to other inorganic materials such as silicon carbide (Morrison and others, 1960), and silicon dioxide (Vecsernyés, 1961).

EXPERIMENTAL FACTORS

Optimum operating conditions

The first application in this laboratory of an argon atmosphere with a direct-current arc was made with the intention of determining Zn at lower concentration levels in tektites. After experimentation with various electrode shapes and arcing conditions, a technique was selected using a 25 ampere d-c arc with the sample electrode held firmly in the vertical axis of a metal and ceramic open-top gas jet (Helz, 1964). Argon gas flowing annularly about the electrodes at the rate of 6.6 liters per minute, or 14 cubic feet per hour, excluded air from the arc gap. An undercut carbon electrode was found satisfactory until some tektite samples from southeast Asia displayed the unusual behavior of upwelling in the electrode shortly after the arc was struck. The incandescent bubble appearing in the optical path produced considerable background on the spectra. This phenomenon was limited to this particular group of tektites. The difficulty was remedied by using a 1/4-inch-diameter graphite electrode with a crater volume of 0.07 cubic centimeter and having a greater cross section than electrodes with a constricted undercut. In addition, the fact that graphite has greater thermal conductivity than carbon permits a more rapid heat transfer to the water-cooled electrode holder and, thereby, minimizes the heat concentration and rapid loss of more volatile constituents which cause upwelling of the sample.

The use of the graphite sample electrode extended

the applicability of the method to a greater variety of silicates. Tests were undertaken with admixtures of Na_2CO_3 or K_2CO_3 buffers, together with powdered graphite to insure smooth volatilization, to evaluate the possibility of simultaneously determining a greater number of elements. Numerous tests have indicated that the best equipment and the optimum conditions for this method are as follows:

Spectrograph: Eagle mounting, 3-meter focal length, 5,900 lines per centimeter grating. Set for second order in (1) the 2,730–3,400-angstrom range for determining Ag, Bi, Cd, Ge, In, Pb, Sb, Tl, and Zn; and in (2) the 2,510–3,180-Å range for determining Au, Bi, Fe, Ge, In, Pb, Sb, and Tl. A cylindrical, 45-cm focal length, quartz lens in front of the 25-micron slit focuses the middle third of the arc gap. A reciprocal linear dispersion of 2.73 Å/mm is obtained at 3,000 Å.

Electrodes: Graphite cup electrodes turned down to 0.225-in. outside diameter from the original 0.242-in. OD. Crater depth of 0.180 in. and width of 0.195 in., and a 120° conical base provide a crater capacity of 0.07 cc. The counter electrode is a blunt end 1/8-in.-diameter graphite rod. The analytical gap is 3 millimeters wide. Twenty milligrams of sample or standard, 30 mg of anhydrous Na_2CO_3 , and 5 mg of powdered graphite are mixed in an aluminum weighing pan with a wood or plastic toothpick and tamped into the electrode cup with a pure graphite rod.

Calibration: Two steps, 50/100 percent filter, Fe spectrum (American Society for Testing Materials, 1964).

Excitation: Total arc time of 120 seconds comprises an initial arc at 8 amp current for 5 sec and the main arc at 25 amp for the remaining 115 sec.

Atmosphere: Argon gas flow at 6.6 liters/min, or 14 cu ft/hr, through gas jet around the electrode.

Photography: Plate. Emulsion, Eastman III-O. Developed in D-19 developer for 4 min at 18°C. Acid fixed for 4 min. Washed in running water for 20 min and dried with warm-air blower.

Standards

Sample 91 (opal glass) from the U.S. National Bureau of Standards was used in preparing a standard for Zn, and pure oxides (Specpure) were used for standards of the other volatile elements. The synthetic tektite-glass base matrix used as a diluent was made from a mixture of highly pure ingredients sintered in a platinum dish at 900°C for 1/2 hour in a muffle furnace (table 1). The NBS-91 was first diluted from its initial Zn concentration of 670 ppm, as determined by X-ray fluorescence and atomic absorption (Frank Cuttitta and M. K. Carron, oral commun., 1966), to 67 ppm Zn by the addition of the matrix. Quantities of the pure oxides SnO_2 , PbO , Ag_2O , CdO , In_2O_3 , GeO_2 , Bi_2O_3 , Tl_2O_3 , and Sb_2O_4 , were then weighed and mixed with the matrix. An initial concentration of 20,000 ppm of each element was reduced to 64 ppm, in 4 steps. Equal quantities of the 67-ppm and 64-ppm standards were mixed. A dilution series

TABLE 1.—Content of constituent oxides, in weight percent, of synthetic tektite base matrix

Constituent oxide	Percent	Constituent oxide	Percent
SiO_2 (Quartz)-----	76	MgO -----	1
Al_2O_3 -----	14	Na_2CO_3 -----	1
Fe_2O_3 -----	3	TiO_2 -----	0.5
K_2CO_3 -----	2.5	Total-----	100
CaCO_3 -----	2		

was made with this new standard and the synthetic matrix to form a series of standards down to 0.26 ppm and 0.25 ppm, respectively. The 0.09 percent Pb content of NBS-91, as reported by the U.S. National Bureau of Standards, was originally included in the calculations for the preparation of our analytical standards. Recently, monitored determinations by atomic absorption have given a value of 1,025 ppm of Pb (M.K. Carron, oral commun., 1966). The corrected value has been used in our determinations (fig. 6).

Volatility

Several jumping-plate spectra were made of different silicates containing various detectable amounts of the volatile elements. These spectra were studied to determine the rates and time required for the elements to volatilize under the selected arcing conditions. The elements Ag, Bi, Cd, Ge, In, Pb, Sb, Tl, and Zn were found to volatilize in less than 100 sec, using the selected conditions and the analytical lines listed in table 2 and shown in figures 1–8. Tin did not completely volatilize all the time, and consequently, this determination was eliminated from the analytical procedure. In addition to the above elements, special interest in the determination of gold led to tests with standards containing the noble elements in a pegmatite base matrix (Bastron and others, 1960). The gold volatilized in less than 100 sec and was detected at a level as low as 0.25 ppm in the standard samples (fig. 2).

TABLE 2.—Analytical lines used, according to wavelength setting of spectrograph

High wavelength setting, 2,730–3,400 Å	Low wavelength setting, 2,510–3,180 Å
Ag, 3382.89 or 3280.68 ¹	Au, 2676.0
Bi, 3067.716	Bi, 3067.716
Cd, 3261.057	Ge, 2651.178 or 3039.064
Ge, 3039.064	In, 3039.356
In, 3039.356	Pb, 2833.069
Pb, 2833.069	Sb, 2877.92
Sb, 2877.92	Tl, 2767.9
Tl, 2767.9	
Zn, 3345.02	

¹ Interference by the strong Mn 3280.01 line. The Ag 3382.89 line is only slightly less intense, but has no noticeable interferences under these conditions (fig. 1).

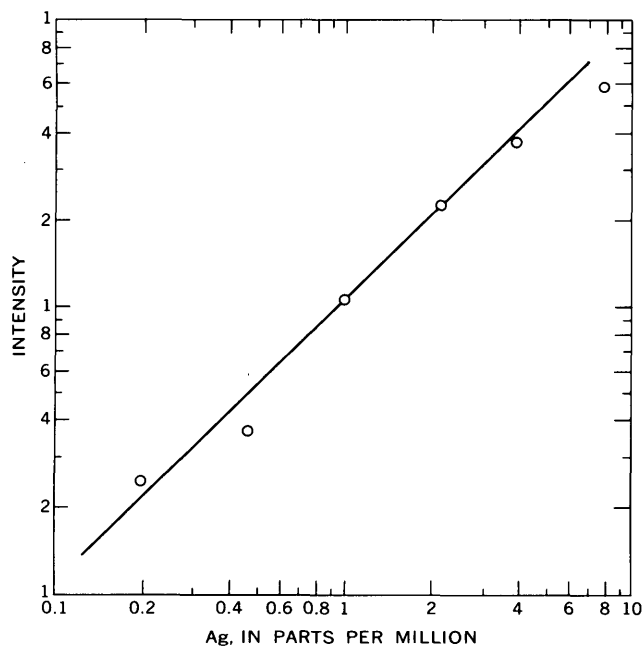


FIGURE 1.—Analytical curve for the Ag 3382.89 line.

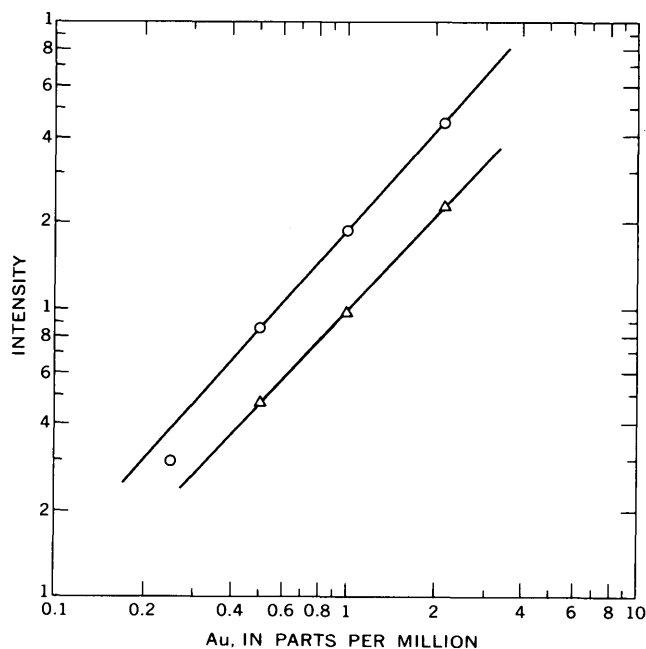


FIGURE 2.—Analytical curves of two gold lines obtained from 20-mg "pegmatite base" standards mixed with 30 mg of Na_2CO_3 and 5 mg of graphite. The Au 2676.0 line, circles, is used in the procedure described in the text. Au 2428.0 line, triangles.

Buffer additive

The effect of buffers on most line intensities of the elements was similar to that found by arcing the sample in air. This was not the conclusion reported by Thiers and Vallee (1956), using lower arc currents. They noted that when samples were arced in argon,

fractional distillation of the elements separated the volatile constituents from the alkali metals, thereby minimizing the effect of the alkalis on their line intensities.

In this work, Na_2CO_3 was found to enhance analytical lines for most of the elements. The lines used for Sb and Zn were not appreciably affected by the buffer, and, in this respect, the Na_2CO_3 acted contrary to where the sample was arced in air. The K_2CO_3 depressed most lines of the volatile elements.

DISCUSSION

Analytical curves

The analytical curves obtained by this procedure are shown in figures 1 through 8. The curves are shown with full background correction as measured in the region adjacent to the analytical line, except for the Ge 2651.2 line, for which three-fourths background is deducted to avoid overcorrection (fig. 5). The curve of the Ge 3039.064 line is used when the high wavelength setting is used (table 2) although the line is not quite as intense and gives a 2-ppm instead of 1-ppm detectability. The residual blank apparent in the Zn curve is due to a superimposed band, and many bands appear in groups of three in the region from approximately 3,330 Å up to 3.371 Å (fig. 8). These bands

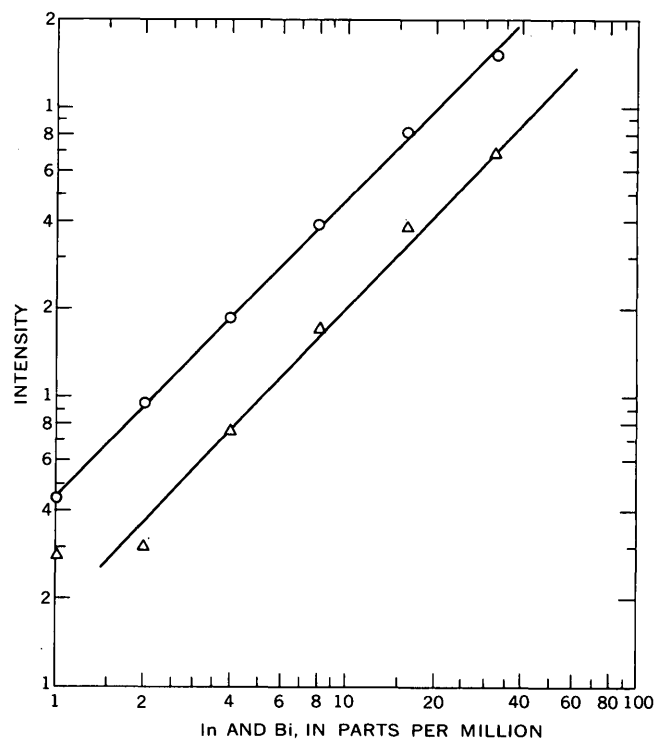


FIGURE 3.—Analytical curves of the Bi 3067.7 line, circles, and the In 3039.356 line, triangles.

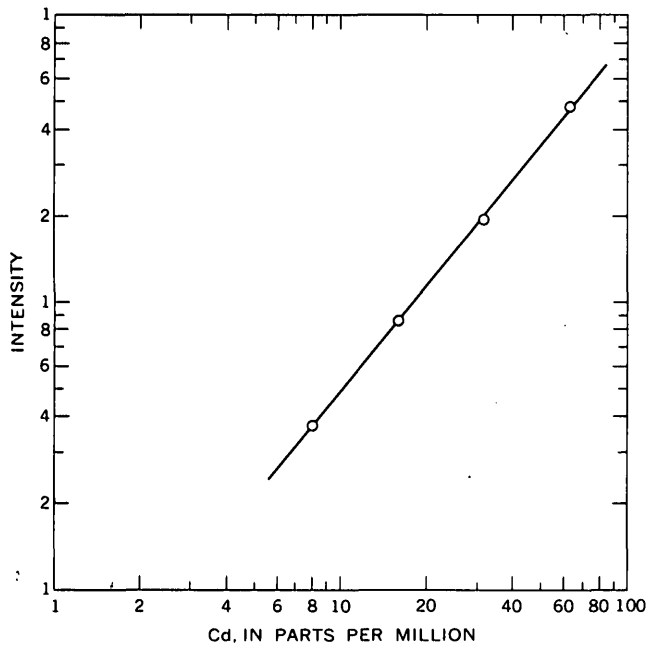


FIGURE 4.—Analytical curve of the Cd 3261.057 line.

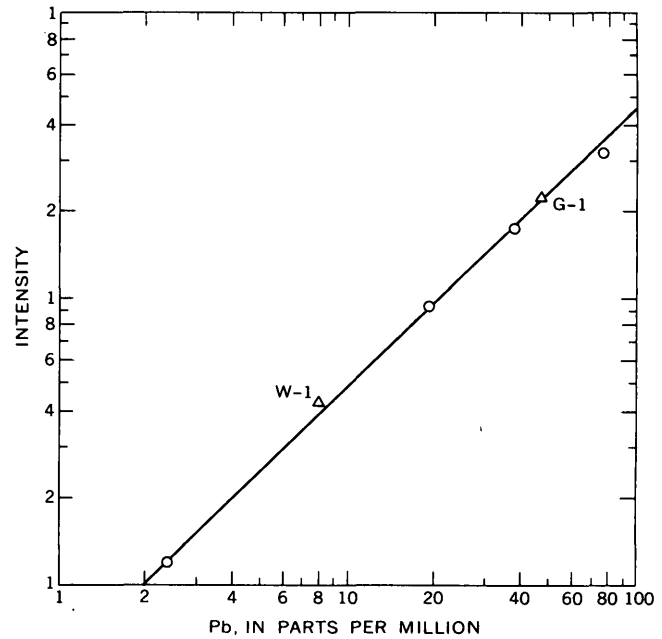


FIGURE 6.—Analytical curve of the Pb 2833.06 line. The suggested Pb values of 49 ppm and 8 ppm (Fleischer, 1965) of USGS reference standards G-1 and W-1, respectively, are included.

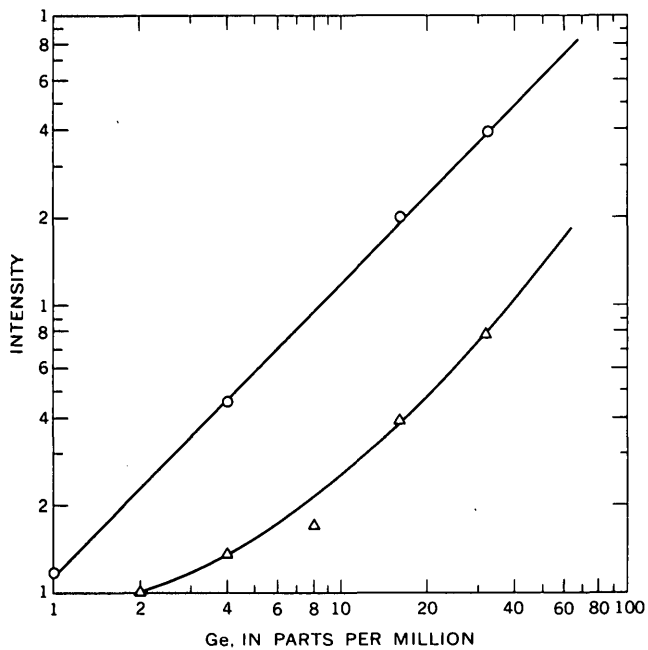


FIGURE 5.—Analytical curves of the Ge 2651.2 line, circles, with three-fourths background deducted, and the Ge 3039.064 line, triangles, with full background deduction.

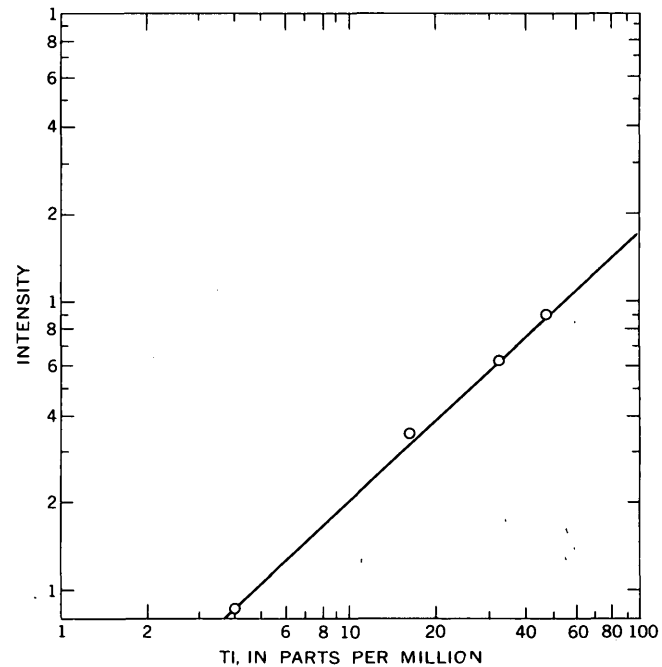


FIGURE 7.—Analytical curve of the Tl 2767.9 line.

are relatively weak and have not been previously described so far as the writer is aware. They seem to be caused by carbon molecules because they appear when blank electrodes are arced in argon.

The curves for the Au 2428 and Au 2676 lines are included, although Au has not been determined rou-

tinely in previous work (fig. 2). The Au 2428 line, which normally gives the best detectability with air arcings, is somewhat less intense than the Au 2676 line with argon arcings.

TABLE 3.—Precision and detection limits for eight volatile elements in argon d-c arc, and comparison with detection limits reported for the general quantitative method

Analytical line	Standard deviation ¹ (ppm) from samples containing—		Coefficient of variation ¹ (percent) from samples containing—		Limit of detection (ppm) from 20-mg samples reported in—	
	15 ppm	5.6 ppm	15 ppm	5.6 ppm	This report	Bastron and others (1960)
Ag 3382.89		0.28		5.0	0.2	1.0
Bi 3067.716	1.253	.35	8.3	6.1	1	10
Cd 3261.057	.756	1.55	5.0	23.4	8	50
Ge 3039.064	3.86	1.91	25.2	35.0	1	10
In 3039.356	1.418	.76	9.5	13.4	1	10
Pb 2833.01	1.03	.34	7.9	6.0	1	10
Tl 2767.9	.87	.75	5.7	13.3	1	50
Zn 3345.02	.87	1.42	5.7	25.0	4	300

¹ Standard deviations and coefficient of variations based on 10 replicate determinations.

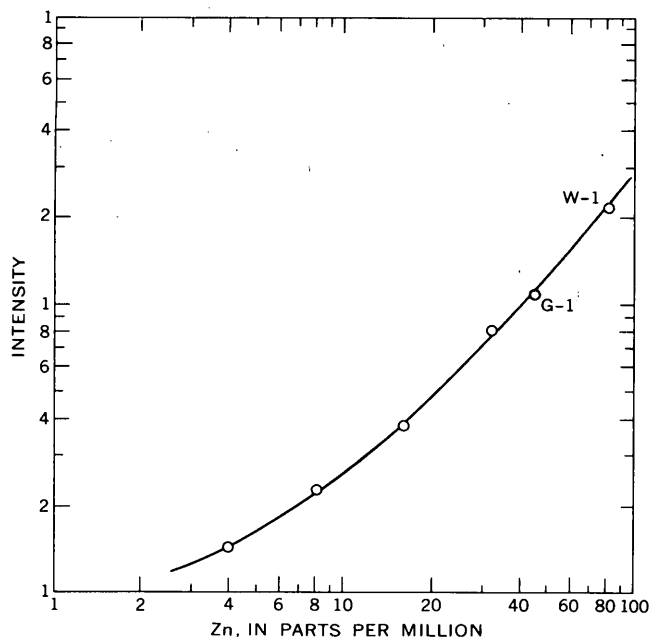


FIGURE 8.—Analytical curve of the Zn 3345.02 line with full adjacent background deducted, but without blank correction. The suggested Zn values of 45 ppm and 82 ppm (Fleischer, 1965) for USGS reference standards G-1 and W-1, respectively, are included.

Detection limit and precision

The precision of this method as shown in table 3 has been determined for the elements by calculating deviations from the average concentrations of 10 replicate arcs with each of 2 specially prepared standards. The standards contained 5.6 ppm and 15 ppm of the elements. Detection limits using this method are also compared with those obtained from the general quantitative method (table 3).

The statistics have not been obtained for the lower wavelength range, which includes the two Au lines and the preferred Ge 2651 line. The relatively poor pre-

cision of the Ge 3039 line is at least partly attributed to background interference of the In 3039.356 line. The limit of detectability for Sb is above the standards used in this test (100 ppm). No improvement in the detection of Sb was obtained by this procedure over that reported in the general quantitative method (Bastron and others, 1960).

REFERENCES

- American Society for Testing Materials, 1964, Methods for emission spectrochemical analysis; 4th ed: Philadelphia, Am. Soc. Testing Materials, 862 p.
- Bastron, Harry, Barnett, P. R., and Murata, K. J., 1960, Method for the quantitative spectrochemical analysis of rocks, minerals, ores, and other materials by a powder d-c arc technique. U.S. Geol. Survey Bull. 1084-G, p. G165-G182.
- Fleischer, Michael, 1965, Summary of new data on rock samples G-1 and W-1, 1962-1965: Geochim. et Cosmochim. Acta, v. 29, p. 1263-1283.
- Helz, A. W., 1964, A gas jet for d-c arc spectroscopy: Art. 159 in U.S. Geol. Survey Prof. Paper 475-D, p. D176-D178.
- Morrison, G. H., Rupp, R. L., and Klecak, G. L., 1960, Spectrographic analysis of high purity silicon carbide: Anal. Chemistry, v. 32, p. 933-935.
- Schnetzler, C. C., and Pinson, W. H., Jr., 1963, The chemical composition of tektites, in O'Keefe, J. A., Tektites: Chicago, Univ. Chicago Press, p. 95-129.
- Thiers, R. E., and Vallee, B. L., 1956, The effect of noble gases on the characteristics of the d.c. arc, in Proceedings of the Colloquium Spectroscopium Internationale VI, Amsterdam, 1956: New York, Pergamon Press, p. 179-185.
- Vallee, B. L., Reimer, C. B., and Loofbourow, J. B., 1950, The influence of argon, helium, oxygen, and carbon dioxide on emission spectra in the d.c. arc: Optical Soc. America Jour., v. 40, p. 751-754.
- Vallee, B. L., and Baker, M. R., 1956, Anode temperatures and characteristics of the d.c. arc in noble gasses: Optical Soc. America Jour., v. 46, p. 77-82.
- Vecsernyés, L., 1961, Spectrochemical determination of 18 trace elements in silicon: Anal. Chemie Zeitschr. v. 182, p. 429-435. [In German]



DETERMINATION OF PHOSPHORUS IN SILICATE ROCKS BY NEUTRON ACTIVATION

By L. PAUL GREENLAND, Washington, D.C.

Abstract.—Phosphorus has been determined in eight U.S. Geological Survey standard rock reference samples by neutron activation. After a 2-hour irradiation of 10-mg samples, phosphorus is separated in a radiochemically pure form by cation exchange, molybdate precipitation, magnesia precipitation, and CuS scavenging. A final magnesia precipitation yields phosphorus in a form suitable for low-level β^- counting. Subsequently, the percentage of recovery for phosphorus is determined spectrophotometrically as the yellow molybdovanadophosphoric acid. The results found by this technique are in good agreement with conventional chemical analyses.

Phosphorus is commonly determined in complete rock analyses, and thus a large quantity of data is available for this element. However, the precision of this determination normally is poor: analyses of standard rock reference samples G-1 and W-1 compiled by Stevens and others (1960), Fleischer and Stevens (1962), and Fleischer (1965) demonstrate standard deviations amounting to 50 percent of the mean. Because of the relatively high accuracy and precision of neutron activation analyses (Bowen and Gibbons, 1963), the determination of phosphorus in the U.S. Geological Survey reference samples of silicate rocks by this technique is pertinent.

The great sensitivity of neutron activation analysis provides a further advantage in that very small samples may be used because phosphorus is a relatively abundant element. When one assumes a 2-hour irradiation in a thermal neutron flux of 10^{13} neutrons per square centimeter per second followed by a 30-day decay period, a 50-percent chemical yield, and a 25-percent counting efficiency, then calculations indicate that as little as 3×10^{-2} micrograms of phosphorus may be reliably determined with the low-level negative beta-emission detector in use by the Geological Survey. Thus, 10 milligrams of sample is entirely adequate for rocks containing as little as 0.001 percent P_2O_5 ; even amounts smaller than this can be deter-

mined by employing longer irradiation times. The analytical problem, therefore, becomes one of representative sampling rather than of analytical determination.

Vincent and Curren (*in* Fleischer and Stevens, 1962, p. 530) have determined phosphorus in G-1 and W-1 by neutron activation analysis, but their procedure apparently has not been published. Atchison and Beamer (1952) and Foster and Gaitanis (1955) have determined phosphorus in magnesium and in aluminum, respectively; these procedures rely solely on the precipitation of ammonium phosphomolybdate to provide radiochemical purity. James and Richards (1955) and Thompson and others (1958) determined phosphorus in pure silicon, but their radiochemical purification procedures appear to be inadequate for silicate rocks. The procedure of Kant and others (1956) for the determination of phosphorus in silicon provides better radiochemical purity by interspersing two hydrogen sulfide scavenges and a lanthanum oxalate scavenger between repeated precipitations of magnesium ammonium phosphate. Because none of these procedures are generally applicable to silicate rocks the author devised a method, involving extensive radiochemical purification, that is suited for most materials of geologic interest.

In a thermal neutron flux, phosphorus undergoes the reaction $P^{31}(n, \gamma)P^{32}$. P^{32} decays by simple β^- emission with a maximum energy of 1.7 million electron volts and a half life of 14.3 days. Interfering reactions which must be considered are: (1) $S^{32}(n, p)P^{32}$, (2) $Cl^{35}(n, \alpha)P^{32}$, and (3) $Si^{30}(n, \gamma)Si^{31} \xrightarrow{\beta^-} P^{31}(n, \gamma)P^{32}$. Calculations indicate that under the irradiation conditions used here, none of these interfering reactions would produce significant amounts of P^{32} in ordinary silicates as compared with the main reaction. Experimental determinations of the degree of interference produced by these three reactions as summarized by Cali (1964, see tables 1 and 2) con-

firm this expectation. It should be noted, however, that the analysis of sulfides and halides may be difficult or impossible by this method.

REAGENTS AND APPARATUS

Phosphate standard: Dry $\text{NH}_2\text{H}_2\text{PO}_4$ at 130°C and weigh out enough to give a final concentration about 5 milligrams per milliliter. Dissolve this in water and acidify slightly with 1:1 HNO_3 before dilution to volume. Standardize this solution by precipitation as magnesium ammonium phosphate and ignition to the pyrophosphate as described by Hillebrand and others (1953, p. 702).

Molybdate reagent: Dissolve 30 grams of NH_4MoO_4 , 28 g NH_4NO_3 , and 23 ml of NH_4OH in 250 ml of H_2O . Filter and dilute the solution to 500 ml.

Magnesia mixture: Dissolve 25 g $\text{MgCl}_2 \cdot 6\text{H}_2\text{O}$ and 50 g NH_4Cl in 250 ml H_2O . Add NH_4OH in slight excess and let the solution stand overnight. Filter if necessary, make just acid with HCl , and dilute to 500 ml.

Copper carrier: Dissolve about 2 g metallic copper in 20 ml 1:1 HCl and dilute to about 500 ml. The exact concentration is unimportant.

Ion exchange column: A cation exchange column 9 centimeters high by 0.5 cm in diameter is prepared with Dowex 50W \times 8, 100–200 mesh, in H^{+1} form.

ANALYTICAL PROCEDURE

Irradiation

Approximately 10 mg of each sample was sealed in a clean polyethylene vial and irradiated for 2 hours in a thermal neutron flux of about $7 \times 10^{12}\text{n/cm}^2/\text{sec}^1$ at the Naval Research Laboratory reactor. After irradiation the samples were left to "cool" for at least 10 days to permit the decay of short-lived radioactive products before starting the radiochemical purification of phosphorus.

Several flux monitors were irradiated simultaneously with each batch of samples. These were prepared by dilution of a standardized $\text{NH}_4\text{H}_2\text{PO}_4$ solution (after Foster and Gaitanis, 1955) to contain 10 parts per million of P; one weighed drop of this was added to 10 milligrams of Specpure SiO_2 in a polyethylene vial. After evaporation, each vial was sealed and they were treated exactly the same as those of the samples.

Radiochemical purification

1. Weigh the sample into a platinum basin and add 1.0 ml phosphorus standard solution, 1 ml HClO_4 , and 5–10 ml Hf. For the monitors, open the vial and place it with its contents, in a platinum basin to which is added phosphorus carrier and HF-

HClO_4 mixture, the same as the samples. After 1 to 2 hours of leaching, remove the vial and treat the monitors henceforth the same as the samples. Evaporate to dryness and fume off the HClO_4 . (Strong fuming with HClO_4 is essential to ensure isotopic exchange of the carrier and radiophosphorus.)

2. Dissolve the residue in 1 ml 2M HNO_3 , dilute the solution with 10 ml H_2O , and pour it through a cation exchange column. Collect the eluent and wash the column with 10 ml 0.1M HNO_3 .
3. To the combined eluent and wash, add 2 ml HNO_3 , warm the solution, and add 5–10 ml of molybdate reagent. After cooling for 20–30 minutes, filter and wash the precipitate with 5 percent NH_4NO_3 .
4. Dissolve the precipitate in a few milliliters of 1:2 NH_4OH , add about 0.5 g citric acid, and make the solution slightly acid with 6M HCl . Add 10–15 ml of magnesia mixture and precipitate phosphorus by adding 1:1 NH_4OH dropwise with constant stirring until the precipitation is complete. Then add 10 ml 1:1 NH_4OH per 100 ml solution. After 20–30 minutes standing, filter and wash the precipitate with 1:20 NH_4OH .
5. Dissolve the precipitate in a few milliliters of 6M HCl , dilute to about 0.5M HCl and add 1 ml of copper carrier. Add a few drops of 2 percent thioacetamide solution and heat until the precipitate coagulates. Filter and boil off excess H_2S from the supernate.
6. Add 1–2 ml of magnesia mixture and precipitate phosphorus as in step 4. Filter the precipitate onto a 25-mm millipore paper disk, and wash with 1:20 NH_4OH followed by a few milliliters of methyl alcohol.
7. Dry the precipitate in air, mount the disk in an aluminum counting planchette, and count the radiophosphorus with a low-level β^- counter. Evidence of the radiochemical purity of the precipitate should be obtained by monitoring the decay for at least 2 weeks to permit a half-life determination.
8. After counting, dissolve the precipitate in 5 ml HClO_4 and dilute to volume with H_2O in a 50-ml volumetric flask. Transfer 2.0-ml aliquots of this in duplicate to 25-ml volumetric flasks and determine the phosphorus content spectrophotometrically as the molybdovanadophosphate complex using the procedure described by Rieman and Beukenkamp (1961, p. 372). The ratio of phosphorus found in the final precipitate to that added originally as carrier allows the observed counting

rate to be corrected for the chemical yield of the procedure.

9. Calculate the concentration of phosphorus in the sample by comparing the corrected sample counting rate with those of the known amounts of phosphorus in the flux monitors.

ANALYTICAL RESULTS

Results of the neutron activation analysis for phosphorus in G-1, W-1, and the six new USGS standard rock reference samples are given in table 1. The average deviation from the mean of the replicate determinations of table 1 is 12.8 percent. This figure may be taken as the empirically observed sum of the total analytical and sampling errors. A conservative estimate of the analytical errors alone suggests a relative deviation of 10 percent. It is not unreasonable to ascribe the discrepancy between these two figures to the difficulties of obtaining representative 10-mg samples. The problem of obtaining representative samples for the determination of an element concentrated in a minor phase (as phosphorus is) has been discussed in detail by Shaw (1961).

TABLE 1.—Comparison of phosphorus content in eight USGS standard rock reference samples determined by different analytical methods

[Quantities are in percentage of P₂O₅]

USGS standard rock reference samples	Sample weight (mg)	Analytical methods			
		Neutron activation (this report)	Chemical (Munson) ¹	Gravimetric (Smith) ¹	Other
Andesite, AGV-1----	9.4	0.40	0.49	0.49	-----
	8.5	.59	-----	-----	-----
Basalt, BCR-1-----	4.7	.30	.35	.35	-----
	11.0	.38	-----	-----	-----
Diabase, W-1-----	7.0	.11	-----	-----	² 0.14
	11.0	.11	-----	-----	³ .15
	10.8	.12	-----	-----	⁴ .15
	8.8	.14	-----	-----	-----
Dunite, DTS-1-----	9.0	.0015	.00	.00	-----
	11.5	.0017	-----	-----	-----
	14.2	.0020	-----	-----	-----
Granite, G-1-----	8.9	.057	-----	-----	² .09
	5.9	.060	-----	-----	³ .078
	15.5	.063	-----	-----	-----
	13.6	.080	-----	-----	-----
	9.5	.13	-----	-----	-----
Granite, G-2-----	7.1	.13	.13	.13	-----
	12.0	.13	-----	-----	-----
Granodiorite, GSP-1	5.0	.24	.28	.28	-----
	12.1	.26	-----	-----	-----
Peridotite, PCC-1---	16.2	.0015	.00	.01	-----
	6.6	.0017	-----	-----	-----

¹ Analyses quoted by F. J. Flanagan (written commun., 1966).

² Recommended values quoted by Fleischer (1965).

³ Neutron activation figures cited by Fleischer and Stevens (1962).

⁴ Isotope dilution figures cited by Fleischer and Stevens (1962).

Table 1 also compares the results of neutron activation analysis with the "recommended values" of G-1 and W-1 and with two conventional chemical analyses of the other rock reference samples. The neutron activation figures are only slightly lower than the "recommended values"; in view of the great scatter of results on which the recommendation is based, the agreement is surprisingly close. The present neutron activation results also compare well with previous neutron activation and isotope dilution data. The agreement of the neutron activation analyses with the chemical analyses of the other six rocks is remarkably good.

Three analyses by rapid chemical procedures of the six new standards are also reported by F. J. Flanagan (written commun., 1966). These have not been included in table 1 because they are not as precise as conventional analyses. In general, rapid analyses give results that are higher than those of gravimetric analyses; this is most notable in the dunite and peridotite samples where rapid analysis reports about 0.04 percent P₂O₅ for each sample as compared with about 0.0015 percent P₂O₅ by neutron activation. In view of the close agreement of the neutron activation and conventional chemical analyses, the rapid chemical analysis values should probably be neglected in any "recommended average."

REFERENCES

- Atchinson, G. J. and Beamer, W. H., 1952, Determination of trace impurities in magnesium by activation analysis: *Anal. Chemistry*, v. 24, p. 1812-1815.
- Bowen, H. J. M., and Gibbons, David, 1963, *Radioactivation analysis: New York and London, Oxford Univ. Press*, 295 p.
- Cali, J. P., 1964, *Trace analysis of semiconductor materials: New York, Macmillan Company*, 282 p.
- Fleischer, Michael, 1965, Summary of new data on rock samples G-1 and W-1, 1962-1965: *Geochim. et Cosmochim. Acta*, v. 29, p. 1263-1283.
- Fleischer, Michael, and Stevens, R. E., 1962, Summary of new data on rock samples G-1 and W-1: *Geochim. et Cosmochim. Acta*, v. 26, p. 525-543.
- Foster, L. M. and Gaitanis, C. D., 1955, Determination of phosphorus in aluminum and aluminum oxide by radioactivation analysis: *Anal. Chemistry*, v. 27, p. 1342-1344.
- Hillebrand, W. F., Lundell, G. E. F., Bright, H. A., and Hoffman, J. I., 1953, *Applied inorganic analysis*, 2d ed.: New York, John Wiley and Sons, 1034 p.
- James, J. A. and Richards, D. H., 1955, Radioactivation analysis of phosphorus in silicon: *Nature*, v. 176, p. 1026.
- Kant, A. R., Cali, J. P., and Thompson, H. D., 1956, Determination of impurities in silicon by neutron activation analysis: *Anal. Chemistry*, v. 28, p. 1867-1871.

- Rieman, William and Beukenkamp, John, 1961, Phosphorus, *in* Kolthoff, I M., Elving P. J., and Sandell, E. B., eds., *Treatise on analytical chemistry*: New York, Interscience Publishers, pt. 2, v. 5, p. 317-402.
- Shaw, D. M., 1961, Element distribution laws in geochemistry: *Geochim. et Cosmochim. Acta* v. 23, p. 116-134.
- Stevens, R. E. and others, 1960, Second report on a cooperative investigation of the composition of two silicate rocks. U.S. Geol. Survey Bull. 1113, 126 p.
- Thompson, B. A., Strause, B. M., and Leboeut, M. B., 1958, Gamma spectrometric and radiochemical analysis for impurities in ultrapure silicon: *Anal. Chemistry*, v. 30, p. 1023-1027.



DETERMINATION OF PALLADIUM IN THE PARTS-PER-BILLION RANGE IN ROCKS

By F. S. GRIMALDI and MARIAN M. SCHNEPF, Washington, D.C.

Abstract.—Acid-soluble palladium in rocks is determined spectrophotometrically with p-nitrosodimethylaniline after its separation by coprecipitation with a small amount of tellurium formed by reduction of tellurite with stannous chloride. The ignition temperature of the tellurium precipitate is critical, because of apparent low recoveries of palladium above 400°C. Higher ignition temperatures can be used, but the tellurium precipitation with palladium must then be made in the presence of microgram amounts of platinum. Palladium contents of 2.5 ppb in reference sample G-1 and 9.0 ppb in W-1 were found. Data for reference sample W-1 suggest that aqua-regia soluble palladium may well represent the total palladium in rocks. Detailed data are given on the behavior of other noble metals.

The serious lack of wet-chemical methods for determining background levels of palladium in rocks has led us to develop a high-sensitivity method applicable to determination of palladium in both the parts-per-billion range and in higher concentrations. The proposed method determines aqua-regia soluble palladium, but our data suggest that this may well represent the total palladium in rocks.

Principal separation of palladium is made by its coprecipitation with a small amount of tellurium formed by reduction of tellurite with stannous chloride (Sandell, 1959, p. 711). Palladium is finally determined spectrophotometrically with p-nitrosodimethylaniline, according to the method described by Yoe and Kirkland, 1954.

The ignition of the tellurium precipitate is a critical step. No losses of palladium occur at 400°C, but apparent low recoveries result if the precipitate is ignited at 700°C. Apparent losses can be prevented at 700°C if microgram amounts of platinum are coprecipitated with palladium. Apparent losses when platinum is absent are thought to result from failure of aqua regia to dissolve strongly ignited products. That these losses are not evident when platinum is present is probably due to the formation of a readily soluble platinum-palladium alloy.

The advantage of high-temperature ignition (700°C) is that carbon and tellurium are quickly eliminated. A disadvantage is that the ignition product cannot be used for determining both palladium and platinum inasmuch as platinum is added. However, with low-temperature ignition (400°C) an additional step, volatilization of tellurium with ammonium iodide at 400°C, is needed; otherwise tellurium would interfere through hydrolysis in the medium used in the spectrophotometric determination. Both low- and high-temperature methods were studied with good results, but the more conservative approach, the use of low-temperature ignition and minimal amounts of added platinum, is proposed.

EXPERIMENTAL METHOD

Reagents

Standard palladium stock solution, 1 milliliter = 100 micrograms of Pd: Dissolve 0.0250 gram of Pd metal by heating with 5 ml of HNO₃. Evaporate the solution to dryness and remove nitrate by several evaporations to dryness with 5-ml portions of HCl. Add 1.6 ml of 1M HCl and a little water, warm to dissolve salts, and make solution to 250-ml volume.

Standard palladium working solution, 1 ml = 1 μg of Pd: Take 5 ml of stock solution, add 3.2 ml of 1M HCl, and dilute to 500-ml volume. The pH of the solution should be 2.25.

Hydrochloric acid solution of pH 2.25: Dilute 3.2 ml of 1M HCl to 500 ml.

Buffer solution: Mix 50 ml of 4M sodium acetate with 53 ml of 4M HCl.

p-Nitrosodimethylaniline solution, 5 milligrams per ml: Dissolve 0.500 g of reagent in 80 ml of absolute ethanol. Filter on a dry paper and adjust to 100-ml volume with absolute ethanol.

Tellurium solution, 1 mg of Te per ml: Dissolve 100 mg of Te metal by heating with a mixture of 2 ml of HNO₃ and 2 ml of HCl. Evaporate the solution to dryness. Remove nitrate by several evaporations with 2 ml of HCl. Dissolve the residue in 10 ml of HCl and dilute to 100 ml with water.

Ammonium iodide solution, 100 mg NH₄I per ml: Prepare fresh as needed.

Stannous chloride solution: Dissolve 20 g of fresh SnCl₂·2H₂O in 17 ml of HCl. Dilute to 100 ml with water.

Solutions of other metals, 1 ml = 100 μg of metal: All solutions were made to have a pH of 2.25 with HCl. For the platinum metals the ammonium chlorosalts were dissolved directly in HCl of pH 2.25. For gold, the metal was dissolved in aqua regia and nitrate removed with hydrochloric acid.

Procedure

- Transfer a 10-g sample ground to -300 mesh to a 400-ml beaker. Add 50 ml of MCl, 10 ml of HNO₃, and a solution of 10 μg of Pt. Cover and digest on the steam bath for 1 hour, mixing the solution periodically by swirling. Evaporate the solution to dryness.
- Add 10 ml of HCl and after a few minutes, 10 ml of water. Cover and digest on steam bath. Add 30 ml of water and digest to dissolve soluble salts. Filter on a medium-porosity 11-centimeter paper, collecting filtrate in another 400-ml beaker. Wash residue with 8 percent by volume HCl. Reject residue. Evaporate the solution to dryness.
- Add 1 g of NH₄Cl and 10 ml of MCl. Cover and place beaker on the steam bath. The ammonium chloride aids in the destruction of nitric acid and other oxidants. After vigorous action subsides, evaporate the solution to dryness.
- Repeat step 3.
- Add 10 ml of HCl, swirl, next add 10 ml of water and digest solution on steam bath. Add 30 ml more of water and digest to dissolve soluble salts. Filter on a 7-cm medium-pore filter, collecting filtrate in a 150-ml beaker. Wash residue with 8-percent v/v HCl until the final volume is approximately 75 ml. The solution should be clear; refilter if necessary.
- Add 1 ml of tellurium solution and heat the mixture to near boiling. Add stannous chloride solution, by graduated pipet, until the color of ferric ion is bleached and tellurium starts to precipitate. Add an additional 5 ml of SnCl₂. Heat on the steam bath for 30 minutes to coagulate the precipitate. The precipitate of tellurium should be black and readily filterable. When removal of nitrate is not as thorough as provided for in the previous steps, a brown colloidal precipitate, which dissolves during the heating, vitiates the analysis. When several samples are processed, the same volume of stannous chloride solution should be added to each sample and blank, the volume being determined by the sample requiring the greatest amount of the reagent.
- Filter on a 7-cm medium-porosity paper and wash well with hot 8-percent v/v HCl. Ignite the precipitate in a small porcelain crucible at 400°C, starting with a cold furnace. Cool.
- Add 10 drops of HCl, 3 drops of HNO₃, and 3 drops of water. Cover the crucible and heat on a steam bath until the reaction subsides. Evaporate solution to dryness.
- Remove nitrogen compounds by evaporating once with 10 drops of HCl and 2 drops of water.
- Add 1 ml of NH₄I solution and evaporate to dryness on the steam bath. Place crucible in a cold furnace, raise temperature to 400°C, and maintain this temperature until all the NH₄I is sublimed. Cool.
- Repeat steps 8 and 9.
- Add 10 drops of HCl and 2 drops of water and evaporate the solution to dryness again.
- Add 0.5 ml of buffer and 2 ml of HCl solution of pH 2.25. Cover and heat for a few minutes on a steam bath.
- Filter the solution on a Fisher filtrator through a fine-porosity fritted glass filter tube of 3-ml capacity, collecting the filtrate in a 25-ml volumetric flask. Using a pipet, wash 3 times with 1-ml portions of HCl solution of pH 2.25. Cool.
- Add to the flask 0.5 ml of p-nitrosodimethylaniline. Wash down neck of the flask with 2.5 ml of absolute alcohol. Mix. Adjust to 25 ml volume with absolute alcohol and mix.
- Determine the absorbance in 5-cm cells at 530 millimicrons against a reagent blank prepared from 5 ml of HCl of pH 2.25 and the other reagents. A slit width of 0.04 millimeter is used with a Beckman DU spectrophotometer. To obviate the slow time-dependent increase in absorbance caused by platinum, add the reagent as in step 15 to one sample and read its absorbance before proceeding to the next sample. A procedural blank is carried through the analysis, starting with step 1. Reference standards for the working curve are prepared by taking 0.1 to 1 μg of Pd through the procedure, starting with step 12. No platinum is added to the reference standards. These standards yield slightly lower absorbances than standards not carried through the steps suggested, thus compensating for very slight losses of palladium that occur by adsorption or other means.

RESULTS

Coprecipitation of palladium with tellurium

Recoveries of 0.1 to 1 μg of palladium from pure solution by coprecipitation with 1 mg of tellurium were found to be quantitative by tracer experiments with radiopalladium. After precipitation and filtration of the palladium and the tellurium, the radioactivity of the filtrate was measured, and it was found to be less than 5 percent of the original palladium activity.

Recoveries of 0.1 to 1 μg of palladium from pure solutions, as determined chemically, ranged from 42 to 79 percent, averaging 58 percent, when ignition of the tellurium precipitate was made at 700°C. Recoveries seemed to be independent of palladium concentration. More than 95 percent of the palladium taken was recovered when ignitions and ammonium iodide treatments were made at 400°C. Again, more than 95 percent of the palladium taken was recovered in tests with 25, 50, and 75 μg of added platinum. Here the ignition was conducted at 700°C, and treatment with ammonium iodide was not made. Similarly, in a single test with 10 μg of platinum, 0.5 μg of palladium was recovered with 94-percent efficiency.

In other experiments without added platinum, where the ammonium iodide volatilization was made at temperatures higher than 400°C, serious apparent low recoveries of 0.1 to 1 μg of palladium resulted.

As examples, for 30-minute heating periods at 500°C, 600°C, and 700°C, respectively 93, 65, and 33 percent of the palladium was recovered when 1 μg was taken.

In experiments where palladium chloride solutions were evaporated in quartz, porcelain, or Vycor vessels, and heated from 500° to 700°C, identically low apparent recoveries of palladium were obtained. It is possible that low results at high ignition temperatures are due to volatilization of palladium or some palladium compound, but we believe that the cause lies in the failure of aqua regia to dissolve strongly ignited residues. For example, similarly treated solutions with 500 μg of palladium as chloride yield a brown residue largely insoluble in aqua regia. This inert behavior of palladium has also been noted by Beamish (1966, p. 4).

On the basis of the above experiments several equivalent procedures are possible. If ignitions are to be made at 700°C, the addition of 25 μg of platinum, prior to the tellurium precipitation step, is recommended. As noted earlier we have taken the more conservative approach in the proposed procedure, combining platinum addition (10 μg) with low-temperature ignition.

Spectral characteristics of the p-nitrosodimethylaniline color system

A plot of the absorbance difference between the palladium-nitrosodimethylaniline and reagent blank solutions as a function of wave length is saddle shaped with peaks at 500 $m\mu$ and 530 $m\mu$, the peak at 500 $m\mu$ being slightly more sensitive. A wavelength of 530 $m\mu$ was selected because the reagent absorbs weakly at this wavelength but very strongly at 500 $m\mu$. Beer's law is followed up to 0.2 parts per million of Pd, the maximum concentration tested. The sensitivity according to Sandell's notation is 0.0014 $\mu\text{g}/\text{cm}^2$ at 530 $m\mu$.

Reaction of other platinum metals and gold

The reaction of the noble elements with p-nitrosodimethylaniline at room temperature (24°C) was tested in pure solution and in the presence of 0.5 or 1 μg of palladium. Results are given in table 1. The absorbances of iridium, osmium, and gold do not change with time (at least 2 hours), and these elements should not interfere because of their low abundance in rocks. Where gold will interfere, it should be removed prior to the tellurium precipitation by extraction of chloroauric acid with an appropriate organic solvent. The absorbance of iridium is probably due to its natural color. Rhodium, ruthenium, and platinum in appreciable concentrations may interfere. Rhodium gives a

TABLE 1.—Reaction of various elements

Element	Amount (μg)	Micrograms of element equivalent to 1 μg of Pd in zero time	Absorbance increase per minute, with 5-cm cells, 24°C
Ir(IV)	100	230	None.
	100+1 μg Pd	230	Do.
	10	230	Do.
Os(IV)	100	No interference	Do.
	100+1 μg Pd	do	Do.
	10	1,200	0.0022
Rh(IV)	100+1 μg Pd	1,200	-----
	10	No interference	.0006
	100	1,500	-----
Rh(III)	100	2.4	Rapid increase.
Ru(IV)	5	38	-----
	4+1 μg Pd	40	.0008
	75	No interference	.00060
	50	do	.00043
	25	do	.00027
	10	do	.00013
Pt(IV)	50+1 μg Pd	do	.00043
	100	380	None.
	50	250	Do.
	10	105	Do.
	50+0.5 μg Pd	160	Do.
	10+0.5 μg Pd	75	Do.
Au(III)	3+0.5 μg Pd	75	Do.

red and ruthenium an olive-green color with time. Ordinarily, rhodium and ruthenium are no problem in rocks, and increase in absorbance due to platinum can be avoided if absorbance measurements are made immediately or at short but definite intervals of time following the addition of reagent. The blank carried through the procedure has added platinum and thus will compensate for the increase in absorbance in the samples. The data in the middle column of table 1 represent immediate absorbance measurements. It is interesting to note that for all ranges of platinum tested a linear relation is obtained for absorbance increase as a function of time, for a time interval of several hours.

Palladium content of reference samples G-1 and W-1

Duplicate determinations gave values of 2.3 and 2.8 parts per billion for the palladium content of G-1. These values are supported by other determinations based on G-1 spiked with various amounts of palladium, discussed below. Absorbances obtained in the 2 determinations were 0.004 and 0.005—practically the limit of detectability. However experience with the method leads us to believe that the uncertainty in absorbances should not exceed 0.002 so that the average of 2.5 ppb should not be off by more than ± 1 ppb.

Twenty determinations were made directly on W-1 and numerous others on W-1 spiked with palladium. The results ranged from 7.5 ppb to 10.0 ppb, averaging 9.0 ppb. This average is lower than 15.8 ppb reported

recently by Crocket and Skippen (1966) who determined palladium by radioactivation analysis.¹

This difference in results cannot be attributed to either the presence in W-1 of discrete palladium minerals resistant to aqua regia or to the occurrence of palladium as minute inaccessible phases in minerals resistant to aqua regia, or to both. Osmium determinations already reported by others on W-1 are so low as to preclude the presence of significant amounts of osmium-iridium, a refractory mineral that conceivably could contain palladium. Wilson and Wilson (1962, p. 703) mention that cooperite, PtS; braggite, (Pt,Pd,Ni)S; laurite, (Ru,Os)S₂; and sperrylite, PtAs₂, are very resistant to attack by aqua regia. However, these minerals should yield their palladium to aqua regia if samples are given a preliminary roast. No additional palladium was found in aqua-regia extracts of roasted material. Finally, several samples were decomposed with aqua regia, and palladium determinations made on the extracts and on the residues. A complete decomposition of the residues was made by treatment with a mixture of aqua regia and hydrofluoric acid. No palladium was found in the residues.

To determine whether the palladium values would be affected by particle size, two samples of W-1 were reduced to submicron-sized particles (determined microscopically), one by grinding for 18 hours automatically in an agate mortar, and the other by grinding for 2 hours in the Wig-L-Bug. Values of 8.3 and

9.7 ppb were obtained on the respective fractions. The average of 9.0 ppb agrees with results obtained on -300-mesh material used for all our other experiments. Of interest is the fact that aqua regia decomposed 50 percent of each of the finely ground samples compared to 36 percent of -300-mesh material.

Recovery of palladium added to reference samples G-1 and W-1

In experiments where palladium was added to G-1 and W-1, an average recovery of 93 percent of 0.1, 0.5, and 1.0 μ g was obtained. For each rock, duplicate runs were made at different times with the indicated spikes. Thus no significant losses of palladium occur either by adsorption, precipitation, or reduction of palladium on glass vessels, or on insoluble residues from the rocks. The palladium content of G-1 and of W-1 is thus further confirmed.

REFERENCES

- Beamish, F. E., 1966, *The analytical chemistry of the noble metals*, 1st ed: New York, Pergamon Press, 609 p.
- Crocket, J. H., and Skippen, G. B., 1966, Radioactivation determination of palladium in basaltic and ultrabasic rocks: *Geochim. et Cosmochim. Acta*, v. 30, p. 129-141.
- Sandell, E. B., 1959, *Colorimetric determination of traces of metals*, 3d ed.: New York-London, Interscience, 1032 p.
- Wilson, C. L., and Wilson, D. W., 1962, *Comprehensive analytical chemistry*: New York, Elsevier Publishing Co., v. 1C, 728 p.
- Yoe, J. H., and Kirkland, J. J., 1954, Separation of platinum and palladium and their subsequent colorimetric determination with p-nitrosodimethylaniline: *Anal. Chemistry*, v. 26, no. 8, p. 1335-1339.

¹ In new determinations, J. H. Crocket finds an average of 13.2 ppb for Pd content of W-1, (written commun., 1966).



GLACIATION AT WALLOWA LAKE, OREGON

By DWIGHT R. CRANDELL, Denver, Colo.

Abstract.—The great compound morainal embankments that enclose Wallowa Lake in northeastern Oregon include the deposits of at least four glaciations, of which three may be represented by two or more stades. Differentiation of drift units is largely based on conspicuous differences in depth of oxidation and the relative amount of secondary clay and calcium carbonate in weathering profiles and on the presence or absence of granodiorite boulders on moraines. The two oldest drifts are probably of pre-Sangamon age. The youngest two are correlated with drift formed during the Salmon Springs and Fraser Glaciations of western Washington.

Wallowa Lake, at the north foot of the Wallowa Mountains, is one of northeastern Oregon's finest scenic and recreational resources. Behind the lake, a precipitous mountain front rises dramatically to the summit of Chief Joseph Mountain, nearly a mile higher than the lake though less than 2 miles to the west (fig. 1). A glacial origin of the lake is revealed by spectacular morainal embankments that enclose it (fig. 2) and by ice-sculptured valleys that lie at its head. The crests of the embankments are as much as 900 feet above the lake, and their bases are hidden beneath the lake, which has a maximum depth of 283 feet (Phillips and others, 1965, p. 65) (fig. 3).

The lake is 3½ miles from north to south, and three-fourths of a mile wide; its surface lies at an altitude of a little less than 4,400 feet. It is fed by the Wallowa River, which splits into two forks above the lake. The West Fork, the largest branch, heads 10 miles upstream from the lake in a broad expanse of cirques, ridges, and peaks between altitudes of 8,000 and 10,000 feet. The East Fork heads 5 miles upstream in a high cirque that encloses Aneroid Lake.

The abrupt northwest-trending front of the Wallowa Mountains is bordered by a plain that is drained by the Wallowa River. Forty-five miles downstream from the lake, the river joins the Grand Ronde River, a tributary of the Snake.

Bedrock of the mountains south of Wallowa Lake consists of greenstone of Permian age and metasedimentary rocks of Triassic age which have been intruded by large plutons of granodiorite and quartz diorite (Smith and Allen, 1941). The Triassic rocks include hornfels, schist, crystalline limestone, and quartzite. The youngest bedrock in the region consists of basalt flows of the Miocene and Pliocene Columbia River Group. Remnants of the flows cap ridges and peaks in the highest parts of the mountains and underlie the region north of the mountain front.

The front of the range in the vicinity of Wallowa Lake roughly coincides with the Wallowa fault, which passes northwestward and southeastward into a monocline (Smith and Allen, 1941, p. 24). The present height of the mountains above the adjacent plains is due to an uplift of at least 5,000 feet along the monocline and normal fault, probably during late Tertiary time.

The compound nature of the morainal embankments bordering Wallowa Lake was first pointed out by Stovall (1929), who recognized eight lateral moraines on the east side of the lake and divided them into two groups. Moraines of the older group lack boulders of granodiorite at their surfaces and have subdued morainal topography, and the younger moraines are strewn with granodiorite boulders and have more pronounced morainal topography. The apparent difference in granodiorite content can be attributed to post-depositional weathering, inasmuch as the successive glaciers all headed in the same areas and should have been carrying granodiorite boulders. Both Stovall (1929) and Lowell (1939) believed that only two episodes of glaciation were recorded by the moraines, and they both suggested that the multiplicity of the moraines was caused by minor glacier advances and recessions during each episode. Stovall (1929, p. 78-80) also recognized two groups of moraines in the valley of Lostine River, about 12 miles northwest

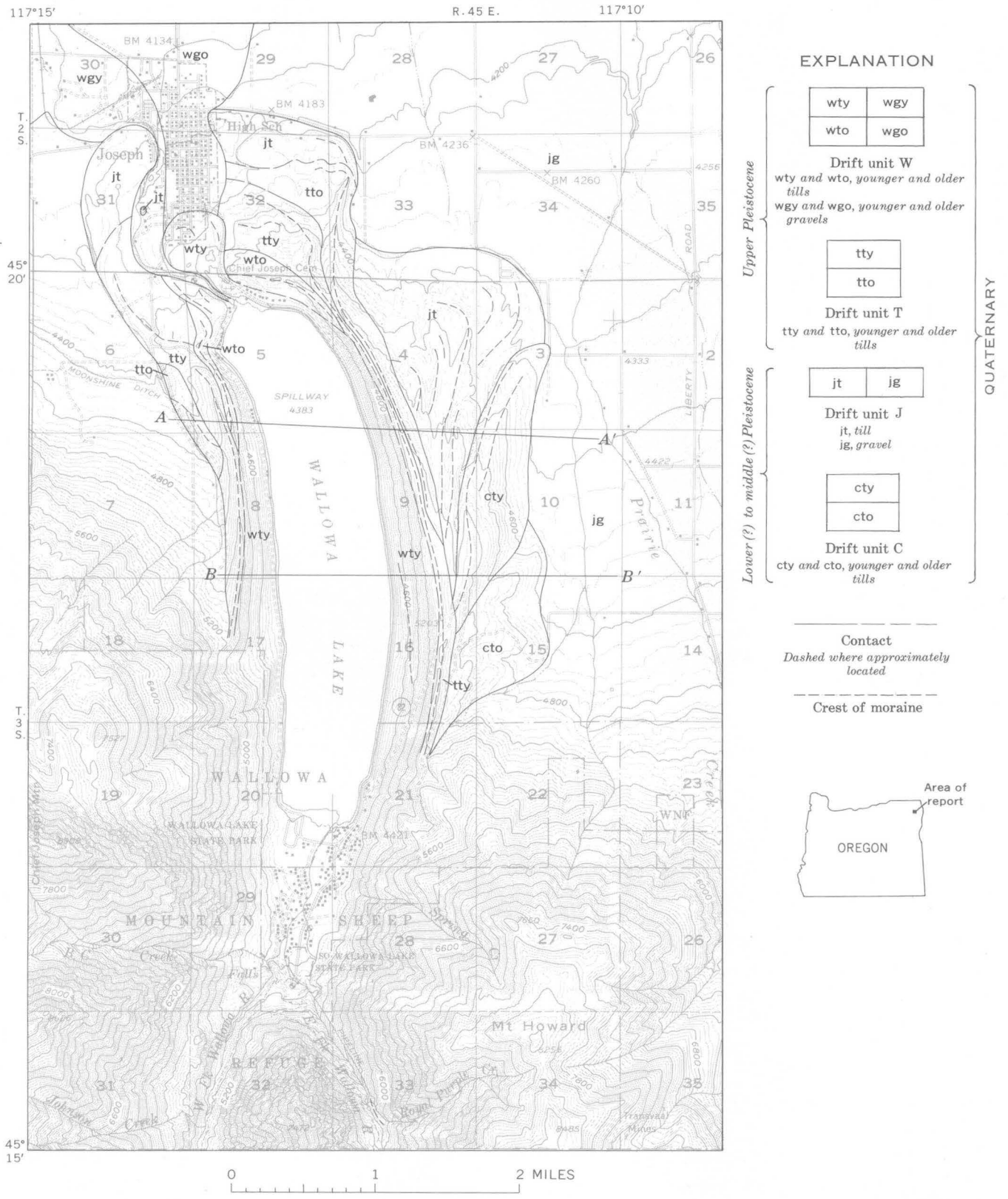


FIGURE 1.—Map of glacial deposits at Wallowa Lake. Nonglacial alluvium of various ages has not been differentiated from the outwash gravels of drift unit J on the map, and postglacial alluvium is grouped with the outwash gravels of drift unit W.

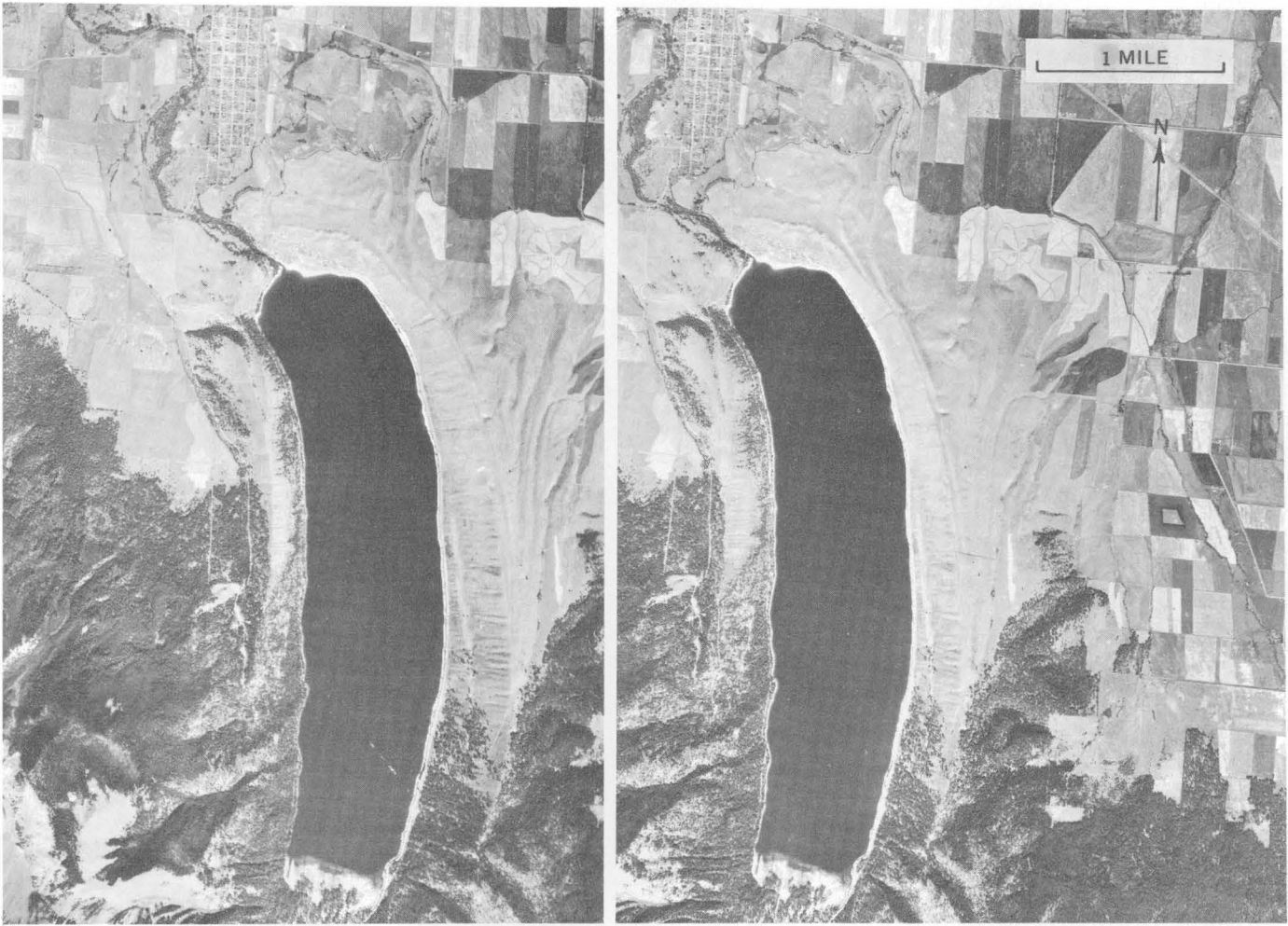


FIGURE 2.—Aerial photographs (stereoscopic pair) of moraines at Wallowa Lake. Compare with geologic map, figure 1. Army Map Service, Western High Altitude Project 109, area F, photographs 19384, 19385.

of Wallowa Lake, which he believed to represent two stages of glaciation. Lowell (1939, p. 52-53), however, suggested that both groups were formed during the same glaciation.

According to the records of the U.S. Weather Bureau, the town of Joseph, Oreg., has an average annual precipitation of about 18 inches; the moisture falls in roughly equal amounts during each month of the year except July and August, which are relatively dry. The average January temperature for 61 years of record is 23.3°F and that of July is 63.7°F. The plain bordering the mountain front is irrigated and farmed; the moraines support native grasses and other herbaceous plants over most of their area, but near the mountain front they bear a coniferous forest.

The plain is underlain by slightly acid to moderately alkaline Chernozem soils, typified by an accumulation of secondary calcium carbonate in the C horizon. The mountains are characterized by medium to very strong-

ly acid podzolic soils that lack the accumulation of calcium carbonate. Soils on the moraines to be described have some features of both Chernozems and podzolic soils. The more mature soils contain secondary calcium carbonate, but are strongly acid in the A and B horizons. A possible explanation of this combination of features is that the moraines are located in the transition zone between the relatively arid, treeless plain and the wetter, forested mountains. During extended periods of slightly increased rainfall in the past, all the moraines may have been covered by a dense coniferous forest, and during intervals less wet than the present, the same areas may have been wholly treeless.

DESCRIPTION OF THE GLACIAL DEPOSITS

The moraines that enclose Wallowa Lake, and the outwash sand and gravel deposits that extend northward beyond the lake, are here subdivided into four

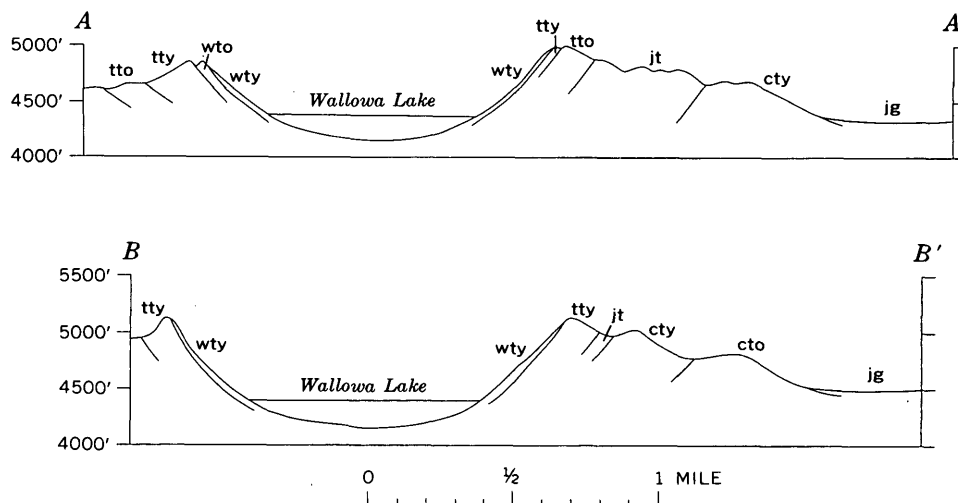


FIGURE 3.—Diagrammatic cross sections of compound morainal embankments that enclose Wallowa Lake. Positions of cross sections are shown on figure 1. Vertical exaggeration is about $\times 2$.

principal drift units which are differentiated by the extent of weathering in the drift. The units are given the arbitrary designations of C, J, T, and W for convenience of reference; drift unit C is the oldest, and unit W the youngest. In addition, some drift units are further divided on the basis of crosscutting relations displayed by their moraines.

Drift unit C

The most extensively weathered drift recognized is on the east side of Wallowa Lake, outside of and lower than the crest of the compound morainal embankment that borders the lake. It is designated on figure 1 as the older till of drift unit C. Shallow excavations in this till revealed a clayey profile of weathering that extends to a depth of more than 4 feet. Basalt fragments as large as 3 inches in diameter in the till can easily be cut through with the blade of a shovel. The till is noncalcareous and consists of a reddish-brown stony clay having a coarse angular blocky structure; this clay grades downward into yellowish-red stony clay. A zone of secondary calcium carbonate was not seen; if present, it is presumably at a depth greater than 4 feet. Boulders exposed at the ground surface are few in number and are all of rock types other than granodiorite. The till is deeply eroded and no longer has morainal topography.

At its northwestern edge, the older till of drift unit C is truncated by a north-trending moraine that continues for about 2 miles and is shown on figure 1 as the younger till of drift unit C. Shallow excavations in the moraine also revealed a clayey profile of weathering, and the widely scattered boulders at its surface are all of rock types other than granodiorite. Because

of these weathering features, the moraine is assigned to drift unit C, although it may represent a separate episode of glaciation.

Drift unit J

Drift unit J includes a series of nested, arcuate end moraines on the northeast side of Wallowa Lake, a terminal moraine at the town of Joseph, and outwash sand and gravel deposits north of the mountain front. The absence of deep clayey profiles of weathering indicates that the drift is younger than unit C. The arcuate moraines were formed by a glacier lobe that extended northeastward for more than a mile beyond the basin of Wallowa Lake. Although gross morainal forms are still recognizable, surface drainage is well integrated and there are no closed depressions.

The outwash plain formed by deposits of drift unit J merges southward with broad compound fans along the mountain front; some of these fans head in glaciated valleys adjacent to that of the Wallowa River. The fans probably include outwash and alluvial deposits of more than one age.

The following profile of weathering on the terminal moraine of drift unit J is exposed in artificial excavations on the south and east sides of the grounds of the Joseph High School, in the SE $\frac{1}{4}$ SW $\frac{1}{4}$ sec. 29:

	Thickness	
	Feet	Inches
4. Sand, silt, and scattered stones; very dark brown (10YR 2/2) at top grading down into dark yellowish brown, noncalcareous, structureless...	2	6
3. Till, clayey, dark-reddish-brown (5YR 3/4), structureless, plastic, slightly sticky; contains disseminated masses of secondary CaCO ₃ (pH 4-5).	6	0
2. Till, strongly impregnated with secondary CaCO ₃ .	2	0
1. Till, sandy and silty, yellowish-brown, calcareous.	>1	0

Because of its generally well sorted character, unit 4 of the measured section is believed to be chiefly of eolian origin; scattered stones in it may have been derived from the underlying till by frost heaving. The eolian deposit probably is much younger than drift unit J. Eolian sand also mantles parts of the arcuate moraines northeast of the lake. The clayey nature of unit 3 in the measured section indicates that it probably is the B horizon of a soil profile; the secondary calcium carbonate in it may have been derived from leaching of the overlying silt and sand during an interval of weathering younger than that which produced the profile in drift unit J.

A weathering profile in till of the terminal moraine is also exposed 0.5 mile west of the Joseph High School. It includes a strongly developed zone of secondary calcium carbonate 2.5 feet thick, which is underlain by a zone of disseminated calcium carbonate also 2.5 feet thick. In this outcrop all boulders of granodiorite within 6 feet of the ground surface are in various states of disintegration, although many similar boulders are still firm at a depth of 10 feet. The B soil horizon is absent here; the Cca horizon is directly overlain by eolian material and colluvium.

Although boulders are abundant at the surface of the terminal moraine, none consist of granodiorite. Granodiorite boulders also are absent at the surface of the arcuate moraines northeast of the lake.

The thick Cca horizon that characterizes drift unit J probably indicates a considerable antiquity. Calcium carbonate seems to make up nearly 100 percent of the bulk of the horizon, a feature that is characteristic of weathering profiles thought to be of pre-Wisconsin age elsewhere in the Western United States (Malde, 1955, p. 247; Scott, 1963, p. 24).

Deposits of sand and gravel that probably are mostly outwash of drift unit J underlie the broad plain northeast of Wallowa Lake. The following profile of weathering is exposed in a gravel pit in these deposits in the SW $\frac{1}{4}$ sec. 21, about 1 mile northeast of Joseph (locality 1, fig. 4):

	Thickness	
	Ft.	In.
4. Sand, silty, black (humic), noncalcareous (pH 4.5), structureless, slightly plastic-----	6	
3. Sand, clayey and silty, dark-brown (10YR 4/3), noncalcareous (pH 5), coarse prismatic structure, plastic, slightly sticky; contains scattered stones.-----	7	
2. Sand and gravel, strongly impregnated with secondary CaCO ₃ -----	2	6
1. Sand and pebble to cobble gravel, brown (10YR 5/8); contains disseminated secondary CaCO ₃ ---	>2	0

Unit 3 of this measured section contains secondary clay and is regarded as the B horizon of a soil profile.

Sand and gravel deposits having a similar profile of

weathering also are exposed at the NE cor. NW $\frac{1}{4}$ SW $\frac{1}{4}$ sec. 3, about 1 mile west of the town of Enterprise (locality 2, fig. 4). The deposit forms a low ridge that is slightly higher than the adjacent surface of younger gravel deposits. Sand and gravel of unit J also is well exposed in the north wall of a pit about 2.5 miles southeast of Enterprise (locality 3, fig. 4); here the gravel is oxidized to a depth of more than 20 feet.

Drift unit T

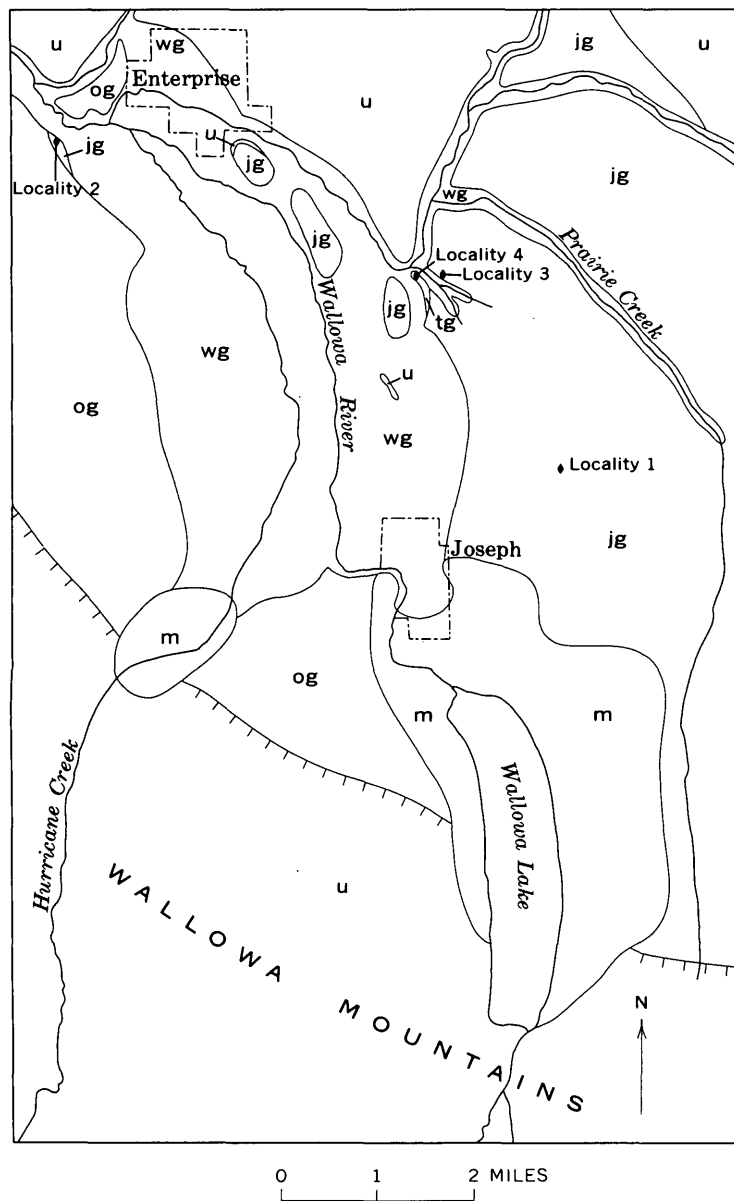
Drift unit T includes paired lateral moraines that form the crest of the two embankments flanking the lake, and two correlative terminal moraines at the north end of the lake. For convenience of reference the two parts of drift unit T are designated older and younger tills. Differences in the altitude of points on the crest of the lateral moraine of the younger till in the NE $\frac{1}{4}$ sec. 16, and on the correlative terminal moraine in the SE $\frac{1}{4}$ sec. 32, indicate that the surface gradient along the lower 3 miles of the glacier was about 280 feet per mile.

The terminal moraine of the older till of drift unit T has smoothly graded slopes, and surface drainage is generally integrated, although a few depressions in the moraine directly east of Joseph are closed. Moraines of the older till are the oldest moraines at Wallowa Lake on which boulders are abundant at the ground surface; 10-30 percent of these are granodiorite boulders, all of which have surfaces roughened by weathering.

A short segment of lateral moraine that is part of the older till lies west of Wallowa Lake in the SE $\frac{1}{4}$ sec. 6. A roadcut exposes the following section at the crest of the moraine. Unit 3 in this measured section probably is colluvium; unit 2 is a clay-enriched B horizon. An accumulation of secondary calcium carbonate was not seen.

	Thickness	
	Ft.	In.
3. Sand, silty and clayey, and scattered stones, dark-brown (7.5YR 5/4), noncalcareous (pH 4), structureless, plastic, slightly sticky-----	4	0
2. Till, clayey, dark-reddish-brown (5YR 4/4), noncalcareous (pH 4), structureless, plastic, sticky; granules break and smear when till is cut with pick-----	3	0
1. Till, sandy, dark-yellowish-brown (10YR 4/4), noncalcareous (pH 4), nonplastic, nonsticky---	>12	0

The following profile of weathering in younger till of drift unit T is exposed in a roadcut 0.7 mile southwest of Joseph, in the SE $\frac{1}{4}$ NE $\frac{1}{4}$ sec. 6. In this cut, nearly all granodiorite boulders within 6 feet of the ground surface are in various stages of disintegration.



EXPLANATION

- m
Moraine deposits
Undifferentiated as to age
 - wg
Outwash sand and gravel deposits of drift unit W, and Recent alluvium
 - tg
Outwash sand and gravel deposits of drift unit T
 - ig
Outwash sand and gravel deposits of drift unit J
Locally include alluvium probably older than till of unit J
 - og
Undifferentiated outwash sand and gravel deposits and alluvium
Probably older than drift unit J
 - u
Bedrock and undifferentiated surficial deposits
- Contact
Approximately located
- North front of the Wallowa Mountains
- Locality 4
 Locality mentioned in text

QUATERNARY

FIGURE 4.—Map showing distribution of glaciofluvial deposits and alluvium between Wallowa Lake and Enterprise, Oreg.

	<u>Thickness</u>	
	Ft	In.
4. Till, sandy, black (humic), noncalcareous (pH 5), structureless, loose, nonplastic.....	1	0
3. Till, silty and clayey, dark-reddish-brown (5YR 3/4), noncalcareous (pH 4), angular blocky structure, slightly plastic, nonsticky.....	2	6
2. Till, sandy and silty, olive-brown (2.5Y 4/4), calcareous; locally contains small amount of secondary CaCO ₃ in horizontal layers as much as half an inch thick in the uppermost 2 in., and as coatings on stones, in veinlets, and in disseminated small irregular masses (pH 7).....	1	6
1. Till, sandy, olive-brown (2.5Y 4/4), locally calcareous (pH 6).....	>4	0

An age difference within drift unit T is expressed by the crosscutting relation displayed, in sec. 6 west of Wallowa Lake, between moraines of the older and younger tills. However, profiles of weathering in the tills of the two moraines do not seem significantly

different, and both moraines probably were deposited during stades of the same glaciation.

Outwash sand and gravel deposits of drift unit T are not found adjacent to the terminal moraines at Wallowa Lake. However, 2.5 miles north of Joseph, the following profile of weathering is exposed in a small remnant of gravel that probably is part of unit T, at the SE cor. sec. 7 (locality 4, fig. 4).

	<u>Thickness</u>	
	Ft	In.
4. Silt, sand, and scattered stones, grayish-brown (10YR 5/2), noncalcareous (pH 5), structureless, nonplastic, nonsticky (may include some spoil from a nearby irrigation ditch).....		8
3. Silt, sand, and scattered stones, grayish-brown (2.5Y 5/2), weak prismatic structure, slightly plastic, nonsticky.....	1	6

- | | <i>Thickness</i>
<i>ft.</i> |
|---|--------------------------------|
| 2. Sand and pebble to cobble gravel that contains scattered boulders, unoxidized; secondary CaCO ₃ partly coats stones in upper 3 feet and weakly impregnates interstitial sand in some zones..... | 3 0 |
| 1. Sand and gravel, unoxidized, noncalcareous..... | >5 0 |

This outwash deposit forms a terrace about 30 feet higher than the adjacent flood plain of Prairie Creek, and about 15 feet lower than an adjacent surface formed by sand and gravel of drift unit J.

Drift unit W

Drift unit W includes two terminal moraines at the north end of Wallowa Lake which are designated the older and younger tills. A gap in the moraine of the older till is partly occupied by a moraine of the younger till, which in turn is breached by the Wallowa River at the lake's outlet. Lateral moraines of the younger till bound both sides of the lake, and an inconspicuous north-sloping lateral moraine descends the east morainial embankment about a mile from the south end of the lake. Within the mountains, a lateral moraine of drift unit W was noted in the valley of the East Fork of the Wallowa River at the mouth of Royal Purple Creek (fig. 1), and a small recessional moraine lies on the valley floor about a mile farther upvalley. Two other moraines in the East Fork valley were described by Stovall (1929, p. 75-76), 1 $\frac{2}{3}$ and 2 $\frac{1}{2}$ miles upstream from the mouth of Royal Purple Creek, respectively. At the first locality, there is an abrupt topographic step in the bedrock floor of the valley. Although till in this area is as much as 100 feet thick, most of the relief is due to the bedrock and not to an end moraine. The feature described by Stovall farther upvalley also is in an area of locally rough bedrock topography and probably is not an end moraine. Aneroid Lake occupies a glacially scoured basin in bedrock at the head of the valley.

Surface drainage on the moraines of drift unit W is poorly integrated or unintegrated, and closed depressions are common. The moraines are distinguished chiefly by relatively immature profiles of weathering in which zones of secondary calcium carbonate and secondary clay are absent.

A profile of weathering in a moraine of the older till on the west side of Wallowa Lake is exposed in a roadcut in the NW $\frac{1}{4}$ SW $\frac{1}{4}$ sec. 5.

- | | <i>Thickness</i>
<i>(feet)</i> |
|--|-----------------------------------|
| 2. Sand and scattered stones, dark-olive-gray (5Y 3/2), noncalcareous (pH 4), structureless, nonsticky, nonplastic..... | 2 |
| 1. Till, sandy, pale-olive (5Y 6/4), grades into olive-gray (5Y 5/2) 4 feet below top of unit, noncalcareous (pH 4), structureless, nonsticky, nonplastic..... | >5 |

The following profile of weathering is exposed in a roadcut in the terminal moraine of the younger till of

drift unit W near Chief Joseph Cemetery, in the NW $\frac{1}{4}$ sec. 5.

- | | <i>Thickness</i>
<i>(feet)</i> |
|--|-----------------------------------|
| 2. Till, sandy, dark-brown (10YR 4/3), slightly darker in uppermost few inches, noncalcareous (pH 4), structureless, nonplastic..... | 3 |
| 1. Till, sandy, olive-gray (5Y 5/2), slightly calcareous (pH 5)..... | >10 |

A count of 100 boulders on the surface of the younger till at the north end of Wallowa Lake revealed 32 of granodiorite. The entire exposed surfaces of all the granodiorite boulders have been roughened by weathering. In a wave-cut cliff in till adjacent to the lake, about 75 percent of the granodiorite boulders larger than 6 inches in diameter are firm at the surface in the upper 6 feet of the till, although most of the smaller stones have disintegrated.

The recessional moraine about 2 miles upstream from Wallowa Lake in the East Fork valley has a similar immature weathering profile. A shallow pit dug in the moraine revealed a slightly humified zone 1-2 inches thick, which has a pH of about 4.5. Beneath this zone is light-olive-brown (2.5Y 5/4) sandy till in which the matrix consists mostly of grus derived from granodiorite. Boulders on the moraine are chiefly granodiorite, although a few are basalt. Here, also, the surfaces of all the granodiorite boulders have been roughened by weathering.

The crosscutting relation displayed by the two terminal moraines of drift unit W at the north end of Wallowa Lake suggests an age difference between them; however, a close similarity in weathering profiles suggests that the two moraines were deposited during stades of the same glaciation.

Outwash sand and gravel deposits belonging to drift unit W underlie the town of Joseph and, merging with outwash heading in the valley of Hurricane Creek, extend northward beneath the flood plain and low terraces along the Wallowa River at least as far as Enterprise (fig. 4). A deposit correlated with the older till forms a broad fan north of Joseph; it is trenched to a depth of about 25 feet by the present valley of the Wallowa River. Sand and gravel deposits of drift unit W are distinguished by the lack of secondary calcium carbonate in the weathering profile.

MORAINES IN THE LOSTINE RIVER VALLEY

A brief reconnaissance was made of the lower part of the valley of Lostine River, 6 miles west of Enterprise, in an attempt to find moraines correlative with the sequence at Wallowa Lake; however, only drifts correlated with units W and J were recognized. A lateral moraine of unit J on the east valley wall

(NE $\frac{1}{4}$ sec. 22 and SW $\frac{1}{4}$ sec. 23, T. 1 S., R. 43 E.) was deposited by a glacier that terminated a little less than half a mile south of the community of Lostine. About 1.5 miles south of Lostine (SE $\frac{1}{4}$ sec. 22), the road along the valley floor crosses the northernmost moraine of a series of three end moraines, in each of which the till bears a profile of weathering like that of drift unit W at Wallowa Lake. The middle moraine of the group (in sec. 27) has several distinct crests. The northernmost moraine of the series ascends the east valley wall, where it directly abuts the lateral moraine of drift unit J; moraines of unit T were not recognized.

CORRELATIONS

Comparisons of weathering profiles and other features of the four major drift units just described suggest that relatively long periods of time elapsed between the formation of the successive drifts, and, moreover, that each drift unit was subjected to substantially less intense weathering than the one which preceded it.

Drift unit W was formed during the last major glaciation of the Wallowa River valley, and is probably correlative with drift formed during the last major glaciation elsewhere in the United States. The shallow and weakly developed profile of weathering in the till of unit W is similar to that in till deposited during the Fraser Glaciation in western Washington, which extended from about 25,000 to 10,000 years ago (Armstrong and others, 1965). This glacial episode is correlative with the Pinedale Glaciation of the Rocky Mountains (see Richmond, 1965) and the Tioga Glaciation of the Sierra Nevada (see Wahrhaftig and Birman, 1965).

The profile of weathering in till of drift unit T is distinguished from that of drift unit W chiefly by the presence of a dark-reddish-brown clay-enriched B horizon and a thin, weak and discontinuous zone of secondary calcium carbonate. These features indicate that drift unit T has been exposed to more intense weathering processes and the drift is thought to represent a distinctly older glaciation. This glaciation is tentatively correlated with the Salmon Springs Glaciation in western Washington (Crandell, 1965, p. 345), which includes at least two glacial advances separated by an episode of warmer climate (Easterbrook and others, 1967). The two moraines of drift unit T may be local correlatives of these two glacial advances. The glaciation responsible for drift unit T is tenta-

tively correlated with the Bull Lake Glaciation of the Rocky Mountains (see Richmond, 1965) and with the Tahoe (older) and Tenaya (younger) Glaciations of the Sierra Nevada (see Wahrhaftig and Birman, 1965).

Drift unit J is readily distinguished from drift units T and W by the absence on it of granodiorite boulders. Profiles of weathering in till of unit J have a dark-reddish-brown clay-enriched B horizon, and a very strongly developed zone of secondary calcium carbonate. The disintegration of granodiorite boulders and the accumulation of such an intense Cca horizon probably represent an episode of weathering greater in intensity than any of those affecting deposits younger than drift unit J. This episode may be correlative with the Puyallup Interglaciation in western Washington (see Crandell, 1965, p. 345) and the Sangamon Interglaciation in the central United States.

Even more intense weathering is indicated by the clayey weathering profile of drift unit C, which probably was largely developed during a pre-Sangamon interglaciation. However, there is no basis for correlating either drift unit C or J with specific glaciations elsewhere.

REFERENCES

- Armstrong, J. E., Crandell, D. R., Easterbrook, D. J., and Noble, J. B., 1965, Late Pleistocene stratigraphy and chronology in southwestern British Columbia and northwestern Washington: *Geol. Soc. America Bull.*, v. 76, p. 321-330.
- Crandell, D. R., 1965, The glacial history of western Washington and Oregon, in Wright, H. E., Jr., and Frey, D. G., eds., *The Quaternary of the United States*: Princeton Univ. Press, p. 341-353.
- Easterbrook, D. J., Crandell, D. R., and Leopold, E. B., 1967, Pre-Olympia Pleistocene stratigraphy and chronology in the central Puget Lowland, Washington: *Geol. Soc. America Bull.* v. 78, p. 13-20.
- Lowell, W. R., 1939, Glaciation in the Wallowa Mountains [Oregon]: Chicago Univ. unpub. M.S. thesis.
- Malde, H. E., 1955, Surficial geology of the Louisville quadrangle, Colorado: U.S. Geol. Survey Bull. 996-E, p. 217-259.
- Phillips, K. N., Newcomb, R. C., Swenson, H. A., and Laird, L. B., 1965, Water for Oregon: U.S. Geol. Survey Water-Supply Paper 1649, 150 p.
- Richmond, G. M., 1965, Glaciation of the Rocky Mountains, in Wright, H. E., Jr., and Frey, D. G., eds., *The Quaternary of the United States*: Princeton Univ. Press, p. 217-230.
- Scott, G. R., 1963, Quaternary geology and geomorphic history of the Kassler quadrangle, Colorado: U.S. Geol. Survey Prof. Paper 421-A, 70 p.
- Smith, W. D. P., and Allen, J. E., 1941, Geology and physiography of the northern Wallowa Mountains, Oregon: Oregon Dept. Geology, Mineral Industries Bull. 12, 64 p.

Stovall, J. C., 1929, Pleistocene geology and physiography of the Wallowa Mountains [Oregon], with special reference to the Wallowa and Hurricane Canyons: Oregon Univ. unpub. M.S. thesis.

Wahrhaftig, Clyde, and Birman, J. H., 1965, the Quaternary of the Pacific mountain system in California, *in* Wright, H. E., Jr., and Frey, D. G., eds., *The Quaternary of the United States*: Princeton Univ. Press, p. 299-340.



OBSERVATIONS ON THE TETON GLACIER, GRAND TETON NATIONAL PARK, WYOMING, 1965 AND 1966

By JOHN C. REED, JR., Washington, D.C.

Abstract.—Resurvey in 1966 of markers placed across the Teton Glacier near the snowline in 1963, 1964, and 1965 indicates that the average rate of ice movement near the center is probably about 28 feet per year. Previously computed and reported movement rates of 30 to nearly 35 feet per year between 1963 and 1964 are too high because of surveying errors. Transverse profiles indicate that the central part of the glacier was 2–8 feet thicker in 1966 than in 1963. Direct measurement in a glacier mill near the surveyed profile indicates that the ice is about 64 feet thick. Locally, the terminus has advanced as much as 30 feet, but most of it remains in virtually the same position as in 1963.

During the summers of 1965 and 1966, surveys on the Teton Glacier were continued to determine the amount and rate of movement, the thickness of the ice, and general regimen of the glacier. Reed (1964, 1965) has reported the results of similar surveys in the summers of 1963 and 1964 and summarized previous observations on the regimen of the glacier. R. Alan Mebane, Assistant Chief Naturalist of Grand Teton National Park, assisted in making the 1965 and 1966 surveys, as well as those in 1963 and 1964; William McKeel assisted in both the 1965 and 1966 surveys. Their able and enthusiastic assistance and the generous cooperation of many other members of the staff of Grand Teton National Park are gratefully acknowledged.

The 1965 survey was made on August 19 with an engineer's transit. Weathering during the survey was extremely bad; much of the lower part of the glacier was still covered by snow so that only one of the stakes placed in previous years was recovered. The reference mark at the north end of the profile along which the 1963 and 1964 marks were placed was also snow covered, and therefore the 1965 markers had to be placed along an arbitrary line from the reference mark on the south wall to a new reference mark on the north

wall. The line of markers was placed as near as possible to the line used in the 1963 and 1964 surveys (line Y–Y', fig. 1), but measurements in 1966, when both the old and new reference points on the north end of the line were visible, showed that the 1965 line was 7.5 feet too far downglacier at point 12, 1,110 feet from the south wall. The location and altitude of the 1965 markers are given in table 1.

TABLE 1.—Location and altitude of markers placed on line across the Teton Glacier on August 19, 1965¹

Point	Distance from red paint mark on south wall (feet)	Altitude of snow or ice surface above arbitrary datum (feet) ²	Depth of snow (feet)
1-----	35	621.5	-----
2-----	87	624.4	1.5
3-----	185	629.3	.6
4-----	310	654.2	.9
5-----	410	651.1	1.5
6-----	510	646.5	1.6
7-----	610	653.9	1.5
8-----	710	653.3	.5
9-----	810	648.0	0
10-----	910	655.2	.1
11-----	1,010	656.8	.8
12-----	1,110	659.8	1.5
Yellow painted cross (+) on boulder in moraine--	1,266	-----	-----

¹ All points, except 9, marked by nails 1 foot long countersunk into snow and surrounded by yellow painted rocks. Point 9 is marked by a cross (+) painted red on top of a large erratic boulder 6.5 feet above the ice surface.

² Arbitrary datum is approximately 9,780 feet above sea level.

The 1966 survey was made on July 25 with a plane-table and telescopic alidade. Weather conditions were ideal. Most of the central part of the glacier was free of snow, and many of the markers placed during previous surveys were found (fig. 2). A new series of stakes was placed along the transverse profile used in the 1963 and 1964 surveys (line Y–Y', figs. 1 and 2); their locations and altitudes are given in table 2. In addition, the longitudinal profile of the glacier along

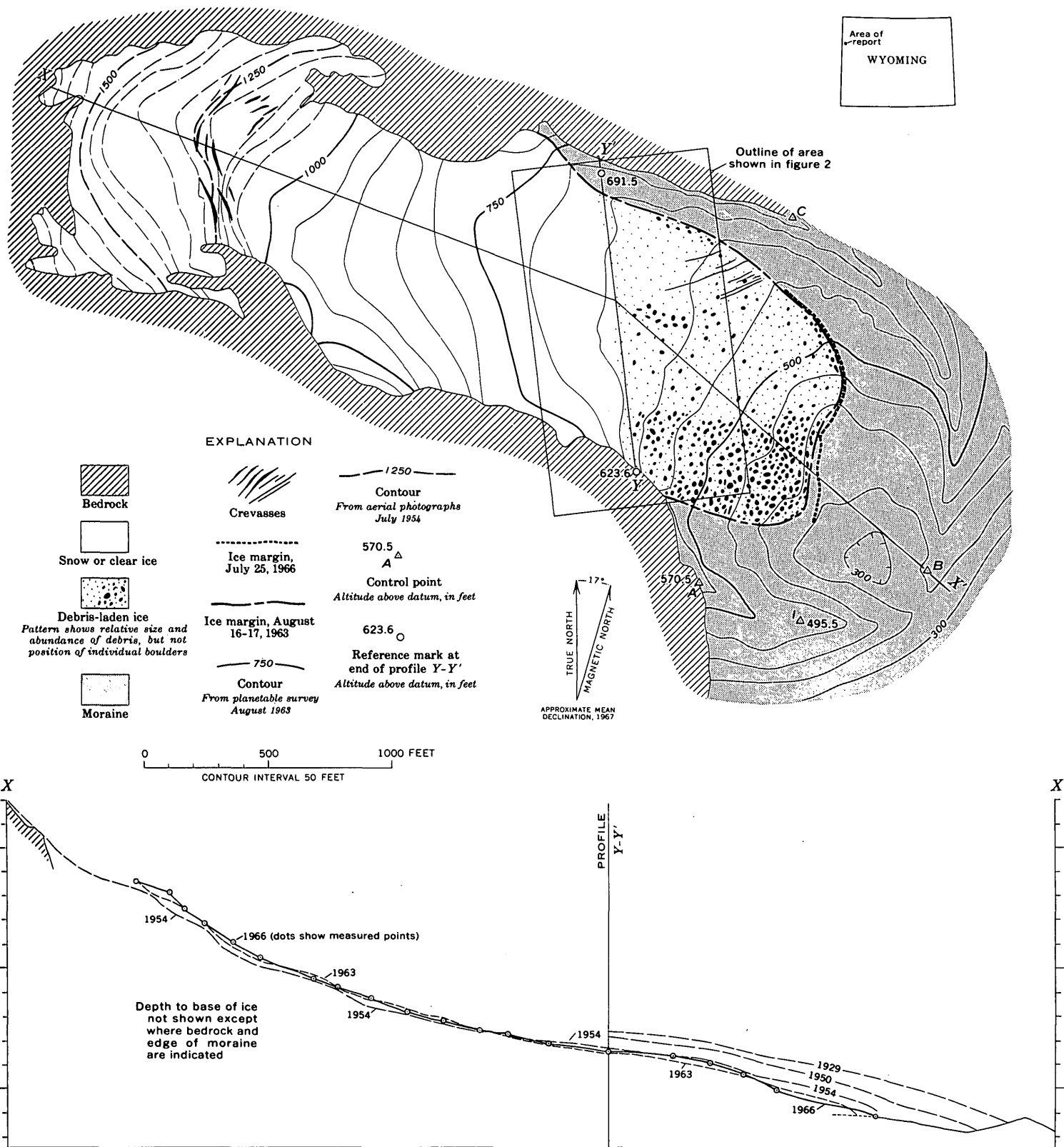


FIGURE 1.—Map and longitudinal profile of the Teton Glacier. Contours show elevation above arbitrary datum, 9,780 feet above sea level.

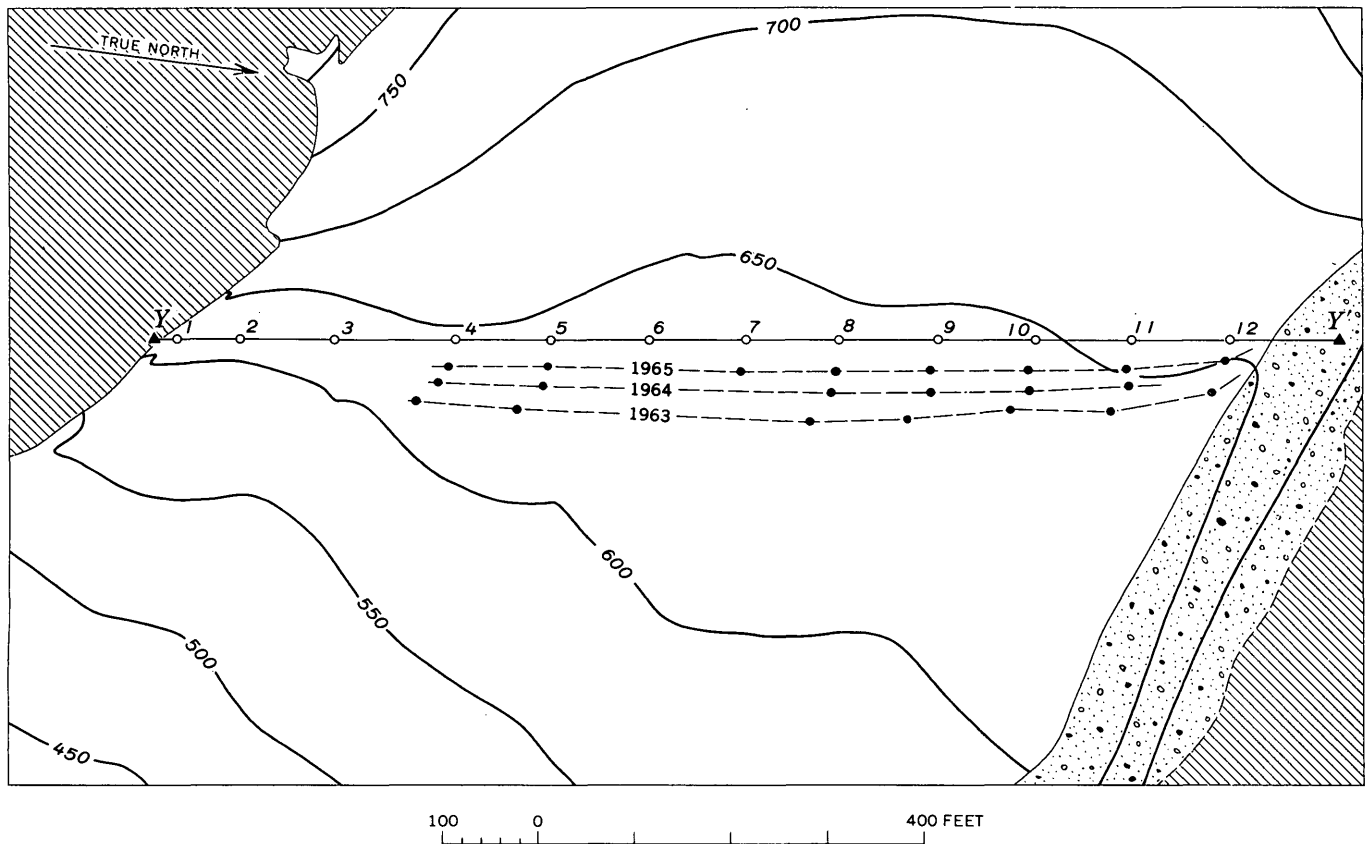


FIGURE 2.—Map showing positions of markers placed along line Y-Y' in 1966 (open circles) and positions of markers from previous years (solid circles). Dashed lines connect positions of markers originally placed along Y-Y' in 1963, 1964, and 1965. Solid triangles show position of fixed reference points marked by red paint '+'. Ruled areas are bedrock; stippled area is moraine. Contours show configuration of ice surface in 1963. Altitude of 1966 points (table 2) therefore cannot be reconciled in detail with contours shown. Contour interval is 50 feet; arbitrary datum is 9,780 feet above sea level.

line X-X' (fig. 1) was resurveyed, and the position of the terminus was redetermined.

All but one of the stakes placed in previous years had melted out of the ice, but each lay with its tip within the group of painted rocks that had been placed around it, so that its position could be recovered within about 2 feet. The location of the old markers with respect to the newly placed 1966 markers was measured with a Brunton compass and steel tape. Their altitudes were measured by leveling to the 1966 marks using a hand level and stadia rod. These data are given in table 3.

The data in table 3 can be used to compute the average annual movement of the ice at each of the points where markers from previous surveys were recovered in 1966, but several adjustments are necessary. Because the 1965 markers were not placed along the same line (Y-Y') as that used in other years, an adjustment in their original positions must be made. The 1965 line was found to have been originally 7.5 feet too far downglacier at point 12, 1,110 feet from

the reference mark on the south wall. The discrepancy in placement of the other 1965 points is:

Distance that 1965 point was originally off line Y-Y' = $\frac{7.5}{1,110} \times \text{distance from south wall}$.

The consistency of the discrepancies in apparent directions of movement of the markers placed in the various previous years suggests that systematic errors were made in measuring the distances from the reference point at the south end of the line when the markers were originally placed. It is very unlikely that the discrepancies are due to an actual change in the direction of movement. To adjust for these measurement errors, the true movement direction at each point must be estimated. The apparent directions of movement of the 1964 and 1965 markers are reasonably consistent and indicate that these markers were more accurately placed than were those in 1963. Because the 1964 markers were originally placed on the correct line and because they represent a longer period of record, it has been assumed that the true direction of movement

at each point is that between the 1964 and 1966 markers. The assumed original positions of the 1963 and 1965 points were found graphically by projecting

their 1966 positions backward along the assumed direction of movement, the 1963 markers into line *Y-Y'* (figs. 1, 2) and the 1965 points into the line along which they were originally placed.

The apparent errors in placement of the 1963 and 1965 markers are given in table 4. The relatively large errors in distance from the south wall of the 1963 markers are probably largely the result of an error in the stadia reading from the reference point to the instrument station on the profile line from which all other distances were taped. Taping errors in the original surveys and errors in estimating the exact positions of stakes which had melted out of the ice probably account for the remaining discrepancies in the placement of the 1963 and 1965 markers.

Average annual movement rates computed from the adjusted original positions of the various markers are given in table 5. These rates of movement are somewhat less than those previously reported (Reed, 1965) because of the errors in the original positions of the 1963 markers, but they confirm the general pattern of movement described in previous papers. The differences between the average movement rates for the various points in table 5 are probably due to discrepancies in the surveys rather than to real changes in the rate of movement in the ice. Detection of changes in the rate of ice movement from year to year would require both more precise surveys and a more satisfactory method of placing the marker stakes.

The only marker stake recovered during the 1966 survey that had not melted free of the ice was the pipe placed at point 5 in 1964. The altitude of the bottom of the stake in 1964 was 642.2 feet (Reed, 1965,

TABLE 2.—Location and altitudes of markers placed on line across the Teton Glacier on July 25, 1966¹

Point	Distance from red paint mark on south wall (feet)	Altitude above arbitrary datum ² (feet)	Remarks
1.....	20	620. 0	Head of stake flush with bare ice surface.
2.....	87	623. 0	Head of stake 1.5 ft below snow and about 1 ft above ice.
3.....	185	629. 7	Head of stake flush with ice surface under 1.5 ft of snow.
4.....	310	656. 4	Head of stake flush with ice surface under 1.0 ft of snow.
5.....	410	651. 7	Head of stake flush with ice surface under 0.5 ft of snow.
6.....	510	645. 6	Head of stake flush with bare ice surface.
7.....	610	652. 9	Head of stake flush with ice surface under 0.4 ft of snow.
8.....	710	651. 7	Head of stake flush with bare ice surface.
9.....	810	650. 5	Do.
10.....	910	657. 5	Do.
11.....	1, 010	662. 5	Head of stake flush with ice surface under 1.7 ft of snow.
12.....	1, 110	665. 4	Head of stake flush with bare ice surface.
Edge of snow on north side of glacier.....	1, 196	678. 2	No mark.

¹ All numbered points marked by telephone-pole cleats about 1 foot long surrounded by blue painted rocks and flagged with small triangular red cloth pennants on wires about 2 feet long.

² Arbitrary datum is approximately 9,780 feet above sea level.

TABLE 3.—Positions of markers placed in 1963, 1964, and 1965 with respect to new markers placed July 25, 1966, on the Teton Glacier

Point	1965 markers			1964 markers			1963 markers		
	Direction	Distance (feet)	Altitude difference (feet)	Direction	Distance (feet)	Altitude difference (feet)	Direction	Distance (feet)	Altitude difference (feet)
¹ 1.....									
¹ 2.....									
¹ 3.....									
4.....	S. 75° E.	28. 0	- 6. 9	S. 69° E.	45. 7	-11. 5	S. 59° E.	75. 0	² -13. 9
5.....	S. 80° E.	29. 0	- 5. 8	S. 80° E.	49. 5	- 9. 6	S. 65° E.	82. 3	-13. 5
¹ 6.....									
³ 7.....	S. 82° E.	32. 8	- 2. 1						
8.....	S. 81° E.	32. 2	- 3. 6	S. 82° E.	55. 0	- 5. 3	S. 72° E.	89. 0	- 5. 7
9.....	S. 82° E.	31. 5	⁴ - 4. 6	S. 84° E.	55. 5	- 7. 7	S. 72° E.	89. 3	-11. 7
10.....	S. 80° E.	32. 0	- 6. 6	S. 84° E.	53. 0	- 9. 8	S. 72° E.	87. 8	-14. 0
11.....	S. 82° E.	31. 5	- 5. 9	S. 87° E.	49. 2	- 8. 2	S. 74° E.	78. 0	-12. 4
⁵ 12.....	S. 82° E.	21. 5	- 4. 4				S. 73° E.	57. 0	- 9. 6

¹ Markers not recovered.

² Difference in altitude refers to ice surface. Mark on an erratic boulder was 5.0 ft above ice surface in 1963 and 6.5 ft above surface in 1966. Mark is control point *E* of 1963 survey.

³ 1964 and 1963 markers not recovered.

⁴ Difference in altitude refers to ice surface. Mark on top of erratic boulder was 6.5 ft above ice surface in 1965 and 11.0 ft above surface in 1966.

⁵ 1964 marker not recovered.

TABLE 4.—*Apparent errors in placement of 1963 and 1965 markers on the Teton Glacier*

Point	1963 marker, error in distance from south wall (feet)	1965 marker	
		Error in distance from south wall (feet)	Distance down-glacier from Y-Y' (feet)
4.....	-14.7	+2.2	2.2
5.....	-22.5	-0.9	2.2
7.....	(¹)	² -1.3	4.2
8.....	-15.7	-1.8	4.9
9.....	-18.9	-2.3	5.6
10.....	-18.7	-3.8	6.2
11.....	-17.2	-3.8	6.8
12.....	-16.0	³ -3.8	7.5

¹ Not determined.² Assumed to be average of errors at points 5 and 8.³ Assumed to be equal to error at point 11.TABLE 5.—*Average movement rates of the Teton Glacier*

Point	Average movement rates, in feet per year, for the period—			
	Aug. 17, 1963, to Sept. 21, 1964 (1.08 years) ¹	Aug. 8, 1965, to July 25, 1966 (0.94 year) ²	Sept. 21, 1964, to July 25, 1966 (1.85 years) ³	Aug. 17, 1963, to July 25, 1966 (2.94 years) ³
4.....	30.2	28.6	24.7	22.7
5.....	32.5	27.6	26.7	24.7
7.....	34.1	29.4	(³)	(³)
8.....	33.9	28.6	29.7	28.4
9.....	34.2	27.1	30.0	28.2
10.....	34.8	26.8	28.6	27.7
11.....	29.0	25.2	26.6	24.8
12.....	24.8	14.1	-----	17.8

¹ Computed from data from previous surveys (Reed, 1965, table 1).² Computed from data from the 1966 survey.³ Marker not recovered.

table 2); in 1966 its altitude was 641.4 feet, only 0.8 foot below its original position. Thus, the inclination of the flow line in the direction of movement was only -1° , appreciably less than the -11° slope of the ice surface in 1966. At this point, at least, relative motion of the ice is upward toward the surface, as would generally be expected in the ablation zone of a glacier.

The longitudinal profile of the glacier in 1966 along with line X-X' (fig. 1) was determined by stadia and

Beaman arc readings from point 8. The profile is little changed from that in 1963. The apparent increase in thickness of the ice in the upper part of the profile may be due to a surveying error but is probably real. Differences between the 1966 and 1963 profiles in the central reach of the glacier are close to the limits of accuracy of the surveys and are probably not significant. The thinning of the ice close to the terminus is apparently real.

More precise transverse profiles along line Y-Y' (figs. 1 and 2) are shown in figure 3. They indicate that the glacier was generally 2-8 feet thick along the line of profile in 1966 than in 1963. Part of the increase in thickness may reflect the fact that the 1966 survey was made much earlier in the ablation season than the previous surveys, but the consistency between the 1965 and 1966 profiles suggests that the thickening is not entirely a seasonal effect.

The northern part of the terminus of the glacier was in virtually the same position in 1966 as in 1963 (fig. 1), but a slight advance (locally as much as 30 feet) of the southern part of the terminus was detected. Whether this advance indicates an end of the long-term retreat of the terminus or is merely a minor oscillation remains to be seen.

A vertical glacier mill, or moulin, 10 feet in diameter and about 200 feet downglacier from point 6 of the 1966 survey, afforded an unusually good opportunity for directly measuring the minimum thickness of the glacier. A heavy stone on the end of a steel tape lowered down the opening encountered rock at a depth of 64 feet. The rock may be an erratic embedded in the ice, but it seems more likely that the mill extended all the way to the floor of the glacier. If so, the ice thickness measured is in rather close accord with the thickness of about 50 feet previously compiled (Reed, 1965) from changes in slope and elevation of the ice surface at this part of the glacier.

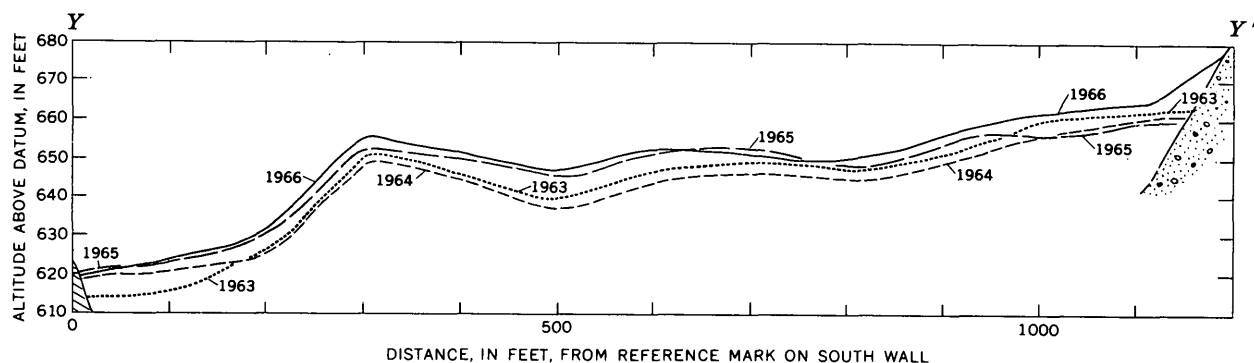


FIGURE 3.—Transverse profiles across the Teton Glacier along line Y-Y' (fig. 1). Arbitrary datum is 9,730 feet above sea level. Ruled area, bedrock; stippled area, moraine.

REFERENCES

- Reed, J. C., Jr., 1964, Recent retreat of the Teton Glacier, Grand Teton National Park, Wyoming, *in* Geological Survey Research 1964: U.S. Geol. Survey Prof. Paper 501-C, p. C147-C151.
- Reed, J. C., Jr., 1965, Rate of ice movement and estimated ice thickness in part of the Teton Glacier, Grand Teton National Park, Wyoming, *in* Geological Survey Research 1965: U.S. Geol. Survey Prof. Paper 525-B, p. B137-B141.



REVISED CORRELATION OF THE NO. 4 (DAWSON SPRINGS NO. 6) COAL BED, WESTERN KENTUCKY COAL FIELD

By T. M. KEHN, J. E. PALMER, and G. J. FRANKLIN, Madisonville, Ky.

Work done in cooperation with the Kentucky Geological Survey

Abstract.—The coal bed in the Dawson Springs area of the Western Kentucky coal field, known locally as the Dawson Springs No. 6 coal bed, lies approximately 200 feet below the No. 6 coal bed of the Carbondale Formation in the Providence-Dekoven area and is herein designated the No. 4 coal bed of the Tradewater Formation. It has been mined extensively in the Dawson Springs and Saint Charles quadrangles for many years and is the source of high-quality stoker and coking coal. Recognition of the correct stratigraphic position of the No. 4 coal bed should aid in exploration for additional minable reserves.

For many years a coal bed in the Dawson Springs–Saint Charles area along the southwestern edge of the Western Kentucky coal field has been called the Dawson Springs No. 6 and correlated with the No. 6 coal bed of the Carbondale Formation, first recognized in the Dekoven area to the northwest (fig. 1). Geologic mapping and studies by the writers, as part of the cooperative geologic mapping program of the Kentucky Geological Survey and the U.S. Geological Survey, have shown that in the Dawson Springs–Saint Charles area the coal bed called Dawson Springs No. 6 is about 200 feet beneath the No. 6 coal bed of the Providence quadrangle to the northwest. The No. 6 bed has been traced from the Providence quadrangle to its type locality at Dekoven.

The Dawson Springs No. 6 coal bed has been redesignated No. 4 in recent geologic quadrangle reports (shown in the caption of fig. 1) and is in the Tradewater Formation. This modification was made to eliminate the use of No. 6 for two coal beds and to give the coal bed a number that fits in the numerical sequence which designates the principal coal beds in the coal field.

The No. 4 coal bed has been mined at numerous localities along the southwestern edge of the coal field. In many places, the No. 4 has not been reached by exploratory holes. Its presence, however, is indicated by electric logs of oil and gas test holes. Recognition of the stratigraphic position of the coal bed should aid in its exploration.

The relation of the No. 4 coal bed to the No. 6 and No. 9 coal beds is shown in figure 1. The position of the No. 4 coal with respect to several coal beds, including Nos. 6 and 9, is shown by columnar sections (fig. 2). Both illustrations cover the area from the Saint Charles to the Providence quadrangles. The columns, except the electric log, are generalized composite sections showing intervals between principal coal beds and a few limestone marker beds. They were drawn from data gathered from measured surface sections and a large number of coal, as well as oil and gas, test holes.

MODIFICATION OF NOMENCLATURE

The application of the term “No. 4” to the Dawson Springs No. 6 coal bed involves modification of pre-existing nomenclature of the Western Kentucky coal field.

The first published geologic studies of the Western Kentucky coal field were made by Owen (1856, 1857) who reported on outcrops of coal beds in the vicinity of the villages of Dekoven and Caseyville, near the Ohio River northwest of the Providence quadrangle. The rocks in this area are considered the type section for Pennsylvanian strata for western Kentucky. Owen proposed both names and numbers for the coal beds of western Kentucky (table 1). Glenn (1912) studied the Tradewater River area, which included Owen’s

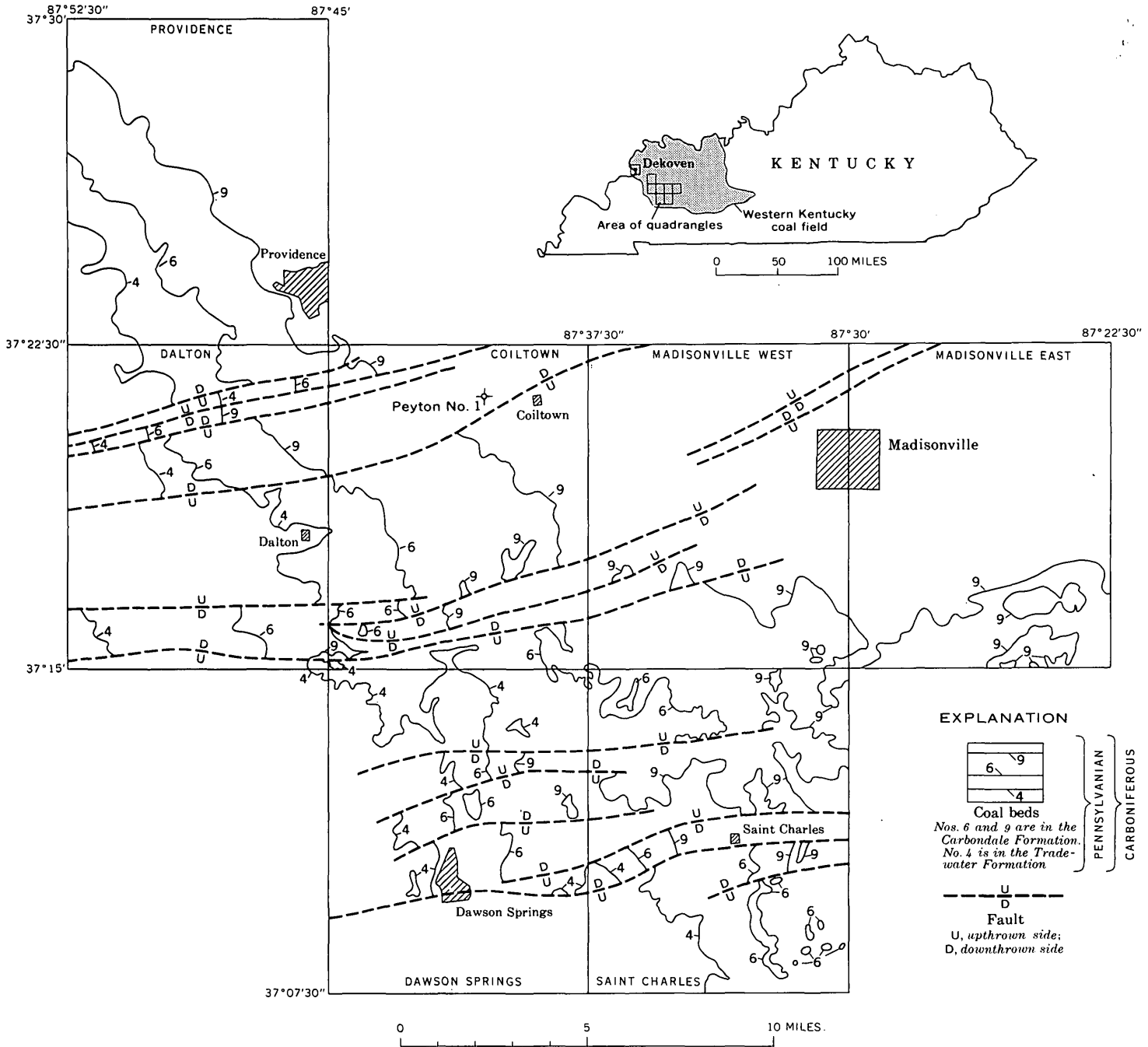


FIGURE 1.—Generalized geologic map of part of the Western Kentucky coal field, showing quadrangles mapped in detail, principal faults, and the Nos. 4, 6, and 9 coal beds. Index map shows location of Western Kentucky coal field, area of geologic quadrangle maps, and the Dekoven, Ky., type area. Maps compiled from the following geologic quadrangle maps: Providence (Kehn, 1966a), Dalton (J. E. Palmer, 1963), Coiltown (G. J. Franklin, unpub. data), Madisonville West (Kehn, 1964), Madisonville East (Kehn, 1963), Dawson Springs (Kehn, 1966b), and Saint Charles (J. E. Palmer, unpub. data). Full name of the dry hole west of Coiltown is Home-Stake Producing Co. Peyton No. 1.

type area and much of the area of this report. Glenn (1912, p. 26, 28) recognized that local usage had substituted No. 7 for Owen's No. 6, and No. 6 for Owen's No. 5, and Lee (1916) adopted these changes in the Shawneetown quadrangle which includes the Dekoven area. Glenn (1922) in a study of coal beds of Webster

County, Ky., which includes the Providence and part of the Dalton quadrangles, continued the use of nomenclature adopted by Lee.

Owen's original numeral designations as modified by Lee (1916) and Glenn (1922) provide a numeral sequence from which the number 5 is absent. The

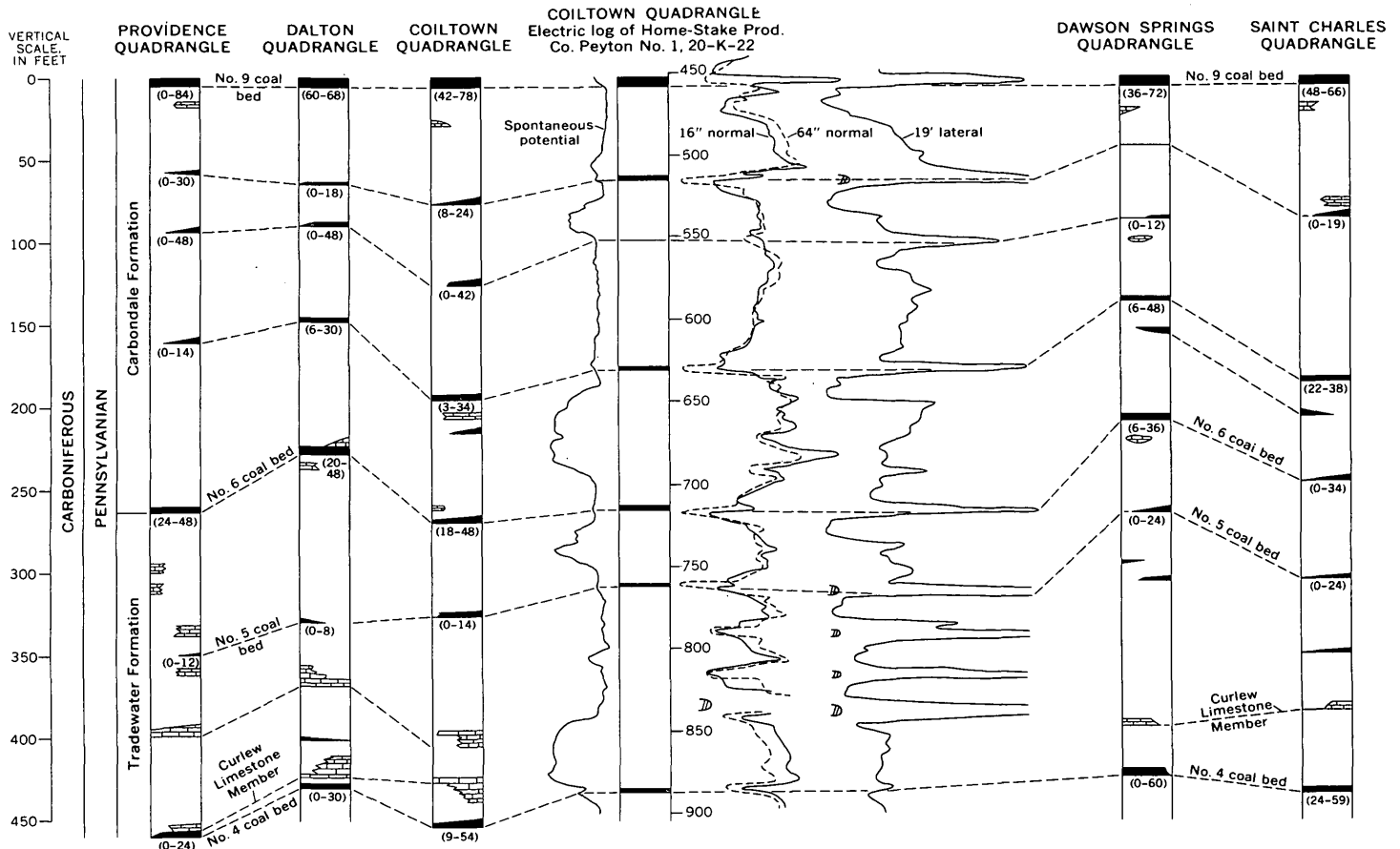


FIGURE 2.—Composite geologic columns and electric log showing correlation of coal beds No. 4 through No. 9 for quadrangles discussed. Datum is top of No. 9 coal bed. Range of coal thickness, in inches, shown in parentheses beneath principal coal beds. Lithologic symbol used for both limestone and chert. Other lithologies not shown.

TABLE 1.—Correlation of names of coal beds in the southwestern part, Western Kentucky coal field

Owen (1856, v. 1, p. 45-46).	Owen (1857, v. 3, p. 21-22).	Glenn (1912, p. 12-13 and 61)	Lee (1916, p. 19, 26, 27 and 31)	Glenn (1922, p. 55 and pl. XXXI)	This report
Main Five Foot, Mulford, or 3d	No. 9 or Main Mulford	No. 9	No. 9 or Springfield	No. 9	No. 9
Well, Water, or 4th	No. 8. Well, or Water			No. 8b	(¹)
	No. 7			No. 8a?	(¹)
Little Vein, Three Foot, or 5th	No. 6, Little Vein, or Three Foot	No. 6	No. 7 or Dekoven	No. 7	(¹)
Four Foot or 6th	No. 5	No. 5	No. 6 or Davis	No. 6	No. 6
	No. 4 or Curlew	No. 4	Curlew	No. 4?	No. 5
		Dawson Springs (position uncertain)			No. 4

¹ Not discussed in this report.

numeral term "No. 5" on geologic maps of quadrangles, shown in figure 1, has been assigned to coal bed No. 4 of Owen (1857), Glenn (1912, 1922), and the Curlew of Lee (1916). The numeral term "No. 4" on figure 1 is assigned to the coal bed previously called the Dawson Springs No. 6 coal bed. This modification restores

No. 5 to coal-bed nomenclature and accurately reflects the lower stratigraphic position of the No. 4 coal bed.

EXTENT, RESERVES, AND QUALITY OF NO. 4 COAL BED

Where the No. 4 is exposed or present at shallow depths, its thickness and extent are fairly well known,

TABLE 2.—Analyses of samples from the No. 4 coal bed

[Data from Cooper and others (1944, table 21, p. 60-92), who called the No. 4 coal bed of the present report the No. 6]

Mines (all abandoned before 1966)	Kind of sample and size ¹	Sample condition ²	Proximate				Ultimate					Heat value (Btu)	Ash softening temperature (°F)	Agglomerating index ³
			Moisture	Volatile matter	Fixed carbon	Ash	Sulfur	Hydrogen	Carbon	Nitrogen	Oxygen			
Dawson Collieries (Dawson Springs, Ky.).	T; 6 in., lump.	A	7.2	39.8	48.8	4.2	2.6	5.8	71.5	1.6	14.3	12,950	2,010	C _F
		B		42.9	52.5	4.6	2.7	5.4	77.0	1.8	8.5	13,950		
		C		45.0	55.0	-----	2.9	5.6	80.7	1.9	8.9	14,620		
Dawson Daylight No. 6 (Charleston, Ky.).	T; 6 in., lump.	A	7.9	38.3	49.2	4.6	2.7	5.7	70.7	1.6	14.7	12,820	2,050	C _F
		B		41.6	53.3	5.1	3.0	5.3	76.8	1.7	8.1	13,920		
		C		43.8	56.2	-----	3.1	5.6	80.8	1.8	8.7	14,650		
Empire (Empire, Ky.)-----	T; 3 in., lump.	A	9.2	37.5	49.5	3.8	2.4	5.9	71.0	1.6	15.3	12,720	2,040	C _F
		B		41.3	54.6	4.1	2.6	5.3	78.2	1.7	8.1	14,000		
		C		43.0	57.0	-----	2.7	5.6	81.6	1.8	8.3	14,600		
Sixth Vein (Charleston, Ky.)-----	T; 6 in., lump.	A	8.3	38.0	49.4	4.3	1.9	-----	-----	-----	-----	12,910	1,970	C _F
		B		41.4	53.9	4.7	2.1	-----	-----	-----	-----	14,070		
Logan (Charleston, Ky.)-----	M-----	A	11.4	37.1	47.9	3.6	2.3	-----	-----	-----	-----	12,620	2,060	-----
		B		41.9	54.0	4.1	2.6	-----	-----	-----	-----	14,250		
		C		43.7	56.3	-----	2.7	-----	-----	-----	-----	14,860		
Workman (Charleston, Ky.)-----	M-----	A	8.3	35.6	50.4	5.7	2.5	-----	-----	-----	-----	12,690	2,010	-----
		B		38.8	54.9	6.3	2.7	-----	-----	-----	-----	13,840		
		C		41.4	58.6	-----	2.9	-----	-----	-----	-----	14,760		

¹ T, tipple sample; M, mine sample.

² A, as received; B, dried at 105°C; C, moisture and ash free.

³ C_F, fair caking.

but where it is at greater depth or displaced in the subsurface by faults, little is known of its extent or thickness. Although many coal test holes have penetrated strata below the No. 9 coal, very few have been drilled to sufficient depth, about 440 feet below the No. 9, to locate the No. 4 coal bed. This lack of deeper drilling may be attributed in part to a lack of understanding of the stratigraphic position of the No. 4 coal bed. Crider (1914, p. 30) reported, for instance, that the interval from the No. 9 coal bed to the No. 4 coal bed (Dawson Springs No. 6) is 276 feet, which is about 160 feet short.

Known reserves of the No. 4 coal bed have been largely depleted in the Dawson Springs and Coiltown quadrangles, and only moderate reserves remain in the Saint Charles quadrangle. Data from deeper drilling below the No. 9 coal bed will be necessary for a reliable estimate of reserves in the deeper parts of the coal field.

The No. 4 coal is of considerable economic importance in the southwestern part of the coal field as a source of high-quality stoker and coking coal. The coal is low in ash content and high in heat value as indicated by analyses of samples from areas where the coal has been extensively mined (table 2).

REFERENCES

- Cooper, H. M., Snyder, N. H., Abernathy, R. F., Tarpley, E. C., and Swingle, R. J., 1944, Analyses of mine, tippie and delivered samples, *in* Analyses of Kentucky coals: U.S. Bur. Mines Tech. Paper 652, p. 40-163.
- Crider, A. F., 1914, Report on the geology and mineral resources of the Dawson Springs quadrangle: Kentucky Geol. Survey, ser. 4, v. 2, pt. 1, p. 7-74.
- Glenn, L. C., 1912, A geological reconnaissance of the Trade-water River region, with special reference to the coal beds: Kentucky Geol. Survey Bull. 17, 75 p.
- 1922, The geology and coals of Webster County: Kentucky Geol. Survey ser. 6, v. 5, 249 p.
- Kehn, T. M., 1963, Geology of the Madisonville East quadrangle, Kentucky: U.S. Geol. Survey Geol. Quad. Map GQ-252.
- 1964, Geology of the Madisonville West quadrangle, Kentucky: U.S. Geol. Survey Geol. Quad. Map GQ-346.
- 1966a, Geologic map of the Providence quadrangle, western Kentucky: U.S. Geol. Survey Geol. Quad. Map GQ-491.
- 1966b, Geologic map of the Dawson Springs quadrangle, western Kentucky: U.S. Geol. Survey Geol. Quad. Map GQ-573.
- Lee, Wallace, 1916, Geology of the Kentucky part of the Shawneetown quadrangle: Kentucky Geol. Survey, ser. 4, v. 4, pt. 2, 73 p.
- Owen, D. D., 1856, Report of the Geological Survey in Kentucky, made during the years 1854 and 1855: Kentucky Geol. Survey, v. 1, 416 p.
- 1857, Third report of the Geological Survey in Kentucky, made during the years 1856 and 1857: Kentucky Geol. Survey, v. 3, 589 p.
- Palmer, J. E., 1966, Geologic map of the Dalton quadrangle, western Kentucky: U.S. Geol. Survey Geol. Quad. Map GQ-490.



KAOLINIZATION OF BEDROCK OF THE BOSTON, MASSACHUSETTS, AREA

By CLIFFORD A. KAYE, Boston, Mass.

Abstract.—Foundation borings show that much of the bedrock beneath Boston and surrounding communities has been altered to a white soft clayey aggregate. Thin-section study and X-ray-diffraction analyses show that kaolinite is the major mineral formed. Siderite also occurs in the altered iron-rich igneous rocks. Intensive alteration is known to occur at depths in excess of 300 feet below the bedrock surface. The alteration is possibly hydrothermal in origin, but more probably it represents the roots of an extensive lateritic regolith that mantled southern New England in the Tertiary.

Deep exploratory borings for new buildings in downtown Boston, Mass., and parts of adjoining Cambridge and Somerville are showing that much of the bedrock beneath the glacial drift is a soft whitish clayey material, quite unlike the hard typically dark argillite, sandstone, conglomerate, and diabase that are known to underlie most of the area. When first found in the exploratory drilling for the Boston Main Drainage Tunnel the material was classified as Cretaceous or Tertiary sediment. (The description appears in unpublished logs of the Metropolitan District Commission; the identity of the classifier is not known.) Later, when it was found in drilling for the new earth-science building of the Massachusetts Institute of Technology, doubt was expressed whether this material was bedrock,¹ although careful inspection of the badly broken core fragments revealed relicts of stratification and slaty cleavage typical of the normal bedrock. Moreover, whatever the material was, its occurrence was believed to be limited. However, as exploration to bedrock for construction of tall and heavy structures went on at an ever-increasing rate during the past several years, it was found that the soft white "rock" was not localized but was widespread under the drift of the Greater Boston area (Kaye, 1961). Because its

¹Lambe, T. W., 1960, Subsoils at the site of the Earth Science Building at Massachusetts Institute of Technology, Cambridge, Mass.: Massachusetts Inst. Technology Soils Eng. Dept. rept., (duplicated) 8 p.

strength as a foundation for heavy structures is questionable, the presence of the soft clayey bedrock has become an important engineering problem in an area experiencing a boom in major construction. Engineers have shown interest in its areal distribution and origin as a clue to discerning its continuity with depth.

Acknowledgments.—The following firms, organizations, and local governmental agencies made available boring logs used in the writer's study of this material: Haley and Aldrich Associates; LeMessurier Associates Inc.; Charles A. Maguire and Associates; Raymond Concrete Pile Division of Raymond International, Inc.; C. L. Guild Drilling and Boring Co., Inc.; Massachusetts Institute of Technology; Harvard University; City of Boston Building Department; Massachusetts Department of Public Works; Massachusetts Bay Transportation Authority; Metropolitan District Commission; and the Massachusetts Turnpike Authority. Pieces of drill core were made available for study by Mr. Alan Gass of LeMessurier Associates and by Dr. Harl P. Aldrich, Jr., and Mr. Donald Reed of Haley and Aldrich Associates.

Professor Marland P. Billings, Harvard University, kindly made available his unpublished notes and maps of the North Metropolitan Relief Tunnel. John C. Hathaway, U.S. Geological Survey, made X-ray-diffraction analyses of several samples of altered rock.

OUTLINE OF GEOLOGY

The soft clayey rocks appear to fall entirely within the outcrop area of the Boston Bay Group, a sequence of relatively unmetamorphosed rocks underlying Greater Boston. These have been described most recently by Rahm (1962), Billings and Tierney (1964), and Billings and Rahm (1966), on the basis of studies of deep tunnels. The rocks are unfossiliferous, but from lithologic analogy with the fossiliferous rocks in the nearby areas they are certainly within the Devonian to Carboniferous age range and in the writer's opinion

are probably Carboniferous. The Boston Bay Group occupies a broad structural basin that is in faulted contact on the north, west, and south with older, more highly metamorphosed rocks. Billings (1929) has shown the generalized structure of the Boston Basin as known at that time, and more recently (*in* Billings and Rahm, 1966) he has described the boundary fault on the north side of the basin, as seen in the Malden Tunnel.

The Boston Bay Group consists of an exceptionally thick accumulation of conglomerates (Roxbury Conglomerate) in the lower part, passing upwards and laterally by intergradation and interdigitation into a thick section of finer grained clastic rocks, mostly argillaceous rocks but including some interbedded sandstones. The accepted formational name for these rocks is the Cambridge Slate, an inappropriate name because slaty cleavage is only locally conspicuous and sandstone is volumetrically important in some places. In the central part of the basin, a broad lenticle of poorly sorted conglomerate—thought by many to be a tillite (Squantum Tillite Member of the Roxbury Conglomerate)—occurs within but near the base of the Cambridge Slate.

Thick accumulations of rhyolite and possibly dacite crop out on the south and north margins of the Boston Basin; most are flows but some are welded tuffs, bedded ash, and coarse-grained pyroclastic rocks. Volcanic rocks in the southern part of the Boston Basin have been called the Mattapan Volcanic Complex (LaForge, 1932), and those on the north the Lynn Volcanic Complex, but both units seem identical. Volcanic rocks (Brighton Melaphyre) also occur higher in the section within the finer grained sediments. These include a variety of dark-green to maroon fine-grained rocks that are commonly vesicular. They occur as flows (some with pillow structure), ash beds, and feeder necks, sills, and dikes.

Unlike most of the sedimentary rocks of eastern Massachusetts, the rocks of the Boston Bay Group are mostly of low metamorphic grade. Locally, the argillaceous rocks have a fairly well developed slaty cleavage. Typically, these rocks are thin bedded or banded, and consist of alternating light- and dark-gray strata ranging from 1 to 100 centimeters in thickness. Bedding parting is absent or poorly developed, and fissility is lacking. Argillite seems the most descriptive name and is preferable to mudstone because of the superior hardness of these rocks. Sandstones that range from fine- to coarse-grained are generally very well indurated but, in spite of the presence of secondary quartz cement, are not quartzites. In the conglomerates the dominant pebble types are impure quartzite, but gran-

ite and several other crystalline rocks make up from 10 to 30 percent of the pebbles. The conglomerates are generally well jointed, and the joints break smoothly across pebbles and matrix alike. Conglomerates are sufficiently indurated to have been widely quarried in the last century as a decorative building stone.

The Boston Bay Group rocks range in color from pink and maroon to gray (medium to dark blue). The red coloration appears to be an oxidation facies that cuts across stratigraphic lines (Billings and Tierney, 1964). In contrast, the altered rock is distinctly lighter, ranging in color from white (dry color) or cream (moist color) for the completely altered rock to light pastel pinks and grays for the partly altered rock.

The Boston Basin is cut by many dikes and sills. The most important intrusive rock is diabase. In addition there are tabular intrusions of other fine-grained mafic rocks and a very coarse grained biotite diabase, typified by the north-trending Medford dike. The diabases have yielded K/Ar ages that range from Pennsylvanian to Permian; a Triassic age (190 ± 6 million years) was obtained for the coarse-grained biotite diabase (H. W. Krueger, Geochron Laboratories, Inc., oral commun., 1966).

The largest structure of the Boston Basin is a complex east-west anticline that plunges east. The conglomerate crops out extensively in the central part of this large fold. The finer grained sediments on the north flank of the fold (fig. 1) are largely covered by glacial deposits. Some idea of the complexity of structural deformation of these beds is conveyed by the tunnel maps made by Rahm (1962) and Billings and Tierney (1964). An attempt is made in figure 1 to show this complexity by indicating strike trends based on the data of the tunnel maps. It is clear that the structure is more complicated than the picture conveyed by the rare outcrops of the fine-grained rocks or by the outcrops of massive conglomerate in the central part of the basin. Many secondary folds are clearly superimposed on the major anticline. The importance of faults in the structural deformation is unknown, mainly because of the scarcity of outcrops and the uncertainty as to the amounts of displacement on the faults seen by Billings and coworkers in the tunnels.

DISTRIBUTION AND STRATIGRAPHIC ASSOCIATION

Knowledge of the areal distribution of the badly altered rock is based on one outcrop, foundation borings, and the tunnels mentioned earlier. Partly kaolinized rock is undoubtedly very widespread, but because of difficulty in separating this rock readily from un-

altered rock, it will not be the subject of the following observations.

The source of the foundation-boring information was the file of boring logs collected by the U.S. Geological Survey for the restudy of the geology of Greater Boston. Although the logs of more than 13,000 borings have been collected from the area, only a very small percentage of the borings reach bedrock, and of these, only a very small percentage were drilled

into bedrock and therefore give information on the nature of the rock. The paucity of drilling data is further affected by the multiplicity of rock- and physical-properties terms used in the drillers' logs. Terms such as "slate," "argillite," "shale," "mudstone," "siltstone," "mica schist," and "rock" have all been used for argillite. Adjectives of consistency such as "decomposed," "soft," and "weathered" are widely used, but here also precise meanings are rarely clear. Super-

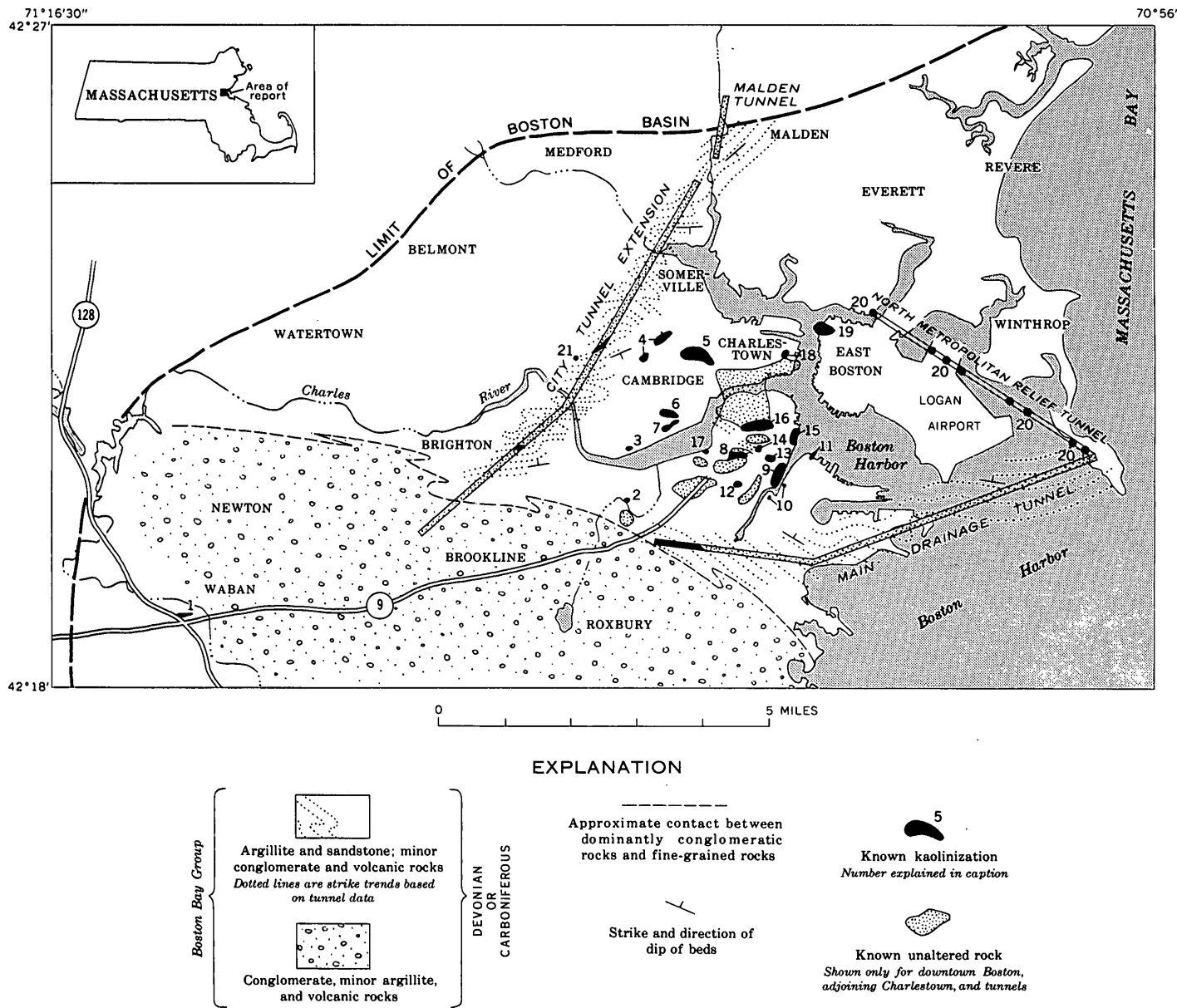


FIGURE 1.—Map of the Boston area showing the areas of known kaolinization, the bedrock tunnels, and the generalized geology of the Boston Bay Group. Occurrences of kaolinization are as follows: 1. Intersection of Routes 128 and 9; 2. Fenway, in front of Sears Roebuck store; 3. Memorial Drive; 4. Inner Belt route; 5. Boston and Maine freight yards; 6. Broad Canal; 7. Green Building, M.I.T.; 8. Boston Common; 9. South Station Postal Annex; 10. Gillette Safety Razor plant; 11. Pier 2; 12. Castle Square; 13. Former site of Stone and Webster Building, and the New England Telephone and Telegraph Building; 14. West side of Washington Street at intersection of Water Street; 15. Atlantic Avenue; 16. Government Center; 17. Beacon and Clarendon Streets; 18. Charlestown Navy Yard; 19. East Boston; 20. Borings for North Metropolitan Relief Tunnel; 21. Memorial Hall, Harvard University.

ficial weathering rather than the more profound hydrothermal alteration may be implied by these adjectives. Of all the clues as to the presence of kaolinized rocks in drillers' logs, perhaps the best is the color white. However, when moist, the kaolinized rocks are commonly light shades of gray or maroon, and this is the condition in which they are generally seen and described by drillers or inspectors; the simple adjectives "gray" or "light gray" are not sufficient to identify them.

It is quite possible that many of the isolated patches of kaolinized rock in figure 1 are in reality contiguous and that, as deep drilling continues in the area, these patches will be found to coalesce into belts which roughly follow the structural trend. Present data suggest that localities 15 and 16 are part of an east-west belt; localities 9 and 13 may also be part of a continuous belt that possibly includes localities 6, 7, 8, and 17. Locality 21 seems to be the same zone as that seen in the City Tunnel Extension in Cambridge.

Only one outcrop of kaolinized rock is known to the writer; it is very close to the western margin of the Boston Basin (loc. 1, fig. 1), where soft partly kaolinized argillite and conglomerate occur together in a road cut. Exposed at the base of the cut are at least 15 feet of soft, very light mauve, laminated clayey silt that can be dug with a shovel. This material is probably altered from argillite. It appears to be a large lens enclosed in massive arkosic conglomeratic sandstone. The sandstone has not been noticeably softened or altered to clay. Overlying, and in sharp contact with the arkosic sandstone, is a massive medium-course conglomerate at least 60 feet thick. The granite pebbles in the conglomerate are fairly soft and clayey; the quartzite pebbles seem relatively unaltered. The matrix of the conglomerate is light-cream to white, broken and friable clayey material, in contrast to the purplish- to brownish-gray, well-cemented arkose typical of the fresh conglomerate.

A few hundred feet to the east of locality 1, just across a small street intersection, a large body of medium-grey, hard igneous rock, containing sparse small phenocrysts set in an aphanitic groundmass, crops out in another roadcut. Although the contact between this igneous rock and relatively unaltered massive conglomerate is exposed in the cut, it is not clear whether this contact is an intrusive contact or a fault. The igneous rock could be intrusive or extrusive, but there is some indication that it is a volcanic neck; it probably is Brighton Melaphyre. Under the microscope the rock is exceedingly fine grained and consists of very fine flakes of white mica and chlorite in a matrix of poorly crystallized albite. Minute mag-

netite crystals and patches of microcrystalline siderite (Fe_2CO_3) are interspersed throughout the matrix. Somewhat similar rocks are found at other localities of kaolinized rock. The siderite is seen in other localities to be a secondary alteration comparable to, and probably formed at the same time as, the kaolinite. Here, however, the sideritized igneous rock has not been noticeably softened.

The tendency of altered rocks to be restricted to certain beds is clearly expressed in the reports by Rahm (1962) and Billings and Tierney (1964) on the tunnels under Boston constructed by the Metropolitan District Commission. In both tunnels studied—the City Tunnel Extension and the Main Drainage Tunnel—soft rock was found, but in both it was limited to certain beds or groups of beds. However, because tunnel observations are limited by the height of the tunnel (about 13 feet for the Boston tunnels), the possibility exists that if viewed on a larger scale, the alteration would be seen to cut across planes of stratification.

In the western 4,300 feet of the Main Drainage Tunnel (fig. 1), altered argillite (called "shale" in the tunnel reports) and sandstone are interbedded with massive conglomerate and arkose, some of which appear from the description to be altered. Three diabase dikes and sills are shown on Rahm's map (1962) as cutting the soft rocks. Except for the absence of the Brighton(?) Melaphyre in the tunnel, the lithologic association in the soft rock zone in this tunnel is similar to that at locality 1.

Billings and Tierney (1964) found "shale" in two places in the City Tunnel Extension (fig. 1). A section 40 feet thick of soft kaolinized argillite, interbedded with thin quartzite beds, purple argillite, sandstone, and conglomerate, was found in the tunnel south of the Charles River at a depth of about 225 feet below the top of the bedrock surface. North of the Charles River, in Cambridge, at a depth of about 300 feet below the bedrock surface, a section about 150 feet thick, consisting of soft light-purplish-gray kaolinized argillite and interbedded sandstone, was found underlain by a soft sideritized magnetite-bearing fine-grained tuffaceous rock. The lithologic relationships here are much like those near locality 1, and the tuff may represent the sideritic magnetite-bearing rock of that locality.

The engineering problems caused by the weak kaolinized rock in the tunnels necessitated use of steel support where this rock occurred.

The North Metropolitan Relief Tunnel (fig. 1) was completed before a geologist had an opportunity to see it. Professor Billings has made available his notes on this tunnel based on a study of the cores of explora-

tory borings and on a very rapid survey of the finished and partly lined bore. Of 33 exploratory borings to bedrock, 8 were in badly altered material. The locations of these latter holes are shown on figure 1. Altered rock was not noticed by Billings in the tunnel and in all likelihood it was covered by the concrete lining. There are about 40 separate lined sections, and most if not all of these may have been built to support altered rock; 24 percent of the tunnel was lined, and exactly the same percentage of rock borings were in altered rock. If this surmise is correct, then, unlike the other tunnels, there was an abundance of altered rock in this tunnel and this material was distributed fairly evenly throughout the length of the bore. The length of the lined sections suggests that altered strata ranged from as little as 10 feet to 100 feet or more in thickness. Between these lined sections are hard argillite and sandstone. Simfilar rock alteration did not occur in the contiguous western end of the Main Drainage Tunnel.

The tunnel observations and the one outcrop are the only places where soft unaltered rocks were seen in place. The identification of other altered rock zones is from samples brought up as cores and from the mention of these rocks in drillers' logs. An interesting example of alteration occurs at the site of the State Street Tower Building, at the south edge of the Government Center development (loc. 16, fig. 1), between the Old State House and the New City Hall. A total of 11 borings into bedrock were made at this site; 3 of these struck diabase and indicate that a fairly thick dike, striking approximately west-northwest and dipping steeply north, cuts diagonally across the site. The argillite on both sides of the dike is badly altered. In one drill hole that probably was at the margin of the dike, diabase was altered to a white soft substance which, from X-ray-diffraction analysis, consists mostly of very fine grained siderite. Several holes penetrated from 6 to 131 feet into soft white altered rock; in these holes the material did not get firmer with depth.

Exploratory borings at locality 13 (fig. 1) found interbedded coarse sandstone, conglomerate, and a very fine grained igneous rock that is texturally similar to that near locality 1. Here too, as beneath the State Street Tower, a diabase dike crosses the site. The buried bedrock surface slopes fairly steeply and was reached at depths of between 71 and 92 feet. The four borings penetrated 37-98 feet into strata that dip at 45°. Fairly good core recovery was obtained from the altered sandstone and conglomerate, but almost none from one interval that is interpreted to have been extensively altered argillite.

All the rocks at the Stone and Webster site (loc. 13, fig. 1) are profoundly altered, and alteration shows no tendency to diminish with depth. Both matrix and pebbles of the conglomerate have been altered to kaolinite. The granitic pebbles are almost entirely kaolinite, and the quartzite pebbles are partly replaced by kaolinite. When seen in the core boxes, the sandstone was white and had a strikingly rough surface—undoubtedly the result of the soft white clayey matrix having been partly flushed away by the wash water during coring. A number of veins, mostly of milky quartz but some partly of drusy milky quartz and partly of massive white kaolin, cut the sandstone. Veinlets of pure white kaolinite as much as 4 millimeters thick were also cored.

The association here of conglomerate, argillite, and fine-grained magnetite-bearing volcanic rock is similar to that observed in the City Tunnel Extension and at the outcrop at locality 1. This similarity suggests that one stratigraphic zone that includes the upper part of the conglomerate and the base of the fine-grained sediment in association with volcanic rocks (Brighton Melaphyre) is susceptible to alteration. However, the distribution of altered rock in the Boston area (fig. 1) seems far too widespread to be restricted to this stratigraphic zone alone. It can be seen from figure 1 that the alteration must have affected rock well above this stratigraphic horizon, unless there are large unrecognized faults and structural complexities in the Boston-Cambridge area that cause a repetition of the same stratigraphic horizon at many places on the bedrock surface.

DEPTH OF ALTERATION

The deepest recorded occurrence of alteration beneath the surface of bedrock was reported by Billings and Tierney (1964) from the City Tunnel Extension under Cambridge; at this point their profile shows about 300 feet of rock overburden. The altered rock obviously extends below the tunnel level to greater depth. No borings yield unequivocal evidence of having reached the base—or maximum depth—of a particular kaolinized zone. The reason for this is that alteration tends to follow certain beds, and because almost everywhere the beds are dipping at some angle other than vertical, a vertical hole may go through a soft rock layer into hard rock beneath and not indicate the downdip extent of alteration. Present data indicate that, in general, rock alteration extends to depths exceeding 100 feet below the present rock surface and in at least one place exceeds 300 feet.

There is one indirect line of evidence that alteration dies out at relatively moderate depths. The distribu-

tion of altered rock is much more restricted in the Main Drainage Tunnel and the City Tunnel Extension than it is under the Boston peninsula and adjoining Cambridge (fig. 1). The average altitude of the rock surface in the altered zones is about -100 feet, whereas the altitude of the tunnels ranges from -290 feet to -380 feet. However, because the tunnels do not pass under the highly altered zone of Boston and Cambridge, it cannot be demonstrated that the sparseness of alteration in the tunnels bears on the depth of alteration. In addition, altered rock is abundant at an altitude of -280 feet in the North Metropolitan Relief Tunnel.

THIN-SECTION STUDY

Thin sections of altered and unaltered rock were studied under the petrographic microscope to identify the minerals in the altered rocks and to try to understand their mode of origin. In rocks having a low content of iron, such as argillite, sandstone, and conglomerate, the alteration consists entirely of the formation of coarsely crystalline kaolinite (fig. 2). In rocks high in iron, such as diabase and volcanic rocks, the alteration products are siderite and kaolinite.

In thin section, normal hard argillite was found to consist largely of an aggregate of very fine grained sericite (fine-grained white mica, or muscovite), chlorite, and very minor kaolinite, with sparse fine quartz

grains. Darker argillite is richer in chlorite, whereas the light-gray argillite has less chlorite and sericite. The white, somewhat firm, partly altered argillite has kaolinite developed through replacement of almost all other minerals. Soft white argillite consists largely of kaolinite with only small relict patches and islands of white mica and quartz.

Thin sections of unaltered sandstone have sand-sized quartz grains and about 10 percent fresh feldspar grains embedded in a cementing matrix that consists of a mosaic of intergrown fine quartz speckled with much fine-grained white mica and chlorite. Light-colored sandstone has little chlorite, and fine-grained kaolinite has replaced some of the matrix quartz and sericite. Thin sections of the very friable white sandstone from locality 13 (fig. 1), having a matrix that consists almost entirely of kaolinite, suggest that the original cement has been replaced by kaolinite (fig. 3). In addition, some of the larger sand-size quartz grains are clouded with minute kaolinite crystals.

The most interesting example of kaolinization is the highly altered conglomerate from locality 13 (fig. 1). Pebbles of granite are altered entirely to kaolinite, and quartzite pebbles are partly replaced by kaolinite. Much of this kaolinite is coarsely crystalline, with indi-

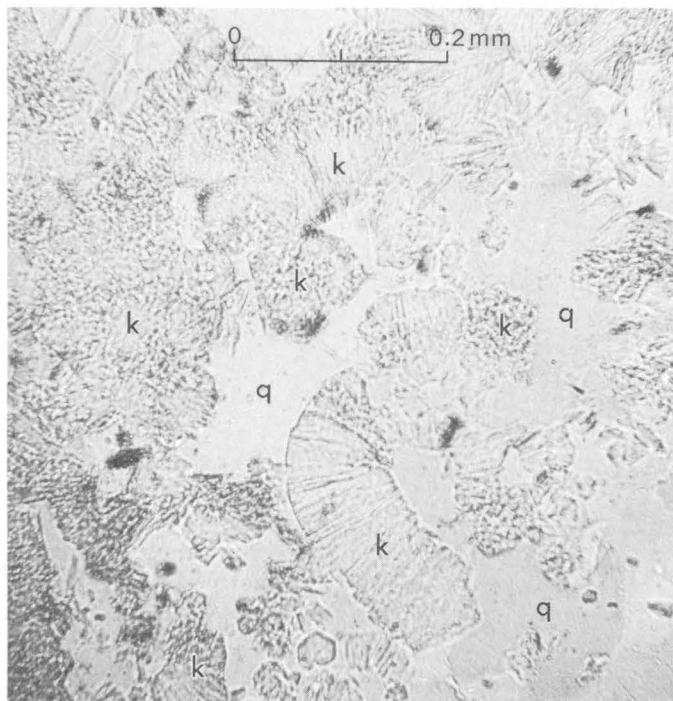


FIGURE 2.—Kaolinized conglomerate, locality 13 on figure 1; large crystals of kaolinite (k) replacing quartz (q). The large curved crystal is 0.275 mm long. Plane polarized light.

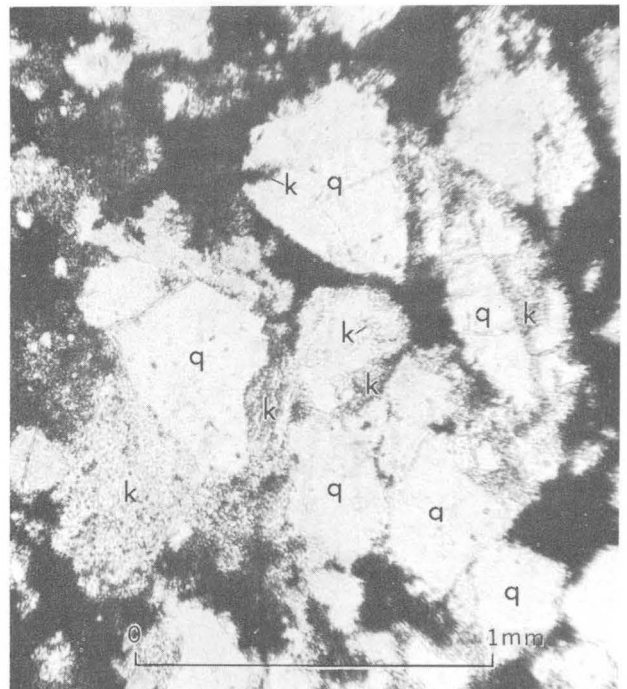


FIGURE 3.—Kaolinized coarse sandstone, locality 13 on figure 1; kaolinite appears as black (opaque) and as clear areas with a peculiar granular texture. Kaolinite (k) has replaced all the matrix of the sandstone and also has embayed some of the sand-sized quartz grains (q). Plane polarized light.

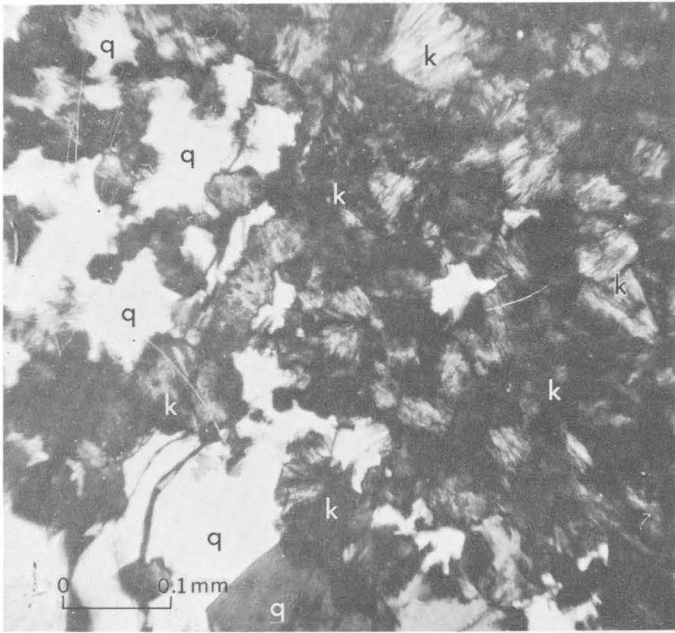


FIGURE 4.—Coarsely crystallized kaolinite (k) replacing quartz (q) in kaolinized conglomerate, locality 13 on figure 1. Crossed nicols.

vidual crystals as much as 0.3 mm long. (fig. 2). The matrix of the conglomerate contiguous to the pebbles consists of coarsely crystalline kaolinite (fig. 4). Small crystals of pyrite were abundant throughout this rock.

The alteration of diabase from the State Street Tower site (loc. 15, fig. 1) was studied in a set of samples that ranged from partly altered hard dark-gray diabase to soft white material. The latter consists largely of very fine grained siderite (average grain size, 0.002 mm) and minor kaolinite. The iron silicates of the original rock (mostly augite and biotite) were completely altered to siderite; the feldspars are somewhat less altered but are densely clouded with sericite and kaolinite.

The fine-grained volcanic rock at locality 13, that megascopically resembles a coherent buff siltstone, appears in thin section to have retained much of its original texture. Almost all its finer grained components, however, have been replaced by a combination of kaolinite and exceedingly fine grained microcrystalline siderite (confirmed by X-ray-diffraction analysis).

ORIGIN

The thin-section study, by showing the replacement of quartz and other minerals by kaolinite, demonstrates the secondary origin of the kaolinite. The question remains as to whether the kaolinization is the result of surface weathering during the long course of preglacial time or whether it was produced in some other way, such as by hot solutions or gaseous emanations

coming from depth or from igneous bodies within the rocks of the Boston Bay Group—that is, a hydrothermal origin.

The origin of the kaolinite in the Boston area is of practical importance to construction engineers because if the alteration is the product of surface processes it should be limited to relatively shallow depths. If, on the other hand, the alteration came about through hydrothermal processes, then there is a good possibility that hard, strong rock cannot be expected at reasonable depths under affected areas. The answer to the problem would be evident if it were known for sure whether the alteration ended at relatively shallow depths, but such information is not now available.

In favor of an origin through weathering or descending ground water are several facts. For one, kaolinitic deposits of this type are known from elsewhere in New England and are common throughout the world. Small deposits of kaolinite associated with limonite are found at a number of points in western Massachusetts and Vermont, generally along the sides and lower slopes of the larger valleys. These deposits are thought to be small relict patches of the late Tertiary clay residuum that for some reason escaped glacial erosion in the Pleistocene (Reis, 1903, 1927).

More impressive is the great blanket of kaolinitic sediments of Cretaceous age that formerly rimmed the shore of preglacial New England and which now is preserved only in the glacial moraines of Martha's Vineyard, Block Island, and Long Island (Woodworth and Wigglesworth, 1934; Fuller, 1914; Kaye, 1964). These preglacial kaolinitic clays, sands, and gravels of New England are identical with sediments of the same age that crop out in the Coastal Plain along the entire eastern seaboard of the United States to the Gulf Coast. The clay in these sediments is almost exclusively kaolinite. Whether the clay formed from the alteration of other minerals after the deposition of these sediments or whether it was deposited as kaolinite is not entirely clear.

If the kaolinite at Boston is the result of weathering, it indicates exceptionally deep weathering. A depth of intense weathering (that is, capable of producing kaolinite) in excess of 300 feet is very rare. In glaciated areas, such as Boston, this depth is even more impressive because one can assume that a considerable thickness of bedrock was eroded by the several ice sheets that occupied the Boston area during the Pleistocene (Kaye, 1961, 1964). Thus, it is fairly certain that just prior to the Pleistocene the kaolinized rock exposed in the City Tunnel Extension lay at a depth beneath the bedrock surface that was consider-

ably in excess of the present 300 feet. Add to this the unknown depth to which alteration extends beneath the tunnel level, and the indications are that kaolinization reached depths of 500 feet or more during the Tertiary. Although this depth is considerable, somewhat comparable depths of weathering have been noted, or deduced, in several other places. According to John Hosterman (written commun., 1967) weathering during the Tertiary reached depths of at least 300 feet, and probably 500 feet, in Idaho and northwestern Washington; and in the piedmont region of southeastern United States, weathering in excess of 300 feet has been noted.

The existence of a period of intense weathering in southern New England during the Tertiary is confirmed by the occurrence of bauxite in the area. The writer has found pebbles of pisolitic bauxite in older drift on Martha's Vineyard. These pebbles were undoubtedly eroded and transported by glacial ice from a deposit located somewhere in southeastern New England. The bauxite consists of the minerals gibbsite, kaolinite, siderite, and quartz, the last named a relict from the parent rock. Deposits of similar bauxite from other parts of the world are commonly accompanied by extensive kaolinitic alteration of the original bedrock. This relation is true of the deposits in Arkansas, the southeastern United States, and Guyana (formerly British Guiana) (Harder, 1952). In these deposits, kaolinite generally underlies the bauxite zone and in places extends to depths of 100 feet or more.

The close association of siderite and kaolinite in the Boston alteration areas also points to a weathering origin. At least the two minerals are commonly closely associated in deposits of this type, for example, the Martha's Vineyard bauxite. Another is the kaolinitic Upper Cretaceous beds of the same island that are locally rich in siderite nodules of large size and of considerable mineralogic purity.

On the other hand, the distribution of kaolinization is difficult to explain by weathering alone. The alteration seems limited to certain beds. The nature of the control for this is not evident because in one place or another all lithologic types (argillite, sandstone, conglomerate, diabase, and other units) have been affected. Why, for example, a certain set of argillite beds is intensively altered whereas adjacent beds of argillite are quite fresh is a question that will require further investigation. In addition, the rather common occur-

rence of igneous rocks in zones of alteration suggests a genetic relationship. One wonders if the Brighton Melaphyre, diabases, and other intrusive rocks may not have played a role in producing the alteration. These rocks, however, are themselves altered. If they were responsible for the alteration, then it was most certainly a deuteritic or late magmatic effect.

The bulk of the evidence indicates that the kaolinization was produced by very deep weathering. If this surmise is correct, then the kaolinized rock found today represents merely the roots of a once extensive and thick lateritic blanket that covered much, if not all, of the region. From the practical standpoint, therefore, there is a good likelihood that alteration dies out at depths shallow enough to be within the range of engineering interest.

REFERENCES

- Billings, M. P., 1929, Structural geology of the eastern part of the Boston Basin: *Am. Jour. Sci.*, 5th ser., v. 18, p. 97-137.
- Billings, M. P., and Rahm, H. A., 1966, Geology of the Malden Tunnel: *Boston Soc. Civil Engineers Jour.*, v. 53, p. 116-141.
- Billings, M. P., and Tierney, F. L., 1964, Geology of the City Tunnel Extension, Greater Boston, Massachusetts: *Boston Soc. Civil Engineers Jour.*, v. 51, p. 111-154.
- Fuller, M. L., 1914, The geology of Long Island, New York: *U.S. Geol. Survey Prof. Paper* 82, 231 p.
- Kaye, C. A., 1961, Pleistocene stratigraphy of Boston, Massachusetts: Art. 34 in *U.S. Geol. Survey Prof. Paper* 424-B, p. B73-76.
- 1964, Outline of Pleistocene geology of Martha's Vineyard, Massachusetts, in *Geological Survey Research 1964*: *U.S. Geol. Survey Prof. Paper* 501-C, p. C134-139.
- Harder, E. C., 1952, Examples of Bauxite deposits illustrating variations in origin, in *American Institute of Mining and Metallurgical Engineers, Problems of clay and laterite genesis—symposium*: New York, Am. Inst. Mining and Metall. Engineers ann. mtg., St. Louis, Mo., 1951, p. 35-64.
- LaForge, Laurence, 1932, Geology of the Boston area, Massachusetts: *U.S. Geol. Survey Bull.* 839, 105 p.
- Rahm, D. A., 1962, Geology of the Main Drainage Tunnel, Boston, Massachusetts: *Boston Soc. Civil Engineers Jour.*, v. 49, p. 319-368.
- Reis, Heinrich, 1903, The clays of the United States east of the Mississippi River: *U.S. Geol. Survey Prof. Paper* 11, 298 p.
- 1927, *Clays, their occurrence, properties, and uses*: New York, John Wiley & Sons, Inc., 613 p.
- Woodworth, J. B., and Wigglesworth, Edward, 1934, Geography and geology of the region including Cape Cod, the Elizabeth Islands, Nantucket, Martha's Vineyard, No Mans Land and Block Island: *Harvard Univ. Mus. Comp. Zoology Mem.* 52, 322 p., 38 pl.



MAY 1963 EARTHQUAKES AND DEFORMATION IN THE KOAE FAULT ZONE, KILAUEA VOLCANO, HAWAII

By WILLIE T. KINOSHITA, Hawaiian Volcano Observatory

Abstract.—An episode of frequent earthquakes with a background of continuous harmonic tremor began at 21^h50^m on May 9, 1963. During the 4 days of this episode 3,000–4,000 earthquakes were recorded on the U.S. Geological Survey Hawaiian Volcano Observatory seismic network. The earthquakes occurred in the western half of the Koae fault system and were accompanied by abundant ground cracking. Tilt measurements on Kilauea Volcano made after the episode showed that the summit had deflated.

After 5 months of relative seismic quiescence, after the December 1962 flank eruption, seismic activity on Kilauea Volcano suddenly increased in the evening of May 9, 1963. Activity began at 21^h50^m Hawaiian standard time with a moderate ($M \approx 1.5$), shallow earthquake that occurred in the Koae fault system near the Ahua seismometer station and shallow harmonic tremor in the Kilauea summit area. More than 3,000 earthquakes were recorded in a 4-day period, and most were located around the western half of the fault system. The earthquakes were accompanied by tremor early in the episode and, in the western part of the system (fig. 1), by abundant ground cracking. All the earthquakes seemed to originate from depths shallower than 5 kilometers, and most were smaller than magnitude 0.5.

The Koae fault system is a zone of northeast-trending faults, 2 or 3 km wide and about 15 km long, that lies about 4 km south of Kilauea Caldera. It is terminated on the west by the southwest rift zone and on the east by the east rift zone of Kilauea. The Koae system is characterized by normal faults having their downthrown side commonly on the north, by open tensional cracks, and by small grabens.

Seismic episodes similar to the one of May 1963 occurred along the Koae fault system in 1938, 1950, and 1962. All these earthquake swarms were accompanied by tremor, subsidence at the summit, and

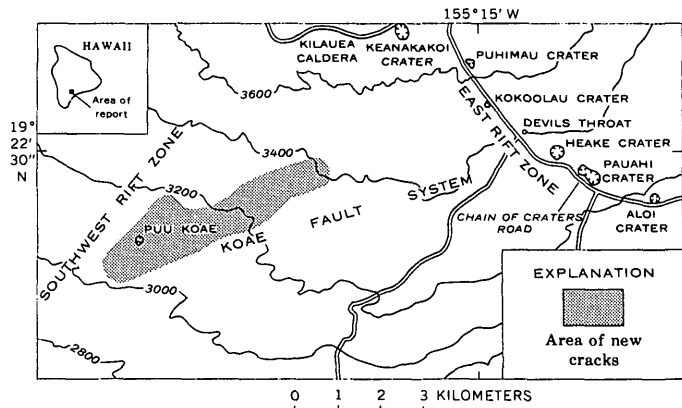


FIGURE 1.—Generalized topographic map showing Koae fault system and the upper parts of the southwest and east rift zones of Kilauea. Pattern shows area where new cracks developed during the May 1963 seismic episode. Area of new cracks mapped by James G. Moore (1963). Contour interval is 200 feet.

ground cracking along the fault system. The various episodes differed, however, in (1) the locations of the most abundant ground cracking and (2) a small eruption that accompanied the 1962 swarm.

According to Jagger (1938), the 1938 episode began on the morning of May 28 and lasted through the evening of the following day. Although he reported only 88 earthquakes and about 7 hours of tremor, his earthquake count and tremor duration are probably low because the seismographs in use at that time were low-magnification mechanical types. Jagger described several east-west-trending cracks that were formed across Chain of Craters Road during the swarm, in an area between Pauahi and Aloi Craters. He also mentioned a hump in the same road near Devils Throat that increased in height noticeably during the seismic activity.

Finch (1950) described a seismic episode in which a very similar series of events occurred in December

1950. Harmonic tremor, however, apparently was not as strong nor as long in duration as in the episode in 1938. He stated that the earthquakes were distributed over a linear distance of about 15 miles from Chain of Craters Road to the upper end of the 1823 lava flow on the Southwest Rift Zone. He described the episode as follows: "During the night of December 8-9, earthquakes continued to originate in the region of the early shakes (near Kokoolau Crater); others showed greater distances as though there was progressive cracking to the southwest." From December 8 to 14, a total of 656 earthquakes were recorded from this region. Finch's estimate of the depth of focus of many of the quakes was $6\frac{1}{2}$ -8 km.

Moore and Krivoy (1964) described a series of events in the December 1962 eruption that, except for the small eruption at Aloi Crater, are apparently similar to the other Koae seismic episodes. The ground cracking in December 1962 in the 0.8-mile zone westward from Aloi Crater is the first Koae seismic swarm that occurred since the installation of an adequately distributed high-gain seismic network.

SEISMIC ACTIVITY

Of the more than 3,000 earthquakes recorded by the U.S. Geological Survey Hawaiian Volcano Observatory seismic network during the May 1963 swarm, less than 30 were of magnitude 2.0 or greater; the greatest was 3.1. The chronological distribution of these earthquakes during the first 50 hours is shown in figure 2. These earthquake-frequency data seem to fit the formula $n = \frac{a}{t+b}$ (Bullen, 1963), where n is number of shocks per hour, t is time in hours, and the constants a and b have the values 1,462.5 and 9.2, respectively, at $t < 1$ hour and $n = 158$, the maximum number of shocks recorded in 1 hour. A magnitude-frequency plot (fig. 3) shows the distribution of earthquakes for increments of $M = 0.5$ for the first 50 hours of the swarm. A least-square fitting of the data to the equation, $\log N = A - bm$ (Richter, 1958), gives the values $A = 3.44$ and $b = 0.98$. The value of b is very close to values obtained by others for earthquakes on Hawaii (Furumoto, 1965; Koyanagi and others, 1966).

The calculated total energy released by the earthquakes during this swarm is 9×10^{15} ergs, based on the formula $\log E = 9.9 + 1.9 M_L - 0.024 M_L^2$ (Richter, 1958), where E is ergs and M_L is magnitude determined from body-wave amplitudes of local earthquakes. About 70 percent of the total energy was released by 5 of the 150 shocks that occurred during the first hour, although there was no clear main shock.

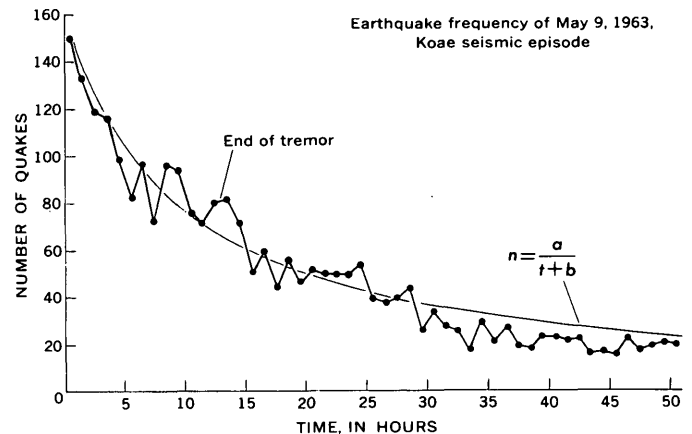


FIGURE 2.—Hourly count of earthquakes recorded at Ahua seismometer station during first 50 hours of seismic episode of May 1963.

The epicenters of the 38 largest earthquakes ($M > 2$) were scattered throughout a 6-, by 6- km area near the west end of the Koae fault system. A plot of the differences in the arrival times of the P-waves at Desert seismometer and Ahua seismometer stations (figs. 4 and 5) shows a shift of earthquake epicenters toward the Desert seismometer station during the first 4-5 hours of the swarm. After about 5 hours there is more scatter in the points, but a tendency to cluster

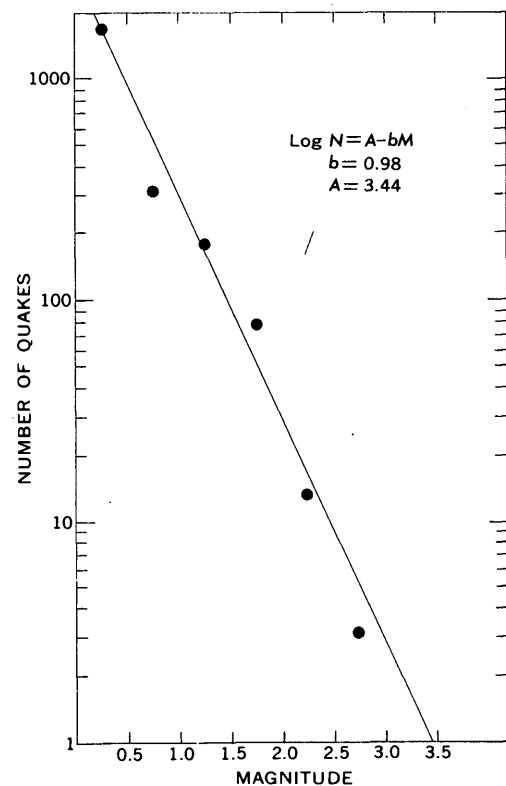


FIGURE 3.—Magnitude-frequency plot of earthquakes during first 50 hours of seismic episode of May 1963.

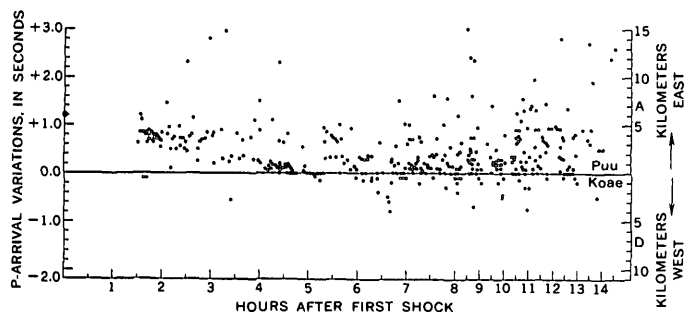


FIGURE 4.—Plot of the differences in the arrival times of the P-waves at Ahua and Desert seismometer stations versus hours after first shock. High-level tremor background obliterated seismograph records for about 1½ hours after first shock. Right ordinate is approximate distance of epicenters, along Koae fault system, from Puu Koa. A, Ahua, and D, Desert stations. Note that time scale is compressed beginning 8 hours after first shock.

near 0.0 time difference indicates that most of the earthquakes originated at nearly equal distances from both the Ahua and Desert stations. After the first shock, and for a period of about 1½ hours thereafter, the earthquake could not be located because the high-level tremor background obliterated the earthquake records. The larger earthquakes in the earlier part of the seismic activity seemed to alternate between the north and south sides of the area of new cracks.

DEFORMATION

The area of obvious deformation lies in the western half of the Koae fault system. Here several new cracks were mapped by Moore (1963) after the seismic episode. Ground tilting at other locations is shown on figure 5. Although the tilt data do not appear to be entirely consistent, in general the summit deflated moderately and the western part of the Koae fault system apparently inflated. The center of apparent inflation shown in figure 5 by the vectors from the bases *Kea*, *Kam*, *Kal*, *KN*, and *HP* almost coincides with the area of new ground cracking. Only data from *Uwe*, which is at the summit, suggest deflation and apparently are in disagreement with data from the *TM* and *SS* bases. However, this apparent disagreement can be explained by considering the daily tilt data from *Uwe*. The short-base tilt measured daily at *Uwe* showed a continued summit inflation after March 18, which was the last time the long-base tilt stations were measured previous to the seismic episode. If the amount of the additional inflation shown by the short-base tilt-meters is added to the March 18 long-base tilt data and a comparison is then made with the post-seismic-episode tilt data, the amount and direction of tilt shown by the dashed lines on figure 5 are obtained. Thus modified, the data clearly indicate a summit de-

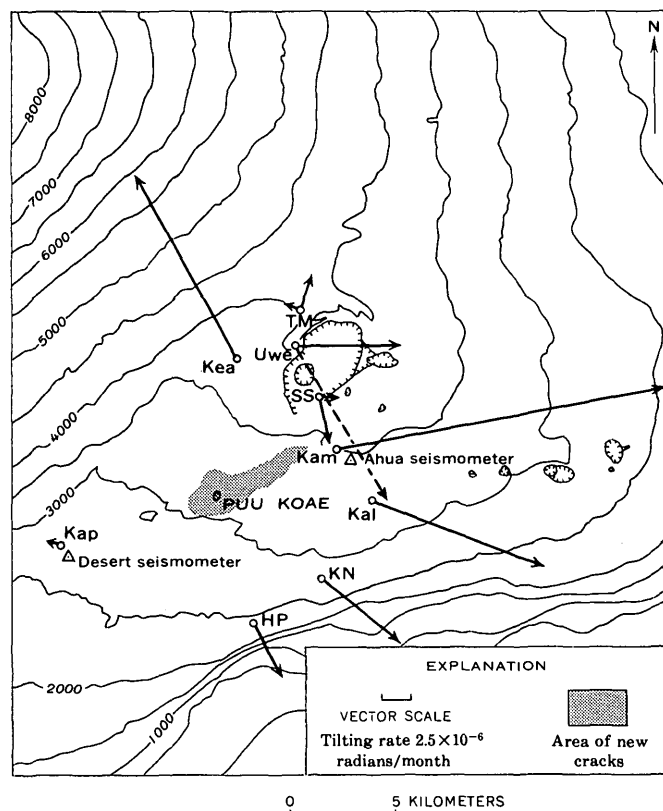


FIGURE 5.—Map showing tilting of the ground at Tree Molds (*TM*), Uwekahuna (*Uwe*), Keamoku (*Kea*), Sand Spit (*SS*), Kapapala (*Kap*), Kamokukolau (*Kam*), Kalihipaa (*Kal*), Kipuka Nene (*KN*), and Hilina Pali (*HP*) tilt bases between March 18 and May 10, 1963, location of Desert and Ahua seismometer stations, and area of new cracks (pattern) formed during episode. The vector depicting tilting at a given base shows the direction of maximum relative subsidence and has a length proportional to the rate of tilting during the measurement interval. Dashed vectors show direction and rate of tilt if probable additional inflation from March 18 to May 9 is considered. Contour interval is 500 feet.

flation at *Uwe* and only small changes at the *SS* and *TM* bases.

SUMMARY

The following events all occurred during the 1938, 1950, 1962, and 1963 earthquake swarms: (1) ground cracking along the Koae fault system, (2) harmonic tremor, (3) large number of earthquakes whose focal depths were probably less than 3 km, (4) a summit deflation accompanied by an apparent upper east rift inflation, and (5) in at least two of the swarms, an apparent westward migration of the earthquake epicenters. The sequence seems to start with an earthquake, not necessarily the largest of the swarm, and shallow harmonic tremor beginning shortly before or at the same time as the earthquake. These events are followed by a rapid summit deflation and a probable inflation in the fault zone. The rate of deflation in the rift zones has not been observed, though in Decem-

ber 1962 ground cracking did not occur until a few hours after the earthquakes and the tremor began. In the May 1963 seismic episode, apparently a slow summit deflation began a few hours before the first earthquake of the swarm followed by rapid deflation after the beginning of the swarm.

Whether these swarms are characterized by only 70 percent of the total energy being released in the first hour is not known. In any case the energy being released is much lower than that released in the first hour of normal tectonic earthquake swarms. The largest quake occurred in the first 2 minutes of the swarm, but it only accounted for about 30 percent of the total energy released, compared to a release of more than 87 percent calculated for other tectonic earthquake swarms (Benioff, 1951).

Both seismic and deformation evidence indicate that these earthquake swarms are intimately associated with volcanic activity, but only one small eruption has occurred during these swarms. Very few eruptions have occurred on the Koa'e fault system, and no historic eruptions, except near the intersections with the southwest and east rift zones. This lack of eruptions

seems peculiar because underground magmatic movement has occurred during each swarm.

REFERENCES

- Benioff, Hugo, 1951, Earthquakes and rock creep, pt. 1, Creep characteristics of rocks and the origin of aftershocks: *Seismol. Soc. America Bull.*, v. 41, no. 1, p. 60.
- Bullen, K. E., 1963, An introduction to the theory of seismology: Cambridge, Cambridge Univ. Press. 381 p.
- Finch, R. H., 1950, The December 1950 subsidence at Kilauea: *The Volcano Letter*, no. 510, Oct.-Dec., 1950, p. 1-3.
- Furumoto, A. S., 1965, Seismicity of Hawaii: Hawaii Univ. Inst. Geophysics Tech. Rept., p. 14.
- Jaggard, T. A., 1938, Hawaiian Volcano Observatory report for May 1938: no. 459, May 1938, p. 2-5.
- Koyanagi, R. Y., Krivoy, H. L., Okamura, A. T., 1966, The Koaiki, Hawaii, earthquake and its aftershocks: *Seismol. Soc. America Bull.*, v. 56, no. 6, p. 1317-1335.
- Moore, J. G., 1963, Hawaiian Volcano Observatory summary: U.S. Geol. Survey Hawaiian Volcano Observatory Summary 31. (July, Aug., and Sept., 1963) 40 p.
- Moore, J. G., and Krivoy, H. L., 1964, The 1962 flank eruption of Kilauea Volcano and structure of the east rift zone: *Jour. Geophys. Research*, v. 69, p. 2033-2041.
- Richter, C. F., 1958, *Elementary seismology*: San Francisco, W. H. Freeman and Co., 768 p.



THE GREAT SAND DUNES OF SOUTHERN COLORADO

By ROSS B. JOHNSON, Denver, Colo.

Abstract.—The Great Sand Dunes National Monument in the San Luis Valley of southern Colorado was set aside to preserve a tract of large spectacular transverse dunes. However, large areas of climbing dunes, barchans, longitudinal dunes, parabolic dunes of accumulation, and parabolic dunes of deflation also occur in and adjacent to the Monument. The geologic setting of the dunes indicates that the whole dune area formed more or less contemporaneously; different processes, operating in different parts of the dune field, formed the various types of dunes. The original source areas of the sand grains in the dunes were the San Juan and Sangre de Cristo Mountains that border the San Luis Valley; the immediate sources are the ancient natural levees and dry oxbow lakes of the Rio Grande.

Prevailing southwesterly winds that have blown for centuries across the flat expanse of the San Luis Valley of south-central Colorado have deposited a great mass of loose sand near the western flank of the Sangre de Cristo Mountains (fig. 1). This mass of sand is made up of several types of dunes whose structure depends upon the amount of sand available for transport, wind speed, and the amount of vegetation. The most spectacular dunes are high transverse dunes that are almost barren of vegetation; a tract of land has been set aside as Great Sand Dunes National Monument (fig. 2) to preserve these dunes.

Although the transverse dunes are among the highest in the United States, they cover only about a fourth of the 150-square-mile area of dunes in the San Luis Valley. The rest of the dunes are less spectacular types, but they, too, contribute to the interesting story of the origin and formation of the dunes in and near Great Sand Dunes National Monument.

GEOGRAPHIC SETTING

The sand dunes are located in the San Luis Valley northeast of Alamosa, Colo., and the greatest accumulation of sand is in a small reentrant in the Sangre de Cristo Mountains north of Sierra Blanca where

Medano Creek emerges from the mountains (fig. 3). Medano Pass is a low pass (about 10,150 feet) in this high rugged range, which in this part of Colorado has many peaks more than 14,000 feet high. Medano Creek flows from the pass to the dunes through a steep canyon that strikes northeast and forms a natural outlet for the high-velocity, southwesterly winds blowing over the dunes from the valley.

The San Luis Valley lies between the Sangre de Cristo Mountains to the east and the San Juan Mountains to the west. The valley is 105 miles long and 40 miles wide at the latitude of the dunes. The valley terminates northward at Poncha Pass, which separates the Rio Grande drainage from that of the Arkansas. Southward the valley extends a short distance into New Mexico (Baltz, 1965, p. 2068) where it merges with the Taos Plateau (Upson, 1939, p. 722).

The valley is exceedingly flat over most of its extent, except for the San Luis Hills southeast of Alamosa (fig. 1). The altitude of the valley floor ranges from 7,400 feet near the Rio Grande at the Colorado–New Mexico boundary to a remarkably consistent 8,000 feet around the periphery of the valley along the bases of the mountain ranges. However, the flat summits of the San Luis Hills are above 9,100 feet and are more than 1,000 feet higher than the highest part of this vast intermontane valley in which they lie.

The principal stream is the Rio Grande, which drains that part of the San Juan Mountains lying east of the Continental Divide. The Rio Grande flows generally eastward in the mountains until it emerges on the San Luis Valley at Del Norte (fig. 1). It meanders slowly in a southeasterly direction past Alamosa across a broad, flat flood plain to the north end of the San Luis Hills. The gradient increases as it flows south through the San Luis Hills into New Mexico.

North of Alamosa is a large area of interior drainage, in which the streams flowing from the mountains

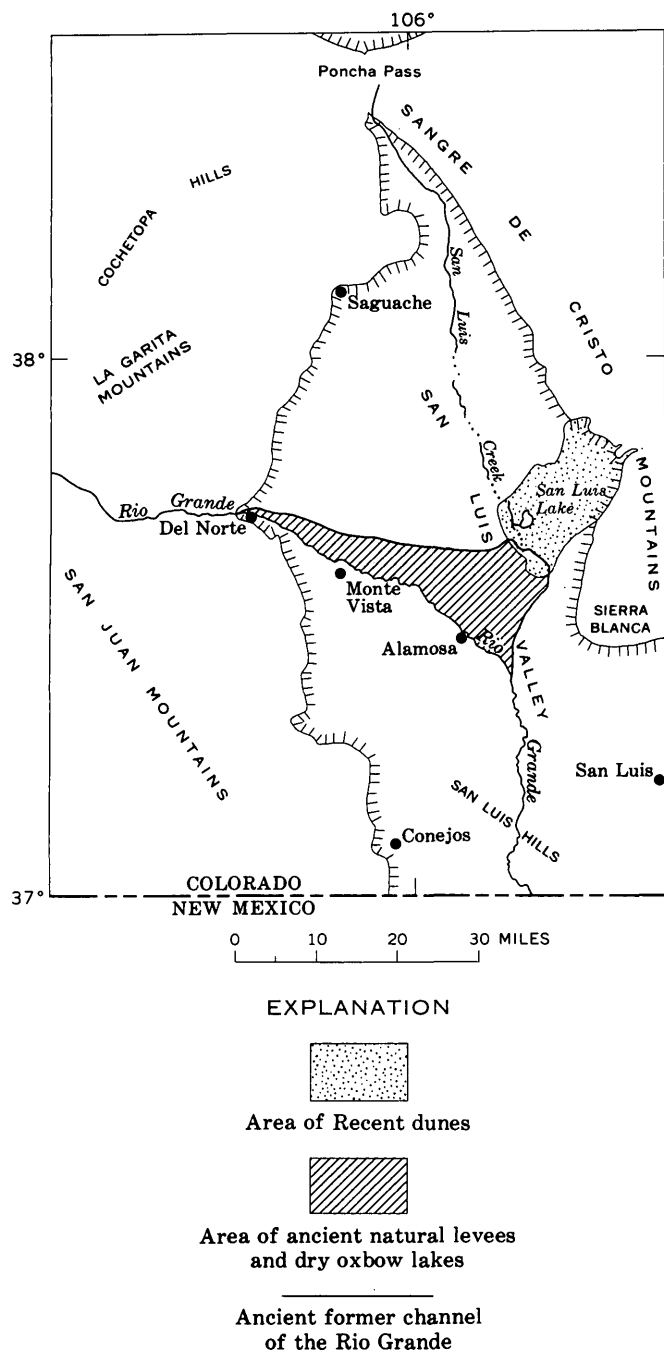


FIGURE 1.—Location map of sand dunes in southern Colorado.

sink into the unconsolidated sediments that floor the valley. The area of interior drainage appears to center in the vicinity of San Luis Lake (fig. 2). San Luis Creek flowing from Poncha Pass and Sand Creek flowing from a cirque in the Sangre de Cristo Mountains terminate in San Luis Lake, which has no outlet. South of Alamosa and east of the Rio Grande, although not in an area of interior drainage, the water of many of the streams sinks beneath the valley floor before reaching the Rio Grande.

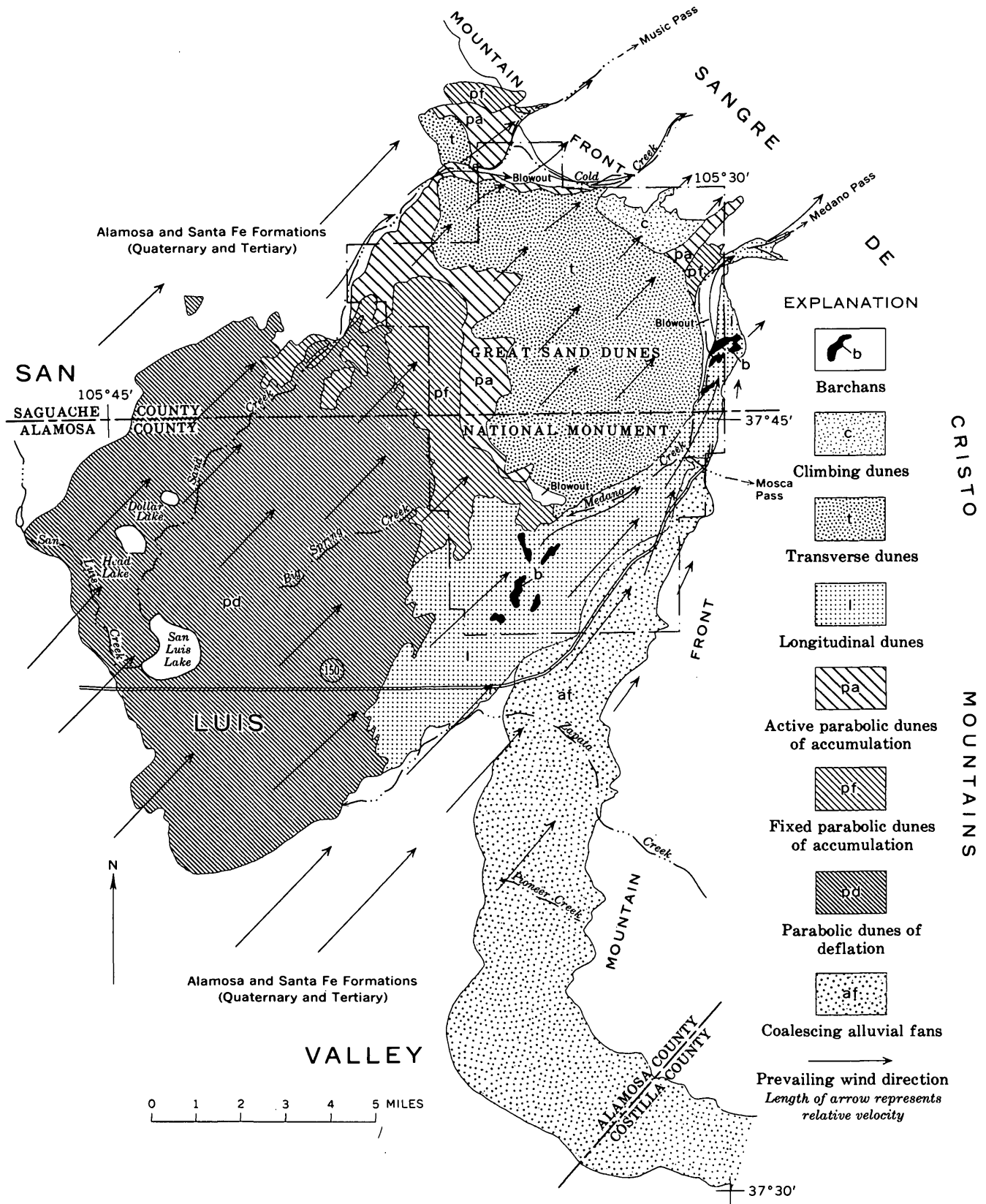
The climate of the San Luis Valley is semiarid. The total normal annual precipitation amounts to 6.56 inches at Alamosa and 9.69 inches at Great Sand Dunes National Monument. Showers are most prevalent in April, and thunderstorms are frequent in July and August. Even during the rainiest months, there are few available hours during which the sun does not shine, and evaporation and transpiration are high. Strong dry winds blow throughout the year from the southwest and dry out the soil and vegetation. During winter storms, high-velocity cold winds blow from the northeast for short periods of time. The strongest winds occur in the spring and early summer when dust storms are fairly common. Occasionally, the winds are so strong that clouds of dust are lifted across the Sangre de Cristo Mountains.

GENERAL GEOLOGY

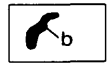
The geologic structure and rock types of the San Luis Valley, the Sangre de Cristo Mountains, and the San Juan Mountains have largely controlled the formation and composition of the sand dunes. The San Luis Valley is a large north-trending structural depression that lies between the two mountain ranges. This depression is filled with 5,000–7,000 feet of alluvial fan gravel, volcanic debris, and interbedded basaltic flows which are here all included in the Pliocene and Pleistocene undifferentiated Santa Fe and Alamosa Formations. Quaternary stream deposits, pediment gravels, and alluvial fan materials mantle most of the valley floor, and a smaller part of the floor is overlain by dune deposits which are younger than most of the alluvium.

The Sangre de Cristo Mountains are composed of a wide variety of igneous and metamorphic rocks of Precambrian age, sedimentary rocks of Paleozoic and Mesozoic age, and igneous intrusive and volcanic rocks of Tertiary age. The bedrock on the western slope of the mountains is mostly Precambrian gneiss, granite, and granodiorite; almost all the debris being eroded from the Sangre de Cristo Mountains into San Luis Valley is derived from these Precambrian rocks. Alluvial fan material, an extension of that filling the San Luis Valley, covers many of the rocks and structural features on the west-facing slopes south of Sierra Blanca (fig. 1).

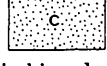
The San Juan Mountains that border the San Luis Valley on the west are composed mainly of volcanic rocks of middle Tertiary age (T. A. Steven, oral commun., 1966). The principal rocks are flows, tuffs, and breccias that range in type from quartz latite to rhyolite (Larsen and Cross, 1956, p. 157).



EXPLANATION



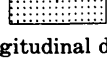
Barchans



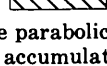
Climbing dunes



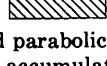
Transverse dunes



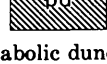
Longitudinal dunes



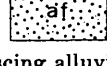
Active parabolic dunes of accumulation



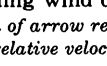
Fixed parabolic dunes of accumulation



Parabolic dunes of deflation



Coalescing alluvial fans



Prevailing wind direction

Length of arrow represents relative velocity

FIGURE 2.—Map showing types of sand dunes in Great Sand Dunes National Monument, Colo., and vicinity, July 1965.



FIGURE 3.—Southeast margin of transverse dunes. Medano Creek in foreground is clogged by eolian sand. View is north toward Sangre de Cristo Mountains. Photograph by W. H. Hill, National Park Service.

DESCRIPTION OF THE DUNES

The sand dunes in and adjacent to Great Sand Dunes National Monument were mapped according to the classification of Hack (1941, p. 240-245) as transverse, parabolic, and longitudinal dunes (fig. 2). Parabolic dunes are divided into parabolic dunes of deflation and parabolic dunes of accumulation (Hack, 1941, p. 242-243). The parabolic dunes of accumulation are further subdivided into fixed and active. Special dune features such as barchans, climbing dunes, and large blowouts are also present (fig. 2). Locally, there is mixing of several types of dunes, and precise delineation is not always possible.

The parabolic dunes of deflation cover a large area southwest, or windward, of all the other dune types (fig. 2), and leeward of an area of ancient oxbow lakes and natural levees (fig. 1) abandoned by the Rio Grande during its lateral migration to the south-

west. The parabolic dunes of deflation consist largely of low mounds of loose sand that are covered by grass and shrubs in most places. Blowouts form on the windward side of the dunes and are the sources of sand being supplied to the actively forming dunes downwind. The blowouts range in size from a few feet to several thousand feet across. Large lakes and barren playas are characteristic of this area of dunes. In fact, the lakes and playas may have originated as blowouts and reached their present size by wind deflation.

Both the longitudinal dunes and the fixed parabolic dunes of accumulation form downwind from the parabolic dunes of deflation. The longitudinal dunes lie in a long, low, and slightly arcuate area south and east of the parabolic and transverse dunes (fig. 2). The longitudinal dunes are lower than the parabolic dunes of deflation, and are only slightly higher than

the duneless valley floor to the south. These dunes are long, low mounds containing a little loose sand at the surface and are covered with grass and a few scattered small shrubs. Although formed here under maximum wind velocities, the longitudinal dunes are stable south and east of Medano Creek. Grains of sand mainly from the parabolic dunes of deflation are piled up by strong winds to form two groups of barchans in the upper and lower reaches of the longitudinal dunes (fig. 2). The upper barchans are now slowly covering a grove of ponderosa pine. Sand and silt are also winnowed from the coalescing alluvial fans nearby to add material to these dunes.

The main area of parabolic dunes of accumulation is leeward of the parabolic dunes of deflation and north of the longitudinal dunes. The fixed parabolic dunes of accumulation are upwind from the active dunes of accumulation. The area of fixed dunes stands generally only a few feet higher than the parabolic dunes of deflation and longitudinal dunes, whereas the active dunes rise for 100–200 feet on a rather steep slope from the fixed dunes to the transverse dunes. Smaller isolated patches of parabolic dunes of accumulation occur near the mouth of the canyons of Medano Creek and Sand Creek (fig. 2). The fixed parabolic dunes are sparsely covered with grass and low shrubs, and the active dunes are even more sparsely covered. The fixed dunes seem to be almost inactive at the present time; only small amounts of sand are collecting on the leeward side of some plants. Most of the sand derived from blowouts in the area of parabolic dunes of deflation seems to be blown across this area to the active parabolic dunes of accumulation.

The transverse dunes from which the Great Sand Dunes National Monument draws its fame (figs. 3, 4) stand 500–600 feet above the parabolic dunes of accumulation to the west and nearly 700 feet above the longitudinal dunes along Medano Creek. The transverse dunes are downwind from the main bulk of the active parabolic dunes of accumulation, which appear to be the immediate source of sand for the transverse dunes. North of Sand Creek (fig. 2) a small patch of transverse dunes is upwind from parabolic dunes. This apparent anomaly may be due to wind eddies. Occasionally strong winds of short duration, especially during the winter (R. L. Burroughs, oral commun., 1966), blow from the northeast and east (Merk, 1960, p. 128) and every winter reverse the crests of the transverse dunes (fig. 4).

The transverse dunes are relatively stable and do not appear to be migrating northeasterly (Merk, 1960, p. 129). Sand blown up from the active parabolic dunes of accumulation appears to be adding mainly

to the bulk of the transverse dunes; a small amount of sand blows beyond to form dunes of other types. These great transverse dunes are almost barren of vegetation; the small amount that is present grows in the interdune hollows where the sand is damp.

Blowouts occur at three places adjacent to the transverse dunes (fig. 2) and are the result of eddying. The blowouts north and east of the transverse dunes appear to be created by strong eddies resulting from sharp changes in wind direction as the prevailing winds funnel into the steep mountain canyons. No reason has been determined for the origin of the eddies that have formed the blowout at the south end of the transverse dunes. Sand is being actively removed from the blowout and moved to the east.

Where Medano Creek emerges from the mountains, strong winds blowing northerly here must turn nearly at right angles to blow easterly up the canyon through Medano Pass. The entire area of the longitudinal dunes is in effect a wind tunnel, and strong eddies are formed where the wind must turn easterly up the canyon. Here these eddies have created a blowout opposite the mouth of the canyon, have piled up high parabolic dunes north of the canyon mouth, and have carried some sand up the canyon to form barren longitudinal dunes with much loose sand. The longitudinal dunes are unstable in the canyon and could be easily converted to other dune types by seasonal variations in wind velocity and sand supply.

Climbing dunes (Hack, 1941, p. 241) are northeast, or leeward, of the transverse dunes between Medano and Cold Creeks (fig. 2). These dunes are piled up against the steep western flank of the Sangre de Cristo Mountains opposite the highest part of the transverse dunes from which the climbing dunes are derived. They rise from about 8,800 feet to 9,500 feet in about a mile. The climbing dunes have no regular dunelike surface features but seem to consist of irregular mounds and swales on a steeply rising slope. They are practically devoid of vegetation, and appear to be accumulating rather rapidly at the present time as the result of the prevailing winds not being able to carry their load of sand over the mountains at this point. However, the turbulence of the eddies that form the large blowouts on either side of the climbing dunes (fig. 2) may have an important influence in containing the dunes laterally.

HISTORY OF THE DUNES AND SOURCES OF THE SAND

Eolian sand, which makes up the dunes, is derived from alluvium deposited by the Rio Grande in the San Luis Valley. During late Pleistocene time the Rio Grande flowed directly eastward from the San Juan



FIGURE 4.—Transverse dunes showing reversal of crests by strong northeasterly winds of short duration. The eastward-facing slopes are steeper than westward-facing slopes and indicate that predominant winds are from the west. Lag gravels cover floor of blowout in foreground. View is north toward Sangre de Cristo Mountains. Photograph by W. H. Hill, National Park Service.

Mountains across the San Luis Valley to the vicinity of San Luis Lake where the river made a 90° bend and flowed directly south through the San Luis Hills (fig. 1). Since that time the Rio Grande has gradually moved southwestward away from this sharp bend until it now occupies a gently curved channel between the east flank of the San Juans and the north end of the San Luis Hills (fig. 1). The area between the oldest and youngest channels now consists of shallow crescent-shaped swales that are abandoned oxbow lakes and low serpentine-shaped mounds of loose sand and silt that are ancient natural levees of the Rio Grande.

The original source area of most of the grains of sand that make up the dunes is the volcanic terrane in that part of the San Juan Mountains drained by the

upper reaches of the Rio Grande and the western tributaries of San Luis Creek. Much smaller amounts of sand were derived from streams flowing into the San Luis Valley from the crystalline and sedimentary rocks of the Sangre de Cristo Mountains north of Sierra Blanca. Alluvial material from these two mountainous terranes was deposited by the Rio Grande and San Luis Creek in the area of ancient natural levees and dry oxbow lakes (fig. 1). This area of loose sand and silt was the ready, immediate source of abundant material for the prevailing southwesterlies to build parabolic dunes to the northeast.

The remnants of these earliest dunes are the parabolic dunes of deflation (fig. 2). The structure of the dunes of deflation appears to have been parabolic when deposited and gives no indication of a history of longi-

tudinal or transverse structures. An increase in vegetation due to an increase in rainfall or relatively low wind velocity has tended to stabilize or fix these early parabolic dunes.

Strong southwesterly winds continued to blow sand out of the Rio Grande flood plain and across the early parabolic dunes. Newly formed parabolic dunes migrated downwind until they reached nearly to the mountain front. There, wind turbulence and eddying were so violent that the sand began to pile up, but a wind-swept valley was kept open along the face of the mountains to the south. As the wind continued to bring in more sand, this sand was piled higher in a transverse pattern, and the interface between the transverse and parabolic dunes gradually moved westward as the large pile of sand stopped the migration of parabolic dunes. A steady and continuous supply of sand accumulated on top of this large pile of transverse dunes and formed climbing dunes against the high barrier formed by the Sangre de Cristo Mountains.

Today, sand is still being derived from the area of natural levees and oxbow lakes and the area of the parabolic dunes of deflation. It is blown across the

fixed parabolic dunes to the active parabolic dunes of accumulation to collect in small amounts; however, most of the sand accumulates in the area of transverse dunes. Excess sand from the transverse dunes forms the climbing dunes. Small amounts of sand blow across the long expanse of longitudinal dunes to collect only temporarily on the barchans, but eventually sand is blown up Medano Pass or piled upon the south side of the climbing dunes as parabolic dunes.

REFERENCES

- Baltz, E. H., 1965, Stratigraphy and history of Raton basin and notes on San Luis basin, Colorado-New Mexico: Am. Assoc. Petroleum Geologists Bull., v. 49, no. 11, p. 2041-2075.
- Hack, J. T., 1941, Dunes of the western Navajo country: Geog. Rev., v. 31, p. 240-263.
- Larsen, E. S., Jr., and Cross, Whitman, 1956, Geology and petrology of the San Juan region, southwestern Colorado: U.S. Geol. Survey Prof. Paper 258, 303 p.
- Merk, G. P., 1960, Great sand dunes of Colorado, in Rocky Mtn. Assoc. Geologists Guide to the geology of Colorado: Denver, p. 127-129.
- Upson, J. E., 1939, Physiographic subdivisions of the San Luis Valley, southern Colorado: Jour. Geology, v. 47, p. 721-736.



MEASUREMENT OF THE ABUNDANCE OF FRACTURE TRACES ON AERIAL PHOTOGRAPHS

By FRANK W. TRAINER, Washington, D.C.

Abstract.—This study illustrates an objective method of investigating the areal abundance of fracture traces seen on aerial photographs. A uniform duration of search, in time per unit area, assures consistent results. The rate of discovery of the traces decreases logarithmically with time. The probable total number of traces per unit area can be estimated from the straightest part of the discovery-time curve, or the number of traces found in a relatively short search can be used as an index of abundance. Contour maps prepared from such index numbers illustrate the areal distribution of abundance. The abundance of the traces and that of their intersections are potentially useful as indices of the near-surface fracture porosity of the rock.

The potential value of aerial-photograph interpretation in areal studies of fractured bedrock is becoming widely recognized. Investigation of the trends of fractures found on aerial photographs is seen as a method of determining structural trends in folded rocks and study of fracture abundance as a guide in estimating fracture porosity. Much of the potential value of the use of photographs lies in their exaggeration of relief under stereoscopic examination. This exaggeration facilitates finding subtly expressed features, especially where the bedrock is so concealed by soil that many of the fractures are missed during studies on the ground. Moreover, study of the photographs provides expeditiously numerical data for statistical study of areal differences in the trends and abundance of fractures. Against these advantages must be weighed the problems of subjectivity inherent in the interpretation of aerial photographs. Lattman (1958, p. 570, 574) discussed several of these problems and described procedures which enable the photointerpreter to avoid mapping manmade linear features as fractures.

In a humid region where the bedrock lies near the land surface the photointerpreter commonly sees the indirect expression of fractures rather than the frac-

tures themselves. Lattman (1958, p. 569) used the terms "fracture trace" and "lineament" for natural linear features, consisting of topographic, vegetation, or soil-tonal alinements, which are visible primarily on aerial photographs. A fracture trace is considered to be less than 1 mile long, whereas a lineament is a mile long or longer. Lattman (1958, p. 570), and other workers whom he cited, believed that fracture traces represent joints, groups of joints, or small faults and that lineaments are faults or shear zones. All the features studied in the present investigation are fracture traces as defined by Lattman.

The two fracture-trace parameters mentioned above—trend and abundance—require different sampling methods. A relatively small sample of fracture traces is adequate to reveal their average trends in a limited area of uniform geology. For example, in another study a sample of 60 or more fracture traces in carbonate rocks was found to be large enough to characterize trends statistically (Trainer and Ellison, 1967); if statistically representative samples are used, it should be feasible to compare results obtained in different areas, in different rocks, or by different workers. The stated abundance of fracture traces, on the other hand, is a function of the time spent in searching for them and of the skill of the interpreter in their recognition. Some standardized method of sampling is required if results are to be consistent within a single area or comparable from one area to another.

This report, which discusses several factors to be considered in such a standardized method, is based on a preliminary study of the abundance of fracture traces in an area of about 10 square miles near Front Royal, Va. (fig. 1). The terrain, part of the floor of the Shenandoah Valley, is gently rolling; local relief is commonly less than 60 feet. The bedrock is chiefly Cambrian and Ordovician limestone and dolomite

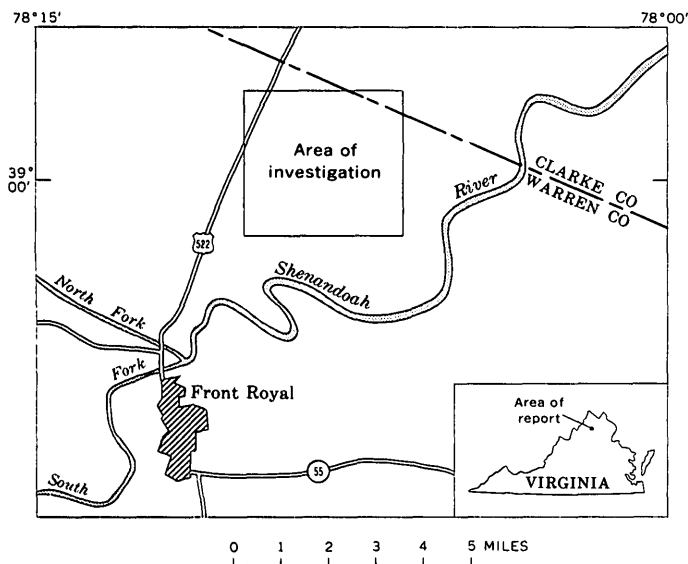


FIGURE 1.—Index map showing location of area studied in the Shenandoah Valley near Front Royal, Va.

lying in a belt of carbonate rocks covered by a thin mantle of residual soil (Hack, 1965, pl. 2). Bedrock is exposed in only a small part of the area—estimated from the aerial photographs to be less than 1 percent—but it probably is within a few feet of the land surface in most of the area.

A count of 661 fracture traces in the Front Royal area shows that about 98 percent of them are topographic features—trenchlike depressions, straight gullies and stream segments, and groups of alined sinkholes. The rest are alinements expressed in soil tone or in vegetation. Probably most of these fractures have been weathered, and some are the sites of extensive solution and removal of rock material.

EXAMINATION OF THE PHOTOGRAPHS

Six adjoining stereopairs of photographs (scale 1:21,100) were examined with a pocket-type stereoscope. Fracture traces were marked on the photographs with a china-marking pencil. So far as possible, all the photographs were studied in the same way and under the same conditions. Periods of study were limited to 2 hours or less in order to minimize the possible effects of fatigue.

A uniform duration of search was adopted so that the abundance of fracture traces might be directly comparable from one part of the area to another. Each pair of photographs was studied for 5 minutes per square mile of area of overlap, which on these photographs is a length of time adequate for one complete scan of the area being examined. After the set of 6 pairs of photographs had been studied, it was

reexamined 5 additional times over a total period of about 4 months, each time at the rate of 5 min per sq mi. Each stereopair was thus examined for a total of 30 min per sq mi. The fracture traces were marked in different colors during successive examinations so that those found during each period of study could be distinguished and separately recorded.

RATE OF DISCOVERY OF FRACTURE TRACES

Fracture traces were found relatively rapidly during the early part of the total period of examination of each pair of photographs, but at a logarithmically decreasing rate as time progressed. Figure 2 illustrates the change in rate of discovery with time, for three of the stereopairs studied.

It is impossible to find all the fracture traces on a given pair of photographs in a practicable period of time. However, the number of traces visible on that pair can be estimated from the trend of the latest and most nearly straight part of the rate-of-discovery curve. For example, it is estimated that totals of about 140, 170, and 180 fracture traces per square mile could be found on the pairs of photographs represented by the graphs in figure 2, if the search were extended sufficiently. Such estimates, when based on graphs of regular form, present an objective basis for comparison of the abundance of fracture traces in different rocks, different structural situations, or different areas. The time required would be prohibitive, however, if a large number of photographs were to be studied. An alternative procedure is use of the number of traces found in less than the total time of

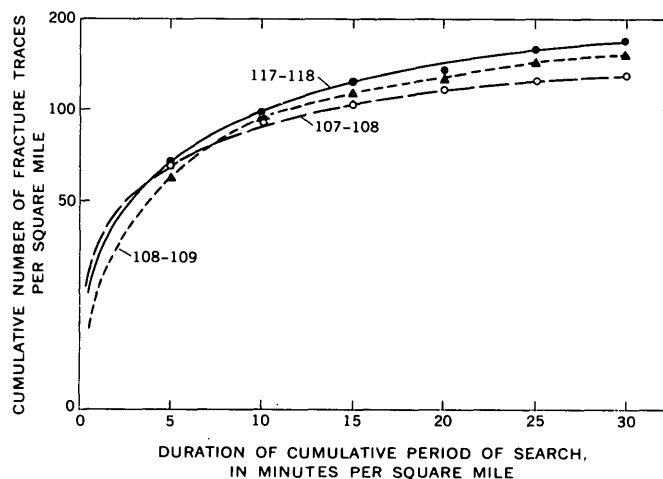


FIGURE 2.—Graphs showing rates at which fracture traces were found on 3 of 6 stereopairs (paired numbers) of vertical aerial photographs studied. The 8 photographs used are DJP-12G-106/109 and 116/119, U.S. Department of Agriculture, scale 1:21,100. Three additional graphs, omitted to avoid crowding, lie between the extremes shown after about 8 min per sq mi of search time.

search as an index of the probable abundance. In the photographs studied, 39–50 percent of the fracture traces found in a cumulative period of search of 30 min per sq mi were found in the first 5 min per sq mi, 57–70 percent in the first 10 min, and 84–89 percent in the first 20 min. The number provided by any one of these periods of examination would be a satisfactory index of the probable abundance for use in comparative studies.

ABUNDANCE OF FRACTURE TRACES

The abundance of fracture traces and lineaments on aerial photographs can be measured as frequency (the total number of features per unit area) or as density (their total length per unit area). Both methods have been used in summarizing data on published maps. Gol'braykh and others (1966, p. 1013) expressed their results in terms of number per unit area; Henderson (1960, p. 58) and Hough (1960, p. 13) used total length per unit area.

Because the population of fracture traces probably represents a variety of physical features (single fractures; groups of parallel, closely spaced fractures; and different kinds of fractures), frequency and density very likely have somewhat different physical significance. However, because both parameters represent the same traces, it is reasonable to assume that in a large population the numerical values of the parameters are proportional to one another. Both were tested in the early part of the present study and were found to provide similar contour maps. Because it is much easier to count traces than to measure their lengths, the parameter frequency was used thereafter.

The procedure used in measuring frequency was as follows: A counting square was moved north to south, and east to west, to successive positions on tracing paper superimposed on a fracture-trace mosaic of the photographs. The side of the counting square represents a length of 0.32 mile; the area of the square represents 0.10 sq mi. Any fracture trace seen inside the square was counted, whether it lay completely within the square or extended into it from beyond its border. The counting square was moved along a square grid which has a spacing of 0.15 mile, and each count was written at the center of the counting square. The result is a square array of numbers, 0.15 mile apart, each of which represents a square that overlaps each adjoining square by about 50 percent. Each number is assumed to be an index of the abundance of weathered fractures in that square. The sizes of the counting square and counting grid were selected to give points considerably nearer one another than the width of outcrop of the thinnest stratigraphic unit in the area.

Thus it should be possible to detect any stratigraphic control of fracture-trace frequency.

The contour maps in figures 3A–3C show the frequency of fracture traces found in searches of 5, 10, and 15 min per sq mi (cumulative totals), respectively. The maps exhibit conspicuous patterns of contour lines with local differences in frequency of two to three times over lateral distances as small as one-sixth of a mile. The principal patterns are generally similar on the three maps. All the maps show linear, north- to northeast-trending zones of high and low values. The approximate parallelism of these zones with the formation contacts suggests stratigraphic control of the frequency. The cause of several conspicuous "gaps" along the trends of these zones (for example, in the north-central and southwestern parts of the area) is not known. The area is entirely in farmland, and there has been little extensive construction by man which would have destroyed fracture traces or rendered them illegible.

Comparison of the maps in figures 3A–3C shows a progressive increase in detail with increasing duration of search. However, the basic pattern of contour lines was established on the first and second maps, and the principal conclusions about the areal distribution of frequency were not significantly altered as a result of the additional information provided by the third map. If these maps had been prepared to determine the locations, dimensions, and relative magnitudes of the principal concentrations of fracture traces, study of the photographs at the cumulative rate of 10 min per sq mi would have been adequate.

FRACTURE TRACES AS INDICES OF FRACTURE POROSITY

More than 99 percent of the fracture traces found in the present study are straight or consist of straight segments which join at an angle. Published maps and descriptions of fracture traces and lineaments found on aerial photographs elsewhere show that these features are commonly straight in plan, regardless of land-surface relief, and therefore that they represent vertical or near-vertical fractures. (See, for example, Boyer and McQueen, 1964, p. 633; Chiang and Skaryatin, 1962, p. 54, 57, 59, 60, 61; Condon, 1965; Henderson, 1960, p. 54; Hough, 1960, p. 10; Marchesini and others, 1963, p. 531; Mollard, 1957, p. 44; Parizek and Drew, 1966, p. 9; and Trainer and Ellison, 1967). This conclusion is significant in regard to the study of fracture porosity because it implies that the abundance of fracture traces represents only part of the total population of fractures and therefore must be considered an indirect indicator of the number of open fractures in the near-surface rock. It seems likely, however,

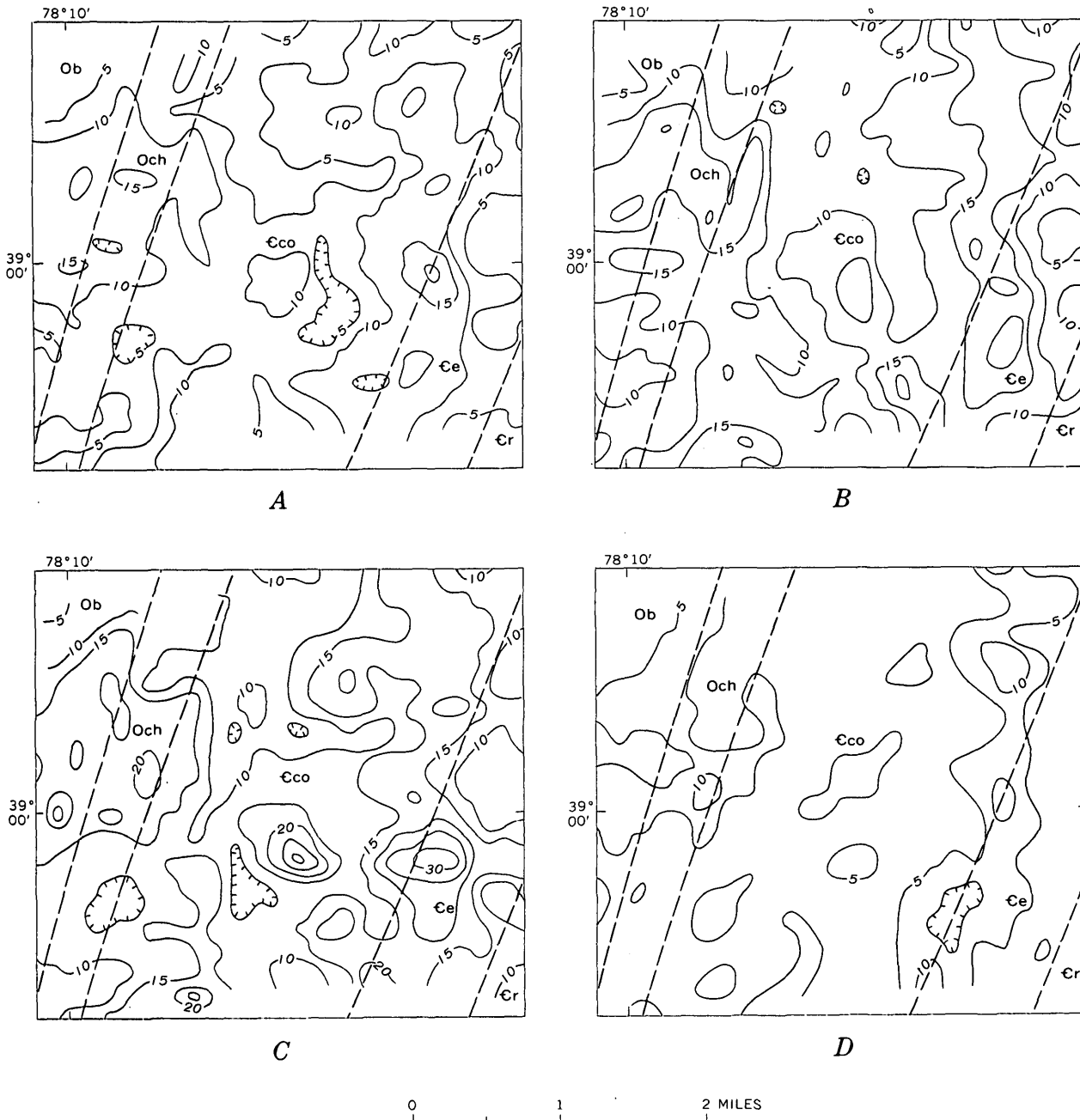


FIGURE 3.—A-D, Maps showing frequency of fracture traces found on vertical aerial photographs after cumulative search periods of (A) 5 min per sq mi, (B) 10 min per sq mi, and (C) 15 min per sq mi. Contour interval, 5 traces per 0.1 sq mi. D, Map showing frequency of fracture-trace intersections after a cumulative search period of 15 min per sq mi. Contour interval, 5 intersections per 0.1 sq mi. Dashed lines indicate approximate positions of stratigraphic boundaries (after Virginia Div. Mineral Resources, 1963). Formations are: Cambrian—Cr, Rome Formation; Ce, Elbrook Dolomite; Eco, Conococheague Limestone; Ordovician—Och, Chepultepec Dolomite; Ob, Beekmantown Group.

that extensive weathering of vertical fractures at the surface is accompanied by subsurface weathering and possible widening of other fractures which are not expressed as fracture traces. The abundance of fracture traces may therefore be proportional to the total number of open fractures, and hence to the near-surface fracture porosity.

Another potential measure of fracture porosity is the frequency of fracture-trace intersections. In a sample of 11 wells in carbonate rocks in central Pennsylvania, Lattman and Parizek (1964, p. 82-83) found that specific capacity is higher in wells on or near fracture traces than in those located between the traces and still higher in wells located at the intersec-

tions of two traces. From these data and from caliper surveys of the wells, they concluded that fracture traces reflect zones of increased solution of the rock (Lattman and Parizek, 1964, p. 86). Figure 3D shows the areal distribution of frequency of intersections in the area near Front Royal, as observed in a cumulative period of search of 15 min per sq mi. The influence of the abundance of traces on the abundance of their intersections, which is logically inferred, is suggested by the similarity of this areal pattern to those shown by the maps in figures 3A-3C. However, differences in the map patterns suggest that the frequency of intersections may be influenced by some additional factor other than abundance of traces.

Further studies should be undertaken in areas having a variety of rock types and structural conditions for which good geologic maps and accurate drillers' logs and other subsurface data are available, so that these potential indices of fracture porosity can be evaluated and the factors which control them can be investigated.

REFERENCES

- Boyer, R. E., and McQueen, J. E., 1964, Comparison of mapped rock fractures and airphoto linear fractures: *Photogrammetric Engineering*, v. 30, no. 4, p. 630-635.
- Chiang, Chiu-Ch'i, and Skaryatin, V. D., 1962, Opyt issledovaniya treshchinovatosti karbonatnykh porod Dagestana s ispol'zovaniyem aerofotosnimkov [Experiment in investigating jointing of carbonate rocks in Dagestan by means of aerial photographs]: *Izvestiya Vysshikh Uchebnykh Zavedeniy, Geologiya i Razvedka*, no. 10, p. 53-62.
- Condon, W. H., 1965, Map of eastern Prince William Sound area, Alaska, showing fracture traces inferred from aerial photographs: U.S. Geol. Survey Misc. Geol. Inv., Map I-453.
- Gol'braykh, I. G., Zabaluyev, V. V., and Mirkin, G. R., 1966, Tectonic analysis of megajointing: A promising method of investigating covered territories: *Internat. Geology Rev.*, v. 8, no. 9, p. 1009-1016. [Translated from *Sovetskaya Geologiya*, 1965, no. 4, p. 63-73.]
- Hack, J. T., 1965, Geomorphology of the Shenandoah Valley, Virginia and West Virginia, and origin of the residual ore deposits: U.S. Geol. Survey Prof. Paper 484, 84 p.
- Henderson, G., 1960, Air-photo lineaments in Mpanda area, Western Province, Tanganyika, Africa: *Am. Assoc. Petroleum Geologists Bull.*, v. 44, no. 1, p. 53-71.
- Hough, V. N. D., 1960, Photogeologic techniques applied to the mapping of rock joints: *West Virginia Geol., Econ. Survey Rept. Inv.* 19, 21 p.
- Lattman, L. H., 1958, Technique of mapping geologic fracture traces and lineaments on aerial photographs: *Photogrammetric Engineering*, v. 24, no. 4, p. 568-576.
- Lattman, L. H., and Parizek, R. R., 1964, Relationship between fracture traces and the occurrence of ground water in carbonate rocks: *Jour. Hydrology*, v. 2, p. 73-91.
- Marchesini, E., Pistolesi, A., and Bolognini, M., 1963, Fracture patterns of the natural steam area of Larderello, Italy, from airphotographs: *Internat. Archives Photogrammetry*, v. 14, Symposium on photo interpretation, Delft, 1962, Trans. p. 524-532.
- Mollard, J. R., 1957, Aerial mosaics reveal fracture pattern on surface materials in southern Saskatchewan and Manitoba: *Oil in Canada*, v. 9, no. 40, p. 26-50.
- Parizek, R. R., and Drew, L. J., 1966, Random drilling for water in carbonate rocks: Pennsylvania State Univ. Inst. Research Land, Water Resources, Water Resources Research Pub. 3-66.
- Trainer, F. W., and Ellison, R. L., 1967, Fracture traces in Shenandoah Valley, Virginia: *Photogrammetric Engineering*, v. 33, no. 2, p. 190-199.
- Virginia Division of Mineral Resources, 1963, Geologic map of Virginia, 1:500,000.



USE OF AN INFILTRATION GALLERY TO OBTAIN FRESH WATER AT OCEAN CAPE, ALASKA

By ALVIN J. FEULNER, HENRY H. HEYWARD, and CLIFFORD G. ANGELO, Anchorage, Alaska

Work done in cooperation with the

U.S. Air Force, Alaskan Air Command, through the Radio Corporation

of America White Alice Communications Project, Alaska, 1966

Abstract.—Sufficient water for a military facility at Ocean Cape has been obtained during the past 3½ years from a horizontal infiltration gallery that taps a layer of fresh water resting on saline water. The gallery, which is 5 feet above mean sea level and 250 feet inland from the shoreline, supplants a well at the same general location. When first installed, the well yielded water of satisfactory quality, but within 2 years the chloride content of the water increased to more than 500 ppm.

Ocean Cape is the westernmost point of land on the Phipps Peninsula, which juts out from the south coast of Alaska between the Gulf of Alaska and Yakutat Bay. The village of Yakutat, at the head of Monti Bay (an arm of Yakutat Bay), is about 5 miles east of Ocean Cape. The location of the Phipps Peninsula area in Alaska is shown on the index map in figure 1, and the relations of the land and water surfaces on the peninsula are shown on the larger scale map in figure 1 and on an aerial photograph (fig. 2).

To supply water for a military facility at Ocean Cape, a 10-inch-diameter well was drilled in 1960 to a depth of 76 feet. The materials penetrated in drilling were gravel, sand, and silt, and the static water level was about 24 feet below the land surface. The well is about 250 feet east of the Gulf of Alaska and only a few hundred feet west of the Anka Saltchucks, which are bodies of saline water that connect with Monti Bay. The land surface at the well is about 30 feet above sea level; the general elevation of the land surface in the vicinity of the well ranges from about 25 to 50 feet above sea level. The location of the well

and storage tank is shown in the aerial view of the Ocean Cape facility (fig. 3).

Pumping tests indicated that yields of from 50 to 70 gallons per minute could be obtained with a drawdown of about 30 feet. Following test pumping and development work, it was suggested that the well be pumped at rates of no more than 20 gpm, at which rate the drawdown would be about 15 feet, to avoid problems of saltwater intrusion to the well. Despite its nearness to open bodies of salt water, the well produced water ranging in chloride content from 95 to 116 parts per million in several tests conducted in 1960. However, when pumped in 1962 at a rate of approximately 25 gpm, the chloride content had increased to 515 ppm, which is double the limit recommended by the U.S. Public Health Service (1962, p. 7) for drinking water supplies. Because the bottom of the well is about 46 feet below sea level and the water level is drawn down to about 10 feet below sea level when the well is pumped at 25 gpm, it appeared that higher concentrations of saline water could be expected if pumping continued. As pumping at a lower rate did not seem practical, another source of water was needed.

Several nearby streams and lakes were sampled for chemical quality. Of these, only two lakes contained water that would be suitable. A small lake near the road and about 1.3 miles from the facility (shown as lake 1 on fig. 1) had a chloride content of 88 ppm, and a very small lake about 300 feet north of the site (figs. 1 and 3) had a chloride content of 10 ppm. Development of a supply from the farther lake was considered not feasible because a pipeline would be too costly;

GROUND WATER

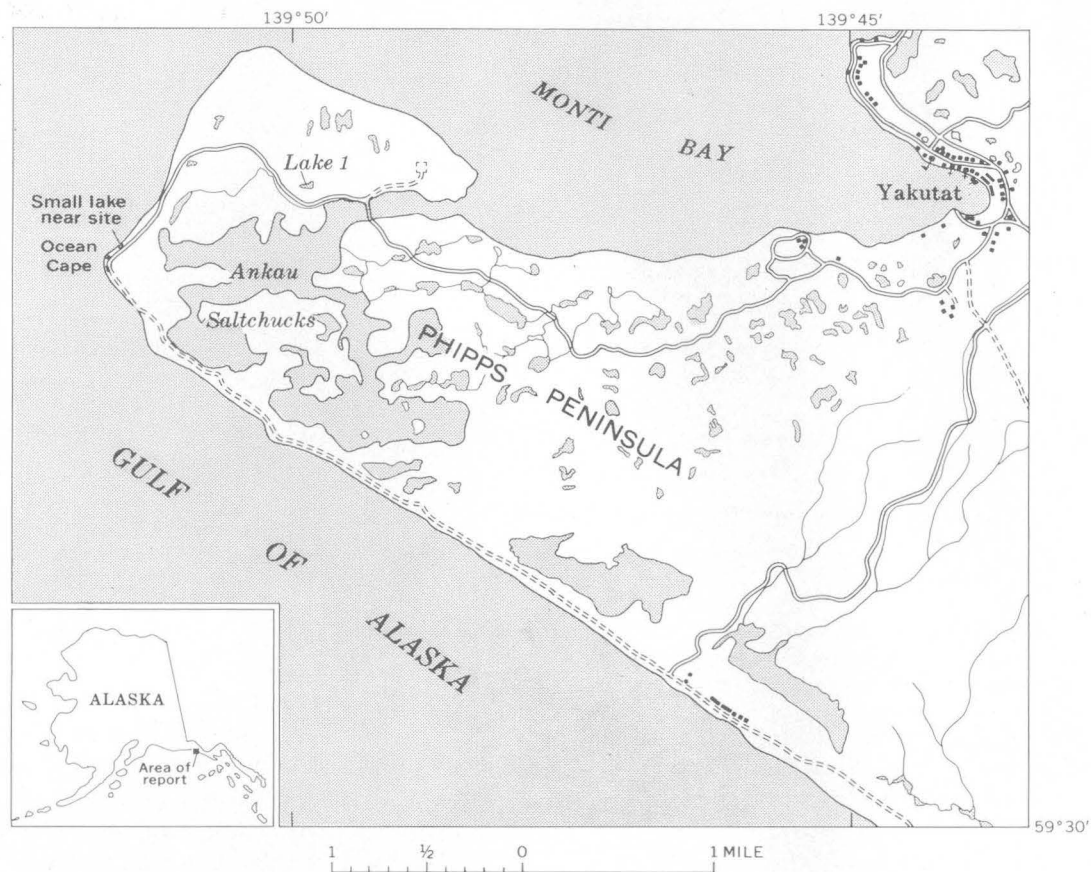


FIGURE 1.—Map of the Ocean Cape area on Phipps Peninsula, southern Alaska.

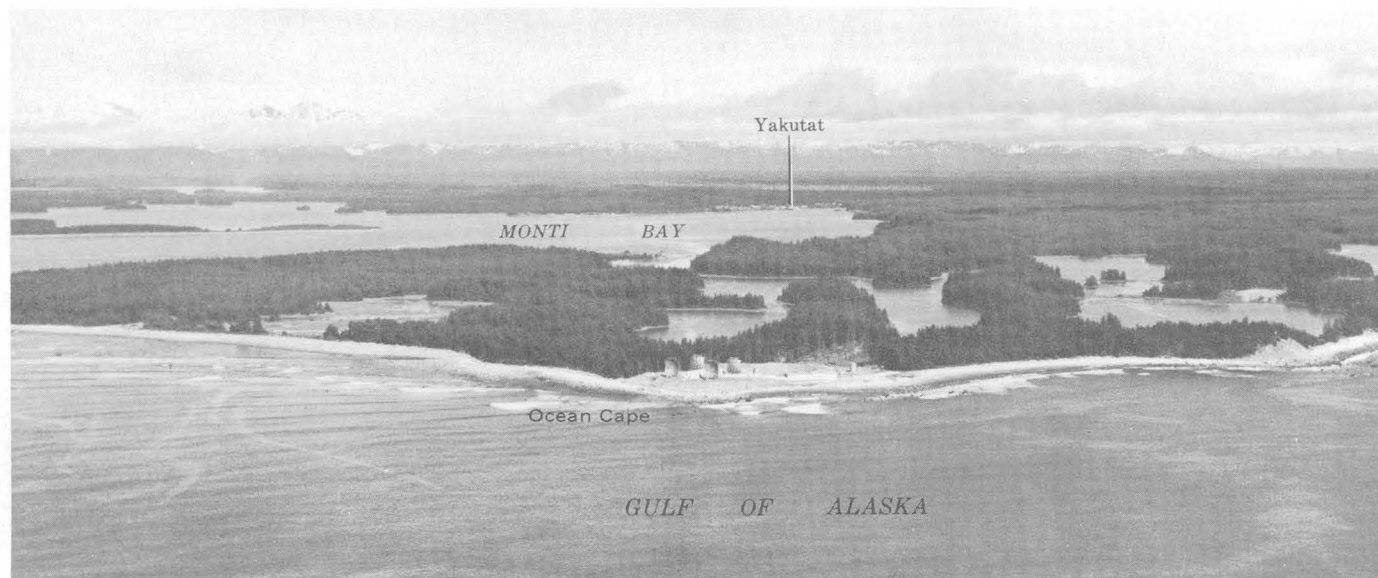


FIGURE 2.—Location of Ocean Cape with respect to the Gulf of Alaska, Monti Bay, and Yakutat. Photograph courtesy of Radio Corporation of America.



FIGURE 3.—View of drilled well, storage tanks, and lake where gallery is located at the Ocean Cape facility. Photograph courtesy of Radio Corporation of America.

development of a supply from the nearer lake was not considered because the water contained too much organic material.

As development of another supply from ground water seemed the only practical alternative, it was decided that a horizontal infiltration gallery tapping only the uppermost water-bearing sediments would be less likely to yield saline water than would a vertical well that necessarily would extend below sea level. The gallery, constructed in 1962, consists of an 80-foot-long corrugated perforated intake pipe and a vertical access pipe connecting the intake pipe with the land surface. The diameters of the intake and access pipes are 4 and 3 feet, respectively. The ditch in which the intake pipe was laid was excavated to 4.3 feet above mean sea level and then backfilled with about 1 foot of graded gravel. After the intake pipe had been laid, more graded gravel was added until the pipe was covered to a depth of about 2 feet. A 1-foot layer of sand, a similar thickness of gravel, and a 2-foot layer of sand completed the filling of the ditch. The details of the installation are illustrated in figure 4.

Observations of the depth to water in a well between the gallery site and the nearby lake indicated that the water table fluctuated seasonally between levels of about 9 and 13 feet above mean sea level (fig. 4). Thus,

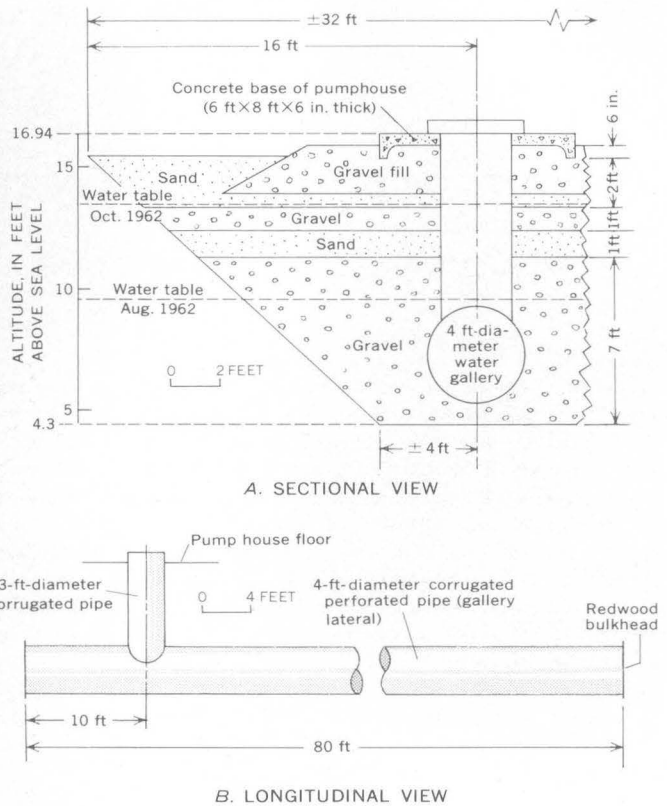


FIGURE 4.—Sectional and longitudinal views of gallery installation.

the intake pipe would be below the water table and high enough above the contact of fresh and saline water to permit withdrawal of fresh water without causing a progressive encroachment of the saline water.

The gallery was placed in operation in late 1962 and the water sampled for chemical quality periodically from 1962 through 1966. During the 3½ years following the installation, the chloride content of the water fluctuated seasonally within the range of 22 to 34 ppm. Sufficient water to maintain the facility was supplied constantly during this entire period.

It appears from this history of development at Ocean Cape that other coastal areas having similar geologic and hydrologic conditions could make use of horizontal galleries for water-supply development.

REFERENCE

U.S. Public Health Service, 1962, Public Health Service drinking water standards: Public Health Service pub. 956.



IMMOBILITY OF CONNATE WATER IN PERMEABLE SANDSTONE

By G. EDWARD MANGER and W. T. WERTMAN,¹ Washington, D.C., Morgantown, W. Va.

Abstract.—Some natural-state cores of moderately permeable Eocene sandstone, obtained by drilling with oil-base mud in Karnes County, Tex., appear to be saturated and other cores appear to be partially unsaturated. The variation of interstitial water chlorinity is related to the depositional environment of the different sandstone strata. These results suggest that a small fraction of connate water has remained immobile in the sandstone since the Eocene. Such immobility agrees with that found experimentally by Wyckoff and Botset and discussed theoretically by Irmay for a small fraction of fluid in a saturated permeable porous medium. Absence of significant diffusion over geologic ages seems to be necessary to explain the present results; reasons for this are not yet evident.

In apparently saturated and partially unsaturated natural-state cores of moderately permeable Eocene sandstone in Karnes County, Tex., variation of interstitial water chlorinity is related to depositional environment of the sandstone strata (see table 1). Thus the suggestion is that a fraction of the connate water has remained immobile since the Eocene. The cores were obtained by drilling with oil-base mud.

To a depth of about 40 or 50 feet, the chloride ion is concentrated because of surface evaporation, but below this depth chlorinity of the interstitial water in permeable sandstone in both dominantly sandy and in dominantly argillaceous beds is greater where sediments were deposited under marine conditions. The lowest mean chlorinity, 167 milligrams per liter, is in the nonmarine part of the DuBose Member of the Whitsett Formation. This nonmarine part lies below fine-grained sandstone and siltstone correlated with coarse-grained sandstone that crops out locally and is called the Tordilla sandstone bed. The lowest chlorinity values for all core samples are found near the bottom of this nonmarine part of the DuBose Member; the highest chlorinity in this part of the member, 404 mg/liter, is found 15 feet below the con-

tact with the Tordilla sandstone bed and probably reflects an upward transition to marine conditions of deposition. The next lowest mean chlorinity, 242 mg/liter, is found in cores of permeable sandstone from the Manning Clay Member of the McElroy Formation, where the depositional environment is described as nonmarine or lagoonal. Although these permeable sandstones apparently are saturated or partially unsaturated, flushing by ground water probably did not remove all connate water.

The question arises, therefore, of how a fraction of connate water could be retained since Eocene time in pores of permeable sandstone. In their experimental study of simultaneous flow of practically immiscible gas and liquid through clay-free sand packings of widely different permeability in the darcy range, Wyckoff and Botset (1936) found that flow of either phase decreased in a complex fashion as liquid saturation decreased. The following is quoted from the Wyckoff and Botset paper (1936, p. 332):

When the liquid saturation of the sand is still about 10 percent the gas permeability has, within observational accuracy, reached 100 percent; the flow is entirely gas. This indicates that the liquid left in the pores of the sand body is retained in the sharp angles between sand grains and that in normal homogeneous-fluid flow this fraction of the pore volume makes an insignificant contribution to the total flow. These sharp angles retaining liquid are thus comparatively dead spaces in which there is never any appreciable amount of flow, consequently their plugging or filling by a solid or incompressible material has a negligible effect on the apparent permeability of the sand.

In considering Wyckoff and Botset's results as related to the hydraulic conductivity of soils, Irmay (1954) emphasized that in regard to liquid flow a fraction of pore water is "always stagnant or dead water . . . [and] might even be replaced by a filler of solid or incompressible material without altering the flow." Irmay (1954, equation 12) developed a correction factor that takes into account this immobile fraction of

¹ U.S. Bureau of Mines, Morgantown Petroleum Research Laboratory.

TABLE 1.—*Depositional environment and chlorinity of interstitial water in natural-state cores of permeable Eocene sandstone of the Jackson Group, Karnes County, Tex.*

[Stratigraphy and depositional environment from Eargle (1959)]

Formation	Member	Unit	Depositional environment	Depth of cores (feet)	Chlorinity (mg/liter)			Permeability (millidarcys)		
					Mean	Range	No. of samples	Logarithmic mean	Range	No. of samples
Whitsett	DuBose	Tordilla sandstone bed	Marine, a temporary return of marine conditions.	16-59	3,020	329-9,490	24	404	1.4-3,730	14
			Nonmarine.	45-128	167	8-404	33	110	0-1,530	10
	Stones Switch Sandstone		Locally marine, transitional from marine Conquista beds below to nonmarine DuBose beds above.	16-36 115-170	1,751 533	500-4,680 76-1,200	38 71	72 63	0-854 0-651	22 17
McElroy	Conquista Clay		Marine or lagoonal above the basal few feet.	38-98 172-214	493 416	105-795 233-802	20 15	60 91	----- 41-199	1 3
	Dilworth Sandstone		Marine at base, grades into nonmarine.	101-293	353	60-1,060	46	57	1.3-831	29
	Manning Clay		Nonmarine or lagoonal.	179-243	242	70-438	21	14	0-270	14

pore water when estimating permeability from grain size, porosity, and other textural properties of saturated porous media. The authors and their colleagues find that by use of this correction factor measured and estimated permeability agree closely for some Jurassic sandstones in the range of 3 to 1,300 millidarcys.

Other lines of evidence also suggest that not all connate water has been removed from permeable sandstone because of flushing by ground water. Chlorinity is independent of a wide range of permeability. Also, below the capillary fringe, salinity of the formation ground water expressed as equivalent chlorinity (obtained from induction-log resistivity, and core porosity and saturation) shows a range of from 4,150 to 1,380 ppm, or a ratio of 3, whereas chlorinity (obtained by extraction of chloride from cores) shows a greater range, from 840 to 43 ppm, or a ratio of 20. The greater variation in chlorinity may be due to differences in composition of original connate waters, fractions of which perhaps have remained to the present even in moderately permeable sandstone. The more limited range in equivalent chlorinity, on the other hand, is due to variation in the salinity of present-day ground water.

In addition to immobility as a necessary condition for the preservation of connate water in the fine interstices in permeable sandstone, absence of significant diffusion seems to be necessary. Reasons for this are

as yet not evident. Although flow of fresher ground water into blind capillary interstices that are already filled (with salty water) does not seem likely, it is not apparent why ions of salty water would not move from these interstices into fresher ground water contained in larger pore openings.

There is also the question of why leaching in the laboratory was effective for recovering water that was not removed by flowing ground water throughout geologic time. No answer to this question is evident, but a possible explanation is that the original structure of the generally soft and unconsolidated sandstones was destroyed when samples were packed into the porous extraction thimbles, thereby permitting access of hot distilled water to connate water previously immobilized in sharp angles between sand grains. Another possible explanation is that continuous flow of hot distilled water through a specimen over a 24-hour period in the laboratory produced more efficient removal of small residual amounts of connate water by displacement or by diffusion than did the flow of ground water under natural-state conditions.

In sandstone of low permeability some connate water and its ions may be retained because of sorption by clays. The present results, however, suggest that in shallow moderately permeable sandstone, a fraction of connate water is retained for geologic ages in sharp angles between sand grains.

REFERENCES

- Eargle, D. H., 1959, Sedimentation and structure, Jackson Group, south-central Texas: Gulf Coast Assoc. Geol. Societies Trans., v. 9, p. 31-39.
- Irmay, S., 1954, On the hydraulic conductivity of unsaturated soils: Am. Geophys. Union Trans., v. 35, p. 463-467.
- Wyckoff, R. D., and Botset, H. C., 1936, The flow of gas-liquid mixtures through unconsolidated sands: Physics, v. 7, p. 325-345.



THE UNDERSIDE OF RIVER ICE, ST. CROIX RIVER, WISCONSIN

By KEVIN L. CAREY, Madison, Wis.

Abstract.—Ripplelike and dunelike features have been found during a second winter on the underside of the ice cover on the St. Croix River, Wis. Profiles of the features and measurements of ablation and accretion show that the features began to form when the underside of the ice was accreting, and continued their development during ablation. The Belokon-Sabaneev formula, $n_t = (2n^{1/2} - n_b^{1/2})^{2/3}$, satisfactorily shows the relationship between the roughness coefficients for the ice, the bed, and the total channel. Calculations of the roughness coefficient for the underside of the ice, n_t , range from 0.0039 to 0.0142, except for one calculation which indicates no retardation of the flow by the ice cover. This anomaly is believed to be caused by an incorrect estimate of the effective size of the roughness projections of the bed. Caution is therefore given that the computed (published) values of the ice-roughness parameters are slightly smaller than actual.

Relief features that appear analogous to some of the bed forms of alluvial streams have been observed on the underside of river ice in a half-mile reach of the St. Croix River near Danbury, Wis. These observations were reported by Carey (1966), along with the method for calculating the roughness coefficient of the underside of the ice. This report presents the findings of an additional winter's study (1965-1966) which supplement the data already reported for the winter of 1964-65.

The first winter (1964-1965) of the study presented conditions that are normally found at the St. Croix River study site except for slightly low monthly average discharges. The second winter's (1965-66) conditions were unusual in two respects: fairly high flow at greater than average depths throughout the winter, and the presence of frazil (slush) ice in the channel beneath the solid ice cover during the first part of the winter.

OBSERVATIONS OF UNDERSIDE OF ICE, 1965-66 WINTER

The frazil ice that was located immediately below the solid ice cover, was stationary or moving imper-

ceptibly. It varied in thickness in different places from several tenths of a foot to several feet and extended to the streambed in some localities. The amount of frazil ice increased downstream through the half-mile reach in which the river widens and velocities diminish slightly. The proportion of the volume of the channel beneath the ice cover that was occupied by frazil ice decreased with time until midwinter, when some frazil ice had become incorporated into the solid ice cover, and the remainder had melted or had been flushed downstream. The frazil ice and (or) greater effective depths of the river (averaging 3-4 feet), compared to those of the previous winter (when depths averaged 2-2.5 feet), apparently did not favor the formation of relief configurations on the underside of the ice during the early part of the winter.

Observations of the underside of a block of ice were made on seven occasions (table 1), spaced at intervals of 6-12 days, and were made in the same part of the reach where ice blocks had been examined the previous winter. The first two observations were made at times when frazil ice was adhering to the underside of the solid ice cover. The underside of this frazil ice was irregular, but had no discernible pattern. On the occasion of the third observation, frazil ice was not present beneath the solid ice cover in the vicinity of the ice block observations; the underside of the observed ice block was fairly smooth and showed no pattern of subtle irregularities. The four succeeding observations (4-7, table 1) showed significant relief on the underside of the ice.

Ripple configurations found on the underside of the four blocks of ice that showed relief during the second winter (4-7, table 1) were no different in form from those observed the first winter. The configurations resembled the ripple and dune patterns found in the bed forms of an alluvial stream flowing over medium to fine sand. However, the first two of these blocks, Nos. 4 and 5, had configurations that were more

TABLE 1.—Winter measurements of stream discharge and channel geometry, computed hydraulic parameters, observations of configuration of the underside of the ice, and amount of frazil ice on the St. Croix River near Danbury, Wis.

[Subscripts B and I refer to bed-section and ice-cover section]

No.	Date (1966)	Discharge Q (cfs)	Mean velocity V (fps)	Cross-sectional area ¹			Wetted perimeter			Hydraulic radius		
				A (ft ²)	A _B (ft ²)	A _I (ft ²)	P (ft)	P _B (ft)	P _I (ft)	R (ft)	R _B (ft)	R _I (ft)
1	Jan. 13	1,123	1.79	627	434	193	463	230	233	1.35	1.89	0.828
2	24	920	1.66	555	427	128	456	227	229	1.22	1.88	.559
3	Feb. 3	908	1.77	514	² 522		451	225	226	1.14	² 2.32	
4	15	1,402	1.98	707	581	126	453	226	227	1.56	2.57	.555
5	21	1,090	1.84	593	585	35	454	227	227	1.31	2.46	.154
6	Mar. 4	1,230	1.95	631	559	72	454	227	227	1.39	2.46	.317
7	10	1,300	1.86	700	507	193	455	228	227	1.54	2.22	.850

No.	Date (1966)	Energy gradient S _s × 10 ⁴ (ft/ft)	Darcy-Weisbach friction factor			Manning roughness coefficient			Ripples on underside of solid ice		Portion of volume of the reach under solid ice cover that was occupied by frazil ice (percent)
			f	f _B	f _I	n	n _B	n _I	Wavelength (ft)	Amplitude (ft)	
1	Jan. 13	3.79	0.0412	0.0575	0.0252	0.0198	0.0247	0.0142	(3)	(3)	27
2	24	3.27	.0373	.0576	.0171	.0186	.0247	.0110	(3)	(3)	18
3	Feb. 3	2.76	.0260	² .0530		.0152	² .0245		None	None	13
4	15	3.01	.0308	.0507	.0109	.0175	.0244	.0088	Approx.	Approx.	2
5	21	2.76	.0275	.0517	.0032	.0160	.0244	.0039	0.4	0.02	1
6	Mar. 4	3.09	.0291	.0516	.0066	.0167	.0244	.0062	0.5-0.7	0.06-0.08	0
7	10	3.24	.0372	.0538	.0206	.0192	.0245	.0129	0.6-0.7	0.07-0.09	0

¹ Includes only flow area, not area occupied by frazil ice.² See discussion in text.³ Frazil ice present under solid ice cover.

subdued than any examined the previous winter. The wavelength and amplitude of the features increased progressively from about 0.4 foot and about 0.02 foot, respectively, for block 4, to as much as 0.6-0.7 foot and 0.07-0.09 foot, respectively, for the last block, No. 7. As shown in table 1, the discharge and mean cross-sectional area (an approximate indicator of mean depth when divided by the width) were largest for block 4, dropped to low values for block 5, and then increased for blocks 6 and 7. The mean velocity, however, was highest for the first of the four observations of configured ice (No. 4), dropped for the second, rose for the third, and dropped again for the final observation. In short, then, the progressive increase in the textural roughness of the four configured blocks is not readily explained by progressively increasing or decreasing velocities or depths, on the basis of this limited data.

Profiles of the features, and data on ablation and accretion of the underside of the ice, discussed later, indicate that during the time interval between the first two block observations (Nos. 4 and 5), accretion of ice occurred. Net ablation of the ice surface took place during the time intervals between the second, third, and fourth of these observations.

Changes in the ice ripples

An attempt was made during the 1965-66 winter season to study more closely the change of the ice ripples with time. Profiles (longitudinal to the stream) of the ripples (transverse to the stream) on the underside of the ice were obtained at various intervals of time at fixed locations on the ice cover. This was done by passing a graduated J-shaped steel bar through a slot cut in the ice by a chainsaw on a line parallel to the flow direction. The bar was turned at right angles to the slot, and pulled up so the tip of the J was in contact with the underside of the ice. The distance from the bottom of the ice to a common datum (that is, the value of the graduation on the J-shaped bar where it intersected the common datum) was noted at a number of equally spaced points along the slot. Thus a profile of the underside of the ice along a line parallel to, and 15 inches away from the slot (15 inches is the width of the J) could be drawn through these points plotted on graph paper. The common datum (with respect to the ice) and horizontal control were maintained by two vertical wood posts frozen in place in the ice about 7 feet apart, across the top of which a graduated rod was placed. The posts extended about 2 feet above the ice top surface. The location of the

rod was fixed by a pin in one post and a corresponding hole in the horizontal graduated rod. The slot, cut by the chainsaw each time a profile was obtained, was about 6 feet long and located between the vertical posts; thus it was directly below the horizontal graduated rod.

By this procedure outlined above, the underside of the ice was profiled along the same line each time, and ablation or accretion, as well as any possible migration of the ripples, could be detected.

Because the ripples that first developed were so subtle, accurate profiles were difficult to obtain. By the time that the amplitude of the ripples increased, general ablation of the underside of the ice had begun. An example of a portion of the profiles is shown in figure 1. The available data appear to indicate that during the period of ablation, melting on the upstream faces of the ripples may be greater than on the downstream faces. This lends some support to the hypothesis that during a period of little net ablation or net accretion, the ripples may migrate downstream by means of melting on the upstream faces and freezing on the downstream faces, closely analogous to the migration of sediment ripples and dunes by erosion on the upstream faces and deposition on the downstream faces. Downstream migration could also occur if melting on the upstream faces took place while the downstream faces neither froze nor melted; this would result in general ablation of the underside of the ice.

Net ablation or accretion

In addition to the detailed studies of the ice ripples during the 1965-66 winter season, a record was obtained of the net ablation or accretion at the top and the bottom of the ice at given points, over successive intervals of time. This was done with ablation-accretion (A-A) gages. Each gage was made up of

a 1/4-inch-diameter wooden dowel 3 feet long and equipped with a 5-inch length of 0.045-inch-diameter stainless steel stranded wire, which pierced the dowel perpendicularly 6 inches from one end. The dowel was graduated in both directions from the crosswire. In use, a vertical hole was drilled through the ice with a carpenter's brace and wood bit with bit extension. Then the dowel was inserted into the hole, with the end having the wire pointing downward. The ends of the flexible wire bent back parallel to the dowel until they passed through to the bottom of the hole, then they sprang out and the wire was horizontal. The dowel was lifted up to a position, determined by feel, where the wire was just touching the bottom of the ice, and the dowel was secured in this position with a clothes pin at the top surface of the ice. The thickness of the ice was noted by the location of the clothes pin on the graduated dowel. After an interval of time during which the A-A gage froze into place (usually the period between discharge measurements), a block containing the A-A gage was cut out. Any net ablation or accretion of the top surface was measured relative to the clothes pin, and after the block was turned over, net ablation or accretion of the underside was measured relative to the wire. At this time, another A-A gage was installed in previously undisturbed ice near the first gage, to be cut out at the end of the next interval of time.

Minor accretion occurred at the top of the ice during two of the six intervals in the 1965-66 season. This was the result of the snow cover becoming saturated in the bottom portion, and then freezing. Accretion at the bottom was a total of 0.9 foot from early January to early February. Little change occurred at the bottom through late February, and net ablation from then until early March amounted to 0.4 foot.

CALCULATIONS OF ROUGHNESS, 1965-66 WINTER

Roughness coefficients and friction factors for the underside of the ice during the 1965-66 winter were computed by a method previously reported (Carey, 1966). In 1964-65, values of the Manning roughness coefficient for the underside of the ice, n_I , ranged from 0.0100 to 0.0281, being generally lower in the early part of the period of ice cover. That winter the value of the Manning roughness coefficient for the streambed, n_B , was nearly constant at 0.0251. For 1965-66, the values of n_I in 6 of 7 discharge measurements ranged from 0.0039 to 0.0142; n_B was again nearly constant, but had values averaging 0.0245. The computation of n_I for 1 (Feb. 3, 1966) of the 7 measurements gave unrealistic results (discussed later), and implied that n_I was in a sense negative. In this second winter, n_I was

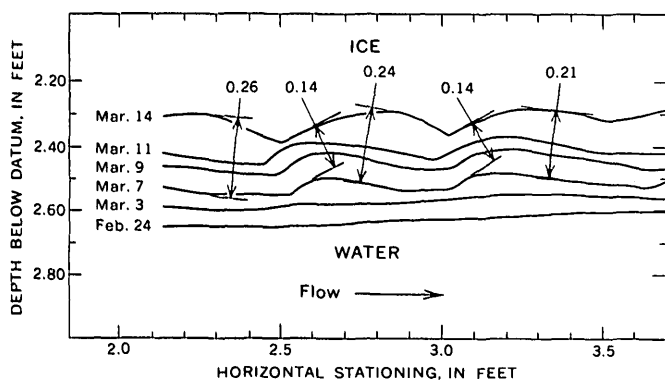


FIGURE 1.—Example of a portion of ice-ripple profiles obtained by the method described in text. Dimensions, in feet, are amount of ablation (Feb.-Mar., 1966) measured approximately perpendicular to the ice surface at points on the upstream and downstream faces of the ripples.

not at all times a meaningful parameter of ice roughness, being more a coefficient for the combined effect of the solid ice undersurface and the variable amounts of frazil, when the latter was present.

A formula showing the relationship between bed roughness, ice roughness, and the total, composite, or combined roughness would be useful in determining the Manning roughness coefficient for the underside of river ice, in that it would eliminate the need for the computational method previously developed (Carey, 1966). Nezhikhovskiy (1964), in a review of this topic, presented three such empirical formulas. One is a general average formula:

$$n = \frac{n_B + n_I}{2} \text{ or } n_I = 2n - n_B,$$

another is known as the Pavlovskiy formula:

$$n_I = \sqrt{(2n^2 - n_B^2)},$$

and the third is the Belokon-Sabaneev formula:

$$n_I = (2n^{3/2} - n_B^{3/2})^{2/3}.$$

The data from both years of this study are described well by the Belokon-Sabaneev formula. For 20 discharge measurements and the corresponding roughness calculations, the values of n_I computed by this formula differ by no more than ± 2.6 percent from the values determined by the method of the writer. The average absolute error is only 0.6 percent. Thus the use of the Belokon-Sabaneev formula appears entirely justified, if a satisfactory mean value of n_B is known.

DISCUSSION

In the previously developed computational method (Carey, 1966) the mean cross section of the reach is assumed to be divided into two parts: one section (the bed section) exerting shear on the streambed, and the other section (the ice-cover section) exerting shear on the underside of the ice. The analysis of the anomalous data from the discharge measurement of February 3, 1966 indicated that A_B , the area of the bed section, was larger than A , the area of the entire cross section. Since the geometry of the situation requires that $A_B + A_I = A$ (A_I being the area of the ice-cover section), a negative value of A_I was indicated. If A_I were zero, it would mean the ice cover was offering no resistance to flow, and so a negative value of A_I would lead to the absurd conclusion that the ice cover was actually spurring the flow rather than retarding it. This would imply that n_I was in a sense negative.

The explanation for the above anomaly can be found in the method by which the values of n_I are computed. A full development of this method, which is outlined below, is given in the author's previous paper (1966).

It is assumed that the Kármán-Prandtl resistance equation for turbulent flow in rough pipes, a relationship between the Darcy-Weisbach friction factor and the relative roughness of a conduit, can be applied to the flow in the bed section of the ice-covered stream. This equation takes the form

$$\frac{V_B}{\sqrt{8gR_B S_e}} = 2 \log_{10} \left(\frac{2R_B}{k_B} \right) + 1.74,$$

in which V_B is the mean velocity in the bed section (assumed equal to the mean velocity in the entire cross section), g is the acceleration of gravity, R_B is the hydraulic radius of the bed section, S_e is the energy gradient of the flow in the reach, and k_B is the effective size of the roughness projections of the bed. The value of k_B is determined from discharge measurements made during open-water periods and is assumed constant throughout the winter. Thus for each discharge measurement made during ice-cover periods, all the terms of the above equation are known except R_B , which can be solved for by trial and error. With R_B known for a particular discharge measurement, A_B is found by the common relation $A_B = R_B P_B$, where P_B is the wetted perimeter of the bed section, a quantity determined by the field data for the discharge measurement. Then, as indicated earlier, A_I is found by the requirement that $A_B + A_I = A$. With A_I known, R_I (the hydraulic radius of the ice-cover section) follows from the common relation $R_I = A_I / P_I$, where P_I is the wetted perimeter in the ice-cover section. With R_I evaluated, n_I follows from the Manning equation.

The values of n_I depend entirely upon an accurate estimate of k_B . In this and the previous report (Carey, 1966), a value of $k_B = 0.23$ foot was used; as mentioned in the previous report the ice-roughness parameters must be termed provisional, inasmuch as k_B was estimated from limited data.

In the data of February 3, 1966, A_B exceeded A because R_B was too large. A smaller value of k_B would produce a smaller value of R_B , so it is evident that the estimate $k_B = 0.23$ foot is too large. A value at least as small as 0.20 foot would be needed to produce a positive value of A_I for the discharge-measurement data in question.

On the assumption that k_B is constant for the streambed of the St. Croix River in the study reach, and that its correct value is as small or smaller than 0.20 foot, the values of n_I and the Darcy-Weisbach friction factor for the ice, as published in this and the previous reports, are slightly lower than the correct values. Correspondingly, the values of the bed roughness parameters are too high. The published ice-roughness parameters are nonetheless useful for comparing one

observation with another, even though they are slightly inaccurate in an absolute sense.

REFERENCES

Carey, K. L., 1966, Observed configuration and computed roughness of the underside of river ice, St. Croix River,

Wisconsin, in Geological Survey Research 1966: U.S. Geol. Survey Prof. Paper 550-B, p. B192-B198.

Nezhikhovskiy, R. A., 1964, Coefficients of roughness of bottom surface of slush-ice cover: State Hydrol. Inst. Trans. (Trudy GGI), v. 110, p. 54-82, Leningrad [in Russian]; translated in Soviet Hydrology, Selected Papers, Am. Geophys. Union, no. 2, 1964, p. 127-150.



ANALYTICAL APPROACHES TO COMPUTATION OF DISCHARGE OF AN ICE-COVERED STREAM

By KEVIN L. CAREY, Madison, Wis.

Abstract.—Two analytical methods for computing winter discharge of an ice-covered stream have recently been developed from observations on the St. Croix River, Wis. One method is based on pipe-flow equations, and the other method on an analogy with methods used to compute open-water discharge for streams affected by backwater. Accuracy of computed discharge in the first method is within ± 19 percent of measured discharge, whereas the second method gives results within ± 9 percent. Relationships in both methods are developed with data either recorded or measured in the field. After the relationships have been developed for a particular stream-gaging station, only recorded data (water-surface stage at both ends of a reach) are needed to compute discharge.

Improving existing instrumentation and (or) techniques used to obtain streamflow records during periods of ice cover has been one objective of a study of ice-covered streams. For most streams, a record of stage is usually adequate for determining the record of discharge during open-water periods. But when ice is in the channel, a record of stage is generally insufficient to determine discharge by a purely hydraulic approach. Additional data—such as winter discharge measurements, the flow of other streams, records of air temperature and precipitation, and hydroelectric plant records—have been used for many years as a basis for estimating streamflow at a station during the winter. This report describes two methods for computing winter discharge that are based solely on hydraulic parameters measured or recorded at the gaging station. These methods have been developed from field data obtained on the St. Croix River near Danbury, Wis., during the 1964–65 and 1965–66 winter seasons. Their applicability to other streams or to other years at the Danbury station is as yet untested.

BACKGROUND

For a given discharge, an ice-covered river must maintain stages that are higher than those for an un-

covered river, for two reasons: First, the presence of a buoyant ice cover of thickness t raises the free surface (stage) of the water, such as in a gage well or a hole in the ice, by an amount approximately $0.9t$; the numerical coefficient depends upon the ice density, which varies slightly according to the number of air bubbles in the ice. Second, the contact between the ice cover and the water adds to the frictional resistance that the flow must overcome in traveling down the channel. This additional resistance varies according to the roughness of the underside of the ice, but its general effect is to reduce the velocity of the water from what it would be for a like discharge during open water. To compensate for the lower velocity, the cross-sectional area of flow must increase, causing an increase in stage in addition to the $0.9t$ increase mentioned above. The total increase in stage associated with an ice cover, over the stage for the same open-water discharge, is usually termed backwater. Since the ice is a variable feature in the channel, it causes backwater to be variable. The random and unpredictable variation in backwater is the reason that stage alone is not a unique indicator of discharge, in contrast with common open-water conditions. Therefore, any analytical solution for discharge under an ice cover cannot be based on stage alone as a parameter, but must in addition include some other variable such as the slope, which, together with the stage, can be related to the discharge.

When a stream is covered with an ice sheet and the stream's width is great enough that the ice cannot bridge the water but remains in floatation on the water, the stream becomes, in a sense, a low-pressure closed conduit. Thus, the flow of an ice-covered stream can be described roughly by pipe-flow or modified pipe-flow equations. In these equations, discharge is generally a function of the size of the pipe, of the slope

of the energy gradient, and of some factor related to the roughness or irregularity of the inside surface of the pipe. In applying pipe-flow equations to an ice-covered stream, the slope of the energy gradient (the slope of the stream, in a uniform channel) can easily be obtained by operating two water-stage recorders, one at each end of an appropriate reach of the channel. When set to the same datum, the difference in stage between these two gages, divided by the reach length, provides the slope of the free water surface through the reach. The other parameters in flow equations (the terms describing the size of the conduit and the roughness of the boundaries) vary much in rivers, if not in pipes. The cross-sectional area (size of the pipe) varies with the flow because the ice cover rises or falls to accommodate more or less water. The roughness also changes, at least in part, because the underside of the ice can have an irregular surface that varies with time [Carey, 1966; 1967 (p. C195-C199, this chapter)]. These cross-section and roughness parameters are not recordable, but must be obtained from field data.

To check the foregoing concepts in the field, part of the St. Croix River was used to study the functional relationships between stage and slope and the non-recordable parameters of the flow equations. These functional relationships can be used to obtain estimates of the values of the nonrecordable parameters on days when no discharge measurements are made. These estimates, combined with the recorded data, when used in flow equations, will then yield values of estimated flow for daily or other chosen intervals.

APPROACH

After a thorough search of northern Wisconsin streams, a reach of the St. Croix River downstream from the gaging station near Danbury, Wis., was selected for field study because it seemed to fit most closely criteria that would adequately test methods for computing discharge under ice cover. These criteria are:

1. The stream should be wide enough that the ice cover is sufficiently flexible to remain in floatation; that is, the ice should contact the water rather than bridge the flow and leave an air space in between. A stream 100 feet or more in width will meet this requirement very well. Narrower streams can also have ice covers in floatation, if the ice is not too thick.
2. The channel should be fairly uniform in cross section throughout the reach, and it should be free of islands or bars that would control the stage.
3. The bed should be stable and not subject to significant erosion or deposition.

4. Slope should be fairly uniform throughout the reach and great enough so that the fall of the water through the reach can be measured within ± 20 -percent accuracy.
5. The average period of ice cover should be long enough so that data can be gathered over a period of several months; the ice cover should not be liable to breakup due to midwinter thaws.
6. The stream should have a history of being relatively free from frazil (slush) ice under the ice cover.
7. Little or no artificial regulation of the flow should be present.
8. The stream should have a natural heat regime.

The St. Croix River near Danbury, Wis., drains an area of 1,588 square miles. The average discharge for the 51 years of record through 1965 is 1,278 cubic feet per second; the flow is subject to slight diurnal regulation caused by power generation upstream. In the study reach, the St. Croix River is 200-240 feet wide and 2.3-3.2 feet in mean cross-sectional depth at average flow. The channel expands slightly downstream and is quite straight. The bed is composed of gravel, scattered small boulders, and minor amounts of sand.

In the 10 winters from 1953-54 to 1962-63, there was a single continuous ice cover each winter season, except for 2 years, during each of which a midwinter thaw broke up the initial ice cover; after these thaws, second ice covers formed. Duration of ice cover ranged from 72 to 112 days with a mean of 95 days. Usually the ice cover forms in early to mid December and lasts until early to mid March.

An auxiliary gage was installed about half a mile downstream from the base gage in November 1964, and it was read at the time of discharge measurements. Using conventional current-meter techniques, many discharge measurements through the ice were obtained as soon as the ice would safely support a man and through the winter until the ice was no longer safe. Each time the discharge at the upstream end of the reach was measured, two cross sections of the river, one at the middle and one at the downstream end of the reach, were obtained. Gage heights applicable to the discharge measurements were obtained at both ends of the reach. These data permitted calculation of geometric mean values of the hydraulic parameters effective within the reach.

FIELD OBSERVATIONS

In the 1964-65 winter season, 14 discharge measurements were made. The depth of the water, the thickness of the ice, and the middepth velocity of the flow

were measured at an average of 31 vertical sections in a cross section about 200 feet wide at the upstream end of the reach. Vertical-velocity profiles, however, were also obtained at four vertical sections, and from these profiles, coefficients were computed that reduce the middepth velocity to mean velocity at each of the four vertical sections. Then, on the basis of these computed coefficients, estimated coefficients were obtained for the other vertical sections. Thus, by using computed coefficients from a few vertical sections and estimated coefficients for the others, the mean velocity of the flow was determined for each vertical section although at most of the sections only the middepth velocity was measured.

During the 1965-66 winter season, seven discharge measurements were made, but deeper water under the ice at the discharge measuring cross section permitted two velocity determinations at each vertical section. These velocities, measured at 0.2 and 0.8 of the effective depth of flow, were averaged to give the mean velocity at each vertical section. Thus, during this winter no velocity profiles were needed. Each discharge measurement was composed of an average of 32 vertical sections.

A vertical vane-type current meter was used for all velocity observations. It was connected to a rod which was supported by a tripod placed over the hole in the ice. The tripod insured that the meter remained in the desired position during the velocity readings.

After each measurement of discharge, data were also obtained at the middle and the lower cross sections. The middle cross section is about 220 feet wide, and the lower about 240 feet wide. The thickness of the ice, the total depth of water, and the effective depth of water were measured at 10-foot intervals. These data were needed because changes in stage and in ice thickness during the time between measurements would result in changes in the cross-sectional areas.

DISCHARGE COMPUTATION METHODS

Pipe-flow-equation method

Although any sort of flow equation could be used, the Manning and Darcy-Weisbach equations are most attractive because they are well known and widely used. The Manning equation, which is generally used for open-channel flow, is adaptable to describing closed-conduit flow, but the Darcy-Weisbach equation is most frequently used for closed-conduit flow.

As used for the discharge (Q) of an ice-covered stream the Darcy-Weisbach equation is

$$Q = \sqrt{\frac{8g}{f}} AR^{\frac{3}{2}} S_e^{\frac{1}{2}}$$

where g is acceleration of gravity, f is the Darcy-Weisbach friction factor, A and R are the area and hydraulic radius, respectively, of the geometric mean cross section of flow under the ice in the reach, and S_e is the slope of the energy gradient through the reach.

The energy gradient is customarily used in uniform-flow equations, but determining the energy gradient for a natural river would require knowledge of the velocity heads at each end of the reach. Although these heads are known for the 21 discharge measurements made during this study, they are not known for the time intervals between discharge measurements. Thus a modification of the flow equation can be made whereby the readily determined water-surface slope (S) is used in lieu of the energy gradient (S_e). The value of S differs from S_e in the studied reach of the St. Croix River because the flow is not strictly uniform. In short, the use of a uniform flow equation, and its modification by the use of S rather than S_e , are simplified approximations. Any error thus introduced is believed to be small; a table presented later in this report (table 2) provides some quantitative measures of the accuracy of the pipe-flow-equation method as well as the stage-fall-relation method, described later.

The modification of the Darcy-Weisbach equation permitting the use of S was done by making the computations for f in the 21 measurements using S , rather than S_e . This f is then termed the modified Darcy-Weisbach friction factor, or f_{MOD} . Thus, the modification of the slope value is compensated for by the modification of the friction factor, and the equation

$$Q = \sqrt{\frac{8g}{f_{MOD}}} AR^{\frac{3}{2}} S^{\frac{1}{2}} \quad (1)$$

will produce the correct value of discharge for a particular discharge measurement when the values of A , R , S , and f_{MOD} from that measurement are used. The values of the important parameters for each discharge measurement are given in table 1.

The values of the hydraulic parameters from the 21 discharge measurements made during the two winters were plotted in various combinations on logarithmic paper, in a search for functional relationships. It was evident that cross-sectional area (A) and hydraulic radius (R) varied in a general way with river stage (G) and that the Darcy-Weisbach friction factor (either as f or f_{MOD}) varied generally with water surface slope (S) or energy gradient (S_e). For the cross-section properties, the Darcy-Weisbach section factor ($AR^{\frac{3}{2}}$) provided a convenient term with which to express the relationship with stage in a single equation.

When plotted on logarithmic paper, a relation between f_{MOD} and S and a relation between $AR^{\frac{3}{2}}$ and

TABLE 1.—Winter measurements of stream discharge, observed and computed hydraulic parameters, and discharge computed by two methods described in text, St. Croix River near Danbury, Wis.

Date	1 Q (cfs)	2 A (ft ²)	3 R (ft)	4 G _A (ft)	5 AR ^{1/2} (ft ^{1/2})	6 SX10 ⁴ (ft/ft)	7 f _{MOD}	8 Q _{LB} (cfs)	9 Q/Q _{LB}	10 G _B (ft)	11 F (ft)	12 F _{LB} (ft)	13 F/F _{LB}	Computed discharge	
														14 Darcy-Weisbach relation Q (cfs)	15 Stage-fall method Q (cfs)
1964															
Dec. 15----	700	446	1.01	0.48	449	3.57	0.0378	700	1.000	1.45	0.97	0.94	1.032	701	657
21----	716	465	1.06	.58	478	3.53	.0406	716	1.000	1.54	.96	.99	.970	728	756
30----	837	518	1.18	.76	563	4.26	.0495	837	1.000	1.92	1.16	1.16	1.000	711	837
1965															
Jan. 5----	722	463	1.05	.68	475	4.15	.0463	795	.908	1.81	1.13	1.11	1.018	703	768
18----	754	471	1.07	.64	487	3.97	.0427	765	.986	1.72	1.08	1.07	1.009	710	752
26----	703	464	1.06	.63	477	4.12	.0488	774	.908	1.75	1.12	1.08	1.037	694	719
Feb. 3----	699	445	1.01	.55	448	4.34	.0459	768	.910	1.73	1.18	1.08	1.093	657	637
11----	666	453	1.03	.62	460	4.74	.0583	833	.800	1.91	1.29	1.16	1.112	624	666
18----	664	472	1.07	.93	489	4.67	.0653	973	.682	2.20	1.27	.86	1.477	702	675
24----	746	525	1.20	1.08	574	4.38	.0668	1,013	.736	2.27	1.19	.76	1.566	778	702
Mar. 6----	855	588	1.34	1.38	680	4.52	.0736	1,230	.695	2.61	1.23	.73	1.685	841	852
12----	788	543	1.24	1.23	604	4.26	.0644	1,085	.726	2.39	1.16	.70	1.657	834	752
20----	752	527	1.20	1.34	577	4.38	.0665	1,175	.640	2.53	1.19	.72	1.653	849	814
30----	928	580	1.32	1.56	666	4.56	.0605	1,365	.680	2.80	1.24	.76	1.632	888	946
1966															
Jan. 13----	1,123	627	1.35	2.12	730	3.75	.0408	1,615	.695	3.14	1.02	.82	1.244	1,206	1,163
24----	920	555	1.22	1.71	612	3.24	.0369	1,216	.757	2.59	.88	.73	1.205	1,088	891
Feb. 3----	908	514	1.14	1.62	549	2.68	.0252	1,060	.857	2.35	.73	.71	1.028	1,061	972
15----	1,402	707	1.56	2.08	884	2.83	.0290	1,402	1.000	2.85	.77	.77	1.000	1,244	1,402
21----	1,090	593	1.31	1.70	678	2.57	.0256	1,090	1.000	2.40	.70	.70	1.000	1,085	1,090
Mar. 4----	1,230	631	1.39	1.94	744	2.94	.0277	1,323	.930	2.74	.80	.75	1.067	1,186	1,156
10----	1,300	700	1.54	2.11	869	3.09	.0355	1,476	.881	2.95	.84	.79	1.063	1,253	1,300

1. Discharge, Q.
2. Cross-sectional area, A.
3. Hydraulic radius, R.
4. Auxiliary gage stage, G_A.
5. Darcy-Weisbach section factor, AR^{1/2}.
6. Water surface slope, SX10⁴.
7. Modified Darcy-Weisbach friction factor, f_{MOD}.
8. Discharge for least backwater due to ice at given base gage stage, Q_{LB}.

9. Discharge ratio, Q/Q_{LB}.
10. Base gage stage, G_B.
11. Fall of water surface through reach, F.
12. Fall associated with least backwater due to ice at given base gage stage, F_{LB}.
13. Fall ratio, F/F_{LB}.
14. Computed discharge by Darcy-Weisbach relation, using auxiliary gage stage, Q.
15. Computed discharge by stage-fall method, Q.

G_A, the auxiliary-gage (downstream) stage, for the 21 discharge measurements are both curved lines. It is desirable to obtain these expressions,

$$f_{MOD} = \text{function}(S), \tag{2}$$

and

$$AR^{1/2} = \text{function}(G_A), \tag{3}$$

as linear functions. For equation 2, making the S scale linear rather than logarithmic and introducing constant negative shift to the f_{MOD} scale produces a straight line (fig. 1). For equation 3, only a transfer from logarithmic to linear scales for G_A is needed to achieve a straight line (fig. 2).

The scatter of points in figure 1 is due to the dependence of f_{MOD} on relative roughness and, to a lesser extent, on variations in velocity, in addition to the dependence on slope. The scatter of points in figure 2 is due to variations in ice thickness and also to variations in slope. At a given stage, a large ice thickness

would correspond to a small section factor, whereas a smaller ice thickness would correspond to a larger section factor. Furthermore, for a given auxiliary-gage (downstream) stage, a large slope would cause a large section factor, whereas a smaller slope would lead to a smaller section factor.

The lines of best fit in figures 1 and 2, determined by the method of least squares, are expressed by

$$f_{MOD} = [(1.430 \times 10^{-3})10^{3.330S}] + 0.0160 \tag{4}$$

and

$$AR^{1/2} = (384)10^{0.148G_A}. \tag{5}$$

Equations 4 and 5 are substituted in equation 1 for f_{MOD} and AR^{1/2}, and give the following result after simplification:

$$Q = \frac{(162,800)10^{0.148G_A}}{(10^{3.330S} + 11.19)^{1/2}} S^{1/2}. \tag{6}$$

The independent variables of equation 6, G_A and S, are easily obtained from data recorded by the two

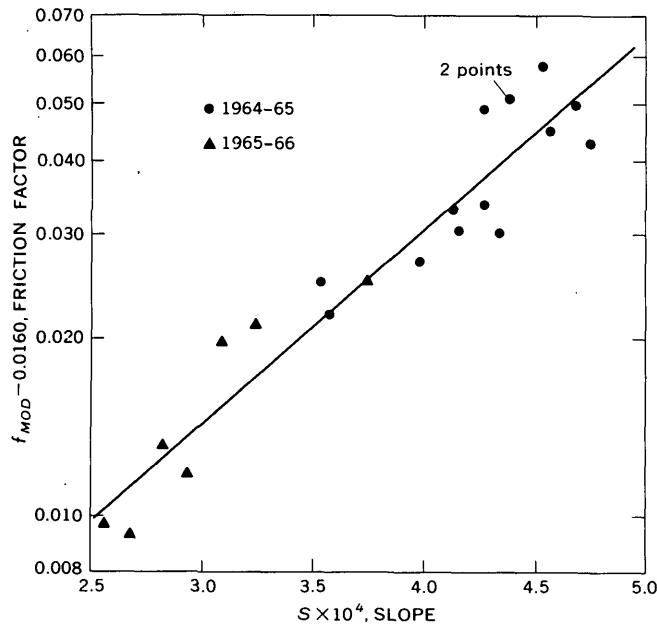


FIGURE 1.—Relation between water surface slope and modified Darcy-Weisbach friction factor. Equation 4 is represented by the straight line.

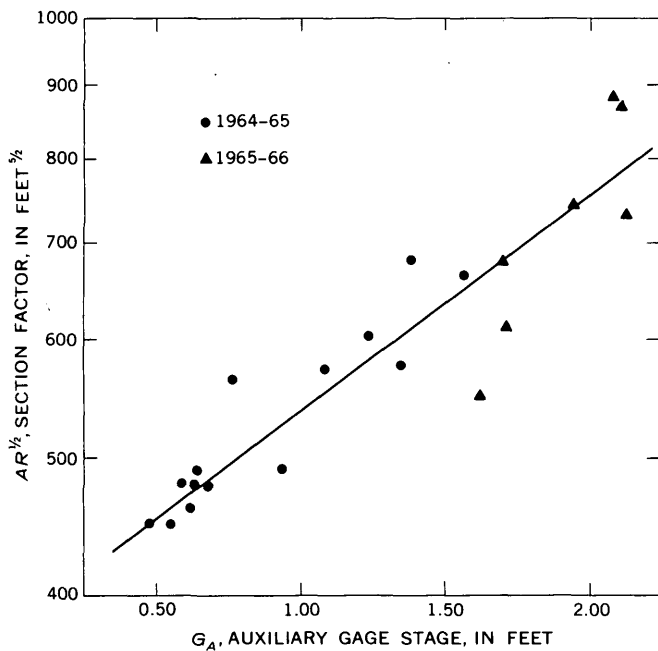


FIGURE 2.—Relation between auxiliary gage stage and Darcy-Weisbach section factor. Equation 5 is represented by the straight line.

gages. Thus equation 6 could be used to compute Q for periods between actual discharge measurements.

Some idea of the accuracy of equation 6 can be gotten by examining figure 3, a plot of measured discharge versus computed discharge. If equation 6 were perfect, all points would lie on the solid line of figure 3. But, of course, the points are scattered about this

line for the reasons already given to explain the scatter in figures 1 and 2. All computed discharges are within ± 19 percent of the corresponding measured discharges, and 16 of 21 (about 75 percent) computed discharges are within ± 10 percent of the corresponding measured discharges.

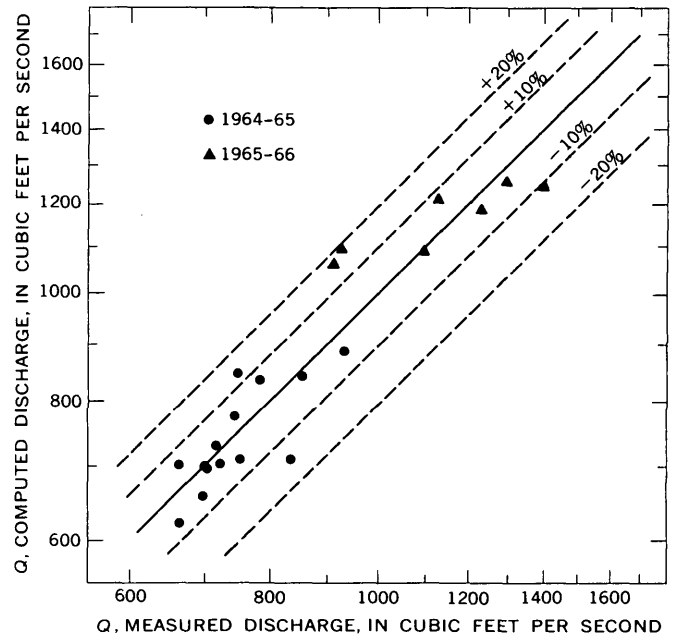


FIGURE 3.—Comparison of measured discharge with discharge computed by the pipe-flow-equation method using the modified Darcy-Weisbach equation and auxiliary-gage stage. Dashed lines indicate error of computed discharge relative to measured discharge.

Stage-fall-relation method

An entirely different approach to the computation of stream discharge under an ice cover is based on an analogy between ice-covered streams and streams having variable slopes caused by backwater during periods of open water. The method of computing discharge for the latter streams, by means of slope-stage-discharge relations, is described by Corbett and others (1943, p. 132-151). Basically, this method involves two graphical relationships: (1) a relation between stage and discharge for some fixed condition of fall of the water surface through the reach (a fixed condition of fall may be either a constant fall or a variable fall associated with minimum backwater), and (2) a relation between discharge ratios (actual discharge at a particular stage divided by the discharge at the same stage for the fixed condition of fall) and corresponding fall ratios (observed fall divided by the fall for the fixed condition of fall). At some sites an additional graphical relationship is needed between stage and the fall for the fixed condition of fall, when

this fall is not a constant with stage. The method depends on the principle that

$$\frac{Q_1}{Q_2} = \text{function} \left(\frac{F_1}{F_2} \right),$$

where Q_1 and Q_2 are different discharges, and F_1 and F_2 are their corresponding falls of the water surface, all at a given stage.

The application of this method to an ice-covered stream is illustrated with data presented in table 1. Figure 4 is a stage-discharge plot (using base-gage stage, G_B) of all winter discharge measurements from both years of the study. A curve has been drawn through the points having the lowest stage within each increment of discharge. These points each have the least backwater of the points within both their respective increments of discharge and their respective small intervals of stage. In other words, they lie closer than the other points to the open-water stage-discharge relation (which is not shown). The curve can be considered as a limit or boundary to the region on the plot in which would appear the points representing all possible measurements of discharge under conditions of complete ice cover. The existence of such a boundary is reasonable, because in a uniform (or approximately uniform) channel, backwater due to an ice cover must always be greater than about $0.9t$, and t must have some minimum value below which the ice

cover would be unstable and would break up. Thus the curve of figure 4 is a relation between stage and discharge for the fixed condition of fall defined as the fall associated with least backwater due to ice cover at the given stage. Of course, the curve could be revised in the light of future data. The value of fall associated with least backwater due to ice cover (F_{LB}) is not a constant, but varies with G_B , in the manner shown in figure 5.

For each discharge measurement, the following ratios can be determined:

$$\text{discharge ratio} = \frac{Q}{Q_{LB}}$$

and

$$\text{fall ratio} = \frac{F}{F_{LB}}$$

where Q and F are the discharge and fall actually measured in the field, Q_{LB} is the discharge associated with least backwater due to ice cover for the same stage as the measurement (determined from the curve of fig. 4), and F_{LB} is the fall associated with least backwater due to ice cover for the same stage as the measurement (determined from fig. 5). A plot of the discharge ratio and the corresponding fall ratio for each measurement is shown in figure 6. A smooth curve fitted by eye expresses the relation between discharge ratios and fall ratios.

To compute discharge during periods between actual discharge measurements, daily mean values of stage

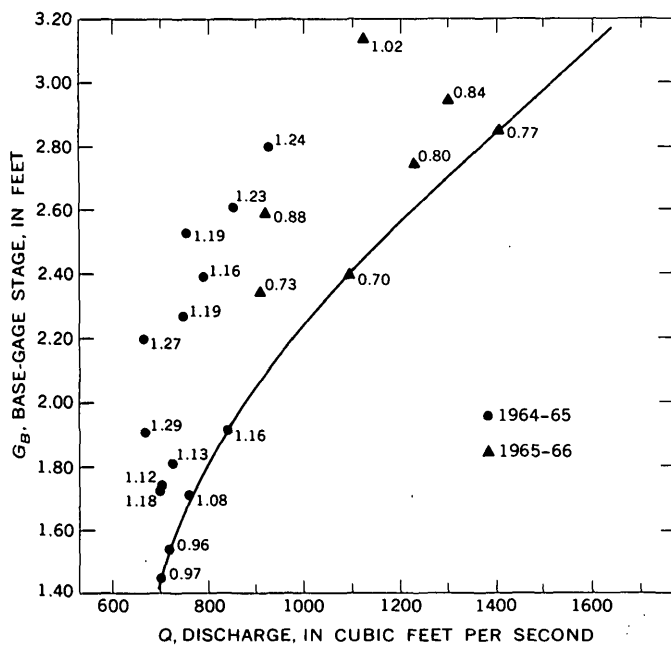


FIGURE 4.—Discharge versus base-gage-stage plot of discharge measurements. Numbers next to points are the fall (in feet) of the free water surface ($G_B - G_A$) within the reach at the time of each measurement. Curve represents the stage-discharge relation for the condition of least backwater due to ice cover.

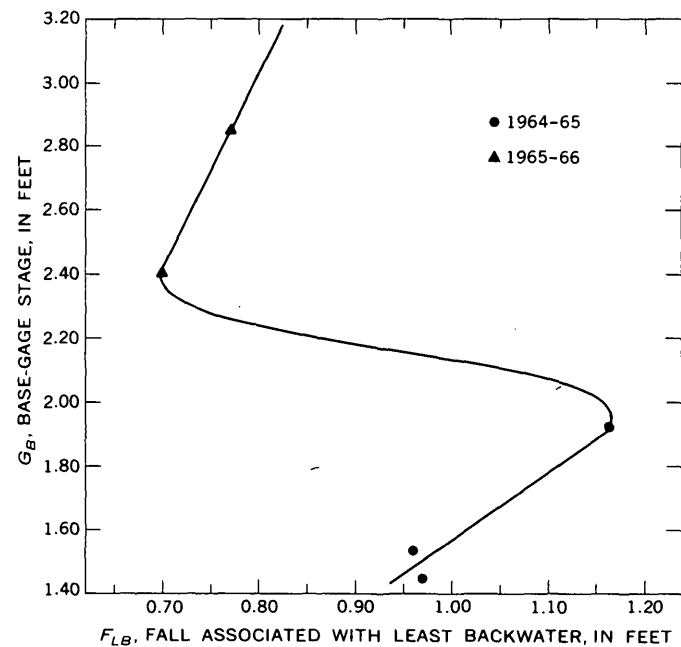


FIGURE 5.—Relation between the fall associated with the condition of least backwater (due to ice cover) and base-gage stage.

recorded at the two gages yield values of F' (by subtraction), values of F_{LB} (by reference to fig. 5), and values of Q_{LB} (by reference to fig. 4). The fall ratio (F/F_{LB}) can be computed, and then the fall ratio is used to determine the discharge ratio (Q/Q_{LB}) with the aid of figure 6. Discharge is then computed by the simple relation

$$Q = \left(\frac{Q}{Q_{LB}} \right) Q_{LB}$$

The accuracy of this method is indicated by figure 7, a plot of measured discharge versus computed discharge. Perfect results of this method would result in all points being on the solid line of figure 7. However, the points are scattered about this line; all computed discharges are within ± 9 percent of the corresponding measured discharges, and 13 of 21 (about 60 percent) of the computed discharges are within ± 5 percent of the corresponding measured discharges.

DISCUSSION

Numerical measures of accuracy for the two methods for computing discharge under ice cover discussed in this paper are shown in table 2, together with similar measures for three methods not discussed. It must be stressed that these methods were developed from data taken from only one stream. Applicability to other ice-covered streams must be determined by future work. Study sites on other streams should be selected to represent a wide range of hydraulic and winter-weather conditions. Probably at least 20 winter-

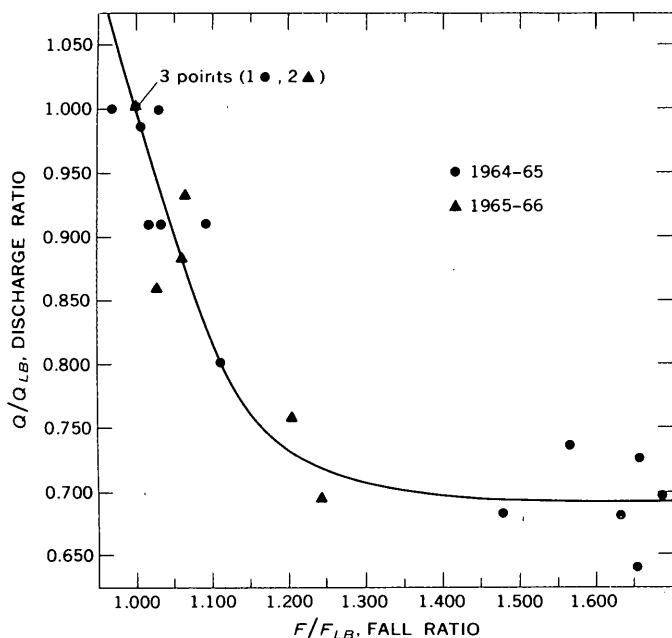


FIGURE 6.—Relation between fall ratio and discharge ratio.

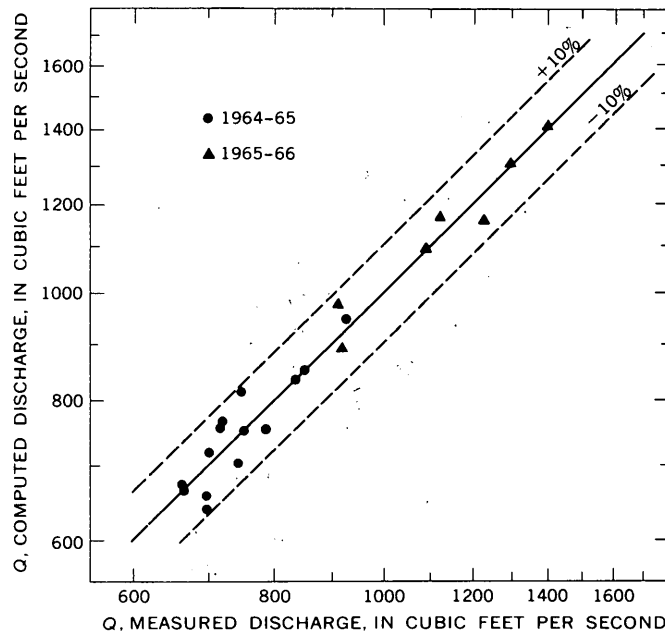


FIGURE 7.—Comparison of measured discharge with discharge computed by the stage-fall-relation method. Dashed lines indicate error of computed discharge relative to measured discharge.

TABLE 2.—Measures of accuracy of various methods of computing discharge of ice-covered streams

Method	Coefficient of correlation	Standard error of estimate (cfs)	Average absolute error (percent)
Stage-fall	0.985	37.3	3.45
Modified Darcy-Weisbach relation method using auxiliary-gage stage			
Average of method using auxiliary-gage stage and method using base-gage stage in modified Darcy-Weisbach relation	.939	77.3	6.43
Modified Darcy-Weisbach relation method using base-gage stage	.927	80.7	6.64
Modified Manning relation method using base-gage stage	.896	94.8	7.54
Modified Manning relation method using base-gage stage	.893	103.0	8.66

discharge measurements over at least two winters would have to be obtained on each stream to develop the "rating" relationships—shown in figures 1 and 2 and (or) figures 4, 5, and 6—needed to compute discharge. Further, these measurements would have to cover the range in discharge, fall, and stage likely to be found at the stream during any period of ice cover. Once a stream had been satisfactorily rated for flows under ice cover, digital stage recorders could supply input data for a very simple computer program for obtaining discharge by either the pipe-flow-equation method or by the stage-fall-relation method. Dis-

charge measurements made during a particular winter could be used to check and refine the ratings.

The stage-fall-relation method is more attractive than the pipe-flow method, first, because it is more accurate, and second, because much less field and office work are called for in its development; this is true because extra cross-section measurements of the stream in the study reach are not needed and the mean hydraulic parameters such as A , R , or f do not have to be calculated.

REFERENCES

- Carey, K. L., 1966, Observed configuration and computed roughness of the underside of river ice, St. Croix River, Wisconsin, *in* Geological Survey Research 1966: U.S. Geol. Survey Prof. Paper 550-B, p. B192-B198.
- 1967, The underside of river ice, St. Croix River, Wisconsin, *in* Geological Survey Research 1967: U.S. Geol. Survey Prof. Paper 575-C, p. C195-C199.
- Corbett, D. M., and others, 1943, Stream-gaging procedure: U.S. Geol. Survey Water-Supply Paper 888, 245 p., 33 pls.



TWO METHODS OF ESTIMATING BASE FLOW AT UNGAGED STREAM SITES IN KANSAS AND ADJACENT STATES

By L. W. FURNESS and M. W. BUSBY, Lawrence, Kans., Albany, N.Y.

Work done in cooperation with the Kansas Water Resources Board

Abstract.—In investigating a satisfactory technique for estimating base flow (a component of total stream flow) at ungaged stream sites, two different methods were studied and the results were compared. By the first method, base flow was estimated from six physical and hydrologic basin characteristics. These 6 characteristics were resolved from regression analyses of about 1,000 combinations of 27 basin characteristics in relation with the base-flow data of 84 long-term streamflow stations in Kansas and adjacent States. The second, and more reliable, method was developed by correlating base-flow current-meter measurements made at the ungaged stream site with data from the records of an established gaging station. Base-flow values estimated by the second method had a smaller standard error than values estimated by the first method in 62 percent of the comparisons made of the results.

Base flow, as used herein, is that part of total streamflow that would exist if all the direct runoff were abstracted and precipitation continued to supply the usual accretions of flow via the ground (Busby and Armentrout, 1965). Typical of the midcontinent areas, the total flow of unregulated streams in Kansas is virtually that of base flow during 40–80 percent of the days. But interspersed between these days are days when storm runoff may occur in large amounts. The frequency of total flow of Kansas streams below certain low amounts has been previously defined (Furness, 1960). Except for the extreme lowest discharge, some storm runoff may be included in these amounts. Ideally, the actual direct runoff should be included in the investigation of low-flow problems so long as the river basins remain unregulated. When the rivers become regulated, however, total flow is depleted by varying amounts depending on local conditions.

For example, in Kansas 20 large Federal reservoirs are completed or under construction; also there are

124 small lakes, 70,000 farm ponds, and organized watershed districts covering a third of the eastern part of the State. The number of these developments will undoubtedly continue to grow. With the exception of the large Federal reservoirs, influent channels will be so small that storage will consist primarily of surface runoff that will be depleted by evaporation and consumptive use. Thus surface runoff will not be a dependable source of water supply farther downstream, and future low-flow problems in these basins should be answered by an analysis of the expected magnitude of base flow instead of by an analysis of low total flow.

Base-flow determinations are needed at a large number of selected sites in Kansas for several reasons. The following three are among the most important: First, many water-right holders under the Kansas Water Appropriation Act are entitled to use the firm supply as represented by base flow. Thus, it is necessary to determine the quantity of base flow in evaluating new water-right applications and in determining the rights of the existing water-right holders to water in new developments and watershed districts.

Second, because base flow is largely derived from ground-water sources, the quantity of such flow is an indication of the potential ground-water yield. Extensive ground-water development for irrigation has or will extract an appreciable part of the base flow. Therefore, base-flow determinations are needed to evaluate how streamflow and downstream development may be affected by pumpage.

Third, because of the change of regimen of flow resulting from surface-water impoundments, it is essential that information about base flow be obtained as

soon as possible for sensible water-supply planning. Such information can be conveniently determined from existing records for sites of long-term streamflow stations, but other methods are needed for ungaged sites.

This article discusses two methods for defining base flow at ungaged sites on Kansas streams where the drainage areas are between 100 and 5,000 square miles. The study is part of a more extensive investigation of the relation of ground- and surface-water resources by the Geological Survey in cooperation with the Kansas Water Resources Board. Although the data apply to the streams in Kansas and adjacent areas, the principles and methods have much more widespread application.

Although total streamflow conforms to a conveniently mapped geographical distribution in Kansas, the base-flow part of total flow varies considerably between adjacent basins (Furness, 1965, fig. 7). Obviously a more intensive method than simple geographic distribution is needed to estimate base flow at ungaged sites. The first method describes the relation of mean base flow and monthly probability of base flow to six basin characteristics. The second method shows how a series of current-meter measurements of base flow at an ungaged site can be related to base-flow data from a nearby established gaging station to determine the monthly probability of base flow at the ungaged site.

ESTIMATING BASE-FLOW VALUES FROM BASIN AND FLOW CHARACTERISTICS

Base-flow information available for investigating the causative characteristics consisted of base flows for each month 1923-62 (in most instances) at each of 84 gaging stations (Busby and Armentrout, 1965). By regression analyses on a digital computer, 27 possible causative characteristics were investigated in more than 1,000 combinations to develop the equations. Of the 27 possible characteristics, 6 characteristics were found significant at the 95-percent confidence level, or higher, to define 39 equations of base flow as follows: mean annual, mean winter, and mean summer base flow, and base flow for each calendar month expected to be exceeded 20, 50, and 80 percent of the time. The 39 equations have the following general form:

$$\log Q = a + b_1 \log L + b_2 \log W + b_3 \log qm + b_4 \log Rsw + b_5 v + b_6 R1m,$$

where Q is base flow in cubic feet per second at any site of 100-5,000 sq mi in area in Kansas; a and b are coefficients whose values are evaluated for 39 different categories of Q ; L is main channel length; W is basin width, equivalent to drainage area divided by main

channel length; qm is mapped mean total streamflow; Rsw is mapped ratio of summer to winter base flow; v is a mapped variability index; and $R1m$ is mapped ratio of 1-percent flow to mean flow. The mapped values are defined by isopleths on maps prepared by Furness and others (1966). The computed values of monthly base flow at 20, 50, and 80 percent points of frequency distribution may be plotted on a log-normal graph and connected by a curve that may be extended to define monthly base flow of other probabilities between 5 and 95 percent.

A study was made of the likely errors resulting from using these equations of base-flow relations, considering that the errors are not direct errors because base flow, by definition, is a part of the total streamflow and cannot be directly or precisely measured. Statistical computations showed that the standard error of estimate for mean annual base flow was +40, -28 percent; for winter base flow (January-March) +34, -25 percent; and for summer base flow (July-September) +43, -30 percent. The standard error for the winter period was the smallest of these, probably because losses are at a minimum during this period.

The magnitudes of standard errors for computing monthly values corresponding to particular probabilities of exceedance are much larger and are illustrated schematically in figure 1. If the true value of monthly base flow were centered within the shaded area, the value computed by formula would be within the shaded area two-thirds of the time. Figure 2 includes a comparison of the typical differences between monthly base flow, of 5-, 50-, and 90-percent chance exceedance as determined for the period 1923-62 from actual records at a gaging station and the comparable values computed by formulas.

ESTIMATING BASE-FLOW VALUES FROM CURRENT-METER MEASUREMENTS

The current-meter method—using on-the-spot current-meter measurements is a more direct method than the basin-and-flow-characteristics method. In order to evaluate the accuracy of the method, records of daily flow at 16 long-term streamflow stations were examined to select flows of different magnitudes but only at times when total flow was known to be all base flow. These daily base-flow values were used as if they were current-meter measurements at an ungaged site and were plotted against the known base flow at a nearby established gaging station. Figure 3 shows how base flow on the Verdigris River near Coyville, Kans., may be related to that at the established station on Fall River near Eureka. Extremely low and extremely

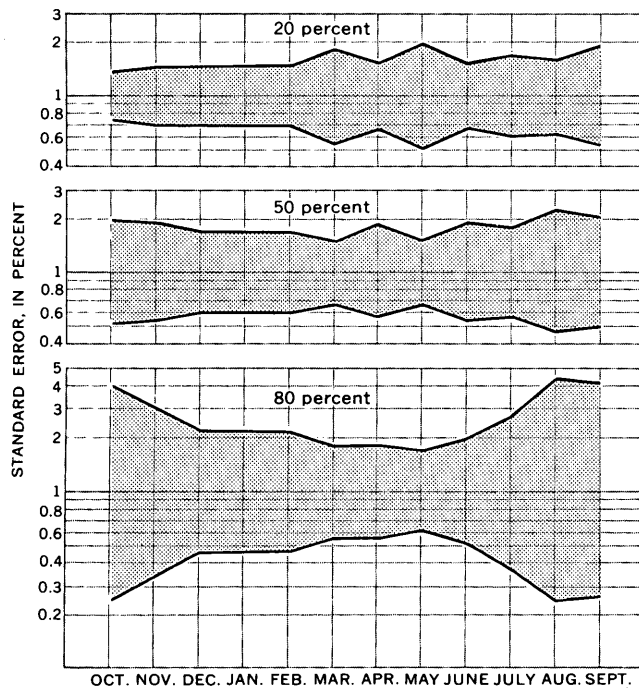


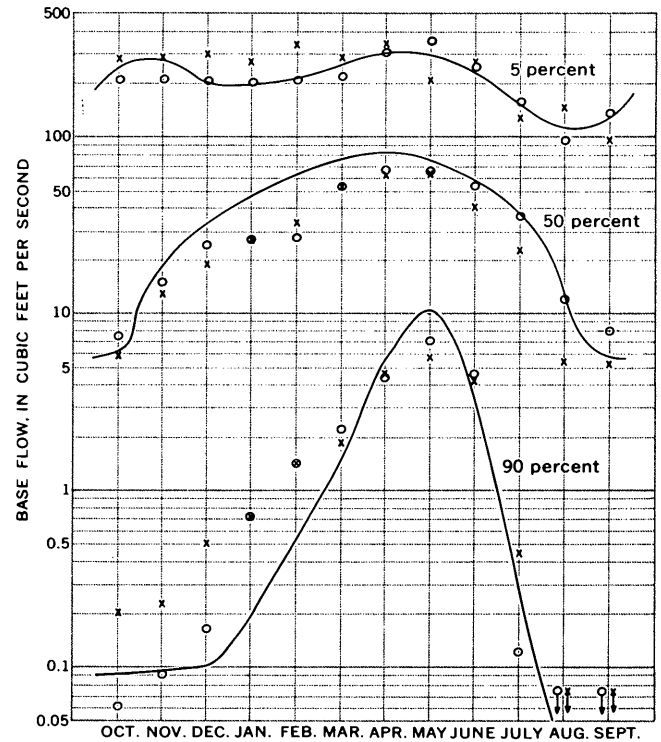
FIGURE 1.—Limits of standard error in computing by formula the monthly base flow for 20-, 50-, and 80-percent chance exceedance.

high values within the required range occurred rarely. In most instances, it was necessary to search back as far as 5 years in the records to find 20–25 values of adequate range and definition. At an actual ungaged site, engineers would need to be extremely alert to the rare times when high and low base flows occur in order to complete the correlation within a 5-year period.

By using figure 3 in combination with the known graph of monthly base-flow exceedance values at the nearby established gaging station, similar monthly base flows corresponding to 5-, 50-, and 90-percent exceedance values were computed for the so-called ungaged site and plotted as circles on figure 2.

Figure 2 shows the comparison of actual probability curves defined from complete streamflow records at a site with the point values that would be computed by formula and also by use of current-meter measurements. Considering that the actual probability curves based on complete streamflow records are correct, four computations of base flow by the formula and by the current-meter methods are defined equally close to the actual curves. Of the rest of the computed points, those obtained by the current-meter method (21 of 32, or 66 percent) are closer to the actual curves.

The comparison just described was repeated for 16 gaging stations distributed throughout Kansas. Comparisons were made of individual and group departures of each monthly point from the established curves



EXPLANATION

o Discharge computed by correlation with Station 107
x Discharge computed by formula

FIGURE 2.—Base flow computed from formulas and from partial-record data compared with actual base-flow curves defined from gaging-station records, Verdigris River near Coyville, Kans. (station 105).

of 5-, 10-, 20-, 50-, 80-, 90-, and 95-percent exceedance. Results showed that the individual departures from the 5-, 10-, 20-, 50-, and 80-percent curves were statistically more reliable 95 percent of the time by the current-meter method than by the formula method and that where the points were combined in groups, the departures by current-meter method were closer to the actual curves 62 percent of the time. The comparison, however, should be somewhat qualified because the actual curves are for a previous 40-year period and may not necessarily represent future probability.

CONCLUSIONS

Annual, seasonal, and monthly values of base flow corresponding to various probabilities of exceedance were related to six basin and streamflow characteristics. The standard errors of the regressions defining annual and seasonal base flows are +43 and -30 percent, or less. Standard errors of monthly base flows are larger. A useful degree of areal generalization of

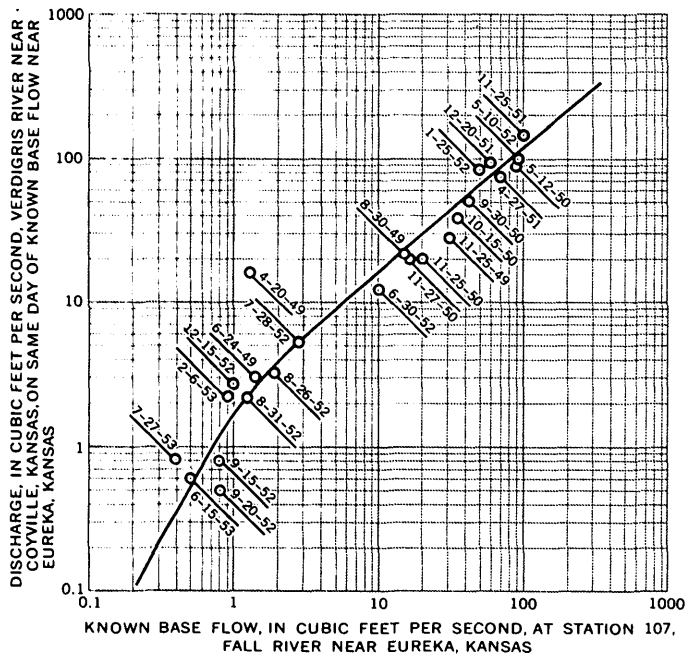


FIGURE 3.—Method of developing relation of base flow at an ungauged site, using base flow at an established gaging station. (See text for an explanation of plotted values.)

base flows is attained by the regressions even though it was not possible to find a factor describing the basin geology.

By use of current-meter measurements, the magnitude of base flow expected to be equalled or exceeded in any month can be defined more closely than by use of formulas. However, much work, money, and about 5 years probably would be required to collect current-meter measurements throughout the range of values needed for meaningful estimates.

REFERENCES

Busby, M. W., and Armentrout, G. W., 1965, Kansas streamflow characteristics, pt. 6A, Base-flow data: Kansas Water Resources Board Tech. Rept. 6A, 207 p.

Furness, L. W., 1960, Kansas streamflow characteristics, pt. 2, Low-flow frequency: Kansas Water Resources Board Tech. Rept. 2, 179 p.

— 1965, Discussion of areal variations of mean annual runoff: Am. Soc. Civil Engineers Proc. 4304, May 1965, p. 336-341.

Furness, L. W., Burns, C. V., and Busby, M. W., 1966, Kansas streamflow characteristics, pt. 6B, Base-flow distribution: Kansas Water Resources Board Tech. Rept. 6B, 139 p.



CHARACTERISTICS OF SUMMER BASE FLOW OF THE POTOMAC RIVER

By RONALD L. HANSON, Washington, D.C.

Abstract.—A relation defining the rate of depletion of summer base flow during periods of negligible precipitation, and a relation expressing the monthly increase in summer base flow due to precipitation have been defined for a virtually unregulated stream. Testing these relations in a combined form using known values of monthly precipitation gives reasonable estimates of summer base flow for subsequent 1- to 4-month periods. A poor correlation was found to exist between monthly precipitation and corresponding increase in base flow. Consideration of variations in monthly evapotranspiration rates and antecedent ground-water conditions should help to explain much of the scatter in this relation; however, additional ground-water data are needed in the basin before a significant improvement in this relation can be expected.

Base flow of a stream may be defined as that flow furnished primarily by the ground-water reservoirs. For many streams, base flow constitutes the major portion of streamflow during the summer months. In regions where water supply is dependent on base flow, and demand approaches supply, a knowledge of base-flow characteristics becomes important. This report describes the development of relations which define (1) the rate of depletion of summer base flow during periods of negligible precipitation, and (2) the increase in summer base flow due to monthly precipitation for a virtually unregulated stream, the Potomac River at Point of Rocks, Md. These two relations are combined to provide expressions for summer base flow during the subsequent 1- to 4-month period, in terms of beginning base flow and the ensuing monthly precipitation.

DATA USED

Streamflow and precipitation data for the 14 years of 1928 to 1930 and 1941 to 1951 were used to derive the base-flow relations. Data for the subsequent 14-year period, 1952 to 1965, were then used to evaluate these relations. Only the months of June through September were considered in this analysis.

Hydrographs of daily streamflow at the U.S. Geological Survey gaging station on the Potomac River at

Point of Rocks were used to study summer base-flow characteristics. Drainage area of the basin above Point of Rocks is 9,651 square miles, of which only 1.2 per cent is regulated by reservoirs. This regulation has had a negligible effect on low flow at Point of Rocks and, therefore, was disregarded in this analysis. Published streamflow records for short periods during 1928 to 1930 were adjusted for upstream diversions into the Chesapeake and Ohio Canal.

Monthly precipitation totals used in this study are basin-average values for the Potomac River basin above Washington, D.C. Each monthly value was computed by the U.S. Weather Bureau on the basis of a weighting, according to areal contribution, of precipitation at each of 88 weather stations located in and adjacent to the basin. These average values were furnished by the U.S. Weather Bureau for the calendar years 1928-30 and 1941-65, thus establishing the study periods used in this analysis. Even though these monthly precipitation totals include the effect of precipitation downstream from the study area, they are considered representative of precipitation on the basin above Point of Rocks.

DEVELOPMENT OF RELATIONS

The base-flow recession curve, plotted in figure 1 with the 1930 hydrograph for the Potomac River at Point of Rocks, represents the rate of depletion of base flow for periods of negligible precipitation. It was drawn to average the lower segments of several base-flow recessions estimated from hydrographs for those summer months having little or no precipitation (Riggs, 1963). As indicated in the figure, this curve does not coincide with the hydrograph recession until several days beyond a significant peak discharge, during which direct runoff becomes depleted. In this analysis, base flow is assumed to consist primarily of ground-water flow, but probably includes some flow from channel and bank storage. The base-flow recess-

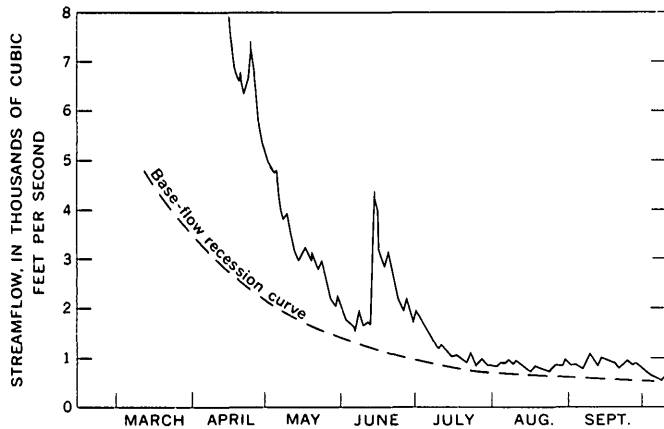


FIGURE 1.—Hydrograph of the 1930 summer flow, and the base-flow recession curve for the Potomac River at Point of Rocks, Md.

sion curve applies only to the period June 1 to October 1, but is not restricted to the position shown in the figure—for example, it may be shifted horizontally to coincide with the base-flow recession of any given hydrograph. Better definition of the rate of depletion of base-flow may be possible by considering variations in evapotranspiration rates for each month; however, for this analysis one curve representing the entire 4-month study period was considered adequate.

The recession curve of figure 1 may be expressed as

$$Q' = 0.57Q_0 + 190, \quad (1)$$

where Q_0 is the base flow, in cubic feet per second, at any point on the curve, and Q' is the corresponding base flow, in cubic feet per second, 30 days later for the condition of no precipitation during the period. Equation (1) is limited to the range $550 \text{ cfs} < Q_0 < 5,000 \text{ cfs}$, and is considered applicable to any 30-day period between June 1 and October 1.

The second relation developed in this study defines the increase in base flow at the end of a given 30-day period due to precipitation during the period. The method of determining monthly increase in base flow is illustrated in figure 2. Base-flow values are selected from the hydrograph for August 1 and September 1. The August 1 base flow is then projected to the end of the month along the base-flow recession curve. The increase in base flow at the end of August is the difference between the September 1 base flow and the projected August 1 base flow.

Monthly increases in base flow were thus determined for June, July, August, and September during the years 1928–30 and 1941–51. These values were plotted against corresponding monthly precipitation totals to

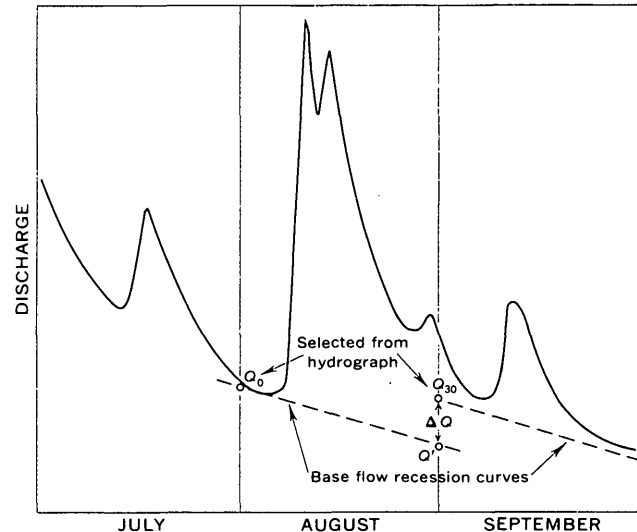


FIGURE 2.—Variables used in determining monthly increase in base flow, ΔQ , due to precipitation, where Q_0 and Q_{30} are beginning month base flows selected from the hydrograph and Q' is the end-of-the-month base flow projected from the beginning of the month along the base-flow recession curve.

define the curve shown in figure 3. This curve may be expressed as

$$\Delta Q = 8.45P^{2.69} \quad (2)$$

where ΔQ is the increase in base flow, in cubic feet per second, at the end of a 30-day period due to precipitation, P , in inches, during the period. Equation (2) is limited to $P \leq 7$ inches and is considered applicable to any 30-day period between June 1 and October 1.

The relation in figure 3 indicates that increase in base flow is negligible when monthly precipitation over the basin is less than 2 inches. The amount of increase in base flow, however, becomes poorly defined with higher precipitation values. In an attempt to explain the wide scatter of points in the relation of figure 3, four factors were considered: (1) variation in the relation from month to month, (2) distribution of precipitation during each month, (3) variations in the ΔQ values due to inconsistencies in selecting observed based flows from the hydrograph, and (4) antecedent runoff and precipitation. None of these four factors significantly reduced the scatter of points in figure 3. Possibly, some of this scatter could be explained by variations in monthly evapotranspiration rates and antecedent ground-water conditions, but insufficient data on these items precluded their consideration in this analysis.

The relations defined in figures 1 and 3 may be combined to define an equation for computing base flow 30 days hence. Thus, base flow at the end of a 30-day period is the sum of equations (1) and (2) or

$$Q_{30} = 190 + 0.57Q_0 + 8.45P_1^{2.69}, \quad (3)$$

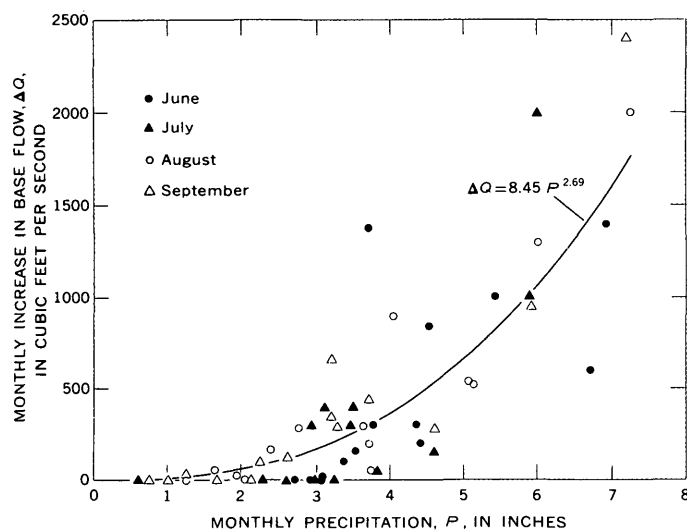


FIGURE 3.—Relation between monthly precipitation, P , and monthly increase in base flow, ΔQ , for June, July, August, and September of 1928–30 and 1941–51.

where Q_{30} is base flow, in cubic feet per second, at the end of the 30-day period, Q_0 is base flow, in cubic feet per second, at the beginning of the period, and P_1 is the total basin precipitation, in inches, during the period.

An expression for base flow 60 days hence may be derived from equation (3) by substituting base flow at the end of the 30-day period for Q_0 and substituting precipitation during the second 30-day period for P_1 . Continued substitution in equation (3) of computed base flow and subsequent 30-day precipitation defines equations for base flow 90 and 120 days hence. Equations for base flow 30, 60, 90, and 120 days hence are summarized below:

$$Q_{30} = 190 + 0.57Q_0 + 8.45P_1^{2.69}, \quad (3)$$

$$Q_{60} = 298 + 0.33Q_0 + 4.82P_1^{2.69} + 8.45P_2^{2.69}, \quad (4)$$

$$Q_{90} = 360 + 0.19Q_0 + 2.75P_1^{2.69} + 4.82P_2^{2.69} + 8.45P_3^{2.69}, \quad (5)$$

and

$$Q_{120} = 395 + 0.11Q_0 + 1.57P_1^{2.69} + 2.75P_2^{2.69} + 4.82P_3^{2.69} + 8.45P_4^{2.69}, \quad (6)$$

where Q_{30} , Q_{60} , Q_{90} , and Q_{120} are base flows, in cubic feet per second, at the end of 30-, 60-, 90-, and 120-day periods respectively; Q_0 is the observed base flow, in cubic feet per second, at the beginning of the computation period; and P_1 , P_2 , P_3 , and P_4 are precipitation totals, in inches, during the first, second, third, and fourth consecutive 30-day periods, respectively. The hydrologic conditions defining equations (3) to (6) are assumed to not change during the period June 1 to

October 1; therefore, equation (3) is applicable during any 30-day period between June 1 and October 1. Similarly, equations (4) and (5) are applicable during any 60- and 90-day period, respectively, between June 1 and October 1.

Equations (3) to (6) were checked by applying them to the 14 years of data (1928–30 and 1941–51) used in their derivation. Comparisons of these computed values with corresponding observed values, selected from the hydrographs, are shown in figure 4. Two-thirds of the 1-month computed base flows (fig. 4A) are within 8 percent of the observed values; the comparable spread for 4-month computed base flows (graph D) is 22 percent. Much of this spread reflects the scatter of points shown in the plot of figure 3. Nevertheless, the spread between observed and computed values in figure 4 is not considered appreciable. The fairly uniform scatter of points about the dashed line on each graph (fig. 4) also indicates no significant bias in equations (3) to (6).

The difference between computed and observed base-flow values can be determined rapidly on the figure by scaling off the vertical distance from the center of

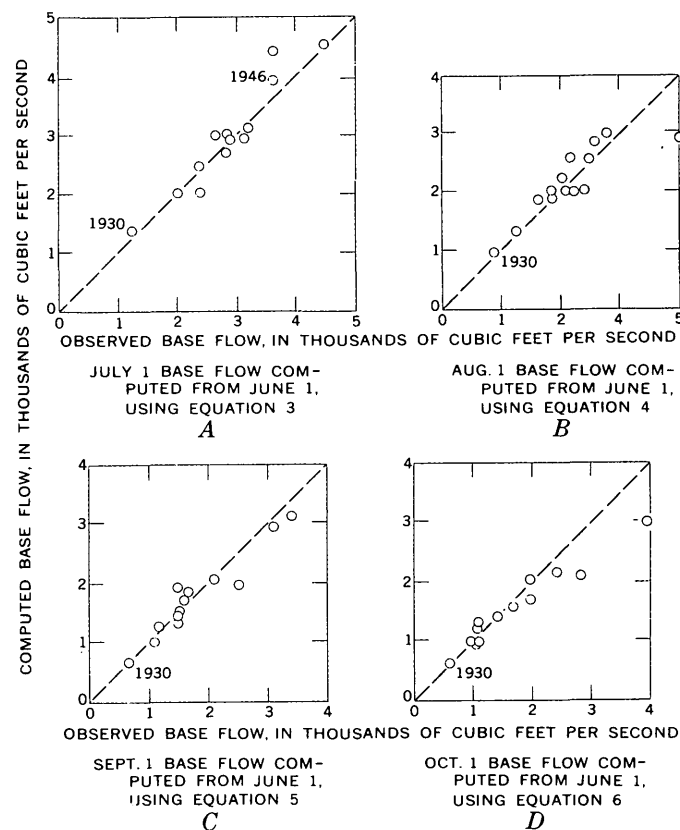


FIGURE 4.—Relation of observed base flows (from hydrographs) to computed base flows (from equations 3–6) for the period used to derive the equations indicated, 1928–30 and 1941–51.

each circle to the dashed line. For example, in figure 4A, the computed July 1, 1946, base flow of 3,900 cfs was about 300 cfs greater than the observed base flow of 3,600 cfs for that day.

To determine whether equations (3) to (6) would be applicable to more recent data, they were tested using streamflow and precipitation data for the period 1952-65. As before, beginning-of-month base flows were computed from the equations using monthly precipitation above Washington, D.C., and June 1 observed base flows selected from the hydrographs of daily stream-

flow. Comparisons of observed and computed base flows for July 1, August 1, September 1, and October 1 are shown in figure 5. The September 1, 1955 (fig. 5C), and October 1, 1955 (fig. 5D), computations are exceptionally high owing to an unusually high August precipitation of 10.1 inches; these points should be disregarded because the precipitation exceeds the prescribed limits of $P \leq 7$ inches. As would be expected, the scatter of points is more pronounced in figure 5 than in figure 4 because figure 4 is based on data used in deriving the equations. However, the relatively good agreement between computed and observed values in figure 5 suggests that equations (3) to (6), based on data prior to 1952, are also applicable to data after 1952. For example, the excellent agreement between computed and observed points for 1930 (fig. 4) and again for 1965 (fig. 5) indicates that a change in the relations with time is unlikely.

CONCLUSIONS

The equations developed in this analysis appear to have practical significance in describing the base-flow recession characteristics and the response of base flow to monthly precipitation. It should not be assumed, however, that base flow as identified in this analysis is necessarily that flow only from principal groundwater sources. Many sources of groundwater contribution apparently exist in the Potomac River basin, and some of these are shallow ephemeral aquifers. The amount of water stored in these aquifers at the beginning of the growing season may have significant effect on the subsequent base-flow increase and recession characteristics. Until sufficient ground-water data become available, significant refinement of the relation between monthly precipitation and corresponding base-flow increase is not likely.

REFERENCE

- Riggs, H. C., 1963, The base-flow recession curve as an indicator of ground water: *Internat. Assoc. Sci. Hydrology*, Pub. 63, p. 352-363.

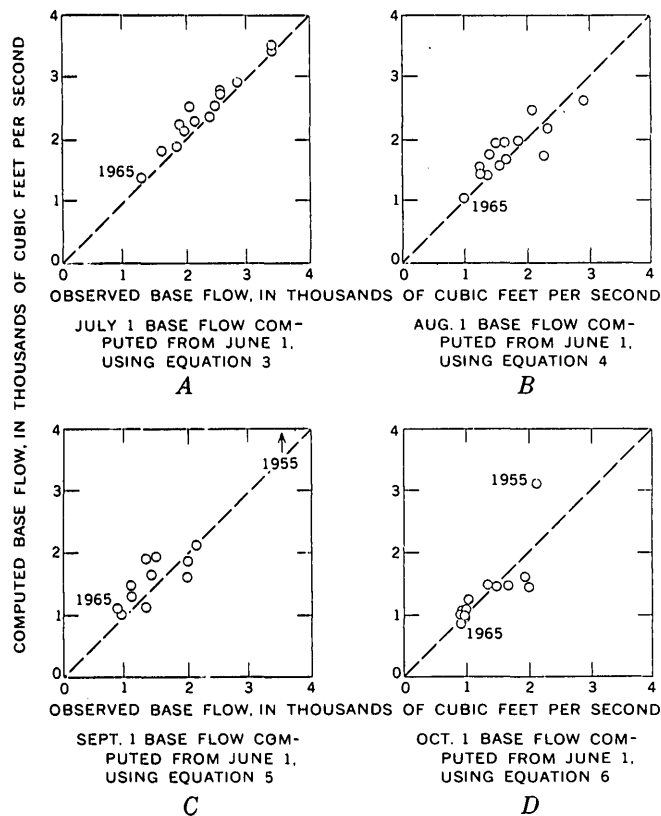


FIGURE 5.—Relation of observed base flows (from hydrographs) to computed base flows (from equations 3-6) for the period 1952-65.



THE CONSTRUCTION AND USE OF FLOW-VOLUME CURVES

By E. G. MILLER, Trenton, N.J.

*Work done in cooperation with the New Jersey Department of Conservation and Economic Development,
Division of Water Policy and Supply*

Abstract.—Flow-volume curves, dealing with the volume of water flowing in a stream, are similar in form to flow-duration curves and are computed from the same arrays of streamflow discharge records used in computing flow-duration curves. They provide an additional tool for preliminary and general studies of the feasibility of using or storing water for various purposes.

Flow-duration curves have been in use for over 50 years to portray streamflow characteristics (Searcy, 1959, p. 1). This paper presents a method of using the same basic data used in constructing a flow-duration curve to construct a “flow-volume” curve that can solve problems dealing with the volume of water flowing in a stream instead of the rate of flow. This type of curve was first suggested by R. H. Tice (written commun., 1958).

The rapidly growing practice of off-stream storage for water supply, low-flow augmentation, and electric-power generation makes this concept an increasingly useful tool. Likewise, the increasing number of permits for diversion of streamflow that specify a minimum flow that must be allowed to remain in the river adds impetus to flow-volume studies.

CONCEPT OF FLOW-VOLUME CURVES

A flow-volume curve shows the percentage of volume of streamflow that occurred at discharges of a specified or greater rate in a given period. Figure 1 presents the flow-volume curve for South Branch Raritan River at Stanton, N.J., for the reference period 1931–60 (Miller, 1966, p. 31). For comparison, the more familiar flow-duration curve for the same station and period is also drawn on figure 1. The same form may be used for both curves. The ordinate scale represents discharge rates in both cases, but, whereas the abscissa

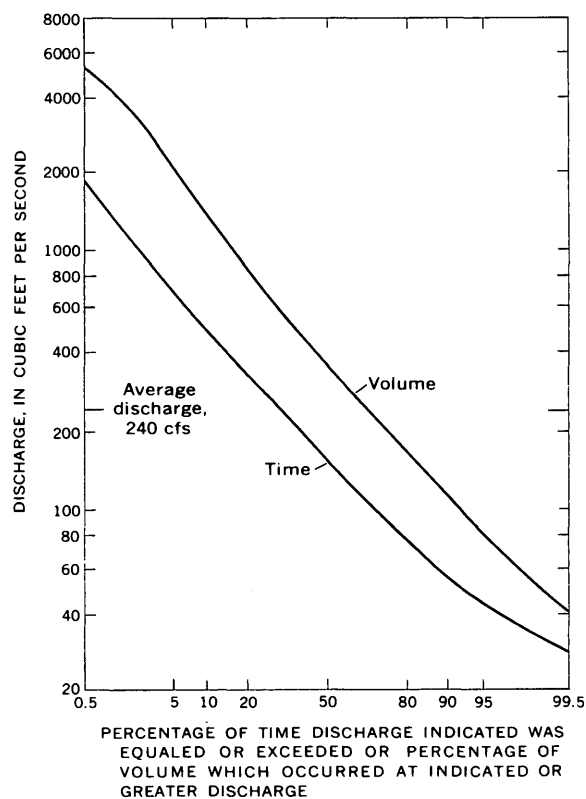


FIGURE 1.—Comparison of flow-duration (lower) curve and flow-volume (upper) curve for South Branch Raritan River at Stanton, N.J., 1931–60.

represents percentage of time for flow-duration curves, it represents percentage of volume for flow-volume curves.

The volume of water which flows past a point in the stream during 1 day expressed as cfs-days is the most convenient unit for compiling flow-volume data, although other units such as million gallons or acre-

feet could be used. The daily mean flows (representing daily volumes) during the given period are arranged according to magnitude, and the percentages of the total volume of streamflow during the period that occurred at discharges of a specified or greater rate are computed.

The technique for computing percentage of volume for flow-volume curves is more complicated than that for computing percentage of time for flow-duration curves. In the procedure commonly used for computing a flow-duration curve, ranges of discharge (called classes) are established and the numbers of days during the period with discharges in each range of discharge are totaled. Each day has equal weight in this computation. In the computation of percentage of volume, however, it is necessary to total the volume of water in each class or range, not the number of days. The use of an electronic computer would make it feasible to total the actual discharge figures of the array and compute percentage of the total volume at convenient intervals, but an approximate method is to count the number of days in a class and multiply this number by an average value of discharge for the class. Experience has shown that the use of the arithmetical average of the highest and lowest discharges of each class frequently produces totals that do not check well with the known total volumes of streamflow. Therefore, it must be decided whether the approximate method is accurate enough for each specific project. In any event, the actual discharge values should be used for the highest few days to prevent gross errors.

A flow-volume curve is based on a specific period of past record that should comprise a large number of whole years. The curve then represents the average for the entire period. If the streamflow for the period of the past record used is representative of the long-term streamflow, the flow-volume curve may be considered a probability curve to estimate the percentage of volume to be expected in the future at various rates of discharge. The results will be reliable if the total volume of future streamflow is taken as the average annual volume times a large number of whole years. The use of whole years eliminates the effect of the annual runoff cycle. The shorter the period in the future being considered, the greater is the possibility of variation from the average curve. The amount that the volume of streamflow for any one year can vary from the average can be determined from an examination of the streamflow records.

A convenient means of providing absolute values of volume without limiting the curve to a definite period is to place a tick mark on the discharge scale (ordinate) showing the average discharge. Then the volume of

water to be expected under normal conditions for any period of years can be computed by multiplying the average discharge by the length of the period.

USES OF FLOW-VOLUME CURVES

Pumped-storage investigations

The curves of figure 1, for example, show that a discharge rate of 200 cubic feet per second or greater for South Branch Raritan River at Stanton, N.J., occurred on only 40 percent of the days during 1931-60, but during that 40 percent of the days 74 percent of the total volume of streamflow of 1931-60 occurred. The curves also show that 35 percent of the total volume of streamflow occurred during the 9 percent of the days when streamflow was 500 cfs or greater, and nearly 98 percent of the total volume of streamflow occurred during the 87 percent of the days when streamflow was 60 cfs or greater. These examples indicate that the combination of curves is useful in preliminary studies of the feasibility of pumping water from a river at times of high water or when streamflow is above a given base.

If the problem is to pump water from the river for water-supply storage, but a minimum of 200 cfs must be permitted to flow down the river, the flow-volume curve can be used to compute the volume of water theoretically available for pumping during a given number of years (74 percent of the total volume of streamflow during the period minus 200 times the number of days when the flow was 200 cfs or greater). To capture all this streamflow available for pumping would require equipment with a pumping capacity equal to the difference between 200 cfs and the maximum rate of discharge. Because it would not be practical or economical to have equipment with capacity equal to the greatest possible demand, the curves are helpful in studying the economics of various-sized pumps and transmission pipelines. Although the maximum instantaneous discharge at Stanton during 1931-60 was 18,000 cfs and the maximum daily mean discharge during that period was 8,060 cfs, the flow-volume curve shows that only 5 percent of the volume of water passed Stanton when the daily discharge was 2,100 cfs or greater and 10 percent of the volume passed when the daily discharge was 1,400 cfs or greater. Such figures can then be used to study the relationship between cost of various-sized pumping equipment and the value of the water that can be diverted with given equipment.

Water-use investigations

Various physical- and chemical-quality parameters are often related to water discharge. Usually the

chemical quality improves with increased discharge. Assuming the chemical quality of the water in South Branch Raritan River at Stanton is suitable for a particular purpose at discharge rates of 200 cfs or greater, usable water would be expected on only 40 percent of the days during an extended period of years, but 74 percent of the total volume would be usable.

On the other hand, sediment concentrations usually increase with increased discharge. Thus, if it is assumed that sediment content in the water is too high for a particular use at discharge rates of 200 cfs or greater, usable water would be expected on 60 percent of the days, but only 26 percent of the total volume could be used.

Thus the combination of flow-duration and flow-volume curves facilitates preliminary investigations of the suitability of water supplies for various purposes. This combination also lends itself readily to economic analysis of the various alternative plans that may be studied, including costs and benefits of each.

Computation of dissolved-solid and suspended-sediment loads

The flow-volume curve can be used instead of the flow-duration curve in certain circumstances to facilitate the computation of dissolved-solid and suspended-sediment loads. The prerequisites for this procedure are usable relations between dissolved-solid content and water discharge and between sediment content and water discharge. Loads for increments of rate of discharge are then simply the product of the volume of

the increment and the average dissolved-solid or sediment content for the increment. This procedure is simpler than the method sometimes used of integrating a flow-duration curve with curves showing the relation between water discharge and dissolved-solid or sediment content.

SUMMARY

Flow-volume curves can be computed from stream-flow discharge records to show the percentage of volume of streamflow that occurred at discharges of a specified or greater rate in a given period. These curves are similar in concept to flow-duration curves and are computed from the same arrays used in computing flow-duration curves.

Flow-volume curves can be used in the engineering and economic analysis of many problems dealing with the volume of water flowing in streams. They can be used directly in the study of dissolved-solid and suspended-sediment loads. In combination with flow-duration curves, flow-volume curves are a flexible tool in preliminary and general studies of the feasibility of using water for various purposes and of pumping water from streams for water-supply use or storage.

REFERENCES

- Miller, E. G., 1966, Flow probability of New Jersey streams: New Jersey Dept. Conserv. Econ. Devel. Water Resources Circ. 15, 61 p.
- Searcy, J. K., 1959, Flow-duration curves: U.S. Geol. Survey Water-Supply Paper 1542-A, 33 p.



BED-MATERIAL MOVEMENT, MIDDLE FORK EEL RIVER, CALIFORNIA

By JOHN R. RITTER, Sacramento, Calif.

Abstract.—The Middle Fork Eel River, at a discharge of about 3,750 cfs and an average velocity of about 6 fps, moved bed material of cobble size. The size of the transported material was determined by actually noting, through the use of photographs, which individual rocks had been removed from painted areas on the riverbed; particle size of these rocks is proportional to average velocity and to tractive force.

The Middle Fork Eel River, a major tributary of the Eel River, flows from the western slopes of the Coast Ranges in northwestern California (fig. 1). The river is about 70 miles long and drains an area of 770 square miles. The section of the river studied is at the U.S. Geological Survey gaging station, 8.6 miles

east of Covelo, Calif. This study was made to determine maximum particle size of bed material moved at different velocities of flow and also to relate the results to similar studies by others.

Only one discharge was used because the study section was destroyed during the flood of Christmas 1964, when the river reached a stage of 31.7 feet, a discharge of about 133,000 cubic feet per second. The study began on October 5, 1964, and the highest river stage occurring between October 5 and the time when the site was revisited on November 16, 1964, was used in the study. This stage was 7.82 feet or a discharge of about 3,750 cfs, a flow equaled or exceeded 8 percent of the time (Rantz, 1964).

METHOD OF STUDY

The following preliminary work was done at a time of low flow in the river. At intervals of 10–20 feet along a cross section beneath the cableway at the gaging station, twelve 1-foot squares of bed material painted bright pink were established as stations and were given numbers corresponding to their distance from the right bank. On October 5, 1964, the squares were photographed (fig. 2) so that the size of transported material could be determined by noting which rocks were subsequently removed from the squares.

A point count, using a grid plotted from a table of random numbers, was made of the size of bed material on photographs of each station. Because photographs provide only two dimensions, the observed dimensions of the bed material were taken as the longitudinal (length) and intermediate (width) axes and the hidden axis was assumed to be the shortest of the three. Analysis (fig. 3) showed that in this section of the river, bed material ranged in size from sand (0.062–2 millimeters) to boulders (>256 mm) and averaged pebble size (4–64 mm).

Material was removed from approximately 50 percent of the area of the painted squares by the peak dis-

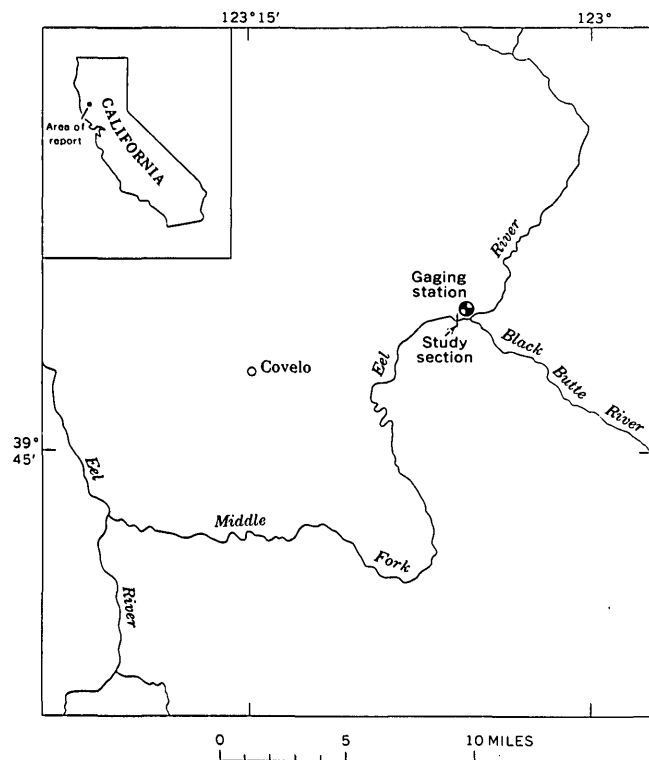


FIGURE 1.—Index map of Middle Fork Eel River, Calif., showing location of study section.

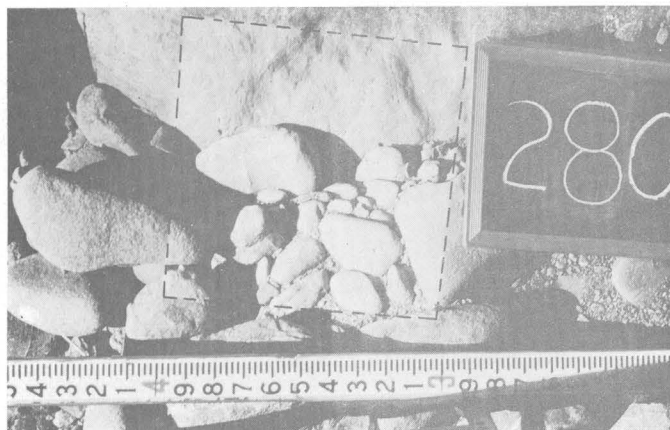


FIGURE 2.—Bed material at station 280 in the study section, before movement of material. Painted area is area within dashed lines. Bed material at this site is typical of the entire section. Scale is in feet and tenths of feet.

change between October 5 and November 16. The amount and dimensions of rocks removed at each station were determined from the photographs taken before the peak discharge. Dimensions of the largest rocks removed and the velocity assumed to have moved these rocks are given in table 1. Except for station 240, where the intermediate axis of one rock and the longitudinal axis of another were used, the dimensions given are those of a single rock. The dimensions of the smallest rock not transported also are shown in the table to indicate the range in size of the transported bed material. Average velocity for each station was determined from a discharge measurement made at a gage height of 7.82 feet.

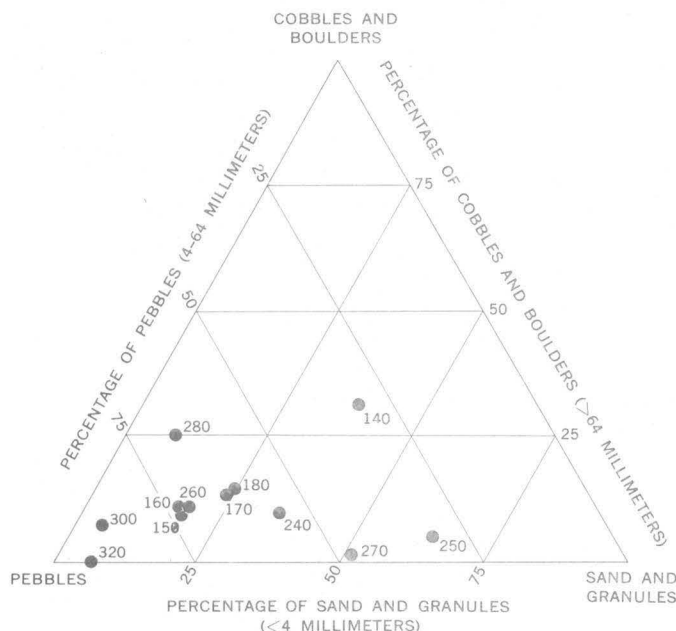


FIGURE 3.—Ternary diagram of particle size at each station in the cross section (Wentworth scale).

TABLE 1.—Assumed stream velocity and the size of transported material,¹ Middle Fork Eel River, Calif.

Station	Average velocity (fps)	Length of maximum size of material transported (mm)		Length of minimum size of material not transported (mm)	
		Longitudinal axis	Intermediate axis	Longitudinal axis	Intermediate axis
140-----	1.90	13.7	9.2	6.7	6.7
150-----	4.14	88.5	58.0	34.4	29.6
160-----	4.73	53.4	32.0	26.8	18.3
170-----	5.53	² 94.5 62.5	² 91.5 51.8	20.7	18.3
180-----	5.84	54.9	33.6	3.7	3.7
240-----	7.49	189.0	82.3	(³)	(³)
250-----	6.46	144.3	91.5	64.0	40.8
260-----	6.73	² 182.9 152.4	² 121.8 97.6	39.6	21.3
270-----	5.45	36.6	24.4	110.4	36.6
280-----	6.17	67.2	45.7	5.5	5.5
300-----	4.80	106.7	64.1	42.7	15.8
320-----	2.54	73.2	42.7	17.7	15.2

¹ Dimensions are those for a single rock, except for station 240 where the longitudinal axis of one rock and the intermediate axis of another were used.
² Rotated, but not transported.
³ All particles removed.

RESULTS

As shown in table 1, the relation between average velocity and the size of material moved varies greatly. This variation probably is due to different factors at different stations, such as the shielding effect of boulders, an absence of material of the maximum size which could have been moved, and local differences in the intensity of turbulence. The relation of force to particle size and to particle height above the floor for laminar flow at the bed of the stream was stated by Rubey (1937): “. . . the force acting upon a particle increases rapidly with the dimensions of the particle or the height to which it stands above the stream floor . . .” Nevertheless, if the average velocity at a station is plotted against the intermediate axis of the largest observed rock removed at that velocity, a relation between the two can be seen. Thus, the line in figure 4 indicates the largest particle size that velocities are capable of moving at this stage (7.82 ft).

The lengths of the intermediate axes also are used to show the relation between tractive force and the maximum particle size moved at each station. Tractive force (τ) is defined as $\tau = \lambda s d$, where λ is the specific weight of water, d is the depth of water, and s is the slope of the water surface (0.00755 ft per ft for a reach of 700 ft at a stage of 1.73 ft). For comparison, these data (fig. 5) are added to a plot of three other sets of data compiled by Fahnestock (1963, p. A29-A32). On the plot, the Middle Fork Eel River River data points fall below the data points of Fahnestock, but they are fairly consistent with the trend indicated by the data points of Nevin (1946) and

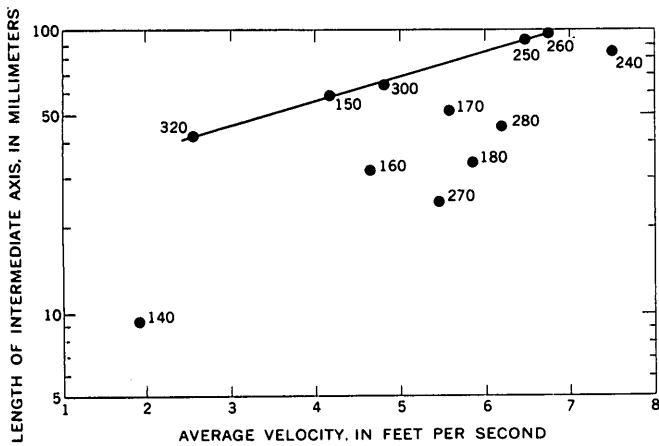


FIGURE 4.—Relation between average velocity and intermediate axis of largest particle transported at each station. The line indicates the largest particle size that velocities are capable of moving at this stage (7.82 ft).

Lane (1955). The relation to Fahnestock's data points was to be expected because his data are for material that is being transported and thus requires less tractive force for movement than material that is being eroded. Although the other data plotted in figure 5 are for material that is being eroded from the bed, Lane's data (1955, p. 1244) are for the particle diameter for which 25 percent of the material is larger by weight, and Nevin's data (1946, p. 667) in part are based on the average of the longest and shortest right-angle diameters. Nevertheless, Lane's and Nevin's results are comparable to the results of this study.

SUMMARY

The maximum particle size transported during a discharge of 3,750 cfs was measured at 12 points in a cross section where the average velocity of flow in the verticals ranged from 1.90 to 7.49 feet per second. Data plots of particle size versus (1) average velocity and versus (2) tractive force indicate that they are related. The second relation is consistent with the results of other investigations done in different areas by several researchers.

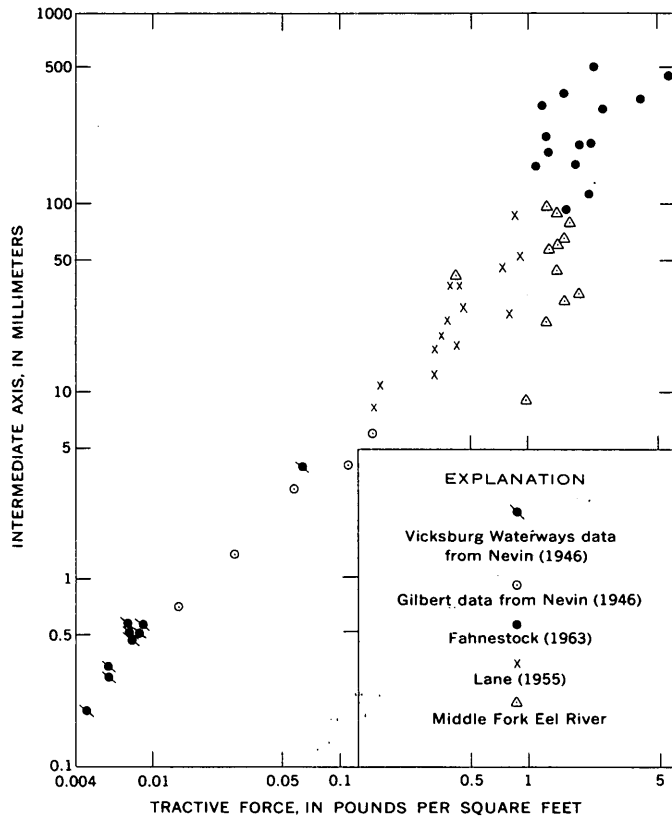


FIGURE 5.—Relation of particle size (intermediate axis) to tractive force. After Fahnestock (1963).

REFERENCES

- Fahnestock, R. K., 1963, Morphology and hydrology of a glacial stream—White River, Mount Rainier, Washington: U.S. Geol. Survey Prof. Paper 422-A, p. A1-A70.
- Lane, E. W., 1955, Design of stable channels: Am. Soc. Civil Engineers Trans., v. 120, p. 1234-1260.
- Nevin, C. M., 1946, Competency of moving water to transport debris: Geol. Soc. America Bull., v. 57, p. 651-674.
- Rantz, S. E., 1964, Surface-water hydrology of coastal basins of northern California: U.S. Geol. Survey Water-Supply Paper 1758, 77 p.
- Rubey, W. W., 1937, The force required to move particles on a streambed: U.S. Geol. Survey Prof. Paper 189-E, p. 121-141.



CHEMICAL CHARACTERISTICS OF BULK PRECIPITATION IN THE MOJAVE DESERT REGION, CALIFORNIA

By J. H. FETH, Menlo Park, Calif.

Abstract.—Analyses of 41 samples of bulk precipitation from 12 places in the Mojave Desert region show wide ranges of dissolved-solids concentration and a variety of chemical types, although the calcium bicarbonate type water dominates. Specific conductance of the solutions analyzed ranged from 8.9 to 823 micromhos and shows strong inverse correlation with quantities of rain but no discernible correlation with time of exposure of the gage between samples. Dust that locally includes saline materials appears directly to govern the chemical type and concentration of a few samples. Bulk precipitation in the Mojave is closely similar to bulk precipitation sampled at Menlo Park, Calif., near the coast, in the San Francisco Bay area.

In a study of the chemical composition of precipitation in desert areas, for which information generally is scanty, analyses were made of 39 samples of bulk precipitation from 12 places in the Mojave Desert region, California (fig. 1). Of the total, 22 samples were from storage-type gages where a layer of oil was used to retard evaporation and 17 from standard U.S. Weather Bureau gages serviced after each rain. The data indicate that concentration by evaporation was probably negligible and that most of the variations in gross concentration as well as concentration of individual constituents resulted from variations in the kind and amount of dry fallout and in the quantity of rainwater that collected in the gages between samples.

Bulk precipitation has been defined by Whitehead and Feth (1964, p. 3320) as the solution that results when "melting snow, or rain falling on the land surface—whether in its native state or modified by man—collects and incorporates the products of dry fallout." The same authors commented further that "Bulk precipitation displays the combined effects of all water-soluble airborne components of precipitation. It is the most significant fluid to study in evaluating contributions of atmospheric mineralization to the chemical quality of natural water [and] * * * is the geochemically active agent in rock weathering and formation

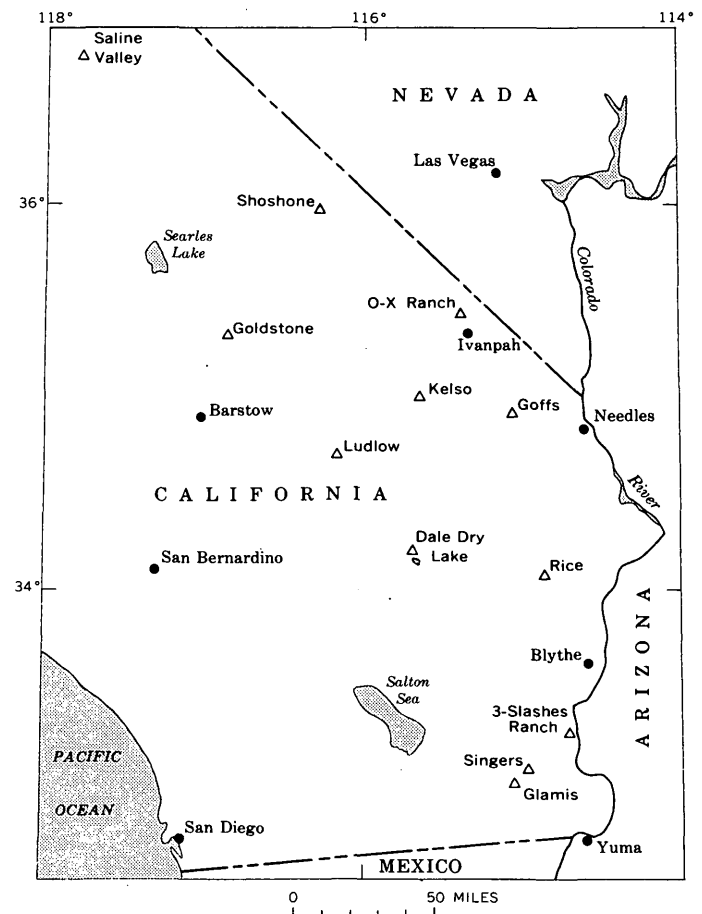


FIGURE 1.—Sketch map of the Mojave Desert region, California, and adjacent areas, showing locations of rain gages (triangles).

of soil and is the solution that provides moisture to growing vegetation."

Acknowledgments.—Collection of the samples was made possible by my colleague, C. T. Snyder, who established the network of rain gages in connection with his own investigations. Mr. Snyder collected many of the samples during periodic rounds of the network,

and arranged with members of the guard force at Goldstone Tracking Station, with several ranchers, and with other individuals to collect samples periodically. The chemical analyses were made at the U.S. Geological Survey laboratory, Sacramento, Calif. The cooperation of all is much appreciated.

ANALYTICAL RESULTS

The samples from the Mojave (table 1) show in their variations in dissolved-solids concentration and chemical type some of the expected effects of saline dust from local sources, but they do not depart from

the overall dominance of calcium bicarbonate type water that is generally characteristic of precipitation throughout the world.

The influence of saline dust is most apparent in the single sample from Saline Valley (table 1). The dominant constituents of the saline materials in Saline Valley are sodium sulfate and sodium chloride (G. I. Smith, oral commun., 1966); sodium, sulfate, and chloride are dominant in the water analysis. The gage was exposed continuously for 11 months, and concentration by evaporation might have contributed to the relatively high salinity. However, 8 other

TABLE 1.—Chemical composition of samples of bulk precipitation from the Mojave Desert region, California, March 1965–March 1966

[Chemical constituents in parts per million. Stations are arranged in order from north to south]

Period of exposure	Silica (SiO ₂)	Calcium (Ca)	Magnesium (Mg)	Sodium (Na)	Potassium (K)	Bicarbonate (HCO ₃)	Sulfate (SO ₄)	Chloride (Cl)	Nitrate (NO ₃)	Specific conductance (in micromhos at 25° C)	Remarks ¹
Saline Valley, lat 36°45' N., long 117°47' W.											
Apr. 29, 1965– Mar. 23, 1966.	3.4	35	4.5	132	18	179	108	90	0.3	823	Near spring northeast of salt flats. Rain, 2.1 in. Boron, 1.3.
Shoshone, lat 35°58' N., long 116°16' W.											
Apr. 28–Oct. 13, 1965	-----	-----	68	-----	-----	330	-----	2.8	1.5	642	Southeast end of airstrip. Water, 0.05 in., Apr. 28–July 17, 1965 (not poured up); 0.6 in., July 18–Oct. 13, 1965. Boron, 0.8.
Oct. 13, 1965–Mar. 22, 1966.	1.6	16	1.2	11	6.0	58	11	5.9	.2	158	Rain, 5 in. Boron, 0.3; fluoride, 0.7.
Goldstone, lat 35°17' N., long 116°48' W.											
Mar. 31–April, 1965	-----	-----	-----	1.7	0.6	-----	2.6	1.3	4.0	34	Rain, 0.19 in.
Mar. 1–Apr. 4, 1965	0.1	1.6	0.0	.2	.1	35	.8	.3	.5	8.9	Rain, 0.90 in. Boron, 0.0.
Apr. 4–8, 1965	-----	-----	-----	.5	.6	3	2.0	.6	1.0	14	Rain, 0.32 in. Boron, 0.0.
Apr. 8–11, 1965	.5	-----	-----	.4	.2	6	1.2	.5	.7	15	Rain, 0.58 in. Boron, 0.1.
Apr. 11–12, 1965	.1	-----	-----	1.0	1.0	7	1.1	1.4	1.2	22	Rain, 0.55 in. Boron, 0.1.
Apr. 12–May 24, 1965	-----	-----	-----	3.8	1.0	-----	-----	1.4	12	70	Rain, 0.10 in.
May 24–25, 1965	-----	-----	-----	3.8	1.0	-----	-----	3.8	10	81	Rain, 0.18 in.
Apr. 25–July 17, 1965	-----	-----	-----	2.0	1.9	-----	-----	3.6	-----	199	Rain, 0.08 in.
July 17–30, 1965	-----	-----	-----	1.2	.9	-----	1.0	2.8	-----	122	Rain, 0.11 in.
July 30–Nov. 14, 1965	-----	1.0	.0	.3	.2	8	1.4	1.0	.9	19	Rain, 1.20 in.
Nov. 14–23, 1965	-----	2.0	.0	.2	.2	4	1.0	.4	.8	12	Rain, 1.20 in. Boron, 0.0.
Nov. 23–Dec. 10, 1965	-----	-----	-----	.2	.2	5	1.6	.4	.9	15	Rain, 1.16 in. Boron, 0.0.
Dec. 10–29, 1965	.0	1.6	.0	.6	.2	5	3.6	.5	1.7	16	Rain, 0.82 in., Dec. 29, 1965. Boron, 0.0.
O-X Ranch, lat 35°12' N., long 115°12' W.											
Mar. 21–Apr. 1, 1965	1.2	-----	-----	8.3	3.7	74	27	17	0.9	218	Rain, Apr. 1, 1965. Boron, 0.1.
Apr. 1–4, 1965	.2	2.4	0.0	.6	.8	12	2.3	1.8	.3	36	Rain, 1.35 in., Apr. 4, 1965. Boron, 0.0.
? –Dec. 9, 1965	.0	2.0	-----	.2	.2	5	4.6	.2	.4	16	Boron, 0.0.
Dec. 4–16, 1965	.1	1.2	.0	.2	.2	4	3.0	.2	.4	11	Snow. Boron, 0.0.

QUALITY OF WATER

TABLE 1.—Chemical composition of samples of bulk precipitation from the Mojave Desert region, California, March 1965–March 1966—Continued

Period of exposure	Silica (SiO ₂)	Calcium (Ca)	Magnesium (Mg)	Sodium (Na)	Potassium (K)	Bicarbonate (HCO ₃)	Sulfate (SO ₄)	Chloride (Cl)	Nitrate (NO ₃)	Specific conductance (in micromhos at 25° C)	Remarks ¹
Kelso, lat 35°01' N., long 115°39' W.											
Mar. 24–Apr. 22, 1965...	0.8	7.6	0.7	8.0	4.9	34	12	3.9	2.3	118	Rain, 1.30 in. Boron, 0.2. Rain, 3.4 in. Boron, 0.2; fluoride, 0.0.
Oct. 13, 1965–Mar. 22, 1966.	1.9	9.2	1.0	.8	1.1	16	5.0	2.2	3.1	77	
Goffs, lat 34°55' N., long 115°03' W.											
Mar. 24–Apr. 23, 1965...	0.4	3.9	1.9	4.1	3.9	19	10	2.6	0.9	70	Rain, 2.4 in. Boron, 0.1. Rain, 0.8 in. Boron, 0.6. Rain, 6.4 in. Boron, 0.1.
Apr. 23–Oct. 13, 1965...	-----	-----	-----	4.5	8.0	26	15	2.2	4.7	144	
Oct. 13, 1965–Mar. 22, 1966.	.5	2.8	.0	.4	.6	6	1.0	1.2	1.2	31	
Ludlow, lat 34°43' N., long 116°10' W.											
Mar. 17–Apr. 8, 1965...	-----	-----	6.8	2.3	-----	40	20	7.8	13	179	Rain, 1.22 in., Mar. 31–Apr. 8, 1965. Boron, 0.1. Rain, 0.70 in., Apr. 13–14, 1965. Rain, 0.60 in. No data. No data.
Apr. 8–14, 1965.....	-----	-----	1.6	1.2	-----	22	4.2	2.4	1.4	57	
Apr. 14–July 17, 1965...	-----	-----	8.4	6.2	-----	-----	21	16	-----	281	
July 17–Nov. 17, 1965...	-----	-----	10	5.0	-----	58	16	14	29	250	
Nov. 17–Dec. 31, 1965...	1.1	6.8	.7	1.2	.8	21	1.0	2.1	.6	46	
Dale Dry Lake, lat 34°09' N., long 115°44' W.											
Mar. 17–Oct. 14, 1965...	-----	7.0	3.0	8.4	5.4	30	16	4.8	1.4	142	Rain, 1.1 in., Mar. 17–July 19, 1965; additional 0.5 in., July 19–Oct. 14, 1965. Boron, 0.3. Rain, accumulated, 2.7 in.
Oct. 14, 1965–Mar. 21, 1966.	0.7	4.8	.7	2.9	4.5	10	6.0	4.5	.1	60	
Rice, lat 34°05' N., long 114°50' W.											
Mar. 17–Oct. 13, 1965...	-----	9.6	2.2	6.3	6.6	12	9.4	3.0	4.3	115	Rain, 2.5 in., Mar. 17–July 18, 1965. No rain to Oct. 13, 1965, when sampled. Boron, 2.3. Rain, 3.2 in. Boron, 0.3; fluoride, 0.0.
Oct. 13, 1965–Mar. 22, 1966.	0.3	2.8	.0	1.1	1.3	14	4.0	3.2	1.0	85	
3-Slashes Ranch, lat 33°17' N., long 114°43' W.											
Mar. 17–Apr. 18, 1965...	0.2	10	1.0	4.6	3.8	10	13	4.8	8.7	111	Boron, 0.0. Rain, 0.35 in., Nov. 17, 1965; 0.85 in., Nov. 23, 1965.
Apr. 4–Nov. 23, 1965...	-----	18	1.7	12	11	94	16	16	2.5	259	
Singers, lat 33°03' N., long 114°43' W.											
Mar. 17, 1965–Mar. 21, 1966.	1.0	4.8	0.0	1.0	0.8	8	4.0	0.8	1.5	44	Rain, 3.8 in. Plastic gage. Boron, 0.0.
Glamis, lat 33°00' N., long 115°04' W.											
Mar. 17–Apr. 4, 1965...	0.6	-----	-----	5.0	2.0	29	18	4.1	4.5	99	Boron, 0.0. Fluoride, 0.0.
Apr. 4, 1965–Jan. 20, 1966.	.3	8.8	0.5	1.0	1.8	2	8.0	3.8	12	72	

¹ U.S. Weather Bureau 8-in. standard gages used at Goldstone and O-X Ranch; U.S. Geological Survey–Bureau of Land Management 5-in. pipe gages used at other locations.

samples in which specific conductance was less than 100 micromhos came from gages exposed for periods of from 5 to 8 months between samplings. It appears, therefore, that dust blowing from the saline playa accounts for most of the concentration found in the single sample from Saline Valley. As will be shown below (see fig. 2), the accumulation of 2.1 inches of water in the Saline Valley gage should have sufficed to put that sample in the lower range of concentrations rather than at the top. The fact that similar concentrations were not obtained from the gage at Dale Dry Lake, where salt was harvested in the past and saline residues remain on the surface, is puzzling. As the Dale Dry Lake gage was located at the chemical plant north of the playa, it may be that prevailing winds kept saline dust away from the gage.

The wind-movement recording station nearest to Saline Valley is at Bishop, Calif., 40 miles away, on the other side of a high range of mountains. The wind-movement recording stations nearest to Dale Dry Lake are at Thermal, Calif., 40 miles away, and at Daggett, Calif., 80 miles away. Therefore, it is not feasible to estimate the degree to which prevailing wind directions and movement actually account for the differences observed at the two collection sites involved.

The high (158 micromhos) and very high (642 micromhos) conductances recorded from samples gathered at Shoshone most likely resulted from the location of the gage near an airstrip where propwash from airplanes contributed to movement of dust in the vicinity. The differences in concentration in the other samples, as indicated by specific conductance, cannot, from the available data, be explained by dust movement except, perhaps, the low concentrations of all but two samples from Goldstone. The generally low concentrations of the group of samples from Goldstone reflect the fact that the gage at Goldstone was serviced after each precipitation event, so there was less chance for dry fallout to accumulate there than at the stations which were equipped with storage-type gages.

The close resemblance between bulk precipitation sampled on the Mojave Desert and that sampled at Menlo Park, Calif., near the coast, in the San Francisco Bay area, is shown in table 2. The somewhat lesser content of chloride in the general run of desert samples may be due to the fact that the Mojave stations are farther from the sea than is Menlo Park. The dominance of sulfate over chloride in both median and mean values of the Mojave samples is not readily explained. Whitehead and Feth (1964, p. 3326) attributed much of the sulfate content of bulk precipitation at Menlo Park to the influence of industry in

TABLE 2.—Comparison of values of selected constituents and specific conductance in bulk precipitation samples from the Mojave Desert region and Menlo Park, Calif.

[Menlo Park data from Whitehead and Feth, 1964, p. 3326; specific conductance values calculated from p. 3323-3324]

Values	Sulfate (ppm)	Chloride (ppm)	Specific conductance (micromhos at 25° C)
Mojave Desert region; 41 samples, 1965-66¹			
Maximum.....	108	90	832
Median.....	4.2	2.6	70
Mean.....	10.7	5.85	118
Minimum.....	0.8	0.2	8.9
Mojave Desert region; 40 samples, 1965-66, omitting Saline Valley²			
Maximum.....	27	17	642
Median.....	4.0	2.4	70
Mean.....	8.03	3.50	101
Minimum.....	0.8	0.2	8.9
Menlo Park; 25 samples, 1957-59			
Maximum.....	106	30	540
Median.....	2.8	3.0	45
Mean.....	12.2	7.28	93.7
Minimum.....	0.4	0.2	7.0

¹ Sulfate, 37 determinations.

² Sulfate, 36 determinations.

the San Francisco Bay region. Such influences certainly are not close at hand in the Mojave Desert. The sulfate in the Mojave samples may in part result from movement of sulfur-laden airmasses from the Los Angeles-San Diego metropolitan complex over the desert, but more likely the sulfate is caused by local sources of sulfate-bearing dust. There is no obvious regional pattern to distribution of the sulfate or chloride when their values are plotted on a map.

The maximum exposure of the sampling surface at Menlo Park between collection of samples was about 2 months, but the duration of exposure commonly ranged from 1 day to about 2 weeks. In the Mojave, sample containers were exposed from 1 day to 11 months between samples. Average exposure time for 23 samples (time exceeding 1 month) was 4.5 months; for the remaining 14, exposure time was about 4 days. The resemblances suggested by table 2 are remarkable. Indeed, the comparison—considering exposure times—suggests that the rates of dry fallout in the San Francisco Bay area exceed those on the Mojave Desert. If—as is thought—the Bay area fallout is derived largely from industry, the conclusion that dry fallout is greater in the Bay area may be warranted.

The concentrations of the Mojave samples, indicated by their respective specific conductances, bear a close inverse correlation with the quantity of water that

accumulated between samplings (fig. 2), but have no discernible correlation with duration of exposure between samplings—in other words, a dilution effect is apparent. To what extent those relations represent rainout of mineral constituents in the early part of a heavy storm followed by accumulation of more dilute water, and to what extent they represent mere dilution of approximately constant amounts of dry fallout, cannot be determined. The data in figure 2 plot, for the most part, in two fields. The lower field represents samples collected at Goldstone, and the upper field, the remainder of the samples for which depth of water in the collector was reported. The differences in collecting procedures, described below, explain the groupings.

COLLECTION AND ANALYSIS OF SAMPLES

The samples of bulk precipitation used in this study were collected under two sets of circumstances. Those from Goldstone and the O-X Ranch were collected in 8-inch standard U.S. Weather Bureau rain gages, and were poured into shipment containers immediately after each precipitation event. Accumulation of dry fallout between sampling was less than that at the other stations where, in general, the collectors remained for weeks and even months between sampling. The collectors at the other stations were U.S. Geological Survey-Bureau of Land Management gages made of lengths of 5-inch soft-steel pipe welded to a steel base

plate. All the rain gages were thoroughly washed with distilled water before being put into service. The storage-type gages were serviced upon installation with a small volume of transformer oil (Shell DIALA-AX) that floated on the surface of the rainwater in the gage and retarded evaporation. After each sampling, a new charge of oil was placed in the gage.

The possibility that the transformer oil contributed to contamination of the samples was considered. The oil was reported to be highly refined, with only organic inhibitors added. A test for possible contamination was made in the laboratory by shaking 10 milliliters of the oil with 200 ml of deionized water in a separatory funnel. After standing for a week, a specific conductance determination showed no contamination when the aqueous fraction was compared with a blank not in contact with oil. The oil may have trapped some dry fallout. However the turbulence and mixing as raindrops fell into the collector must have incorporated most of the fallout in the aqueous phase, otherwise the chemical concentrations of the under-oil samples would not have been as large or as variable as those that were determined.

Many of the samples were reported to be "rusty" when received in the laboratory, and they included part or all of the oil that had protected them from evaporation. Under the circumstances, it was not feasible to analyze the samples for iron. Values for pH are not reported in table 1. Those for bicarbonate and nitrate are indicative only, and not necessarily representative of the rain as it fell. Bicarbonate, pH, and nitrogen compounds in water are notoriously unstable during storage (Roberson and others, 1963; Feth, 1966).

The samples were analyzed by methods (Rainwater and Thatcher, 1960) standard in the U.S. Geological Survey, except that chloride was determined by the more sensitive method (for low concentrations) described by Bergman and Sanik (1957) and by Iwasaki and others (1952). The alkalinity end point was chosen from the titration curve, and sulfate was determined by a method described by Gambell and Fisher (1964).

CONCLUSIONS

The results of this study show that bulk precipitation throughout the Mojave Desert region is strikingly similar in concentration and chemical type to bulk precipitation in the far different environment of Menlo Park, Calif., near the coast. The unavoidably crude collecting procedures seem not to have vitiated the results, although the present study yields values that must be considered first approximations only. Locally, dust that contained saline materials appears over-

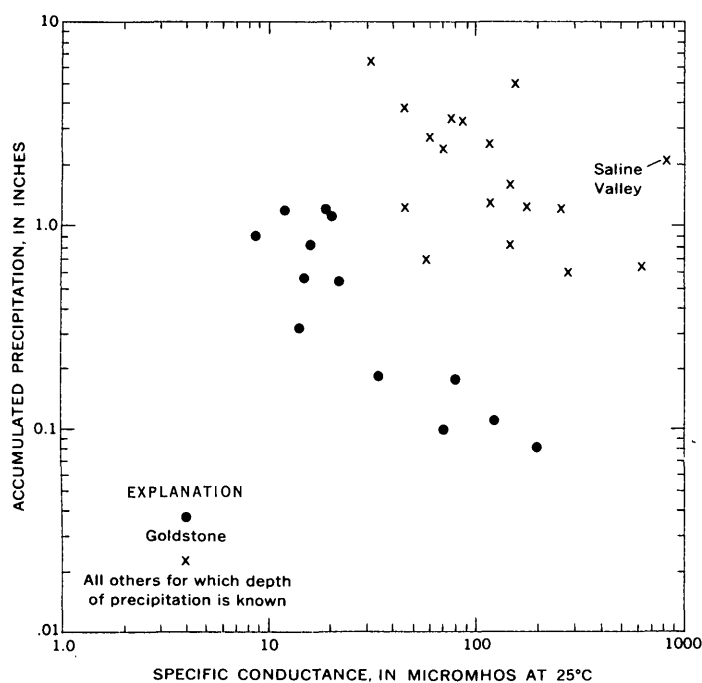


FIGURE 2.—Relation of specific conductance of samples to depth of precipitation at Goldstone and at other sites in the Mojave Desert region.

whelmingly to have governed the composition and concentration of bulk precipitation. Some variations among the samples cannot be explained from present knowledge. The fairly high concentrations of sulfate in the desert samples remain unexplained. The influence of the sea in contributing chloride to precipitation is perhaps less apparent in the desert samples than in those from Menlo Park. Bulk precipitation in the desert varies widely from place to place and with time (see especially Goldstone samples, table 1) but is mostly a calcium bicarbonate type as is precipitation generally, except at stations within range of the immediate influence of the sea.

REFERENCES

- Bergman, J. F., and Sanik, J., Jr., 1957, Determination of trace amounts of chloride in naphtha: *Anal. Chemistry* v. 29, p. 241-243.
- Feth, J. H., 1966, Nitrogen compounds in natural water—a review: *Water Resources Research*, v. 2, p. 41-58.
- Gambell, A. W., and Fisher, D. W., 1964, Occurrence of sulfate and nitrate in rainfall: *Jour. Geophys. Research*, v. 69, p. 4203-4210.
- Iwasaki, I., Utsumi, S., and Ozawa, T., 1952, New colorometric determination of chloride with mercuric thiocyanate and ferric iron: *Chem. Soc. Japan Bull.*, v. 25, p. 226.
- Rainwater, F. H. and Thatcher, L. L., 1960, Methods for collection and analysis of water samples: U.S. Geol. Survey Water-Supply Paper 1454, 301 p.
- Roberson, C. E., Feth, J. H., Seaber, P. R., and Anderson, Peter, 1963, Differences between field and laboratory determinations of pH, alkalinity, and specific conductance of natural waters: Art. 115 in U.S. Geol. Survey Prof. Paper 475-C, p. C212-C215.
- Whitehead, H. C., and Feth, J. H., 1964, Chemical composition of rain, dry fallout, and bulk precipitation at Menlo Park, California, 1957-1959: *Jour. Geophys. Research*, v. 69, p. 3319-3333.



WINTER LOSS AND SPRING RECOVERY OF DISSOLVED SOLIDS IN TWO PRAIRIE-POTHOLE PONDS IN NORTH DAKOTA

By JAMES H. FICKEN, Lincoln, Nebr.

Abstract.—A temporary loss of more than 25 percent of dissolved-solids tonnage was detected in two prairie-pothole ponds in each of several winters. Analyses of ice, water beneath the ice, and water in the bed material suggest that "lost" dissolved solids were stored temporarily in the bed material. Probably dissolved solids migrate by diffusion into the bed as the ice thickens and migrate back after the ice melts. Full recovery of the loss required at least several weeks. The slowness of recovery may be due to a slow rate of diffusion from the bed material.

A prairie pothole commonly is defined as a shallow depression in the prairie in which water becomes ponded. There are several hundred thousand of them in North Dakota, and they range in size from a fraction of an acre to more than a hundred acres. Until recently, little was known about the hydrology of prairie potholes even though they constitute a significant part of the water resources of the glaciated part of the northern Great Plains. They are particularly important as breeding and resting places for migratory waterfowl.

The present study of the hydrology of prairie potholes was begun in 1960. Attention was first given to water losses by evapotranspiration and seepage (Shjeflo and others, 1962). As a part of the study, measurements of the dissolved solids in nine pothole ponds were obtained about monthly, except during the periods of ice cover. Examination of the measurements indicated that the tonnage of dissolved solids in some of the ponds decreased significantly between the last sampling before freezeup in the fall and the first sampling after melting in the spring. The dissolved solids seemingly lost during winter were recovered gradually in the spring, generally within a period of about 2 months. This paper describes the loss and subsequent recovery of dissolved solids from two ponds in which this phenomenon was especially noticeable, and offers a probable explanation.

GEOHYDROLOGY AND QUALITY-OF-WATER CHANGES

The two pothole ponds are in Dickey and Stutsman Counties, N. Dak. (fig. 1), and have been designated "5" and "C-1" for the pothole-study program. Both are located on the Coteau du Missouri, which is "a topographically high belt of hummocky dead-ice morainal material" (Lemke and others, 1965, p. 15). The land surface is characterized by depressions and grassy hills; maximum local relief is a little more than 250 feet. The ponds studied have gently sloping bottoms and average depths of 4–5 feet. The surface area of pond 5 is about 20 acres and that of pond C-1 about 40 acres. In both ponds, the upper 0.5 foot of bed material is loosely packed and contains much organic matter. This material is so highly porous that it is about 75 percent water by volume and thus stores about a third of a acre-foot of water per acre of pond surface. Both ponds are considered to be clear of vegetation, although a very narrow band of emergent vegetation is present around the edge of each.

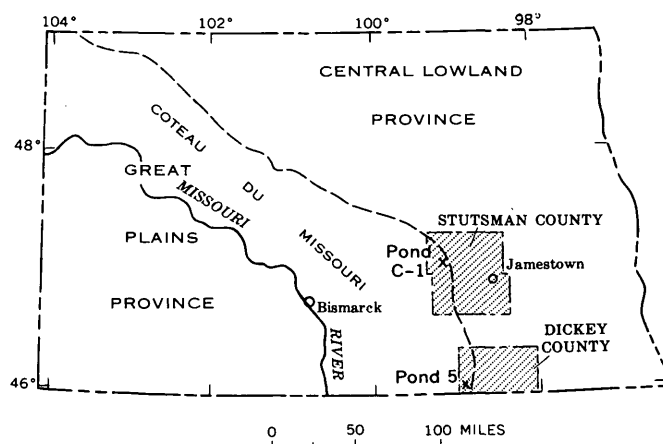


FIGURE 1.—Map of North Dakota, showing physiographic provinces and locations of the prairie-pothole ponds studied.

TABLE 1.—Typical analyses of water from prairie-pothole ponds 5 and C-1, North Dakota

Constituent	Pond 5 ¹ (sample P-5950)		Pond C-1 ² (sample P-8781)	
	Parts per million	Equivalents per million	Parts per million	Equivalents per million
Calcium (Ca)-----	147	7.34	68	3.39
Magnesium (Mg)---	234	19.26	90	7.39
Sodium (Na)-----	105	4.57	252	10.96
Potassium (K)-----	32	.82	50	1.28
Alkalinity (as HCO ₃)-----	288	4.72	324	5.30
Sulfate (SO ₄)-----	1,270	26.44	790	16.45
Chloride (Cl)-----	12	.34	38	1.07
Dissolved solids (residue at 180° C)-----	2,130	-----	1,520	-----

¹ Specific conductance (micromhos at 25°C) was 2,390.

² Specific conductance (micromhos at 25°C) was 2,260.

Typical analyses of water from ponds 5 and C-1 are given in table 1. Expressed as equivalents, magnesium and sulfate are the chief constituents in the water in pond 5, whereas sodium, magnesium, and sulfate are the chief constituents in the water in pond C-1. Water similar in composition to the water in these two ponds characterizes many potholes in this region.

The water volumes (from capacity tables) and the tonnages of dissolved solids for ponds 5 and C-1 are shown graphically in figure 2. These graphs show that during the winter of 1963-64 approximately 25 percent of the dissolved solids in both ponds was in some manner lost, only to be recovered during the first few months of spring. Additional measurements (not shown) for pond 5 indicate that the losses and recoveries that occurred during the winters of 1961-62 and 1962-63 were about the same. None of the decreases from fall to spring can be attributed to spillage because neither pond overflowed its outlet. In neither of the ponds studied could much, if any, of the change in the computed tonnages of dissolved solids be attributed to seepage, although large tonnages might be gained or lost by some ponds in this way. According to W. S. Eisenlohr, Jr. (written commun., July 1, 1965), the results of permeability tests on core samples from the vicinity of pond C-1 and evapotranspiration studies at both ponds indicate that there is virtually no seepage.

SEASONAL VARIATIONS IN DISSOLVED SOLIDS

Because the loss in dissolved solids from the ponds seemed to be closely associated with freezing, measurements of dissolved solids in the ice, water beneath the ice, and bed material were made for both ponds in February 1965. At that time, the ice ranged in thickness

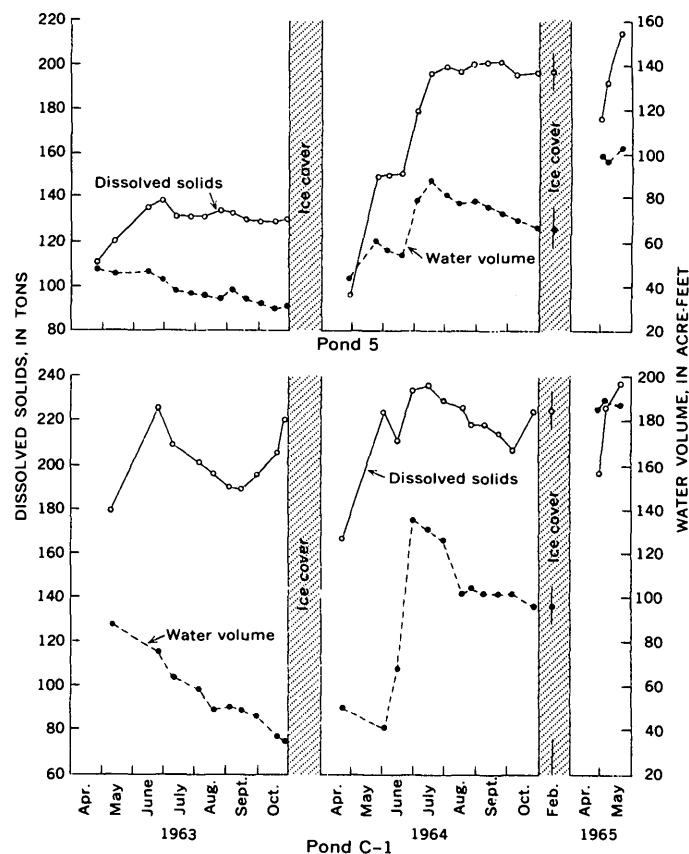


FIGURE 2.—Water volume and tonnage of dissolved solids for ponds 5 and C-1 from April 1963 to May 1965.

from 2.5 to 3.0 feet, and the depth of water under the ice was less than a foot. At some sampling points, there was no water and even the bed material was frozen.

The locations of the sites sampled in February and the concentrations of dissolved solids in the ice at several depths, in the water, and in the bed material are shown in figure 3. In both ponds, the concentration of dissolved solids in the top foot of ice was somewhat erratic, but very low. Below the top foot, the concentration increased sharply with depth, and that of the water beneath the ice was greater than that in the lowest layer of ice. The concentration of dissolved solids in the water from the bed material, however, was less than that in the water above the bed.

Although water constituted only about 10 percent of the total pond volume (ice plus water) for pond C-1 and about 30 percent for pond 5, it contained about 90 percent of the dissolved solids. Obviously, the dissolved-solids concentration in the water under the ice increased progressively and appreciably as the ice cover thickened during the winter.

The average concentrations of dissolved solids (fig. 3) were used to estimate the total tonnages of

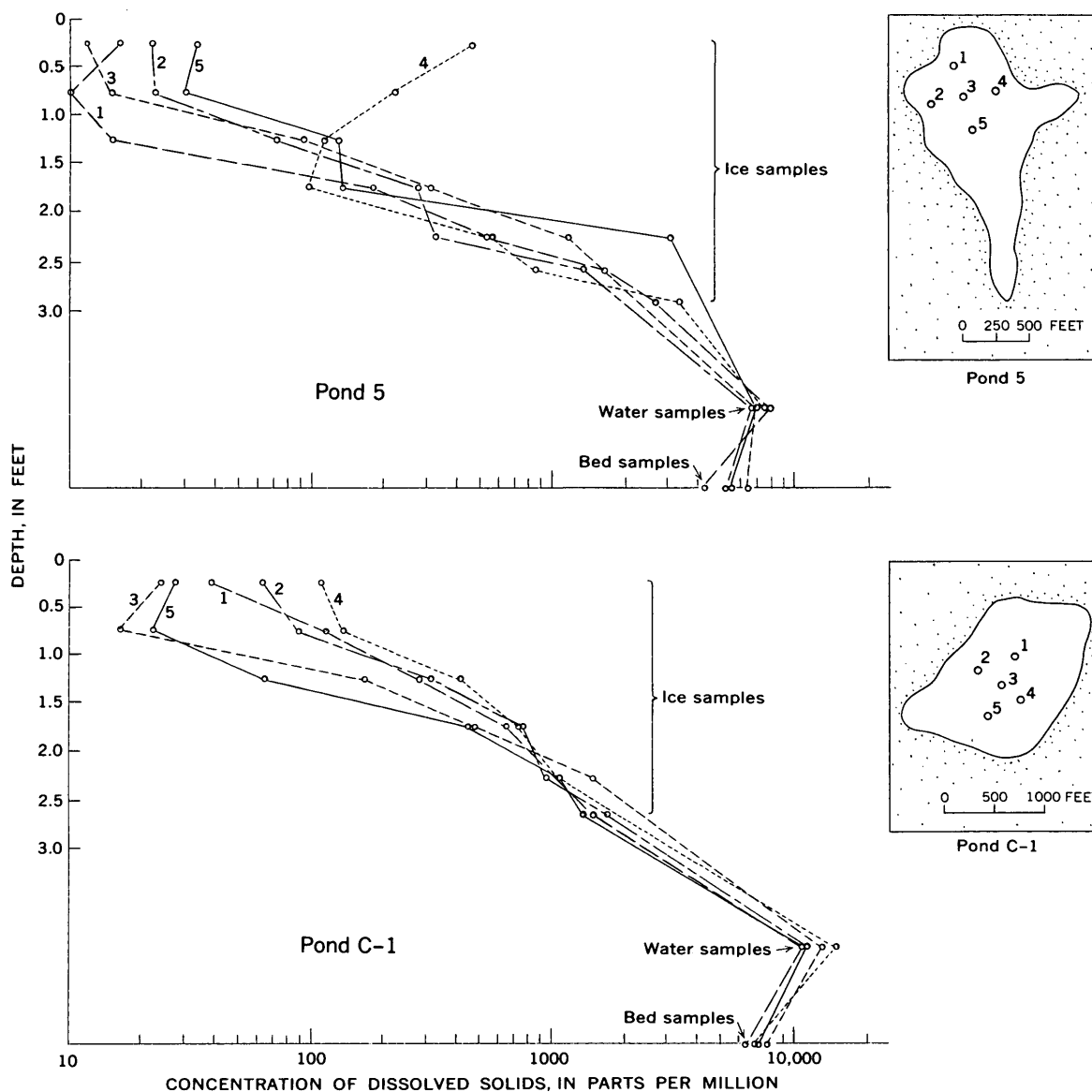


FIGURE 3.—Distribution of dissolved solids in ice, water, and bed material in ponds 5 and C-1 in February 1965. Insert maps show locations of sampling sites. Points on the graphs, except those indicated as water or bed samples, represent samples taken from the ice cover.

dissolved solids in the water and ice of the two ponds in mid-February 1965. These tonnages—197 for pond 5 and 223 for pond C-1—were in close agreement with the tonnages of 197 and 225 computed for late October 1964. The amount of rainfall from October to February was small, so any inflow that may have entered the ponds during the period most likely was from snowmelt, which was low in dissolved solids and relatively small in volume. No significant amounts of water left either of the ponds as runoff over the ice, and, as mentioned earlier, seepage losses were negligible. Consequently, no significant amounts of dissolved

solids either entered or left the pond waters during the period.

The concentrations of dissolved solids in the top half a foot of ice at some places in both potholes (fig. 3) were higher than at slightly greater depths. This unexpected condition may have been the result of one or more of the following: contributions of dissolved solids in small inflows from snowmelt on occasional warm days; increased concentrations due to evaporation from the surface of the ice; and deposition of windblown dust. Whatever the reason, the tonnages of dissolved solids in the top half a foot of ice

were less than 1 percent of the total tonnages and, therefore, had little effect on gains or losses of dissolved solids in the pond waters.

In April 1965, shortly after all the ice had melted, the total tonnage of dissolved solids in pond 5 was 174 and in pond C-1 was 196, decreases of about 15 percent from the tonnages in both October 1964 and February 1965. These tonnages were based on the results for two samples taken from each pond, one near the surface and the other near the bottom. Differences in dissolved-solids concentration between the top and bottom samples from either pothole were insignificant. Similar samples obtained in early May also showed no evidence of stratification in the ponds. It seems reasonable to conclude that most of the decrease in tonnages of dissolved solids occurred after mid-February 1965, presumably during the time the potholes were freezing solid or nearly solid. Of special significance is the fact that the tonnages of dissolved solids in April 1965 were lower than in the previous October and February even though pond volumes were at least 50 percent greater.

The distribution and concentration of dissolved solids in ponds 5 and C-1 were determined again in mid-May 1965. Water samples from several different depths were taken at 6 widely separated verticals in pond 5 and at 4 in pond C-1 for measurement of specific conductance. No differences among the samples greater than that which could be attributed to experimental error were detected; all measurements for pond 5 were $1,800 \pm 20$ micromhos and all for pond C-1 were $1,310 \pm 10$ micromhos. The small range in measurements indicates that in mid-May 1965 the water in both ponds was well mixed both areally and vertically. At this same time the concentrations of dissolved solids in the bed material from 4 sampling points in pond 5 averaged 4,730 parts per million and from 5 sampling points in C-1 averaged 7,870 ppm. These concentrations are much greater than the concentrations in the pond water, which were 1,540 ppm and 929 ppm for ponds 5 and C-1, respectively. Thus, after the ice thawed, the concentration of dissolved solids in the water was less than that in the bed material, the opposite of the condition that existed in February 1965.

INTERPRETATION OF SEASONAL VARIATIONS

Some of the loss and recovery of dissolved solids may be due to precipitation of salts as the pond water

freezes in the fall and to re-solution of the salts as the ice melts in the spring. Precipitation and re-solution, however, are not likely to be the principal causes of the loss and recovery. No salt crystals were observed on cursory examination of the bed-material samples. Possibly some crystals formed in the ice phase where the ice extended into the bed of the pond. In any case, had salt crystals been present, they most likely would have been relatively soluble sulfate salts that would have redissolved quickly.

A more likely explanation, then, for the apparent decrease in the tonnages of dissolved solids from fall to spring and the slow recovery of the tonnages in the spring is temporary storage of dissolved solids in a water or ice phase of the bed material. As indicated by the analyses of the February 1965 samples, freezing of the ponds results in a gradual increase in the concentration of dissolved solids in the water beneath the ice and establishment of a gradient favorable for an increase in the concentration of dissolved solids in the bed material. So long as ice continues to form, the gradient may induce migration of dissolved solids, probably by diffusion, into the bed material. Then, when the ice has melted, the gradient is reversed and dissolved solids in the bed material may migrate back into the water.

Under certain circumstances, diffusion can be a slow process; a rather slow rate of diffusion could account for the long time required for recovery by the water of the tonnages "lost" in the late winter. It is also possible that formation of ice within the bed material increases the length of time needed for recovery of dissolved solids by the pond water. At least in some parts of the ponds, ice in the bed material is the last to melt in the spring and may exist for some time after the pond ice has melted. Obviously, dissolved solids trapped in or below the frozen bed material cannot diffuse into the pond water until the bed material also thaws.

REFERENCES

- Lemke, R. W., Laird, W. M., Tipton, M. J., and Lindvall, R. M., 1965, Quaternary geology of northern Great Plains in the Quaternary of the United States: Princeton, N.J., Princeton Univ. Press, p. 15-25.
- Shjeflo, J. B., and others, 1962, Current studies of the hydrology of prairie potholes: U.S. Geol. Survey Circ. 472, 11 p. [1963].



HYDROGEOLOGIC SIGNIFICANCE OF CALCIUM-MAGNESIUM RATIOS IN GROUND WATER FROM CARBONATE ROCKS IN THE LANCASTER QUADRANGLE, SOUTHEASTERN PENNSYLVANIA

By HAROLD MEISLER and ALBERT E. BECHER, Harrisburg, Pa.

Work done in cooperation with the Pennsylvania Geological Survey

Abstract.—The ratios in equivalents of calcium to magnesium in ground water from the limestones and dolomites of the Lancaster quadrangle in southeastern Pennsylvania correlate well with the composition of the carbonate source rocks. The lowest calcium-magnesium ratios occur in water from dolomite; the ratios are very close to the stoichiometric proportion of calcium to magnesium in the mineral dolomite. The highest calcium-magnesium ratios are in water from limestone. In ground water from interbedded limestone and dolomite, the calcium-magnesium ratios are between those in water from limestone and those in water from dolomite. When applied with caution, calcium-magnesium ratios in ground water can be an aid to geologic mapping of a limestone and dolomite terrane.

During a study of the geology and hydrology of the carbonate rocks of the Lancaster quadrangle in southeastern Pennsylvania (see fig. 1), a close relationship

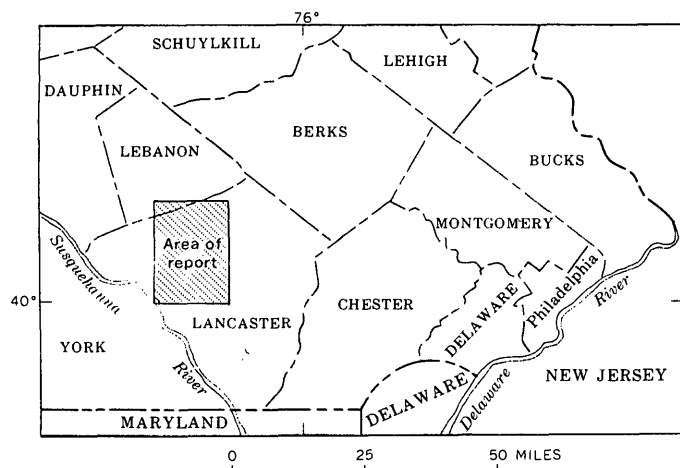


FIGURE 1.—Map of southeastern Pennsylvania, showing the Lancaster quadrangle (patterned).

was observed between the ratio of equivalents of calcium to magnesium in ground water and in the composition of the source rocks. Data from this study substantiate Hem's (1959, p. 82) suggestion that high calcium-magnesium ratios are obtained from relatively pure limestones and that low ratios are obtained from dolomitic rocks. The data also corroborate Foster's (1942, p. 651) statement that "dolomite yields water that contains practically equivalent amounts of calcium and magnesium."

The carbonate rocks studied are of Cambrian and Ordovician age and occupy a broad belt that trends east-west across the Lancaster quadrangle (see fig. 2). The structure of the rocks is complex, as the strata are intensely folded and, in places, intricately faulted. In general, progressively younger strata crop out northward across the area, although faulting has caused some stratigraphic units to be repeated. The Conestoga Limestone, possibly the youngest carbonate-rock formation in the quadrangle, unconformably overlies older formations in the southern part of the quadrangle.

Chemical analyses of ground water from 45 wells tapping 5 stratigraphic units furnish the calcium-magnesium data used in this paper. The five stratigraphic units studied in this paper are described in table 1. The descriptions are based on field examinations.

GEOLOGIC DISTRIBUTION OF CALCIUM-MAGNESIUM RATIOS

Cumulative-frequency-distribution plots of the ratios of calcium to magnesium (equivalents per million) in ground waters from the carbonate rocks are shown in



FIGURE 2.—Generalized geologic map of the Lancaster 15-minute quadrangle, Pennsylvania.

TABLE 1.—Description of stratigraphic units in the Lancaster quadrangle, Pennsylvania

System	Stratigraphic unit ¹	Description	Number of ground-water samples
Ordovician	Conestoga limestone	Medium-gray limestone containing shaly partings locally; schistose limestone; limestone conglomerate near the base; dolomite present locally near the base.	14
	Epler Formation	Very light gray to medium-gray limestone, contains some interbedded medium-gray dolomite and calcareous dolomite.	13
	Stonehenge Formation	Medium-gray limestone; scattered shale laminae; dolomite rare.	7
Cambrian	Unnamed dolomite ²	Light- to medium-gray dolomite; sandy dolomite abundant locally; scattered sandstone beds; limestone rare but occurs locally.	5
	Ledger and Vintage Dolomites ³	Very light gray to medium-gray, mottled, massive pure crystalline dolomite.	6

¹ Stratigraphic units not referred to in this report are not shown in this table.
² Geologic mapping is not completed; hence some stratigraphic units have not been named yet.
³ The Ledger and Vintage Dolomites are similar in appearance in the Lancaster quadrangle and are combined in this paper.

figure 3. The ratios are grouped by stratigraphic unit and show that the lowest calcium-magnesium ratios occur in the dolomite units, the highest ratios occur in the limestone units, and intermediate ratios occur in interbedded limestone and dolomite.

Within stratigraphic units, no areal trends of calcium-magnesium ratios appear to be present. The presence of vertical trends cannot be ascertained because of a lack of pertinent data.

The plot on a single straight line of the dolomite units indicates that they are normally distributed and have been drawn from a single population. The flat slope of the line indicates the small variability of the data. The mean calcium-magnesium ratio is 1.09, and the standard deviation is 0.10.

Calcium-magnesium ratios in ground water from the dolomite units are very close to the stoichiometric proportion of calcium to magnesium in the mineral dolomite. Thus the scarcity of calcite observed in field mapping is corroborated by the chemistry of the ground water.

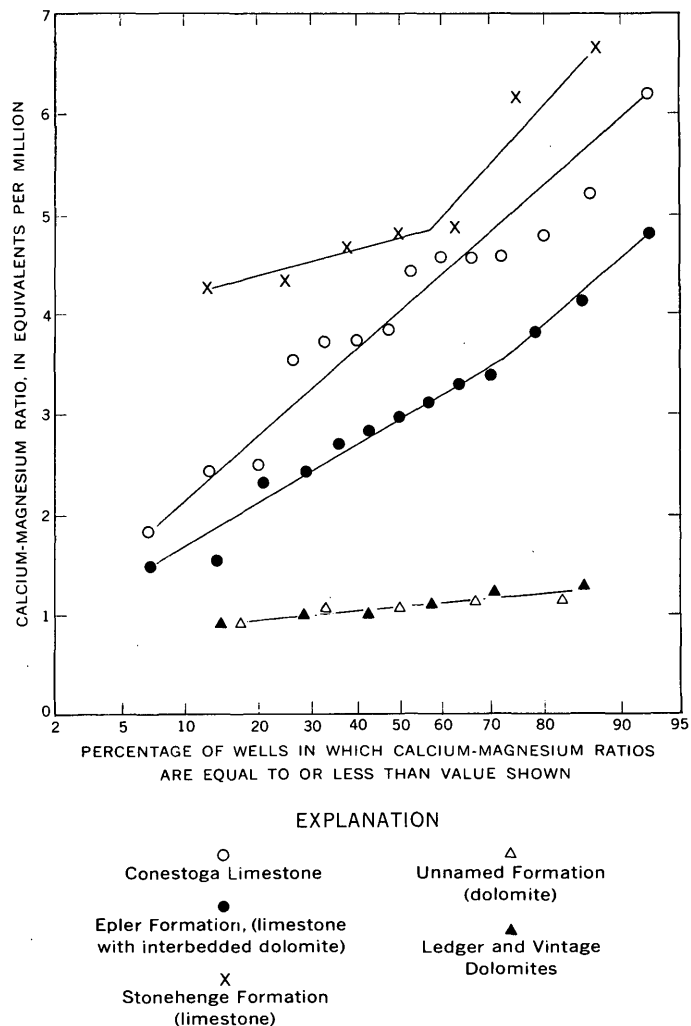


FIGURE 3.—Cumulative-frequency distribution of calcium-magnesium ratios in ground water from wells grouped according to stratigraphic unit.

Calcium-magnesium ratios of water from the limestones are considerably higher than those of water from the dolomites and are more variable. Their distribution is also less normal. In ground water from the Conestoga Limestone, the mean calcium-magnesium ratio is 4.00 and the standard deviation is 1.13. In the Stonehenge Formation, the mean calcium-magnesium ratio is 5.09 and the standard deviation is 0.85.

The relatively large variation of calcium-magnesium ratios in ground water from the limestone wells may be attributed to more than one reason, though variability in the magnesium content of the rocks is probably the principal reason. In addition, the magnesium content of shale laminae, which are locally abundant, may lower the calcium-magnesium ratio. Magnesium enrichment may also occur in ground water which has traveled long distances and reached equilibrium with

respect to the more soluble calcite but not with respect to the less soluble dolomite. In such waters the minor amounts of dolomite in the rocks may continue to be dissolved while little or no calcite is being dissolved. Such a mechanism may explain the low calcium-magnesium ratios reported from predominantly limestone terranes in Florida (Hsu, 1963, p. 288).

Calcium-magnesium ratios of ground water from the interbedded limestone and dolomite of the Epler Formation are intermediate between the ratios of limestone waters and the ratios of dolomite waters. The plot of calcium-magnesium ratios on a nearly straight line indicates a normal distribution. The mean calcium-magnesium ratio is 2.98 and the standard deviation is 0.91.

CONCLUSIONS

Calcium-magnesium ratios in ground water in the Lancaster quadrangle are clearly related to the composition of the carbonate source rock. This close relationship makes possible the use of calcium-magnesium ratios as a valuable tool in the study of carbonate rocks.

In areas where the carbonate rocks are unmapped, the calcium-magnesium ratios are of value both in mapping geologic formations and in delineating lateral facies changes within a formation. The ratios can be used only where it is known that the rocks through which the water moved are predominantly of one rock type and that the water has not traveled far enough to allow saturation and subsequent precipitation of calcite.

In areas where the geology is already known, the calcium-magnesium ratios are helpful in identifying the aquifer from which the water is obtained or in recognizing that the water is from two or more aquifers.

REFERENCES

- Foster, M. D., 1942, Chemistry of ground water, in Meinzer, O. E., ed., *Physics of the earth*, pt. 9, Hydrology: New York, McGraw Hill Book Co., p. 646-655.
- Hem J. D., 1959, Study and interpretation of the chemical characteristics of natural water: U.S. Geol. Survey Water-Supply Paper 1473, 269 p.
- Hsu, K. J., 1963, Solubility of dolomite and composition of Florida ground waters: *Jour. Hydrology*, v. 1, no. 4, p. 288-310.



SHORELINE FEATURES AS INDICATORS OF HIGH LAKE LEVELS

By DARWIN D. KNOCHENMUS, Ocala, Fla.

Work done in cooperation with the Florida Geological Survey

Abstract.—A relation between certain shoreline features (tree line of the slash pine, beach scarp, beach ridge) and high lake levels was found on eight Florida lakes. For the lakes studied, the features were above the lake level an average of 95 percent of the time. An estimate of former high levels of ungaged lakes can be made from this relation. Grain-size analyses of the material comprising the various geomorphic features show a consistent relation between median diameter and the type of feature. In order of decreasing median grain size, material of the high beach ridge is followed by that of the low beach ridge, the upland, and the base of the beach scarp. This relation helps separate areas which have been under the influence of wave action from those which have been above the water level.

It has been variously reported that Florida has about 30,000 natural lakes (Florida Water Resources Study Commission, 1956, p. 24). Records show that a few of these lakes have wide ranges in level, whereas some range but little. During the past 20 years, many of the lake shores have been developed for homesites, and this development is increasing steadily. On some lakes that have a wide range in levels, homes have been built during periods of low level, and later, at high lake levels, lawns, buildings, and septic tanks have suffered from flooding. Criteria are needed for determining the approximate level of past high stages at ungaged lakes.

Preliminary observations suggested that certain shoreline features that are related to lake level could be recognized and could be used to delineate the position of former high lake levels. To define the relation between these features and lake levels, eight Florida lakes were selected for study on the basis of their diverse physical characteristics and the availability of a long-term record. The eight lakes are located in figure 1, and their characteristics and periods of record are listed in table 1.

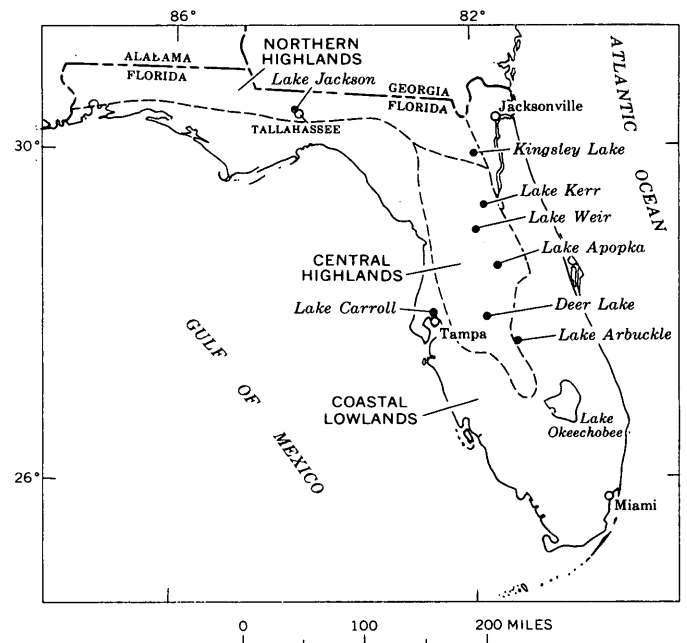


FIGURE 1.—Map of Florida, showing location of selected lakes and physiographic divisions.

The growth pattern of slash pine and the elevations of beach scarp and beach ridges were studied in relation to lake levels. Elevations of the shoreline features were measured to the nearest one-tenth of a foot with a hand level and range pole. Numerous measurements were made on each lake to obtain an average elevation for each type of feature. Samples of surficial material were collected for size analysis along profiles from the beach ridges to the upland. A stage-duration curve was prepared from the long-term record for each of the eight lakes. The duration curve shows, for the period of record involved, the percentage of time that the lake surface was at or above a given level.

TABLE 1.—Characteristics of selected lakes in Florida

Name	Location		Area (sq mi)	Shape ²	Depth (ft)	Elevation (feet above mean sea level)		Records used	Control of outlet	Remarks
	County	Physiographic division ¹ (fig. 1)				Maxi-mum	Mini-mum			
Kingsley	Clay	NH	2.5	C	85	177.8 (1950)	174.3	1947-63 weekly mean.	Concrete weir at elevation of 176 ft.	Circular sinkhole lo- cated on the east- ernmost ridge of the Northern Highlands. Shore is highly developed with private homes and a military post.
Kerr	Marion	CH	4.0	I	15	26.6 (1948)	19.9	1936-51, 1956- 65 weekly mean.	No outlet; con- nected to another lake by narrow canal.	Lake on a broad gen- eral upland on the east flank of the Central Highlands.
Weir	do	CH	8.5	C	30	59.6 (1938)	53.5	1937-63 month- ly mean.	Broad crested weir at eleva- tion of 57.4 ft.	Sink surrounded by smaller sinkhole lakes on a broad general upland of the Central High- lands.
Apopka	Orange and Lake.	CH	48	C	15	69.3 (1936)	64.0	1943-63 daily mean.	Lock and dam structure with fixed weir at eleva- tion of 67 ft.	Lake at the end of a large valley, sur- rounded on three sides by ridges of the Central High- lands.
Deer	Polk	CH	.2	C	-----	141.9 (1960)	138.1	1947-64 weekly mean.	18-in. culvert at elevation of 139.2 ft.	Lake surrounded by numerous sinkhole lakes on a ridge which rises above the general uplands of the Central Highlands.
Arbuckle	do	CL	5.9	E	10	58.3 (1948)	51.4	1942-64 daily mean.	None; Arbuckle Creek flows out of lake.	Lake located on up- land of the Coastal Lowlands.
Carroll	Hillsborough	CL	.3	I	-----	40.1 (1947)	32.4	1946-64 weekly mean.	Partial control by culvert.	Lake on a karst plain. Development around lake is com- plete. Shoreline has been completely re- worked and changed.
Jackson	Leon	NH	6.2	I	-----	³ 95.2 (1965)	75.7	1950-65 5-day read- ings.	No outlet	Lake with a highly ir- regular shoreline surrounded by high hills interspersed with smaller lakes and depressions.

¹ After Puri and Vernon (1964). NH, Northern Highlands; CH, Central Highlands; CL, Coastal Lowlands.

² C, circular; I, irregular; E, elongate.

³ Level was higher in 1966.

PATTERN OF SLASH PINE GROWTH

One of the most prominent biologic features that is influenced by the lake level is the growth pattern of the slash pine (*Pinus elliotte* Egeln). The pattern of the tree line runs parallel to the shoreline. An aerial photograph of a lake in central Florida (fig. 2) shows the tree line distinctly. Landward of this line, mature slash pine grow; lakeward of the line, only immature trees, both living and dead, are present. The tree line develops during periods of high water when the trees

are killed below a certain elevation. During periods of low water the slash pines germinate and grow on an area of the shore which previously was under water. Before the seedlings can grow to maturity at this lower level, they are killed during the next period of high water which may or may not affect the mature trees established at the higher level. After the seedlings are killed they remain standing for a few years. New seedlings germinate, giving rise to the presence of both living and dead immature trees below the tree line.

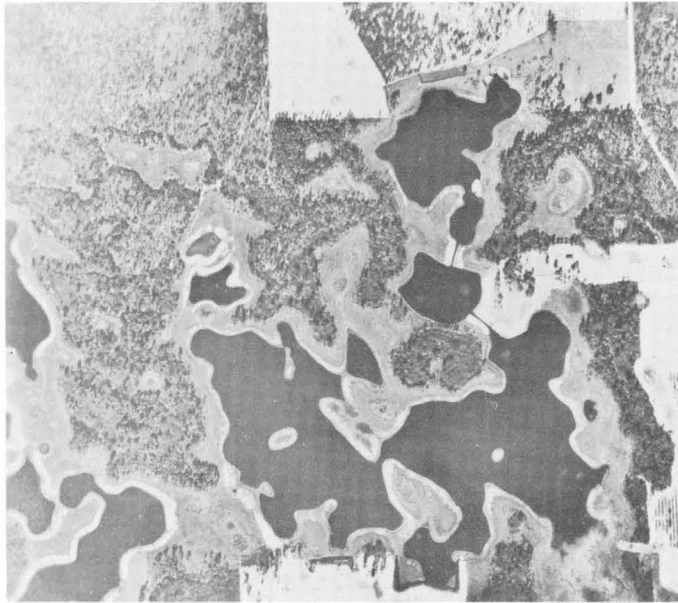


FIGURE 2.—Aerial photograph showing tree line around central Florida lakes.

BEACH SCARPS AND RIDGES

Two miniature geomorphic features, a beach scarp and a beach ridge, both of which have counterparts on large bodies of water, were found on Florida lake-shores (fig. 3). Their origins also can be attributed to the stand of the lake at that particular level.

The beach scarp is a miniature cliff cut into the lake-shore by wave action. A scarp developed at a low lake level would soon be obliterated by erosion and deposition during periods of higher levels. The beach scarp which remains records the highest level at which the lake eroded the shore, but it is not necessarily the highest level attained by the lake. The base of the scarp is developed at a level slightly below the maximum lake level attained. In this study, the highest beach scarp was found to coincide with a high level infrequently reached by the lake. Above the beach scarp—which has an almost vertical slope—is a more

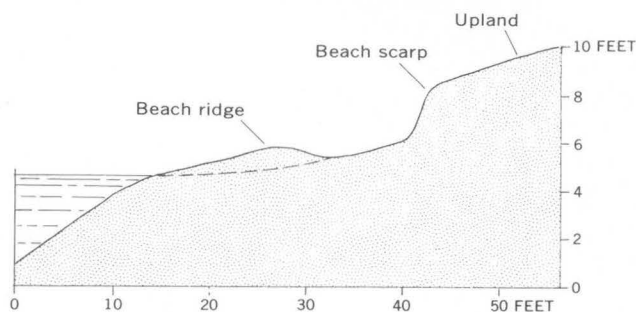


FIGURE 3.—Typical profile of the beach of Kingsley Lake. Arbitrary datum.

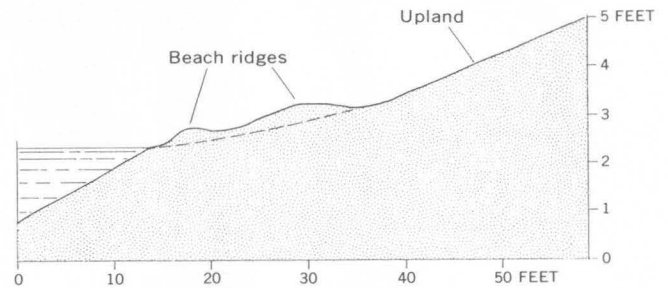


FIGURE 4.—Typical profile of beach ridges on Lake Kerr. Arbitrary datum.

gentle upland slope, which was developed by mass movement; below the base of the beach scarp the surface also has a gentle slope, which is smooth to undulating where beach ridges have formed (see fig. 3).

Beach ridges are found at all levels (fig. 4), but only the highest ridge is of importance in determining former high lake levels. The beach ridge is a depositional feature on the wave-cut slope. It has a convex shape and is asymmetrical with its apex offset landward. The average height of a typical ridge is about half a foot. Between ridges, and landward of the highest ridge, are shallow troughs, much like the depression that is found landward of the berms along large bodies of water. The crest of the highest ridge is slightly lower in elevation than the maximum lake level attained. However, as with the beach scarp, the crest elevation of the highest ridge coincides with a high level infrequently reached by the lake.

Not all the above described features are found near every lake. Where man has developed and changed the shoreline, the natural features are either absent or have been so altered that they no longer bear the same relation to the lake level.

DISCUSSION OF RELATION BETWEEN SHORELINE FEATURES AND LAKE LEVELS

The development of a shoreline feature involves an element of time. For example, in the development of the tree line, the water must remain at or near the tree line long enough to kill the trees. In Florida, most lakes do not stand at their maximum level but for a brief period; therefore, the most pronounced shoreline features develop at a level lower than the maximum. The relation between the maximum lake level and the occurrence of the more prominent shoreline features is somewhat dependent upon the character of the lake. A closed lake will remain near its maximum level for a longer time than a lake which has a surface drainage outlet. Even though the shoreline features studied here develop most prominently at levels lower

than the maximum level, they were found to coincide with relatively high lake levels.

The average elevation for each type of shoreline feature, when plotted on a stage-duration curve, falls toward the upper end of the curve (fig. 5). The average percentage of time that the lake level equalled or exceeded the tree line is 5 percent, determined by averaging the percentage of time corresponding to the elevation of the tree line on all curves. The average percentage of time that the lake level equalled or exceeded the level of the beach scarp was 5 percent, and for the beach ridge it was 6 percent. These features are indicators of a relatively high water level because they are, on the average, above the water level 95 percent of the time.

The elevation of the tree line on Kingsley Lake was the only feature to plot above the stage-duration curve. It averaged three-tenths of a foot above the 0.1 percent on the stage-duration curve. With the exception of Lake Carroll, the elevation of the beach ridge on Lake Weir plotted lowest on the stage-duration curve (highest percentage). It was reached or exceeded by the lake level 12 percent of the time. The elevation of the beach ridge on Lake Carroll (fig. 5) plots near the middle of the curve. Within the past 5 years the shoreline has been developed for a residential area and, therefore, the tree line, beach scarp, and beach ridges have been destroyed, and the existing beach ridge indicates high water only during the last 5 years.

At least 2 types of shoreline features were mapped at 6 of the 8 selected lakes. Lake Carroll, which was one of the lakes where only one type of feature was found, has a shoreline altered by manmade construction. At a particular lake, each type of feature was found to differ slightly in elevation from the other types. This small difference in elevation, between the feature having the lowest elevation and that having the highest elevation, ranged from 0.1 foot at Lake Kerr to 1.9 feet at Lake Jackson. With the exception of Lake Jackson, at all the lakes where two or more features were found there was less than 0.8 foot of difference in elevation between them. Small differences such as these are believed to result from the various types of shoreline features that develop at different times and under different conditions. Water must be in motion to form the geomorphic features, while either quiescent or turbulent water may be involved in the formation of a tree line. The time interval necessary to develop a geomorphic form is dependent upon the energy level of the water. Under low-energy conditions it may take longer to develop the geomorphic scarps or ridges than to develop the tree line, and under high-energy conditions the converse may be

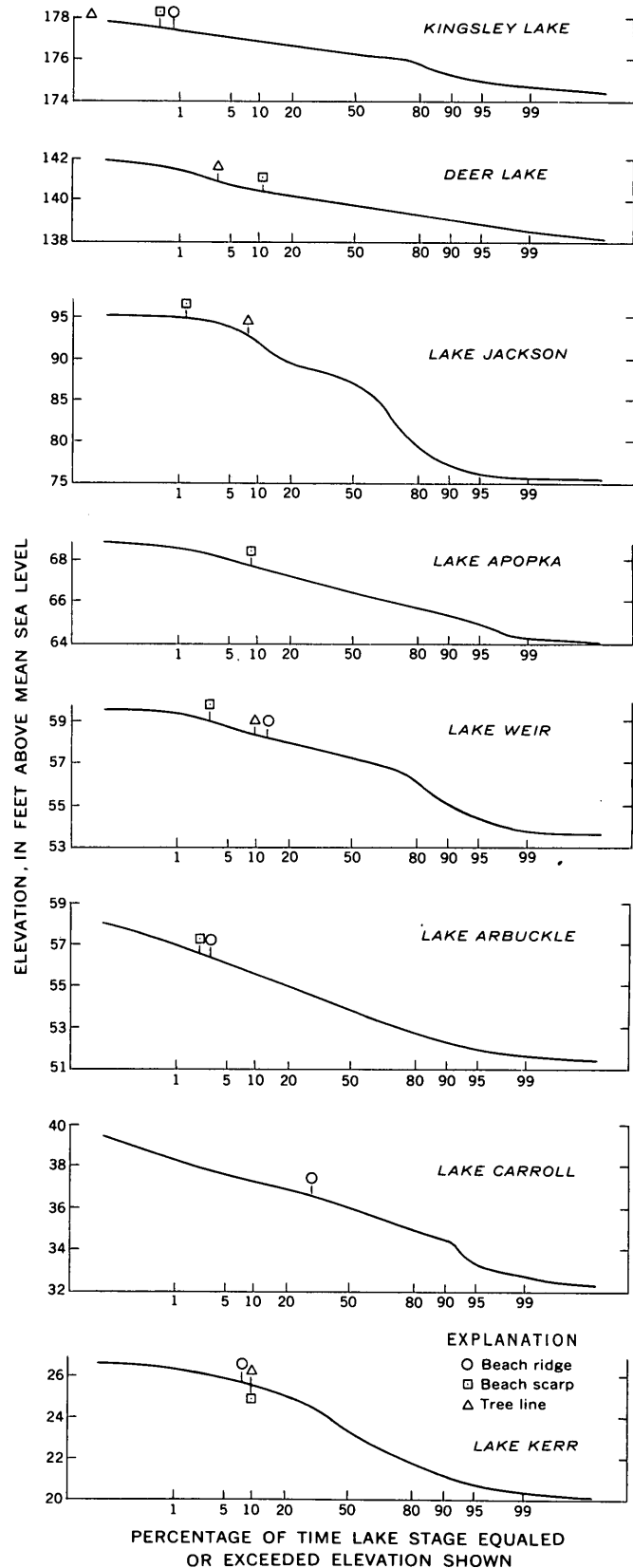


FIGURE 5.—Stage-duration curves of selected lakes, showing the relationship between lake stage and shoreline features.

true. This could account for the geomorphic features being at a slightly higher level than the tree line on some lakes and at a slightly lower level on others. Lake Jackson has a relatively large range in stage, more than 25 feet, which could account for the greater difference in the elevations of its shoreline features.

SIZE ANALYSES OF GEOMORPHIC FEATURES

In addition to the elevation of geomorphic features, the character of the material of the features was investigated. Borings were hand augered in the low beach ridges, high beach ridges, bases of beach scarps, and on the upland; along profiles normal to the lake shore. Samples of the surficial material were collected, and mechanical analyses were made from which size frequency curves were drawn. The surficial material in Florida is predominantly well-sorted sand. The average sorting coefficient for all samples analyzed is 1.32, which indicates well-sorted material. A sample which has a sorting coefficient of 1.0 would contain grains of only one size. The geomorphic features were developed from well-sorted parent materials having characteristic median grain sizes. The median is that size for which 50 percent of the material, by weight, is larger and 50 percent is smaller or, on a cumulative frequency curve, the size corresponding to the point where the 50-percent line crosses the curve (Pettijohn, 1957, p. 36). A relation between median grain size and geomorphic feature was determined from 10 profiles at 5 lakes. The material in the high beach ridge has the largest median grain diameter, followed by material from the low beach ridge, the upland, and the base of the beach scarp, which is composed of grains of the smallest median diameter (fig. 6). An average of all the samples shows a median grain diameter of 0.45 mm for the high beach ridge; 0.38 mm for the low beach ridge; 0.30 mm for the base of the beach scarp, and 0.34 mm for the upland.

The sorting of material by size is accomplished by the geologic processes of mass wasting and wave action. The geomorphic features are made up of material derived from the upland. As the waves cut into the upland forming the beach scarp, the material is moved downslope, it is reworked, and some is deposited as the beach ridge. The highest beach ridge consists of the coarsest material because some of the finer material is moved farther downslope. Therefore, the low beach ridge consists of finer material than that in the

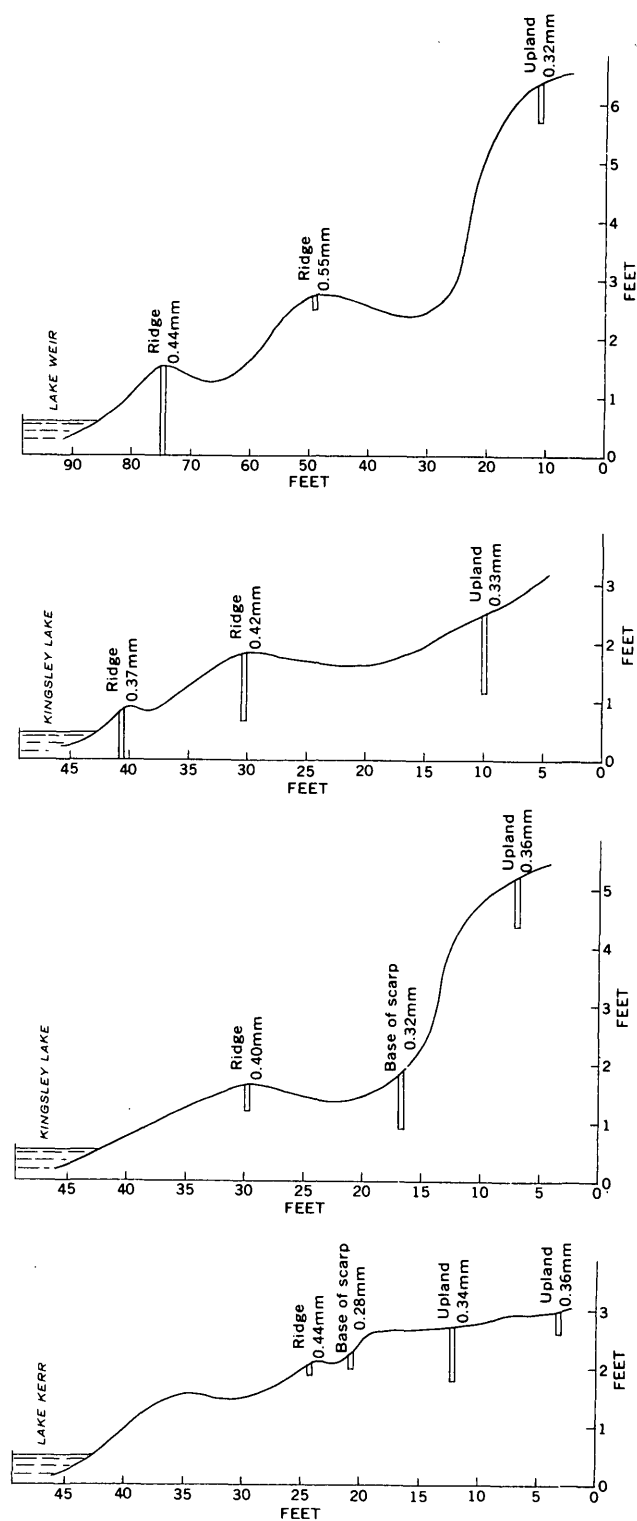


FIGURE 6.—Selected profiles of lake shores, showing the median diameter of the sediment from various geomorphic features. Arbitrary datum.

high beach ridge, and the finest material is found at the base of the beach scarp. After the scarp is developed and the lake level falls, fine material moves down the slope by mass wasting, and it is deposited at the base of the beach scarp.

The usefulness of the median grain size for determining former high lake levels is in identifying obscure shoreline features and in locating the transition zone between the upland area and the area which has been under the influence of the wave action.

CONCLUSIONS

Certain shoreline features—the tree line, the beach scarp, and the high beach ridge—develop when there is a relatively high water level on lakes in Florida. During the period of record for the 8 lakes studied, the level of the shoreline features was equalled or exceeded an average of only 5 percent of the time. Thus the shoreline features may be used to estimate the elevation of former high water levels for natural lakes where long-term records are lacking. Furthermore, a consistent relationship was found among the median grain diameters of the sands comprising the various geomorphic features of the shoreline. The finest material is found at the base of the beach scarp, followed

by the low beach ridge, upland, and the high beach ridge, which contains the coarsest material. This relation helps identify obscure shoreline features and may be used to distinguish the zone which has been reworked by the waves from that which has been above the lake level.

The shoreline features are somewhat temporary and are suggested as high-water indicators only for historic time. They cannot be used to indicate high water levels during recent geologic time. Perhaps the features can be used to indicate high water during the past century. Numerous measurements and observations of each type of feature should be made, and the most logical interpretation of all the features should be used. On lakes where man has destroyed the natural shoreline features, however, this method of determining former highwater levels will not work.

REFERENCES

- Florida Water Resources Study Commission, 1956, Florida's water resources: 94 p.
- Pettijohn, F. J., 1957, Sedimentary rocks, 2d ed.: New York, Harper and Brothers, 718 p.
- Puri, H. S., and Vernon, R. O., 1964, Summary of the geology of Florida and a guidebook to the classic exposures (revised): Florida Geol. Survey Spec. Pub. 5, 312 p.



MAGNETIC TAPE RECORDING OF GEOPHYSICAL LOGS

By W. SCOTT KEYS, Denver, Colo.

Abstract.—An inexpensive magnetic tape system has been developed and used for recording geophysical well logs. The unmodified signal from a logging probe is recorded simultaneously with the conventional graphic log. During tape playback, all adjustments normally made during logging are possible. These include independent changes in horizontal scale, vertical scale, zero positioning, and time constant. Use of this system reduces the time spent at the well. Correction of operator errors and equipment malfunctions can be done in the office, and logs can be plotted at any time in a format consistent with the planned use. This system also provides for the economical storage and retrieval of data.

The standard method of recording geophysical data derived from logs of drill holes is a graphic analog representation. This is usually a pen-and-ink record of the signal received from the probe, modified by the logger electronics at the surface, and plotted against hole depth. The graphic log is subject to many control adjustments, operator errors, and equipment malfunctions and is not amendable to correction or modification. In order to make better use of data from oil wells, logging service companies within the last few years have introduced digital tape recording of logs. Punched paper tape was used at first; now (1967), however, the trend is toward digital magnetic tape that is compatible with most computer systems (Tinch and others, 1966). At present, these multichannel digital tape systems are not widely used in hydrology. Also they cost more than the conventional electric and gamma loggers employed by the U.S. Geological Survey in water-resources studies. For this reason, an inexpensive magnetic tape recording system that will permit the rapid conversion of logs to a digital format at a later time was developed; it provides advantages not inherent in the existing digital systems. Because such equipment was not available commercially it was developed within a U.S. Geological Survey research project on borehole geophysics as applied to geohydrology. The system was developed and built

by Edwin R. Bullard, Jr. (written commun., 1966). Basically it differs from the service company taping system in that it records raw pulses instead of digitizing an analog signal.

Since feasibility studies and preliminary tests in 1965, the system has been permanently installed in the U.S. Geological Survey research logging equipment illustrated in figure 1. It is used routinely to record and modify natural gamma, gamma-gamma, neutron-gamma and neutron-epithermal neutron logs. The equipment also makes it possible to record fluid temperature, fluid-resistivity, short and long normal resistivity, sonic velocity, and impeller-flowmeter logs. In addition, planned modifications to the equipment will permit the recording of caliper, single point resistivity, and spontaneous potential logs.

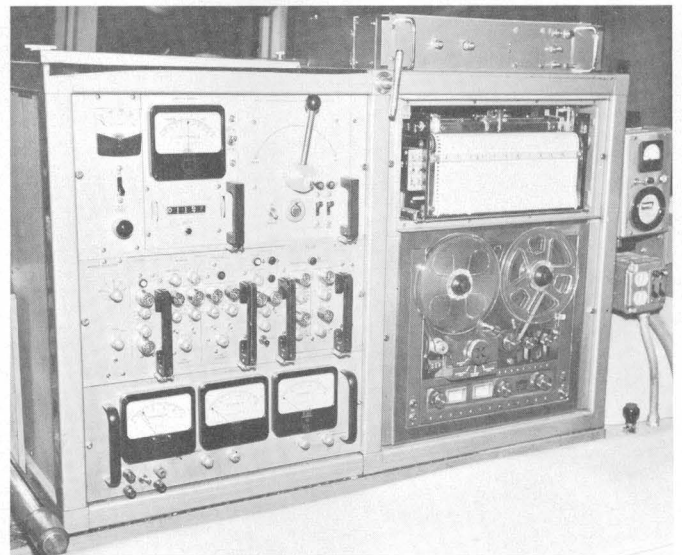


FIGURE 1.—Control panel for research logging equipment. Control modules (center left) are used for adjusting original graphic logs and tape playback logs. On the right side, from bottom to top, are the tape recorder, graphic recorder, and pulse-to-footage converter.

DESCRIPTION OF EQUIPMENT

With the exception of the pulse-to-footage converter, the tape recording and playback system is relatively simple. An inexpensive two-track stereo tape recorder is used without modification. Pulses as received from the various probes are recorded on the data track (or channel) and a cable-footage signal is recorded on the other channel. The logging-equipment operator records a vocal description of the well and the logging parameters on either channel.

The basic principles of the tape recording and playback system are shown in figure 2. The raw-data output, in the form of pulses from a logging probe, is split between the tape and graphic recorders at the upper end of the cable. Pulses from the cable are recorded on the data track of the tape, unmodified by any operator adjustments. At the same time, equivalent

pulses are also input to the logger control module, which is essentially a pulse to direct-current converter. The operator can make adjustments that will modify the conventional graphic log, which include recorder amplifier gain, resistor-capacitor time constant, pulse energy discrimination, basing or zero positioning, sensitivity or horizontal scale, and vertical scale in feet of hole per inch of paper. None of the adjustments affect the data being put on the tape at the well, and all the adjustments may be made during later playback of the magnetic tape. Whenever the equipment is operating, the graphic log is always made along with the tape recording because of its value in preliminary field interpretations.

A most important part of the system is devoted to synchronizing the position of a probe in the hole with the data being recorded on tape. A cam and switch are driven by the cable measuring sheave on the logger. The switch activates a 1-kilocycle oscillator that produces a beep on the footage track of the tape for each 6 inches of hole traversed by a probe. For example, the radiation pulses received when the probe travels from a depth of 100 feet to 99.5 feet are recorded on the data track between two beeps on the adjacent footage track. In this manner, the pulse data representing a given interval of hole are properly tagged in space regardless of how fast the tape is moving.

Playback from the tape may be done in the field or the office with either a large research logger or a recently designed "minilogger" that is mounted in a suitcase. Once the controls are set, a new graphic log is automatically plotted without being attended. The graphic recorder starts and stops at the proper places exactly as it did under operator control at the well. Controls adjusted during tape playback are the same ones that the operator used to make the original log. The only part of the tape system that required considerable developmental research is the pulse-to-footage converter through which the 1-kc beeps from the footage track are fed to automatically drive the graphic recorder.

The electronic section of the pulse-to-footage converter receives the 1-kc signal from the preamplifiers of the tape recorder and converts it to a d-c voltage that operates a relay which in turn starts a mechanical train in motion. The train is powered by a free-running 120-revolutions-per-minute motor which is coupled to an electric clutch, an electric brake, and a cam, with two valleys, which turns a selsyn transmitter. When a 1-kc beep is received from the tape, a relay is opened which in turn opens a second relay.

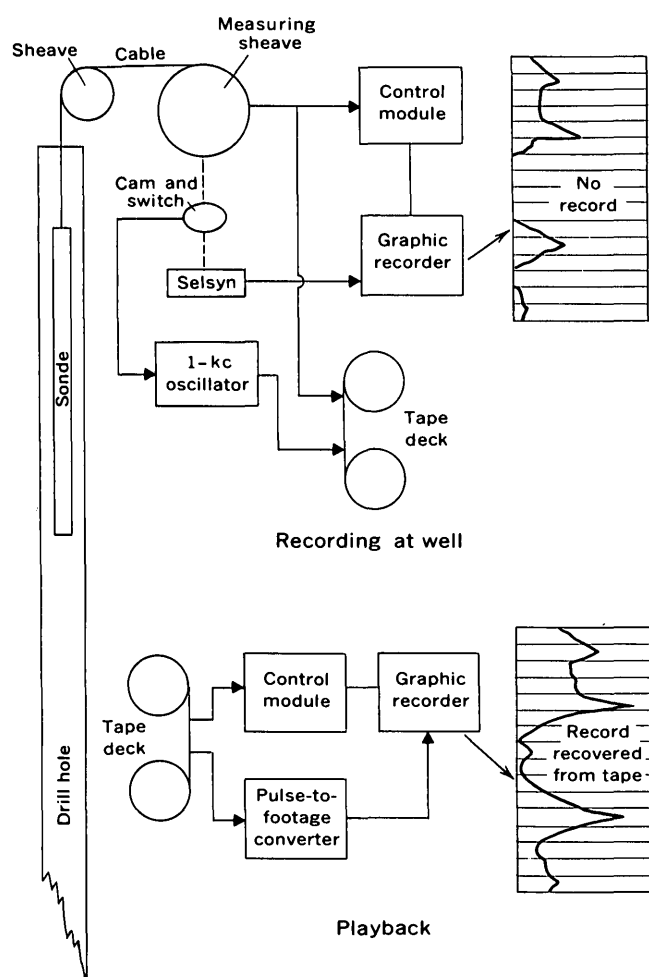


FIGURE 2.—Magnetic tape recording and playback system. Sample logs show how information lost by operator basing, or zero-adjustment, error can be recovered from tape.

The second relay switches power from the electric brake to the electric clutch, allowing the cam to turn. While the cam is turning toward the next valley, the first relay closes; when the cam arrives at the next valley, the second relay is closed and power is switched from the clutch back to the brake. This cam has the same number of valley positions as the cam on the logger and is directly coupled to a selsyn transmitter. Therefore, each half revolution of the selsyn is equal to half a foot of hole depth, as on the logger. The selsyn transmitter drives the receiver selsyn on any graphic recorder exactly as it does when logging a well.

The pulse-to-footage converter is mounted in the panel-width case shown in the upper right of figure 1. It is not necessary to take the converter into the field unless playback is planned. A simple check with an earphone enables the operator to tell if data is being recorded on both channels. Since no modifications were made to the tape recorder, recording and later playback may be accomplished with any good quality stereo recorder that uses $\frac{1}{4}$ -inch tape.

APPLICATIONS

The magnetic taping system was first applied to neutron logs made in the upper Brazos River Basin in Texas. The problem in this area was to locate the interface between fresh water and underlying brine behind both plastic and steel casing. It was planned to do this by a collation of neutron-epithermal-neutron and neutron-gamma logs (Dewan and others, 1961). The neutron-epithermal-neutron sonde has a minor response to the chemical composition of the rock matrix and interstitial fluid. In contrast, the neutron-gamma device is affected significantly by the chemical composition of the rock and fluid, and thus by the amount of chloride present. A comparison of the two logs should, therefore, reveal the presence of any large quantities of sodium chloride. One of the problems in the utilization of this technique has been the recording of the two different types of logs with the same horizontal amplitude in rocks saturated with fresh water. This can be done in the field by time-consuming relogging, or it may be readily accomplished in the office during playback of the magnetic tape.

A more common application is the recovery of log data lost by operator basing error (fig. 2). Without a tape system this information is not recoverable unless the hole is relogged. Because the raw data from the probe are on the tape, off scale information may be retrieved at any time. All control module adjustments normally made by the operator at the well may also be made during playback. Changes in both horizontal or

vertical scale may be made simultaneously or independently. Although this is possible with special photographic or pantographic techniques a source of error is introduced by them and a log copy derived from tape is more accurate and economical than a copy made by other techniques.

A unique advantage of the magnetic taping system is that when a log is expanded from tape, detail not present on the original becomes apparent. For example, most natural gamma logs recorded in the vicinity of Anchorage, Alaska, at the conventional sensitivity did not clearly indicate lithologic changes that were shown on neutron and gamma-gamma logs. This situation is usually caused by operator error or by the desire to eliminate rebasing or off scale deflections. Figure 3 shows a field copy of a gamma log made in Anchorage compared with an office tape playback made on a very sensitive, continuously variable scale. Lithologic changes which are obvious on the tape playback log were not thought to be significantly above statistical fluctuations when the field log was first examined.

Important new techniques for derivation of porosity corrected for hole and matrix effects and for interpretation of lithology are based on a cross plot of porosities derived from gamma-gamma and neutron log derived porosities or a comparison of a reversed gamma-gamma log and a neutron log (Alger and others, 1963; Tittman and others, 1965). Figure 4 is an example of these two types of logs from the Anchorage, Alaska, area; it demonstrates that they may be played back from magnetic tape at approximately the same amplitude as an aid to composite log interpretation.

Proper calibration and field standardization are essential to the quantitative interpretation of geophysical logs. Logs on magnetic tape have proven to be invaluable as an aid in quantitative interpretation. All logger calibration runs on the research logging equipment were made at the American Petroleum Institute neutron and gamma calibration facilities in Houston, Tex., and were recorded on tape. The tapes were later played into a laboratory radiation scaler, and counts per second averaged over a long period of time were used to construct calibration curves. The count rates were then compared with values for the neutron or gamma field standards measured in the same way. If two neutron field standard values are recorded immediately after logging a well, tape playback is an excellent means for standardizing logging system response and reducing all the logs for an area to the same porosity scale. Most changes in system response are due to temperature drift and nonlinearity. Standardizing is accomplished by adjusting base and sensitivity on

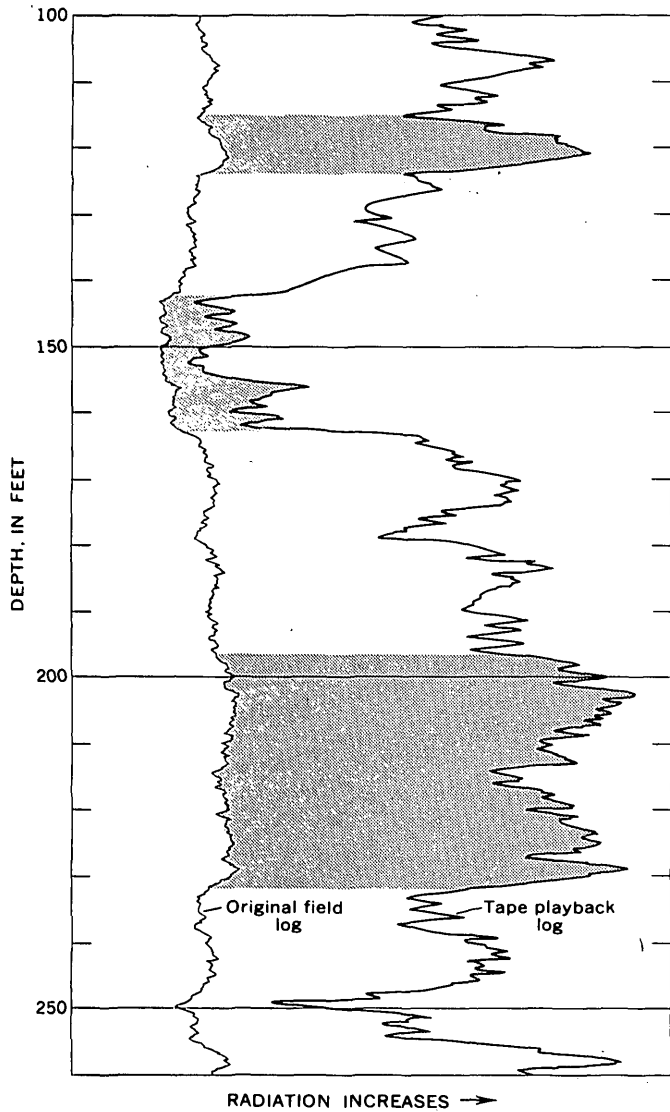


FIGURE 3.—Comparison of original gamma log run at normal sensitivity and tape playback at very high sensitivity (well 280, Anchorage, Alaska). Several important lithologic units are stippled as an aid in comparison of logs.

tape playback until the graphic record for two field standard values coincides with predetermined values. This procedure compensates for changes in source strength, spacing, detector sensitivity, and system gain, but not for hole diameter or casing size. When correction factors for these hole parameters are known, they may also be introduced during tape playback.

The number of logs that can be placed on a spool of tape is a function of both logging and tape speed. During the Anchorage project, more than 150 geophysical logs of wells averaging more than 200 feet in depth were recorded on four 7-inch spools of magnetic tape. These same logs required about 500 linear feet of graph paper 12 inches wide. Logging speed was 40 feet per minute, and tape speed was $3\frac{3}{4}$ inches

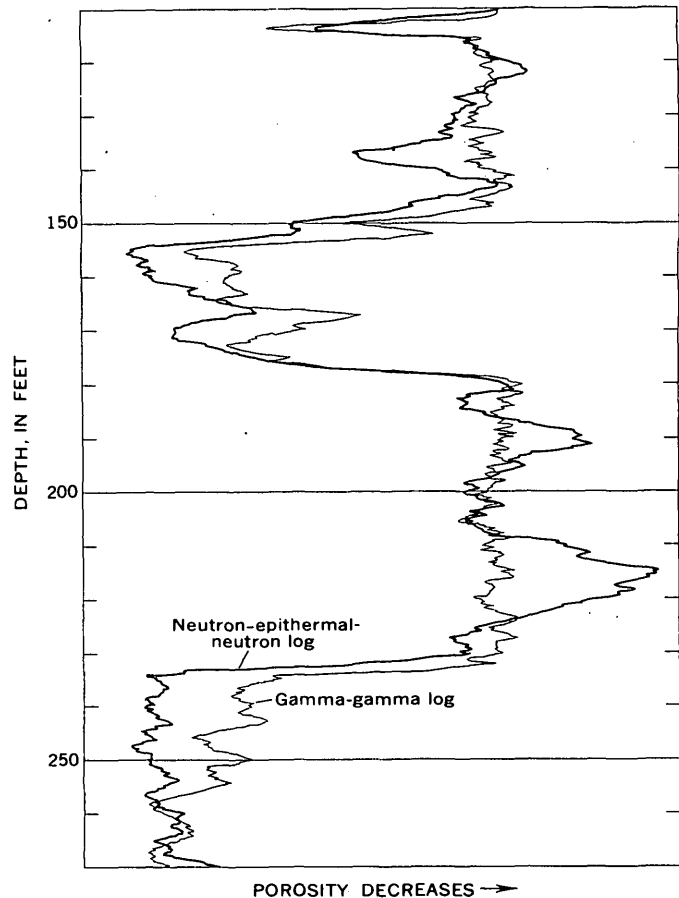


FIGURE 4.—Comparison of neutron log and reversed gamma-gamma log on about the same sensitivity (well 111A, Anchorage, Alaska). Collation of the two logs is the basis for a new technique for determining lithology and porosity corrected for hole and matrix effects.

per second. In order to simplify recovery of data, only one side of the four-track tape was used. If both sides had been used and if recording had been done at $17\frac{1}{8}$ inches per second, all the Anchorage logs could have been stored on one spool of tape. Work to date suggests that accuracy of log reproduction is not affected by tape speed.

It is apparent that geophysical logs recorded on tape can be stored in a fraction of the space presently required for logs on paper and they may be recovered at any time in a format consistent with the planned use.

POTENTIAL USES

Several new applications of magnetic taping of raw data from geophysical logging tools are possible. The present equipment feeds unmodified pulses from the tape directly into the control module or through a pulse shaper which simulates the actual pulses received at the top of the cable. Logs exactly duplicating the original are made by either method. New control or

signal-modification equipment that can be developed in the future may be used on raw data from logging sondes to produce better quality logs and to facilitate log interpretation.

Another possible application of the tape system may be the comparison of logs made before and after pumping. In granular aquifers, extensive pumping or surging is often required to reduce the silt in suspension and to develop the well properly. Most of the fine-grained material produced by this pumping ordinarily comes from the aquifers yielding most of the water. Furthermore, removal of this fine-grained material causes an increase in porosity in the producing zones. Beds in which this increase has taken place can be identified by comparing neutron or gamma-gamma logs made before and after well development. Some of the high-porosity zones, shown by deflections to the left on the logs in figure 4 may be due to the removal of fines during pumping. The use of tape as a means of standardizing the graphic logs facilitates the interpretation of logs made after a time lapse.

In addition the possibility of taping variable height radiation pulses with the equipment is being studied. If this recording proves feasible, tapes can be played back through a multichannel analyzer in the office, and the radiation-energy spectrum can be plotted. This procedure will be more economical and satisfactory than attempting to adapt expensive multichannel analyzers to rough field conditions, and tapes could be used as input to any analyzer. Studies of radiation energy distribution can be used in the following ways: (1) natural gamma—lithologic units may be identified by the differences in naturally occurring radioisotopes, and radioactive wastes may be identified; (2) gamma-gamma—log quality may be improved by discrimination against photon energies derived mostly from inhole scatter; (3) neutron—log quality may also be improved by energy discrimination but more important is its use for inhole neutron-activation analysis. The application of each of these spectral techniques will

be greatly facilitated if the energy distribution can be tape recorded in the field and analyzed in the office.

SUMMARY

The magnetic tape system has the following advantages and capabilities:

1. Logs can be recorded on tape regardless of whether all surface control modules and the graphic recorder are functioning.
2. Many types of operator errors and equipment malfunctions can be corrected in the office, thus reducing time spent in the field and drill-rig standby time. The magnetic tape system also provides a means of salvaging data which might otherwise be lost in cases where it is impossible to relog the hole.
3. Changes in horizontal and vertical scales, time constant, and basing can be made to produce playback logs conforming with these characteristics on other logs in the area.
4. Storage and retrieval of data are more economical.
5. Conversion to digital form for computer input is more rapid and economical.
6. When new control or signal-modification systems are developed, data obtained previously will be available for reprocessing.
7. Logs on magnetic tape can be transmitted by radio or telephone.

REFERENCES

- Alger, R. P., Raymer, L.L., Hoyle, W. R., and Tixier, M. P., 1963, Formation density log applications in liquid-filled holes: *Jour. Petroleum Technology*, v. 15, no. 3, p. 321-332.
- Dewan, J. T., Stone, O. L., and Morris, R. L., 1961, Chlorine logging in cased holes: *Jour. Petroleum Technology*, v. 13, no. 6, p. 531-537.
- Tinch, D. H., Miller, G. K., Carpenter, B. N., and Warren, E. J., 1966, Application of magnetic tapes to well logging: *Jour. Petroleum Technology*, v. 18, no. 6, p. 687-696.
- Tittman, J., Sherman, H., Nagel, W. A., and Alger, R. P., 1965, The sidewall epithermal neutron porosity log: *Soc. Petroleum Engineers Preprint 1180*, 20 p.



SUBJECT INDEX

[For major headings such as "Economic geology," "Geochemistry," "Paleontology," see under State names or refer to table of contents]

A	Page	C	Page		Page
Activity coefficients, determination from emf measurements.....	106	Calcium-magnesium ratios, in ground water from carbonate rocks.....	232	Dunes, San Luis Valley, Colo., geomorphology.....	177
Aerial photographs, measurement of bedrock fractures on.....	184	California, bed-material movement, Middle Fork Eel River.....	219	E	
Alaska, military water supply, southeastern part....	189	bulk precipitation, Mojave Desert.....	222	Earthquakes, Hawaii.....	173
Andesite flow, petrology.....	55	marine geology and bathymetry, southern part..	97	Echo sounding, use in marine geology studies.....	97
Arikaree Formation, Wyoming, heavy-minerals studies.....	42	metamorphism, northwestern Coast Ranges....	1	Electrochemical methods, measurement of activity coefficient values....	106
Arizona, structural geology, Yavapai County.....	60	spheroidal weathering, White Mountains.....	32	Emf measurements, activity coefficients from.....	106
Arroyo Formation, Texas, plant fossils.....	120	Cambrian, Pennsylvania, quality of ground water.....	232	Eocene, Texas, permeability of sandstone.....	192
Atlantic Coastal Plain, New England, subsurface morphology.....	92	Canyons, submarine, California..	97	Equilibria studies, method for activity coefficient measurements.....	106
Atlantic slope, underwater television studies.....	72	Carbonate rocks, calcium-magnesium ratios in ground water from...	232	Equipment, tape recording system for geophysical well logs.....	242
Atomic ratios, in micas, comparison of.....	17	Carbonates, spectrographic determination of elements in.....	132	underwater television system for marine geology studies.....	72
B		Carbondale Formation, Kentucky, stratigraphy..	160	Evaporites, rare-earth mineral in.....	38
Bacteria, sulfur-oxidizing, Steamboat Springs, Nev... 110	110	Celadonite, analysis, Reno, Nev. 17	17	F	
Basalt, grouped spectrographic analyses..... 113	113	Coal beds, western Kentucky, stratigraphy..... 160	160	Faults, wrench-type, Arizona... 60	60
Base flow, estimation at ungaged stream sites..... 208	208	Colorado, geomorphology, Great Sand Dunes National Monument..... 177	177	<i>See also</i> Fractures.	
summer, Potomac River... 212	212	volcanism and tectonism, northeastern part.... 42	42	Florida, lake studies, central part..... 236	236
Bed-material movement, California..... 219	219	Computer, use in deriving mineral formulas..... 23	23	Flow-volume curves, use in planning off-stream storage..... 216	216
Block Island Sound, subsurface morphology studies.. 92	92	Connate water, immobility in sandstone..... 192	192	Formulas, minerals, computer program for deriving.. 23	23
Bonneville Salt Flats, Utah, geochemistry of brine... 116	116	Conodonts, Mississippian, Idaho. 127	127	Fractures, abundance measured on aerial photographs.. 184	184
Boston Basin, Massachusetts, engineering geology.. 165	165	Continental Shelf, underwater television studies.... 72	72	Franciscan Formation, metamorphism, California-Oregon..... 1	1
Boston Bay Group, Massachusetts, engineering geology..... 165	165	Cretaceous, California-Oregon, stratigraphy..... 1	1	Fraser Glaciation, Wallowa Lake, Oreg..... 145	145
Breccia pipes, stratigraphy and structural geology, Utah..... 66	66	Current meters, use in estimating base steamflow... 208	208	Freezing, effect on dissolved solids in prairie-pothole ponds..... 228	228
Brines, geochemistry, Utah.... 116	116	D		G	
Bulk precipitation, California, chemical characteristics..... 222	222	Deformation, Koaie fault system, Hawaii..... 173	173	Gardena Sand, California, marine geology..... 97	97
Buzzards Bay, New England, subsurface morphology..... 92	92	Discharge, ice-covered streams, computation..... 200	200	Geophysical well data, tape recording system..... 242	242
		Dissolved solids, prairie-pothole ponds, North Dakota.. 228	228	Georgia, marine studies, Atlantic coastal area..... 72	72
		Dolomite, spheroidal weathering.. 32	32		

	Page	M	Page		Page
Glacial deposits, correlation, Wallowa Lake, Oreg.	145	Maine, heavy minerals, coastal rivers.....	77	Muscovite, in metamorphic rock, northwestern North Carolina.....	10
Glaciers, movement and ablation, Wyoming.....	154	Marine evaporites, rare-earth-mineral occurrence..	38	N	
Grand Teton National Park, Wyo., glaciology.....	154	Maryland, base flow, Potomac River.....	212	Nebraska, volcanism and tectonism, western part..	42
Great Sand Dunes National Monument, Colo., geomorphology.....	177	Massachusetts, engineering geology, Boston area....	165	Neutron activation method, phosphorus determination in silicate rocks.....	137
Gulf of Maine, heavy minerals..	77	heavy minerals, coastal rivers.....	77	Nevada, mineralogy, Reno area..	17
H		Menlo Park, Calif., bulk precipitation.....	222	sulfur-oxidizing bacteria, Steamboat Springs..	110
Hawaii, earthquakes.....	173	Mesozoic. <i>See</i> Jurassic, Cretaceous.		New Hampshire, heavy minerals, coastal rivers.....	77
Heavy minerals, in Gulf of Maine.....	77	Metagraywacke, textural zones, California-Oregon...	1	New Jersey, surface water, South Branch Raritan River.....	216
use in detecting volcanism and tectonism.....	42	Metamorphic rocks, carbonate, weathering.....	32	North Carolina, metamorphic rocks, Grandfather Mountain area.....	10
Hot Springs, sulfuric acid production.....	110	iron-rich, northwestern North Carolina.....	10	North Dakota, quality of pond water, southeastern part.....	228
I		zonation, California-Oregon..	1	volcanism and tectonism, southwestern part....	42
Ice, river, underside configuration.....	195	Methods and techniques, computation of discharge of ice-covered streams.....	200	O	
Ice-covered streams, computed discharge.....	200	electrochemical measurement of activity coefficient values.....	106	Ogallala Formation, Wyoming, heavy-minerals studies.....	42
Idaho, stratigraphy, east-central part.....	127	neutron activation determination of phosphorus.....	137	Ordovician, Pennsylvania, quality of ground water..	232
Infiltration gallery, as freshwater source.....	189	spectrographic determination of volatile elements.....	132	Oregon, glaciation, Wallowa County.....	145
Instruments and equipment. <i>See</i> Equipment.		spectrophotometric determination of palladium..	141	metamorphism, southwestern Coast ranges....	1
Ion activity products, calculation for brine.....	116	X-ray analysis of celadonite. <i>See also</i> Computer, Echo sounding, Tape recorder, Television.	17	Oxidation, iron-rich metamorphic rock, northwestern North Carolina.....	10
J		Micas, comparison of analyses..	17	P	
Jurassic, California-Oregon, stratigraphy and mineralogy.....	1	Microbiology, Steamboat Springs, Nev.....	110	Paleobotany, north-central Texas, Arroyo Formation....	120
K		Middle Fork Eel River, Calif., bed-material movement.....	219	Paleozoic, Utah, stratigraphy and structural geology...	66
Kansas, methods for estimating base flow of streams..	208	Milligen Formation, Idaho, stratigraphy.....	127	<i>See also</i> Cambrian, Ordovician, Mississippian, Pennsylvanian, Permian.	
Kaolinization, bedrock, Boston, Mass., area.....	165	Minerals, computer program for deriving formulas...	23	Palladium, spectrophotometric determination.....	141
Kentucky, stratigraphy and economic geology, western coal field.....	160	Mississippian, Idaho, stratigraphy.....	127	Palos Verdes Hills fault, California.....	97
Kilauea Volcano, Hawaii, earthquakes.....	173	Mojave Desert, Calif., bulk precipitation.....	222	Paradox Member, Hermosa Formation, Utah, rare-earth mineral.....	38
Koae fault system, Hawaii.....	173	Montana, volcanism and tectonism, eastern part...	42	Pennsylvania, quality of ground water, Lancaster quadrangle.....	232
L		Monterey Shale, California, marine geology.....	97	Pennsylvanian, Utah, rare-earth mineral.....	38
Lake studies, shoreline features, Florida.....	236	Moraines, correlation, Wallowa Lake, Oreg.....	145		
Limestone, spheroidal weathering.....	32	Mount Adams, Wash., andesite flow.....	55		
Long Island Sound, New York-New England, subsurface morphology..	92				
Lost River Range, Idaho, paleontology.....	127				

SUBJECT INDEX

C249

	Page
Permian, Texas, plant fossils....	120
Phosphorus, determination by neutron activation....	137
Piercement structure, in area of wrench fault.....	60
Porosity, fractured rocks, deter- mination from aerial photographs.....	184
Potentials, measurement of, emf cells.....	106
Potomac River, Maryland-Vir- ginia, base flow.....	212
Prairie-pothole ponds, North Da- kota, dissolved solids in.....	228
Precambrian, Arizona, wrench fault.....	60
Utah, stratigraphy and struc- tural geology.....	66
Precipitation, chemical quality, California.....	222
Precipitation of soluble salts, method of predicting..	116
Profiling, subbottom, high-effi- ciency method.....	81
Q	
Quaternary, California, marine geology.....	97
Colorado, geomorphology..	177
Washington, petrology of andesite flow.....	55
R	
Rare-earth mineral, in evaporites, Utah.....	38
Redondo submarine canyon, Cal- ifornia, origin.....	97
Reed Dolomite, California, spher- oidal weathering....	32
Rhode Island Sound, subsurface morphology.....	92
Riverbed material, movement, Middle Fork Eel Riv- er, Calif.....	219
Rivers, computation of discharge under ice cover.....	200
underside configuration of ice cover.....	195
S	
St. Croix River, Wis., ice studies..	195
Salmon Springs Glaciation, Wal- lowa Lake, Oreg.....	145
Sandstone, immobile connate water in.....	192

	Page
Seismic studies, subsurface pro- filing, Long Island Sound area.....	92
<i>See also</i> Earthquakes.	
Sheeprock Mountains, Utah, breccia pipes.....	66
Shoreline features, as indicators of lake levels.....	236
Silicate rocks, determination of phosphorus in.....	137
Silicates, spectrographic deter- mination of elements in.....	132
South Dakota, volcanism and tectonism, western part.....	42
South Fork Mountain Schist, metamorphism, Cali- fornia-Oregon.....	1
Spectrographic analyses, basaltic rocks.....	113
volatile elements.....	132
Spectrophotometric determina- tion, palladium.....	141
Statistics, regression analyses for estimating base streamflow.....	208
Streamflow, base flow, methods for estimating.....	208
base flow, characteristics...	212
flow - volume distribution studies.....	216
Streams, ice-covered, computed discharge.....	200
underside configuration of ice cover.....	195
Subbottom profiling, high- efficiency method....	81
Submarine canyons, California..	97
T	
Tape recorder, use in geophysical well studies.....	242
Tectonism and volcanism, Wyo- ming, heavy minerals indicating.....	42
Television, use in marine geology..	72
Tertiary, California, marine geology.....	97
Utah, stratigraphy and structural geology...	66
Wyoming, history of vol- canism and tec- tonism.....	42
<i>See also</i> Eocene.	
Teton Glacier, Wyo., surveys...	154
Texas, permeability of sandstone, Karnes County.....	192
plant fossils, Baylor County..	120

	Page
Trace elements, in celadonite, Reno, Nev.....	17
spectrographic determina- tion of.....	132
Tradewater Formation, Ken- tucky, stratigraphy..	160
Transport, movement of river- bed material.....	219
U	
Utah, geochemistry, Bonneville Salt Flats.....	116
rare-earth mineral, south- eastern part.....	38
stratigraphy and struc- tural geology, Juab County.....	66
V	
Virginia, aerial-photograph studies, Shenandoah Valley.....	184
Volcanic rocks, Utah, stratig- raphy and structural geology.....	66
Washington, petrology of andesite flow.....	55
<i>See also</i> Basalt.	
Volcanism and tectonism, Wyo- ming, heavy minerals indicating.....	42
W	
Washington, petrology, Mount Adams andesite flow..	55
Water supply, Alaska, use of infiltration gallery...	189
Weathering, spheroidal, limestone and dolomite.....	32
Well logs, tape recording system..	242
West Tintic Mountains, Utah, breccia pipes.....	66
White River Formation, Wyo- ming, heavy-minerals studies.....	42
Wisconsin, studies of ice-covered St. Croix River...	195, 200
Wyman Formation limestone, California, spheroidal weathering.....	32
Wyoming, glaciology, Teton Glacier.....	154
volcanism and tectonism, heavy minerals indi- cating.....	42
X	
X-ray analysis, celadonite, Reno, Nev.....	17

AUTHOR INDEX

	Page
A	
Anderson, C. A.....	60
Angelo, C. G.....	189
Annell, Charles.....	132
B	
Becher, A. E.....	232
Blake, M. C., Jr.....	1
Bowen, R. W.....	23
Bradley, Edward.....	72
Bryant, Bruce.....	10
Busby, M. W.....	208
C	
Carey, K. L.....	195, 200
Christ, C. L.....	106
Coleman, R. G.....	1
Crandell, D. R.....	145
D	
Denson, N. M.....	42
E	
Eddy, J. E.....	72
Ehrlich, G. G.....	110
F	
Feth, J. H.....	222
Feulner, A. J.....	189
Ficken, J. H.....	228
Foster, M. D.....	17
Franklin, G. J.....	160
Furness, L. W.....	208
G	
Gorsline, D. S.....	97
Graves, M. L.....	113

	Page
Greenland, L. P.....	137
Grimaldi, F. S.....	141
Groves, H. L., Jr.....	38
Gude, A. J. 3d.....	38
H	
Hanson, R. L.....	212
Henry, V. J.....	72
Heyward, H. H.....	189
Hostetler, P. B.....	106
Hoyt, John.....	72
Huddle, J. W.....	127
I	
Irwin, W. P.....	1
J	
Jackson, E. D.....	23
Johnson, R. B.....	177
K	
Kaye, C. A.....	165
Kehn, T. M.....	160
Keys, W. S.....	242
Kinoshita, W. T.....	173
Knochenmus, D. D.....	236
Kopf, R. W.....	66
L	
LaMarche, V. C., Jr.....	32
Lovering, T. G.....	113
M	
Mamay, S. H.....	120
Manger, G. E.....	192
Mapel, W. J.....	127
Meisler, Harold.....	232

	Page
Miller, E. G.....	216
Morris, H. T.....	66
N	
Niles, M. S.....	113
P	
Palmer, J. E.....	160
Polzer, W. L.....	116
R	
Raup, O. B.....	38
Reed, J. C., Jr.....	154
Ritter, J. R.....	219
Roberson, C. E.....	116
Ross, D. A.....	77
Rusnak, G. A.....	81, 97
S	
Sandberg, C. A.....	127
Sato, Yoshiaki.....	42
Schnepfe, M. M.....	141
Schoen, Robert.....	110
Sheppard, R. A.....	55
Stevens, R. E.....	23
T	
Tagg, A. R.....	92
Trainer, F. W.....	184
U	
Uchupi, Elazar.....	92
W	
Wertman, W. T.....	192
Y	
Yerkes, R. F.....	97